Universitat
de Girona

MODEL ARYL HALIDE MACROCYCLIC SUBSTRATES FOR THE ELUCIDATION OF COINAGE METAL CATALYSED CROSS-COUPLING REACTION MECHANISM

Marc Font Molins

Dipòsit legal: Gi. 351-2015
http://hdl.handle.net/10803/285975

ADVERTIMENT. L'accés als continguts d'aquesta tesi doctoral i la seva utilització ha de respectar els drets de la persona autora. Pot ser utilitzada per a consulta o estudi personal, així com en activitats o materials d'investigació i docència en els termes establerts a l'art. 32 del Text Refós de la Llei de Propietat Intel·lectual (RDL 1/1996). Per altres utilitzacions es requereix l'autorització prèvia i expressa de la persona autora. En qualsevol cas, en la utilització dels seus continguts caldrà indicar de forma clara el nom i cognoms de la persona autora i el títol de la tesi doctoral. No s'autoritza la seva reproducció o altres formes d'explotació efectuades amb finalitats de lucre ni la seva comunicació pública des d'un lloc aliè al servei TDX. Tampoc s'autoritza la presentació del seu contingut en una finestra o marc aliè a TDX (framing). Aquesta reserva de drets afecta tant als continguts de la tesi com als seus resums i índexs.

ADVERTENCIA. El acceso a los contenidos de esta tesis doctoral y su utilización debe respetar los derechos de la persona autora. Puede ser utilizada para consulta o estudio personal, así como en actividades o materiales de investigación y docencia en los términos establecidos en el art. 32 del Texto Refundido de la Ley de Propiedad Intelectual (RDL 1/1996). Para otros usos se requiere la autorización previa y expresa de la persona autora. En cualquier caso, en la utilización de sus contenidos se deberá indicar de forma clara el nombre y apellidos de la persona autora y el título de la tesis doctoral. No se autoriza su reproducción u otras formas de explotación efectuadas con fines lucrativos ni su comunicación pública desde un sitio ajeno al servicio TDR. Tampoco se autoriza la presentación de su contenido en una ventana o marco ajeno a TDR (framing). Esta reserva de derechos afecta tanto al contenido de la tesis como a sus resúmenes e índices.

WARNING. Access to the contents of this doctoral thesis and its use must respect the rights of the author. It can be used for reference or private study, as well as research and learning activities or materials in the terms established by the 32nd article of the Spanish Consolidated Copyright Act (RDL 1/1996). Express and previous authorization of the author is required for any other uses. In any case, when using its content, full name of the author and title of the thesis must be clearly indicated. Reproduction or other forms of for profit use or public communication from outside TDX service is not allowed. Presentation of its content in a window or frame external to TDX (framing) is not authorized either. These rights affect both the content of the thesis and its abstracts and indexes.

Universitat de Girona

DOCTORAL THESIS

Model aryl halide macrocyclic substrates for the elucidation of coinage metal catalysed cross-coupling reaction mechanisms

Marc Font Molins

2015

Doctoral programme in Chemistry

Supervised by: Dr. Xavi Ribas Salamaña and Dr. Miquel Costas Salgueiro

Tutor: Dr. Xavi Ribas Salamaña

This manuscript has been presented to opt for the doctoral degree from the University of Girona

Dr. Xavi Ribas Salamaña and Miquel Costas Salgueiro, from the Universitat de Girona,

WE DECLARE:

That the thesis entitled “Model aryl halide macrocyclic substrates for the elucidation of coinage metal catalysed cross-coupling reaction mechanisms” presented by Marc Font Molins to obtain a doctoral degree, has been completed under our supervision and meets the requirements to opt for an International Doctorate.

For all intents and purposes, we hereby sign this document.

Dr. Xavi Ribas Salamaña Dr. Miquel Costas Salgueiro

Girona, 16th January 2015

La ment que s'obre a una nova idea
mai tornarà a la seva mida original

Albert Einstein

FULL LIST OF PUBLICATIONS

This thesis is based on a compendium of the followed publications:

Chapter III

Catalytic C-S, C-Se, and C-P Cross-Coupling Reactions Mediated by a Cu^{I}/Cu^{III} Redox Cycle. Font, M., Parella, T., Costas, M., Ribas, X. *Organometallics* **2012**, 31(22), 7976-7982. (Impact factor: 4.253, position 5/44 in Chemistry, Inorganic & Nuclear, 1st quartile)

Chapter IV

Direct Observation of Two-Electron Ag(I)/Ag(III) Redox Cycles in Coupling Catalysis. Font, M., Acuña-Parés, F., Parella, T., Serra, J., Luis, J. M., Lloret-Fillol, J., Costas, M., Ribas, X. *Nat. Commun.* **2014**, 5:4373, DOI: 10.1038/ncomms5373. (Impact factor: 10.742, position 3/55 in Multidisciplinary Sciences, 1st quartile)

All these papers have been published in journals that belong to the first quartile according to JCR.

LIST OF ABBREVIATIONS

ºC	Degree(s) Celsius
Å	Angstrom(s)
AcFc	Acetylferrocene
AcFc$^+$	Acetylferrocinium cation
AD	Adduct
Abs	Absorbance
Ac	Acetyl
Ar	Aryl
AT	Atom Transfer
B	Base
BDE	Bond Dissociation Energy
cat	Catalyst
CFL	Compact Fluorescent Light
CHD	Cyclohexadiene
COSY	Correlation Spectroscopy
CV	Cyclic Voltammetry
DDQ	2,3-Dichloro-5,6-dicyano-1,4-benzoquinone
DFT	Density Functional Theory
DMEDA	*N*,*N*′-Dimethylethylenediamine
DMF	Dimethylformamide
DMSO	Dimethyl Sulfoxide
E^0	Standard potential
equiv	Equivalent
EPR	Electron Paramagentic Ressonance
ESI-MS	Electrospray Mass Spectrometry
Et	Ethyl
exc	Excess
FT-IR	(Fourier Transform) Infrared spectroscopy
G	Gibbs free energy
h	Hour(s)
HMBC	Heteronuclear Multiple Bond Correlation
HRMS	High Resolution Mass Spectrometry
HSQC	Heteronuclear Single Quantum Coherence Spectroscopy
Hz	Hertz
ICP-MS	Inductively Coupled Plasma Mass Spectrometry
*i*Pr	Isopropyl
IPrAuOH	1,3-bis(2,6-diisopropylphenyl)-1H-imidazol-2(3H)-ylidene gold(I) hydroxide
J	Magnetic scalar coupling
HSQMBC-IPAP	In-Phase Anti-Phase Heteronuclear Single Quantum Multiple Bond Correlation
K	Degree(s) Kelvin
kg	Kilogram(s)
L	Ligand

M	Molar
Me	Methyl
MHz	Megahertz
Min	Minute(s)
mL	Millilitre(s)
mM	Millimolar
m/z	Mass/charge
*n*Bu	Butyl
NCP	*N*-Confused Porphyrin
NIH	National Institutes of Health
nm	Nanometer(s)
NMP	*N*-Methyl-2-Pyrrolidone
NMR	Nuclear Magnetic Resonance
NOESY	Nuclear Overhauser effect spectroscopy
Nu	Nucleophile
OTf	Trifluoromethanesulphonic anion
OTs	*p*-Toluenesulphonic anion
P	Product
PCET	Proton Coupled Electron Transfer
PET	Positron Emission Tomography
Ph	Phenyl
phen	1,10-Phenanthroline
ppm	Part(s) per million
py	Pyridine
R	Residue
rds	Rate determining step
rt	Room temperature
s	Second(s)
SCE	Saturated Calomel Electrode
S_EAr	Aromatic Electrophilic Substitution
SET	Single electron transfer
stoich	Stoichiometric
t	Time
T	Temperature
*t*Bu	*Tert*-butyl
TEMPO	2,2,6,6-Tetramethylpiperidine 1-oxyl
THF	Tetrahydrofuran
Tol	Toluene
TS	Transition State
UVC	Ultraviolet C
UV-Vis	Ultraviolet-Visible spectroscopy
V	Volt(s)
W	Watt(s)

LIST OF FIGURES

Figure I. 1. X-ray structures of **2**$_{Cl}$, **2**$_{Br}$ and **2**$_{I}$ complexes (ellipsoid representation at 50% probability). Hydrogen and corresponding halide counterions are omitted for clarity. 27

Figure I. 2. X-ray structures of complex **47** (ellipsoid representation at 50% probability). Hydrogen and perchlorate counterions are omitted for clarity... 27

Figure I. 3. UV-Vis monitoring of the sequential interconversion between Cu^{III}/Cu^{I} redox states with complex **2**$_{Br}$ through addition of acid or base... 29

Figure V. 1. **A**) Low temperature ^{1}H NMR monitoring of the reaction of complex **1**-Cu^{III} with 1-butanethiol revealing the formation of an adduct (**AD**) before reaching the formation of the reaction product (**P**). Conditions: [**1**-Cu^{III}] = 4 mM, [1-butanethiol] = 3.6 mM, CD_3CN, 0 ºC. **B**) Low temperature UV-Vis monitoring of the reaction of **1**-Cu^{III} with 1-butanethiol exhibiting the formation of an adduct species. Conditions: [**1**-Cu^{III}] = 0.8 mM, [1-butanethiol] = 0.72 mM, CH_3CN, 0 ºC............................... 81

Figure V. 2. ORTEP thermal ellipsoid diagram (at 50 % probability level) of the cationic moiety of **1**-Ag^{III} complex. The hydrogen atoms and the two perchlorate counteranions have been omitted for clarity. Selected bond lengths (Å) and angles (º) for **1**-Ag^{III}: Ag-C(16) 1.974(2), Ag-N(3) 2.084(2), Ag-N(1) 2.085(5), Ag-N(2) 2.153(2); C(16)-Ag-N(3) 82.03(10), C(16)-Ag-N(1) 81.6(1), N(3)-Ag-N(2) 98.2(1), N(1)-Ag-N(2) 98.4(1), C(16)-Ag-N(2) 178.2(1), N(3)-Ag-N(1) 162.1(1)... 85

Figure V. 3. Comparison of the benzylic region of **1**-Ag^{III} in the ^{1}H NMR and ^{1}H{^{109}Ag} NMR experiments (298 K, CD_3CN, 400 MHz)... 87

LIST OF TABLES

Table V. 1. Reaction of **1**-Cu^{III} with sulphur-, selenium- and phosphorus-based nucleophiles resulting in the formation of the corresponding C-S, C-Se and C-P coupling products.. 79

Table V. 2. Reactivity of **1**-Cu^{III} complex with bifunctional thiol/alcohol and thiol/carboxylic acid substrates.. 80

Table V. 3. Copper-catalysed C-S, C-Se, C-P bond forming cross-coupling reactions........................... 83

Table V. 4. Stoichiometric coupling of the aryl-Ag^{III} complex **1**-Ag^{III} with nucleophiles....................... 88

Table V. 5. Silver-mediated fluorination of aryl bromide model substrates. 90

Table V. 6. Silver-catalysed C-O and C-C bond forming cross-coupling reactions within **L$_1$-X** model aryl halide substrates.. 92

LIST OF SCHEMES

Scheme I. 1. Novel silver-based methodologies for organic synthesis 16

Scheme I. 2. Radical and non-radical reaction intermediates postulated to operate in Ullmann-Goldberg-type coupling reactions 19

Scheme I. 3. Proposed mechanistic pathways for the Ullmann-Goldberg reaction following radical Cu^{I}/Cu^{II} catalytic cycles initiated by a SET 20

Scheme I. 4. Ligand-directed chemoselective copper-catalysed N-arylation and O-arylation of 5-amino-1-pentanol using 3-bromoiodobenzene and bidentate ligands 20

Scheme I. 5. **A**) Photoinduced Ullmann C-N coupling reactions of Cu^{I}-carbazolide complex **24** with aryl halides. **B**) Formation of the cyclisation plus C-N bond formation product **31** in a photoinduced Ullmann protocol using an allyloxyiodobenzene as radical probe substrate. **C**) Stereochemistry study of the cyclised products obtained using allyloxyiodobenzene substrates. **D**) Substrate competition experiment in a photoinduced Ullmann methodology 22

Scheme I. 6. **A**) Photoinduced copper-catalysed alkylation of aromatic amides. B) General mechanistic proposal for the photoinduced Ullmann-Goldberg coupling methodology by J. Peters and G. Fu 24

Scheme I. 7. Proposed mechanistic pathways for the Ullmann-Goldberg reaction following oxidative addition/reductive elimination fundamental steps 25

Scheme I. 8. Reactivity of an heteroleptic phenanthtroline Cu^{I}-amidate complex with *p*-iodotoluene 26

Scheme I. 9. **A**) Copper-catalysed C-O bond forming cross-coupling reaction within a macrocyclic model aryl halide substrate. **B**) General mechanistic scenario operating in Cu-catalysed C-N, C-O cross-coupling reactions and halide exchange reactions within triazamacrocyclic model aryl halide platforms 30

Scheme I. 10. Glaser-type homocoupling of silver phenylacetylide 32

Scheme I. 11. Silver-catalysed homocoupling reaction of alkyl Grignard reagents 32

Scheme I. 12. Competition experiment of the alkylation of secondary and tertiary alkyl bromides 33

Scheme I. 13. Silver-catalysed intramolecular cyclisation plus benzylation of (2-iodocyclohexyloxy)vinylsilane 34

Scheme I. 14. Silver-mediated homocoupling reaction of boranes 34

Scheme I. 15. Silver-catalysed cross-coupling reactions traditionally operated through two-electron redox cycles by their analogous Pd- and Cu-catalysed reactions 35

Scheme I. 16. Silver-promoted fluorination of arenes bearing transmetallating agents 36

Scheme I. 17. Mechanistic proposal for the silver-catalysed fluorination of arylstannanes Mechanistic proposal for the silver-catalysed fluorination of arylstannanes 37

Scheme I. 18. Silver-mediated pyridination of benziporphyrin 37

Scheme I. 19. Mechanistic proposal involving aryl-Ag^{III} species to rationalise the regioselective pyridination of benziporphyrin **75** 38

Scheme I. 20. A) Phosphanylation of the furanone-Ag^{III} complex **79** through reductive elimination. **B**) Phosphanylation of the NCP-Ag^{III} complex **82** through reductive elimination and dephosphorylative insertion of AgOAc over product **84** to restore complex **82** 39

Scheme I. 21. General mechanism for the gold-catalysed oxidative coupling reactions promoted by sacrificial external oxidants........ 40

Scheme I. 22. Gold-catalysed cascade heterocyclisation plus oxidative arylation of alkenes........ 40

Scheme I. 23. A) Gold-catalysed intermolecular allylation of arylboronic acids proposed to operate through Au^{II}-Au^{II} bimetallic intermediate species **90**. **B**) Model stepwise intramolecular allylation of arylboronate ester **92** via allyl-Au^{III} species **94** formed upon monometallic oxidative addition. 42

Scheme II. 1. General mechanistic arena for the copper and silver-catalysed model cross-coupling reactions........ 50

Scheme V. 1. Proposed catalytic cycle by Shyu and co-workers for the copper-catalysed arylation of thiophenol 77

Scheme V. 2. Mechanistic proposal for the C-S cross-coupling between aryl-Cu^{III} complex **1**-Cu^{III} and thiol nucleophiles 82

Scheme V. 3. General proposed mechanism of copper-catalysed C-S, C-Se and C-P bond forming cross-coupling reactions through the intermediacy of aryl-Cu^{III} complexes within a model triazamacrocyclic aryl bromide substrate 84

Scheme V. 4. Silver-catalysed bromination of model aryl iodide **L_1-I** substrate 93

Scheme V. 5. Mechanistic proposal for the catalytic cycle of the model silver-catalysed cross-coupling reactions operating via aryl-Ag^{III} species 94

ACKNOWLEDGEMENTS

This work would not have been possible without the following collaborations:

- Serveis Tècnics de Recerca from Universitat de Girona for technical support.
- Dr. Julio Lloret, Dr. Josep M. Luis and Ferran Acuña Parés from the Institut de Química Computacional i Catàlisi of Universitat de Girona for DFT calculations.
- Dr. Teodor Parella from Servei de RMN at Universitat Autònoma de Barcelona for NMR experiments and fruitful discussions.
- Dr. Santi Sala and Mr. José Amable Bernabé from Institut de Ciència dels Materials de Barcelona (ICMAB-CSIC) for turbidity measurements.
- Prof. Dr. John F. Hartwig from University of California at Berkeley for hosting a scientific visit and the collaborative research in the mechanistic investigations on Ullmann-type biaryl ether formation in the presence of anionic ligands.
- European Research Council (ERC) for financial support through project ERC-2011-StG-277801.
- MINECO of Spain for financial support through projects CTQ2009-08464/BQU, CTQ2012-37420-C02-01/BQU, CTQ2012-32436/BQU and for the Ph.D. FPI grant BES-2010-030894.

GRAPHICAL ABSTRACT

Summary (p.10)

Chapter I. General Introduction (p.13)

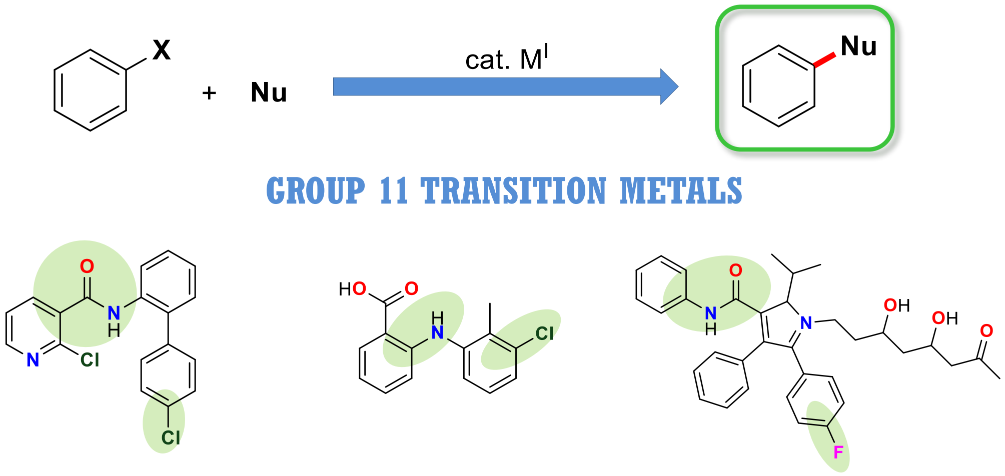
X
+
Nu
cat. M^I
Nu
GROUP 11 TRANSITION METALS
O
N
H
N
Cl
Cl
HO
O
H
N
Cl
O
N
H
N
OH
OH
O
F

Chapter II. Main Objectives (p.47)

Chapter III. Catalytic C-S, C-Se, and C-P Cross-Coupling Reactions Mediated by a Cu^{I}/Cu^{III} Redox Cycle (p.51)

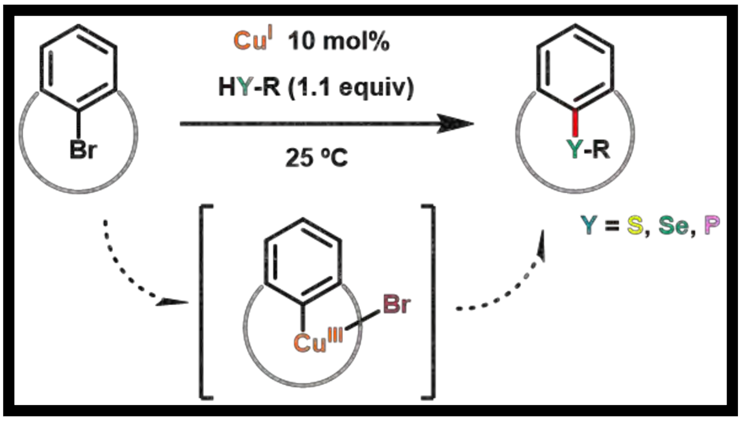
Cu^I 10 mol%
HY-R (1.1 equiv)
25 °C
Br
Y-R
Br
Cu^III
Y = S, Se, P

Chapter IV. Direct Observation of Two-Electron Ag(I)/Ag(III) Redox Cycles in Coupling Catalysis (p.61)

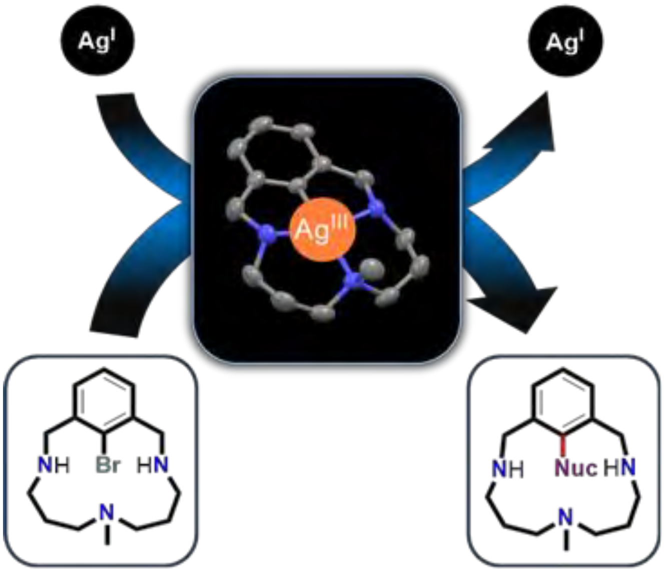
Ag^I
Ag^I
Ag^{III}
NH
Br
HN
N
NH
Nuc
HN
N

Chapter V. Results and discussion (p.73)

Chapter VI. General Conclusions (p.97)

ANNEX I (p.101)

ANNEX II (p.169)

TABLE OF CONTENTS

Summary 10

Resum 11

Resumen 12

Chapter I. General Introduction 13

I.1. Coinage Metals in Organic Synthesis 15

I.2. Cross-Coupling Catalysis 17

I.3. Copper in Cross-Coupling Catalysis 18

I.3.1 Mechanistic aspects on copper cross-coupling reactions 18

I.3.2 One electron redox Cu^{I}/Cu^{II} proposal 19

I.3.2.1. Photoinduced Ullmann-type couplings operating via SET mechanism 21

I.3.3 Oxidative addition/reductive elimination Cu^{I}/Cu^{III} proposal 24

I.3.3.1. Chelation-assisted stabilisation of high-valent copper species 26

I.3.3.2. Application of stable aryl-Cu^{III} complexes to the fundamental understanding of Cu redox processes 28

I.3.3.3. Mechanistic insights on Ullmann-Goldberg-type coupling reactions 29

I.3.4 General outlook on Ullmann-type condensations 31

I.4. Silver in Coupling Reactions 32

I.4.1 Silver-promoted homocoupling reactions 32

I.4.2 Silver-promoted oxidative coupling reactions 35

I.4.3 Silver-promoted coupling chemistry via Ag^{I}/Ag^{III} redox cycles 37

I.5. Gold in Coupling Catalysis 39

I.6. References 43

Chapter II. Main objectives 47

Chapter III. Catalytic C-S, C-Se, and C-P cross-coupling reactions mediated by a Cu^{I}/Cu^{III} redox cycle 51

Chapter IV. Direct observation of two-electron Ag(I)/Ag(III) redox cycles in coupling catalysis 61

Chapter V. Results and discussion 73

V.1. ..Catalytic C-S, C-Se, and C-P cross-coupling reactions mediated by a Cu^{I}/Cu^{III} redox cycle 76
V.2. Direct observation of two-electron Ag(I)/Ag(III) redox cycles in coupling catalysis 84
V.3. References........95

Chapter VI. General conclusions 97

Annex I........101
A. 1. Supplementary information Chapter III........103
Annex II 169
A. 2. Supplementary information Chapter IV........171

SUMMARY

Transition metal-catalysed cross-coupling reactions in organic synthesis have revolutionised the design of retro-synthetic strategies for the preparation of new organic compounds. Despite such methodologies have been extensively developed for copper, especially for the generation of C_{sp2}-nucleophile coupling products, fundamental pathways that govern such processes are still under debate. The number of examples of related methodologies promoted by the other two coinage metals, silver and gold, are much scarcer due to several impediments. With regard to silver redox chemistry, its engagement on two-electron transitions switching from Ag^{I}/Ag^{III} redox states has been rarely proposed and never properly proven. Owing to the otherwise well-established M^{n}/M^{n+2} mechanistic nature of classical cross-coupling chemistry the possibility that silver could carry out parallel transformations has been disregarded. Gold oxidative couplings, on the other hand, are often invoked to occur through Au^{I}/Au^{III} redox cycles in which a sacrificial oxidant drives the first oxidation step to produce key Au^{III} species. Nonetheless, challenging oxidative additions over C-halide bonds have precluded gold-catalysed cross-coupling reactions in the absence of oxidants.

The first part of this thesis deals with the reactivity of a well-defined aryl-Cu^{III} complex bearing a triazamacrocyclic ligand that serves as a platform to study the nature of copper-catalysed C-S, C-Se and C-P bond forming reactions. The results obtained set rational ground for the implication of aryl-Cu^{III} species in such reactions and provide insights on the key parameters that dominate these transformations.

We subsequently explored the possibility that analogous reactivity could take place on silver centres. The analogous aryl-Ag^{III} complex was isolated upon monometallic oxidative addition of Ag^{I} over aryl halide substrates bearing an anchor with three amine coordination sites available to assist the stabilization of silver in a high-valent state. **1**-Ag^{III} complex showed coupling in the presence of a broad range of nucleophiles of different nature via reductive elimination. The aforementioned fundamental steps can occur consecutively achieving Ullmann-type and Hurtley-type cross-coupling reactions under silver catalysis. The results discussed herein validate the plausibility of oxidative addition and reductive elimination steps on silver centres and unravels a mechanism based on two-electron redox cycles Ag^{I}/Ag^{III} in silver-catalysed cross-coupling reactions.

RESUM

Les reaccions d'acoblament creuat catalitzades per metalls de transició han revolucionat el disseny de les anàlisis retrosintètiques per a la preparació de nous compostos orgànics. Encara que el desenvolupament d'aquestes estratègies ha estat extens per al coure, especialment per a la formació de productes d'acoblament del tipus C_{aril}-nucleòfil, els passos fonamentals que regeixen aquests processos continuen encara generant controvèrsia. Tanmateix, els exemples de metodologies relacionades promogudes pels dos altres metalls d'encunyació, són molt més escassos degut a certs impediments. Pel que fa a la química redox de la plata, la possibilitat que pugui participar en processos de dos electrons amb transicions Ag^{I}/Ag^{III} ha estat rarament proposada i mai ha estat demostrada inequívocament. Degut a que la química tradicional d'acoblament creuat té lloc a través de mecanismes ben establerts M^{n}/M^{n+} de dos electrons, la possibilitat que la plata pugui portar a terme transformacions anàlogues no s'ha tingut en compte. Per altra banda, la química d'acoblament oxidatiu promoguda per sals d'or(I), s'associa generalment amb cicles redox Au^{I}/Au^{III} en què l'oxidant de sacrifici porta a terme el primer pas d'oxidació per a generar les espècies clau d'Au^{III}. Malauradament, el desenvolupament de la química d'acoblament creuat catalitzada per or en absència d'oxidants ha estat impossibilitat degut a la reticència que presenta l'or a patir addicions oxidants.

La primera part d'aquesta tesi estudia la reactivitat d'un complex ben definit aril-Cu^{III} que conté un lligand triazamacrocíclic. Aquest complex ha estat utilitzat com a model per a l'estudi de la natura mecanística de les reaccions d'acoblament creuat catalitzades per coure resultants en la formació d'enllaços C-S, C-Se i C-P. Els resultats obtinguts estableixen una base racional per a la implicació d'espècies aril-Cu^{III} en aquestes reaccions i aporten coneixement sobre els paràmetres clau que dominen aquestes transformacions.

Seguidament vam explorar la possibilitat que una reactivitat anàloga pugués tenir lloc en centres metàl·lics de plata. El complex anàleg aril-Ag^{III} va poder ser aïllat després d'una etapa d'addició oxidant de Ag^{I} sobre substrates halur d'aril connectats a un residu amb tres posicions de coordinació amíniques disponibles per tal assistir l'estabilització d'alts estats d'oxidació de la plata. El complex **1**-Ag^{III} exhibeix reaccions d'acoblament en presència d'una gran varietat de nucleòfils de diferent natura mitjançant etapes d'eliminació reducitva. Les etapes fonamentals esmentades anteriorment poden ocórrer consecutivament donant lloc a reaccions d'acoblament creuat del tipus Ullmann i Hurtley catalitzades per plata. Els resultats presentats aquí dónen suport a un mecanisme basat en cicles redox Ag^{I}/Ag^{III} de dos electrons en reaccions model d'acoblament creuat catalitzades per plata.

RESUMEN

Las reacciones de acoplamiento cruzado catalizadas por metales de transición han revolucionado el diseño de los análisis retrosintéticos para la preparación de nuevos compuestos orgánicos. Aunque estas metodologías han sido desarrolladas extensamente para el cobre, especialmente para la formación de productos de acoplamiento del tipo C_{arilo}-nucleófilo, los pasos fundamentales que rigen estos procesos siguen generando controversia. Asimismo, los ejemplos de metodologías relacionadas promovidas por los dos otros metales de acuñación, son mucho más escasos debido a ciertos impedimentos. Con respecto a la química redox de la plata, la posibilidad que pueda participar en procesos de dos electrones con transiciones Ag^{I}/Ag^{III} ha sido raramente propuesta y nunca demostrada inequívocamente. Debido a que la química tradicional de acoplamiento cruzado se da mediante mecanismos bien establecidos M^{n}/M^{n+} de dos electrones, la posibilidad de que la plata puede llevar a cabo transformaciones análogas no se ha considerado. Por otra parte, la química de acoplamiento oxidativo promovida por sales de oro(I), se asocia generalmente con ciclos redox Au^{I}/Au^{III} en los que el oxidante de sacrificio lleva a cabo el primer paso de oxidación para generar las especies clave de Au^{III}. Por el contrario, el desarrollo de la química de acoplamiento cruzado catalizada por oro en ausencia de oxidantes se ha visto imposibilitada por la reticencia del oro a sufrir adiciones oxidantes.

La primera parte de esta tesis estudia la reactividad de un complejo bien definido arilo-Cu^{III} que contiene un ligando triazamacrocíclico. Este complejo ha sido empleado como modelo para el estudio de la naturaleza mecanística de las reacciones de acoplamiento cruzado catalizadas por cobre resultantes en la formación de enlaces C-S, C-Se y C-P. Estos resultados establecen una base racional para la implicación de especies arilo-Cu^{III} en dichas reacciones y aportan conocimiento sobre los parámetros clave que dominan estas transformaciones.

Seguidamente se exploró la posibilidad que una reactividad análoga pueda darse en centros de plata. El complejo análogo arilo-Ag^{III} pudo ser aislado tras una etapa de adición oxidante de Ag^{I} sobre sustratos haluro de arilo, conectados a un residuo con tres posiciones de coordinación amínicas disponibles para asistir en la estabilización de altos estados de oxidación de la plata. El complejo **1**-Ag^{III} reacciona mediante etapas de eliminación reductora en presencia de gran variedad de nucleófilos de naturaleza distinta dando lugar a los correspondientes productos de acoplamiento. Las etapas de adición oxidante y eliminación reductora pueden ocurrir consecutivamente originando reacciones de acoplamiento cruzado del tipo Ullmann y Hurtley catalizadas por plata. Dichos resultados, apoyan mecanismos basados en ciclos redox Ag^{I}/Ag^{III} de dos electrones en reacciones modelo de acoplamiento cruzado catalizadas por plata.

CHAPTER I.

GENERAL INTRODUCTION

I. GENERAL INTRODUCTION

I.1. Coinage Metals in Organic Synthesis

The term coinage metal applies to the non-radioactive elements of the group 11, *i.e.* copper, silver and gold, used by mankind for millennia. The use of coinage metals is strongly linked to the progress of many disciplines of science, of which synthetic chemistry is no exception. Chemists have employed copper, silver and gold in organic transformations for more than a century, especially in catalysis, leading to the development of greener approaches towards organic molecules. Among the three elements, copper is the one with the richest history in organometallic chemistry. Copper is able to catalyse in an enantioselective fashion numerous reactions of great importance such as 1,4-conjugate additions[1,2] and 1,2-additions[3], allylic substitutions,[1,2] hydrosilylations[4] and many other processes. Further, 1,3-dipolar cycloadditions[5] and particularly copper-catalysed Huisgen azide-alkyne cycloadditions, the most popular reaction catalogued within the Click chemistry concept, that give access to triazoles in a very simple and orthogonal manner, are another prominent example of the richness of copper chemistry.[6-8]

On the other hand, silver has also had a notable presence on synthetic organic protocols. Still today, silver maintains a relevant role in the industrial production of chemicals as heterogeneous catalyst for oxidation processes. Interestingly, it promotes the oxidation of ethylene to ethylene oxide in the ethylene glycol synthesis, a molecule with high demand (about 6.7 billion kg are produced annually). Moreover, the application of this reaction can be extended to the propylene and butadiene oxidation.[9] In homogeneous transformations, silver has had an important role as stoichiometric additive serving as a one electron oxidant, transmetallating agent (commonly of alkynyl residues or after decarboxylation processes) and halide abstractor, taking advantage of the inherent insolubility of its corresponding halide salts. Very often transition metal-catalysed reactions are conducted in the presence of silver(I) salts to trigger the displacement of the halide from coordinatively saturated metal centres precipitating as its corresponding AgX (X = Cl, Br, I) salts.[10] Besides, it has also contributed to organic synthesis as reaction promoter in silver-catalysed and mediated protocols, mainly exploiting its ability to activate multiple C-C bonds. Classically, these methods include cycloadditions, C-C bond forming reactions *via* nucleophilic attack over carbonyl and imine groups,[9,10] and also cover numerous examples of intramolecular heterocyclisations,[11] with enantioselective control in most of these classes of transformations. These days silver chemistry is attracting the interest of more and more research groups and is becoming a growing area of research. The last lustrum has seen the appearance of very powerful tools for organic transformations based on silver chemistry that tackle two of the most challenging and ambitious goals of modern synthetic chemistry: the C-H functionalisation and the fluorination of organic substrates. These advances include a very straightforward route to furnish polysubstituted furans *via* coupling through double C-H activation and subsequent heterocyclisation,[12] trifluoromethylation of aromatic C-H bonds,[13] hydrotrifluoromethylation of terminal alkenes,[14] ring closing aminofluorinations,[15] a direct route towards the *ortho* C-H fluorination of pyridines and diazines,[16] and the germinal difluorination of styrenes (**Scheme I. 1**).[17]

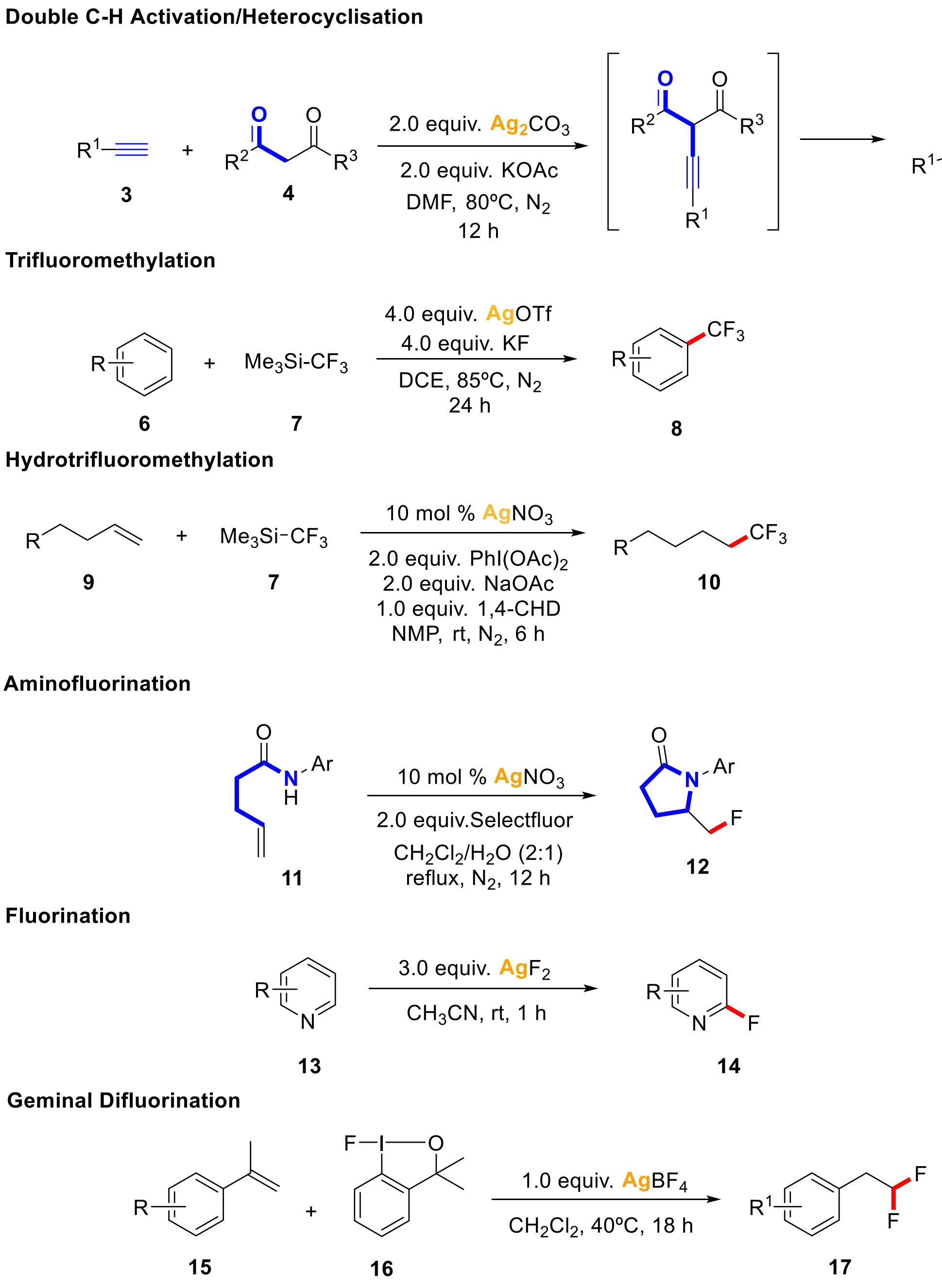
Double C-H Activation/Heterocyclisation
R1
+
O
O
R2
R3
3
4
2.0 equiv. Ag2CO3
2.0 equiv. KOAc
DMF, 80°C, N2
12 h
R1
5
Trifluoromethylation
R
+
Me3Si-CF3
6
7
4.0 equiv. AgOTf
4.0 equiv. KF
DCE, 85°C, N2
24 h
CF3
8
Hydrotrifluoromethylation
9
10 mol % AgNO3
2.0 equiv. PhI(OAc)2
2.0 equiv. NaOAc
1.0 equiv. 1,4-CHD
NMP, rt, N2, 6 h
10
Aminofluorination
N
H
Ar
11
10 mol % AgNO3
2.0 equiv.Selectfluor
CH2Cl2/H2O (2:1)
reflux, N2, 12 h
F
12
Fluorination
13
3.0 equiv. AgF2
CH3CN, rt, 1 h
14
Geminal Difluorination
F—I—O
15
16
1.0 equiv. AgBF4
CH2Cl2, 40°C, 18 h
17

Scheme I. 1. Novel silver-based methodologies for organic synthesis.

The chemistry of the heaviest of the coinage metals, gold, has seen a tremendous development during the past decade, especially for gold catalysis. As for silver(I), gold(I) exhibits strong Lewis acidity toward unsaturated C-C bonds and this inherent property has been intensely exploited by chemists to facilitate the straightforward formation of new bonds with high enantioselectivity. Notable examples are the intra and intermolecular nucleophilic addition of N, O, S, and C-based nucleophiles to C-C unsaturations,[18-20] and the cycloisomerisation of enynes and heteroenynes.[21]

Finally, the three metals share common reactivity patterns in some cases. First, coinage metals are able to effect carbene, nitrene and silylene insertions into C-H bonds, affording readily the functionalisation of non-prefunctionalised hydrocarbons.[22-24] Moreover, and although copper is the most well-known coinage metal capable of catalysing cross-coupling reactions either through C-H or C-X (X = halide, metal) bond activation, examples of silver and gold-catalysed coupling processes have been also reported. While silver-catalysed cross-coupling development is still in its infancy, gold-catalysed protocols, especially in the cutting edge area of C-H bond functionalisation have already resulted on significant advances to access functionalized arenes through simple and direct routes.[25]

I.2. Cross-Coupling Catalysis

Cross-coupling processes, consisting of the assembling of two coupling partners aided by a transition metal promoter, have been known for more than one century. However, it was not until the early seventies, when the first reports on palladium-catalysed cross-coupling reactions appeared, that the enormous potential that this transformations enclose in synthetic chemistry was realised. Since then, cross-coupling technology has revolutionized organic synthesis by providing chemists with valuable tools towards the synthesis of molecules such as pharmaceuticals, agrochemicals, polymers and other relevant compounds finding extensive industrial application.[26-28] Indeed, the significance of palladium-catalysed C-C couplings was recognised in 2010 with the Nobel Prize in Chemistry awarded to Akira Suzuki, Ei-ichi Negishi and Richard F. Heck.[29] The palladium-catalysed methodologies developed before the 1990's were limited to the coupling of aryl halides and vinyl halides with metalloorganic fragments but importantly provided direct access to scaffolds such as biaryls, aryl alkenyls, aryl alkynyls, conjugated alkenes and many others that had only been accessed *via* multistep reactions until that point.[30] In the beginning of the 1990's, the groups of Buchwald and Hartwig developed cross-coupling protocols for the formation of C-N bonds, specifically for the arylation of amines, extending the variety of the architectures accessible through cross-coupling to a wide range of aromatic amines.[31,32]

I.3. Copper in Cross-Coupling Catalysis

Recently, the National Institutes of Health (NIH) emphasised the necessity of advancing towards a greener approach for renewable energy production and automotive catalyst systems that to date require large amounts of precious metals but also for the production of material goods in the pharmaceutical and agricultural industries.[33] In their statement they encouraged chemical sciences to find alternatives to critical resources such as precious metal-based catalysts. Specifically, the change of direction that cross-coupling arena has been experiencing since the beginning of the 21st century, leading to methodologies for the replacement of palladium with first-row transition metals, most frequently nickel and copper, in these transformations was highlighted. In fact, the seeds for the blooming of copper-catalysed cross-coupling chemistry were planted long before this field was taken by palladium, as the first examples of copper-mediated cross-coupling reactions date back to the beginning of the 20th century. For instance, the arylation of active methylenes[34] and acetylenes[35] were first reported in 1927 and 1963 respectively, and even a catalytic version of this palladium-free Sonogashira-type coupling appeared more than 20 years ago.[36] Also, copper-mediated C_{aryl}-heteroatom bond forming cross-coupling reactions, known as Ullmann-type condensations, have been known for more than a century.[37-39] Although these last protocols emerged as a powerful tool to effect the arylation of amines, amides and phenols, the practicality of these processes was very limited until the late 1990's, when the major drawbacks of these reactions, such as the usual need for stoichiometric amounts of copper, harsh reaction conditions (temperatures above 200 ºC), long reaction times as well as the narrow range of nucleophiles tolerated as coupling partners were improved by introducing auxiliary ligands.[40-42] More recently, another strategy consisting on performing the reactions using photoirradiation is found to allow operation of these transformations under unusually mild conditions.[43-48] Despite the extensive development of Ullmann-type methodologies since the late 1990's, the fundamental steps governing the coupling reactions remained obscure.

I.3.1 Mechanistic aspects of copper-catalysed cross-coupling reactions

In order to further develop Ullmann-type chemistry based on rational grounds, understanding of the mechanism was required. As a result, many proposals were drawn, including radical and non-radical processes (**Scheme I. 2**).[49] The two radical pathways postulate the formation of aryl radicals that can recombine with a Cu^{II}-nucleophile species to form the coupling product and copper(I).[43-48,50-56] Among the non-radical processes, σ-bond metathesis[57-59] and S_EAr processes[60-62] driven by the π-complexation of copper(I) have been proposed but the most invoked mechanism postulates that these reactions proceed through oxidative addition/reductive elimination processes[63-71] (**Scheme I. 2**).

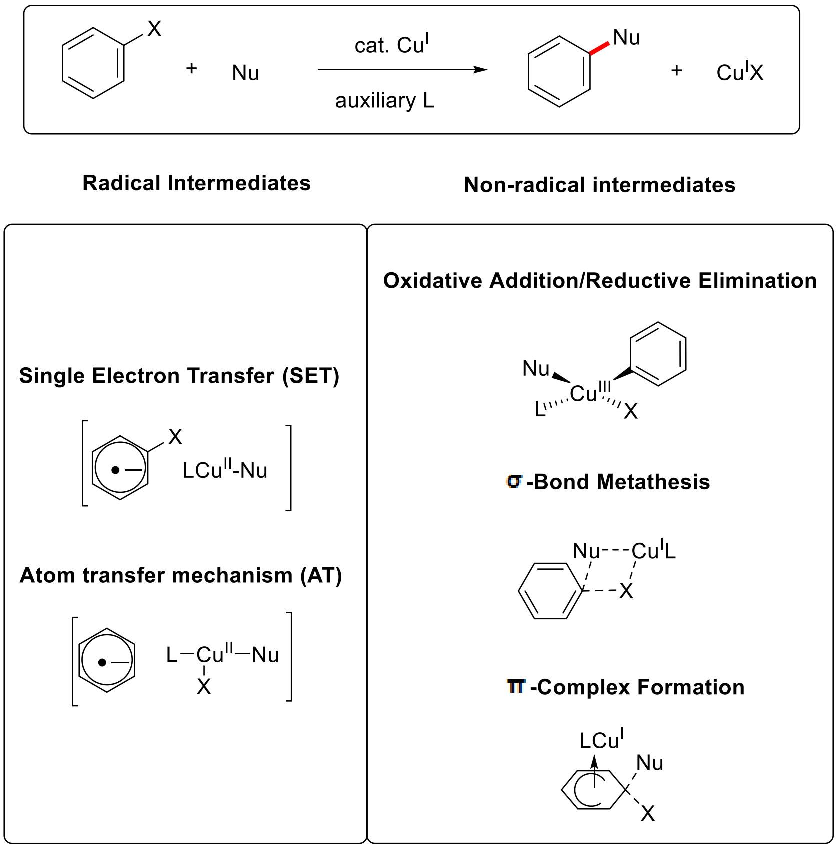
X
+
Nu
cat. Cu^I
auxiliary L
Nu
+
Cu^{I}X
Radical Intermediates
Non-radical intermediates
Single Electron Transfer (SET)
X
LCu^{II}-Nu
Atom transfer mechanism (AT)
L–Cu^{II}–Nu
X
Oxidative Addition/Reductive Elimination
Nu
Cu^{III}
L
X
σ-Bond Metathesis
Nu---Cu^{I}L
X
π-Complex Formation
LCu^I
Nu
X

Scheme I. 2. Radical and non-radical reaction intermediates postulated to operate in Ullmann-Goldberg-type coupling reactions.

Although the literature on this topic indicates that the nature of Ullmann-type couplings significantly depend on the ligands and the conditions employed in each particular reaction, there are no clear rules to predict the operative mechanism in each case. However, among all proposals, radical pathways initiated by a first single electron transfer (SET) process and Cu^I/Cu^{III} catalytic cycles based on two-electron redox steps are the most often invoked mechanisms in Ullmann-type protocols.

I.3.2 One electron redox Cu^I/Cu^{II} proposal

Studies supporting Cu^I/Cu^{II} cycles involving radical species generated *via* SET have often been proposed. These studies postulate that the copper(I) complex transfers one electron to the aryl halide leading to the formation of a haloarene radical anion. This radical eventually recombines with the copper-nucleophile complex to furnish the coupling product and regenerate the copper(I) species (**Scheme I. 3**).

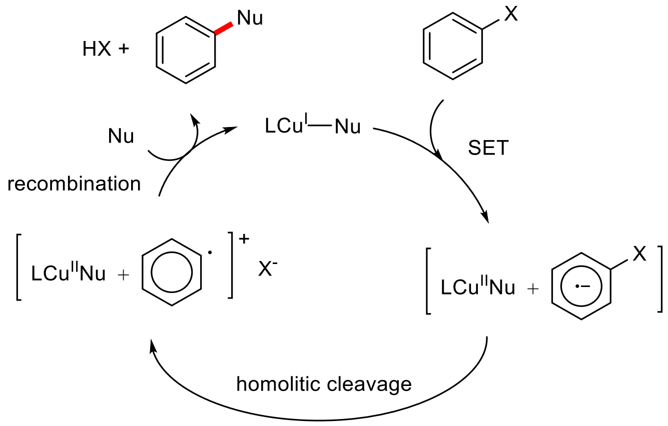
HX +
Nu
X
Nu
LCu^I—Nu
SET
recombination
LCu^{II}Nu +
+
X$^-$
LCu^{II}Nu +
X
homolitic cleavage

Scheme I. 3. Proposed mechanistic pathways for the Ullmann-Goldberg reaction following radical Cu^I/Cu^{II} catalytic cycles initiated by a SET.

In 2010, Buchwald and Houk studied the mechanism and the origin of the ligand-directed selectivity in the copper(I)-catalysed N- vs. O-arylation of aminoalcohol bifunctional substrates developed by Buchwald three years before.[72] In this report, the authors described the ability of β-diketone (**20**) and tetramethylphenanthroline (**21**) ligands to discriminate between the arylation of the N-terminus (using β-diketone) or the O-terminus (using tetramethylphenanthroline) of the substrate (**Scheme I. 4** for the application of this methodology to the coupling of 5-amino-1-pentanol).

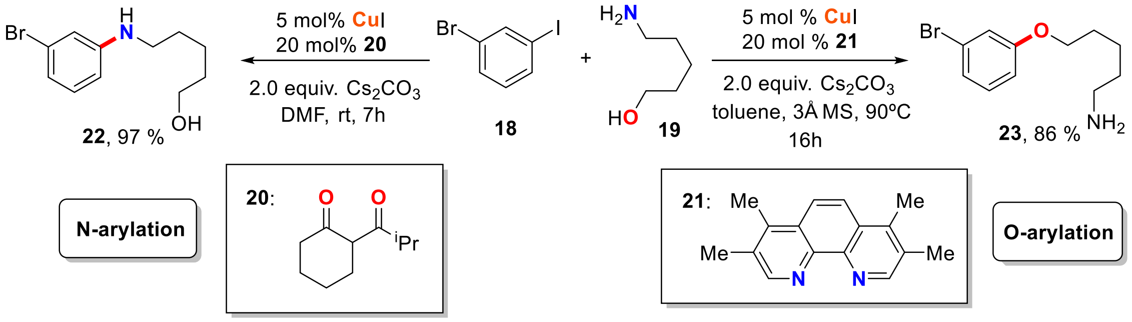
Br
H
N
OH
22, 97 %
5 mol% CuI
20 mol% 20
2.0 equiv. Cs$_2$CO$_3$
DMF, rt, 7h
Br
I
18
+
H$_2$N
HO
19
5 mol % CuI
20 mol % 21
2.0 equiv. Cs$_2$CO$_3$
toluene, 3Å MS, 90°C
16h
Br
O
NH$_2$
23, 86 %
N-arylation
20:
O
O
^{i}Pr
21:
Me
Me
Me
Me
N
N
O-arylation

Scheme I. 4. Ligand-directed chemoselective copper-catalysed N-arylation and O-arylation of 5-amino-1-pentanol using 3-bromoiodobenzene and bidentate ligands.

In this study, the authors, building their conclusions on DFT calculations, established that the most favoured pathway for these couplings among σ-bond metathesis, oxidative addition and SET mechanism is the SET pathway involving aryl radicals.[54] Later that year, Y. Fu and co-workers, in another computational study, proposed an alternative mechanism for these reactions based on two-electron Cu^I/Cu^{III} redox cycles, using the actual 5-amino-1-pentanol substrate employed in the reactions instead of theoretical model MeOH and $MeNH_2$ substrates.[70]

This serves as a good example to show that subtle changes introduced in the DFT calculation can drastically influence the conclusions extracted. Hence, mechanistic proposals only based on DFT calculations have to be taken carefully and their consistency is improved when complemented by experimental evidence.

I.3.2.1. Photoinduced Ullmann-type couplings operating *via* SET mechanism

The first authors to provide convincing experimental evidence of Cu^I/Cu^{II} catalytic cycles in Ullmann-Goldberg protocols were J. Peters and G. Fu. In their first report on photoinduced Ullmann-Goldberg-type couplings they investigated the nature of the C-N couplings between a photoluminescent (*bis*-monophosphino)copper-carbazolide complex and aryl halides (**Scheme I. 5A**).[43] EPR measurements indicated the formation of a copper-containing radical upon photoirradiation with a standard 13 W compact fluorescent light (CFL) bulb of a sample of $((m\text{-Tol})_3P)_2Cu^I$-carbazolide complex **24** and iodobenzene evidencing that one electron processes take place. Exclusive observation of cyclised compounds when complex **24** is reacted with 2-(allyloxy)iodobenzene (**29**), a radical probe often used by Bowman and Hartwig to demonstrate non-radical processes in Ullmann-Goldberg mechanistic investigations,[63,67-69] further substantiated the radical nature of these couplings. Rapid cyclisation (9.6×10^9 s^{-1} in DMSO) of radical species **30** furnishes the cyclised products obtained (**31**) that are indicative of a homolytic cleavage of the C-I bond after a SET step (**Scheme I. 5B**). Moreover, if the same test is carried out employing the deuterated analogue of the aryl halide radical probe substrate (**29’**), produces a 1:1 mixture of cyclised diastereomer products (**31’** and **31’’**) fully consistent with radical pathways (**Scheme I. 5C**). Also, a competition experiment, consisting of subjecting **24** to reaction in the presence of 1-bromonaphtalene and 4-chlorobenzonitrile in the standard reaction conditions, served to corroborate the radical nature of the described methodology. Complex **24** showed faster reaction rates for the coupling with 4-chlorobenzonitrile, thus leading to the predominant formation of product **35**. Since the more favourable reduction potential of 4-chlorobenzene (-2.03 V for 4-chlorobenzene; -2.17 V for 1-bromonapthalene vs. SCE in DMF), despite having a higher C-halogen bond dissociation energy (BDE), makes it more susceptible to the homolytic cleavage of its C-halogen bond when compared to 1-bromonaphtalene this observation supports a mechanism involving radical species (**Scheme I. 5D**).

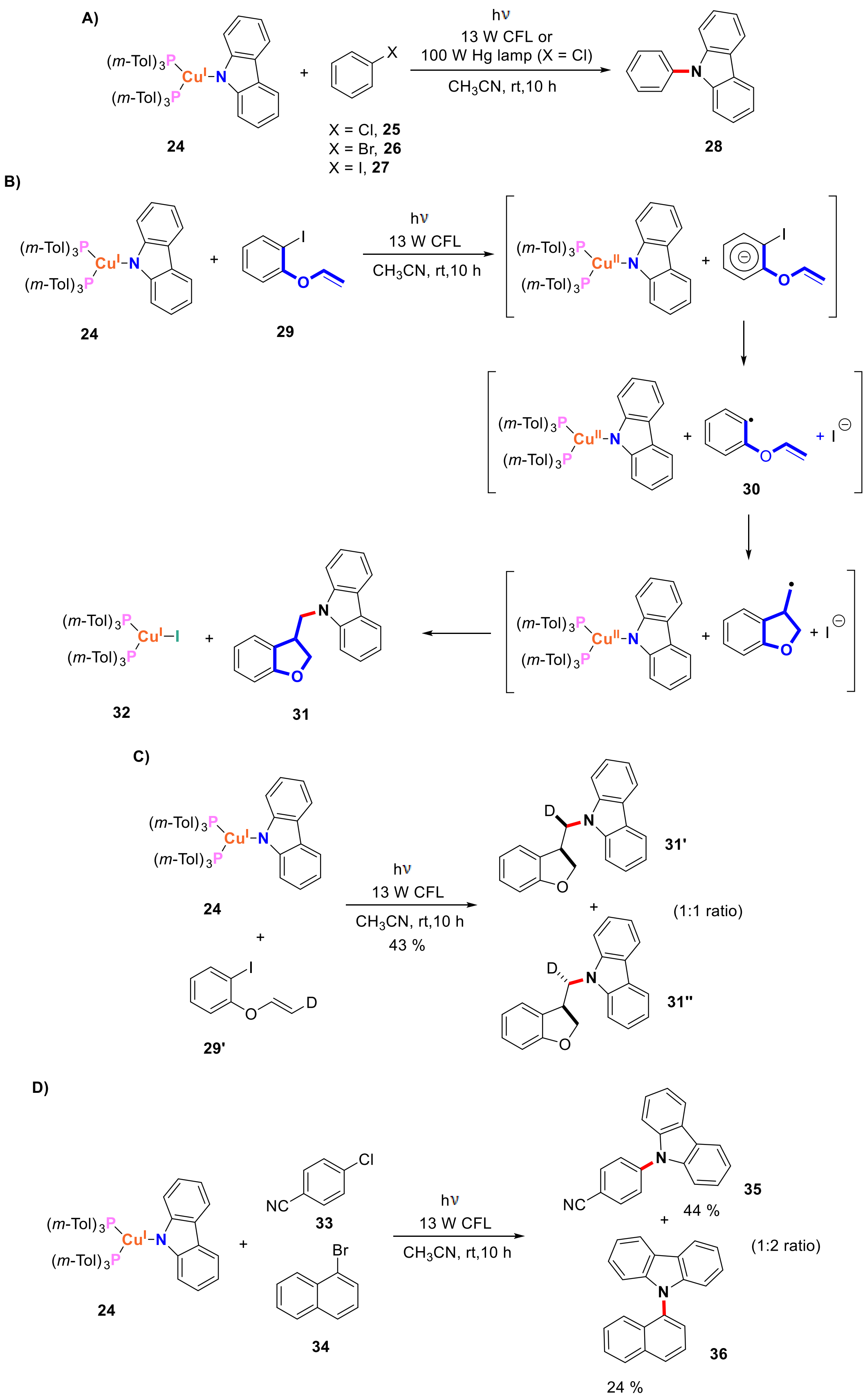
A)
(m-Tol)3P
Cu^I–N
24
+
X
X = Cl, 25
X = Br, 26
X = I, 27
hν
13 W CFL or
100 W Hg lamp (X = Cl)
CH3CN, rt,10 h
28
B)
24
29
hν
13 W CFL
CH3CN, rt,10 h
Cu^II–N
+ I⊖
30
32
31
Cu^I–I
C)
24
29'
hν
13 W CFL
CH3CN, rt,10 h
43 %
31'
31''
(1:1 ratio)
D)
24
33
34
NC
Cl
Br
hν
13 W CFL
CH3CN, rt,10 h
35
44 %
36
24 %
(1:2 ratio)

Scheme I. 5. A) Photoinduced Ullmann C-N coupling reactions of Cu^{I}-carbazolide complex **24** with aryl halides. **B**) Formation of the cyclisation plus C-N bond formation product **31** in a photoinduced Ullmann protocol using an allyloxyiodobenzene as radical probe substrate**.** **C**) Stereochemistry study of the cyclised products obtained using allyloxyiodobenzene substrates. **D**) Substrate competition experiment in a photoinduced Ullmann methodology.

The interest of the outlined system not only lies in its potential to deliver information on mechanistic pathways involving one electron processes and formation of aryl radicals otherwise favoured by photoirradiating conditions, but it could also be converted into a practical methodology for C-N, C-O and C-S bond forming couplings.[43-48] Since their first discovery in 2012, photoinduced strategies have proven to be a mild alternative to the standard Ullmann-type condensations and offer a new approach to realise the desired C-heteroatom transformations (**Scheme I. 6A**). The scope of these methodologies has also been broadened demonstrating application with a wide range of nucleophiles and electrophiles. Among the nucleophiles explored that stand out are nitrogen heterocyclic scaffolds[44,46] such as indoles, benzimidazoles, imidazoles and carbazoles, alkyl and aryl amides,[47] thiophenols[45] and phenols.[48] Concerning the scope of the electrophiles it was demonstrated that aryl iodides, aryl bromides and aryl chlorides, secondary and hindered primary alkyl iodides and bromides, and vinyl and alkynyl iodides and bromides can be engaged in such transformations. To rationalise the observed reactivity, the authors propose a common catalytic cycle shared in all the couplings described (see **Scheme I. 6B**). The mechanism is initiated by the photoexcitation of a *bis*-ligated copper(I)-nucleophile species that triggers a transfer of one electron from the copper complex to the electrophile promoting the homolytic cleavage of its C-halogen bond and generating a radical organic fragment. The radical subsequently recombines with one of the nucleophiles coordinated to the copper(II) centre to produce the desired coupling product and regenerate copper(I) species that upon coordination of another molecule of deprotonated nucleophile restart the catalytic cycle.

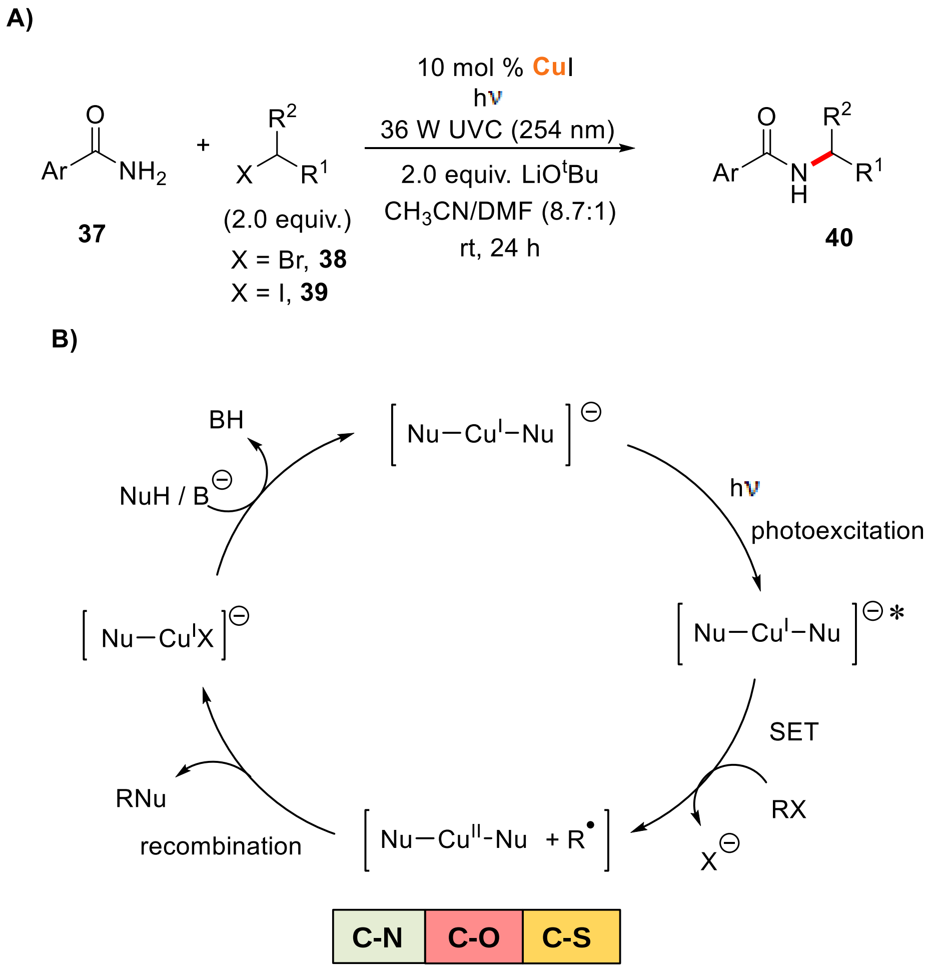
A)
10 mol % CuI
hν
36 W UVC (254 nm)
2.0 equiv. LiOtBu
CH3CN/DMF (8.7:1)
rt, 24 h
Ar
NH2
O
37
+
R2
X
R1
(2.0 equiv.)
X = Br, 38
X = I, 39
N
H
R1
R2
40
B)
[Nu−CuI−Nu]⊖
hν
photoexcitation
[Nu−CuI−Nu]⊖*
SET
RX
X⊖
[Nu−CuII-Nu + R•]
RNu
recombination
[Nu−CuIX]⊖
NuH / B⊖
BH
C-N
C-O
C-S

Scheme I. 6. **A**) Photoinduced copper-catalysed alkylation of aromatic amides. **B**) General mechanistic proposal for the photoinduced Ullmann-Goldberg coupling methodology by J. Peters and G. Fu.

I.3.3 Oxidative addition/reductive elimination Cu^{I}/Cu^{III} proposal

Cu^{I}/Cu^{III} catalytic cycle proposals based on two-electron redox steps in Ullmann-type couplings implicate an initial aryl halide oxidative addition at copper(I) to form an aryl-Cu^{III} intermediate. Then, after coupling of the nucleophile and the aryl moiety, the coupling product is obtained *via* reductive elimination thus regenerating the copper(I) catalyst. To date, two different mechanistic pathways have been postulated depending on the position of the coordination step of the nucleophile in the catalytic sequence (**Scheme I. 7**). The coordination of the base-deprotonated nucleophile to copper may occur in the first step, before the cleavage of the C-halide bond (pathway A) or on the contrary it may take place after the oxidative addition step (pathway B).

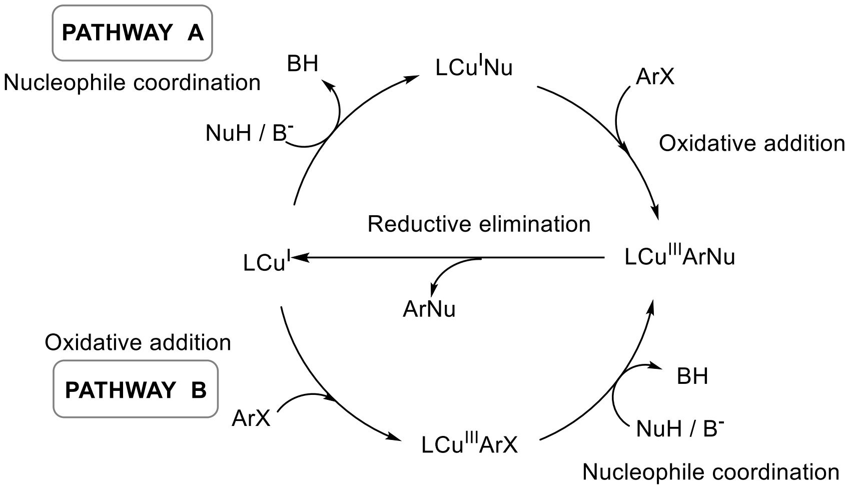
PATHWAY A
Nucleophile coordination
BH
NuH / B⁻
LCuᴵNu
ArX
Oxidative addition
Reductive elimination
LCuᴵ
ArNu
LCuᴵᴵᴵArNu
Oxidative addition
PATHWAY B
ArX
LCuᴵᴵᴵArX
BH
NuH / B⁻
Nucleophile coordination

Scheme I. 7. Proposed mechanistic pathways for the Ullmann-Goldberg reaction following oxidative addition/reductive elimination fundamental steps.

Pathway A is the most frequently invoked mechanism in Ullmann-type couplings which proceed *via* two-electron pathways. Hartwig and coworkers systematically synthesised and characterised a series of neutral tridentate LCu^{I}-imidate,[68] LCu^{I}-amidate[67] and LCu^{I}-phenoxide[69] heteroleptic complexes bearing N,N and P,P bidentate auxiliary ligands (L) such as phenanthroline, bipyridine, diamines and diphosphines. Even though some of these complexes tend to form dimeric homoleptic complexes displaying $[L_2Cu^{I}][Cu^{I}(Nu)_2]$ structures in the solid state, it has been shown by NMR spectroscopy and conductivity measurements that the neutral heteroleptic species, such as complex **45**, are the predominant species in solution. The authors subsequently studied the reactivity of these copper(I) complexes with aryl halides concluding that the neutral tricoordinated copper(I) species are chemically and kinetically competent intermediates in N-arylation and O-arylation coupling processes (see **Scheme I. 8** for an example of arylation of a Cu^{I}-amidate complex). Moreover, kinetic data obtained for these systems revealed no dissociation of the nucleophile from the copper(I) centre during the reaction, suggesting that the nucleophile coordination step occurs prior to the oxidative addition in the scope of methodologies explored in their reports.

The oxidative addition step is thus usually rate-limiting, and to date, no experimental example of an Ullmann-type coupling operating by pathway B has been demonstrated.

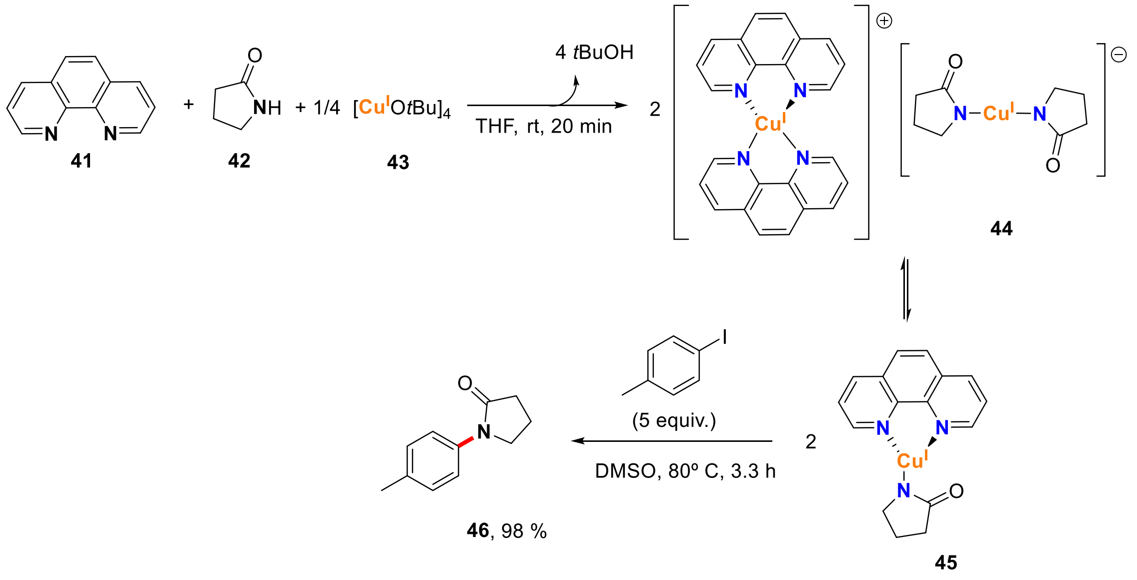

Scheme I. 8. Reactivity of an heteroleptic phenanthtroline Cu^{I}-amidate complex with *p*-iodotoluene.

I.3.3.1. Chelation-assisted stabilisation of high-valent copper species

The mechanistic aspects of Ullmann-type catalysis today generates still intense debate and depends on the features of each individual catalyst system. Until 2010, studies aimed at unravelling its reaction pathways lacked direct experimental evidence to provide confirmation of a mechanistic hypothesis. For instance, the aforementioned work by Hartwig supported their Cu^{I}/Cu^{III} proposal on DFT calculations and a set of experiments that ruled out the formation of radicals during the reaction timecourse. Key reaction intermediates such as high-valent copper species had remained elusive due to the short-lived nature of the intermediate species generated after the C-halogen bond cleavage, which is generally the rate-limiting step of the reaction as revealed by computational studies.

In 2010, Ribas in collaboration with Stahl and later Wang began to work on a line of research focused on the fundamental understanding of Ullmann-Goldberg-type couplings by pursuing the detection and identification of the key intermediate species that drive these reactions. In this regard, Ribas pioneered a new strategy based on using model substrates bearing an anchor with three amine coordination sites available to assist the stabilization of putative high valent copper species by chelation. Square pyramidal aryl-Cu^{III}-X (X = Cl, Br, I) organometallic species $\mathbf{2}_{\mathrm{Cl}}$, $\mathbf{2}_{\mathrm{Br}}$ and $\mathbf{2}_{\mathrm{I}}$ were prepared by reacting Cu^{II}X$_2$ salts with a triazamacrocyclic ligand containing an arene moiety *via* a proton coupled electron transfer (PCET) C-H activation process.[73-75] These structures are bench-top stable thus allowing exhaustive spectroscopic and crystallographic characterisation (see **Figure I. 1** for X-ray structures).

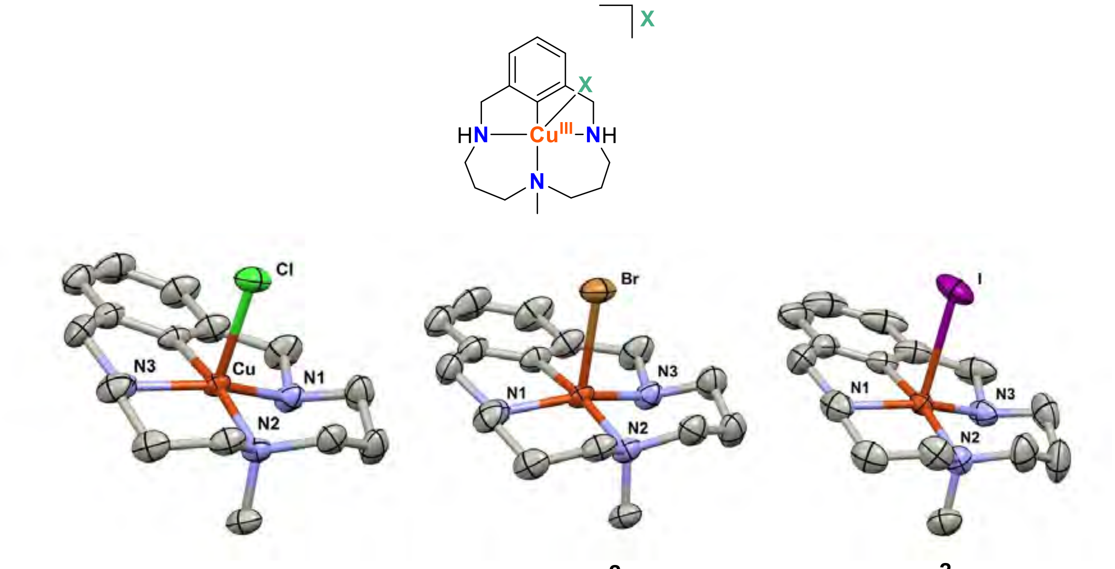
X
X
HN
Cu^III
NH
N
Cl
N3
Cu
N1
N2
Br
N1
N3
N2
I
N1
N3
N2

2_{Cl} 2_{Br} 2_{I}

Figure I. 1. X-ray structures of $\mathbf{2_{Cl}}$, $\mathbf{2_{Br}}$ and $\mathbf{2_{I}}$ complexes (ellipsoid representation at 50% probability). Hydrogen and corresponding halide counterions are omitted for clarity.

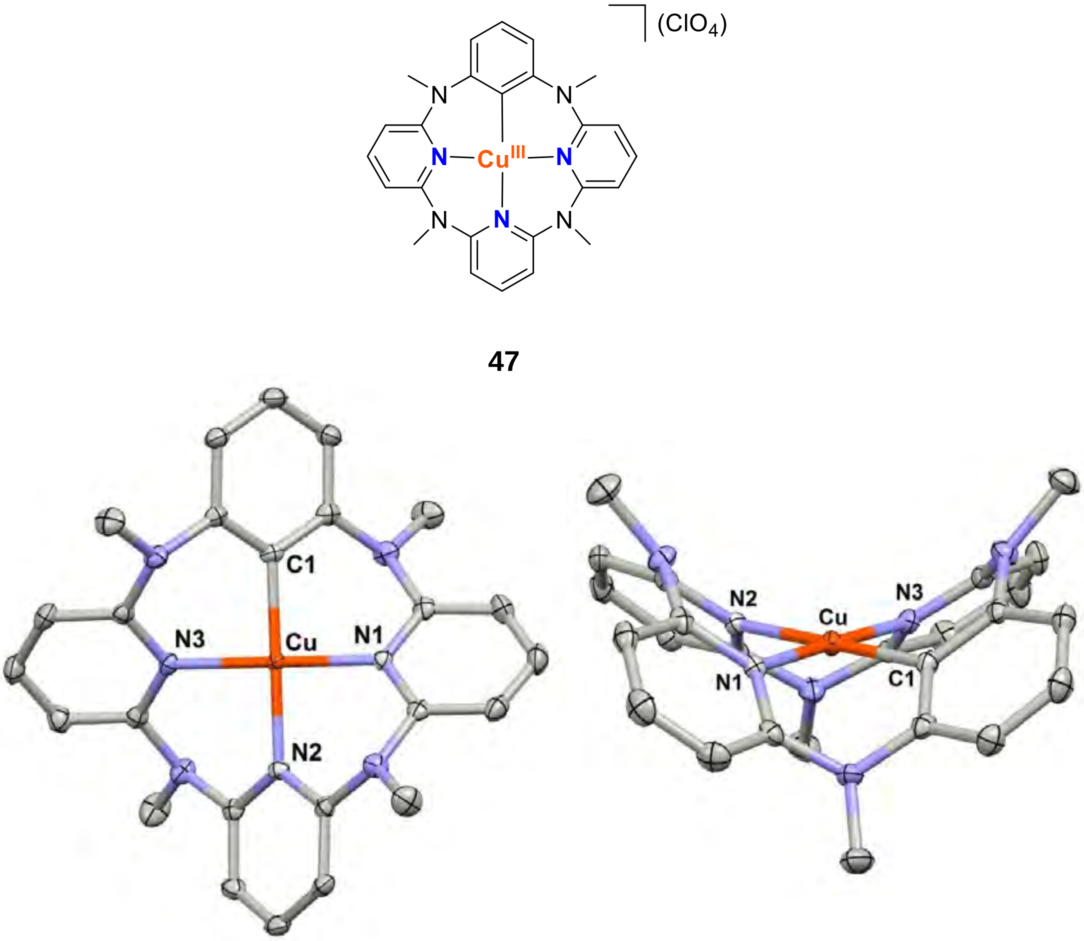
(ClO4)
N
N
N
Cu^III
N
N
N
N
N
C1
N3
Cu
N1
N2
N2
Cu
N3
N1
C1

47

Figure I. 2. X-ray structures of complex **47** (ellipsoid representation at 50% probability). Hydrogen and perchlorate counterions are omitted for clarity.

Similar protocols to those employed for the synthesis of **2_X** complexes using copper(II) salts bearing non-coordinating anions as perchlorates leaded to the analogous square planar **1-**Cu^{III} complex.

Also, Wang used the chelation-assisted stabilization of high-valent metal species to obtain complex **47**. In their case the copper(III) cation is embedded within heterocalixarene architectures that provide an electron-donating environment suitable for the stabilisation of the high-valent species (see **Figure I. 2** for X-ray structure of the complex).[76]

I.3.3.2. Application of stable aryl-Cu^{III} complexes to the fundamental understanding of copper redox processes

Most importantly, complexes **2_X** allowed the characterisation of a reductive elimination step from a copper(III) centre resulting in the formation of a C_{aryl}-halide bond. Moreover, the reversibility of this process and the feasibility of the aryl halide oxidative addition to copper(I) resulting in the regeneration of the initial aryl-Cu^{III}-X complex were demonstrated. Through monitoring of the characteristic UV-Vis band at 420 nm corresponding to **2_{Br}** it was demonstrated that the addition of triflic acid triggered the reductive elimination, effecting the bromination of the phenyl moiety and releasing the copper(I) from the macrocyclic pocket. The band at 420 nm was fully recovered by addition of Proton-sponge® (base) to the solution, being the first reported of aryl halide oxidative addition to copper(I) (**Figure I. 3**). The interconversion between copper(I) and copper(III) redox states by sequential addition of acid and base was repeated several times without significant loss of the **2_X** complex (**Figure I. 3**).[75]

A detailed computational study served to reason that the protonation of one of the amines of the macrocyclic ligand causes its decoordination from the very electron deficient copper(III) centre, thus strongly destabilising the complex and triggering the reductive elimination.[77]

An equally effective strategy to trigger the reductive elimination and displace the equilibrium towards the halogenated ligand and copper(I) species is the use of 1,10-phenanthroline. The presence of excess of 1,10-phenanthroline, that presents a large affinity for copper(I) ions, drives the formation of the **2_X** (X = Cl, Br, I) coupling products and $[Cu^I(phen)_2]$ from the corresponding aryl-Cu^{III}-X species exhibiting increasing reaction rates as the strength of the C-X bond formed increases.[78]

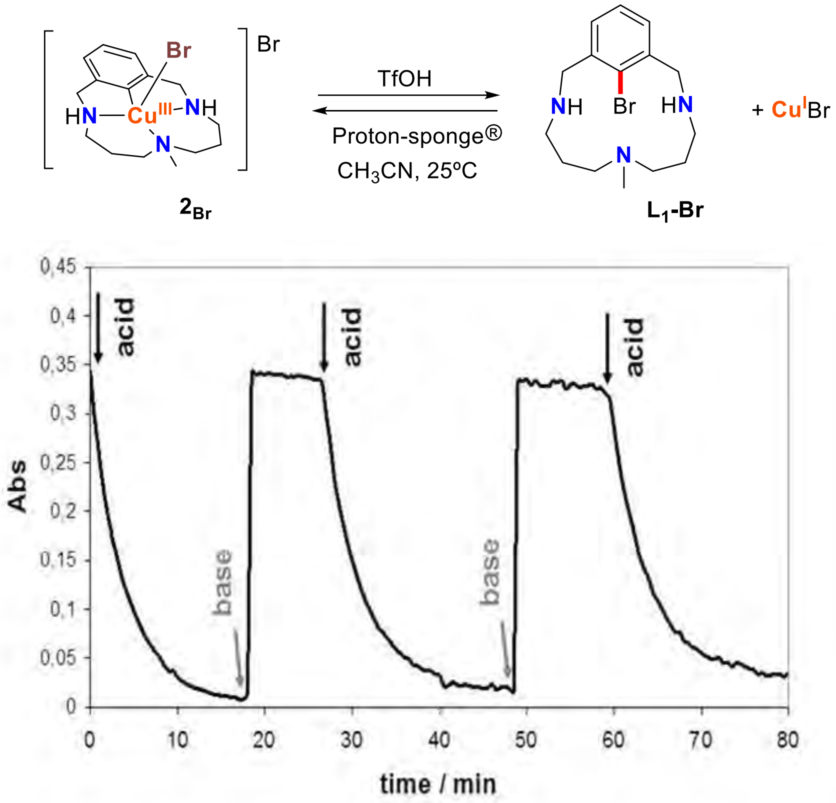

Figure I. 3. UV-Vis monitoring of the sequential interconversion between Cu^{III}/Cu^{I} redox states with complex **2**$_{\mathbf{Br}}$ through addition of acid or base.

Moreover, Wang also described in 2009 the ability of aryl-Cu^{III} heterocalixaromatic **47** complex to undergo very fast halogenation reactions except fluorination upon reaction with equimolar amounts of the corresponding Et$_4$NX (X = Cl ,Br, I).[76]

I.3.3.3. Mechanistic insights on Ullmann-Goldberg-type coupling reactions

The advent of stable aryl-Cu^{III} compounds allowed the study of the reductive elimination and oxidative addition steps independently. Stahl and Ribas demonstrated the capability of aryl-Cu^{III} complexes to generate C$_{aryl}$-nucleophile products *via* reductive elimination upon reaction with nitrogen- and oxygen-based nucleophiles.[79,80] In an initial report, Stahl studied the reactivity of the perchlorate salt of the triazamacrocyclic aryl-Cu^{III} complex and *N*-nucleophiles such as lactams, imides, sulphonamides, oxazolidone and benzamides to furnish the C-N coupling products under mild conditions (25 to 50 ºC).[79] The rates of the reaction increased with the acidity of the *N*-nucleophile indicating that the deprotonation of the nucleophile takes place before or during the rate-determining step. Similarly, Stahl and Ribas demonstrated that the aryl-Cu^{III} also undergoes coupling in the presence of carboxylic acids, phenols and aliphatic alcohols.[80] These coupling steps can be envisioned to occur through at least two possible mechanisms: 1) a three-centered C-nucleophile reductive elimination from the unobserved aryl-Cu^{III}-(nucleophile) intermediate; 2) a bimolecular nucleophilic attack of a deprotonated nucleophile on the ipso carbon of the aryl ligand. While for halogenation reactions is clear that the first pathway is functional, being aryl-Cu^{III}-X complexes isolated and fully characterized,[75] for C-nucleophile couplings the authors have only been able to detect aryl-Cu^{III}-(nucleophile) adducts prior to the nucleophile deprotonation step by low temperature UV-Vis and NMR techniques.[80]

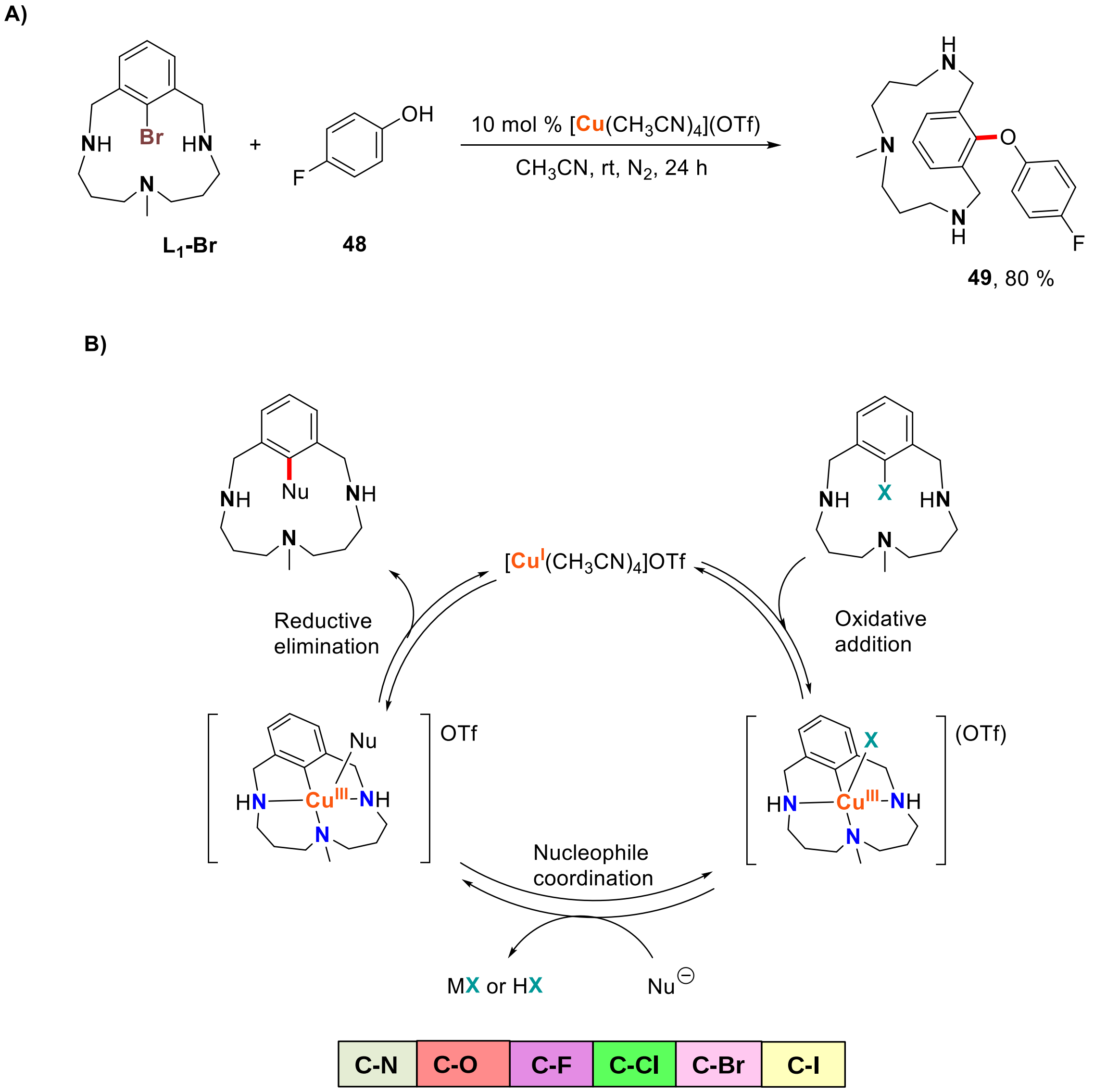
A)
L1-Br
48
NH Br HN
N
OH
F
+
10 mol % [Cu(CH3CN)4](OTf)
CH3CN, rt, N2, 24 h
49, 80 %
B)
Nu
X
[CuI(CH3CN)4]OTf
Reductive elimination
Oxidative addition
OTf
(OTf)
HN—CuIII-NH
Nucleophile coordination
MX or HX
Nu⊖
C-N
C-O
C-F
C-Cl
C-Br
C-I

Scheme I. 9. A) Copper-catalysed C-O bond forming cross-coupling reaction within a macrocyclic model aryl halide substrate. **B**) General mechanistic scenario operating in copper-catalysed C-N, C-O cross-coupling reactions and halide exchange reactions within triazamacrocyclic model aryl halide platforms.

Further, both oxidative addition and coupling steps could be merged to realise a catalytic process with nucleophiles ranging from halides[78] to alcohols[80] and aromatic amides[75] (**Scheme I. 9A** for C-O bond forming cross-coupling catalysis). In all cases, aryl-Cu^{III}-halide intermediate species have been identified as the resting state of the catalysis and thus have been unequivocally characterised under catalytic conditions. These studies were proof of principle to prove the feasibility of Cu^{I}/Cu^{III} catalytic redox cycles in Ullmann-Goldberg-type chemistry and that this mechanism is found to be general within the triazamacrocyclic aryl halide model system investigated. Moreover, these reports proved that aryl-Cu^{III}-halide species are plausible key intermediates in Ullmann-Goldberg-type condensations for the formation of C-N, C-O and C-halide bonds (**Scheme I. 9B**). Indeed, these reports represent the first experimental examples of an operative pathway B mechanism (**Scheme I. 7**) favoured by the facile oxidative addition step within the macrocyclic aryl halide substrate environment.

I.3.4 General outlook on Ullmann-type condensations

Since the discovery of the Buchwald-Hartwig palladium-catalysed amine arylation reactions, which caused a notable impact in synthetic organic chemistry, researchers have aimed to develop methods for constructing C-heteroatom bonds in a greener fashion. The last two decades have witnessed a blooming of the Ullmann-type condensations and the development of practical more sustainable alternatives to palladium chemistry for coupling halide-containing hydrocarbons and nucleophiles. The development of methodologies capable of competing with palladium chemistry came hand in hand with the use of ancillary bidentate ligands that enabled these transformations to proceed under more attractive mild conditions.[81] Indeed, the pharmaceutical industry has realised the high potential that Ullmann-type methodologies possess and successfully applied these reactions to the synthesis of numerous precursors and pharmaceuticals.[82] More recently, an approach based on a photoinduced variant of Ullmann-type chemistry has emerged as a powerful tool to effect C-nucleophile couplings with a broad range of electrophiles and nucleophiles under very mild conditions. Further, photoinduced Ullmann-type reactions complement the richness of the field and extend its versatility remarkably as they can engage coupling partners such as alkyl halides, which are unreactive under non-photoinduced conditions. However, although these protocols are advantageous in many aspects, they suffer from functional group susceptibility issues related to their radical nature. This fact becomes evident by the limited functional group tolerance of these reactions, especially for the electrophilic coupling partner. Therefore, this might become a limiting factor in exploiting its applicability to the late stage transformation of complex molecules such as pharmaceuticals or natural products, transformations in which non-photoinduced methods have already proven to be efficient. In conclusion, the wide variety of available methods developed over the last twenty years has significantly boosted Ullmann-type chemistry turning it into a reliable and versatile transformation that can be appropriately adapted to particular necessities depending on the requirements of the molecule that is being targeted.

I.4. Silver in Coupling Reactions

I.4.1 Silver-promoted homocoupling reactions

In contrast to the other two coinage metals, silver holds a rather unexplored redox chemistry that is poorly understood.[9,10,83] Silver has been rarely the metal of choice in classical transition metal-catalysed cross-coupling reactions. In fact, silver redox chemistry has been long assumed to stem exclusively from one-electron processes, thus attracting very little attention in the cross-coupling field, typically operated by a metal catalyst that undergo two-electron redox processes such as oxidative addition and reductive elimination.[84,85]

Nevertheless, silver-promoted coupling reactions are traced back to 1870, with the work on Glaser-type coupling of acetylenes in the presence of metal salts. These early reports revealed that silver(I) salts mediate the dimerisation of phenylacetylide (**Scheme I. 10**).[86]

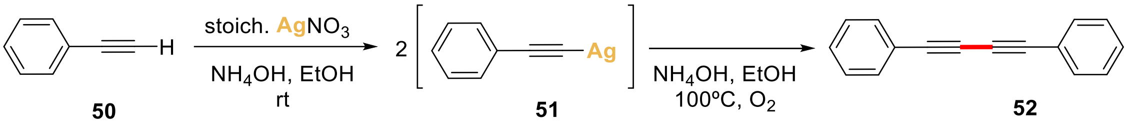

Scheme I. 10. Glaser-type homocoupling of silver phenylacetylide.

Later, at the end of 1920's, silver's ability to promote Wurtz-type coupling reactions of Grignard reagents was discovered. Research focused on such chemistry showed that silver(I) salts mediate the homocoupling of aryl and alkyl Grignard reagents as well as unselective cross-coupling reactions through the formation of the corresponding organic radical fragments.[87,88] Alkyl homocoupling reactions from the parent alkyl Grignard analogues have been recently performed in a catalytic process by using low loadings of silver tosylate and 1,2-dibromoethane as reoxidant (**Scheme I. 11**).[89]

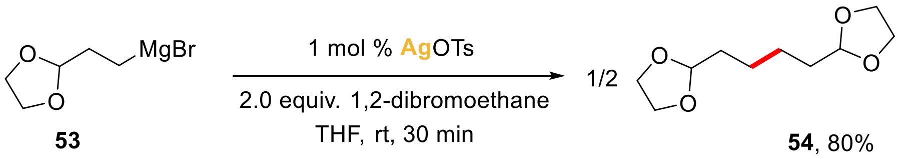

Scheme I. 11. Silver-catalysed homocoupling reaction of alkyl Grignard reagents.

Four decades after the first discovery of the silver-catalysed homocoupling of Grignard reagents, Kochi showed that these reactions also proceed readily using alkyl halides as one of the coupling partners.[90,91] Parallel results concerning the Grignard cross-couplings were obtained when the alkyl fragments on the Grignard reagent and the alkyl halide were different showing the formation of the three possible coupling products. Studies on the reaction mechanisms also revealed that the formation of the products occur through alkyl radicals.[92]

The limitations of the very narrow scope of these transformations were not overcome until recently. Oshima contributed to the extension of the limits of these reactions by showing that benzyl, allyl, alkyl and aryl Grignards can efficiently couple with challenging alkyl halides including tertiary alkyl halides, thus providing access to quaternary carbon centres.[93,94]

The authors discussed the mechanistic pathways hypothesised by Kochi and made efforts to validate the radical nature of their couplings. A competition experiment in which secondary **55** and tertiary **56** alkyl bromides were reacted with benzylmagnesium bromide using catalytic amounts of silver nitrate yielded predominantly product **59** resulting from the alkylation of the tertiary alkyl bromide **56**. These results suggested the formation of sp^2-hybridised carbon centres as carbocations or carbon-centred radicals, more favourably generated for tertiary than for secondary carbons (**Scheme I. 12**).[93]

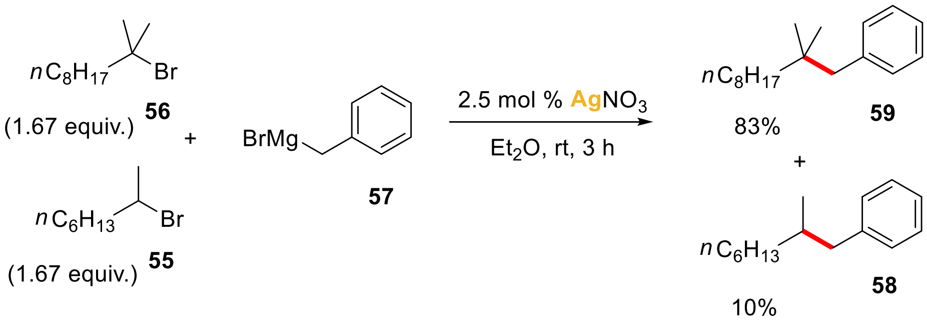

Scheme I. 12. Competition experiment of the alkylation of secondary and tertiary alkyl bromides.

Also, a radical probe experiment was performed subjecting (2-iodocyclohexyloxy)vinylsilane **60** to the silver-catalysed benzylation reaction. After 3 hours of reaction, compound **61**, resulting from the homolytic cleavage of the C-I bond plus recombination of the generated radical with the vinyl moiety, was formed (**Scheme I. 13**). To reliably characterise the products of the reaction, **61** was converted *in situ* into its diacetylated derivative **62** owing to the spontaneous decomposition of **61** by hydrolytic processes.[93]

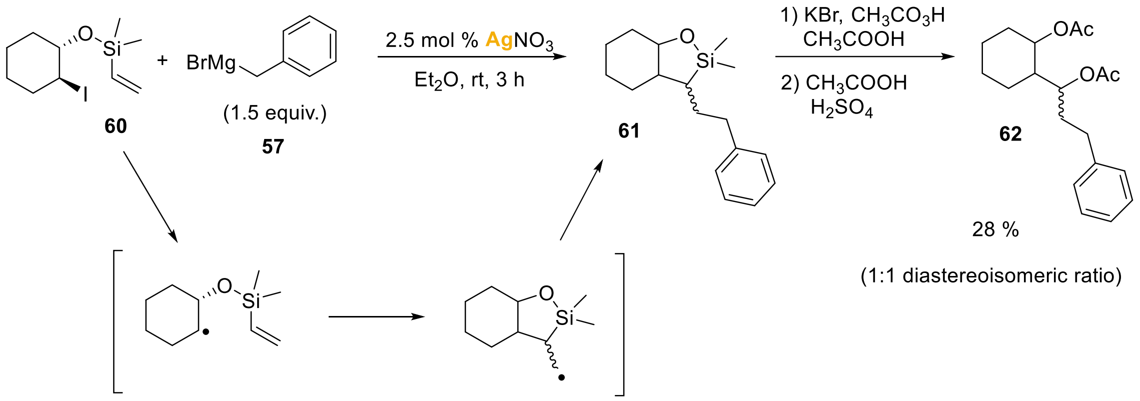

Scheme I. 13. Silver-catalysed intramolecular cyclisation plus benzylation of (2-iodocyclohexyloxy)vinylsilane.

Similar reactivity was discovered by Brown in the 1960's but using boranes instead of Grignard reagents as transmetallating agents. In their reports, they described the stepwise hydroboration of terminal and internal alkenes and subsequent homocoupling triggered by the addition of an excess of a silver salt (**Scheme I. 14**).[95,96] When these reactions were conducted using two different coupling partners, *i.e.* two alkenes, a mixture of products resulting from the homocoupling and the cross-coupling processes was formed.[97]

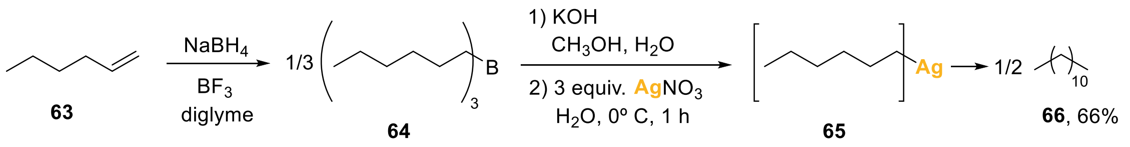

Scheme I. 14. Silver-mediated homocoupling reaction of boranes.

In similarity to the proposals for the related reactions with Grignard reagents, the authors hypothesised the formation of alkylsilver species that decompose at ambient temperature to generate alkyl radicals that afford the coupling products after recombination.

Since these pioneering studies on silver-promoted couplings, this area of chemistry has seen little progress. Nevertheless, sporadic examples have been reported on silver-promoted cross-coupling reactions. For instance, it has been described that palladium or copper can be replaced by silver in some examples of Sonogashira,[98] Suzuki,[99] and Ullmann-type[100] reactions (**Scheme I. 15**). Moreover, a silver-catalysed coupling of arylboronic acids with thiols has been recently documented in a transformation that reminds its analogous copper-catalysed transformation known as Chan-Lam coupling.[99] The authors of these studies ruled out the possibility that trace amounts of the original palladium or copper were carrying out these transformations based on the ICP-MS analysis of all starting materials being too low to be effective. Even though the mechanistic aspects of the original reactions have been thoroughly studied and are well-defined, no mechanistic ground has been reported on silver-catalysed cross-coupling reactions, hampering the development and design of new synthetic methodologies based on silver.

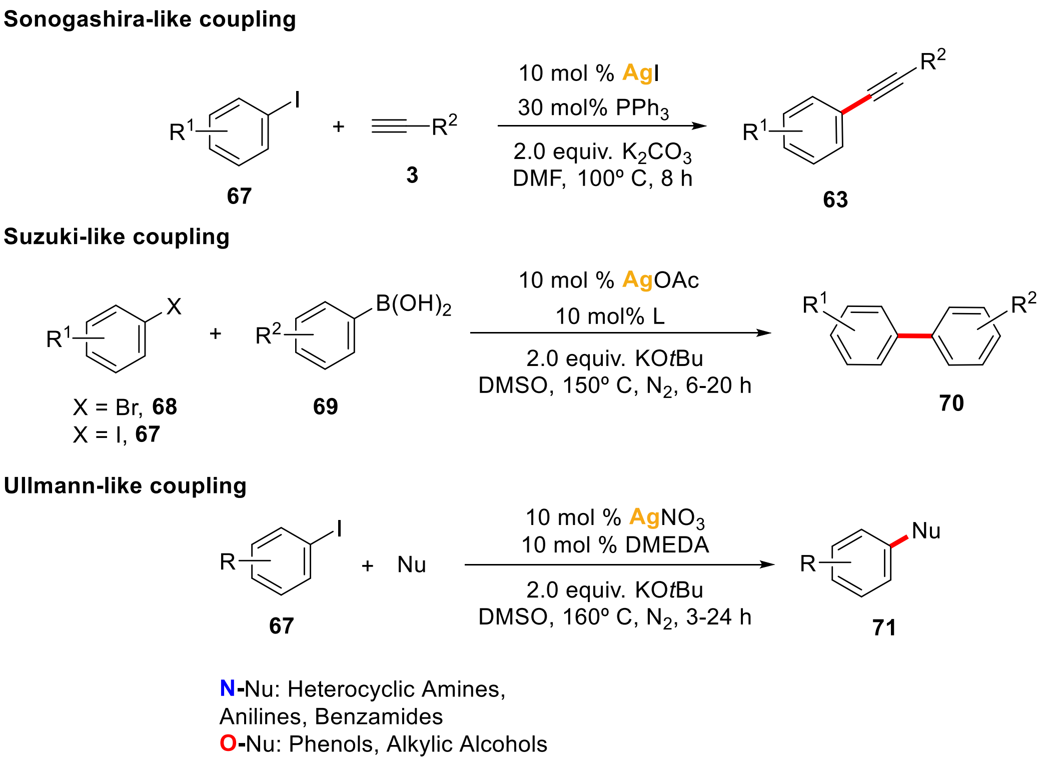
Sonogashira-like coupling
10 mol % AgI
30 mol% PPh3
2.0 equiv. K2CO3
DMF, 100° C, 8 h
67
3
63
Suzuki-like coupling
10 mol % AgOAc
10 mol% L
2.0 equiv. KOtBu
DMSO, 150° C, N2, 6-20 h
X = Br, 68
X = I, 67
69
70
Ullmann-like coupling
10 mol % AgNO3
10 mol % DMEDA
2.0 equiv. KOtBu
DMSO, 160° C, N2, 3-24 h
67
71
N-Nu: Heterocyclic Amines, Anilines, Benzamides
O-Nu: Phenols, Alkylic Alcohols

Scheme I. 15. Silver-catalysed cross-coupling reactions traditionally operated through two-electron redox cycles by their analogous palladium- and copper-catalysed reactions.

I.4.2 Silver-promoted oxidative coupling reactions

Silver has been also applied to oxidative couplings to provide access to aryl fluoride molecules. Progress in fluorinating technologies of organic chemistry is of pivotal importance for the agrochemical and pharmaceutical industries. Fluorinated compounds are of unique biological relevance due to their enhanced solubility, bioavailability, metabolic stability as well as rate and extent of blood-brain barrier penetration in comparison to non-fluorinated analogues.[101-107] All these features lead to an enhancement of drug efficacy that allows for a lowering of the needed dosage reducing undesirable secondary effects. At present, up to a 30-40 % of agrochemicals and 20-30% of pharmaceuticals contain at least one fluorine atom, usually located at arene rings.[105-108] Furthermore, radioactive ^{18}F-labeled organic compounds are used as tracers for Positron Emission Tomography (PET), a very powerful tool used in Medicine for the diagnosis of diseases.[109-111] Despite the appreciation of fluorine's importance, the existing methods for the fluorination of organic molecules, including arenes, still lack generality and practicality. In the last few years the transition metal-promoted conversion of arene and arene derivatives to furnish the corresponding aryl fluoride compounds have emerged as milder and functional group tolerant alternatives to traditional methods such as the Balz-Schiemann reaction[112] (conversion of anilines to aryl fluorides), the Halex process[113] (conversion of aryl halides to aryl fluorides) and others.[105] Among these novel fluorination technologies, transition metal-promoted electrophilic fluorinations, that afford fluorinated arenes from arenes bearing transmetallating agents as arylborates and stannanes using electrophilic fluoride sources have proven to be very efficient.[114-117]

Notably, Ritter discovered the first silver-mediated fluorination of arylstannanes in 2009, when transition metal-promoted fluorination began to be conceived as a real alternative to traditional methods.[118] This methodology was brought one step further with the achievement of the catalytic late-stage fluorination of complex molecules from its corresponding arylstannanes.[84] This example constitutes one of the most reliable methods to access fluorinated arenes having the broadest substrate scope to date. Notwithstanding, working with arylstannanes as starting materials presents major drawbacks such as their high toxicity and their proclivity to protodestannylation. Hence, the authors developed silver-mediated routes towards electrophilic fluorination of arenes that utilize less toxic arylboronic acids and arylsilanes.[119,120]

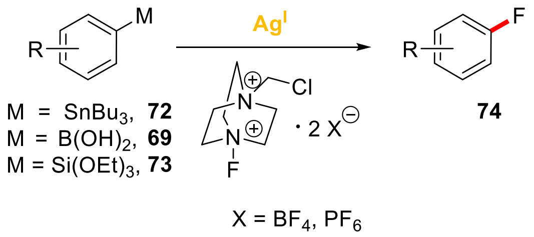

Scheme I. 16. Silver-promoted fluorination of arenes bearing transmetallating agents.

The authors, based on few and inconclusive results, drew a tentative mechanism for the catalytic cycle of the C-F bond formation of arylstannanes that involves dinuclear silver(II) species (**Scheme I. 17**). The cycle starts with a transmetallation step to form aryl-Ag^{I} species **I** or its corresponding aggregates with other silver(I) cations. Subsequent oxidation of **I** by Selectfluor® provides the dinuclear Ag^{II}-Ag^{II}-F high-valent species **II** responsible for the C-F coupling after a two-centred reductive elimination step. The authors proposed analogous bimetallic key intermediate species for the related reactions with arylboronic acids and arylsilanes although no further studies were performed to confirm their mechanisms.

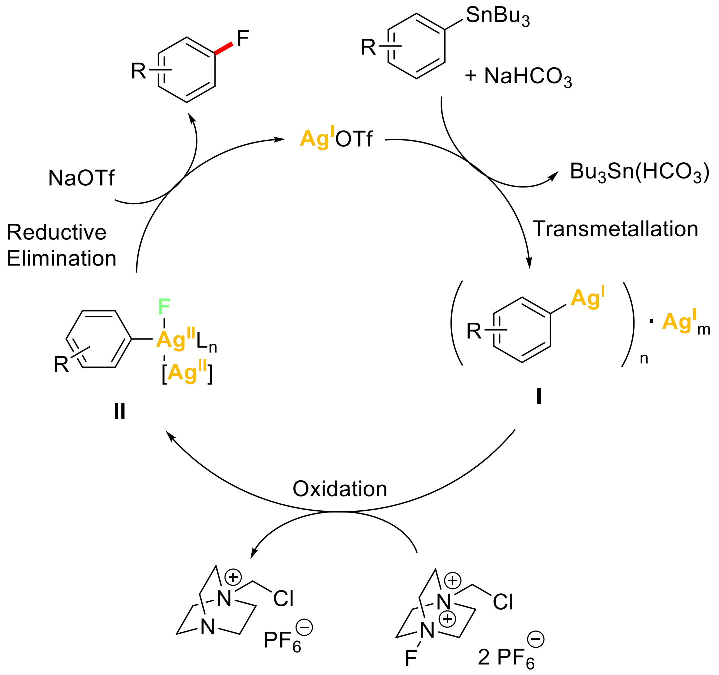
SnBu3
R
+ NaHCO3
F
R
AgIOTf
Bu3Sn(HCO3)
NaOTf
Reductive Elimination
Transmetallation
F
AgIILn
[AgII]
R
II
R
AgI
n
· AgIm
I
Oxidation
N
N
Cl
PF6
N
N
F
Cl
2 PF6

Scheme I. 17. Mechanistic proposal for the silver-catalysed fluorination of arylstannanes.

The authors, though, were unable to identify any high-valent species in the reaction and none of the experiments carried out to unravel its mechanistic pathways rules out the involvement of monomeric Ag^{III}-F key intermediates, analogous to the Cu^{III}-F intermediates directly observed by Hartwig and co-workers by means of mass spectrometry and NMR techniques in their related copper-mediated fluorination of arylboronate esters.[115]

I.4.3 Silver-promoted coupling chemistry *via* Ag^{I}/Ag^{III} redox cycles

Aryl-Ag^{III} species had been proposed previously to operate in the pyridination and acetoxylation of carboporphyrinoids, porphyrin-related molecules resulting from the replacement of one or more of the pyrrolic rings by other carbocyclic moieties. These examples showed that treatment of the benziporphyrin scaffold **75** with a large excess of $AgBF_4$ in refluxing pyridine produced the product of pyridination of the inner C-H bond of the arene moiety to afford the aryl-pyridinium **76** product (**Scheme I. 18**).[121] Similarly, when the reaction was carried out with excess of AgOAc the analogous acetoxylation product was obtained.[122]

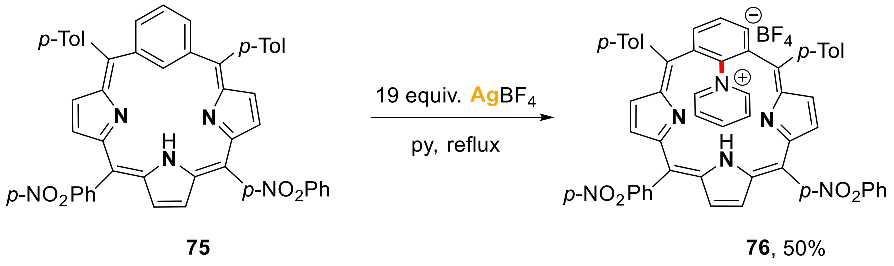
p-Tol
p-Tol
N
N
H
N
p-NO2Ph
p-NO2Ph
75
19 equiv. AgBF4
py, reflux
BF4
p-Tol
p-Tol
N
N
N
H
N
p-NO2Ph
p-NO2Ph
76, 50%

Scheme I. 18. Silver-mediated pyridination of benziporphyrin.

Radical pathways were ruled out on the basis of the complete regioselectivity on the inner carbon of the carbaporphyrin. Hence, a mechanism operated through aryl-Ag^{III} intermediates was invoked despite no evidence being provided to support these proposals. First, C-H activation of the inner C-H bond of the aryl moiety was proposed to take place generating an aryl-Ag^{III} species, which after coordination of the pyridine and subsequent reductive elimination afforded product **76** (**Scheme I. 19**). The metallic silver formed during the reaction might suggest that the large excess of silver(I) is needed to reach silver(III) redox states by a disproportionation process.

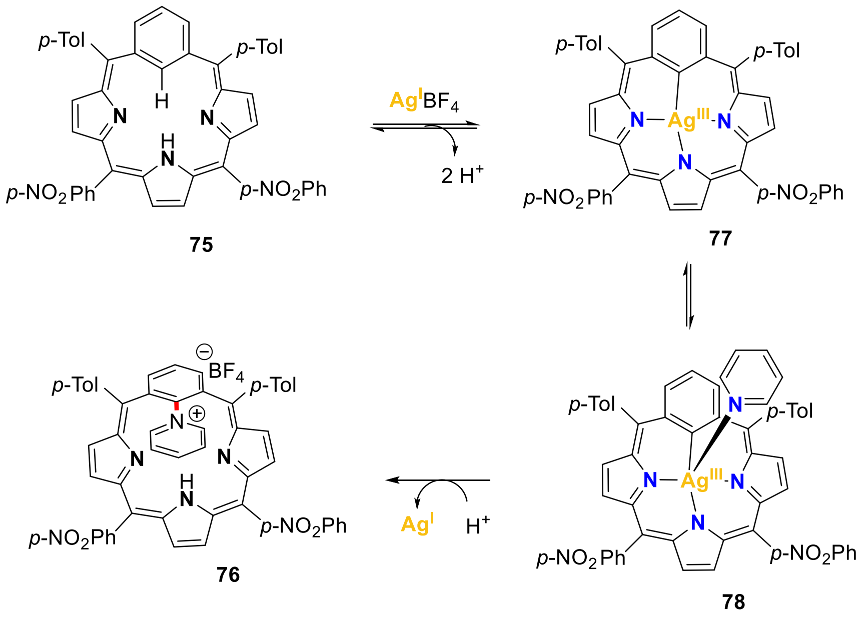
p-Tol
p-Tol
H
N
N
H
N
p-NO2Ph
p-NO2Ph
75
AgIBF4
2 H+
p-Tol
p-Tol
N
AgIII
N
N
p-NO2Ph
p-NO2Ph
77
BF4
p-Tol
p-Tol
N
N
N
H
N
p-NO2Ph
p-NO2Ph
76
AgI
H+
p-Tol
N
p-Tol
N
AgIII
N
N
p-NO2Ph
p-NO2Ph
78

Scheme I. 19. Mechanistic proposal involving aryl-Ag^{III} species to rationalise the regioselective pyridination of benziporphyrin **75**.

The observation of reductive elimination processes in organometallic silver(III) complexes including related porphyrinoid-Ag^{III} systems support their proposal. The first study that proposed a reductive elimination was reported in 1997 and described the decomposition of the *tris*(trifluoromethyl)halide argentates(III) of $[Ag^{III}(CF_3)_3X]^-$ (X = Cl, Br, I) general formula to $[Ag^{I}(CF_3)_2]^-$ and CF_3X. However, the CF_3X reaction products were not characterised.[123] The plausibility of key aryl-Ag^{III} intermediate species in the pyridination of **75** (**Scheme I. 19**), though, was bolstered by another study of the same research group in which a reductive elimination step from organometallic Ag^{III}-C$_{sp2}$ species resulting in the coupling of a nucleophile in the frame of the furanone-Ag^{III} complex **79** (**Scheme I. 20A**). They reported the phosphonylation of complex **79** upon treatment with potassium diphenylphosphide to furnish the desired formation of product **80** and its corresponding diphenylphosphoryl analog (**81**) generated by oxidation of **80**.[124]

Three years later, another example of reductive elimination was reported using related complexes. Organometallic silver(III) complex **82**, where silver is embedded in an *N*-confused porphyrin (NCP) ligand, that is, a porphyrin isomer wherein one of the four pyrrole rings is inverted, thus placing one carbon atom into the inner cavity of the macrocycle, presented favoured reductive eliminations in the presence of nucleophilic substrates. In fact, phosphorylation reaction is effected in the same conditions employed for **82** and also the products of thiophosphorylation of the complex are accessible by parallel routes affording a family of rare NCP hybrid ligands (**Scheme I. 20B**).[125] It is worth noting that the phosphorylation reaction can be reverted by reacting an excess of AgOAc with compound **84** in a process that resembles an oxidative addition process that the authors did not consider studying further to characterise it as such.

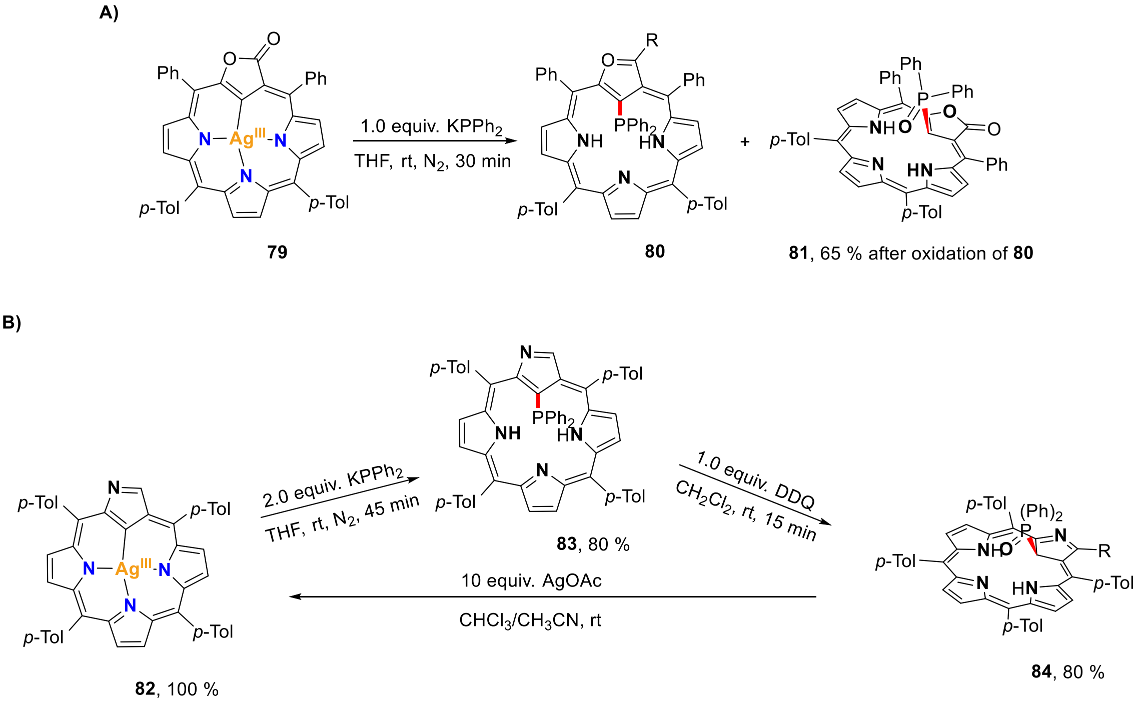
A)
O
Ph
Ph
N
Ag^{III}
N
N
p-Tol
p-Tol
79
1.0 equiv. KPPh$_2$
THF, rt, N$_2$, 30 min
R
O
Ph
Ph
NH
PPh$_2$
HN
N
p-Tol
p-Tol
80
+
Ph
Ph
P
Ph
p-Tol
NH
O
O
O
N
HN
Ph
p-Tol
81, 65 % after oxidation of 80
B)
p-Tol
N
p-Tol
N
Ag^{III}
N
N
p-Tol
p-Tol
82, 100 %
2.0 equiv. KPPh$_2$
THF, rt, N$_2$, 45 min
p-Tol
N
p-Tol
NH
PPh$_2$
HN
N
p-Tol
p-Tol
83, 80 %
1.0 equiv. DDQ
CH$_2$Cl$_2$, rt, 15 min
p-Tol
(Ph)$_2$
P
p-Tol
NH
O
N
R
N
HN
p-Tol
p-Tol
84, 80 %
10 equiv. AgOAc
CHCl$_3$/CH$_3$CN, rt

Scheme I. 20. A) Phosphanylation of the furanone-Ag^{III} complex **79** through reductive elimination. **B)** Phosphanylation of the NCP-Ag^{III} complex **82** through reductive elimination and dephosphorylative insertion of AgOAc over product **84** to restore complex **82.**

I.5. Gold in Coupling Catalysis

A scarce number of gold-catalysed protocols for classical cross-coupling catalysis, typically proceeding through M^n/M^{n+2} redox cycles, have arisen despite the fact that gold chemistry has been a major focus of research during the past two decades. Indeed, studies that demonstrated catalytic activity in the presence of ppm levels of palladium have generated intense debate on the actual metal that promotes the transformations, especially for Sonogashira-like couplings.[126,127] Even though +1 and +3 are stable oxidation states for gold, switching between them during the course of a reaction is not trivial. This reluctance to engage in two-electron redox oxidations is due to the high oxidation potential of the Au^I/Au^{III} redox couple (E_0 = + 1.41 V in water).[128] Thus, the oxidative addition of gold(I) species to organic halides or pseudoaryl halides is a critical impediment that limits the applicability of gold(I) in cross-coupling chemistry. To overcome this obstacle gold(I) coupling chemistry has evolved towards oxidative coupling transformations in which the use of a sacrificial external oxidant allows the oxidation to gold(III) species and thereby enabling the access to Au^I/Au^{III} catalytic cycles (see **Scheme I. 21** for a general mechanistic overview).[129]

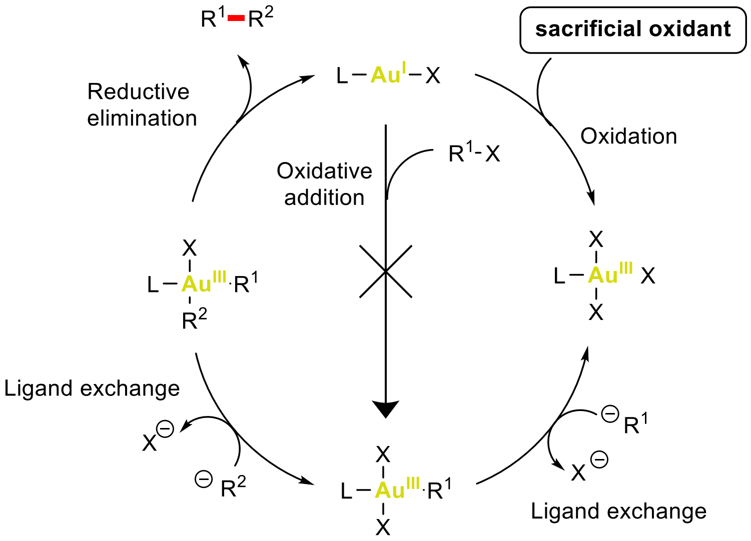

Scheme I. 21. General mechanism for the gold-catalysed oxidative coupling reactions promoted by sacrificial external oxidants.

Remarkably, the two most unique reactivity patterns mediated by gold; the hydrofunctionalisation of C-C multiple bonds driven by π-activation and the oxidative coupling have been combined to develop gold-catalysed tandem routes capable of building molecular complexity in a very step-economical manner (see **Scheme I. 22** for an example of gold-catalysed tandem heterocyclisation/oxidative arylation of alkenes).[130]

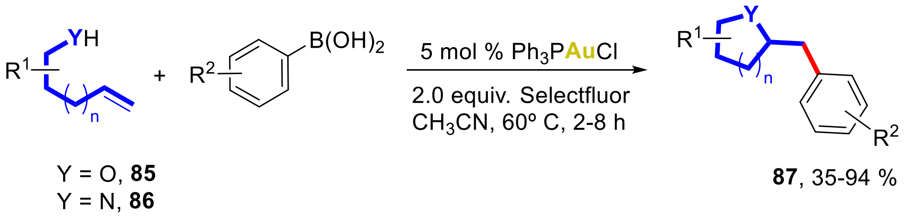

Scheme I. 22. Gold-catalysed cascade heterocyclisation plus oxidative arylation of alkenes.[130]

On the other hand, whilst oxidative addition over gold(I) centres is remarkably challenging it has proven plausible, especially if triggered by chelating groups that direct the C-halide bond towards the gold(I) centre, as the studies from the groups of Kochi and Schmidbaur in the 1970's and more recently Bourissou and Amgoune demonstrate.[131-136]

Continued efforts pursuing oxidant-free gold-catalysed cross-coupling methodologies have resulted in the first gold-catalysed allylation of arylboronic acids reported by Toste.[137] These examples follow two different strategies to attain the allylation reaction; the first exploits the potential cooperation of two metal centres to favour bimetallic oxidative addition steps that according to the authors could generate Au^{II}-Au^{II} key intermediate species **90** yielding an overall intermolecular allylation of arylboronic acids *via* reductive elimination (**Scheme I. 23A**). The authors, though, were unable to provide conclusive evidence to neither support the proposed mechanism nor detect any intermediate species likely due to the fast reaction rates of the reductive elimination. The second strategy implies the design of an arylboronic acid substrate bearing a pendant allyl bromide arm that places the gold(I) centre in close proximity to the targeted C-halide bond resulting in the formation of the corresponding gold(III) complex **94**, characterised by single crystal X-ray diffraction. The complex underwent subsequent reductive elimination in the presence of a halide abstractor to afford the intramolecular coupling product **95** (**Scheme I. 23B**). Albeit the reaction requires stoichiometric amounts of gold and the final net allylation only takes place in a stepwise manner, it validates the idea of an operative Au^{I}/Au^{III} redox cycle in the arylation of allyl bromide **92**.

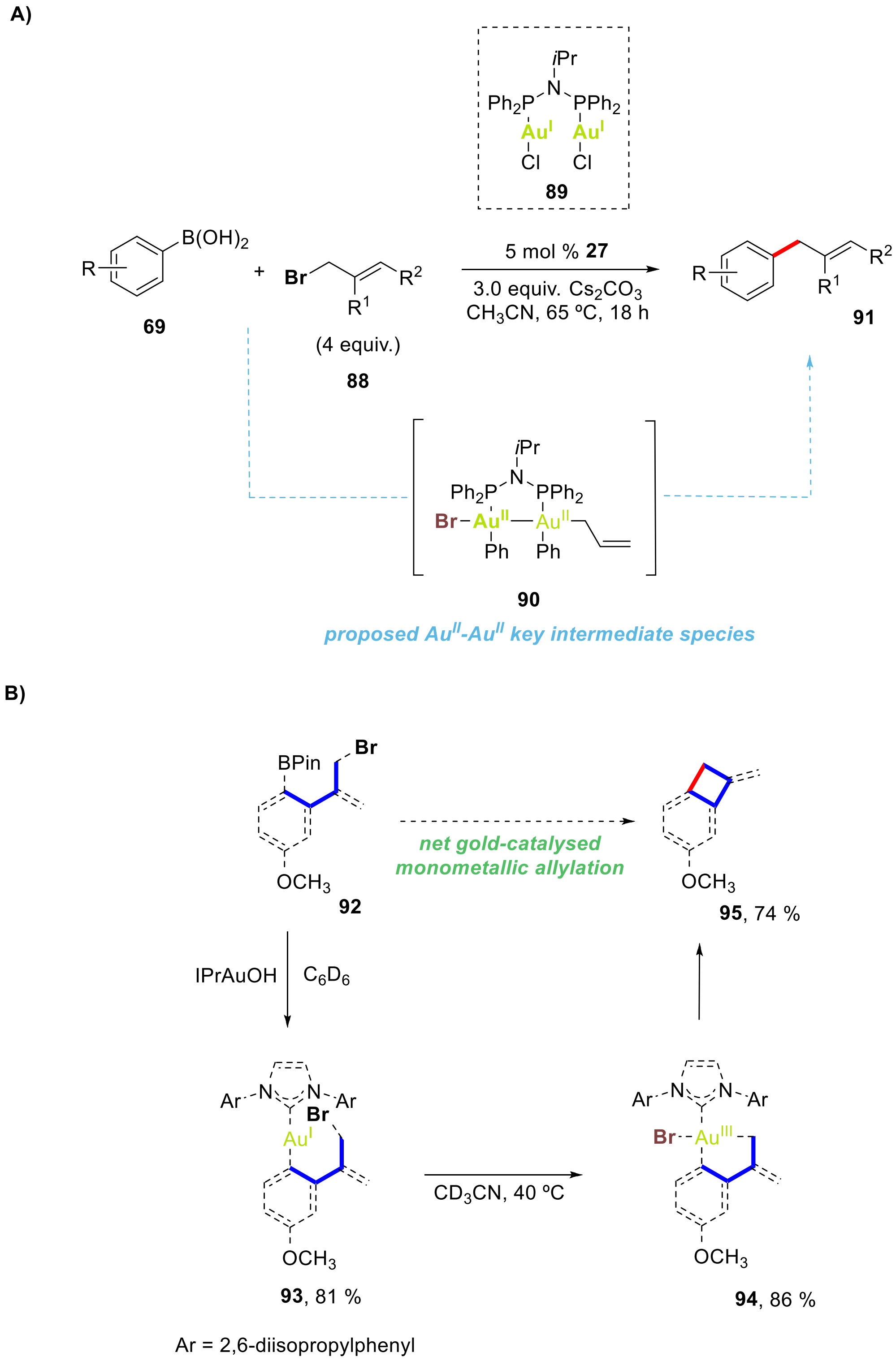
A)
iPr
Ph2P N PPh2
AuI AuI
Cl Cl
89
B(OH)2
R
69
+
Br R2 R1
(4 equiv.)
88
5 mol % 27
3.0 equiv. Cs2CO3
CH3CN, 65 °C, 18 h
R R2 R1
91
iPr
Ph2P N PPh2
Br AuII AuII
Ph Ph
90
proposed AuII-AuII key intermediate species
B)
BPin Br
OCH3
92
net gold-catalysed monometallic allylation
OCH3
95, 74 %
IPrAuOH C6D6
Ar N N Ar
Br
AuI
OCH3
93, 81 %
CD3CN, 40 °C
Ar N N Ar
Br AuIII
OCH3
94, 86 %
Ar = 2,6-diisopropylphenyl

Scheme I. 23. A) Gold-catalysed intermolecular allylation of arylboronic acids proposed to operate through Au^{II}-Au^{II} bimetallic intermediate species **90**. **B**) Model stepwise intramolecular allylation of arylboronate ester **92** via allyl-Au^{III} species **94** formed upon monometallic oxidative addition.

I.6. References

(1) Alexakis, A.; Bäckvall, J.-E.; Krause, N.; Pàmies, O.; Diéguez, M. *Chem. Rev.* **2008**, *108*, 2796.
(2) Harutyunyan, S. R.; den Hartog, T.; Geurts, K.; Minnaard, A. J.; Feringa, B. L. *Chem. Rev.* **2008**, *108*, 2824.
(3) Shibasaki, M.; Kanai, M. *Chem. Rev.* **2008**, *108*, 2853.
(4) Deutsch, C.; Krause, N.; Lipshutz, B. H. *Chem. Rev.* **2008**, *108*, 2916.
(5) Stanley, L. M.; Sibi, M. P. *Chem. Rev.* **2008**, *108*, 2887.
(6) Bock, V. D.; Hiemstra, H.; van Maarseveen, J. H. *Eur. J. Org. Chem.* **2006**, 51.
(7) Meldal, M.; Tornøe, C. W. *Chem. Rev.* **2008**, *108*, 2952.
(8) Kolb, H. C.; Finn, M. G.; Sharpless, K. B. *Angew. Chem. Int. Ed.* **2012**, *40*, 2004.
(9) Naodovic, M.; Yamamoto, H. *Chem. Rev.* **2008**, *108*, 3132.
(10) Weibel, J.-M.; Blanc, A.; Pale, P. *Chem. Rev.* **2008**, *108*, 3149.
(11) Álvarez-Corral, M.; Muñoz-Dorado, M.; Rodríguez-García, I. *Chem. Rev.* **2008**, *108*, 3174.
(12) He, C.; Guo, S.; Ke, J.; Hao, J.; Xu, H.; Chen, H.; Lei, A. *J. Am. Chem. Soc.* **2012**, *134*, 5766.
(13) Ye, Y.; Lee, S. H.; Sanford, M. S. *Org. Lett.* **2011**, *13*, 5464.
(14) Wu, X.; Chu, L.; Qing, F.-L. *Angew. Chem. Int. Ed.* **2013**, *52*, 2198.
(15) Li, Z.; Song, L.; Li, C. *J. Am. Chem. Soc.* **2013**, *135*, 4640.
(16) Fier, P. S.; Hartwig, J. F. *Science* **2013**, *342*, 956.
(17) Ilchenko, N. O.; Tasch, B. O. A.; Szabó, K. J. *Angew. Chem. Int. Ed.* **2014**.
(18) Li, Z.; Brouwer, C.; He, C. *Chem. Rev.* **2008**, *108*, 3239.
(19) Hashmi, A. S. K.; Toste, F. D. *Modern Gold Catalyzed Synthesis*; Wiley-VCH: Weinheim, 2012; p. 402 pp.
(20) Wang, Y.-M.; Lackner, A. D.; Toste, F. D. *Acc. Chem. Res.* **2014**, *47*, 889.
(21) Obradors, C.; Echavarren, A. M. *Acc. Chem. Res.* **2014**, *47*, 902.
(22) Li, Z.; He, C. *Eur. J. Org. Chem.* **2006**, 4313.
(23) Rasika Dias, H. V.; Lovely, C. J. *Chem. Rev.* **2008**, *108*, 3223.
(24) Díaz-Requejo, M. M.; Pérez, P. J. *Chem. Rev.* **2008**, *108*, 3379.
(25) Boorman, T. C.; Larrosa, I. *Chem. Soc. Rev.* **2011**, *40*, 1910.
(26) Schlummer, B.; Scholz, U. *Adv. Synth. Catal.* **2004**, *346*, 1599.
(27) Buchwald, S. L.; Mauger, C.; Mignani, G.; Scholz, U. *Adv. Synth. Catal.* **2006**, *348*, 23.
(28) Magano, J.; Dunetz, J. R. *Chem. Rev.* **2011**, *111*, 2177.
(29) For an historical contextual perspective to the 2010 Nobel prize in Chemistry see: Johansson Seechurn, C. C. C.; Kitching, M. O.; Colacot, T. J.; Snieckus, V. *Angew. Chem. Int. Ed.* **2012**, *51*, 5062.
(30) Corbet, J.-P.; Mignani, G. *Chem. Rev.* **2006**, *106*, 2651.
(31) Wolfe, J. P.; Wagaw, S.; Marcoux, J.-F.; Buchwald, S. L. *Acc. Chem. Res.* **1998**, *31*, 805.
(32) Hartwig, J. F. *Acc. Chem. Res.* **2008**, *41*, 1534.
(33) Friedman, D.; Masciangioli, T.; Olson, S. *The Role of Chemical Sciences in Finding Alternatives to Critical Resources. A Workshop Summary.*; The National Academies Press: Washington, D.C., 2012; p. 59 pp.
(34) Hurtley, W. R. H. *J. Chem. Soc.* **1929**, 1870.
(35) Stephens, R. D.; Castro, C. E. *J. Org. Chem.* **1963**, *28*, 3133.
(36) Okuro, K.; Furuune, M.; Enna, M.; Miura, M.; Nomura, M. *J. Org. Chem.* **1993**, *58*, 4716.
(37) Ullmann, F. *Ber. Dtsch. Chem. Ges.* **1903**, *36*, 2382.
(38) Ullmann, F.; Sponagel, P. *Ber. Dtsch. Chem. Ges.* **1905**, *38*, 2211.
(39) Goldberg, I. *Ber. Dtsch. Chem. Ges.* **1906**, 1691.
(40) Evano, G.; Blanchard, N.; Toumi, M. *Chem. Rev.* **2008**, *108*, 3054.
(41) Ma, D.; Cai, Q. *Acc. Chem. Res.* **2008**, *41*, 1450.
(42) Casitas, A.; Ribas, X. *Chem. Sci.* **2013**, *4*, 2301.
(43) Creutz, S. E.; Lotito, K. J.; Fu, G. C.; Peters, J. C. *Science* **2012**, *338*, 647.
(44) Ziegler, D. T.; Choi, J.; Muñoz-Molina, J. M.; Bissember, A. C.; Peters, J. C.; Fu, G. C. *J. Am. Chem. Soc.* **2013**, *135*, 13107.
(45) Uyeda, C.; Tan, Y.; Fu, G. C.; Peters, J. C. *J. Am. Chem. Soc.* **2013**, *135*, 9548.
(46) Bissember, A. C.; Lundgren, R. J.; Creutz, S. E.; Peters, J. C.; Fu, G. C. *Angew. Chem. Int. Ed.* **2013**, *52*, 5129.
(47) Do, H.-Q.; Bachman, S.; Bissember, A. C.; Peters, J. C.; Fu, G. C. *J. Am. Chem. Soc.* **2014**, *136*, 2162.
(48) Tan, Y.; Muñoz-Molina, J. M.; Fu, G. C.; Peters, J. C. *Chem. Sci.* **2014**, *5*, 2831.

(49) For a review that discusses the proposed reaction mechanisms governing Ullmann-type chemistry see: Sperotto, E.; van Klink, G. P. M.; van Koten, G.; de Vries, J. G. *Dalton Trans.* **2010**, *39*, 10338.
(50) Kochi, J. K. *J. Am. Chem. Soc.* **1957**, *79*, 2942.
(51) Kochi, J. K.; Subramanian, R. V. *J. Am. Chem. Soc.* **1965**, *87*, 1508.
(52) Arai, S.; Yamagishi, T.; Ototake, S.; Hida, M. *Bull. Chem. Soc. Jpn.* **1977**, *50*, 547.
(53) Arai, S.; Hida, M.; Yamagishi, T. *Bull. Chem. Soc. Jpn.* **1978**, *51*, 277.
(54) Jones, G. O.; Liu, P.; Houk, K. N.; Buchwald, S. L. *J. Am. Chem. Soc.* **2010**, *132*, 6205.
(55) Sperotto, E.; van Klink, G. P. M.; de Vries, J. G.; van Koten, G. *Tetrahedron* **2010**, *66*, 9009.
(56) Sperotto, E.; van Klink, G. P. M.; de Vries, J. G.; van Koten, G. *Tetrahedron* **2010**, *66*, 3478.
(57) Bacon, R. G. R.; Hill, H. A. O. *J. Chem. Soc.* **1964**, 1097.
(58) Bacon, R. G. R.; Hill, H. A. O. *J. Chem. Soc.* **1964**, 1108.
(59) Bacon, R. G. R.; Hill, H. A. O. *J. Chem. Soc.* **1964**, 1112.
(60) Weingarten, H. *J. Org. Chem.* **1964**, *29*, 977.
(61) Weingarten, H. *J. Org. Chem.* **1964**, *29*, 3624.
(62) Ma, D.; Zhang, Y.; Yao, J.; Wu, S.; Tao, F. *J. Am. Chem. Soc.* **1998**, *120*, 12459.
(63) Bowman, W. R.; Heaney, H.; Smith, P. H. G. *Tetrahedron Lett.* **1984**, *25*, 5821.
(64) Zhang, S.; Liu, L.; Fu, Y.; Guo, Q. *Organometallics* **2007**, *26*, 4546.
(65) Ouali, A.; Spindler, J.-F.; Jutand, A.; Taillefer, M. *Adv. Synth. Catal.* **2007**, *349*, 1906.
(66) Ma, D.; Cai, Q. *Acc. Chem. Res.* **2008**, *41*, 1450.
(67) Tye, J. W.; Weng, Z.; Johns, A. M.; Incarvito, C. D.; Hartwig, J. F. *J. Am. Chem. Soc.* **2008**, *130*, 9971.
(68) Tye, J. W.; Weng, Z.; Giri, R.; Hartwig, J. F. *Angew. Chem. Int. Ed.* **2010**, *49*, 2185.
(69) Giri, R.; Hartwig, J. F. *J. Am. Chem. Soc.* **2010**, *132*, 15860.
(70) Yu, H.-Z.; Jiang, Y.-Y.; Fu, Y.; Liu, L. *J. Am. Chem. Soc.* **2010**, *132*, 18078.
(71) Chen, C.; Weng, Z.; Hartwig, J. F. *Organometallics* **2012**, *31*, 8031.
(72) Shafir, A.; Lichtor, P. A.; Buchwald, S. L. *J. Am. Chem. Soc.* **2007**, *129*, 3490.
(73) Ribas, X.; Jackson, D. A.; Donnadieu, B.; Mahía, J.; Parella, T.; Xifra, R.; Hedman, B.; Hodgson, K. O.; Llobet, A.; Stack, T. D. P. *Angew. Chem. Int. Ed.* **2002**, *41*, 2991.
(74) Ribas, X.; Calle, C.; Poater, A.; Casitas, A.; Gómez, L.; Xifra, R.; Parella, T.; Benet-Buchholz, J.; Schweiger, A.; Mitrikas, G.; Solà, M.; Llobet, A.; Stack, T. D. P. *J. Am. Chem. Soc.* **2010**, *132*, 12299.
(75) Casitas, A.; King, A. E.; Parella, T.; Costas, M.; Stahl, S. S.; Ribas, X. *Chem. Sci.* **2010**, *1*, 326.
(76) Yao, B.; Wang, D.-X.; Huang, Z.-T.; Wang, M.-X. *Chem. Commun.* **2009**, 2899.
(77) Casitas, A.; Poater, A.; Solà, M.; Stahl, S. S.; Costas, M.; Ribas, X. *Dalton Trans.* **2010**, *39*, 10458.
(78) Casitas, A.; Canta, M.; Solà, M.; Costas, M.; Ribas, X. *J. Am. Chem. Soc.* **2011**, *133*, 19386.
(79) Huffman, L. M.; Stahl, S. S. *J. Am. Chem. Soc.* **2008**, *130*, 9196.
(80) Huffman, L. M.; Casitas, A.; Font, M.; Canta, M.; Costas, M.; Ribas, X.; Stahl, S. S. *Chem. Eur. J.* **2011**, *17*, 10643.
(81) For a review that illustrates the complementarity of copper-catalysed and palladium-catalysed methodologies for C-N cross-coupling reactions see: Beletskaya, I. P.; Cheprakov, A. V. *Organometallics* **2012**, *31*, 7753.
(82) Surry, D. S.; Buchwald, S. L. *Chem. Sci.* **2010**, *1*, 13.
(83) Hashmi, A. S. K. In *Silver in Organic Chemistry*; Harmata, M., Ed.; John Wiley & Sons, Inc: Hoboken, New Jersey, 2010; pp. 357–379.
(84) Tang, P.; Furuya, T.; Ritter, T. *J. Am. Chem. Soc.* **2010**, *132*, 12150.
(85) Seo, S.; Taylor, J. B.; Greaney, M. F. *Chem. Commun.* **2013**, *49*, 6385.
(86) Glaser, C. *Ann. Chem. Pharm.* **1870**, *154*, 137.
(87) Gardner, J. H.; Borgstrom, P. *J. Am. Chem. Soc.* **1929**, *51*, 3375.
(88) Bickley, E. A.; Gardner, J. H. *J. Org. Chem.* **1940**, *5*, 126.
(89) Nagano, T.; Hayashi, T. *Chem. Lett.* **2005**, *34*, 1152.
(90) Tamura, M.; Kochi, J. *Synthesis (Stuttg).* **1971**, 303.
(91) Kochi, J. K. *J. Organomet. Chem.* **2002**, *653*, 11.
(92) Takamura, M.; Kochi, J. *J. Am. Chem. Soc.* **1971**, *93*, 1483.
(93) Someya, H.; Ohmiya, H.; Yorimitsu, H.; Oshima, K. *Org. Lett.* **2008**, *10*, 969.
(94) Someya, H.; Yorimitsu, H.; Oshima, K. *Tetrahedron Lett.* **2009**, *50*, 3270.
(95) Brown, H. C.; Snyder, C. H. *J. Am. Chem. Soc.* **1961**, *83*, 1002.
(96) Brown, H. C.; Hébert, N. C.; Snyder, C. H. *J. Am. Chem. Soc.* **1961**, *83*, 1001.
(97) Brown, H. C.; Verbrugge, C.; Snyder, C. H. *J. Am. Chem. Soc.* **1961**, *83*, 1001.

(98) Li, P.; Wang, L. *Synlett* **2006**, 2261.
(99) Das, R.; Chakraborty, D. *Tetrahedron Lett.* **2012**, *53*, 7023.
(100) Das, R.; Mandal, M.; Chakraborty, D. *Asian J. Org. Chem.* **2013**, *2*, 579.
(101) Jeschke, P. *ChemBioChem* **2004**, *5*, 570.
(102) Gerebtzoff, G.; Li-Blatter, X.; Fischer, H.; Frentzel, A.; Seelig, A. *ChemBioChem* **2004**, *5*, 676.
(103) Müller, K.; Faeh, C.; Diederich, F. *Science* **2007**, *317*, 1881.
(104) Yamazaki, T.; Taguchi, T.; Ojima, I. In *Fluorine in Medicinal Chemistry and Chemical Biology*; Ojima, I., Ed.; Wiley-Blackwell: Chippenham, Wiltshire, 2009; pp. 1–46.
(105) Furuya, T.; Kamlet, A. S.; Ritter, T. *Nature* **2011**, *473*, 470.
(106) Liang, T.; Neumann, C. N.; Ritter, T. *Angew. Chem. Int. Ed.* **2013**, *52*, 8214.
(107) Wang, J.; Sánchez-Roselló, M.; Aceña, J. L.; Del Pozo, C.; Sorochinsky, A. E.; Fustero, S.; Soloshonok, V. A.; Liu, H. *Chem. Rev.* **2014**, *114*, 2432.
(108) Grushin, V. V. *Acc. Chem. Res.* **2010**, *43*, 160.
(109) Phelps, M. E. *Proc. Natl. Acad. Sci.* **2000**, *97*, 9226.
(110) Ametamey, S. M.; Honer, M.; Schubiger, P. A. *Chem. Rev.* **2008**, *108*, 1501.
(111) Tredwell, M.; Gouverneur, V. *Angew. Chem. Int. Ed.* **2012**, *51*, 11426.
(112) Balz, G.; Schiemann, G. *Ber. Dtsch. Chem. Ges.* **1927**, *60*, 1186.
(113) Finger, G. C.; Kruse, C. W. *J. Am. Chem. Soc.* **1956**, *78*, 6034.
(114) Furuya, T.; Kaiser, H. M.; Ritter, T. *Angew. Chem. Int. Ed.* **2008**, *47*, 5993.
(115) Fier, P. S.; Luo, J.; Hartwig, J. F. *J. Am. Chem. Soc.* **2013**, *135*, 2552.
(116) Ye, Y.; Sanford, M. S. *J. Am. Chem. Soc.* **2013**, *135*, 4648.
(117) Mazzotti, A. R.; Campbell, M. G.; Tang, P.; Murphy, J. M.; Ritter, T. *J. Am. Chem. Soc.* **2013**, *135*, 14012.
(118) Furuya, T.; Strom, A. E.; Ritter, T. *J. Am. Chem. Soc.* **2009**, *131*, 1662.
(119) Furuya, T.; Ritter, T. *Org. Lett.* **2009**, *11*, 2860.
(120) Tang, P.; Ritter, T. *Tetrahedron* **2011**, *67*, 4449.
(121) Stepień, M.; Latos-Grażyński, L. *Org. Lett.* **2003**, *5*, 3379.
(122) Stepień, M.; Latos-Grazyński, L. *Chem. Eur. J.* **2001**, *7*, 5113.
(123) Eujen, R.; Hoge, B.; Brauer, D. J. *Inorg. Chem.* **1997**, *36*, 1464.
(124) Grzegorzek, N.; Pawlicki, M.; Szterenberg, L.; Latos-Grazyński, L. *J. Am. Chem. Soc.* **2009**, *131*, 7224.
(125) Grzegorzek, N.; Latos-Grażyński, L.; Szterenberg, L. *Org. Biomol. Chem.* **2012**, *10*, 8064.
(126) González-Arellano, C.; Abad, A.; Corma, A.; García, H.; Iglesias, M.; Sánchez, F. *Angew. Chem. Int. Ed.* **2007**, *46*, 1536.
(127) Lauterbach, T.; Livendahl, M.; Rosellón, A.; Espinet, P.; Echavarren, A. M. *Org. Lett.* **2010**, *12*, 3006.
(128) Bratsch, S. G. *J. Phys. Chem. Ref. Data* **1989**, *18*, 1.
(129) Hopkinson, M. N.; Gee, A. D.; Gouverneur, V. *Chem. Eur. J.* **2011**, *17*, 8248.
(130) Zhang, G.; Cui, L.; Wang, Y.; Zhang, L. *J. Am. Chem. Soc.* **2010**, *132*, 1474.
(131) Tamaki, A.; Kochi, J. K. *J. Organomet. Chem.* **1972**, *40*, C81.
(132) Tamaki, A.; Kochi, J. K. *J. Organomet. Chem.* **1973**, *51*, C39.
(133) Tamaki, A.; Kochi, J. K. *J. Organomet. Chem.* **1974**, *64*, 411.
(134) Shiotani, A.; Schmidbaur, H. *J. Organomet. Chem.* **1972**, *37*, C24.
(135) Guenther, J.; Mallet-Ladeira, S.; Estévez, L.; Miqueu, K.; Amgoune, A.; Bourissou, D. *J. Am. Chem. Soc.* **2014**, *136*, 1778.
(136) Joost, M.; Zeineddine, A.; Estévez, L.; Mallet-Ladeira, S.; Miqueu, K.; Amgoune, A.; Bourissou, D. *J. Am. Chem. Soc.* **2014**, *136*, 14654.
(137) Levin, M. D.; Toste, F. D. *Angew. Chem. Int. Ed.* **2014**, *53*, 6211.

CHAPTER II.

MAIN OBJECTIVES

II. MAIN OBJECTIVES

The progress of chemical sciences involves the evolution of synthetic methods towards greener approaches to synthesise organic molecules at industrial scale. In this line, the replacement of precious metal-based catalysts for less environmentally hazardous first-row transition metals is a long sought and highly desirable goal that modern chemistry will need to tackle in the near future. Of growing interest are the copper-catalysed cross-coupling reactions that have provided environmentally friendly alternatives to a field dominated by palladium. Even though the number of cross-coupling methods based on copper has increased exponentially during the last decade, especially for the creation of C-heteroatom bonds, the fundamental comprehension of these reactions has been limited for a long time due to the challenging identification of the elusive intermediate species operating in these transformations. In order to optimise the reaction conditions and design new ligands to improve the efficiency and practicality of Ullmann-type condensations, a profound understanding of the mechanistic aspects of these transformations is essential.

On the other hand, silver-promoted coupling chemistry is still on its infancy and the nature of these reactions has been almost unexplored. In fact, the two-electron oxidations and reductions, typically involved in coupling chemistry, lack consistent precedent in silver chemistry considering that silver redox chemistry is thus assumed to arise only from one-electron processes. In order to design new coupling methodologies relying on silver(I) salts, that might lead to complementary chemistry to *inter alia* palladium, gold, copper, nickel and iron routes, it is of major importance to study the fundamental pathways that drive these reactions.

The first part of this thesis will be aimed at characterising the mechanisms that govern the copper-catalysed C-S, C-Se and C-P bond forming cross-coupling reactions. For this purpose we will study the reactivity of a well-defined macrocyclic aryl-Cu^{III} model complex that resembles the elusive key intermediate species often proposed to be operative in Ullmann-type condensations in the presence of sulphur, selenium and phosphorus-based nucleophiles (**Scheme II. 1**). Our research group and others have previous experience on the investigation of mechanistic pathways of copper-catalysed aromatic C-H functionalizations, and copper-catalysed cross-coupling reactions including Ullmann-type condensations (mainly with nitrogen and oxygen-based nucleophiles), halide exchange and fluorination reactions within this macrocyclic model system. [1]

---

[1] (a) Ribas, X. Ph.D. Dissertation, Universitat de Girona, Girona, **2001**. (b) Casitas, A. Ph.D. Dissertation, Universitat de Girona, Girona, **2012**.

The second part of the thesis will explore the chemistry of the analogue macrocyclic aryl-Ag^{III} model complex in the presence of a wide range of nucleophiles of different nature (nitrogen, oxygen, sulphur and carbon-based nucleophiles as well as halides) and will evaluate the plausibility of two-electron processes such as oxidative addition and reductive elimination in silver-catalysed model cross-coupling reactions (**Scheme II. 1**).

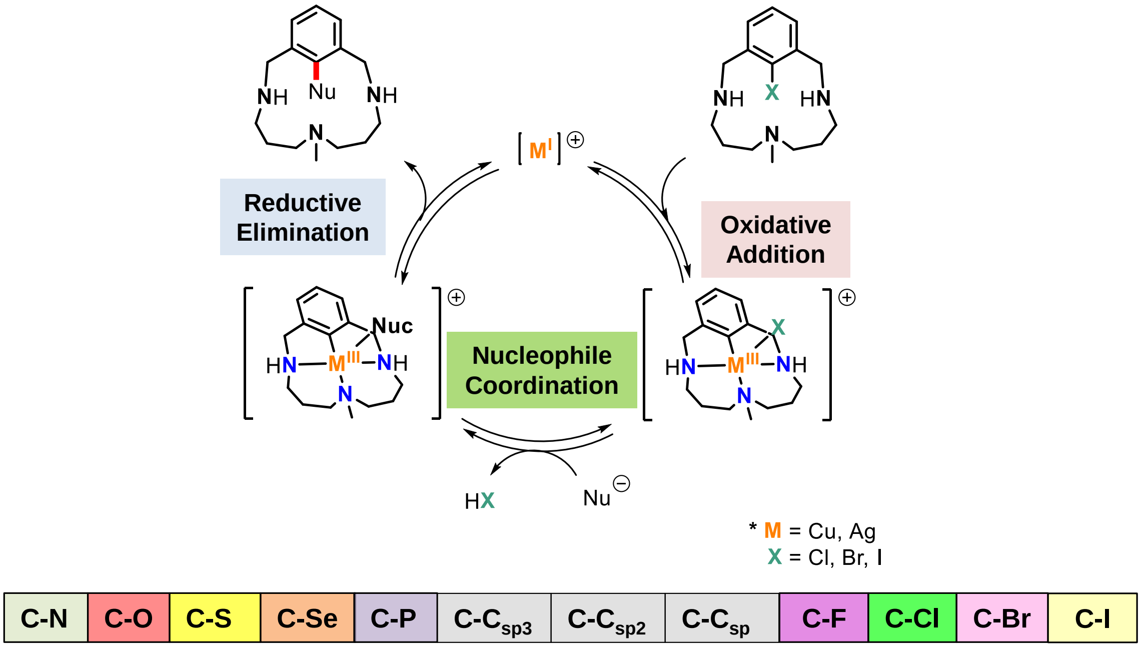
NH Nu NH
N
[M^{I}]$^{\oplus}$
NH X HN
N
Reductive Elimination
Oxidative Addition
Nuc
HN—M^{III}—NH
N
Nucleophile Coordination
X
HN—M^{III}—NH
N
HX
Nu$^{\ominus}$
* M = Cu, Ag
X = Cl, Br, I
C-N
C-O
C-S
C-Se
C-P
C-C$_{sp3}$
C-C$_{sp2}$
C-C$_{sp}$
C-F
C-Cl
C-Br
C-I

Scheme II. 1. General mechanistic arena for the copper and silver-catalysed model cross-coupling reactions.

The data gathered for these two systems will enable us to compare the different reactivity features that each metal confers to the nature of the cross-couplings.

CHAPTER III.

CATALYTIC C-S, C-Se, AND C-P CROSS-COUPLING REACTIONS MEDIATED BY A Cu^I/Cu^{III} REDOX CYCLE

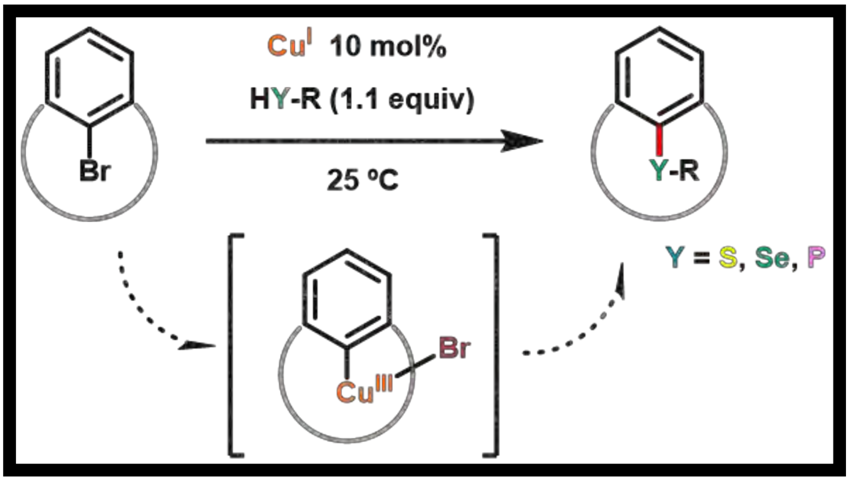

This chapter corresponds to the following publication:

Marc Font, Dr. Teodor Parella, Dr. Miquel Costas, Dr. Xavi Ribas. *Organometallics* **2012**, 31(22), 7976-7982.

M. F. performed all the experimental work concerning with this publication. Besides, he was involved in argumentations and discussions. M. F. contributed in approximately 85 %.

Published version cannot be used

Font, Marc, Parella, Teodor, Costas, Miquel, Ribas, Xavi. Catalytic C–S, C–Se, and C–P Cross-Coupling Reactions Mediated by a Cu^{I}/Cu^{III} Redox Cycle. *Organometallics*, 31 (22) : 7976-7982 (2012)

Copyright © 2012 American Chemical Society

http://dx.doi.org/10.1021/om3006323

http://pubs.acs.org/doi/abs/10.1021/om3006323

Publication Date (Web): August 2, 2012

Abstract

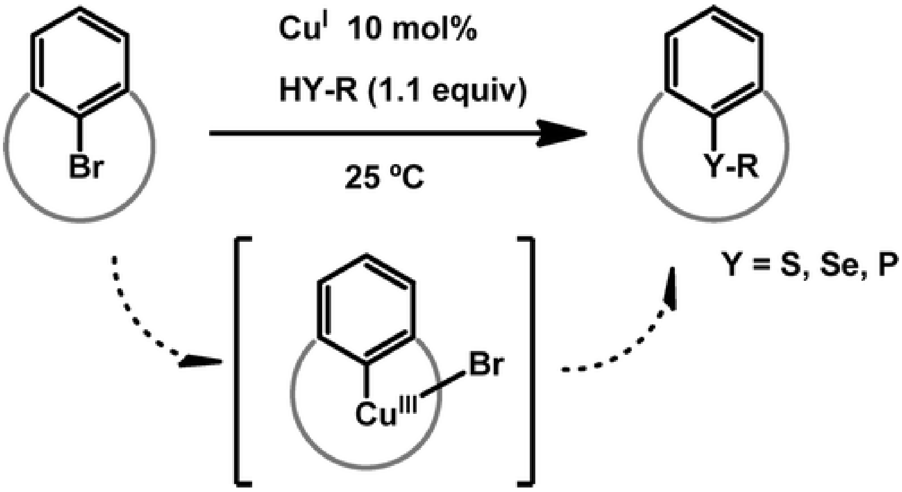

A well-defined macrocyclic aryl-Cu^{III} complex (**1**) readily reacts with a series of R–SH, Ar–SH, Ar–SeH, and $(RO)_2(O)$–PH (R = alkyl) nucleophiles to quantitatively afford the corresponding aryl alkyl thioethers, biaryl thioethers, biaryl selenide, and aryl dialkyl phosphonates, respectively. Competition experiments using bifunctional substrates revealed the important impact of lower pK_a values in order to discriminate between functional groups, although other influencing parameters such as steric effects have been identified. The catalytic version of these reactions is achieved using aryl bromide and aryl chloride model substrates, affording C–S, C–Se, and C–P coupling compounds in excellent to moderate yields. Low-temperature UV–vis and NMR monitoring of the reactions of complex **1** with a variety of nucleophiles support the formation of a ground-state **1**–nucleophile adduct. A mechanistic proposal for reaction of **1** with S-nucleophiles involving key nucleophile deprotonation and aryl-nucleophile reductive elimination steps is finally described.

CHAPTER IV.

DIRECT OBSERVATION OF TWO-ELECTRON Ag(I)/Ag(III) REDOX CYCLES IN COUPLING CATALYSIS

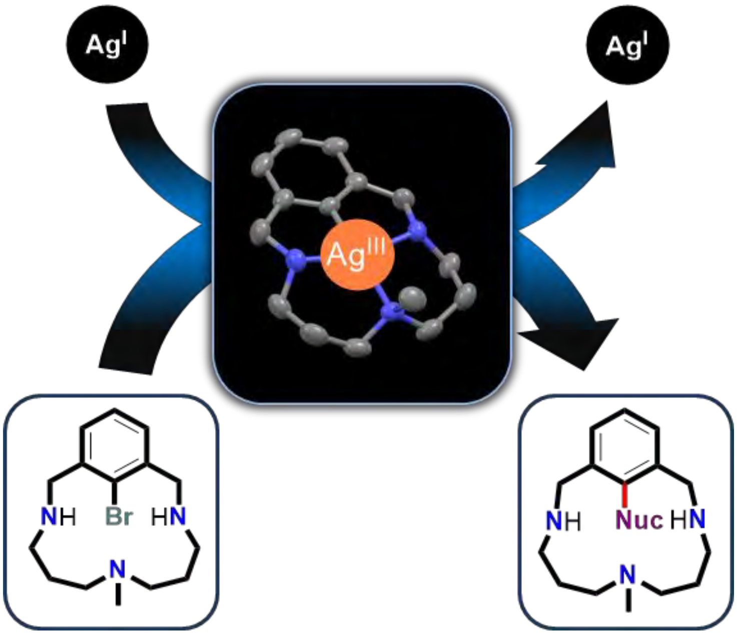

This chapter corresponds to the following publication:

Marc Font, Ferran Acuña-Parés, Dr. Teodor Parella, Jordi Serra, Dr. Josep M. Luis, Dr. Julio Lloret-Fillol, Dr. Miquel Costas, Dr. Xavi Ribas. *Nat. Commun*. **2014**, 5:4373, DOI: 10.1038/ncomms5373.

M. F. performed all the experimental work concerning with this publication. Besides, he wrote the manuscript and was involved in argumentations and discussions. M. F. contributed in approximately 80 %.

nature COMMUNICATIONS

ARTICLE

Received 11 Mar 2014 | Accepted 11 Jun 2014 | Published 11 Jul 2014

DOI: 10.1038/ncomms5373

Direct observation of two-electron Ag(I)/Ag(III) redox cycles in coupling catalysis

Marc Font[1], Ferran Acuña-Parés[1], Teodor Parella[2], Jordi Serra[1], Josep M. Luis[1], Julio Lloret-Fillol[1], Miquel Costas[1] & Xavi Ribas[1]

Silver is extensively used in homogeneous catalysis for organic synthesis owing to its Lewis acidity, and as a powerful one-electron oxidant. However, two-electron redox catalytic cycles, which are most common in noble metal organometallic reactivity, have never been considered. Here we show that a Ag(I)/Ag(III) catalytic cycle is operative in model C–O and C–C cross-coupling reactions. An aryl-Ag(III) species is unequivocally identified as an intermediate in the catalytic cycle and we provide direct evidence of aryl halide oxidative addition and C–N, C–O, C–S, C–C and C–halide bond-forming reductive elimination steps at monometallic silver centres. We anticipate our study as the starting point for expanding Ag(I)/Ag(III) redox chemistry into new methodologies for organic synthesis, resembling well-known copper or palladium cross-coupling catalysis. Furthermore, findings described herein provide unique fundamental mechanistic understanding on Ag-catalysed cross-coupling reactions and dismiss the generally accepted conception that silver redox chemistry can only arise from one-electron processes.

---

[1] Institut de Química Computacional i Catàlisi (IQCC) and Departament de Química, Universitat de Girona, Campus Montilivi, Girona E-17071, Catalonia, Spain. [2] Servei de RMN, Facultat de Ciències, Universitat Autònoma de Barcelona, Campus UAB, Bellaterra E-08193, Catalonia, Spain. Correspondence and requests for materials should be addressed to X.R. (email: xavi.ribas@udg.edu).

© 2014 Macmillan Publishers Limited. All rights reserved.

Organic chemistry has taken advantage of the catalytic transformations promoted by most transition metals, although some of them, such as silver, have only gained interest in the past few years. Silver holds the most unexplored chemistry among the coinage metals and its redox chemistry is the least understood[1–5]. Ag(I) salts are commonly employed in organic transformations by exploiting three main properties (Fig. 1). First, its moderate Lewis acidity has found application in activating allenes and alkynes to promote a nucleophilic attack over the unsaturation to render, for instance, the cyclization of allenols, allenones and allenoic acids[4,5]. The π-activation of terminal acetylenes can also produce silver(I)-acetylides[6,7], which are known as efficient transmetallating agents and have been widely utilized in organopalladium catalysis[8–10]. The second important characteristic of Ag(I) chemistry is the insolubility of its corresponding halide salts (halogenophilicity). A large number of transition metal-catalysed reactions are conducted in the presence of Ag(I) salts to trigger the precipitation of Ag*X* salts (*X* = Cl, Br, I) from coordinatively saturated metal centres, for instance, in Pd-catalysed cross-coupling reactions involving aryl or alkenyl halides[5], or in Au-catalysed C–C bond-forming reactions[11]. Finally, Ag(I) salts are extensively used as one-electron oxidant, for instance in the preparation of carbonyls from the corresponding alcohols under mild conditions[2,12]. More recently, an increasing number of oxidative C–C bond-forming reactions of arenes require the use of a sacrificial outer-sphere oxidant, and Ag(I) is often the oxidant of choice[13].

It is generally accepted that silver involves exclusively one-electron redox chemistry[4,14–17], in contrast to the other two group-11 metals, copper and gold, which can undergo two-electron redox chemistry. Copper and gold have been directly implicated in M(I)/M(III) oxidative addition and reductive elimination processes[18–25], whereas such chemistry has never been considered for silver. Nevertheless, silver has been reported as an effective catalyst in cross-coupling reactions such as Ag-catalysed Sonogashira couplings[26] and Ag-catalysed Ullmann-type C-heteroatom bond-forming reactions[27]. However, no mechanistic studies have been carried out so far to rationalize these transformations. Ritter and co-workers proposed recently the presence of bimetallic aryl-Ag(II)-Ag(II)-F species in silver(I)-mediated electrophilic fluorination of aryl stannanes[14]. Instead, Li and co-workers suggest in their studies on Ag(I)-catalysed radical aminofluorinations that electrophilic fluoride sources are capable of generating monometallic Ag(III)-F intermediate species[28], although the C–F bond formation is proposed to occur through reaction of a Ag(II)-F and a carbon-centred radical species, following a one-electron redox sequence. No direct evidence of the intermediates proposed is reported, thus mechanistic comprehension of silver-catalysed processes stands as its Achilles heel for future design of new synthetic methodologies.

Herein we report the discovery that silver can be engaged in two-electron oxidative addition and reductive elimination processes and that, indeed, a Ag(I)/Ag(III) catalytic cycle is operative in model C-O and C-C cross-coupling reactions (Fig. 1d). We provide direct spectroscopic and crystallographic

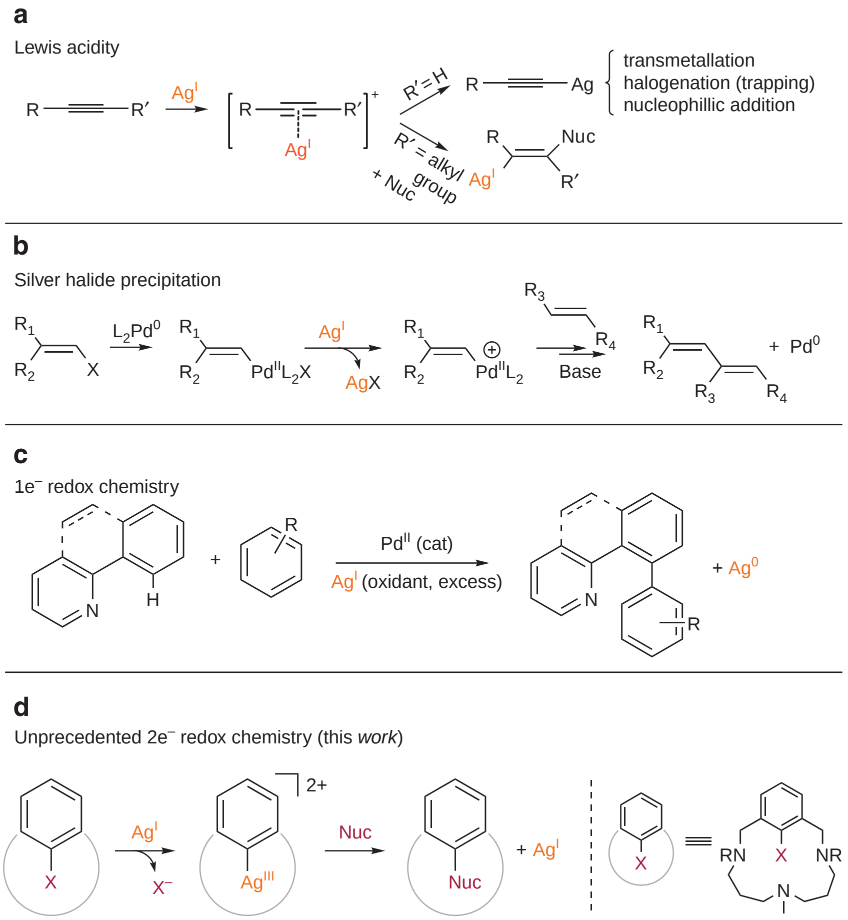

Figure 1 | Canonical reactivity of silver. (**a**) Activation of C-C insaturations due to its Lewis acid character. (**b**) Halogenophilicity to drive reactions by forming insoluble halide salts (AgX). (**c**) Use as sacrificial oxidant by promoting the one-electron oxidation of the metal catalyst. (**d**) Novel two-electron-based reactivity described in this work involving Ag(I)/Ag(III) redox processes.

© 2014 Macmillan Publishers Limited. All rights reserved.

characterization of a well-defined aryl-Ag(III) species, which is identified as the catalytically active species.

Results

Synthesis and full characterization of the Ag(III) complex. The synthesis of aryl-Ag(III) complex $\mathbf{1_{ClO4}}$ was achieved by reacting the model aryl-halide ligand **L_1-Br** with 2 equiv. of Ag(I)ClO_4, affording [Ag(III)$\mathbf{L_1}$]$(ClO_4)_2$ ($\mathbf{1_{ClO4}}$, 68% yield) and AgBr that precipitates from the solution (Fig. 2a). This complex is bench-top stable and has been fully characterized spectroscopically and crystallographically. The structure obtained by X-ray diffraction studies of compound $\mathbf{1_{ClO4}}$ shows that the Ag(III) centre is tetracoordinated and exhibits a nearly square planar geometry, in which the aryl moiety and three amine N atoms are coplanar with the silver centre (Fig. 2b).

The Ag–C bond length is 1.974 Å, the shortest in the silver coordination sphere of $\mathbf{1_{ClO4}}$, and also among the scarce number of organometallic Ag(III) complexes reported in the literature[29–32]. The short Ag–C bond distance along with the charge balance of the complex, its diamagnetic nature and density functional theory (DFT) (B3LYP-D_2/6-311 + G**) spin densities indicate that the metal centre is best described as Ag(III). Indeed, $\mathbf{1_{ClO4}}$ is isostructural with the previously described and fully characterized aryl-Cu(III) complex[33,34], and the DFT optimized geometry is also in agreement with the crystallographic characterization (see Supplementary Fig. 1). NMR studies (^{1}H-NMR and one-dimensional (1D) ^{109}Ag-decoupled ^{1}H-NMR, see Fig. 2c and Supplementary Figs 2–9) and high-resolution mass spectrometry (HRMS) analysis ($[C_{15}H_{24}N_3AgClO_4]^+$, $m/z = 454.0495$; Supplementary Fig. 10) are conclusive to state that the aryl-Ag(III) maintains the same structure in solution than in the solid state. Moreover, a ^{1}H-^{109}Ag heteronuclear multiple bond correlation (HMBC) experiment allowed the determination of the ^{109}Ag chemical shift (2,127 p.p.m.), which is in close agreement to that reported for other Ag(III) complexes (Supplementary Fig. 5)[32]. For further discussion on the NMR analysis of $\mathbf{1_{ClO4}}$, see Supplementary Discussion 1.

Reactivity of the Ag(III) complex. Once $\mathbf{1_{ClO4}}$ was fully characterized, we turned our attention towards its reactivity. We speculated that this complex could show a similar reactivity to its analogous copper complex, that is, to undergo reductive eliminations to functionalize the C_{sp2}-M(III) (M = Cu or Ag) bond in the presence of nucleophiles of different nature[19,35]. The reaction of $\mathbf{1_{ClO4}}$ with sulfonamides, aromatic and aliphatic carboxylic acids, phenols and thiophenols resulted in the formation of C_{aryl}–nucleophile coupling products in excellent yields, characteristic of a reductive elimination reaction (products **2a-2g**, Table 1). *p*-Thiocresol is the substrate that exhibits the fastest reactivity with the aryl-Ag(III) complex, reaching completion after only 1 min (Table 1, entry 7). Furthermore, NaCN also reacts with $\mathbf{1_{ClO4}}$ to form the C–C coupling product (**L_1-CN**, Table 1, entry 8) in good yield. Strikingly, C–C coupling products were also obtained in excellent yields when malononitrile[36] and aryl boronic acids were used as coupling partners (Table 1, entries 9–11). The above reductive elimination processes rendered the C–nucleophile coupling products and Ag(I) species; the latter was detected by performing the reaction of $\mathbf{1_{ClO4}}$ with 1 equiv. of *p*-nitrophenol to full conversion and subsequently adding 3 equiv. of PPh_3 to form Ag(I)$(PPh_3)_n$ species. ^{31}P{^{1}H} NMR showed a broad doublet at

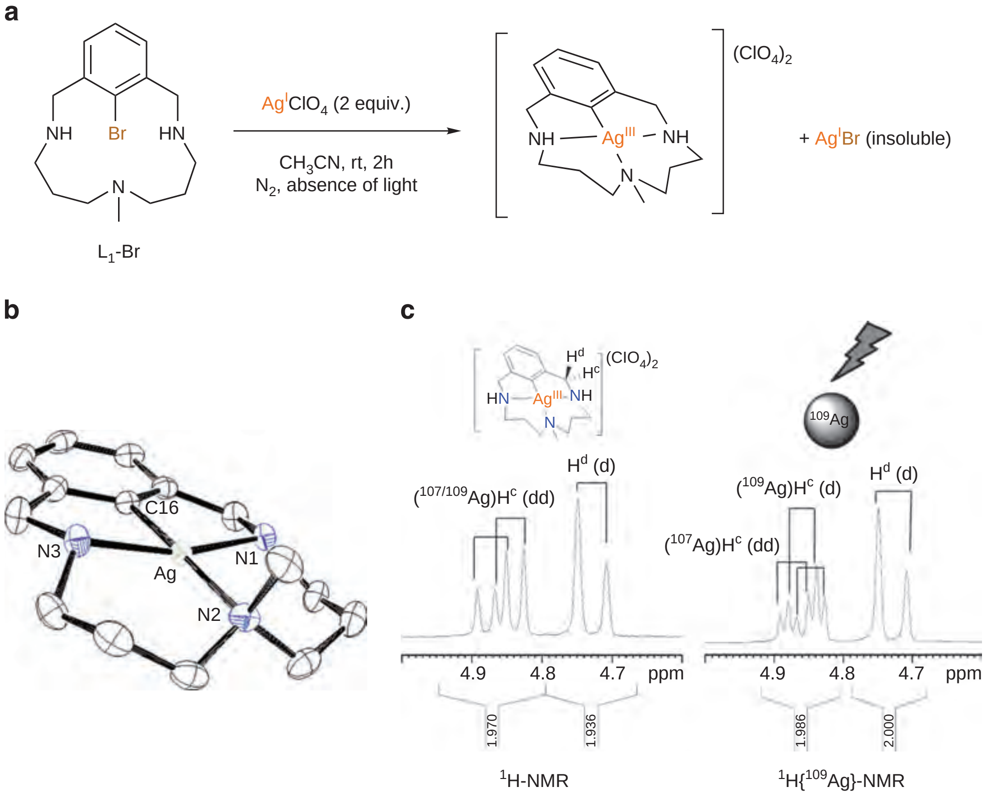

Figure 2 | Synthesis and characterization of the aryl-Ag(III) complex ($\mathbf{1_{ClO4}}$). (**a**) Synthesis of the aryl-Ag(III) species ($\mathbf{1_{ClO4}}$). (**b**) X-ray diffraction: thermal ellipsoid diagram (at 50% probability level) of the cationic moiety of $\mathbf{1_{ClO4}}$. The hydrogen atoms and the two perchlorate anions have been omitted for clarity. Selected bond lengths [Å] and angles [°] of $\mathbf{1_{ClO4}}$: Ag-C(16) 1.974(2), Ag-N(3) 2.084(2), Ag-N(1) 2.085(5), Ag-N(2) 2.153(2); C(16)-Ag-N(3) 82.03(10), C(16)-Ag-N(1) 81.6(1), N(3)-Ag-N(2) 98.2(1), N(1)-Ag-N(2) 98.4(1), C(16)-Ag-N(2) 178.2(1), N(3)-Ag-N(1) 162.1(1). (**c**) Comparison of the benzylic region of $\mathbf{1_{ClO4}}$ in the ^{1}H NMR and ^{1}H{^{109}Ag} NMR experiments (298 K, CD_3CN, 400 MHz NMR; see Supplementary Information).

© 2014 Macmillan Publishers Limited. All rights reserved.

Table 1 | Stoichiometric coupling of nucleophiles with $\mathbf{1}_{\mathbf{ClO_4}}$ complex*.

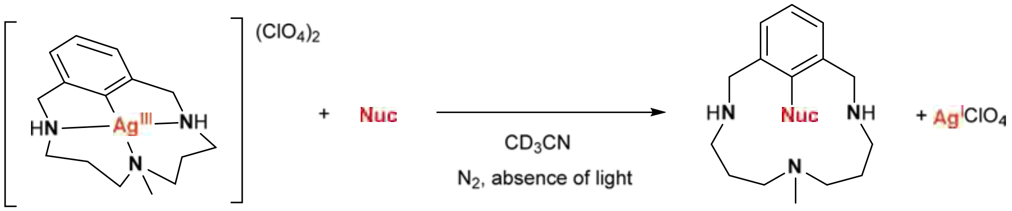

Entry	Nuc	Equiv.	T°	pKa (DMSO)	Reaction time	Yield (product label)†
1	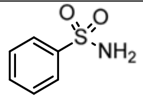	10	50°C	16.1	72 h	94% (**2a**)
2	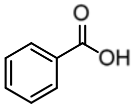	3	40°C	11	6h	85% (**2b**)
3	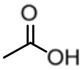	3	40°C	12.6	24h	92% (**2c**)
4	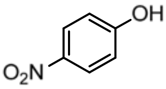	2	40°C	10.8	3 h	100% (**2d**)‡
5	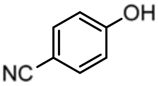	2	40°C	13.2	3 h	100% (**2e**)
6	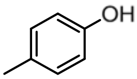	10	70°C	18.9	7 h	100% (**2f**)
7	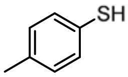	3	25°C	10.3-11.2	1 min	100% (**2g**)
8§	NaCN	10	25°C	—	2 h	81% (**L_1-CN**)
9	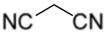	3	25°C	11.1	18 h	97% (**2h**)‖
10¶	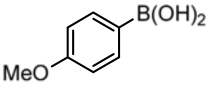	5	50°C	—	12 h	97% (**2i**)
11¶	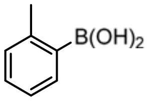	5	50°C	—	12h	89% (**2j**)
12	nBu_4NI	2	25°C	—	1 min	97% (**L_1-I**)
13	nBu_4NBr	2	25°C	—	30 min	99% (**L_1-Br**)
14	nBu_4NCl	2	40°C	—	3.5 h	97% (**L_1-Cl**)
15	$nBu_4NF·3H_2O$	2	40°C	—	24 h	39% (**L_1-F**)

DMSO, dimethyl sulphoxide.

*General conditions: [$\mathbf{1}_{\mathbf{ClO_4}}$] = 12 mM, [Nuc] = 24–120 mM, 0.7 ml CD_3CN.

†Calculated by ^{1}H-NMR spectroscopy using 1,3,5-trimethoxybenzene as internal standard.

‡90% in the presence of 1 equiv. of TEMPO.

§10% $\mathbf{1}_{\mathbf{ClO_4}}$(remaining starting material).

‖**2h** consists of the expected C–C coupling followed by intramolecular reorganization, see Table 2 and ref. 36.

¶Mixture of solvents CD_3CN:CD_3OD 1:1.

7.93 p.p.m. ($J(^{31}P\text{-}^{109}Ag) = 343$ Hz), which exactly matched the signal observed in a sample prepared by reacting Ag(I)ClO_4 with 3 equiv. of PPh_3 (Supplementary Figs 11 and 12). Moreover, these reactions were unaffected by the addition of TEMPO radical; this observation disfavours a radical-mediated process (Table 1, entry 4). To the best of our knowledge, these are the first examples of fully characterized two-electron reductive elimination processes from a well-defined Ag(III) complex.

We then explored the C–halide reductive elimination reaction by treating $\mathbf{1}_{\mathbf{ClO_4}}$ with 2 equiv. of nBu_4NX (X = I, Br, Cl) salts,

© 2014 Macmillan Publishers Limited. All rights reserved.

and found that the corresponding **L$_1$–X** coupling products were obtained quantitatively (Table 1, entries 12–14). Aryl fluorination was also attempted, affording a 39% yield of the desired fluorinated arene (**L$_1$–F**) when the reaction was run in the presence of 2 equiv. of nBu$_4$NF · 3H$_2$O at 40 °C in acetonitrile (Table 1, entry 15). Detrimental deprotonation of **1$_{ClO4}$** by the basic fluoride anion was avoided by using the *N*-permethylated **L$_5$–Br** aryl bromide model substrate, obtaining quantitative formation of **L$_5$–F** product (Fig. 3; see also Supplementary Figs 13–15 for additional information in fluorination reactions)[37–39]. DFT calculations show that the reductive elimination of **L$_5$**–Ag(III) is strongly exergonic ($\Delta G = -25.8\,\mathrm{kcal \cdot mol^{-1}}$) and has a very low barrier ($\Delta G^{\neq} = 8.6\,\mathrm{kcal \cdot mol^{-1}}$; for computed reaction profile see Supplementary Fig. 16).

Study of the Ag(III) complex synthesis. Concerning the aryl halide oxidative addition step (Supplementary Table 1), we found that for aryl-Br (**L$_1$–Br**) and aryl-I (**L$_1$–I**) model substrates, yields of **1$_{ClO4}$** were almost quantitative when 2 equiv. of AgOTf were used (25 °C). On the contrary, if only 1 equiv. of AgOTf was used, yields no higher than 50% were observed. We rationalized these results by considering that 1 equiv. of silver(I) loading is consumed to form the desired aryl-Ag(III) product, whereas the second Ag(I) equivalent traps the halide to precipitate as Ag*X* (*X* = Br, I). However, a bimetallic centred process similar to Ritter's proposal could not be ruled out at this point[14]. Addition of Tl(OTf) as an additive to directly compete for the formation of extremely insoluble thalium halide salts, afforded **1$_{OTf}$** in 68% yield by using 1 equiv. of AgOTf, 1 equiv. of Tl(OTf) and **L$_1$-I**, thus strongly supporting our monometallic oxidative addition proposal (Supplementary Table 1). We additionally tested these reactions with **L$_1$–Cl** as model substrate, but no aryl-Ag(III) product was observed. The DFT-computed reaction profiles for the oxidative addition of Ag(I) over **L$_1$–F**, **L$_1$–Cl**, **L$_1$–Br** and **L$_1$–I** show a decrease of the Gibbs energy barriers ($\Delta G^{\neq}$ (**L$_1$–*X***) = 33.2, 18.1, 14.4, 11.2 kcal · mol^{-1} for *X* = F, Cl, Br, I, respectively) and reaction Gibbs energies (ΔG (**L$_1$–*X***) = 17.6, 1.8, 0.8, −7.5 kcal · mol^{-1} for *X* = F, Cl, Br, I, respectively; for computed reaction profiles see Supplementary Fig. 17). The trends extracted from DFT calculations nicely agree with the observed formation of the Ag(III) complex with **L$_1$–Br** and **L$_1$–I** but not with **L$_1$–Cl** and **L$_1$–F**.

Model C–O bond-forming cross-coupling reactions. Provided that the fundamental details of two-electron Ag(I)/Ag(III) oxidative addition and reductive elimination redox steps were understood individually, we merged both steps in a single C-heteroatom cross-coupling reaction. We selected *p*-nitrophenol as the nucleophile to be reacted with **L$_1$–*X*** (*X* = I, Br, Cl) in the presence of 1 equiv. of AgOTf at 50 °C (Table 2). The C–O coupling product **2d** was obtained in 75% and 64% yield when **L$_1$–I** and **L$_1$–Br** were used, respectively (Table 2, entries 1, 10). In the case of **L$_1$–I**, if a slight excess of AgOTf is used (1.1 equiv.), a 95% yield of **2d** is obtained (Table 2, entry 2). These results suggest that after initial oxidative addition, a 50% of the silver precipitates as AgI, whereas the other 50% produces Aryl-aryl-Ag(III) that reacts with the nucleophile and reductively eliminates the coupling product **2d**, thus a 50% Ag(I) is set free again (assuming quantitative reductive elimination) to react again with more **L$_1$–I**. The same reactivity pattern is repeated after each cycle with the remaining free Ag(I) in solution. However, we cannot exclude the potential beneficial effect of using excess of nucleophile (20 equiv.) as we have observed that it severely prevents the precipitation of AgI (*vide infra*). Moreover, when **L$_1$–Cl** was used we could obtain a 37% yield of the desired product (Table 2, entry 13), thus in agreement with the computed kinetic feasibility of the oxidative addition of **L$_1$–Cl** ($\Delta G^{\neq} = 18.1\,\mathrm{kcal \cdot mol^{-1}}$).

Catalytic cross-coupling reactions via silver(III) species. The positive results for the C–O cross-coupling reactions stoichiometric in silver(I) prompted us to explore the catalytic version of these processes (Table 2). The first attempts employing **L$_1$–I** (1 equiv.), *p*-nitrophenol (2 equiv.) and 10 mol% of AgOTf as the catalyst (in CH$_3$CN, absence of light) failed to provide more than 1 catalytic cycle as only 9% of the desired biaryl ether product **2d** was obtained (Supplementary Table 2), along with a yellow precipitate. The undesired precipitation of catalytic silver as AgI was prevented by increasing the amount of nucleophile up to 20 equiv. and we observed that the C–O coupling product yield increased up to 37% (Table 2, entry 3). We optimized the reaction in the presence of phosphines with distinct electron donor strength to further stabilize the Ag(I) cations in solution (Table 2, Supplementary Discussion 2 and Supplementary Table 2). Among the auxiliary ligands tested, PPh$_3$ (10 mol%) was the best choice giving a 46% yield of the biaryl ether product **2d** (Table 2, entry 4). We were pleased to find that a 74% yield of the desired product **2d** was achieved by increasing the catalyst loading to 20 mol% and employing a 20 mol% of PPh$_3$ (Table 2, entry 5). Under the same conditions, *p*-cyanophenol afforded a 70% yield of the desired product **2e** (Table 2, entry 6), confirming that the C–O coupling catalysis can be extended to other phenols. The catalytic reactivity could be additionally extended to C–C couplings, as demonstrated by the 68% yield of **2h** coupling product obtained by the catalysis with **L$_1$–I**, malononitrile (10 equiv.), 10 mol% of AgOTf and 10 mol% of PPh$_3$ (Table 2, entry 8). On the other hand, when the substrate **L$_1$–I** is replaced by **L$_1$–Br**, containing a stronger C$_{aryl}$–halide bond, the yields of the catalytic

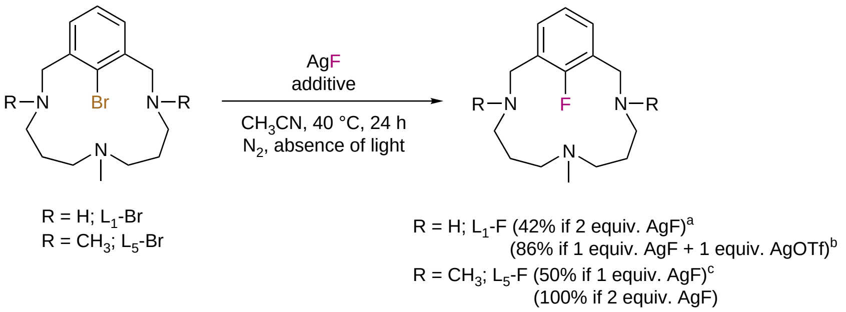

Figure 3 | Silver(I)-mediated fluorination of model aryl halide substrates. General conditions: model aryl halide (**L$_n$-*X***) 12–14 μmol, AgF 12–28 μmol, AgOTf 0–12 μmol, 2 ml CH$_3$CN, 40 °C. Yields calculated by ^{1}H-NMR spectroscopy using 1,3,5-trimethoxybenzene as internal standard. [a]13% of intramolecular C-N coupling product.[39] [b]8% of intramolecular C-N coupling product.[39] [c]20% **L$_5$-Br** (remaining starting material).

© 2014 Macmillan Publishers Limited. All rights reserved.

Table 2 | Silver-catalysed C-O and C-C bond-forming cross-coupling reaction with L_1-X model substrates*.

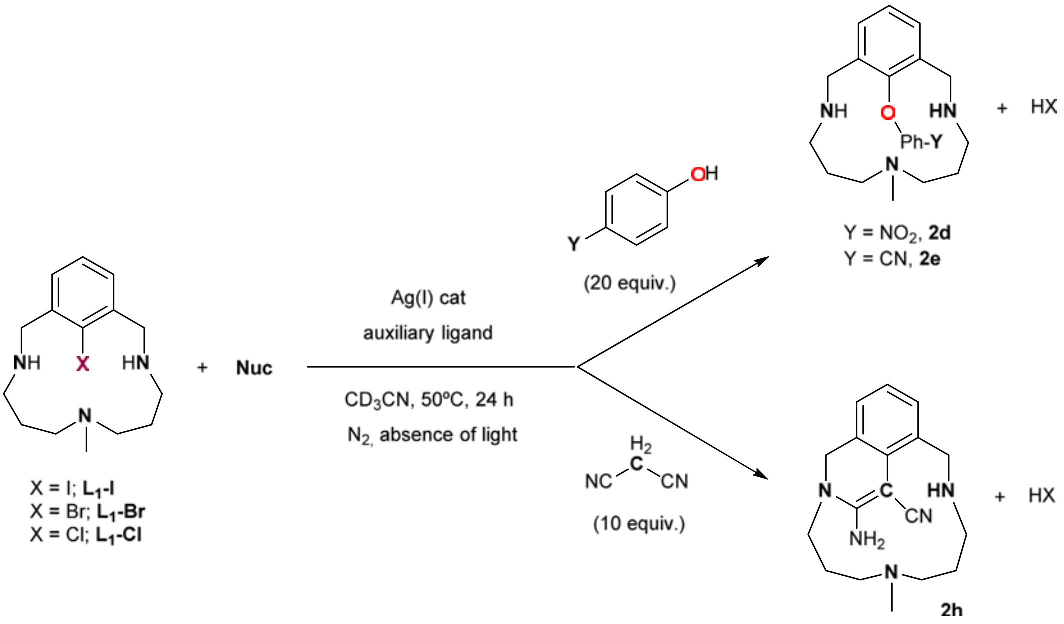
NH
X
HN
N
X = I; L1-I
X = Br; L1-Br
X = Cl; L1-Cl
+
Nuc
Ag(I) cat
auxiliary ligand
CD3CN, 50ºC, 24 h
N2, absence of light
Y
OH
(20 equiv.)
NH
O
HN
Ph-Y
N
+ HX
Y = NO2, 2d
Y = CN, 2e
H2
C
NC
CN
(10 equiv.)
N
C
HN
CN
NH2
N
+ HX
2h

Entry	Substrate	Additive (mol%)	AgOTf (mol%)	2d (% Yield)†
1‡	**L_1-I**	-	100	75
2‡		-	110	95
3		-	10	37
4		PPh_3 (10)	10	46
5		PPh_3 (20)	20	74
6		PPh_3 (20)	20	70, **2e**
7		-	10	44, **2h**
8		PPh_3 (10)	10	68, **2h**
9		PPh_3 (10)	$\mathbf{1}_{\mathbf{ClO4}}$ (10)	48
10‡	**L_1-Br**	-	100	64
11		PPh_3 (10)	10	21
12		PPh_3 (10) + (Tl(OTf) (2 equiv.)	10 (25 °C)	43
13‡	**L_1-Cl**	-	100	37

*General conditions: [**L_1-X**] = 5 mM, [Nuc] = 50–100 mM, 3 ml CH_3CN, 50 °C.
†Calculated by ^{1}H-NMR spectroscopy using 1,3,5-trimethoxybenzene as internal standard.
‡[**L_1-X**] = 15 mM, [*p*-NO_2phenol] = 300 mM, [NaOTf] = 45 mM, 1 ml CH_3CN, 50 °C, 6 h.

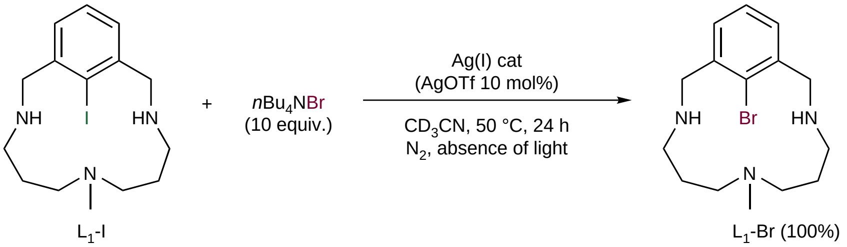
NH
I
HN
N
L1-I
+
nBu4NBr
(10 equiv.)
Ag(I) cat
(AgOTf 10 mol%)
CD3CN, 50 °C, 24 h
N2, absence of light
NH
Br
HN
N
L1-Br (100%)

Figure 4 | Silver(I)-catalysed bromination of model aryl iodide substrate. Conditions: [**L_1-I**] = 5 mM, [nBu_4NBr] = 50 mM, [AgOTf] = 0.5 mM, 3 ml CD_3CN, 50 °C; yield calculated by ^{1}H-NMR spectroscopy using 1,3,5-trimethoxybenzene as internal standard.

reactions were reduced to a maximum of 21% of **2d** (Table 2, entry 11). As expected, these low yields were clearly enhanced by using 2 equiv. of Tl(OTf) as additive under the same catalytic conditions, obtaining a 43% yield of **2d** (Table 2, entry 12). More importantly, the implication of the aryl-Ag(III) species as competent catalytic intermediate species was demonstrated by performing the catalytic coupling of **L_1–I** and *p*-nitrophenol using 10 mol% of $\mathbf{1}_{\mathbf{ClO4}}$ and 10 mol% of PPh_3 under the standard catalysis conditions (Table 2, entry 9), to find that the same yield as in the catalysis with 10 mol% AgOTf was finally obtained. ^{1}H-NMR monitoring of the catalytic reaction corroborated the formation of the aryl-Ag(III) (4%) as active species during the course of the reaction (see Supplementary Fig. 18).

A key aspect to rationalize the observed catalysis consists of the ability to prevent the precipitation of AgI so that catalytic turnover becomes possible. We observed that the large excess of *p*X-phenol used in the catalysis delayed the precipitation of AgI (for turbidity monitoring experiments see Supplementary

© 2014 Macmillan Publishers Limited. All rights reserved.

Fig. 19) and might form coordination complexes with silver(I) (by HRMS, see Supplementary Figs 20 and 21), thus preventing the precipitation of AgI. On the other hand, we realized that excess of iodide caused the formation of monoanionic AgI_2^- in solution (by HRMS, see Supplementary Figs 22 and 23) and completely quenched the precipitation of AgI (Supplementary Fig. 19)[40,41]. To further substantiate that monoanionic dihalide silver(I) species can participate in the cross-coupling reactions described, we attempted a halide exchange catalysis starting with **L_1–I** model substrate, 10 mol% AgOTf and 10 equiv. of *n*Bu_4NBr. The substrate was quantitatively converted to **L_1–Br** in 24 h without any sign of precipitation during the catalytic reaction (see Fig. 4). In addition, AgI_2^-, $AgBrI^-$ and $AgBr_2^-$ monoanionic species were detected by HRMS (Supplementary Fig. 24). In addition, the slight beneficial effect of PPh_3 might be related to the formation of monocationic $[Ag(PPh_3)_2]^+$ species, which was detected by HRMS (Supplementary Fig. 25) under the catalytic conditions of entry 3, Table 2, thus also contributing to prevent the precipitation of silver(I) out of the solution.

Discussion

Further investigations were performed to evaluate the possibility that coupling reactions involve an initial single electron transfer (SET) step. Cyclic voltammetry experiments indicate that the Ag(III)/Ag(II) reduction is electrochemically irreversible and has a reduction potential of -0.6 V versus non-aqueous Ag/$AgNO_3$ reference electrode (Supplementary Fig. 26). As the oxidation potential of *p*-nitrophenol is $E^0_{ox} > 1.3$ V (versus Ag/$AgNO_3$)[42,43], SET from the latter to the Ag(III) complex is highly disfavoured (1.9 V difference, $\Delta G^0 = 43.8\ \mathrm{kcal \cdot mol^{-1}}$). Moreover, DFT calculation of the first SET from *p*-nitrophenol to Ag(III) to afford a phenoxyl radical and aryl-Ag(II) is thermodynamically endergonic ($\Delta G = 41.6\ \mathrm{kcal \cdot mol^{-1}}$, in close agreement to the value deduced from cyclic voltammetry data, see Supplementary Fig. 27 for computed reaction profile), thus clearly disproving SET in our mechanism. In addition, the DFT-calculated pathway for the reductive elimination of aryl-Ag(III)-(*p*NO_2-phenolate) species to afford the *p*NO_2-Ph-O-Aryl coupling product and Ag(I) provides theoretical evidence for a single transition state with a small energy barrier of 16.6 kcal · mol^{-1} (Supplementary Fig. 28). Furthermore, the activation parameters for the reaction of **1_{ClO4}** with *p*-cyanophenol could be determined by ultraviolet–visible monitoring of the decay of the aryl-Ag(III) providing a $\Delta G^{\neq}(298\mathrm{K}) = 24.5 \pm 0.6\ \mathrm{kcal \cdot mol^{-1}}$ (for the Eyring plot of the reaction see Supplementary Fig. 29). This value is in reasonable agreement with that computed for our proposal of a two-electron reductive elimination process (Supplementary Fig. 28). Therefore, a general two-electron-based Ag(I)/Ag(III) mechanistic proposal that accommodates all the experimental data collected in this study is depicted in Fig. 5.

In summary, we have demonstrated that the canonical one-electron redox reactivity of silver can be surpassed. The fundamental oxidative addition and reductive elimination steps involved in Ag(I)/Ag(III) redox chemistry have been clarified and this provides a solid mechanistic understanding of a completely new reactivity for silver. These results represent a breakthrough in the fundamental understanding of silver's redox chemistry, and opens potential new avenues for designing Ag-catalysed synthetic tools in organic synthesis, in a direct parallel to the well-known Pd(0)/Pd(II) and Cu(I)/Cu(III) catalysis[20].

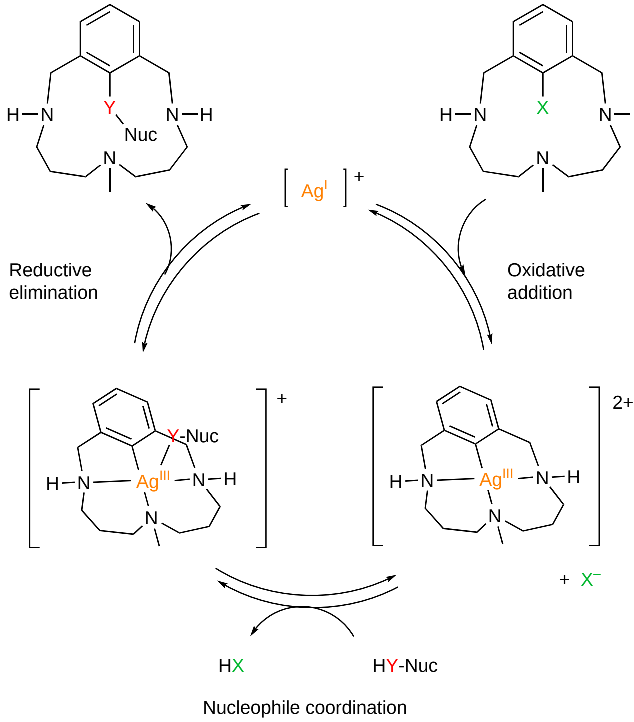

Figure 5 | Mechanistic proposal operating via aryl-Ag(III) species. General proposed mechanism of Ag(I)-catalysed cross-coupling reactions through the intermediacy of aryl-Ag(III) complexes using model aryl halide substrates.

Methods

General materials and methods. Reagents and solvents used were commercially available reagent quality unless indicated otherwise. Solvents were purchased from SDS-Carlo Erba and Scharlab and were purified and dried by passing through an activated alumina purification system (MBraun, SPS-800). Preparation and handling of air-sensitive materials were carried out in a N_2 drybox (JACOMEX) with O_2 and H_2O concentrations <1 p.p.m. NMR data were collected on a BRUKER 400 or 300 AVANCE spectrometer (BRUKER or AVANCE) in the corresponding deuterated solvent ($CDCl_3$ or CD_3CN) and calibrated relative to an external ^1H reference (1,3,5-trimethoxybenzene). Conventional 1D ^1H, $^{13}C\{^1H\}$, $^{19}F\{^1H\}$, $^{31}P\{^1H\}$ and two-dimensional (2D) ^1H–^1H correlation spectroscopy (COSY), ^1H–^1H nuclear Överhauser enhancement spectroscopy (NOESY), ^1H–^{13}C heteronuclear single quantum coherence (HSQC) experiments were recorded under routine conditions. ^{109}Ag NMR experiments were collected in a broadband fluorine observation (BBFO) probe using a sample of 1 M $AgNO_3$ as an external chemical shift reference and for pulse and frequency calibration. The 1D $^1H\{^{109}Ag\}$ spectrum was recorded with the pulse programme zgig (included in the TOPSPIN v2.1 software package), using a recycle delay of 1 s. 2D ^1H-^{109}Ag HMBC spectrum was collected using the standard pulse programme hmbcgpndqf, with a defocusing period of 65 ms (optimized to 8 Hz) and using a relative gradient ratio of G1:G2:G3 = 70:30:44.7, which was established as a function of the gyromagnetic ratios between ^1H and ^{109}Ag nuclei. Equivalent 2D ^1H-^{109}Ag HSQMBC-IPAP and HSQMBC-COSY-IPAP experiments were acquired using the pulse schemes and general acquisition conditions described in the literature[44].

The relevant parameters concerning Ag-NMR studies are listed below[45]: ^{109}Ag; spin ½, natural abundance 51.82%, gyromagnetic moment/γ $-1.087 \cdot 10^7\ \mathrm{radT^{-1}\,s^{-1}}$, relative receptivity 0.197 ^{107}Ag; spin ½, natural abundance 48.18%, gyromagnetic moment/γ $-1.250 \cdot 10^7\ \mathrm{radT^{-1}\,s^{-1}}$, relative receptivity 0.279.

HRMS were recorded on a Bruker MicrOTOF-Q IITM instrument (Bruker) using electrospray ionization (ESI) or Cryospray ionization sources at Serveis Tècnics de Recercaof the University of Girona. C, H, N elemental analyses were performed on a ThermoFinnigan Flash-EA1112 analyzer.

Electrochemical measurements of **1_{ClO4}** were carried out on a Workstation CH-600E series (CH Instruments). The compound (1 mM) was dissolved in a degassed solution of nBu_4NPF_6 (0.1 M) in CH_3CN. The measurements were performed under constant flux of N_2 employing a three-electrode setup: 3-mm-diameter Teflon-shrouded glassy carbon working electrode, a Pt wire auxiliary electrode and a non-aqueous Ag/$AgNO_3$ reference electrode (purchased from CH Instruments). All potential values are reported with respect to non-aqueous Ag/$AgNO_3$ reference electrode.

Turbidity measurements to monitor the precipitation of silver as AgI in the presence and absence of *p*-nitrophenol were performed by multiple light scattering techniques on a Turbiscan LAB instrument.

All reagents used for stoichiometric and catalytic experiments were weighed in a precision balance (legibility 0.01 mg) and then brought in an inert-atmosphere glove box to perform the reactions.

© 2014 Macmillan Publishers Limited. All rights reserved.

Synthesis and characterization of complex $[\mathbf{Ag^{III}(L_1)}](\mathbf{ClO_4})_2$ ($\mathbf{1_{ClO4}}$). Complex $[\mathbf{Ag^{III}(L_1)}](\mathbf{ClO_4})_2$ was prepared by dropwise addition of a solution of $AgClO_4$ (2 equiv.) in CH_3CN to a vigorously stirred solution of $\mathbf{L_1–Br}$ in CH_3CN under inert atmosphere. After few seconds, the solution became cloudy turning bright yellow and a precipitate appeared. After 2 h, the reaction mixture is centrifuged, filtered through Celite and then through an Acrodisc filtre. Slow diethyl ether diffusion over the resulting solution afforded yellow crystals of the desired complex.

$[\mathbf{Ag^{III}(L_1)}](\mathbf{ClO_4})_2$ ($\mathbf{1_{ClO4}}$): (68% yield) ^{1}H-NMR (400 MHz, CD_3CN, 25 °C) δ, p.p.m.: 7.27 (t, 1H, $J=7.58$ Hz, H^a), 7.06 (d, 2H, $J=7.52$ Hz, H^m), 6.66 (bb, 2H, **NH**), 4.86 (dd, $J=16.32$ Hz, $^3J(H^c\text{-}^{109}Ag)=11.5$ Hz, 2H, H^c), 4.73 (d, $J=16.2$ Hz, $^3J(H^d\text{-}^{109}Ag)=1.5$ Hz, 2H, H^d), 3.44–3.37 (m, 2H, H^e or H^f), 3.33–3.27 (m, 2H, H^e or H^f), 3.15–3.08 (m, 2H, H^i or H^j), 2.81–2.78 (m, 2H, H^i or H^j), 2.64 (s, 3H, H^k), 2.20–2.11 (m, 4H, H^g or H^h). ^{13}C-NMR (100 MHz, CD_3CN, 25 °C) δ, p.p.m.: 186.47 (dd, $JC\text{-}^{107}Ag$, $JC\text{-}^{109}Ag=32.60$ Hz, 36.72 Hz), 147.90 (C_2), 129.65 (C_4), 123.19 (C_3), 65.35 (C_5), 59.35 (C_6), 53.42 (C_8), 42.55 (C_9), 25.58 (C_7); ^{109}Ag NMR (18.62 MHz, CD_3CN, 25 °C, extracted from the indirect dimension of a ^{1}H-^{109}Ag HMBC spectrum, and taking a sample of 1 M $AgNO_3$ in D_2O as a external reference) δ, 2,127 p.p.m. HRMS electrospray ionization-time of flight (ESI-TOF), (m/z) calculated for $[C_{15}H_{24}AgClN_3O_4]^+$, $[Ag^{III}(\mathbf{L_1})](ClO_4)$, 454.0484, found: 454.0495. Ultraviolet–visible (CH_3CN): $\lambda_{max}(\epsilon)=390$ nm (sh, 540).

For the computed structure and spectroscopic and electrochemical data for the characterization of $\mathbf{1_{ClO4}}$ see Supplementary Figs 1–10 and Supplementary Fig. 26.

Oxidative addition over $\mathbf{L_1}$–Cl and $\mathbf{L_1}$–Br. A sample of the $\mathbf{L_1}$–X ($X=$ Br, Cl) model substrate (25.4 mg for $\mathbf{L_1}$–**Cl**, 29.4 mg for $\mathbf{L_1}$–**Br**, 0.090 mmol) and 1,3,5-trimethoxybenzene as internal standard were dissolved in CH_3CN (0.6 ml). A portion of this solution (0.1 ml) was loaded into an amber vial containing 0.5–2 equiv. of the Ag (I) salt (AgOTf) and 0–10 equiv. of the corresponding additive (NaOTf or TlOTf; Supplementary Table 1). The mixture was subsequently diluted with 0.9 ml of CH_3CN and the vial was sealed with a screw-cap. The mixture was allowed to react for 2 h at room temperature. After that time, the reaction mixture is centrifuged, filtered through Celite and then through an Acrodisc filtre. The resulting solution was evaporated and dried under vacuum. The crude mixture was then redissolved in 0.5 ml of CD_3CN and transferred to an amber NMR tube and analysed by ^{1}H-NMR. Final concentrations: $[\mathbf{L_1\text{-}X}]=15$ mM, $[Ag^I$ salt$]=7.5$–30 mM, [additive] $=0$–150 mM. Reaction yields were obtained by integration of the ^{1}H-NMR spectra of the crude reaction mixtures relative to 1,3,5-trimethoxybenzene as internal standard (5 mM in CD_3CN; see Supplementary Table 1).

Synthesis and characterization of C–N, C–O, C–S and C–C coupling products. A sample of the aryl-Ag(III) complex $\mathbf{1_{ClO4}}$ (16.3 mg, 0.029 mmol) was dissolved in CD_3CN (2.1 ml) and 0.2 ml of a solution of 1,3,5-trimethoxybenzene was added as internal standard. A portion of this solution (0.6 ml) was loaded into an amber NMR tube, and 2–10 equiv. of the corresponding nucleophile was added to the tube (0.1 ml, 0.168–0.84 M). Final concentrations: $[\mathbf{1_{ClO4}}]=12$ mM and [Nuc] $=24$–120 mM. The tube was sealed with a septum, and the reaction was allowed to proceed at the corresponding temperature monitoring it by ^{1}H-NMR spectroscopy until completion. ^{1}H, ^{13}C, COSY, NOESY, ^{1}H–^{13}C HSQC NMR spectra and HRMS analysis were obtained without isolation of the C-Nuc coupling product. Spectra corresponding to the monoprotonated form of the products are labelled with $HClO_4$. Reaction yields were obtained by integration of the ^{1}H-NMR spectra of the crude reaction mixtures relative to the internal standard.

Synthesis and characterization of the coupling products of boronic acids and $\mathbf{1_{ClO4}}$. A sample of the aryl-Ag(III) complex $\mathbf{1_{ClO4}}$ (13.3 mg, 0.024 mmol) was dissolved in CD_3CN (0.9 ml) and 0.1 ml of a solution of 1,3,5-trimethoxybenzene was added as internal standard. A portion of this solution (0.35 ml) was loaded into an amber NMR tube, and 5 equiv. of the corresponding arylboronic acid in CD_3OD was added to the tube (0.35 ml, 0.12 M). Final concentrations: $[\mathbf{1_{ClO4}}]=12$ mM and [arylboronic acid] $=60$ mM. The tube was sealed with a septum, the reaction was allowed to proceed at 50 °C and was monitored by ^{1}H-NMR spectroscopy until completion. ^{1}H, ^{13}C, COSY, NOESY, ^{1}H–^{13}C HSQC NMR spectra and HRMS analysis were obtained without isolation of the C-Nuc coupling product. Reaction yields were obtained by integration of the ^{1}H-NMR spectra of the crude reaction mixtures relative to the internal standard.

Halogenation of complex $\mathbf{1_{ClO4}}$. A sample of the aryl-Ag(III) complex $\mathbf{1_{ClO4}}$ (15.5 mg, 0.028 mmol) was dissolved in CD_3CN (2 ml) and 0.2 ml of a solution of 1,3,5-trimethoxybenzene was added as internal standard. A portion of this solution (0.6 ml) was loaded into an amber NMR tube, and 2 equiv. of the corresponding tetrabutylammonium halide was added to the tube (0.1 ml, 0.168 M). Final concentrations: $[\mathbf{1_{ClO4}}]=12$ mM and $[nBu_4NX]=24$ mM ($X=$ Cl, Br, I). Upon addition of the halides, the solution rapidly turns deep orange, indicating some degree of deprotonation of the complex. The tube was sealed with a septum, and the reaction was allowed to proceed at the corresponding temperature and was monitored by ^{1}H-NMR spectroscopy until completion. ^{1}H-NMR and HRMS analysis were obtained without isolation of the C–X coupling product. Reaction yields were obtained by integration of the ^{1}H-NMR spectra of the crude reaction mixtures relative to the internal standard. The characterization of the halogenation products ($\mathbf{L_1}$–**Cl**, $\mathbf{L_1}$–**Br** and $\mathbf{L_1}$–**I**) has been achieved by direct comparison with authentic samples synthesized independently[18,39].

Fluorination of complex $\mathbf{1_{ClO4}}$. A sample of the aryl-Ag(III) complex $\mathbf{1_{ClO4}}$ (15.5 mg, 0.028 mmol) was dissolved in CD_3CN (2 ml) and 0.2 ml of a solution of 1,3,5-trimethoxybenzene was added as internal standard. A portion of this solution (0.6 ml) was loaded into an amber vial, and 2 equiv. of $nBu_4NF\cdot 3H_2O$ was added to the tube (0.1 ml, 0.168 M). Final concentrations: $[\mathbf{1_{ClO4}}]=12$ mM and $[F^-]=24$ mM. Upon addition of the fluoride source, the solution rapidly turns deep orange, indicating some degree of deprotonation of the complex. The vial was sealed with a screw-cap and the reaction was allowed to proceed at 40 °C under vigorous stirring. After 24 h of reaction, the crude was centrifuged to remove the black solids generated during the reaction. The resulting solution was evaporated under vacuum and the solids obtained were dried under vacuum for several hours. ^{1}H-NMR yield of the $\mathbf{L_1}$–**F** coupling product was obtained in CD_3CN and calculated using 1,3,5-trimethoxybenzene as internal standard. ^{1}H-NMR, ^{19}F-NMR and HRMS analysis were obtained without isolation of the C–F coupling product.

For spectroscopic data for the characterization of the coupling products and its description, see Supplementary Figs 30–106 and Supplementary Methods.

Catalytic experiments. Stock solutions of $\mathbf{L_1}$–X/1,3,5-trimethoxybenzene (30/10 mM; $x=$ I, Br), AgOTf/ligand (7.5–15/0–37.5 mM) and of the corresponding nucleophile (0.065–0.13 M) were prepared in CD_3CN in the glove box. An amber vial was loaded with 0.2 ml of the AgOTf/ligand stock solution and subsequently 2.3 ml of the nucleophile stock solution and 0.5 ml of the $\mathbf{L_1}$–**X**/1,3,5-trimethoxybenzene stock solution were added. The vial was sealed with a screw-cap and allowed to react at 50 °C for 24 h. Final concentrations: $[\mathbf{L_1\text{–}X}]=5$ mM, [AgOTf] $=0.5$–1 mM, [ligand] $=0$–2.5 mM, [Nuc] $=0.05$–0.1 M. When the reaction time is finished, the crude was transferred to an amber NMR tube and analysed by ^{1}H-NMR. Reaction yields were obtained by integration of the ^{1}H-NMR spectra of the crude reaction mixtures relative to 1,3,5-trimethoxybenbenzene as internal standard (Table 2 main text and Supplementary Table 2). The product obtained in the reaction crude was identified by ESI-TOF spectroscopy.

See Supplementary Methods section for additional experimental procedures not cited in this part.

Crystallographic characterization of $[\mathbf{Ag^{III}(L_1)}](\mathbf{ClO_4})_2$ ($\mathbf{1_{ClO4}}$). Crystals of complex $\mathbf{1_{ClO4}}$ were grown from slow diffusion of diethyl ether in a CH_3CN solution of the compound. All of them were used for low temperature (150(10) K) X-ray structure determination. The measurement was carried out on a Agilent Supernova diffractometer equipped with a 135-mm Atlas detector, and using graphite-monochromated Mo $K\alpha$ radiation (($\lambda=0.71073$ Å) from an X-ray Tube. Programme used for data collection and reduction, CrysAlis pro. Structure solution and refinement were done using SHELXTL Version 6.14 (Bruker, AXS 2000–2003). The structure was solved by direct methods and refined by full-matrix least-squares methods on F^2. The non-hydrogen atoms were refined anisotropically. The H-atoms were placed in geometrically optimized positions and forced to ride on the atom to which they are attached, except N–H hydrogens, which were located in the difference Fourier map and refined without constrains. See Supplementary Table 3 for crystallographic data and structure refinement of $\mathbf{1_{ClO4}}$.

Computational details. The Cartesian coordinates of the X-ray diffraction structure of $\mathbf{1_{ClO4}}$ have been used as starting point in DFT optimizations. An explicit molecule of CH_3CN, which is coordinated in the $\mathbf{L_1}$–$\mathbf{X}$–Ag(I) or $\mathbf{L_5}$–$\mathbf{X}$–Ag(I) complexes ($X=$ F, Cl, Br, I), has been included in all DFT calculations. All the calculations were carried out using the Gaussian09 programme package[46]. The DFT-B3LYP hybrid exchange-correlation functional[47–49] has been employed to model the silver molecular systems. Geometry optimizations were performed with no symmetry restrictions, using the Stuttgart/Dresden (SSD) core pseudopotential pseudopotential and basis set[50] on the heavier atoms (I, Ag) and the 6-311 + G** basis set on all the other atoms. The acetonitrile solvation and London dispersion effects were included in energy and geometry optimization calculations through the solvation model including the role of density (SMD) polarizable continuum model[51] and the B3LYP-D_2 correction[52]. See Supplementary Figs 17 and 18, 26 and 27 and Supplementary Table 4.

Vibrational frequency calculations based on analytical second derivatives to obtain the enthalpy and entropy corrections ($T=298.15$ K) were performed at the same level of theory. The nature of stationary points was also established in solvent-phase, where minima have no imaginary frequencies and transition states have only one.

The free energy of the proton was computed as:

$$G^*(H^+) = G\left(H^+_{gas}\right) + \Delta G^{H+}_{solv} + \Delta G^* \tag{1}$$

where $G\left(H^+_{gas}\right)$ is the gas-phase free energy (-6.3 kcal · mol^{-1})[53] and ΔG^{H+}_{solv} its experimental solvation free energy in acetonitrile (-260.2 kcal · mol^{-1}). The term ΔG^* represents the free energy change associated with the conversion from a standard-state of 1 M in the aqueous phase and 1 atm in gas phase, to 1 M in both phases. Its value is 1.9 kcal · mol^{-1} at 298.15 K.

© 2014 Macmillan Publishers Limited. All rights reserved.

References

1. Lipshutz, B. H. & Yamamoto, Y. Introduction: coinage metals in organic synthesis. *Chem. Rev.* **108,** 2793–2795 (2008).
2. Naodovic, M. & Yamamoto, H. Asymmetric silver-catalyzed reactions. *Chem. Rev.* **108,** 3132–3148 (2008).
3. Álvarez-Corral, M., Muñoz-Dorado, M. & Rodríguez-García, I. Silver-mediated synthesis of heterocycles. *Chem. Rev.* **108,** 3174–3198 (2008).
4. Hashmi, A. S. K. in *Silver in Organic Chemistry*. (ed Harmata, M.) Ch. 12 357–379 (John Wiley & Sons, 2010).
5. Weibel, J.-M., Blanc, A. l. & Pale, P. Ag-Mediated reactions: coupling and heterocyclization reactions. *Chem. Rev.* **108,** 3149–3173 (2008).
6. Létinois-Halbes, U., Pale, P. & Berger, S. Ag NMR as a tool for mechanistic studies of Ag-catalyzed reactions: evidence for in situ formation of alkyn-1-yl silver from alkynes and silver salts. *J. Org. Chem.* **70,** 9185–9190 (2005).
7. Halbes-Letinois, U., Weibel, J.-M. & Pale, P. The organic chemistry of silver acetylides. *Chem. Soc. Rev.* **36,** 759–769 (2007).
8. Proietti Silvestri, I. *et al.* Copper(i)-catalyzed cycloaddition of silver acetylides and azides: incorporation of volatile acetylenes into the triazole core. *Org. Biomol. Chem.* **9,** 6082–6088 (2011).
9. Negishi, E.-i. & Meijere, A. D. *Handbook of Organopalladium Chemistry for Organic Synthesis* (Wiley, 2002).
10. Dillinger, S., Bertus, P. & Pale, P. First evidence for the use of organosilver compounds in Pd-catalyzed coupling reactions; a mechanistic rationale for the Pd/Ag-catalyzed enyne synthesis? *Org. Lett.* **3,** 1661–1664 (2001).
11. Homs, A., Escofet, I. & Echavarren, A. M. On the silver effect and the formation of chloride-bridged digold complexes. *Org. Lett.* **15,** 5782–5785 (2013).
12. Mijs, W. J. & Jong, C. R. H. I. d. *Organic Synthesis by Oxidation with Metal Complexes* (Plenum Press, 1986).
13. Hull, K. L. & Sanford, M. S. Catalytic and highly regioselective cross-coupling of aromatic C − H substrates. *J. Am. Chem. Soc.* **129,** 11904–11905 (2007).
14. Tang, P., Furuya, T. & Ritter, T. Silver-catalyzed late-stage fluorination. *J. Am. Chem. Soc.* **132,** 12150–12154 (2010).
15. Seo, S., Taylor, J. B. & Greaney, M. F. Silver-catalysed trifluoromethylation of arenes at room temperature. *Chem. Commun.* **49,** 6385–6387 (2013).
16. Weibel, J.-M., Blanc, A. & Pale, P. in *Silver in Organic Chemistry*. (ed Harmata, M.) Ch. 10 285–327 (John Wiley & Sons, 2010).
17. Ghosh, S. P., Ghosh, M. C. & Gould, E. S. Electron transfer 122. Reductions of an N4-coordinated complex of silver(III). *Inorg. Chim. Acta* **225,** 83–88 (1994).
18. Casitas, A. *et al.* Direct observation of Cu^{I}/Cu^{III} Redox steps relevant to ullmann-type coupling reactions. *Chem. Sci.* **1,** 326–330 (2010).
19. Casitas, A. & Ribas, X. The role of organometallic copper(III) complexes in homogeneous catalysis. *Chem. Sci.* **4,** 2301–2318 (2013).
20. Hickman, A. J. & Sanford, M. S. High-valent organometallic copper and palladium in catalysis. *Nature* **484,** 177–185 (2012).
21. Boorman, T. C. & Larrosa, I. Gold-mediated C-H bond functionalisation. *Chem. Soc. Rev.* **40,** 1910–1925 (2011).
22. Guenther, J. *et al.* Activation of aryl halides at Gold(I): practical synthesis of (P,C) Cyclometalated gold(III) complexes. *J. Am. Chem. Soc.* **136,** 1778–1781 (2014).
23. Hashmi, A. S. K., Blanco, M. C., Fischer, D. & Bats, J. W. Gold catalysis: evidence for the *in-situ* reduction of Gold(III) during the cyclization of allenyl carbinols. *Eur. J. Org. Chem.* **2006,** 1387–1389 (2006).
24. Hashmi, A. S. K. *et al.* On homogeneous gold/palladium catalytic systems. *Adv. Synth. Catal.* **354,** 133–147 (2012).
25. Yu, Y., Yang, W., Pflästerer, D. & Hashmi, A. S. K. Dehydrogenative Meyer–Schuster-like rearrangement: a gold-catalyzed reaction generating an alkyne. *Angew. Chem. Int. Ed.* **53,** 1144–1147 (2014).
26. Li, P. & Wang, L. A novel silver iodide catalyzed sonogashira coupling reaction. *Synlett.* **2006,** 2261–2265 (2006).
27. Das, R., Mandal, M. & Chakraborty, D. Silver-nitrate-catalyzed N-arylation of amines and O-arylations of phenols and alcohols. *Asian J. Org. Chem* **2,** 579–585 (2013).
28. Li, Z., Song, L. & Li, C. Silver-catalyzed radical aminofluorination of unactivated alkenes in aqueous media. *J. Am. Chem. Soc.* **135,** 4640–4643 (2013).
29. Lash, T. D., Rasmussen, J. M., Bergman, K. M. & Colby, D. A. carbaporphyrinoid chemistry has a silver lining! Silver(III) Oxybenzi-, Oxynaphthi-, Tropi-, and Benzocarbaporphyrins. *Org. Lett.* **6,** 549–552 (2004).
30. Furuta, H., Maeda, H. & Osuka, A. Doubly N-confused porphyrin: a new complexing agent capable of stabilizing higher oxidation states. *J. Am. Chem. Soc.* **122,** 803–807 (2000).
31. Brückner, C., Barta, C. A., Briñas, R. P. & Krause Bauer, J. A. Synthesis and Structure of [meso-Triarylcorrolato]silver(III). *Inorg. Chem.* **42,** 1673–1680 (2003).
32. Eujen, R., Hoge, B. & Brauer, D. J. Preparation and NMR spectra of difluoromethylated silver(I) and silver(III) compounds. Structure of [PNP][Ag(CF2H)4]. *Inorg. Chem.* **36,** 3160–3166 (1997).
33. Ribas, X. *et al.* Aryl C-H activation by Cu(II) to form an organometallic Aryl-Cu(III) species: a novel twist on copper disproportionation. *Angew. Chem. Int. Ed.* **41,** 2991–2994 (2002).
34. Ribas, X. *et al.* Facile C-H bond cleavage via a proton-coupled electron transfer involving a $C\text{-}H \cdots Cu^{II}$ interaction. *J. Am. Chem. Soc.* **132,** 12299–12306 (2010).
35. Huffman, L. M. *et al.* Observation and mechanistic study of facile C-O bond formation between a well-defined aryl-copper(III) complex and oxygen nucleophiles. *Chem. Eur. J.* **17,** 10643–10650 (2011).
36. Rovira, M., Font, M. & Ribas, X. Model C sp 2-C sp 3 Hurtley coupling catalysis that operates through a well-defined CuI/CuIII mechanism. *Chem. Cat. Chem.* **5,** 687–691 (2013).
37. Furuya, T., Kamlet, A. S. & Ritter, T. Catalysis for fluorination and trifluoromethylation. *Nature* **473,** 470–477 (2011).
38. Casitas, A., Ioannidis, N., Mitrikas, G., Costas, M. & Ribas, X. Aryl-O reductive elimination from reaction of well-defined aryl-Cu(III) species with phenolates: the importance of ligand reactivity. *Dalton Trans.* **40,** 8796–8799 (2011).
39. Casitas, A., Canta, M., Solà, M., Costas, M. & Ribas, X. Nucleophilic aryl fluorination and aryl halide exchange mediated by a Cu(I)/Cu(III) catalytic cycle. *J. Am. Chem. Soc.* **133,** 19386–19392 (2011).
40. Helgesson, G. & Jagner, S. Halogenoargentate(I) with unusual coordination geometries. Synthesis and structure of potassium-crypt salts of chloro-, bromo- and iodoargentates(I), including the first example of a two-coordinated chloroargentate(I) in the solid state. *Inorg. Chem.* **30,** 2574–2577 (1991).
41. Della Monica, M., Lamanna, U. & Senatore, L. Silver complexes with I − , Br − and SCN − in sulfolane. *Inorg. Chim. Acta* **2,** 357–362 (1968).
42. Garcia-Bosch, I., Ribas, X. & Costas, M. Electrophilic arene hydroxylation and phenol OH oxidations performed by an unsymmetric μ-η1:η1-O2-peroxo dicopper(II) complex. *Chem. Eur. J* **18,** 2113–2122 (2012).
43. Osako, T. *et al.* Oxidation mechanism of phenols by dicopper − dioxygen (Cu_2/O_2) complexes. *J. Am. Chem. Soc.* **125,** 11027–11033 (2003).
44. Saurí, J. & Parella, T. On the interference of J(HH) modulation in HSQMBC-IPAP and HMBC-IPAP experiments. *Magn. Reson. Chem.* **51,** 509–516 (2013).
45. Penner, G. H. & Liu, X. Silver NMR spectroscopy. *Prog. Nucl. Magn. Reson. Spectrosc* **49,** 151–167 (2006).
46. *Gaussian 09 revision A.1* (Gaussian Inc., Wallingford CT, 2004).
47. Becke, A. D. A new mixing of Hartree–Fock and local density-functional theories. *J. Chem. Phys.* **98,** 1372–1377 (1993).
48. Becke, A. D. Density-functional thermochemistry. III. The role of exact exchange. *J. Chem. Phys.* **98,** 5648–5652 (1993).
49. Lee, C., Yang, W. & Parr, R. G. Development of the Colle-Salvetti correlation-energy formula into a functional of the electron density. *Phys. Rev. B* **37,** 785–789 (1988).
50. Dolg, M., Wedig, U., Stoll, H. & Preuss, H. *J. Chem. Phys.* **86,** 866–872 (1987).
51. Marenich, A. V., Cramer, C. J. & Truhlar, D. G. Universal solvation model based on solute electron density and on a continuum model of the solvent defined by the bulk dielectric constant and atomic surface tensions. *J. Phys. Chem. B* **113,** 6378–6396 (2009).
52. Schwabe, T. & Grimme, S. Double-hybrid density functionals with long-range dispersion corrections: higher accuracy and extended applicability. *Phys. Chem. Chem. Phys.* **9,** 3397–3406 (2007).
53. Winget, P., Cramer, C. J. & Truhlar, D. G. Computation of equilibrium oxidation and reduction potentials for reversible and dissociative electron-transfer reactions in solution. *Theor. Chem. Acc.* **112,** 217–227 (2004).

Acknowledgements

This work was supported by grants from the European Research Council (Starting Grant Project ERC-2011-StG-277801), the Spanish MINECO (CTQ2012-37420-C02-01/BQU, CTQ2012-32436, Consolider-Ingenio CSD2010-00065, INNPLANTA project INP-2011-0059-PCT-420000-ACT1) and the Catalan DIUE of the Generalitat de Catalunya (2009SGR637). M.F and J.L.-F. thank a PhD grant and a RyC contract from Spanish MINECO, respectively. X.R. and M.C. also thank ICREA-Acadèmia awards. We also thank Dr. S. Sala for technical support.

Author contributions

M.F. performed the experimental work and wrote the manuscript; F.A.-P. performed the theoretical calculations; T.P. has performed and supervised all NMR studies; J.S. contributed with the isolation and characterization of $\mathbf{1_{ClO4}}$ complex; J.M.L. and J.L.-F. supervised all theoretical calculations; M.C. supervised experimental work and wrote the manuscript; X.R. designed and directed the project, and wrote the paper.

Additional information

Accession Codes. Supplementary crystallographic data for compound $\mathbf{1_{ClO4}}$ has been deposited at the Cambridge Crystallographic Data Centre under accession number CCDC978368. These data can be obtained free of charge at http://www.ccdc.cam.ac.uk/

© 2014 Macmillan Publishers Limited. All rights reserved.

data_request/cif. Reprints and permissions information is available at www.nature.com/reprints. Readers are welcome to comment on the online version of the paper..

Supplementary Information accompanies this paper at http://www.nature.com/naturecommunications

Competing financial interests: The authors declare no competing financial interests.

Reprints and permission information is available online at http://www.nature.com/reprints/index.html.

How to cite this article: Font, M. *et al.* Direct observation of two-electron Ag(I)/Ag(III) redox cycles in coupling catalysis. *Nat. Commun.* 5:4373 doi: 10.1038/ncomms5373 (2014).

© 2014 Macmillan Publishers Limited. All rights reserved.

CHAPTER V.

RESULTS AND DISCUSSION

V. RESULTS AND DISCUSSION

*Complexes referred as **1** and **1**$_{ClO4}$ in Chapter III and Chapter IV respectively, will be labelled as **1**-Cu^{III} and **1**-Ag^{III} in Chapter IV for clarity reasons.*

Cross-coupling technology has become an indispensable tool in synthetic chemistry and has changed the organic chemist's approach towards the synthesis of target molecules. The first wave of cross-coupling transformations, that provided diverse C-C bond forming reactions, brought a new general route towards the construction of biaryl, bis(heteroaryl) and aryl alkynyl and heteroaryl alkynyl scaffolds, giving rise to the synthesis of a vast number of molecular architectures that had remained inaccessible until the discovery of cross-coupling methodologies.[1] The second wave provided general methodologies for the formation of C-heteroatom bonds that further expanded the scope of cross-coupling to a broader range of compounds including *N*-substituted anilines, *N*-arylamides and biaryl ethers among others. In this context, the occurrence of Buchwald-Hartwig condensation reactions overcame the limitation arising from the availability of resources to access these substructures and broadened the scope of the accessible compounds also to arene products not containing electron-withdrawing activating groups.[2,3] Recent progress in the field of cross-coupling has focused on developing methods for the functionalisation of non-prefunctionalised arenes through coupling reactions, namely C-H functionalisation,[4] and on the replacement of precious metals by more abundant first-row transition metals.[5] These advances are driving the cross-coupling arena towards a more sustainable scenario that is evolving to produce fewer waste products.[6]

In most cross-coupling reactions catalysed by metals other than palladium, the C_{sp2}-halide cleavage is the rate-limiting step and thus the resting state is the species prior to the formation of high-valent aryl-M key intermediate species. This fact, plus the short-lived nature of the high-valent species responsible for driving the coupling of the two partners, precluded their identification for many years. Thus, mechanistic proposals to rationalise such transformations relied on computational and kinetic data for a long time in the case of copper or are otherwise inexistent as occurs for silver.

The work described in this thesis aims to shed light into the mechanistic aspects that govern copper and silver-catalysed C-heteroatom bond forming cross-coupling reactions by designing model aryl halide substrates bearing an appendage containing three amine coordination sites capable of chelating the metal centre, hence facilitating the stabilisation of high-valent metal intermediate species. These studies revealed Cu^{I}/Cu^{III} redox cycles in the formation of biaryl thioethers, aryl alkyl thioethers, biaryl selenide and ary dialkyl phosphonates within model aryl halide macrocyclic substrates. Importantly, these model aryl halide substrates also allowed for the first time direct observation of the engagement of silver in two-electron oxidative addition and reductive elimination processes and unequivocally identified aryl-Ag^{III} as the key intermediate species in catalytic C-O and C-C bond forming cross-coupling reactions. These findings dismiss the widespread conception that silver redox chemistry can only arise from one-electron processes.

The ultimate goal of this work is to widen the understanding of the nature of the copper and silver-catalysed cross-coupling reactions and apply this knowledge to the design of more efficient catalysts that fulfil the structural and electronic requirements that enables these transformations in milder conditions. Moreover, these studies enable the comparison of the reactivity of both metals in cross-coupling transformations and provide insights into their complementarity.

V.1. Catalytic C-S, C-Se and C-P Cross-Coupling Reactions Mediated by a Cu^I/Cu^{III} Redox Cycle

*The compound labelled as **2a** in this section does not correspond to the same compound **2a** in Section V.1.*

Although some steps have been taken towards the application of copper-catalysed cross-coupling methodologies for the formation of C_{aryl}-heteroatom bonds in the synthesis of pharmaceuticals and natural products, still some important challenges remain, such as increasing the scope of the existing reactions and their selectivity which has limited the industrial application of these transformations.[7] The last 10 years have seen a rapid development in the area of copper-catalysed functionalisation of aryl halides, especially for the formation of C_{aryl}-N and C_{aryl}-O bonds.[8-10] Fewer efforts have been devoted to the progress in analogous reactions for the formation of C-S, C-Se and C-P bonds despite the relevant presence of the potentially accessible scaffolds derived from these transformations in biologically active compounds.[11-18] In any case, as a result of interest in these biologically active scaffolds this field has recently attracted significant interest giving rise to important advances.[19-31]

To obtain insights into the mechanism of these transformations, Shyu decided to investigate the intermediate species formed in copper(I)-catalysed condensations of aryl halides with thiophenol by means of *in situ* ESI-MS analysis.[32] To do so, a mixture of thiophenol (1.1 equiv.), iodobenzene (1 equiv.), sodium *tert*-butoxide (1.5 equiv.), CuI (10 mol %) and 1,10-phenanthroline (10 mol %) were reacted in DMF at 120 ºC for 2 h and then injected into an ESI-MS instrument. The ESI-MS spectra obtained in the negative-ion mode revealed the presence of

$[Cu^I(SPh)_2]^-$ and $[Cu^I(SPh)I]^-$ at *m/z* = 280.95 and *m/z* = 298.85 respectively. Peaks at *m/z* = 423.07 and *m/z* = 219.03 corresponding to $[Cu^I(phen)_2]^+$ and $[K(phen)]^+$ were observed in the positive-ion mode ESI-MS spectra in addition to a signal at *m/z* = 396.95 which was attributed to the formation of high-valent $[K[Cu^{III}(SPh)_2(Ph)]^+$ species. This copper(III) fragment may derive from the fragmentation of neutral $[Cu^{III}(SPh)_2(Ph)(I)]$ into the observed peak and I^-, which is indeed observed in the negative-ion mode ESI-MS spectra. Whilst it could be argued that the species formed in the ESI-MS equipment might not correspond to the actual intermediate species formed during the reaction, this is the first direct observation of aryl-Cu^{III} species in copper-catalysed C-S bond forming cross-coupling reactions.

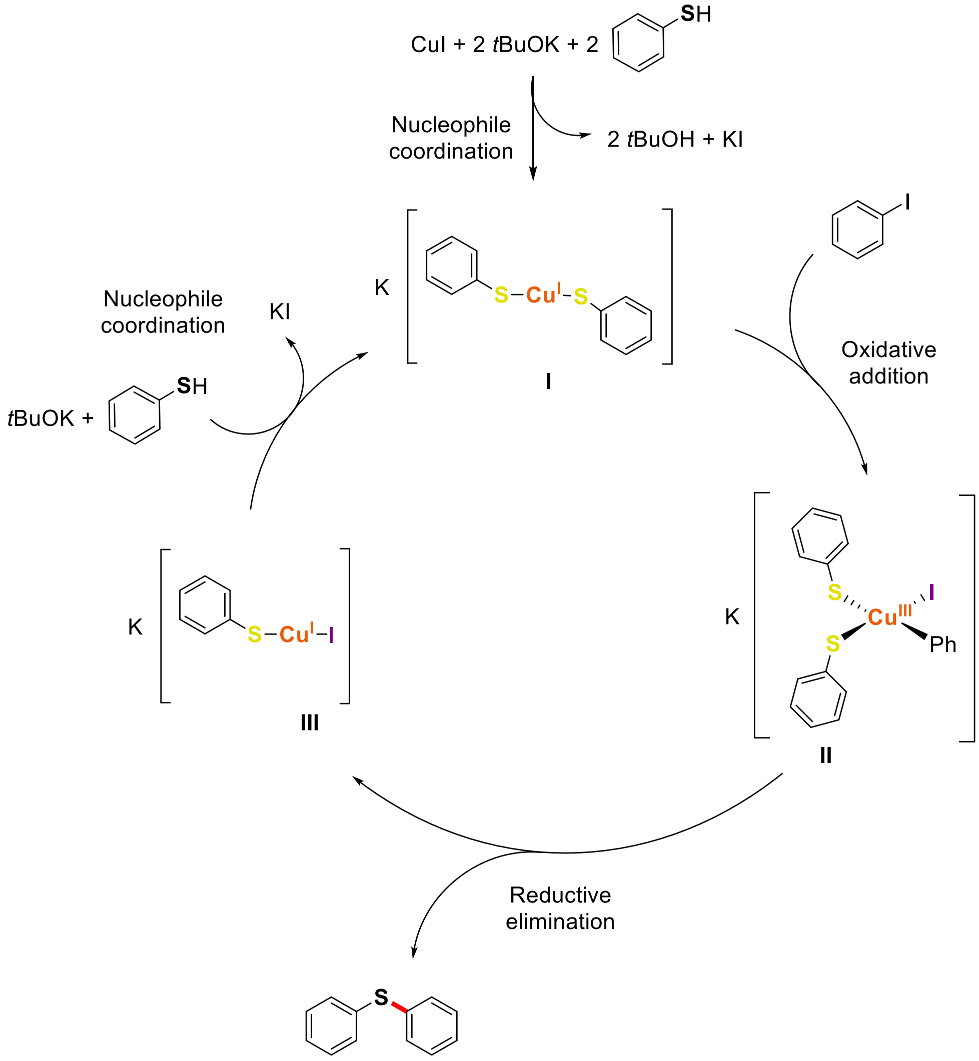
CuI + 2 tBuOK + 2
SH
Nucleophile coordination
2 tBuOH + KI
K
S–Cu^I–S
I
Nucleophile coordination
KI
tBuOK +
SH
Oxidative addition
I
K
S
Cu^III
I
S
Ph
II
K
S–Cu^I–I
III
Reductive elimination
S

Scheme V. 1. Proposed catalytic cycle by Shyu and co-workers for the copper-catalysed arylation of thiophenol.

Based on the identity of the species observed in this work, the authors drew a proposal for the catalytic cycle of the reaction (see **Scheme V. 1**). First, species **I**, detected by ESI-MS is generated *via* coordination of two thiolate molecules. Upon oxidative addition species **I** is transformed into intermediate **II**, as suggested by the detection of a peak corresponding to

$[K[Cu^{III}(SPh)_2(Ph)]]^+$ in the positive-ion mode of the ESI-MS. After a reductive elimination the desired product is formed along with species **III**, which eventually regenerates the catalyst after coordination of a new thiolate.

As a result of not observing copper(I) species containing both 1,10-phenanthroline and thiolate in the ESI-MS, the authors suggest that 1,10-phenanthroline combines with copper(I) to form bulky cations, $[Cu^I(phen)_2]^+$, able to stabilise $[Cu^I(SPh)_2]^-$ anions, rather than directly acting as the auxiliary ligand. Their proposal, though, is in contrast with the importance of 1,10-phenanthroline, that was proven by the fact that in its absence only trace amounts of product were obtained.

Motivated by Shyu's proposal and in light of the absence of akin studies for C-Se and C-P analogous reactions we decided to study the behaviour of our model organometallic copper(III) complex embedded in a trizamacrocyclic arene ligand (**1**-Cu^{III}) in the presence of sulphur, selenium and phosphorus-based nucleophiles in order to evaluate the plausibility of aryl-Cu^{III} key intermediates in these couplings.

Complex **1**-Cu^{III} readily reacts with stoichiometric amounts (0.9-1.5 equiv.) of several thiophenols, aliphatic thiols, benzeneselenol and H-phosphonates in CD_3CN under mild temperatures (25-50 ºC) to afford the corresponding coupling products (**Table V. 1**).

The rates of the coupling reactions of **1**-Cu^{III} complex with the nucleophiles follow the trend benzeneselenol > aromatic thiols > aliphatic thiols > H-phosphonate diesters as revealed by ^1H NMR monitoring of the reactions. While C-Se and C-S coupling reactions take place at room temperature, reaction with H-phosphonate diesters need to be run at 50 ºC to reach completion. The rates of the reactions with selenols and thiols can be correlated to the pK_a of the acidic protons of the nucleophile, although steric factors can also be observed (pK_a values extracted from ref.33). The more easily deprotonated the substrate the faster the reactions with the exception of 2-methyl-2-propanethiol, that despite possessing very similar pK_a values to 1-butanethiol presents longer reaction times (3 h) indicating that steric effects play a role in the reaction rates.

Reactions with dibenzyl phosphite and dimethyl phosphite yielded the desired C-P products that in turn underwent rapid partial dealkylation and phosphite oxide alkylation leading to undesired decomposition products (see full characterisation of the C-P coupling products in **Annex I**).[34] Conversely, dibutyl phosphite did not present such decomposition pathways but exhibited a much slower reactivity than its parent phosphites.

Table V. 1. Reaction of **1**-Cu^{III} with sulphur-, selenium- and phosphorus-based nucleophiles resulting in the formation of the corresponding C-S, C-Se and C-P coupling products.

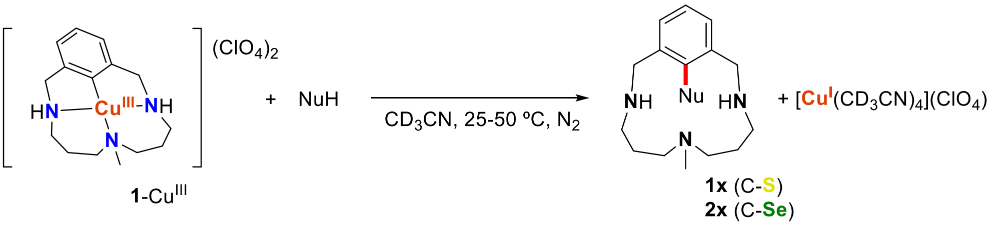

S-Nucleophiles

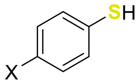

X	pK_a(DMSO)	t	% yield[a]
H	10.3	< 10 min.	100 (**1a**)
CH_3	10.3-11.2	< 10 min.	100 (**1b**)
OCH_3	11.2	< 10 min.	100 (**1c**)
Cl	9.0[b]	< 10 min.	100 (**1d**)

substrate	pK_a (DMSO)	t	% yield[a]
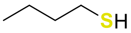	17.0	1.5 h	100 (**1e**)
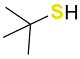	17.9	3 h	100 (**1f**)
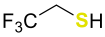	-	1.5 h	100 (**1g**)

Se-Nucleophile

substrate	pK_a(DMSO)	t	% yield[a]
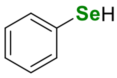	7.1	3 h	100[c] (**2a**)

P-Nucleophiles

Substrate[d]	Equiv.	t	% yield[a]
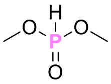	1.1	1.5 h	95 (**3a**)
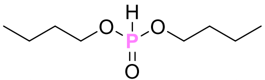	2	18 h	48 (**3b**)
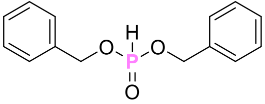	0.9	2 h	95[e] (**3c**)

General conditions: [**1**-Cu^{III}] = 12 mM, [NuH] = 12.5 mM in 0.7 mL CD_3CN at rt. [a] Calculated by ^{1}H NMR spectroscopy using 1,3,5-trimethoxybenzene as internal standard. [b] pK_a(DMSO) value for 4-bromothiophenol (the 4-chlorothiophenol pK_a value is not tabulated; a value close to that of the 4-bromothiophenol is expected).[33] [c] Conditions: [**1**-Cu^{III}] = 12 mM, [NuH] = 18 mM in 0.7 mL CD_3CN at rt, reaction time < 1 min. [d] Conditions: [**1**-Cu^{III}] = 12 mM, [NuH] = 12-24 mM in 0.7 mL CD_3CN at 50 ºC. [e] With respect to limiting nucleophile.

Competition experiments were carried out to test the chemoselectivity of the system and to explore the factors that control it. **1**-Cu^{III} was reacted with selected bifunctional substrates combining thiol/alcohol and thiol/carboxylic acid functional groups in both aromatic and aliphatic moieties (**Table V. 2**).

Table V. 2. Reactivity of **1**-Cu^{III} complex with bifunctional thiol/alcohol and thiol/carboxylic acid substrates.

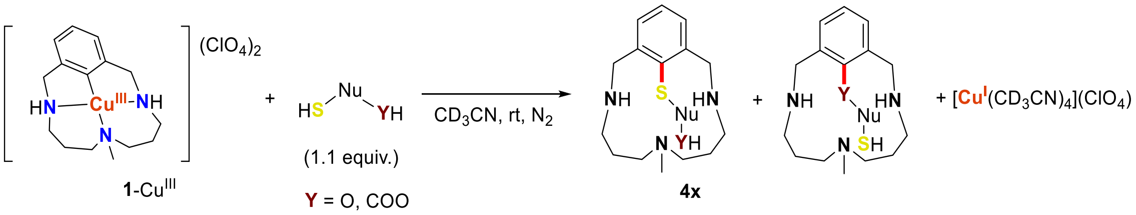

Substrate	pK_a (DMSO) OH / SH[a]	C-O / C-S % yield[b]
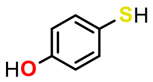	16.7 / 9.0	0 / 100 (**4a**)
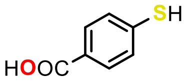	9.1 / 9.0	55 / 45 (**4b**)
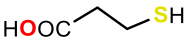	12.6 / 17.0	25 / 75 (**4c**)
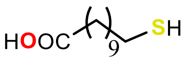	12.6 / 17.0	49 / 51 [c] (**4d**)

General conditions: [**1**-Cu^{III}] = 12 mM, [NuH] = 12.5 mM, in 0.7 mL CD_3CN at r.t. [a] tabulated pK_as of related compounds with similar electronic properties.[33] [b] Calculated by ^{1}H NMR spectroscopy using 1,3,5-trimethoxybenzene as internal standard. [c] 6% of intramolecular C-N reductive elimination product.[35]

Reactions with aromatic bifunctional substrates *p*-mercaptophenol and *p*-mercaptobenzoic acid are in agreement with a critical dependence of the preferred arylated functionality on the pK_a of the functional group. Whilst *p*-mercaptophenol, showing distinct pK_a values for the two functionalities reacted with **1**-Cu^{III} to only produce the C-S coupling product, the reaction with *p*-mercaptobenzoic substrate, possessing similar pK_a values exhibited no discernible chemoselectivity. On the other hand, the behaviour of aliphatic bifunctional substrates diverged from their parent aromatic compounds. Unexpectedly, the related competition experiments employing 3-mercaptopropanoic acid showed preferential S-arylation and in contrast 11-mercaptoundecanoic acid showed equimolar amounts of C-S and C-O coupling products despite the higher acidity of aliphatic acids compared to aliphatic thiols. Thus, these results indicate that the acidity of the functional group is not the only factor governing the selectivity of **1**-Cu^{III} coupling with aliphatic bifunctional substrates. A reasonable explanation for the higher thiol selectivity observed for 3-mercaptopropanoic acid might lie on the fact that shorter chain spacers between functional groups allow for the proper interaction of the carboxylic acid with the ligand amines orienting the substrate in such manner that the C-S coupling is favoured.

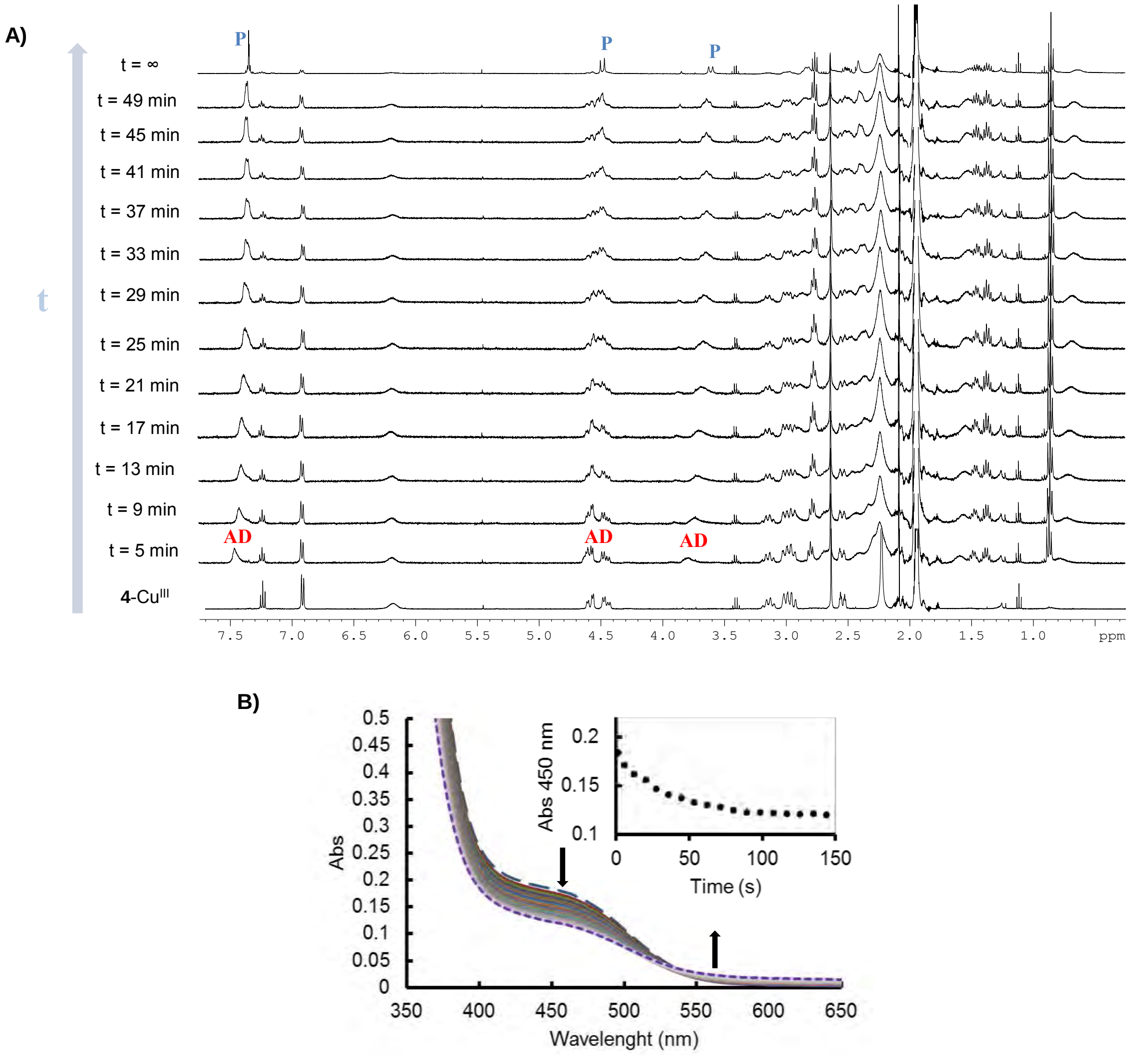

Figure V. 1. A) Low temperature ^{1}H NMR monitoring of the reaction of complex **1**-Cu^{III} with 1-butanethiol revealing the formation of an adduct (**AD**) before reaching the formation of the reaction product (**P**). Conditions: [**1**-Cu^{III}] = 4 mM, [1-butanethiol] = 3.6 mM, CD_3CN, 0 ºC. **B)** Low temperature UV-Vis monitoring of the reaction of **1**-Cu^{III} with 1-butanethiol exhibiting the formation of an adduct species. Conditions: [**1**-Cu^{III}] = 0.8 mM, [1-butanethiol] = 0.72 mM, CH_3CN, 0 ºC.

To attain a better understanding of the mechanism of the reactions described, we monitored the reactions of complex **1**-Cu^{III} with 1-butanethiol, *p*-methoxythiophenol and benzeneselenol at low temperature in order to trap the **1**-Cu^{III}···nucleophile adduct species analogous to the previously species proposed to form upon reaction of **1**-Cu^{III} with carboxylic acids and phenols bearing electron-donating groups.[36] Indeed, low temperature UV-Vis and ^{1}H NMR spectroscopy monitoring showed visible changes upon addition of the nucleophile to **1**-Cu^{III}. The apparent formation of a transient species using 1-butanethiol as substrate became apparent by the appearance of a new set of signals in the ^{1}H NMR spectra within the first 5 min of reaction, especially distinguishable in the aromatic and benzylic region, that shifted visibly as the reaction product formed (**Figure V. 1A**. See **Annex I. Figure S53** for the analogous spectra using *p*-methoxythiophenol). Likewise, low temperature UV-Vis monitoring showed rapid bleaching of the characteristic Cu^{III}-C_{aryl} band at 450 nm which stabilises after 3 min before starting to decay again with the formation of the reaction product (**Figure V. 1B**. See **Annex I. Figure S51** for the analogous spectra using *p*-methoxythiophenol and benzeneselenol respectively). These observations supported our hypothesis that an aryl-Cu^{III}-(HS-*n*Bu) adduct species is generated before it decomposes rapidly to form the corresponding C-S coupling product. Further, the minor changes of the electronic spectra rule out the direct coordination of a new thiolate ligand to the copper centre and suggest a weaker interaction that could be attributed to a **1**-$Cu^{III}\cdots$HS-Nu adduct prior to the deprotonation of the nucleophile.

The detection of the intermediate adduct species added missing pieces to the mechanistic puzzle of the coupling of **1**-Cu^{III} with thiols, selenols and H-phosphonate diesters. Thus, with all the results gathered in this study a mechanistic proposal is disclosed in **Scheme V. 2**, in which only thiol nucleophiles have been depicted for simplification purposes. Our mechanistic proposal starts by formation of the adduct **1**-$Cu^{III}\cdots$HS-Nu, that precedes the rate-limiting deprotonation of the thiol moiety likely by one of the amines of the ligand, which eventually leads to a reductive elimination that furnishes the C-S coupling product and copper(I) cations.

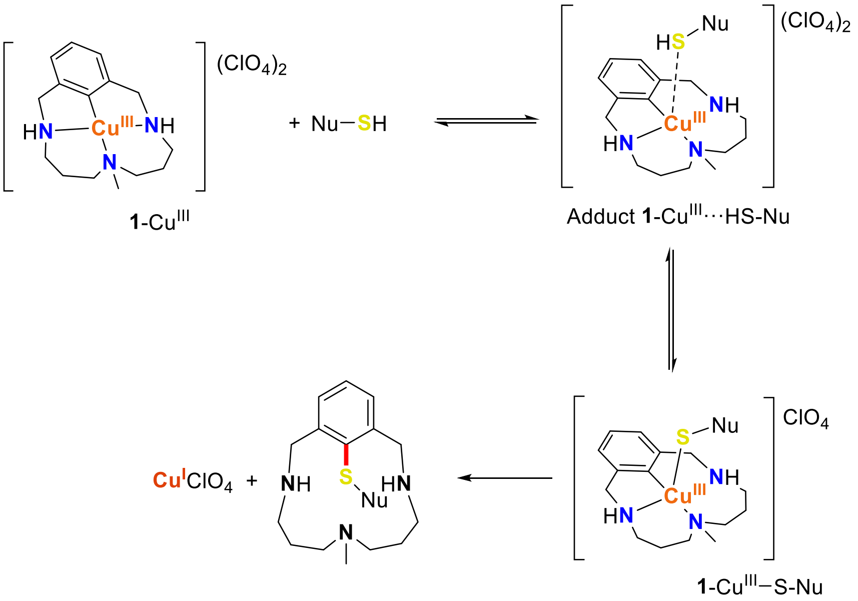

Scheme V. 2. Mechanistic proposal for the C-S cross-coupling between aryl-Cu^{III} complex **1**-Cu^{III} and thiol nucleophiles.

Remarkably, the catalytic copper-catalysed cross-coupling reactions of thiophenols, alkylic thiols, benzeneselenol and H-phosphonate were achieved within the model triazamacrocyclic aryl bromide **L_1-Br** substrate affording the coupling products in quantitative to good yields (**Table V. 3**). Furthermore, analogous C-S cross-coupling by copper catalysis also proceeded with a 96 % yield when more challenging model aryl chloride substrate **L$_1$-Cl** containing a C$_{aryl}$-Cl bond was employed in the presence of 5 mol % of catalyst. In all catalysis experiments slow addition of the substrate proved beneficial for the reaction outcomes either by preventing detrimental precipitation of copper(I) salts with thiolates and selenolates or by minimising the dimethyl phosphite decomposition. Importantly, the UV-Vis monitoring of these reactions demonstrated that the aryl-Cu^{III}-Br complex (**2$_{Br}$**) oxidative addition product is a steady-state intermediate of the reaction suggesting a rate-limiting ligand exchange for the catalytic reaction (**Annex I. Figure S54**).

Table V. 3. Copper-catalysed C-S, C-Se, C-P bond forming cross-coupling reactions.

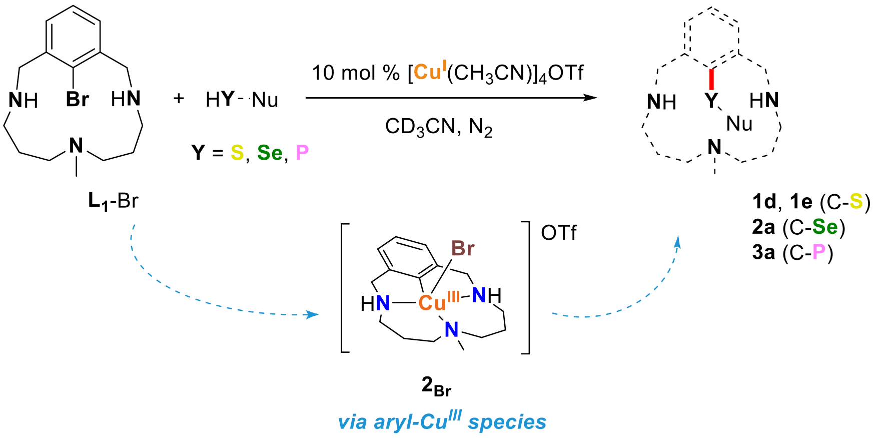

Substrate	Equiv.	T	% yield[a]
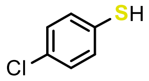	1.1	rt	(96)[b] 100 (**1d**)
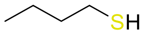	1.1	rt	100 (**1e**)
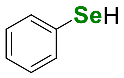	2	rt	72 (**2a**)
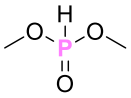	2	50 ºC	46 (**3a**)

General conditions: [**L$_1$-Br**] = 5 mM, [Cu(CH$_3$CN)$_4$OTf] = 0.5 mM, [NuH] = 5.5-10 mM in 3 mL CD$_3$CN.[a] Calculated by ^{1}H NMR spectroscopy using 1,3,5-trimethoxybenzene as internal standard. [b] Employing **L$_1$-Cl** as the substrate and 5 mol % of [Cu(CH$_3$CN)$_4$]OTf.

These observations enabled us to propose a catalytic cycle based on an aryl-Cu^{III} intermediate species depicted in **Scheme V. 3** in consonance to the key intermediate species also proposed by Shyu and co-workers for the copper-catalysed arylation of thiophenol.[32] On the other hand, while our system relies on the chelating effect of the three amines of the substrate anchor to drive the cross-coupling process, Shyu's mechanistic proposal dismisses the formation of a phenanthroline-ligated copper intermediate species, although the reaction outcomes were reduced to trace amounts of the product in the absence of phenanthroline. While ligand-containing copper intermediate species were not detected by ESI-MS experiments, they cannot be ruled out as the active species of the reaction only on the basis of mass spectrometry measurements.

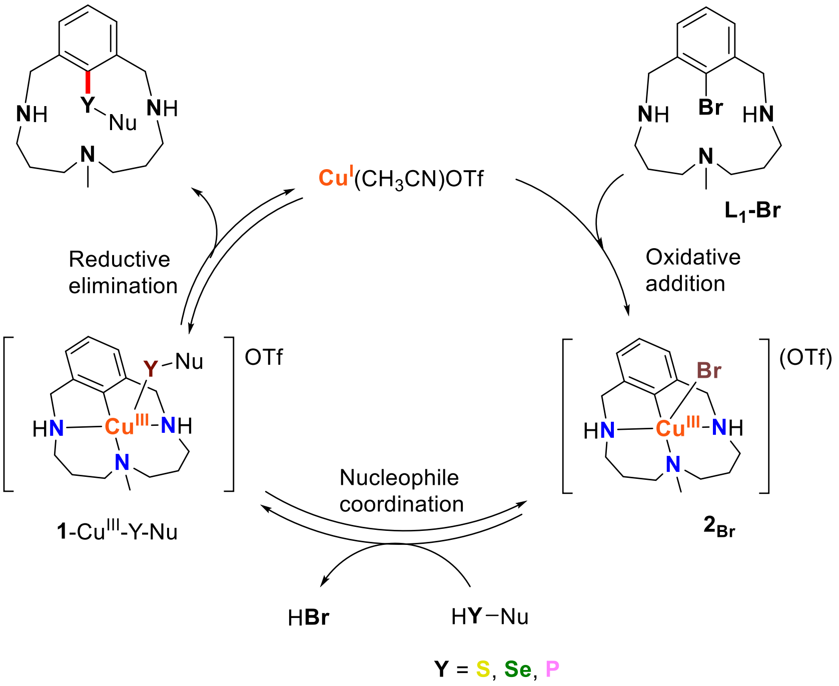

NH
Y
Nu
NH
N
Cu^{I}(CH$_3$CN)OTf
NH
Br
HN
N
L$_1$-Br
Reductive elimination
Oxidative addition
Y-Nu
OTf
HN—Cu^{III}-NH
N
1-Cu^{III}-Y-Nu
Br
(OTf)
HN—Cu^{III}-NH
N
2$_{Br}$
Nucleophile coordination
HBr
HY–Nu
Y = S, Se, P

Scheme V. 3. General proposed mechanism of copper-catalysed C-S, C-Se and C-P bond forming cross-coupling reactions through the intermediacy of aryl-Cu^{III} complexes within a model triazamacrocyclic aryl bromide substrate.

V.2. Direct Observation of Two-Electron Ag(I)/Ag(III) Redox Cycles in Coupling Catalysis

*The compound labelled as **2a** in this section does not correspond to the same compound **2a** in Section V.1.*

Reports on silver coupling chemistry, typically operated through two-electron redox steps in protocols that employ catalysts based on other transition metals, have only started to appear in the recent years and in a very limited number. This consideration is in stark contrast with the numerous breakthroughs described for the other two coinage metals, copper and gold, on coupling catalysis driven by well-established two-electron redox processes. Among the factors that have caused that the development of silver-promoted coupling methodologies to be left behind, is the conception that silver's redox nature is only one-electron-based.[37,38] In order to investigate this possible misconception and provide mechanistic information for the silver-catalysed cross-coupling arena, we decided to utilise our experience in copper(III) systems to synthesise analogous triazamacrocyclic aryl-Ag^{III} model platform that enabled the study of C-heteroatom cross-coupling reactions catalysed by silver salts.

Complex **1**-Ag^{III}, isostructural to its analogous aryl-Cu^{III} complex **1**-Cu^{III},[39] was obtained upon reaction of **L_1-Br** with 2 equiv. of $AgClO_4$. Single crystals suitable for X-ray diffraction analysis were grown by slow diffusion of Et_2O into an CH_3CN solution and the structure of the complex was revealed to be a tetracoordinated silver centre in a nearly square planar environment, in which the metal is bonded to an aryl moiety and three amine nitrogen atoms in the same plane (**Figure V. 2**). The charge balance of the complex in addition to the short Ag-C bond length of 1.974 Å and the DFT (B3LYP-D_2/6-311+G**) calculation of its spin densities indicates that the metal centre is best described as silver(III) (See **Annex II. Supplementary Figure 1.**).

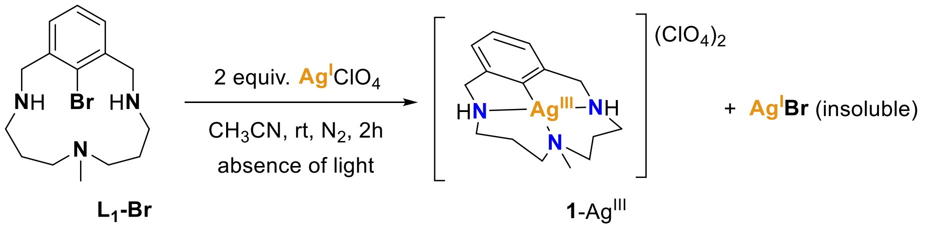

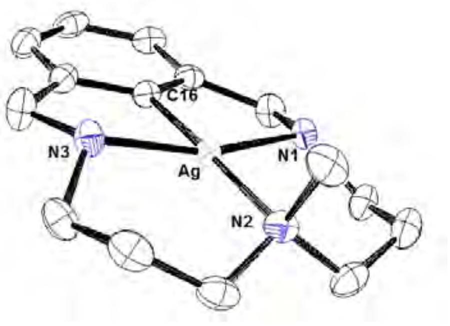

1-Ag^{III}

Figure V. 2. ORTEP thermal ellipsoid diagram (at 50 % probability level) of the cationic moiety of **1**-Ag^{III} complex. The hydrogen atoms and the two perchlorate counteranions have been omitted for clarity. Selected bond lengths (Å) and angles (°) for **1**-Ag^{III}: Ag-C(16) 1.974(2), Ag-N(3) 2.084(2), Ag-N(1) 2.085(5), Ag-N(2) 2.153(2); C(16)-Ag-N(3) 82.03(10), C(16)-Ag-N(1) 81.6(1), N(3)-Ag-N(2) 98.2(1), N(1)-Ag-N(2) 98.4(1), C(16)-Ag-N(2) 178.2(1), N(3)-Ag-N(1) 162.1(1).

^1H NMR and $^1H\{^{109}Ag\}$ NMR studies provided conclusive evidence that in solution **1**-Ag^{III} complex maintains the same structure observed in the solid state. The ^1H NMR spectrum is similar to that of the analogous aryl-Cu^{III} complex but several signals presented different *J* multiplicities (**Figure V. 3**, and **Annex II. Supplementary Figures 2-9**).[39] The two diastereotopic H^c and H^d benzylic protons display a typical AB spin system showing a doublet of doublets and a doublet at 4.86 and 4.73 ppm, respectively (**Figure V. 3**, left). The ^1H NMR spectrum must be understood as a superimposition of two sets of equivalent signals, with similar chemical shifts and coupling sizes, corresponding to the different ^{107}Ag and ^{109}Ag isotopomers.[40] The 1D ^{109}Ag-decoupled ^1H spectrum, referred to $^1H\{^{109}Ag\}$ NMR experiment, showed a pseudo doublet of triplets for H^c whereas a doublet remained for H^d (**Figure V. 3**, right). A detailed analysis of the resulting ^{109}Ag-decoupled multiplets revealed the overlapping of two signals for each resonance, one ^{109}Ag-decoupled doublet and an unaffected doublet of doublets which came from the different ^1H-^{109}Ag and ^1H-^{107}Ag coupling patterns, respectively. To confirm this phenomenon, a ^1H-^{109}Ag HMBC experiment was carried out to check for the presence of scalar coupling interactions between the ^{109}Ag center with protons separated by 3 or 4 bonds, and also to determine indirectly the important value for the ^{109}Ag chemical shift (2,127 ppm), which is in close agreement to those reported for other silver(III) complexes (**Annex II. Supplementary Figure 5**).[41,42] In addition, the quantitative measurement of a complete set of small $J(^1H\text{-}^{109}Ag)$ coupling constants was also performed from HSQMBC-IPAP experiments (**Annex II. Supplementary Figure 6**), where values of $^3J(H^c\text{-}^{109}Ag) = 11.5$ Hz and $^3J(H^d\text{-}^{109}Ag) = 1.5$ Hz were measured. The NMR studies, together with the high resolution mass spectrometry (HRMS) analysis ($[C_{15}H_{24}N_3AgClO_4]^+$, m/z = 454.0495; **Annex II. Supplementary Figure 10**), provide a clear indication that the silver(III) complex has the same structure in solution as in the solid state.

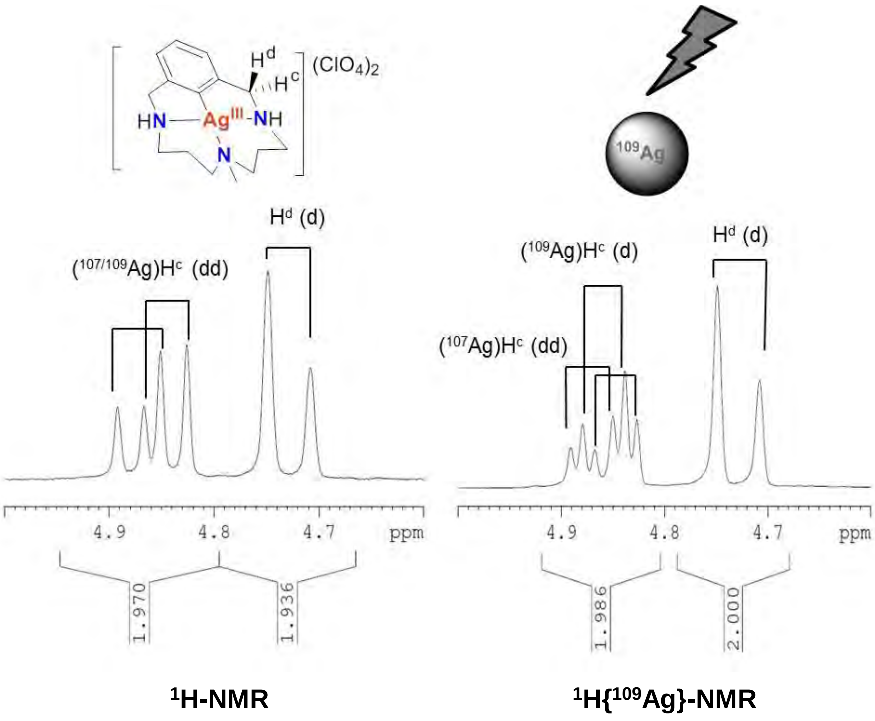

Figure V. 3. Comparison of the benzylic region of **1**-Ag^{III} in the ^{1}H NMR and ^{1}H{^{109}Ag} NMR experiments (298 K, CD_3CN, 400 MHz)

As described, in the reaction for the formation of **1**-Ag^{III} complex, 2 equiv. of silver were needed to reach nearly quantitative yields upon reaction with **L$_1$-Br** and **L$_1$-I** model substrates. We reasoned that this was due to the consumption of the first equivalent for the cleavage of the C-halogen bond and the second equivalent for precipitation of AgX upon trapping of the released halide. These results could also be interpreted as a bimetallic activation of the C-halogen bond. However, when the reaction was carried out with only 1 equiv. of a silver salt in presence of Tl(OTf) to directly compete with silver for the precipitation of the generated halides, yields above 50 % (for instance a 68 % yield of **1**-Ag^{III} from **L$_1$-I**) were obtained ruling out bimetallic pathways and supporting a monometallic oxidative addition process (**Annex II. Supplementary Table 1**). Interestingly, analogous reactions using **L$_1$-Cl** model substrates did not afford the desired aryl-Ag^{III} complex.

DFT-computed reaction profiles for the oxidative addition of silver(I) salts to **L$_1$-F**, **L$_1$-Cl**, **L$_1$-Br** and **L$_1$-I** showed a decrease in the energy barriers ($\Delta G^{\neq}$ (**L$_1$-X**) = 33.2, 18.1, 14.4, 11.2 kcal·mol^{-1} for X = F, Cl, Br, I respectively) and reaction thermodynamics (ΔG (**L$_1$-X**) = 17.6, 1.8, 0.8, -7.5 kcal·mol^{-1} (X = F, Cl, Br, I respectively) as the C-X bond strength decreases (for computed reaction profiles see **Annex II. Supplementary Figure 17**). The trends inferred from DFT calculations nicely agree with the feasible formation of **1**-Ag^{III} complex from reaction with **L$_1$-Br** and **L$_1$-I** but not with **L$_1$-Cl**.

Complex **1**-Ag^{III} in a direct parallel to its analogous copper(III) complex **1**-Cu^{III} underwent coupling with a broad range of nucleophiles of different nature.[43-47] **1**-Ag^{III} reacted readily with sulphonamides, aromatic and aliphatic carboxylic acids, phenols and thiophenols to generate the corresponding C$_{aryl}$-nucleophile coupling products in excellent yields (products **2a-2g**). Reaction of **1**-Ag^{III} with 10 equiv. benzenesulphonamide proceeded slowly at 50 ºC and afforded nearly quantitative yields of the corresponding C-N coupling product after 72 h (**Table V. 4**, entry 1). **1**-Ag^{III} showed faster reaction rates for C-O bond forming couplings with carboxylic acids even employing lower amounts of the substrate and lower temperatures (40 ºC). Benzoic acid, possessing a lower pK_a than acetic acid, reacted much faster leading to 85 % product formation in 6 h, whereas reaction with acetic acid needed 24 h to furnish the C-O coupling product in a 92 % yield (**Table V. 4**, entries 2 and 3). Reaction with phenols having closer acidities compared to the described carboxylic acids were faster, as observed for the couplings of *p*-nitrophenol and *p*-cyanophenol, in which 2 equiv. of the substrates underwent quantitative coupling with **1**-Ag^{III} in only 3 h (**Table V. 4**, entries 4 and 5). For *p*-cresol, having a pK_a of 18.9, coupling required heating the reaction mixture to 70 ºC and increasing the loading of the phenol to 10 equiv. to quantitatively produce **2f** (**Table V. 4**, entry 6). However, *p*-thiocresol was the substrate which exhibited the fastest reactivity with **1**-Ag^{III}, reaching completion after only 1 min. (**Table V. 4**, entry 7) driven by the rapid displacement of the reaction due to the formation of very insoluble Ag^{I}-sulfide species. Importantly, the described coupling reactions took place through pathways not involving the formation of free diffusing radicals as demonstrated by the fact that coupling reactions remained unaffected by the addition of TEMPO (**Table V. 4,** entry 4).

Table V. 4. Stoichiometric coupling of the aryl-Ag^{III} complex **1**-Ag^{III} with nucleophiles.

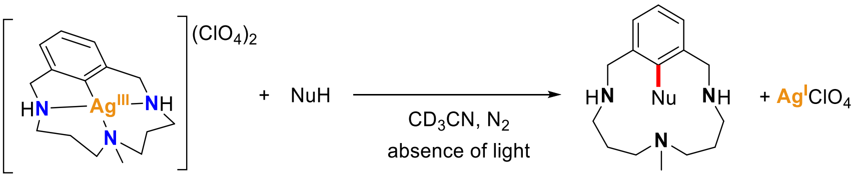

1-Ag^{III}

2x (C-N, C-O, C-S & C-C)
L$_1$-X (C-CN & C-halide)

Entry	Substrate	Equiv.	T	p*K*a (DMSO)	t	% yield[a] (product label)
1	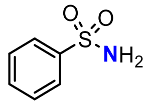	10	50 ºC	16.1	72 h	94% (**2a**)
2	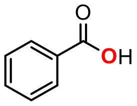	3	40 ºC	11	6h	85% (**2b**)

3	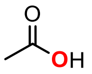	3	40 ºC	12.6	24h	92% (**2c**)
4	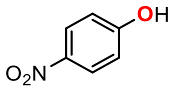	2	40 ºC	10.8	3 h	100% (**2d**)[b]
5	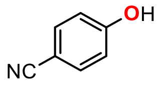	2	40 ºC	13.2	3 h	100% (**2e**)
6	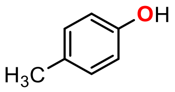	10	70 ºC	18.9	7 h	100% (**2f**)
7	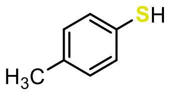	3	rt	10.3-11.2	1 min	100% (**2g**)
8[c]	NaCN	10	rt	-	2 h	81% (**L$_1$-CN**)
9	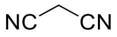	3	rt	11.1	18 h	97% (**2h**)[d]
10[e]	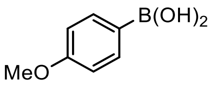	5	50 ºC	-	12 h	97% (**2i**)
11[e]	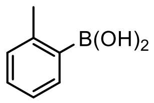	5	50 ºC	-	12h	89% (**2j**)
12[f]	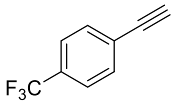	1.5	rt	≈ 28.8	24 h	63% (**2k**)[g]
13	nBu$_4$NI	2	rt	-	1 min	97% (**L$_1$-I**)
14	nBu$_4$NBr	2	rt	-	30 min	99% (**L$_1$-Br**)
15	nBu$_4$NCl	2	40 ºC	-	3.5 h	97% (**L$_1$-Cl**)
16	nBu$_4$NF·3H$_2$O	2	40 ºC	-	24 h	39% (**L$_1$-F**)

General conditions: [**1**-Ag^{III}] = 12 mM, [NuH] = 24-120 mM, 0.7 mL CD$_3$CN. [a] Calculated by ^{1}H NMR spectroscopy using 1,3,5-trimethoxybenzene as internal standard. [b] 90% in the presence of 1 equiv. of TEMPO. [c] 10% **1**-Ag^{III} (remaining starting material). [d] **2h** consists of the expected C-C coupling product followed by intramolecular reorganization, see **Table. V. 6** and ref. 46 [e] Mixture of solvents CD$_3$CN:CD$_3$OD 1:1. [f] 15% **1**-Ag^{III} (remaining starting material). [g] **2k** consists of the expected C-C coupling followed product by intramolecular reorganization, see ref. 47

Notably, this reactivity is not restricted to C-heteroatom couplings but can be extended also to C-C bond forming reactions. Indeed, 10 equiv. of sodium cyanide reacted rapidly with the aryl-Ag^{III} complex at room temperature to furnish an 81 % yield in 2 h (**Table V. 4**, entry 8). Furthermore, when malononitrile or *p*-ethynyl-*α*,*α*,*α*-trifluorotoluene were employed as the coupling partners at room temperature, the corresponding products of coupling plus intramolecular cyclisation were obtained in 97 % and 63 % yields after 18 h and 24 h respectively (**Table V. 4**, entries 9 and 12). This chemistry is analogous to that reported for the aryl-Cu^{III} system.[46,47] Remarkably, upon reaction with 5 equiv.of *o*-tolylboronic acid and *p*-

methoxyphenylboronic acid at 50 °C, the corresponding products containing biaryl scaffolds were produced in excellent yields giving for the first time an indication that boronic acids can effectively transmetallate with silver(III) centres.

Finally, C-halide coupling reactions were explored by treating **1**-Ag^{III} with 2 equiv. of *n*Bu_4NX (X = I, Br, Cl) to furnish quantitative yields of the corresponding **L_1-X** products. Contrarily to the trend observed previously for the aryl-Cu^{III} complex **1**-Cu^{III},[44] its silver analogue **1**-Ag^{III} reacted faster as the halide atomic mass increases.

Table V. 5. Silver-mediated fluorination of aryl bromide model substrates.

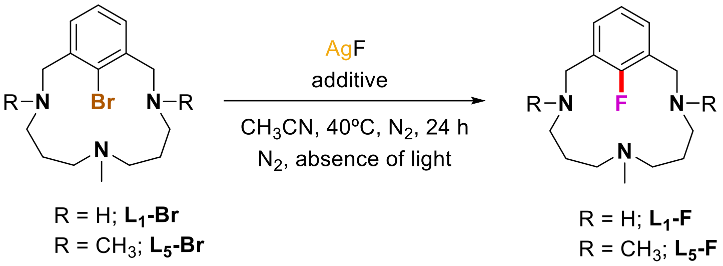

Substrate	Equiv. of AgF	Additive	% yield[a] (product label)
L_1-Br	2	-	42 (**L_1-F**)[b]
L_1-Br	1	AgOTf (1 equiv.)	86 (**L_1-F**)[c]
L_5-Br	1	-	50 (**L_5-F**)[d]
L_5-Br	2	-	100 (**L_5-F**)

General conditions: model aryl halide (**L_n-Br**) 12-14 µmol, AgF 12-28 µmol, AgOTf 0-12 µmol, 2 mL CH_3CN, 40 °C. [a] Calculated by ^1H NMR spectroscopy using 1,3,5-trimethoxybenzene as internal standard. [b] 13 % of intramolecular C-N coupling product.[35] [c] 8 % of intramolecular C-N coupling product. [d] 20 % of **L_1-Br** (remaining starting material).

Aryl fluorination, though, proved more challenging, and the application of the conditions employed for the coupling of the other halides resulted in only a 39 % yield of the desired fluorinated arene (**Table V. 4**, entry 16) due to the detrimental deprotonation of **1**-Ag^{III} complex by the inherently basic fluoride anion (see **Annex II. Supplementary Figures 13 and 14** for the characterisation of the deprotonated complex). To overcome this obstacle and drive the fluorination reactions to full conversion into the fluorinated arene, two strategies were followed: the first consisted in reacting the model aryl bromide substrate **L_1-Br** with an insoluble source of fluoride, such as AgF, to prevent significant deprotonation of the ligand. ^1H NMR monitoring of these reactions revealed that these reactions occur through the formation of **1**-Ag^{III} species (see **Annex II: Supplementary Figure 15**). The second strategy consisted in employing the analogous *N*-permethylated **L_1-Br** aryl bromide model substrate to carry out the fluorination protocol. Both approaches resulted in the generation of the desired C-F coupled products in good to excellent yields (**Table V. 5**). DFT calculations showed a strongly exergonic ($\Delta G = -25.8$ kcal·mol^{-1}) reductive elimination that presents a very low barrier ($\Delta G^{\neq} = 8.6$ kcal·mol^{-1} See **Annex II: Supplementary Figure 16** for computed reaction profile)

At this point it was still not completely clear whether the coupling reactions proceeded through a process involving the formation of radicals or rather a two-electron process. In order to evaluate the possibility of an initial single electron transfer (SET) step in the coupling reactions, Cyclic Voltammetry (CV) measurements of **1**-Ag^{III} were performed. CV experiments indicate that the Ag^{III}/Ag^{II} couple is electrochemically irreversible and has a reduction potential of -0.6 V versus non-aqueous Ag/AgNO$_3$ reference electrode (**Annex II. Supplementary Figure 26**). Given the oxidation potential value of $E^o > 1.3$ V (versus Ag/AgNO$_3$) for *p*-nitrophenol,[48,49] a potential SET step of the *p*-nitrophenol to silver(III) to produce a phenoxyl radical and aryl-Ag^{II} (1.9 V difference, $\Delta G^o = 43.8$ kcal·mol^{-1}) is very disfavoured. DFT calculations are in agreement with a highly endergonic initial SET ($\Delta G = 41.6$ kcal·mol^{-1}) (**Annex II. Supplementary Figure 27** for computed reaction profile), thus disproving a first SET step in the mechanism of these catalytic systems. Furthermore, a small energy barrier of 16.6 kcal·mol^{-1} was found for the reductive elimination of aryl-Ag^{III}-(*p*NO$_2$-phenolate) to furnish its corresponding C-O coupling product and silver(I) when computed by DFT (**Annex II. Supplementary Figure 28**). UV-Vis monitoring of the decay of **1**-Ag^{III} in the presence of *p*-cyanophenol allowed us to elaborate an Eyring plot to determine the activation parameters of the reaction providing a value of $\Delta G^{\neq}$ (298 K) = 24.5 ± 0.6 kcal·mol^{-1}(Eyring plot of the reaction **Annex II. Supplementary Figure 29**). This value matches reasonably that computed for the two-electron reductive elimination process.

Once the nature of the two-electron redox Ag^{I}/Ag^{III} oxidative addition and reductive elimination steps had been demonstrated, the chemistry was further challenged by merging both steps to realise a catalytic process. The first attempts using **L$_1$-I**, *p*-nitrophenol (2 equiv.) and 10 mol % of AgOTf as the catalyst in CH$_3$CN in the absence of light failed to provide catalytic turnover and only 9% of the desired C-O coupling product **2d** was observed together with a yellow precipitate corresponding to AgI (**Table V. 6**, entry 1). A combination of a large excess of the nucleophile and the presence of triphenylphosphine in the reaction mixture was found to prevent the precipitation of the silver(I) cations in solution furnishing the biaryl ether product **2d** in a 46 % yield (**Table V. 6**, entry 3, for the optimisation of the catalytic experiments and its discussion see **Annex II. Supplementary Table 2** and **Supplementary Discussion 1**). Increasing the catalyst and auxiliary ligand loadings to 20 mol % resulted in yields above the 70 % yield of the desired C-O coupling products derived from using *p*-nitrophenol and *p*-cyanophenol as coupling partners (**Table V. 6**, entries 5 and 6). This indicates that the catalysis behaves coherently and this catalytic protocol can be extended to other phenols. Importantly, the catalytic activity could be extended to C-C couplings, as shown by the 68 % yield of **2h** product obtained by replacing phenols by malononitrile as the coupling partner of the reaction and using 10 mol % of AgOTf (**Table V. 6**, entry 8). Moreover, **L₁-I** model aryl halide could be replaced by **L₁-Br**, possessing a stronger C_{aryl}-halide bond, although the yields of the catalysis dropped to a 21 % yield of **2d** (**Table V. 6**, entry 9). However, reaction outcomes were enhanced by using excess of Tl(OTf) as additive (**Table V. 6**, entry 10).

Table V. 6. Silver-catalysed C-O and C-C bond forming cross-coupling reactions within **L₁-X** model aryl halide substrates.

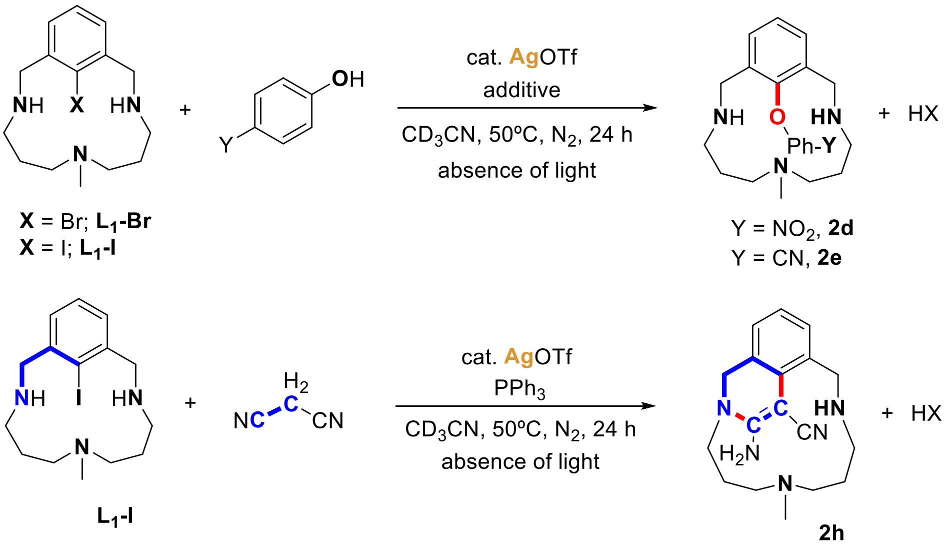
NH X HN
N
X = Br; L1-Br
X = I; L1-I
+
OH
Y
cat. AgOTf
additive
CD3CN, 50°C, N2, 24 h
absence of light
NH O HN
Ph-Y
N
+ HX
Y = NO2, 2d
Y = CN, 2e
NH I HN
N
L1-I
+
H2
NC C CN
cat. AgOTf
PPh3
CD3CN, 50°C, N2, 24 h
absence of light
N C C HN
H2N CN
N
+ HX
2h

Entry	Substrate	Equiv. NuH	mol % AgOTf	Additive (mol %)	% yield[a] (product label)
1	**L₁-I**	2	10	-	9 (**2d**)
2		20	10	-	37 (**2d**)
3		20	10	PPh_3 (10)	46 (**2d**)
4		20	**1**-Ag^{III} (10)	PPh_3 (10)	48 (**2d**)
5		20	20	PPh_3 (20)	74 (**2d**)
6		20	20	PPh_3 (20)	70 (**2e**)
7		10	10	-	44 (**2h**)
8		10	10	PPh_3 (10)	64 (**2h**)
9	**L₁-Br**	20	10	PPh_3 (10)	21 (**2d**)
10[b]		20	10	PPh_3 (10) + TlOTf (2 equiv.)	43 (**2d**)

General conditions: [**L₁-X**] = 5 mM, [NuH] = 50-100 mM, 3 mL CH_3CN, 50 °C. [a] Calculated by ^1H NMR spectroscopy using 1,3,5-trimethoxybenzene as internal standard. [b] Reaction performed at rt.

Finally, a crucial experiment was performed, using **1**-Ag^{III} as the catalyst and under the standard catalysis conditions used for the reactions promoted by silver(I) salts. The experiment resulted in the same yields of C-O coupling product as the catalytic experiments carried out with silver(I) as the catalyst (**Table V. 6**, entry 4), revealing that aryl-Ag^{III} species are competent intermediates in these transformations. Indeed, this experiment is in agreement with the identification of aryl-Ag^{III} species (4%) during the course of the catalysis (See **Annex II. Supplementary Figure 18**).

At this the influence of the excess of the phenol substrate and triphenylphosphine in providing turnover to the catalytic reactions was considered in terms of studying the factors that prevent the precipitation of silver(I) in solution when these components are present in solution. Indeed, turbidity measurements revealed that large excesses of *p*X-phenol delay the precipitation of silver(I) (for turbidity monitoring measurements see **Annex II. Supplementary Figure 19**) most plausibly due to the generation of coordination complexes with silver(I) (see **Annex II. Supplementary Figure 20** and **21** for HRMS experiments). Also, the slight improvement in the catalytic reactions resulting from the addition of triphenylphosphine may relate to the formation of $[Ag^I(PPh_3)_2]^+$ species, detected by HRMS (**Annex II. Supplementary Figure 25**). Interestingly, excess of iodide caused the formation of monoanionic $Ag^II_2^-$, a highly soluble species (see **Annex II. Supplementary Figures 22** and **23** for HRMS experiments). Indeed, monoanionic dihalide silver(I) species can participate in model halide exchange catalysis as demonstrated by reacting **L$_1$-I** with 10 mol % AgOTf in the presence of 10 equiv. of *n*Bu$_4$NBr. The bromination of **L$_1$-I** reaction took place quantitatively in 24 h with no sign of precipitation during the catalysis (**Scheme V. 4**) showing formation of $Ag^II_2^-$, Ag^IBrI^- and $Ag^IBr_2^-$ species during the catalysis as detected by HRMS experiments (**Annex II. Supplementary Figure 25**).

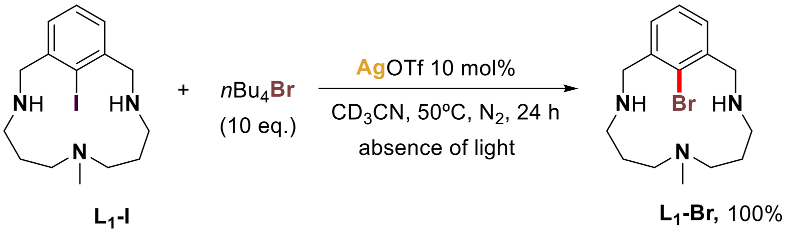

Scheme V. 4. Silver-catalysed bromination of model aryl iodide **L$_1$-I** substrate.

From all the data collected during this study it was possible to propose a general two-electron based Ag^I/Ag^{III} mechanistic proposal as depicted in **Scheme V. 5**.

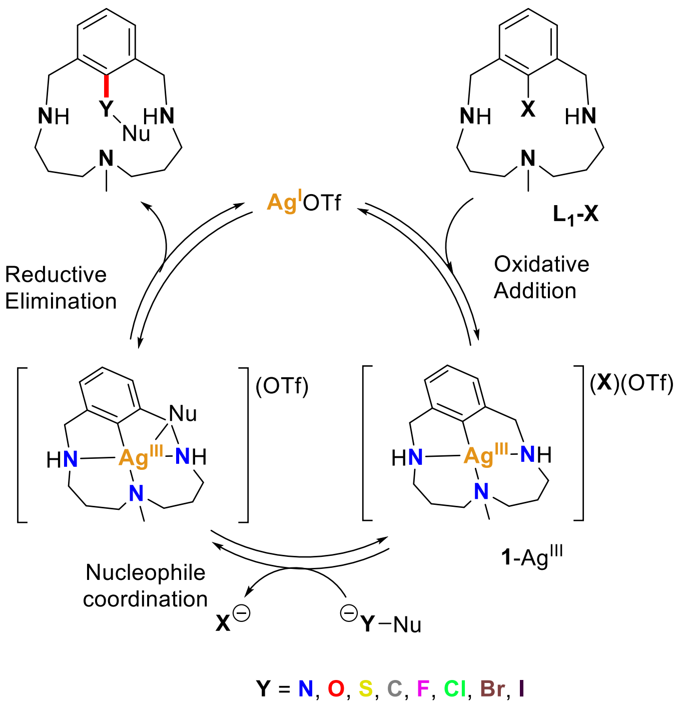

Scheme V. 5. Mechanistic proposal for the catalytic cycle of the model silver-catalysed cross-coupling reactions operating *via* aryl-Ag^{III} species.

Herein the first example of a well-defined Ag^{I}/Ag^{III} redox cycle involving oxidative addition and reductive elimination fundamental steps has been described. This reactivity is operative in model silver-catalysed C-nucleophile cross-coupling reactions with a broad variety of substrates ranging from phenols to arylboronic acids. Hence, this study reveals that silver redox chemistry is not restricted to one-electron processes and provides mechanistic understanding for an unprecedented reactivity for silver parallel to the well-known Pd^{0}/Pd^{II} and Cu^{I}/Cu^{III} catalysis. Interestingly, silver and copper present some different features in the context of the described macrocyclic platform. For instance, silver is only capable of furnishing complex **1**$_{\mathbf{ClO4}}$ upon reaction with macrocyclic aryl halide ligands containing weak C-Br and C-I bonds, while copper can also activate the corresponding **L**$_{\mathbf{1}}$**-Cl** ligand to generate the **1**-Cu^{III} complex. Another fundamental divergence between the behavior of silver and copper originates in terms of selectivity. Analogous complexes **1**-Ag^{III} and **1**-Cu^{III} react upon treatment of aryl boronic acid to form different coupling products. **1**-Ag^{III} affords the corresponding C-C$_{sp2}$ coupling product arising from the transmetallation of the aryl boronic acid and subsequent reductive elimination to produce biaryl scaffolds, whereas **1**-Cu^{III} forms the C-O coupling product resulting from the coupling with methanol, the co-solvent employed in the reaction. Given the revealed inherent complementary reactivity of silver with respect to copper, new perspectives on exploiting the applicability of this potential orthogonality of the two metals towards real synthetic problems arise.

V.3. References

(1) Corbet, J.-P.; Mignani, G. *Chem. Rev.* **2006**, *106*, 2651.
(2) Wolfe, J. P.; Wagaw, S.; Marcoux, J.-F.; Buchwald, S. L. *Acc. Chem. Res.* **1998**, *31*, 805.
(3) Hartwig, J. F. *Acc. Chem. Res.* **2008**, *41*, 1534.
(4) Godula, K.; Sames, D. *Science* **2006**, *312*, 67.
(5) Friedman, D.; Masciangioli, T.; Olson, S. *The Role of Chemical Sciences in Finding Alternatives to Critical Resources. A Workshop Summary.*; The National Academies Press: Washington, D.C., 2012; p. 59 pp.
(6) For an historical overview of cross-coupling reactions see: Johansson Seechurn, C. C. C.; Kitching, M. O; Colacot, T. J.; Snieckus, V. *Angew. Chem. Int. Ed.* **2012**, *51*, 5062.
(7) Surry, D. S.; Buchwald, S. L. *Chem. Sci.* **2010**, *1*, 13.
(8) Evano, G.; Blanchard, N.; Toumi, M. *Chem. Rev.* **2008**, *108*, 3054.
(9) Monnier, F.; Taillefer, M. *Angew. Chem. Int. Ed.* **2009**, *48*, 6954.
(10) Casitas, A.; Ribas, X. *Chem. Sci.* **2013**, *4*, 2301.
(11) Shrift, A. *Bot. Rev.* **1958**, *24*, 550.
(12) Kaldor, S. W.; Kalish, V. J.; Davies, J. F.; Shetty, B. V.; Fritz, J. E.; Appelt, K.; Burgess, J. A.; Campanale, K. M.; Chirgadze, N. Y.; Clawson, D. K.; Dressman, B. A.; Hatch, S. D.; Khalil, D. A.; Kosa, M. B.; Lubbehusen, P. P.; Muesing, M. A.; Patick, A. K.; Reich, S. H.; Su, K. S.; Tatlock, J. H. *J. Med. Chem.* **1997**, *40*, 3979.
(13) Liu, G.; Link, J. T.; Pei, Z.; Reilly, E. B.; Leitza, S.; Nguyen, B.; Marsh, K. C.; Okasinski, G. F.; von Geldern, T. W.; Ormes, M.; Fowler, K.; Gallatin, M. *J. Med. Chem.* **2000**, *43*, 4025.
(14) Liu, L.; Stelmach, J. E.; Natarajan, S. R.; Chen, M.-H.; Singh, S. B.; Schwartz, C. D.; Fitzgerald, C. E.; O'Keefe, S. J.; Zaller, D. M.; Schmatz, D. M.; Doherty, J. B. *Bioorg. Med. Chem. Lett.* **2003**, *13*, 3979.
(15) He, G.-X.; Krise, J. P.; Oliyai, R. In *Prodrugs: Challenges and Rewards Part 1*; Stella, V. J.; Borchardt, R. T.; Hageman, M. J.; Oliyai, R.; Maag, H.; Tilley, J. W., Eds.; Springer New York: New York City, New York, 2007; pp. 923–964.
(16) Narajji, C.; Karvekar, M. D.; Das, A. K. *Indian J. Pharm. Sci.* **2007**, *69*, 344.
(17) Gangjee, A.; Zeng, Y.; Talreja, T.; Mcguire, J. J.; Kisliuk, R. L.; Queener, S. F. *J. Med. Chem.* **2007**, *50*, 3046.
(18) Gu, X.; Zhu, Y.-Z. *Expert Rev. Clin. Pharmacol.* **2011**, *4*, 123.
(19) Wirth, T. *Organoselenium Chemistry: Modern Developments in Organic Synthesis*; Springer-Verlag: Berlin, 2000; p. 259 pp.
(20) Gelman, D.; Jiang, L.; Buchwald, S. L. *Org. Lett.* **2003**, *5*, 2315.
(21) Beletskaya, I. P.; Cheprakov, A. V. *Coord. Chem. Rev.* **2004**, *248*, 2337.
(22) Bates, C. G.; Saejueng, P.; Doherty, M. Q.; Venkataraman, D. *Org. Lett.* **2004**, *6*, 5005.
(23) Rout, L.; Saha, P.; Jammi, S.; Punniyamurthy, T. *Eur. J. Org. Chem.* **2008**, 640.
(24) Sperotto, E.; van Klink, G. P. M.; de Vries, J. G.; van Koten, G. *J. Org. Chem.* **2008**, *73*, 5625.
(25) Sperotto, E.; van Klink, G. P. M.; de Vries, J. G.; van Koten, G. *Tetrahedron* **2010**, *66*, 9009.
(26) Xu, R.; Wan, J.-P.; Mao, H.; Pan, Y. *J. Am. Chem. Soc.* **2010**, *132*, 15531.
(27) Kabir, M. S.; Lorenz, M.; van Linn, M. L.; Namjoshi, O. A.; Ara, S.; Cook, J. M. *J. Org. Chem.* **2010**, *75*, 3626.
(28) Beletskaya, I. P.; Ananikov, V. P. *Chem. Rev.* **2011**, *111*, 1596.
(29) Kao, H.-L.; Lee, C.-F. *Org. Lett.* **2011**, *13*, 5204.
(30) Zhao, M.; Wang, F.; Li, X. *Org. Lett.* **2012**, *14*, 1412.
(31) Alayrac, C.; Gaumont, A.-C. In *Copper-Mediated Cross-Coupling Reactions*; Evano, G.; Blanchard, N., Eds.; John Wiley & Sons, Inc: Hoboken, New Jersey, 2013; pp. 93–112.
(32) Cheng, S.-W.; Tseng, M.-C.; Lii, K.-H.; Lee, C.-R.; Shyu, S.-G. *Chem. Commun.* **2011**, *47*, 5599.
(33) Bordwell, G. *Acc. Chem. Res.* **1988**, *21*, 456.
(34) Zhuang, R.; Xu, J.; Cai, Z.; Tang, G.; Fang, M.; Zhao, Y. *Org. Lett.* **2011**, *13*, 2110.
(35) Casitas, A.; Canta, M.; Solà, M.; Costas, M.; Ribas, X. *J. Am. Chem. Soc.* **2011**, *133*, 19386.
(36) Huffman, L. M.; Casitas, A.; Font, M.; Canta, M.; Costas, M.; Ribas, X.; Stahl, S. S. *Chem. Eur. J.* **2011**, *17*, 10643.
(37) Tang, P.; Furuya, T.; Ritter, T. *J. Am. Chem. Soc.* **2010**, *132*, 12150.
(38) Seo, S.; Taylor, J. B.; Greaney, M. F. *Chem. Commun.* **2013**, *49*, 6385.
(39) Ribas, X.; Jackson, D. A.; Donnadieu, B.; Mahía, J.; Parella, T.; Xifra, R.; Hedman, B.; Hodgson, K. O.; Llobet, A.; Stack, T. D. P. *Angew. Chem. Int. Ed.* **2002**, *41*, 2991.
(40) Penner, G. H.; Liu, X. *Prog. Nucl. Magn. Reson. Spectrosc.* **2006**, *49*, 151.

(41) Eujen, R.; Hoge, B.; Brauer, D. J. *Inorg. Chem.* **1997**, *36*, 1464.
(42) Eujen, R.; Hoge, B.; Brauer, D. J. *Inorg. Chem.* **1997**, *36*, 3160.
(43) Huffman, L. M.; Stahl, S. S. *J. Am. Chem. Soc.* **2008**, *130*, 9196.
(44) Casitas, A.; King, A. E.; Parella, T.; Costas, M.; Stahl, S. S.; Ribas, X. *Chem. Sci.* **2010**, *1*, 326.
(45) Font, M.; Parella, T.; Costas, M.; Ribas, X. *Organometallics* **2012**, *31*, 7976.
(46) Rovira, M.; Font, M.; Ribas, X. *ChemCatChem* **2013**, *5*, 687.
(47) Rovira, M.; Font, M.; Acuña-Parés, F.; Parella, T.; Luis, J. M.; Lloret-Fillol, J.; Ribas, X. *Chem. Eur. J.* **2014**, *20*, 10005.
(48) Osako, T.; Ohkubo, K.; Taki, M.; Tachi, Y.; Fukuzumi, S.; Itoh, S. *J. Am. Chem. Soc.* **2003**, *125*, 11027.
(49) Garcia-Bosch, I.; Ribas, X.; Costas, M. *Chem. Eur. J.* **2012**, *18*, 2113.

CHAPTER VI.

GENERAL CONCLUSIONS

VI. GENERAL CONCLUSIONS

In **Chapter III**, a model aryl-Cu^{III} complex bearing a triazamacrocyclic chelating ligand is the starting point of the study. Stoichiometric reactions of sulphur-, selenium- and phosphorus-based nucleophiles with the **1**-Cu^{III} complex, accessible via oxidative addition from its model aryl halide precursors, result in reductive elimination processes that furnished the corresponding C-S, C-Se, C-P coupling products. UV-Vis and NMR monitoring of these reactions together with competitive experiments employing bifunctional nucleophiles as coupling partners indicate that the pK_a of the nucleophile is a key parameter albeit sterics and other parameters must be taken into account. The plausibility of Cu^{I}/Cu^{III} redox cycles governing the copper-catalysed cross-coupling reactions for the formation of C-S, C-Se and C-P bonds is further supported within our model platform by catalytic experiments that converted **L_1-X** (X = Cl, Br) into their corresponding desired products bearing biaryl thioether, biaryl selenide and aryl dialkyl phosphonate scaffolds using catalytic amounts of copper. Importantly, UV-Vis experiments determined that aryl-Cu^{III}-X (**2_X**) species are the steady-state of the catalytic versions. Overall, these results provide conclusive evidence of the competence of aryl-Cu^{III} species in cross-coupling reactions to form C-S, C-Se and C-P bonds.

In **Chapter IV**, a model aryl-Ag^{III} complex analogous to complex **1**-Cu^{III} described in Chapter III has been synthesised through C_{aryl}-halogen bond activation of model triazamacrocyclic aryl bromide and iodide substrates. **1**-Ag^{III} complex has been exhaustively characterised by crystallographic and spectroscopic techniques showing a monomeric nearly square planar complex that maintains its structure in solution. A combination of experimental and computational studies supported our proposal of monometallic activation of the aryl halides arising from oxidative addition processes that result in the formation of the complex. Further investigations have demonstrated that **1**-Ag^{III} exhibits similar reactivity compared to its aryl-Cu^{III} analogous complex, that is; it undergoes coupling reactions to form a broad range of C-nucleophile new bonds comprising C-N, C-O, C-S, C_{sp2}-C_{sp3}, C_{sp2}-C_{sp2}, C_{sp2}-C_{sp} and C-halide bonds inclusive of C-F bonds. Experiments carried out to unravel the nature of the coupling reactions, including cyclic voltammetry measurements, ruled out mechanistic pathways involving the generation of radical intermediate species. Complementation of the more experimental mechanistic studies with feasible DFT-computed reaction profiles for reductive elimination events driving the couplings clarified the two-electron nature of these couplings. The plausibility of the unprecedented engagement of silver in two-electron redox cycles involving oxidative addition and reductive elimination fundamental steps was confirmed by the formation of C-O and C_{sp2}-C_{sp3} coupling products using catalytic amounts of silver in the frame of the model triazamacrocyclic aryl halide systems through aryl-Ag^{III} species. This work provides unique evidence of two-electron processes occurring at silver centres, a redox chemistry that had not been clearly identified until this study.

ANNEX I

Supplementary Information

Catalytic C-S, C-Se and C-P cross-coupling reactions mediated by a Cu^{I}/Cu^{III} redox cycle

*Marc Font,[a] Teodor Parella,[b] Miquel Costas[a] and Xavi Ribas[a,]**

[a] QBIS Research Group, Departament de Química, Universitat de Girona, Campus Montilivi, Girona E-17071, Catalonia, Spain. [b] Servei de NMR, Facultat de Ciències, Universitat Autònoma de Barcelona, Campus UAB, Bellaterra, E-08193, Catalonia, Spain

CONTENTS

1. **Materials and Methods** 103
    1.1. Materials and methods 103
    1.2. Instrumentation 104
    1.3. Synthesis of aryl-Cu^{III} complex **1** 104
    1.4. Characterization of products with S-nucleophiles 104
    1.5. Characterization of products with Se-nucleophile 108
    1.6. Characterization of products with P-nucleophiles 109
    1.7. Characterization of products with bifunctional groups 111
    1.8. Procedure for catalytic reactions 114
2. **Supporting References** 114
3. **Supporting Figures** 115

1. Materials and Methods

1.1. Materials and methods

Reagents and solvents used were commercially available reagent quality unless otherwise noted. Solvents were purchased from SDS-Carlo Erba and Scharlab and were purified and dried by passing through an activated alumina purification system (MBraun SPS-800). Preparation and handling of air-sensitive materials were carried out in a N_2 drybox (MBraun-Unilab) with O_2 and H_2O concentrations < 1 ppm. Ligands **L1-Cl** and **L1-Br**, and aryl-Cu^{III} complex **1** were synthesized following published procedures.[1,2,3]

1.2. Instrumentation

UV-vis spectroscopy was performed on a Cary-50 (Varian) UV-vis spectrophotometer. Low temperature control was maintained with a cryostat from Unisoku Scientific Instruments, Japan. NMR data concerning product identity were collected on Bruker 600, 400 or 300 AVANCE spectrometer in the corresponding deuterated solvent ($CDCl_3$, CD_3CN) and calibrated relative to an external reference (1,3,5-trimethoxybenzene). ESI-MS experiments were collected and analyzed on a Bruker Daltonics Esquire 6000 spectrometer with acetonitrile or acetonitrile/water (80:20) as the mobile phase.

1.3. Synthesis of aryl-Cu^{III} complex 1

Caution: *Perchlorate salts are potentially explosive and should be handled with care!* Aryl-copper(III) complex **1** was prepared following procedures described in the literature previously.[1,2]

1.4. Synthesis and characterization of C$_{aryl}$-S coupling products

In an inert-atmosphere glove box, a sample of the Cu^{III}-aryl complex **1** (21.4 mg, 42 μmol) was dissolved in CD_3CN (1.6 mL) and 0.4 mL of a solution of 1,3,5-trimethoxybenzene was added as an internal standard. A portion of this solution (0.4 mL) was loaded into an NMR tube, and 1.1 equivalents of the corresponding thiophenol nucleophile were added to the tube (0.3 mL, 29.2 mM). Final concentrations: [**1**] = 12 mM and [S-nucleophile] = 12.5 mM. The tube was sealed with a screw-cap and the reaction was allowed to react at room temperature and monitored by ^{1}H-NMR spectroscopy until reaction completion. ^{1}H, COSY, NOESY, ^{1}H-^{13}C HSQC and ^{13}C-NMR spectra and mass spectrometric analysis were obtained without isolation of the C-O coupling product. Reaction yields were obtained by integration of the ^{1}H-NMR spectra of the crude reaction mixtures relative to 1,3,5-trimethoxybenbenzene.

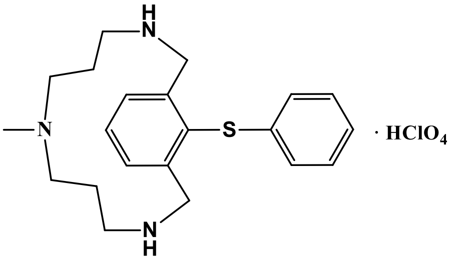

(1a)

1a. **^{1}H-NMR** (400 MHz, CD_3CN, 25 ºC) δ, ppm: 7.41-7.40 (m, 3H, H^a, H^b), 7.30-7.25 (m, 2H, H^m), 7.22-7.18 (m, 1H, H^n), 7.11-7.08 (m, 2H, H^l), 4.16 (d, 2H, *J* = 13 Hz, H^c or H^d), 3.53 (d, 2H , *J* = 13 Hz, H^c or H^d), 3.12-3.06 (m, 2H, H^i or H^j), 2.87-2.81 (m, 2H, H^e or H^f), 2.73-2.66 (m, 4H, H^i or H^j, H^e or H^f), 2.61 (s, 3H, H^k), 1.64-1.54 (m, 2H, H^g or H^h), 0.74-0.67 (m, 2H, H^g or H^h). **^{13}C-NMR** (100 MHz, CD_3CN, 25 ºC) δ, ppm: 144.5 (C_1), 137.6 (C_{10}), 134.2 (C_2), 131.8 (C_3 or C_4), 129.4 (C_{12}), 129.2 (C_3 or C_4), 127.5 (C_{11}), 126.3 (C_{13}), 55.2 (C_8), 52.7 (C_5), 46.2 (C_6), 39.9 (C_9), 24.3 (C_7). **ESI-MS** (CH_3CN, m/z): 356.2 (100) $[C_{21}H_{30}N_3S]^+$.

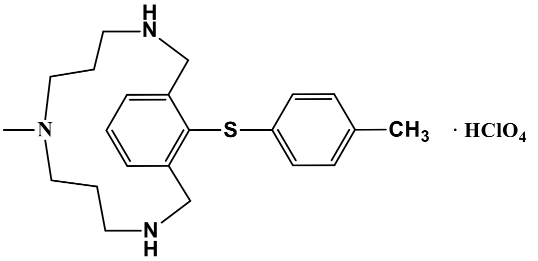

(1b)

1b. **^{1}H-NMR** (400 MHz, CD_3CN, 25 ºC) δ, ppm: 7.39-7.38 (m, 3H, H^a, H^b), 7.11-7.09 (m, 2H, H^m), 7.02-6.99 (m, 2H, H^l), 4.17 (d, 2H, *J* = 13 Hz, H^c or H^d), 3.52 (d, 2H, *J* = 13 Hz, H^c or H^d), 3.10-3.05 (m, 2H, H^i or H^j), 2.87-2.81 (m, 2H, H^e or H^f), 2.72-2.65 (m, 4H, H^e or H^f, H^i or H^j), 2.61 (s, 3H, H^k), 2.27 (s, 3H, H^n), 1.64-1.54 (m, 2H, H^g or H^h), 0.74-0.67 (m, 2H, H^g or H^h). **^{13}C-NMR** (100 MHz, CD_3CN, 25 ºC) δ, ppm: 144.1 (C_1), 136.6 (C_{13}) 134.8 (C_2), 133.8 (C_{10}) 131.8 (C_3 or C_4), 130.1 (C_{12}), 129.0 (C_3 or C_4), 127.9 (C_{11}), 55.0 (C_8), 52.7 (C_5), 46.1 (C_6), 39.9 (C_9), 24.2 (C_7), 20.0 (C_{14}). **ESI-MS** ($CH_3CN:H_2O$ (80:20), m/z): 370.2 (100) $[C_{22}H_{32}N_3S]^+$.

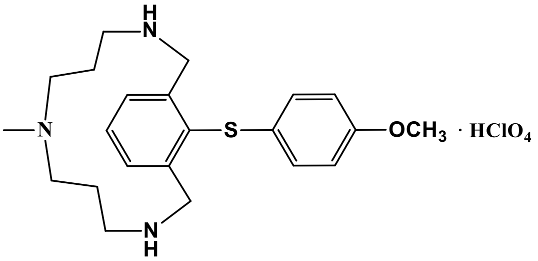

(1c)

1c. **^{1}H-NMR** (400 MHz, CD_3CN, 25 ºC) δ, ppm: 7.39 (s, 3H, H^a, H^b), 7.12-7.08 (m, 2H, H^l), 6.88-6.84 (m, 2H, H^m), 4.23 (d, 2H, *J* = 13.1 Hz, H^c or H^d), 3.75 (s, 3H, H^n), 3.57 (d, 2H , *J* = 13.1 Hz, H^c or H^d), 3.06-3.01 (m, 2H, H^i or H^j), 2.91-2.85 (m, 2H, H^e or H^f), 2.70-2.63 (m, 4H, H^i or H^j, H^e or H^f), 2.60 (s, 3H, H^k), 1.67-1.56 (m, 2H, H^g or

H^h), 0.79-0.73 (m, 2H, H^g or H^h). **^{13}C-NMR** (100 MHz, CD_3CN, 25 ºC) δ, ppm: 158.9 (C_{13}), 143.2 (C_1), 135.7 (C_2), 132.0 (C_3 or C_4), 130.3 (C_{11}), 128.9 (C_3 or C_4), 127.2 (C_{10}), 115.1 (C_{12}), 55.1 (C_{14}), 55.0 (C_8), 52.5 (C_5), 46.1 (C_6), 40.0 (C_9), 24.1 (C_7). **ESI-MS** (CH_3CN, m/z): 386.2 (100) $[C_{22}H_{32}N_3OS]^+$.

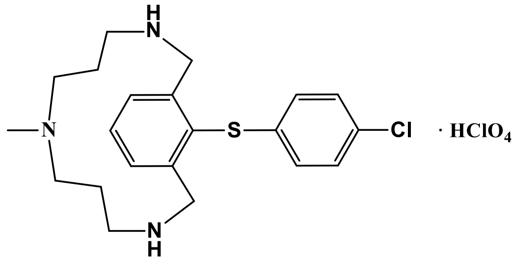

(1d)

1d. **^{1}H-NMR** (400 MHz, CD_3CN, 25 ºC) δ, ppm: 7.47-7.46 (m, 3H, H^a, H^b), 7.31-7.27 (m, 2H, H^l), 7.07-7.04 (m, 2H, H^m), 4.20 (d, 2H, J = 13.2 Hz, H^c or H^d), 3.62 (d, 2H , J = 13.2 Hz, H^c or H^d), 3.04-2.98 (m, 2H, H^i or H^j), 2.93-2.87 (m, 2H, H^e or H^f), 2.70-2.63 (m, 4H, H^i or H^j, H^e or H^f), 2.57 (s, 3H, H^k), 1.68-1.57 (m, 2H, H^g or H^h), 0.78-0.72 (m, 2H, H^g or H^h). **^{13}C-NMR** (100 MHz, CD_3CN, 25 ºC) δ, ppm: 143.6 (C_1), 136.1 (C_{10}), 133.7 (C_2), 132.4 (C_3 or C_4), 131.7 (C_{13}), 129.8 (C_3 or C_4), 129.8 (C_{11}), 128.9 (C_{12}), 55.0 (C_8), 52.4 (C_5), 46.2 (C_6), 39.9 (C_9), 23.9 (C_7). **ESI-MS** ($CH_3CN:H_2O$ (80:20), m/z): 390.2 (100) $[C_{21}H_{29}ClN_3S]^+$.

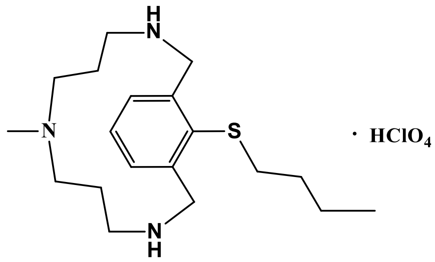

(1e)

1e. **^{1}H-NMR** (400 MHz, CD_3CN, 25 ºC) δ, ppm: 7.37-7.31 (m, 3H, H^a, H^b), 4.51 (d, 2H, J = 13.2 Hz, H^c or H^d), 3.64 (d, 2H, J = 13.2 Hz, H^c or H^d), 2.89-2.77 (m, 6H, H^e or H^f, H^i or H^j, H^l), 2.68-2.60 (m, 2H, H^e or H^f), 2,54-2.47 (m, 2H, H^i or H^j), 2.41 (s, 3H, H^k), 1.59-1.45 (m, 4H, H^g or H^h, H^m), 1.43-1.34 (m, 2H, H^n), 0.86 (t, 3H, J = 7.26, H^o), 0.77-0.68 (m, 2H, H^g or H^h). **^{13}C-NMR** (100 MHz, CD_3CN, 25 ºC) δ, ppm: 144.4 (C_1), 135.6 (C_2), 131.5 (C_3 or C_4), 128.7 (C_3 or C_4), 55.3 (C_8), 52.9 (C_5), 46.2 (C_6), 40.0 (C_9), 37.0

(C_{10}), 31.6 (C_{11}), 24.4 (C_7), 21.5 (C_{12}), 12.9 (C_{13}). **ESI-MS** (CH_3CN, m/z): 336.3 (100) $[C_{19}H_{34}N_3S]^+$.

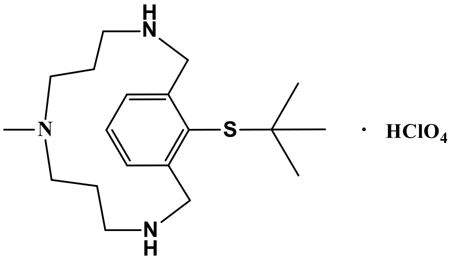

(1f)

1f. **^{1}H-NMR** (400 MHz, CD_3CN, 25 ºC) δ, ppm: 7.47-7.41 (m, 3H, H^a, H^b), 4.72 (d, 2H, *J* = 13.24 Hz, H^c or H^d), 3.70 (d, 2H, *J* = 13.24 Hz, H^c or H^d), 2.92-2.86 (m, 2H, H^e or H^f), 2.72-2.63 (m, 4H, H^i or H^j, H^e or H^f), 2,44-2.37 (m, 2H, H^i or H^j), 2.28 (s, 3H, H^k), 1.63-1.52 (m, 2H, H^g or H^h), 1.26 (s, 9H, H^l), 0.90-0.80 (m, 2H, H^g or H^h). **^{13}C-NMR** (100 MHz, CD_3CN, 25 ºC) δ, ppm: 146.4 (C_1), 132.0 (C_2), 131.6 (C_3 or C_4), 129.9 (C_3 or C_4), 55.8 (C_8), 53.0 (C_5), 50.7 (C_{10}), 46.5 (C_6), 39.4 (C_9), 30.0 (C_{11}), 24.1 (C_7). **ESI-MS** (CH_3CN, m/z): 336.2 (100) $[C_{19}H_{34}N_3S]^+$.

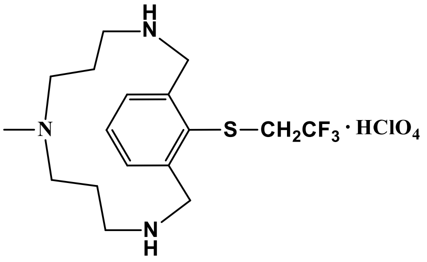

(1g)

1g. **^{1}H-NMR** (400 MHz, CD_3CN, 25 ºC) δ, ppm: 7.51 (s, 3H, H^a, H^b), 4.60 (d, 2H, *J* = 13.4 Hz, H^c or H^d), 3.89 (d, 2H, *J* = 13.2 Hz, H^c or H^d), 3.53 (q, 2H, *J* = 10.1 Hz, H^l), 3.03-2.97 (m, 2H, H^e or H^f), 2.79-2.73 (m, 4H, H^e or H^f, H^i or H^j), 2.56-2.49 (m, 2H, H^i or H^j), 2.39 (s, 3H, H^k), 1.71-1.60 (m, 2H, H^g or H^h), 0.89-0.79 (m, 2H, H^g or H^h). **^{13}C-NMR** (100 MHz, CD_3CN, 25 ºC) δ, ppm: 142.3 (C_1), 134.1 (C_2), 132.9 (C_3 or C_4), 130.7 (C_3 or C_4), 125.8 (q, $J_{C\text{-}F}$ = 276.13 Hz, C_{11}), 55.1 (C_8), 51.8 (C_5), 46.3 (C_6), 39.9 (C_9), 38.4 (q, $J_{C\text{-}F}$ = 31.98 Hz, C_{10}), 23.35 (C_7). **ESI-MS** ($CH_3CN:H_2O$ (80:20), m/z): 362.2 (100) $[C_{17}H_{27}F_3N_3S]^+$.

1.5. Synthesis and characterization of C_{aryl}-Se coupling product

The compound labelled as ***2a*** *in this section does not correspond to the same compound* ***2a*** *in Annex II.*

In an inert-atmosphere glove box, a sample of the Cu^{III}-aryl complex **1** (21.4 mg, 42 µmol) was dissolved in CD_3CN (1.6 mL) and 0.4 mL of a solution of 1,3,5-trimethoxybenzene was added as an internal standard. A portion of this solution (0.4 mL) was loaded into an NMR tube, and 1.5 equivalents of benzeneselenol were added to the tube (0.3 mL, 42 mM). Final concentrations: [**1**] = 12 mM and [HSe-Ph] = 18 mM. The tube was sealed with a screw-cap and the reaction was allowed to react at room temperature and monitored by ^{1}H-NMR spectroscopy until reaction completion. ^{1}H, ^{13}C, COSY, NOESY, ^{1}H-^{13}C HSQC and ^{1}H-^{77}Se HMBC NMR spectra and mass spectrometric analysis were obtained without isolation of the C-Se coupling product. Reaction yields were obtained by integration of the ^{1}H-NMR spectra of the crude reaction mixtures relative to internal standard.

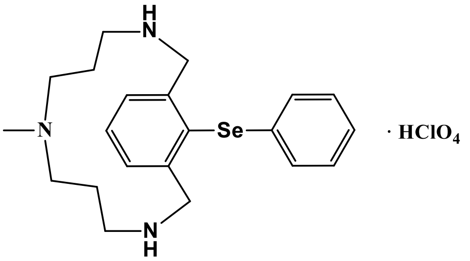

(2a)

2a. **^{1}H-NMR** (400 MHz, CD_3CN, 25 ºC) δ, ppm: 7.55 (m, 3H, H^a, H^b), 7.30 (m, 5H, H^m, H^l, H^n), 4.44 (d, 2H, J = 13.4 Hz, H^c or H^d), 3.87 (d, 2H , J = 13.4 Hz, H^c or H^d), 3.04 (m, 2H, H^e or H^f), 2.77 (m, 4H, H^e or H^f, H^i or H^j), 2.58 (m, 2H, H^i or H^j), 2.49 (s, 3H, H^k), 1.72 (m, 2H, H^g or H^h), 0.99 (m, 2H, H^g or H^h). **^{13}C-NMR** (100 MHz, CD_3CN, 25 ºC) δ, ppm: 140.5 (C_1), 133.8 (C_3 or C_4), 133.0 (C_3 or C_4), 131.7 (C_2), 130.3 (C_{10}), 130.3 (C_{11} or C_{12} or C_{13}), 129.9 (C_{11} or C_{12} or C_{13}), 127.6 (C_{11} or C_{12} or C_{13}), 54.7 (C_8), 53.2 (C_5), 46.1 (C_6), 40.7 (C_9), 23.0 (C_7). **ESI-MS** (CH_3CN:H_2O (80:20), m/z): 404.2 (100) $[C_{21}H_{30}N_3Se]^+$.

1.6. Synthesis and characterization of C$_{aryl}$-P coupling products.

In an inert-atmosphere glove box, a sample of the Cu^{III}-aryl complex **1** (21.4 mg, 42 μmol) was dissolved in CD$_3$CN (1.6 mL) and 0.4 mL of a solution of 1,3,5-trimethoxybenzene was added as an internal standard. A portion of this solution (0.4 mL), 0.25 mL of CD$_3$CN and 0.9-2 equivalents of the corresponding dialkyl phosphite nucleophile were added to the tube (0.05 mL, 0.48-0.34 M). Final concentrations: [**1**] = 12 mM and [dialkyl phosphite] = 10.8-24 mM. The tube was sealed with a screw-cap and the reaction was allowed to react at 50 ºC and monitored by ^{1}H-NMR spectroscopy until reaction completion. ^{31}P, ^{1}H, COSY, NOESY, ^{1}H-^{13}C HSQC and ^{13}C-NMR spectra and mass spectrometric analysis were obtained without isolation of the C-P coupling product. Reaction yields were obtained by integration of the ^{1}H-NMR spectra of the crude reaction mixtures relative to internal standard.

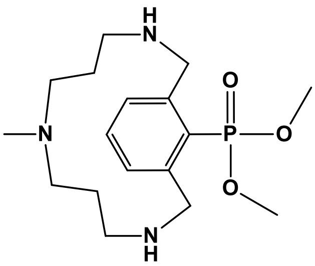

· HClO$_4$ **(3a)**

3a. **^{1}H-NMR** (400 MHz, CD$_3$CN, 25 ºC) δ, ppm: 7.48-7.45 (m, 1H, H^a), 7.34-7.31 (m, 2H, H^b), 4.72 (dd, 2H, J = 13.48 Hz, J = 1.6 Hz, H^c or H^d), 3.72 (d, 6H, J = 11.2 Hz, H^l), 3.50 (d, 2H, J = 13.6 Hz, H^c or H^d), 3.19-3.16 (m, 2H, H^i or H^j), 2.77-2.71 (m, 2H, H^e or H^f), 2.2-2.56 (m, 2H, H^i or H^j), 2.52 (s, 3H, H^k), 2.46-2.39 (m, 2H, H^e or H^f), 2.15 (bs, 3H, NH), 1.59-1.48 (m, 2H, H^g or H^h), 0.78 (bs, 2H, H^g or H^h). **^{13}C-NMR** (100 MHz, CD$_3$CN, 25 ºC) δ, ppm: 131.8 (d, $J_{C\text{-}P}$ = 3.3 Hz, C$_2$), 131.6 (C$_3$ or C$_4$), 130.5 (C$_3$ or C$_4$), 128.6 (d, $J_{C\text{-}P}$ = 146.9 Hz, C$_1$), 54.5 (d, $J_{C\text{-}P}$ = 3.5 Hz, C$_5$), 54.4 (C$_8$), 51.6 (d, $J_{C\text{-}P}$ = 6.6 Hz, C$_{10}$), 46.0 (C$_6$), 39.7 (C$_9$), 24.1 (C$_7$). **^{31}P-NMR** (162 MHz, CD$_3$CN, 25 ºC) δ, ppm: 21.3. **ESI-MS** (CH$_3$CN:H$_2$O (80:20), m/z): 356.2 (100) [C$_{17}$H$_{31}$N$_3$O$_3$P]$^+$. *This product slowly decomposes to generate the byproducts* **3a.1** *and* **3a.2. ESI-MS (**CH$_3$CN:H$_2$O (80:20), m/z): 370.2 [C$_{18}$H$_{33}$N$_3$O$_3$P]$^+$ (**3a.1**), 342.2 [C$_{16}$H$_{29}$N$_3$O$_3$P]$^+$ (**3a.2**).

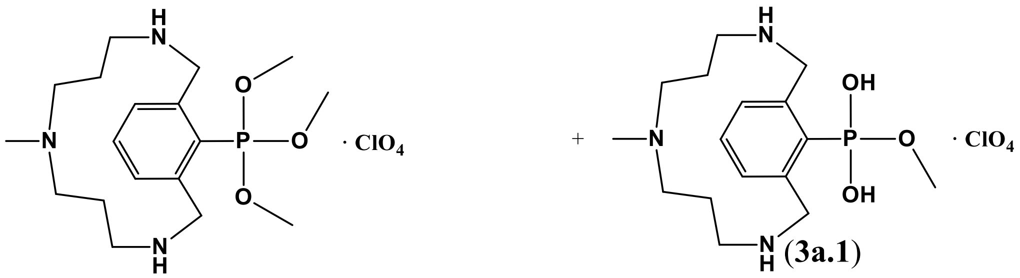

(3a.1)

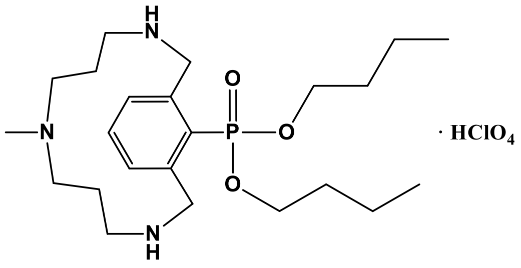

(3b)

3b. **^{1}H-NMR** (400 MHz, CD$_3$CN, 25 ºC) δ, ppm: 7.51-7.42 (m, 1H, H^a), 7.36-7.33 (m, 2H, H^b), 4.78 (d, 2H, *J* = 13.4 Hz, H^c or H^d), 4.06- 3.95 (m, 4H, H^m), 3.56-3.53 (m, 2H, H^c or H^d), 3.15-3.10 (m, 2H, H$^{i\ \mathrm{or}}$ H^j), 2.79-2.72 (m, 2H, H^e or H^f), 2,59-2.52 (m, 2H, H^i or H^j), 2.52 (s, 3H, H^k), 2.49 (s, 3H, H^k), 2.46 (bs, 2H, H^e or H^f), 2.15 (bs, 3H, NH), 1.70-1.60 (m, 4H, H^m), 1.56 (bs, 2H, H^g or H^h), 1.44-1.35 (m, 4H, H^l), 0.93 (dt, 6H, *J* = 7.36 Hz, *J* = 1.48 Hz, H^o), 0.82 (bs, 2H, H^g or H^h). **^{13}C-NMR** (100 MHz, CD$_3$CN, 25 ºC) δ, ppm: 132.2 (d, $J_{C\text{-}P}$ = 13.8 Hz, C$_2$), 132.1 (C$_4$), 132.0 (d, $J_{C\text{-}P}$ = 2.6 Hz, C$_3$), 127.7 (d, J$_{C\text{-}P}$ = 182.2 Hz, C$_1$), 66.6 (d, $J_{C\text{-}P}$ = 6.8 Hz, C$_{10}$), 54.3 (C$_5$), 54.3 (C$_8$), 46.6 (C$_6$), 39.6 (C$_9$), 32.1 (d, $J_{C\text{-}P}$ = 6.4 Hz, C$_{11}$), 23.9 (C$_7$), 18.6 (C$_{12}$), 12.9 (C$_{13}$). **^{31}P-NMR** (162 MHz, CD$_3$CN, 25 ºC) δ, ppm: 18.9. **ESI-MS** (CH$_3$CN, m/z): 440.3 (100) [C$_{17}$H$_{31}$N$_3$O$_3$P]$^+$.

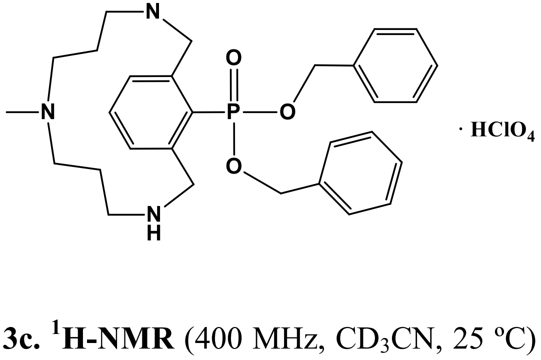

(3c)

3c. **^{1}H-NMR** (400 MHz, CD$_3$CN, 25 ºC) δ, ppm: 7.47 (dt, 1H, *J* = 7.6 Hz, *J* = 1.8 Hz, H^a), 7.39-7.29 (m, 12H, H^b, H^m, H^n, H^o), 5.06-4.96 (m, 4H, H^l), 4.76 (dd, 2H, *J* = 13.4 Hz, *J* = 1.8 Hz, H^c or H^d), 3.72 (d, 6H, *J* = 11.2 Hz, H^l), 3.48 (d, 2H, *J* = 13.4 Hz, H^c or

H^d), 3.23-3.17 (m, 2H, H^i or H^j), 2.77-2.71 (m, 2H, H^e or H^f), 2,63-2.56 (m, 2H, H^i or H^j), 2.52 (s, 3H, H^k), 2.48-2.43 (m, 2H, H^e or H^f), 2.07 (bs, 3H, NH), 1.59-1.49 (m, 2H, H^g or H^h), 0.90-0.80 (m, 2H, H^g or H^h). **^{13}C-NMR** (100 MHz, CD_3CN, 25 ºC) δ, ppm: 136.3 (d, $J_{C\text{-}P}$ = 6.5 Hz, C_{11}), 131.8 (d, $J_{C\text{-}P}$ = 3.5 Hz, C_2), 131.5 (C_4), 131.4 (C_3), 128.7 (C_{12} or C_{13} or C_{14}), 128.5 (C_{12} or C_{13} or C_{14}), 128.4 (C_{12} or C_{13} or C_{14}), 127.5 (d, $J_{C\text{-}P}$ = 165.6 Hz, C_1), 68.1 (d, $J_{C\text{-}P}$ = 6.6 Hz, C_{10}), 54.4 (C_5 or C_8), 54.4 (C_5 or C_8), 46.04 (C_6), 39.8 (C_9), 24.1 (C_7). **^{31}P-NMR** (162 MHz, CD_3CN, 25 ºC) δ, ppm: 19.3. **ESI-MS** (CH_3CN, m/z): 508.3 (100) $[C_{27}H_{35}N_3O_3P]^+$. *This product rapidly decomposes to generate the byproducts* **3c.1** *and* **3c.2. ESI-MS (**CH_3CN, m/z): 598.3 $[C_{36}H_{46}N_3O_3P]^+$ (**3c.1**), 418.2 $[C_{22}H_{33}N_3O_3P]^+$ (**3c.2**).

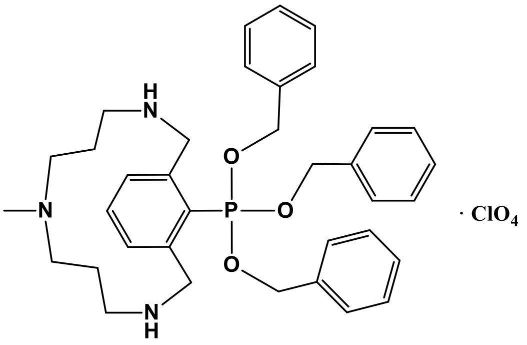

(**3c.1**)

+

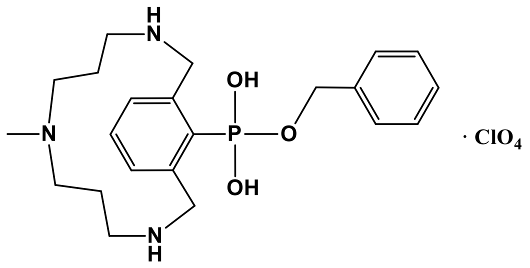

(**3c.2**)

1.7. Characterization of products with bifunctional groups

In an inert-atmosphere glove box, a sample of the Cu^{III}-aryl complex **1** (21.4 mg, 42 μmol) was dissolved in CD_3CN (1.6 mL) and 0.4 mL of a solution of 1,3,5-trimethoxybenzene was added as an internal standard. A portion of this solution (0.4 mL), 0.25 mL of CD_3CN and 1.1 equivalents of the corresponding bifunctional nucleophile were added to the tube (0.3 mL, 0.48-0.34 M). Final concentrations: [**1**] = 12 mM and [Nuc]= 13.2 mM. The tube was sealed with a screw-cap and the reaction was allowed to react at room temperature and monitored by ^{1}H-NMR spectroscopy until reaction completion. ^{1}H, COSY, NOESY, ^{1}H-^{13}C ^{1}H-^{13}C HSQC, ^{1}H-^{13}C HMBC and ^{13}C-NMR spectra and mass spectrometric analysis were obtained without isolation of the C-S coupling product. Reaction yields were obtained by integration of the ^{1}H-NMR spectra of the crude reaction mixtures relative to 1,3,5-trimethoxybenbenzene.

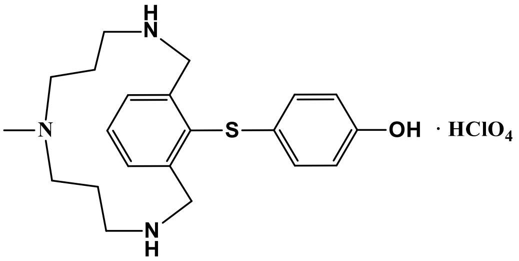

(**4a**)

4a. ^{1}H-NMR (400 MHz, CD_3CN, 25 ºC) δ, ppm: 7.36 (s, 3H, H^a, H^b), 7.05-7.02 (m, 2H, H^l), 6.77-6.73 (m, 2H, H^m), 4.21 (d, 2H, *J* = 13.0 Hz, H^c or H^d), 3.54 (d, 2H, *J* = 13.1 Hz, H^c or H^d), 3.08-3.03 (m, 2H, H^i or H^j), 2.89-2.83 (m, 2H, H^e or H^f), 2.70-2.63 (m, 2H, H^i or H^j), 2.63-2.58 (m, 5H, H^k, H^e or H^f), 1.65-1.55 (m, 2H, H^g or H^h), 0.78-0.69 (m, 2H, H^g or H^h). **^{13}C-NMR** (100 MHz, CD_3CN, 25 ºC) δ, ppm: 156.2 (C_{13}), 143.4 (C_1), 136.0 (C_2), 131.8 (C_3 or C_4), 130.6 (C_{11}), 128.5 (C_3 or C_4), 126.3 (C_{10}), 116.5 (C_{12}), 55.1 (C_8), 52.6 (C_5), 46.1 (C_6), 39.91 (C_9), 24.2 (C_7). **ESI-MS** (CH_3CN, m/z): 372.2 (100) $[C_{21}H_{30}N_3OS]^+$.

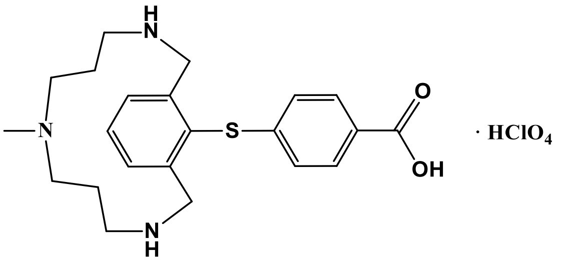

(**4b**)

4b. ^{1}H-NMR (400 MHz, CD_3CN, 25 ºC) δ, ppm: 7.85 (d, 2H, *J* = 8.5 Hz, H^m), 7.49-7.44 (m, 2H, H^b), 7.16-7.13 (m, 1H, H^a), 7.10 (d, 2H, *J* = 8.5 Hz, H^l), 4.16 (d, 2H, *J* = 13.1 Hz, H^c or H^d), 3.62-3.58 (m, 2H , *J* = 13.1 Hz, H^c or H^d), 3.08-3.03 (m, 2H, H^i or H^j), 2.89-2.85 (m, 2H, H^e or H^f), 2.73-2.66 (m, 4H, H^i or H^j, H^e or H^f), 2.59 (s, 3H, H^k), 1.68-1.59 (m, 2H, H^g or H^h), 0.73 (bs, 2H, H^g or H^h). **^{13}C-NMR** (100 MHz, CD_3CN, 25 ºC) δ, ppm: 166.4 (C_{14}), 144.5 (C_1), 132.5 (C_2), 132.2 (C_3), 130.5 (C_{12}), 130.0 (C_{10}), 129.9 (C_{13}), 126.8 (C_4), 126.3 (C_{11}), 55.2 (C_8), 52.6 (C_5), 46.2 (C_6), 39.9 (C_9), 24.1 (C_7). **ESI-MS** ($CH_3CN:H_2O$ (80:20), m/z): 400.2 (100) $[C_{22}H_{30}N_3O_2S]^+$.

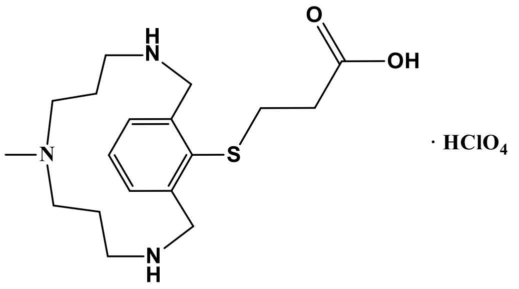

(4c)

4c. ^{1}**H-NMR** (400 MHz, CD_3CN, 25 ºC) δ, ppm: 7.56-7.50 (m, 3H, H^a, H^b), 4.85 (d, 2H, *J* = 13.6 Hz, H^c or H^d), 3.92 (d, 2H, *J* = 13.6 Hz, H^c or H^d), 3.07 (t, 2H, *J* = 6.4 Hz, H^l), 3.05-3.01 (m, 2H, H^e or H^f), 2.78-2.72 (m, 2H, H^e or H^f), 2,64-2.56 (m, 2H, H^i or H^j), 2.54 (t, 2H, *J* = 6.4 Hz, H^m), 2.41-2.35 (m, 2H, H^i or H^j), 2.23 (s, 3H, H^k), 1.70-1.65 (m, 2H, H^g or H^h), 0.95 (bs, 2H, H^g or H^h). ^{13}**C-NMR** (100 MHz, CD_3CN, 25 ºC) δ, ppm: 174.2 (C_{12}), 140.7 (C_1), 134.7 (C_2), 133.4 (C_3 or C_4), 130.5 (C_3 or C_4), 54.5 (C_8), 51.5 (C_5), 45.8 (C_6), 39.8 (C_9), 33.5 (C_{11}), 33.0 (C_{10}), 23.2 (C_7). **ESI-MS** (CH_3CN:H_2O (80:20), m/z): 352.2 (100) $[C_{18}H_{30}N_3O_2S]^+$.

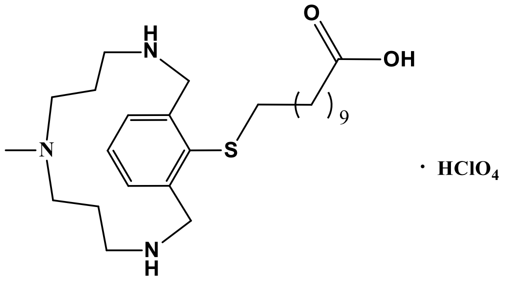

(4d)

4d. ^{1}**H-NMR** (400 MHz, CD_3CN, 25 ºC) δ, ppm: 7.58-7.50 (m, 3H, H^a, H^b), 4.73 (d, 2H, J = 13.56 Hz, H^c or H^d), 3.96 (d, 2H, J = 13.56 Hz, H^c or H^d), 3.11-3.05 (m, 2H, H^e or H^f), 2.84 (t, 2H, J = 7.36 Hz, H^l), 2.82-2.74 (m, 2H, H^e or H^f), 2.61-2.53 (m, 2H, H^i or H^j), 2.40-2.31 (m, 2H, H^i or H^j), 2.28-2.22 (m, 5H, H^k, H^u), 1.72-1.60 (m, 2H, H^g or H^h), 1.58-1.50 (m, 4H, H^m, H^t), 1.39-1.35 (m, 2H, H^n), 1.29-1.24 (m, 10H, H^o, H^p, H^q, H^r, H^s), 1.00-0.96 (m, 2H, H^g or H^h). ^{13}**C-NMR** (100 MHz, CD_3CN, 25 ºC) δ, ppm: 174.3 (C_{13}), 139.9 (C_1), 135.53 (C_2), 133.58 (C_3 or C_4), 130.40 (C_3 or C_4), 54.57 (C_8), 51.51 (C_5), 46.06 (C_6), 39.88 (C_9), 37.81 (C_{10}), 33.25 (C_{12}), 29.11, 29.1, 28.91, 28.81, 28.63, 28.21, 28.04, 24.56 (C_{11}), 22.97 (C_7). **ESI-MS** (CH_3CN:H_2O (80:20), m/z): 464.4 (100) $[C_{26}H_{46}N_3O_2S]^+$.

1.8. General procedure for catalytic reactions

In an inert-atmosphere glove box, a vial was loaded with 0.5 mL of ligand **L1-X (X =** Cl or Br) 30 mM in CH_3CN and 0.5-10 mol % of $Cu(CH_3CN)_4(CF_3SO_3)$ was added (0.2 mL of stock solution 0.75-7.5 mM in CH_3CN). The colourless solution becomes slightly red indicating that oxidative addition takes place obtaining the corresponding complex arylCu^{III}-**X** (**X** = Cl, Br), complex $\mathbf{2_x}$. Then 2.3 mL of HS-nucleophile 7.15-13 mM in CH_3CN was added. Final concentrations: [**L1-Br**] = 5 mM, [Cu] = 0.05-0.5 mM and [nucleophile] = 5.5-10 mM. After stirring the mixture crude, either at room temperature (for thiols and benzeneselenol) or at 50ºC (for phosphites) for 24 hours, 150 μL of trimethoxybenzene 3 mM in CH_3CN as internal standard is added and the solvent is removed. The sample is re-dissolved in 0.5 mL of CD_3CN and NMR yields were obtained by ^{1}H-NMR using integration of benzylic protons respect to trimethoxybenzene.

2. Supporting References

1. Ribas, X.; Jackson, D. A.; Donnadieu, B.; Mahía, J.; Parella, T.; Xifra, R.; Hedman, B.; Hodgson, K. O.; Llobet, A.; Stack, T. D. P. *Angew.Chem. Int. Ed.* **2002**, *41*, 2991.

2. King, A. E.; Huffman, L. M.; Casitas, A.; Costas, M.; Ribas, X.; Stahl, S. S. *J. Am. Chem. Soc.* **2010**, *132*, 12068.

3. Casitas, A.; Canta, M.; Solà, M.; Costas, M.; Ribas, X. *J. Am. Chem. Soc.* **2011**, *133*, 19386.

3. Supporting Figures

Figure S1. ^{1}H-NMR spectrum of compound **1a** in CD_3CN, 400 MHz, at 298 K.

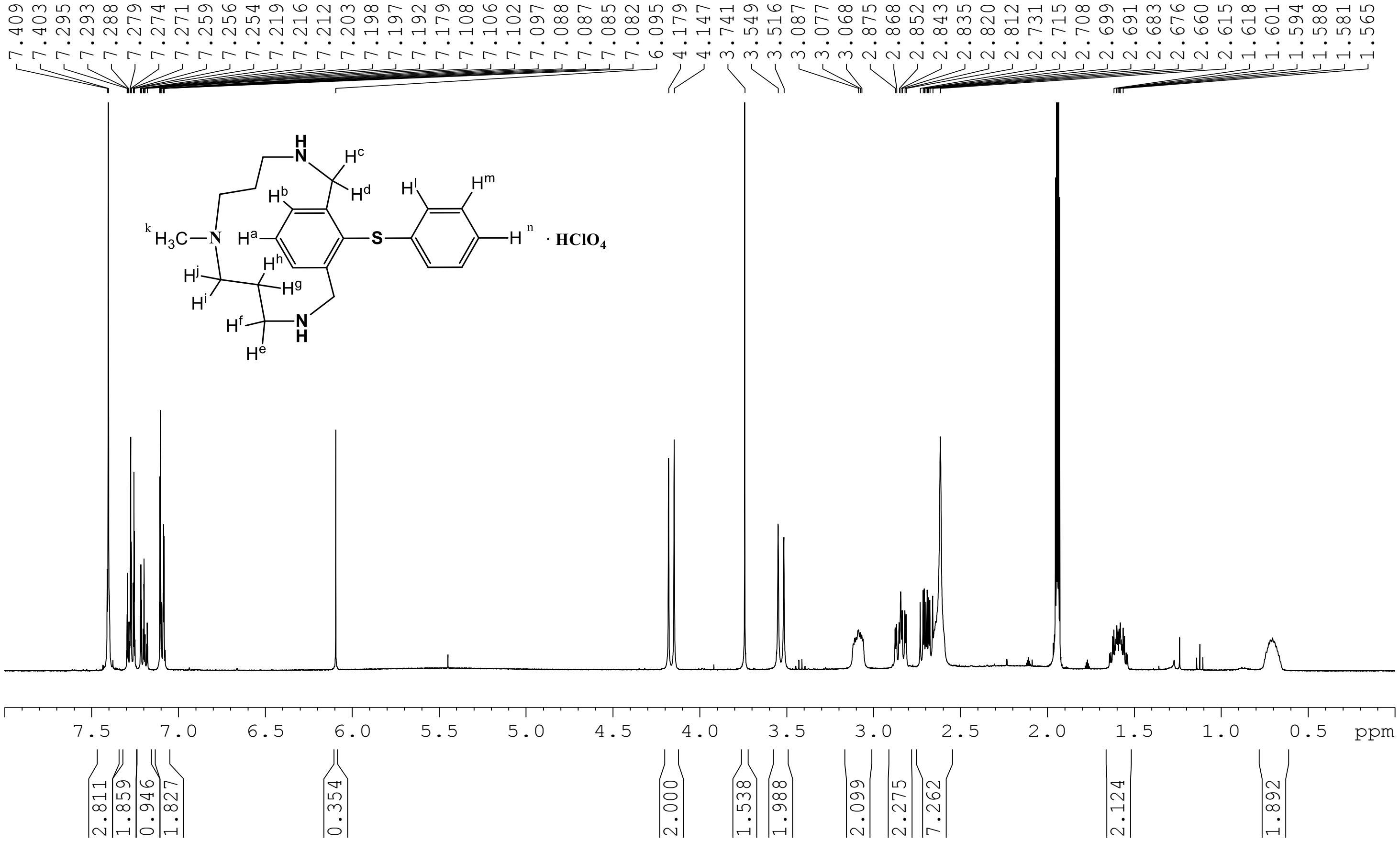

Figure S2. ^{13}C-NMR spectrum of compound **1a** in CD_3CN, 100MHz, at 298 K.

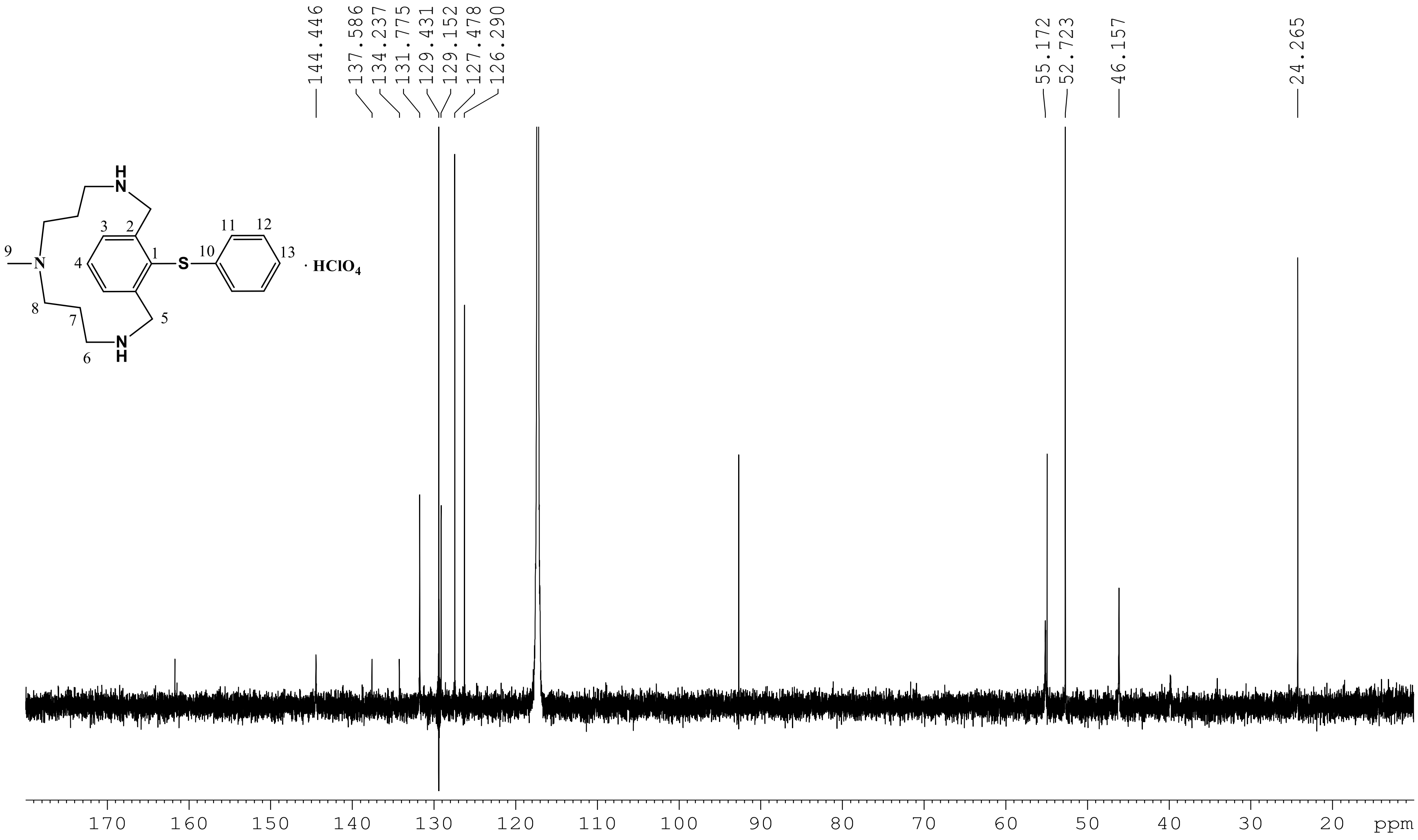

Figure S3. COSY spectrum of compound **1a** in CD_3CN, 400 MHz, at 298 K.

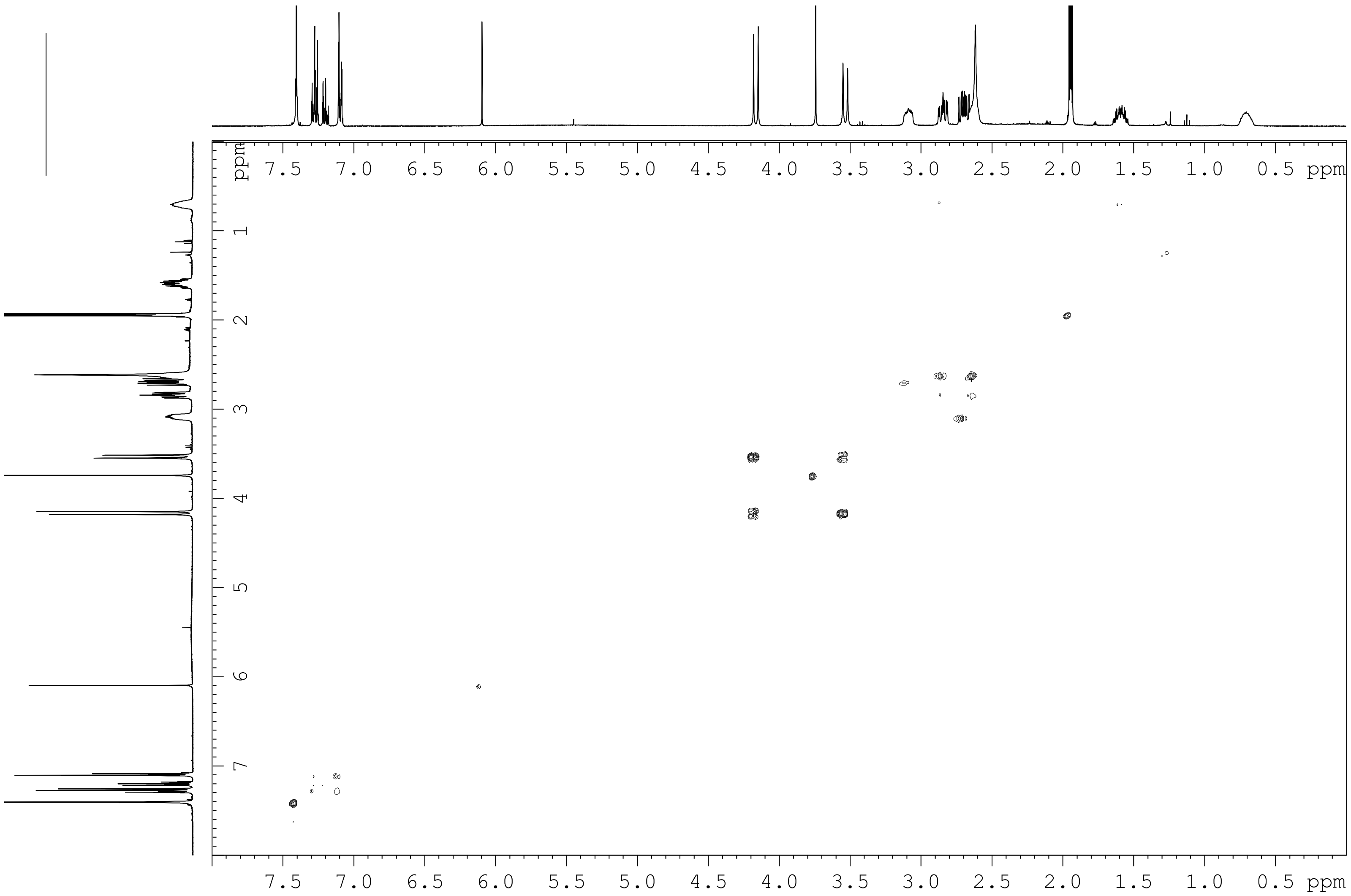

Figure S4. NOESY spectrum of compound **1a** in CD_3CN, 400 MHz, at 298 K.

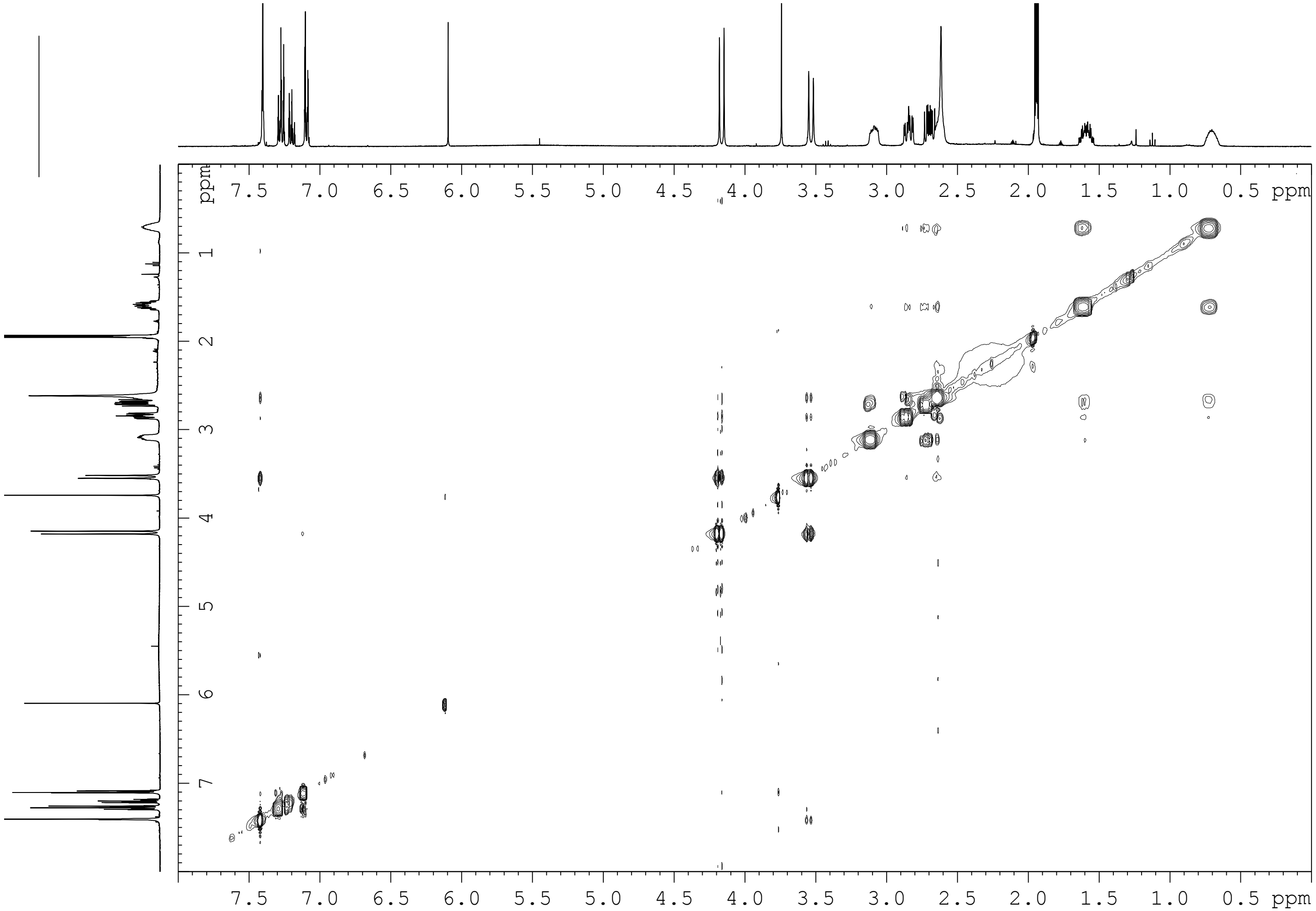

Figure S5. ^{1}H-^{13}C HSQC spectrum of compound **1a** in CD_3CN, 400 MHz, at 298 K.

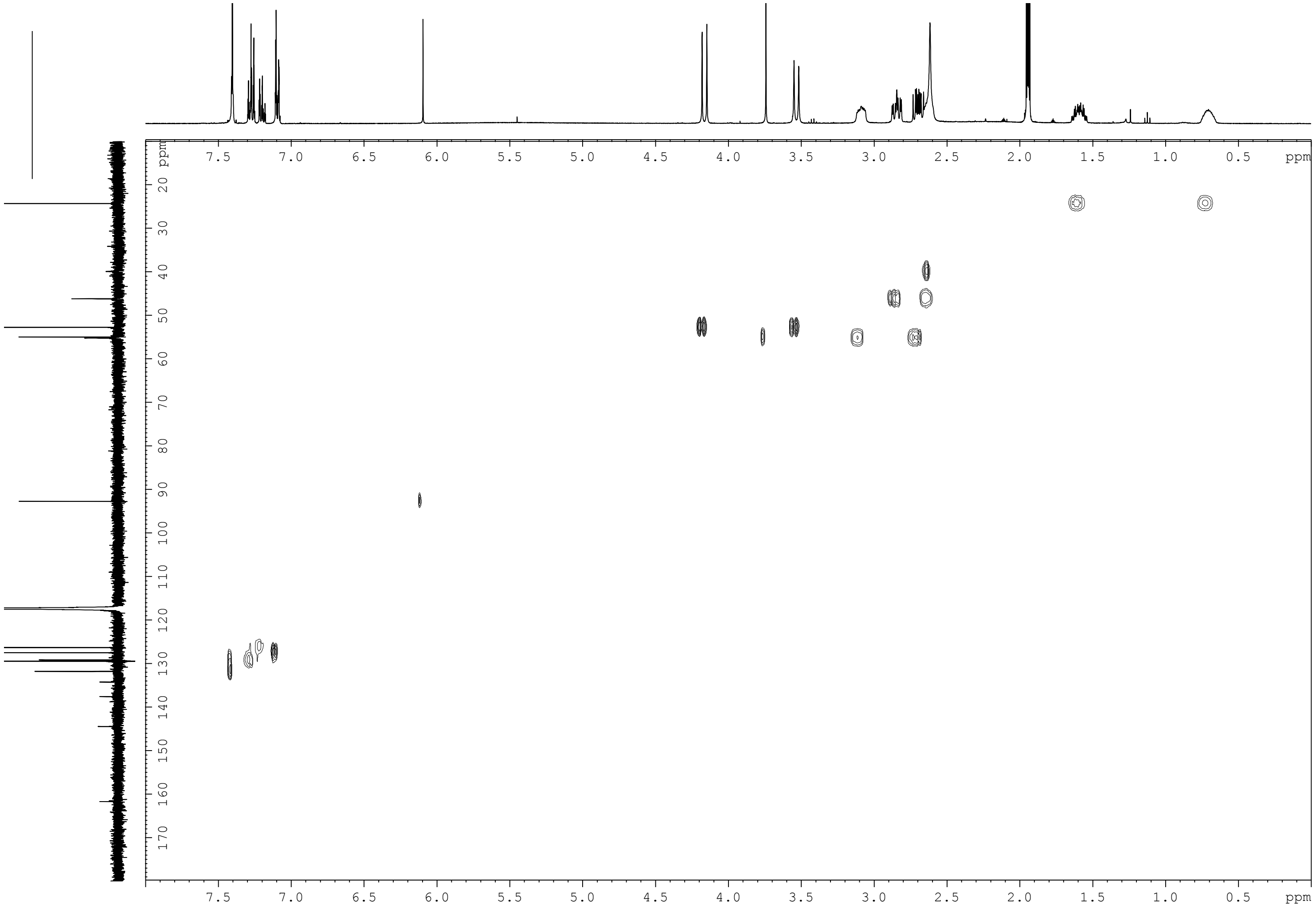

Figure S6. ^{1}H-NMR spectrum of compound **1b** in CD_3CN, 400 MHz, at 298 K.

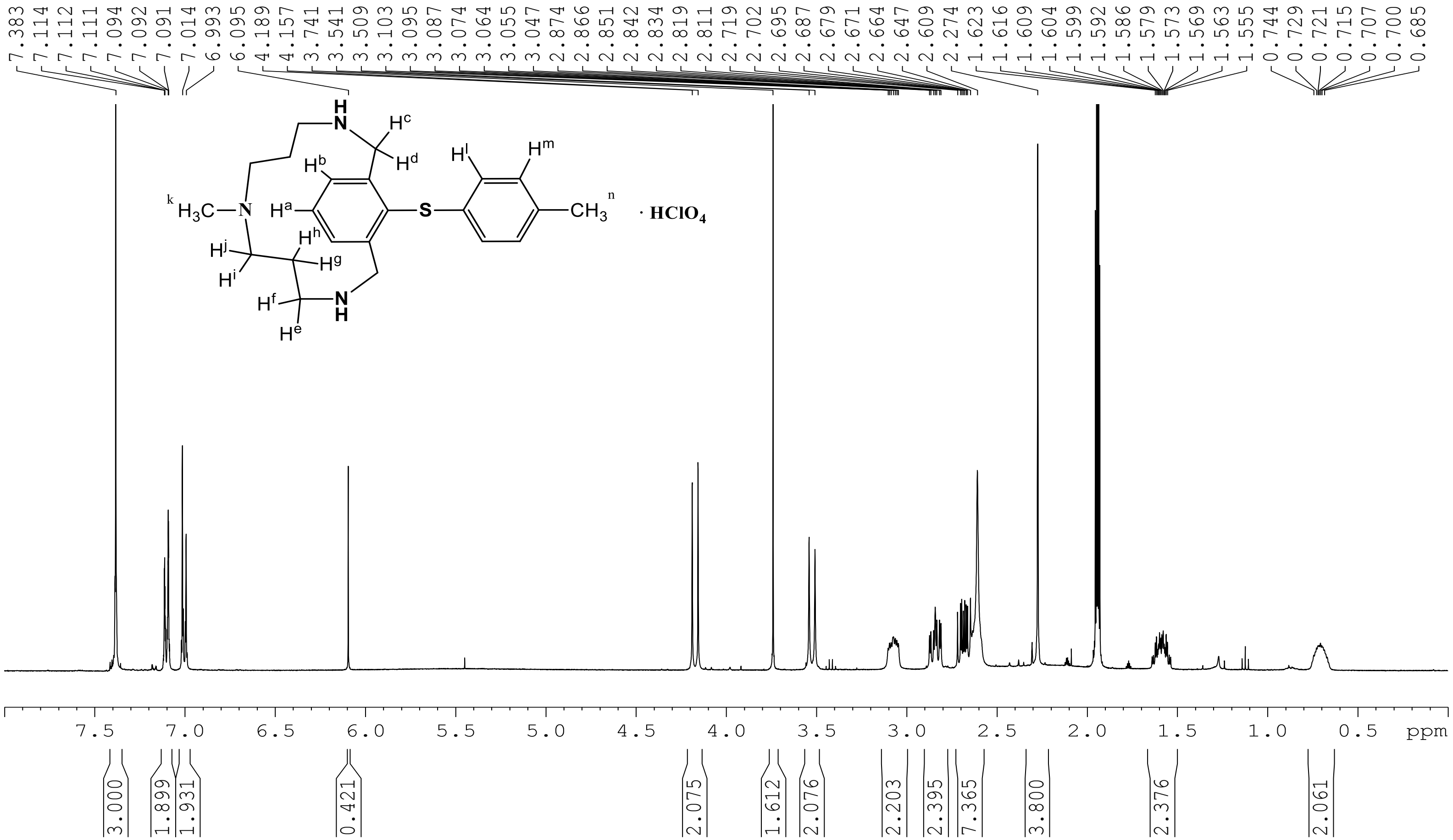

Figure S7. ^{13}C-NMR spectrum of compound **1b** in CD_3CN, 100 MHz, at 298 K.

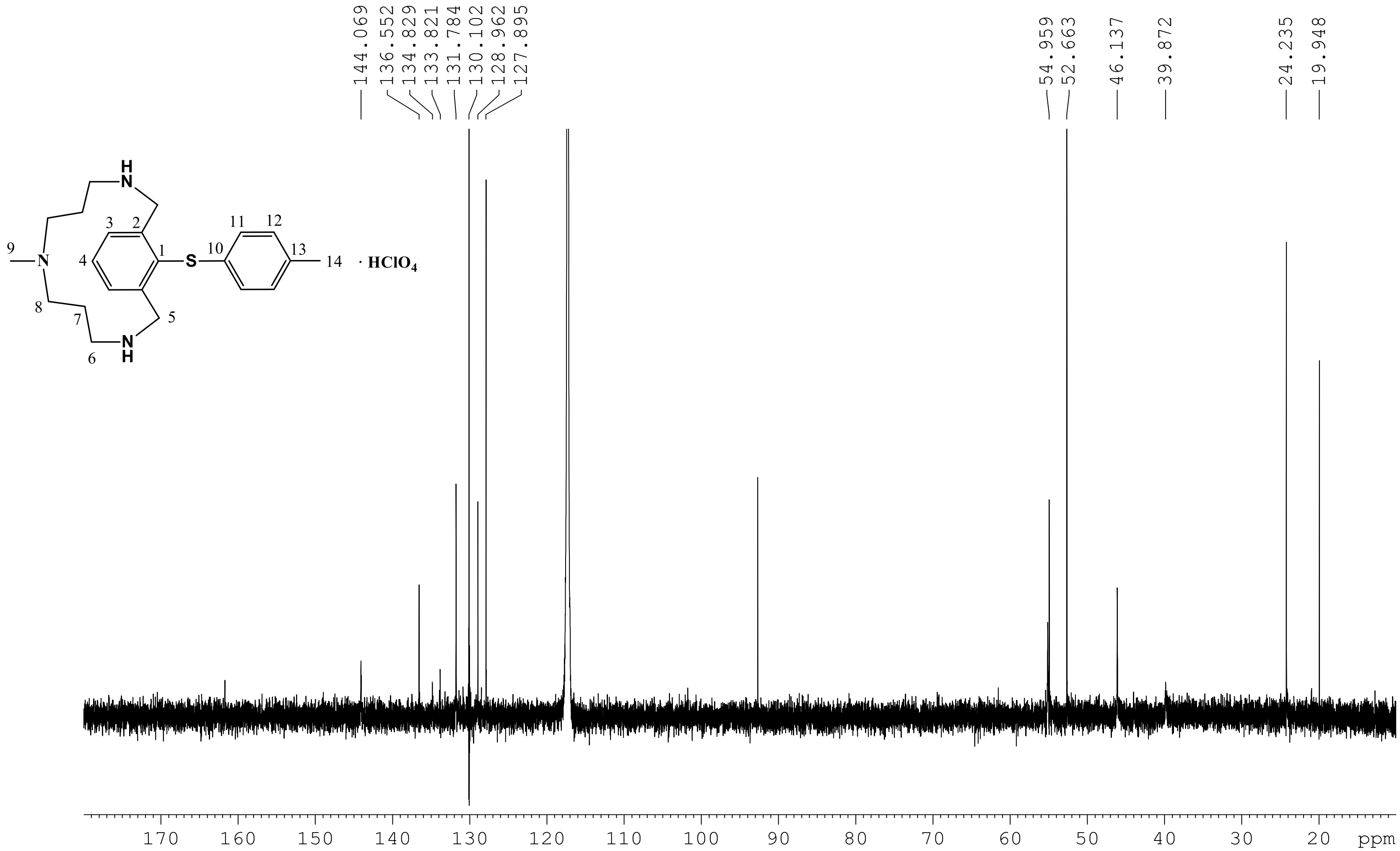

Figure S8. COSY spectrum of compound **1b** in CD_3CN, 400 MHz, at 298 K.

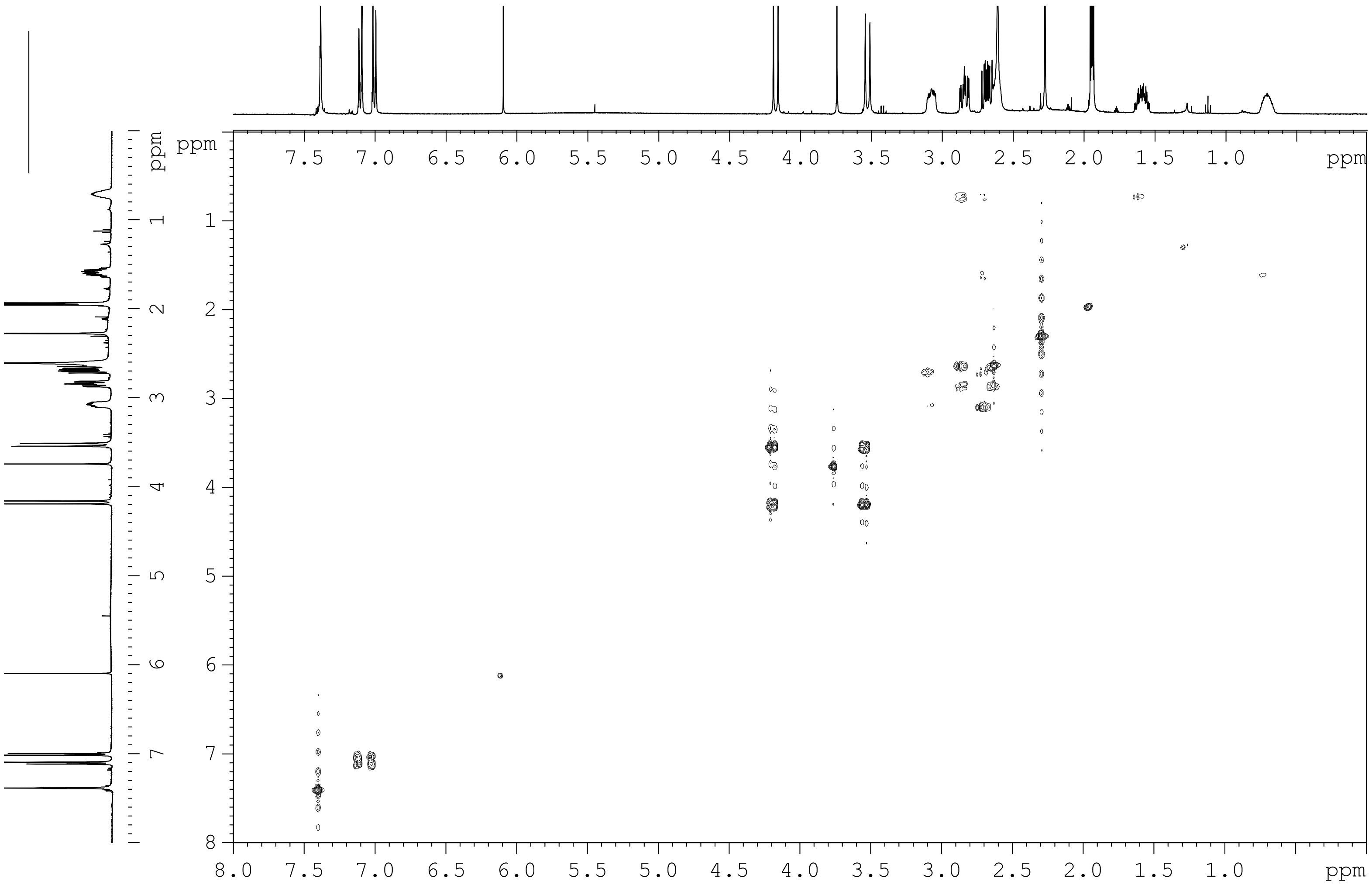

Figure S9. NOESY spectrum of compound **1b** in CD_3CN, 400 MHz, at 298 K.

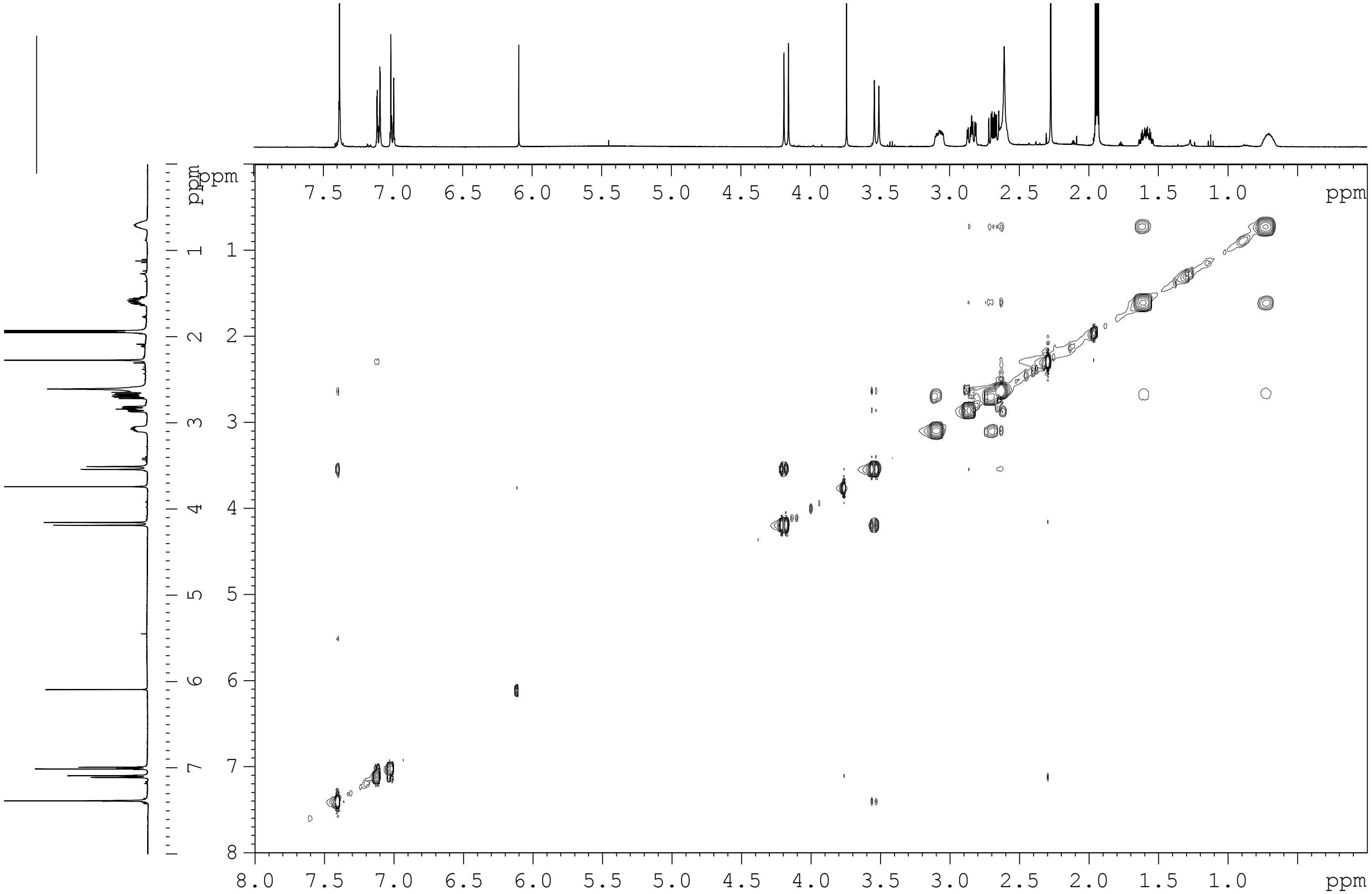

Figure S10. ^{1}H-^{13}C HSQC spectrum of compound **1b** in CD$_3$CN, 400 MHz, at 298 K.

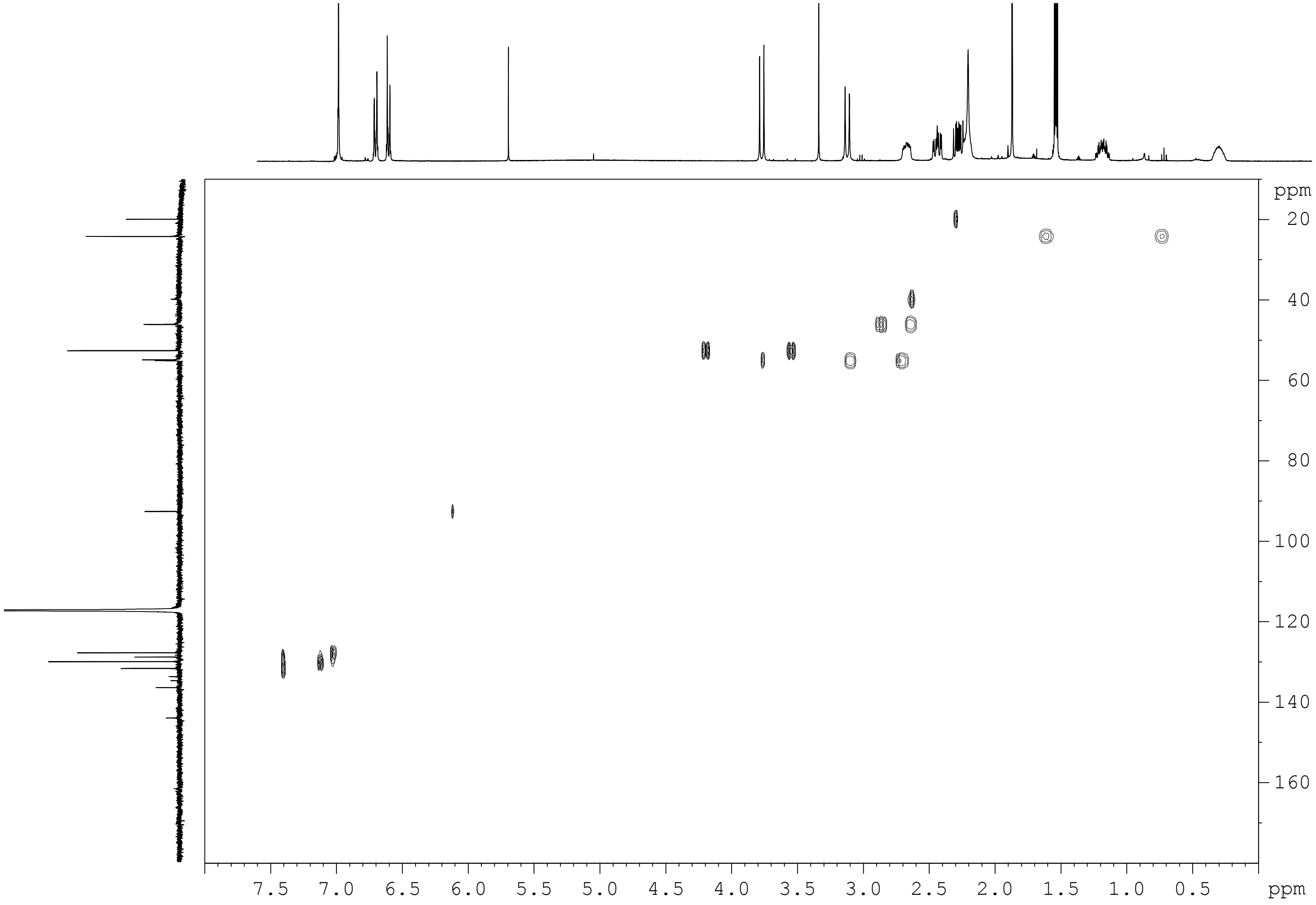

Figure S11. ^{1}H-NMR spectrum of compound **1c** in CD_3CN, 400 MHz, at 298 K.

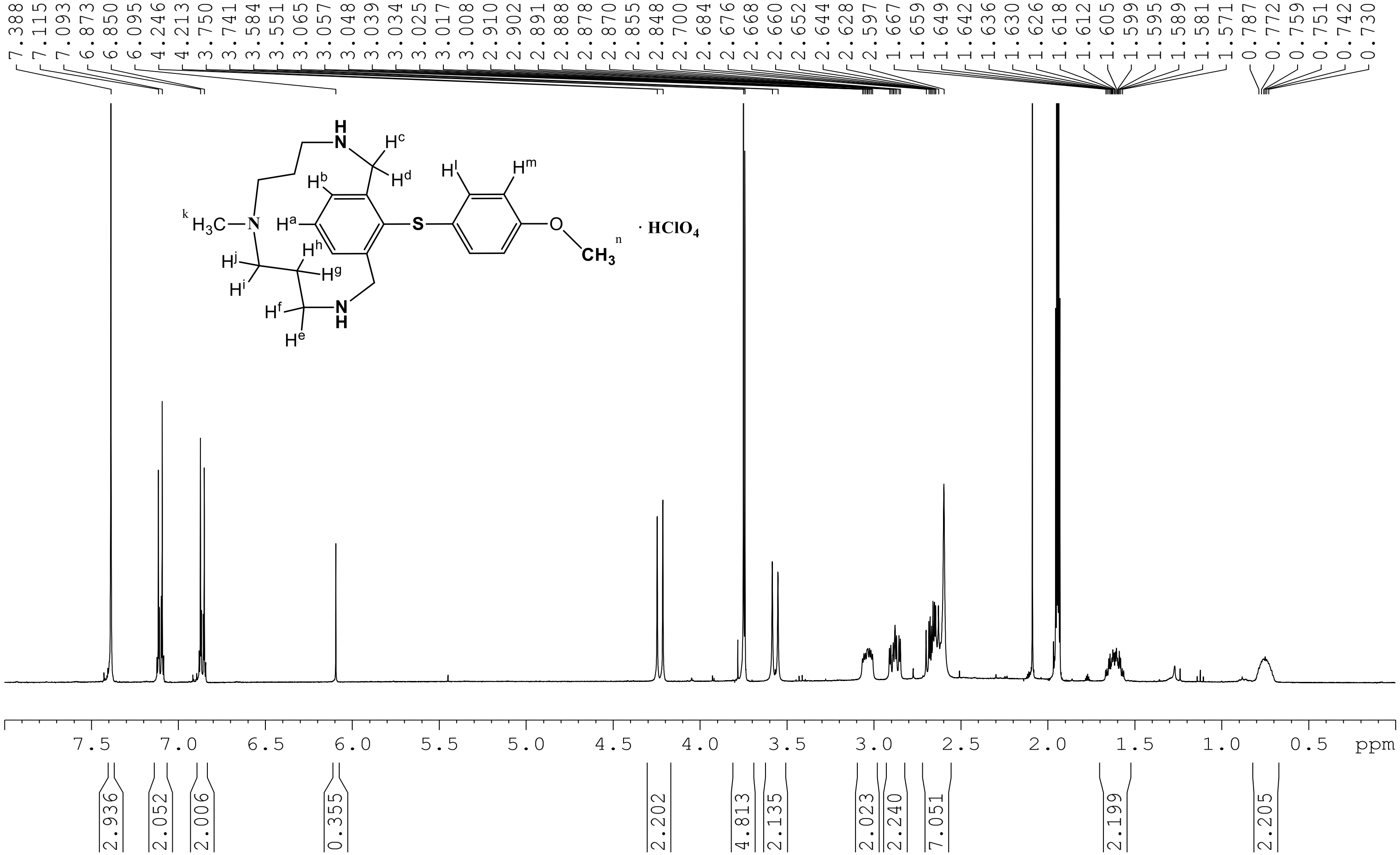

Figure S12. ^{13}C-NMR spectrum of compound **1c** in CD$_3$CN, 100 MHz, at 298 K.

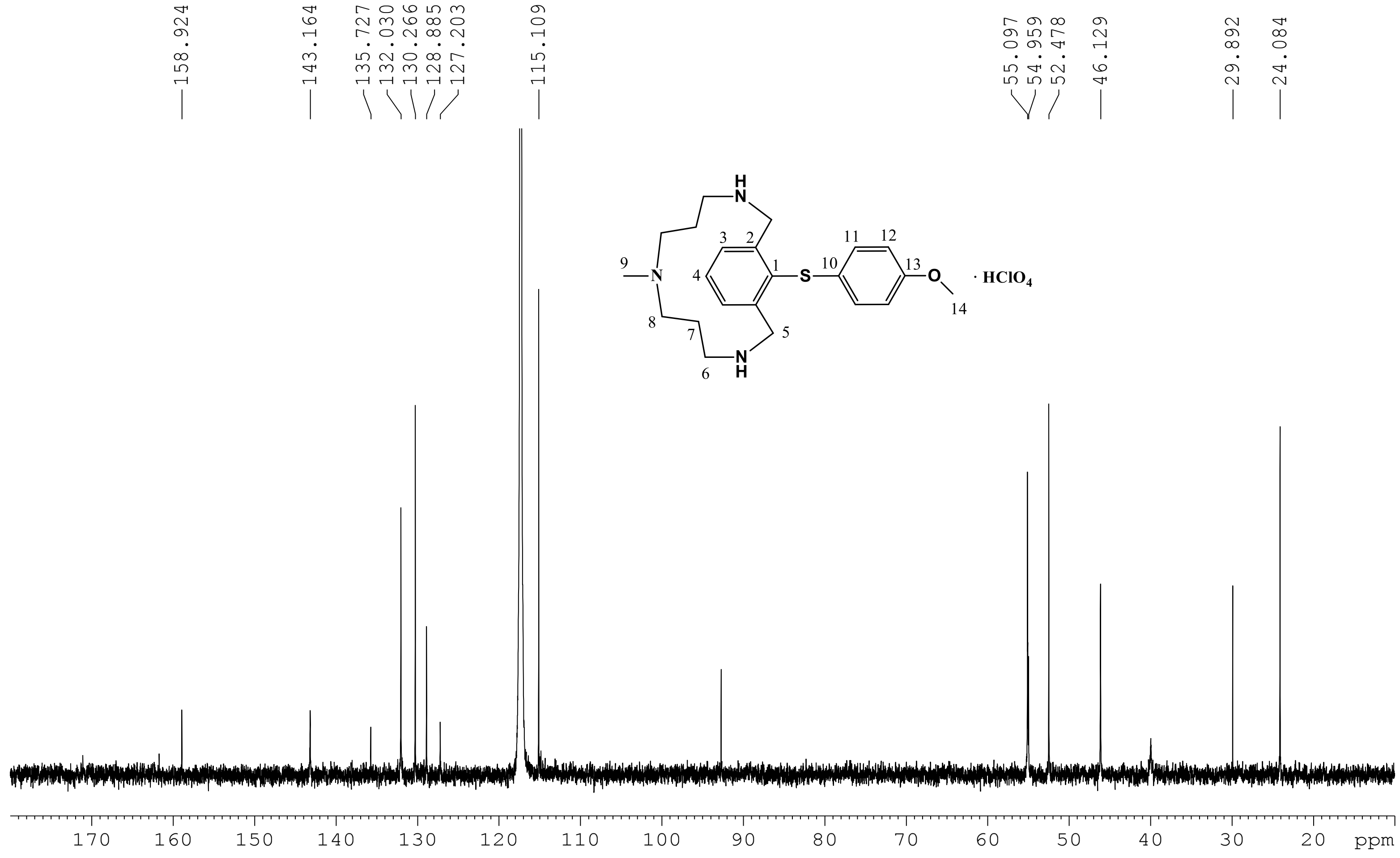

Figure S13. ^{1}H-NMR spectrum of compound **1d** in CD_3CN, 400 MHz, at 298 K.

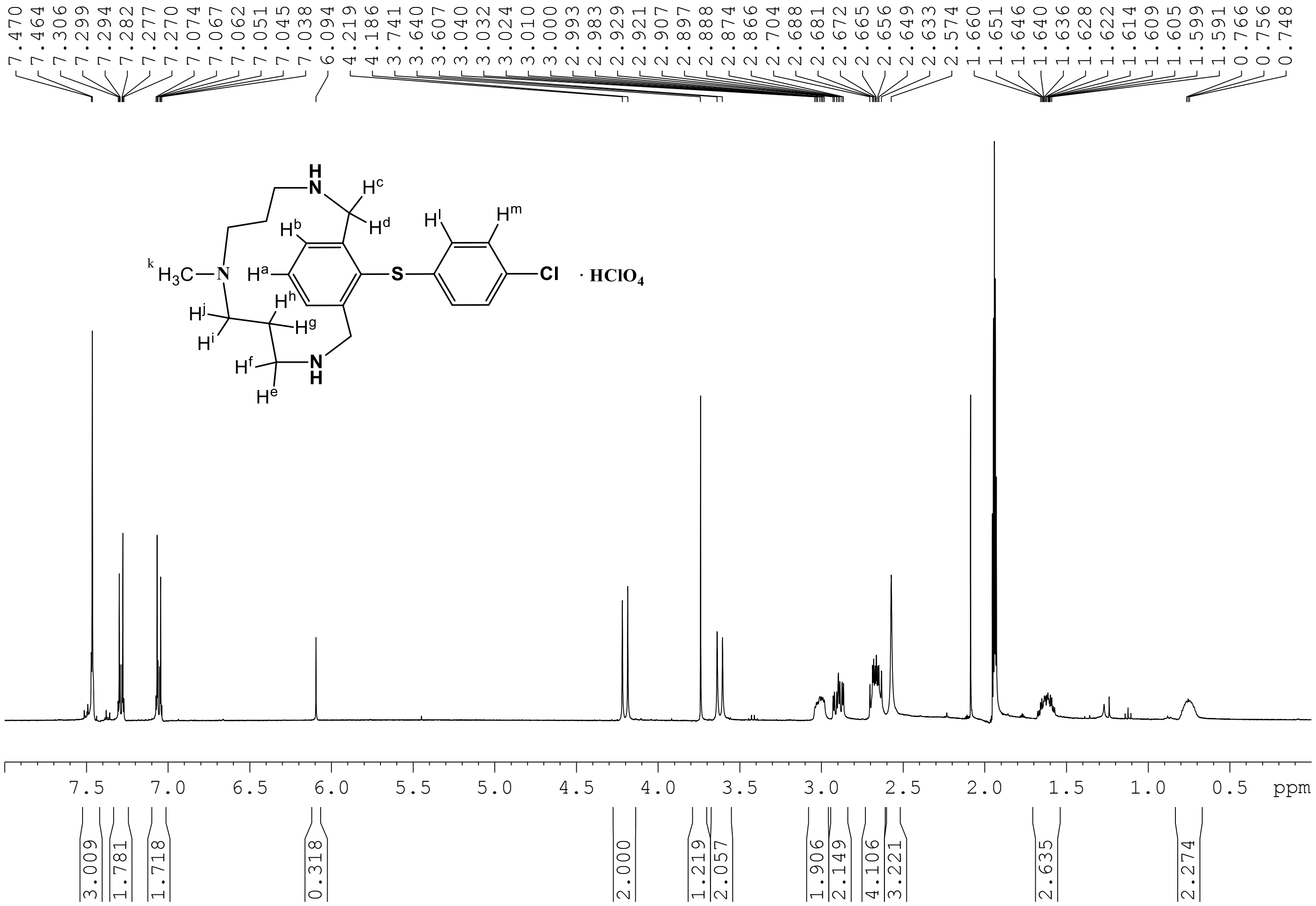

Figure S14. ^{13}C-NMR spectrum of compound **1d** in CD_3CN, 100 MHz, at 298 K.

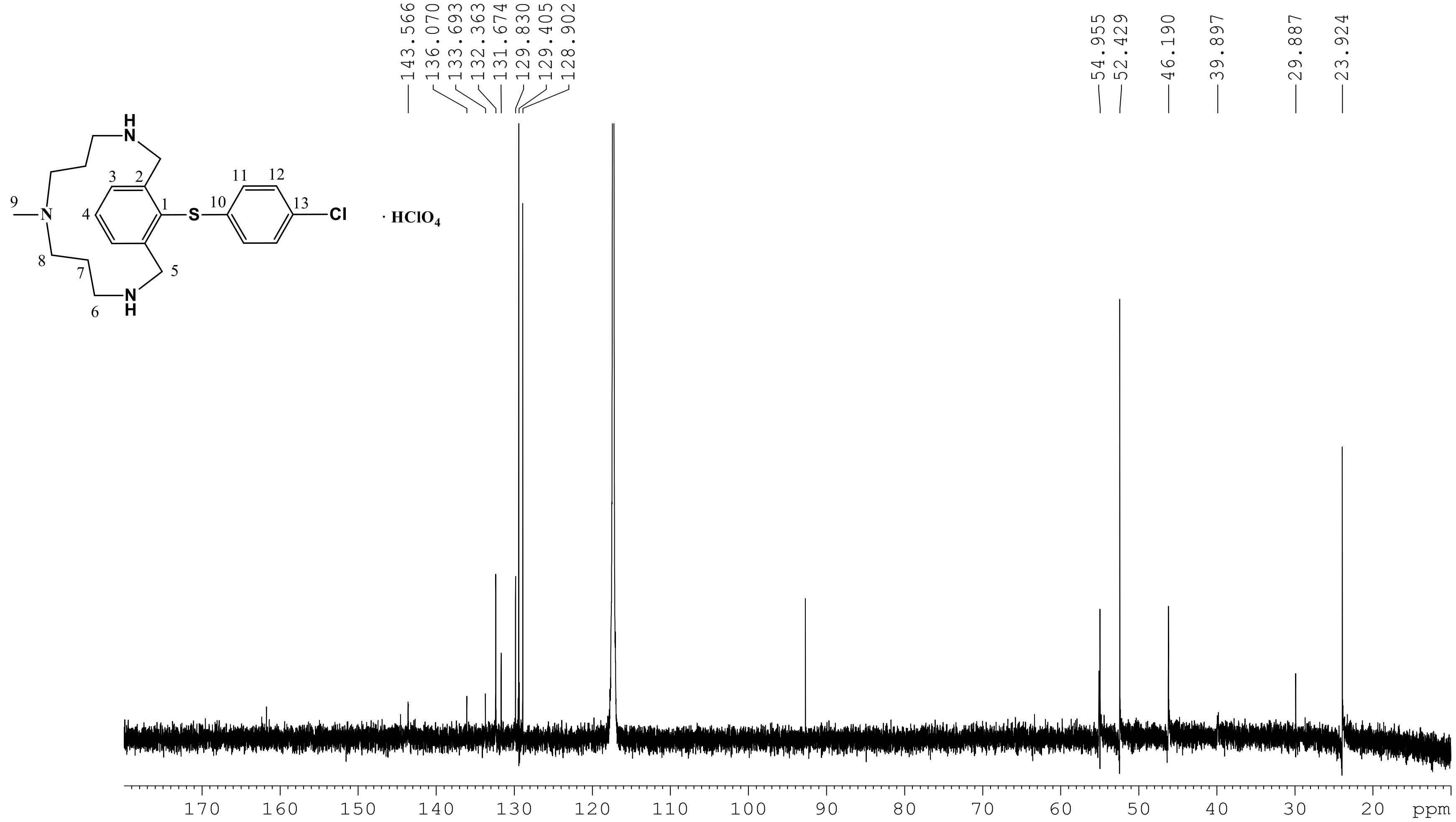

Figure S15. ^{1}H-NMR spectrum of compound **1e** in CD_3CN, 400 MHz, at 298 K.

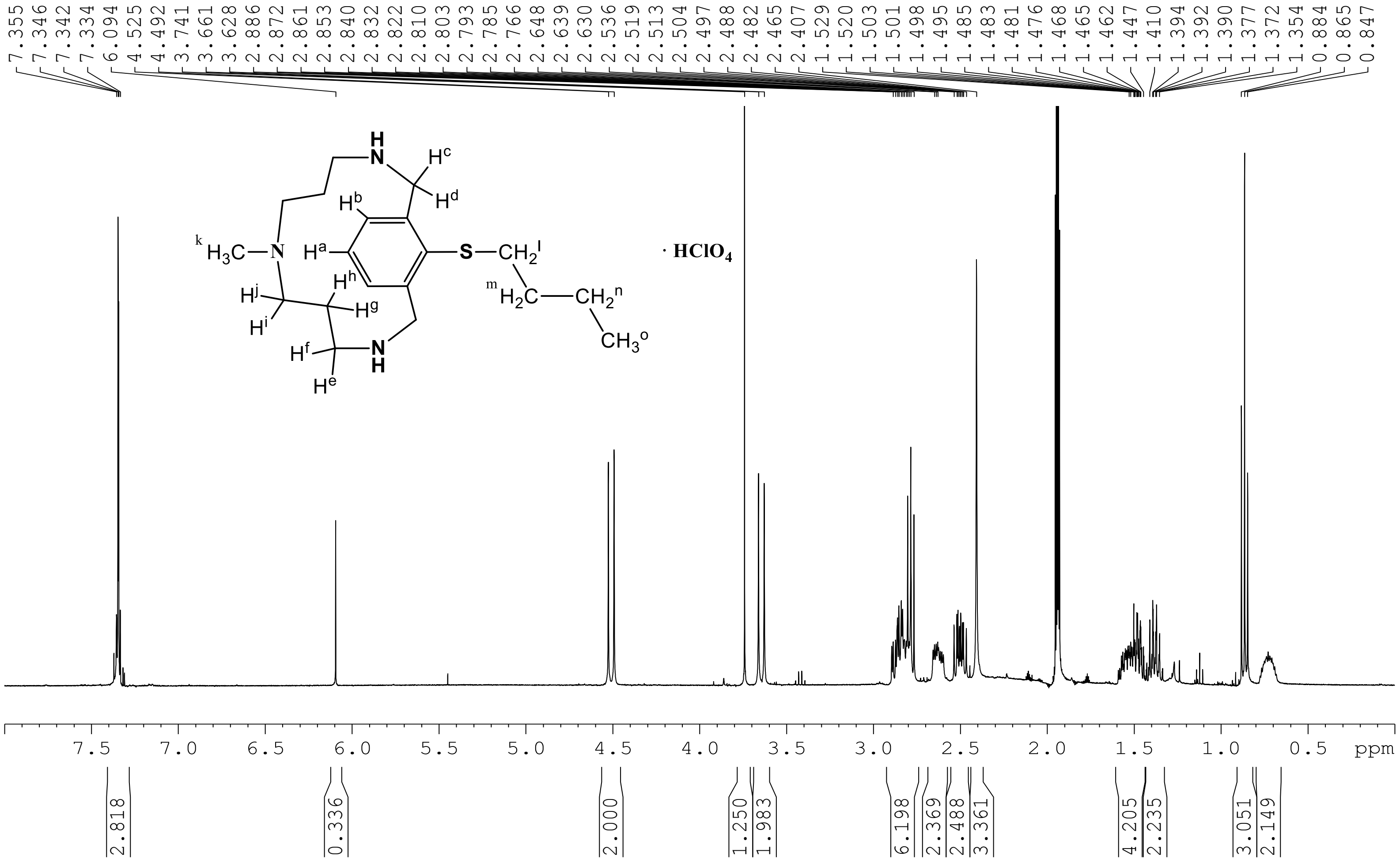

Figure S16. ^{13}C-NMR spectrum of compound **1e** in CD_3CN, 100 MHz, at 298 K.

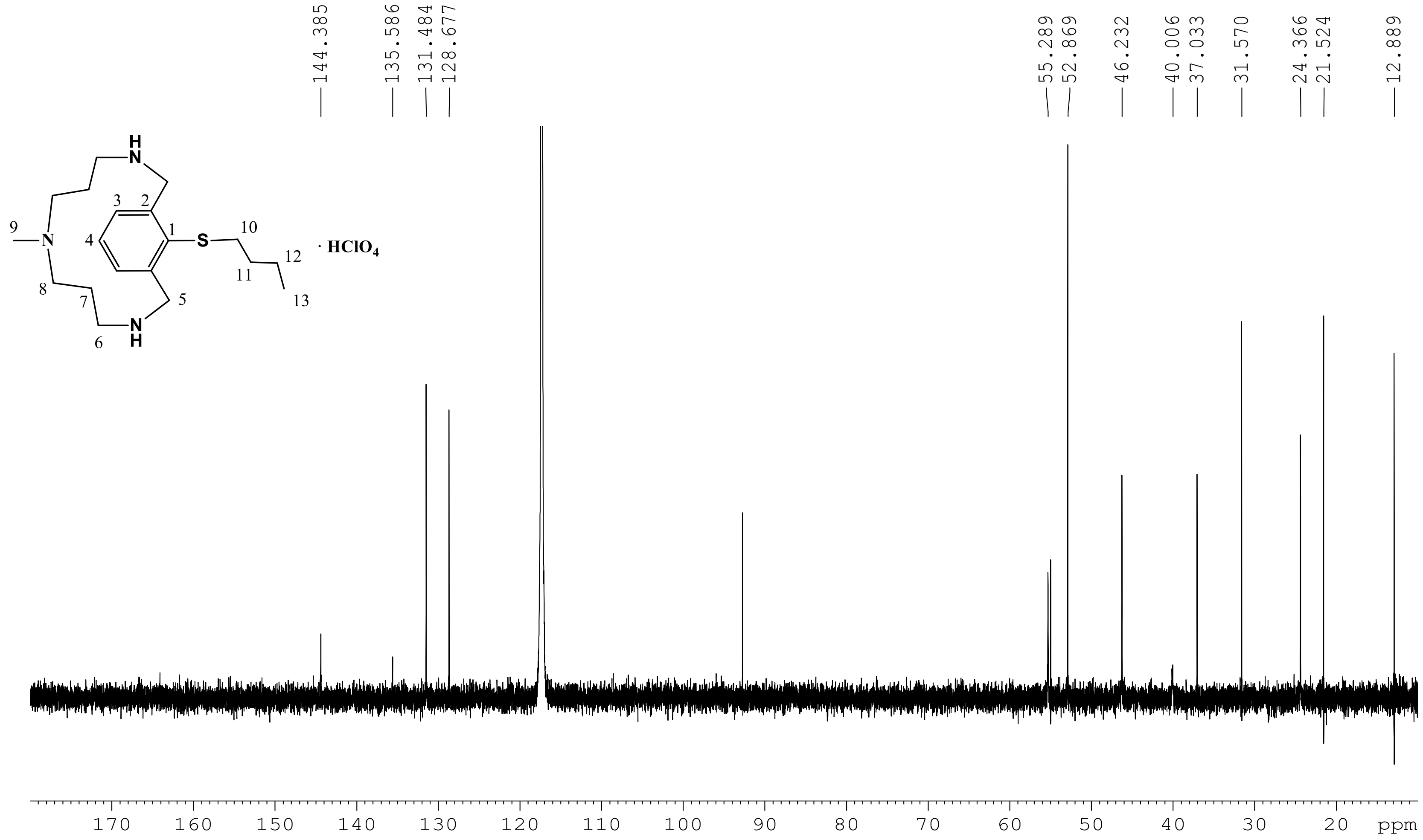

Figure S17. COSY spectrum of compound **1e** in CD_3CN, 400 MHz, at 298 K.

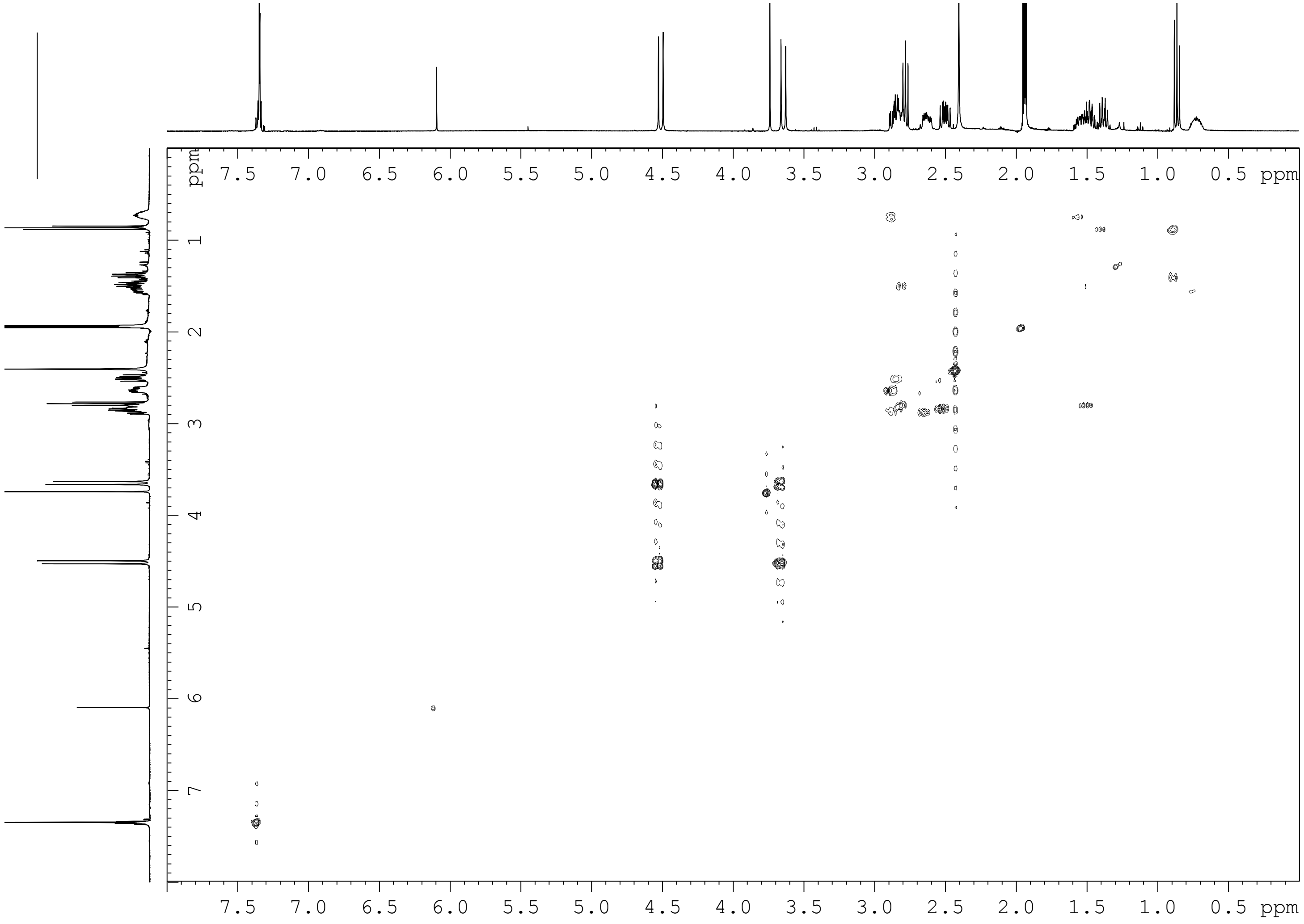

Figure S18. NOESY spectrum of compound **1e** in CD_3CN, 400 MHz, at 298 K.

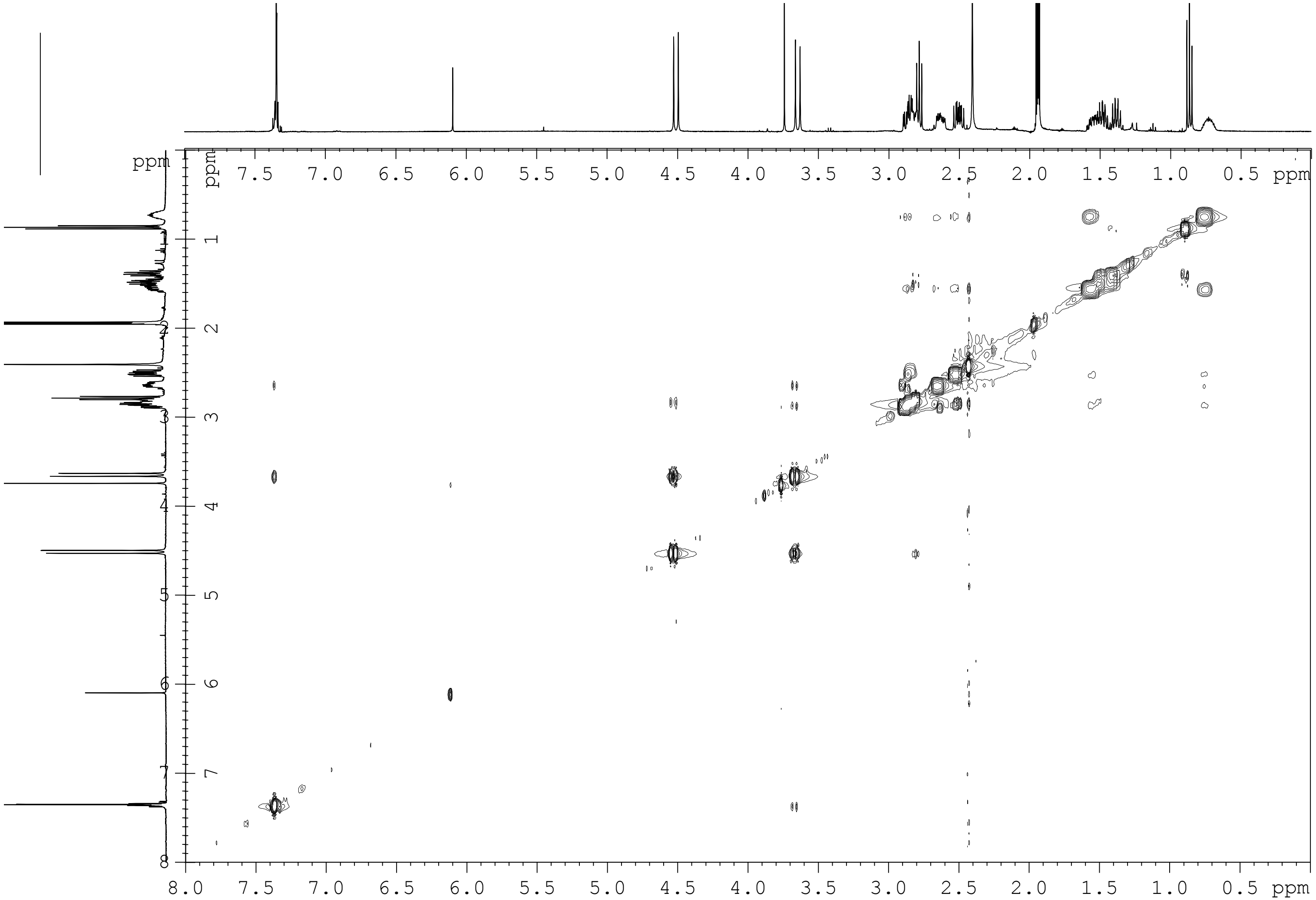

Figure S19. ^{1}H-^{13}C HSQC spectrum of compound **1e** in CD$_3$CN, 400 MHz, at 298 K.

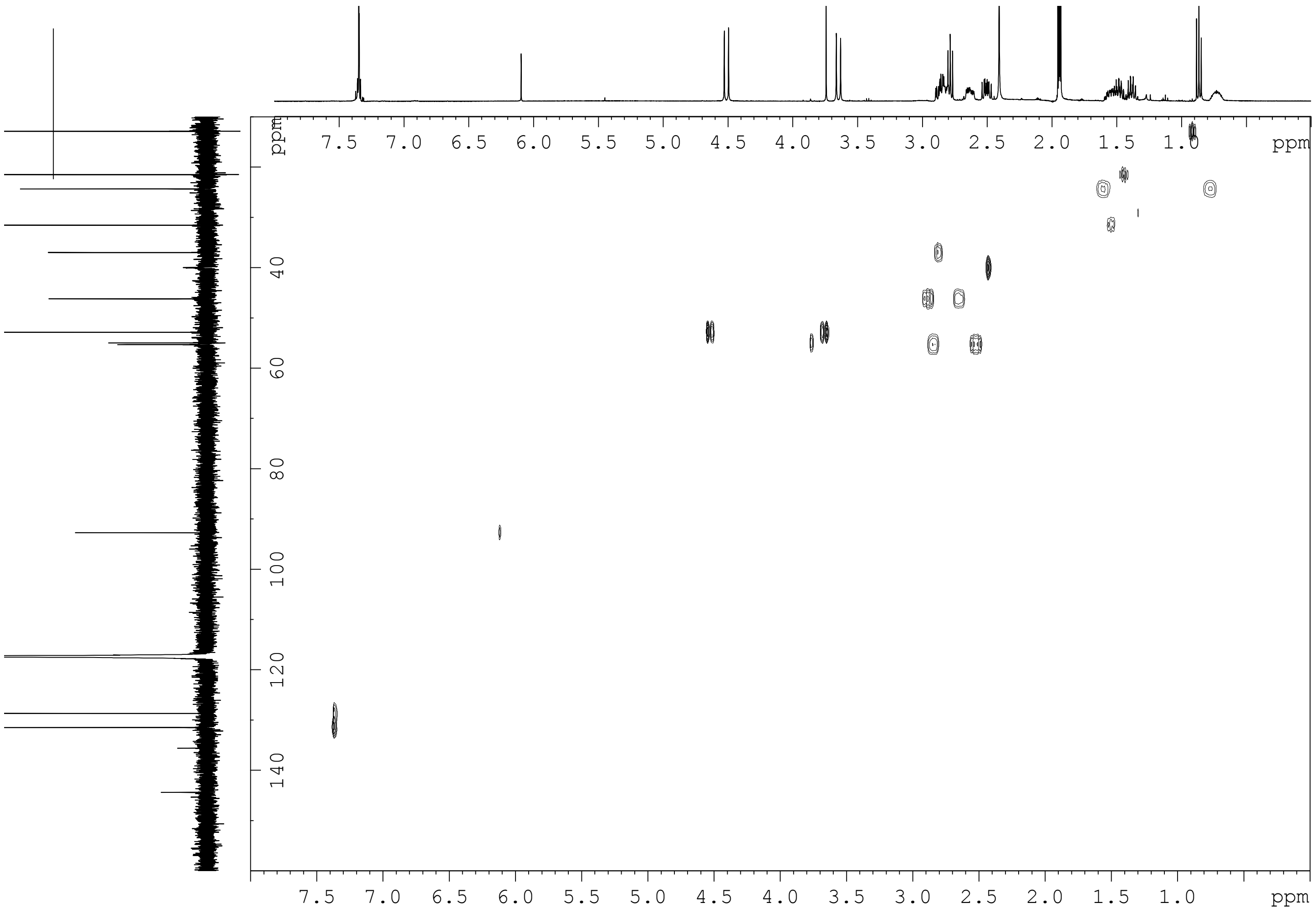

Figure S20. ^{1}H-NMR spectrum of compound **1f** in CD_3CN, 400 MHz, at 298 K.

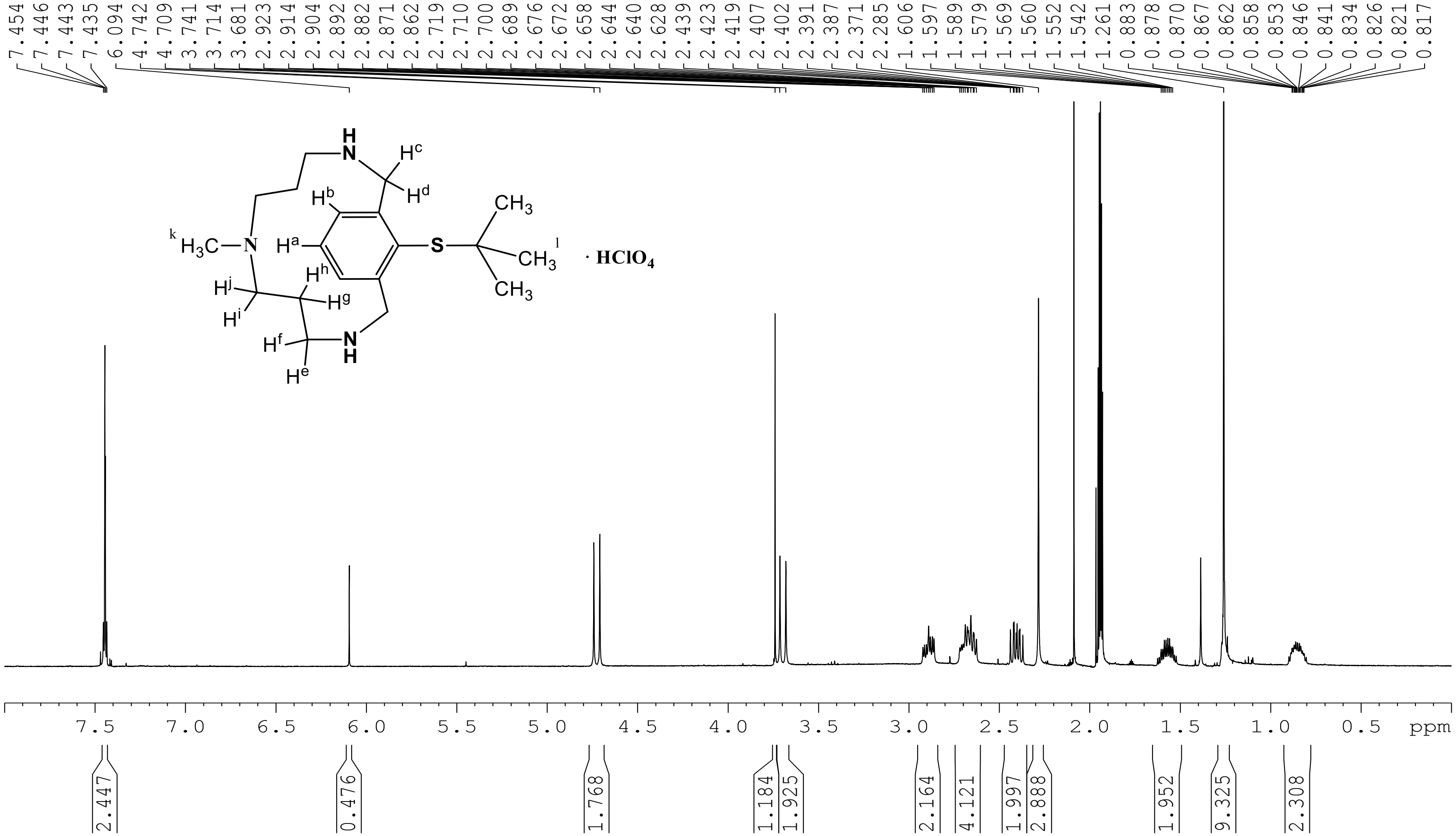

Figure S21. ^{13}C-NMR spectrum of compound **1f** in CD_3CN, 100 MHz, at 298 K.

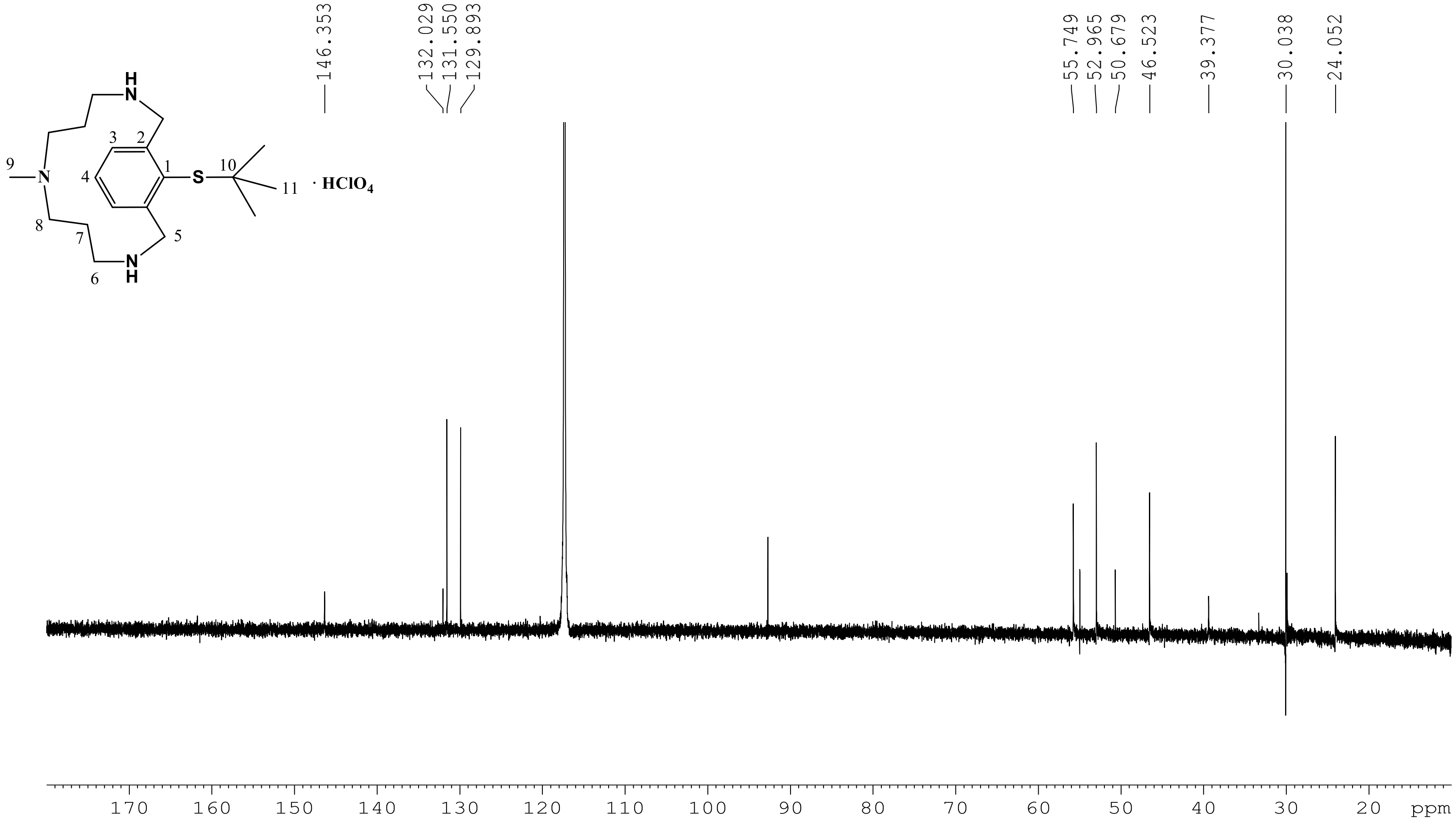

Figure S22. COSY spectrum of compound **1f** in CD_3CN, 400 MHz, at 298 K.

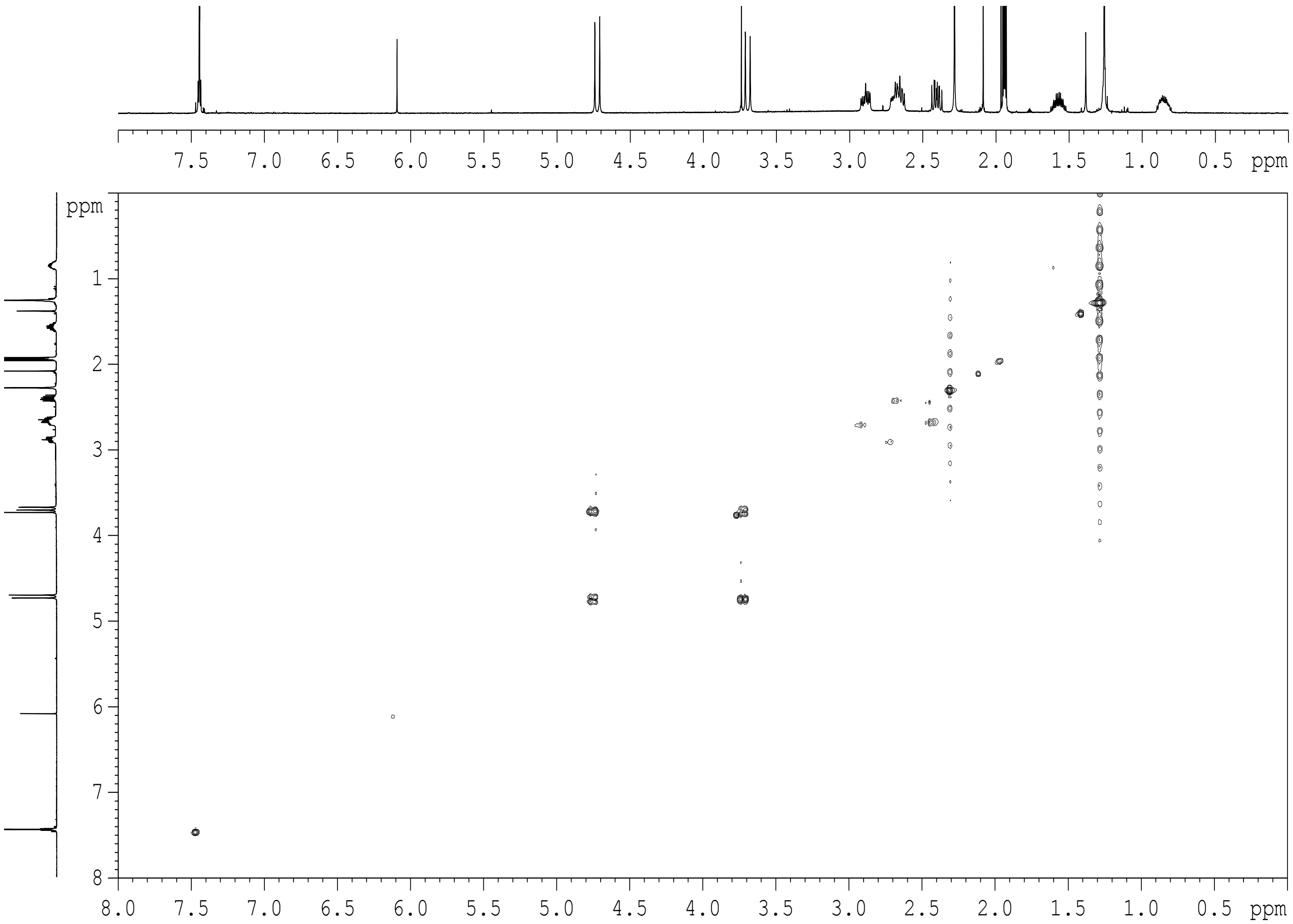

Figure S23. NOESY spectrum of compound **1f** in CD_3CN, 400 MHz, at 298 K.

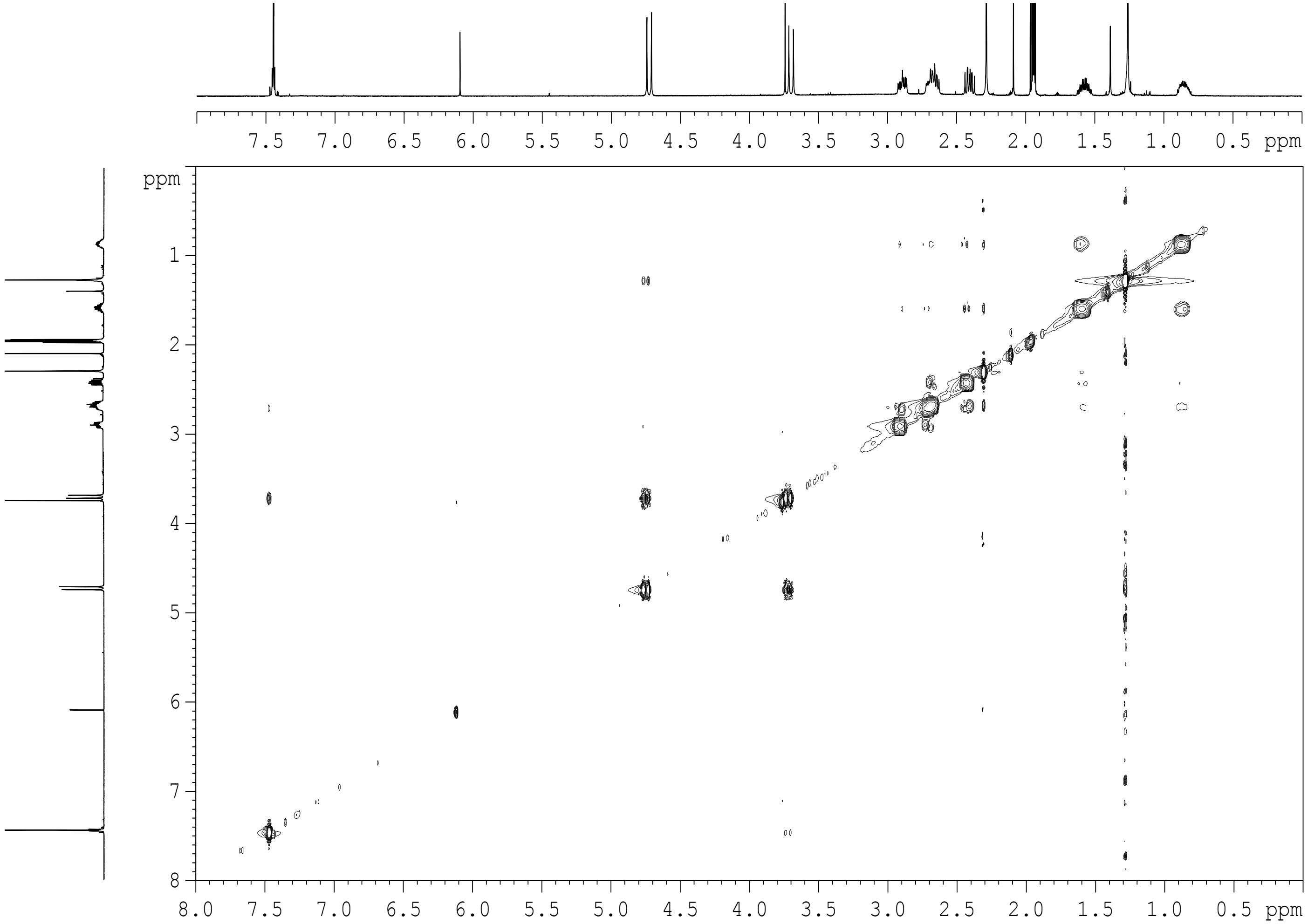

Figure S24. ^{1}H-^{13}C HSQC spectrum of compound **1f** in CD$_3$CN, 400 MHz, at 298 K.

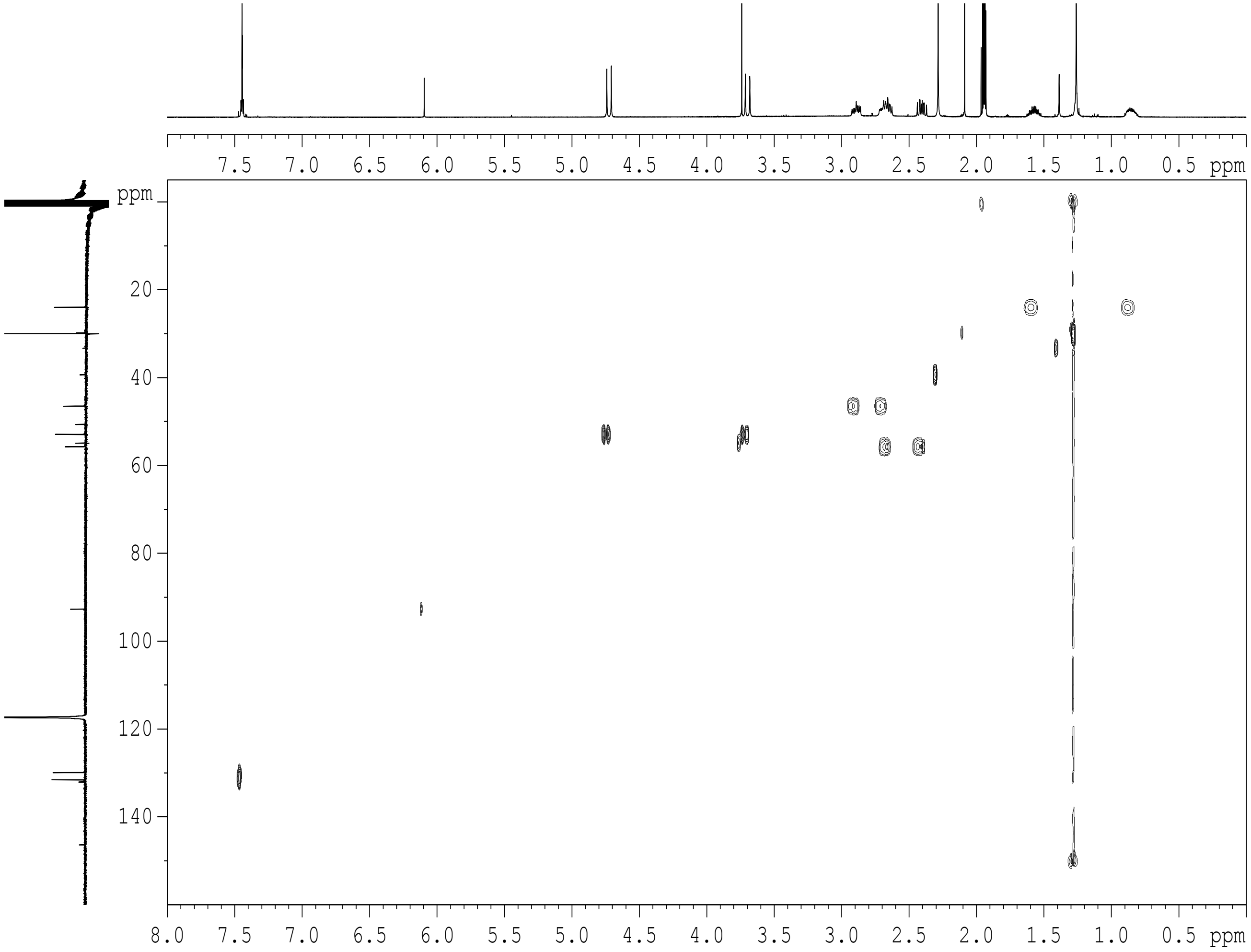

Figure S25. ^{1}H-NMR spectrum of compound **1g** in CD_3CN, 400 MHz, at 298 K.

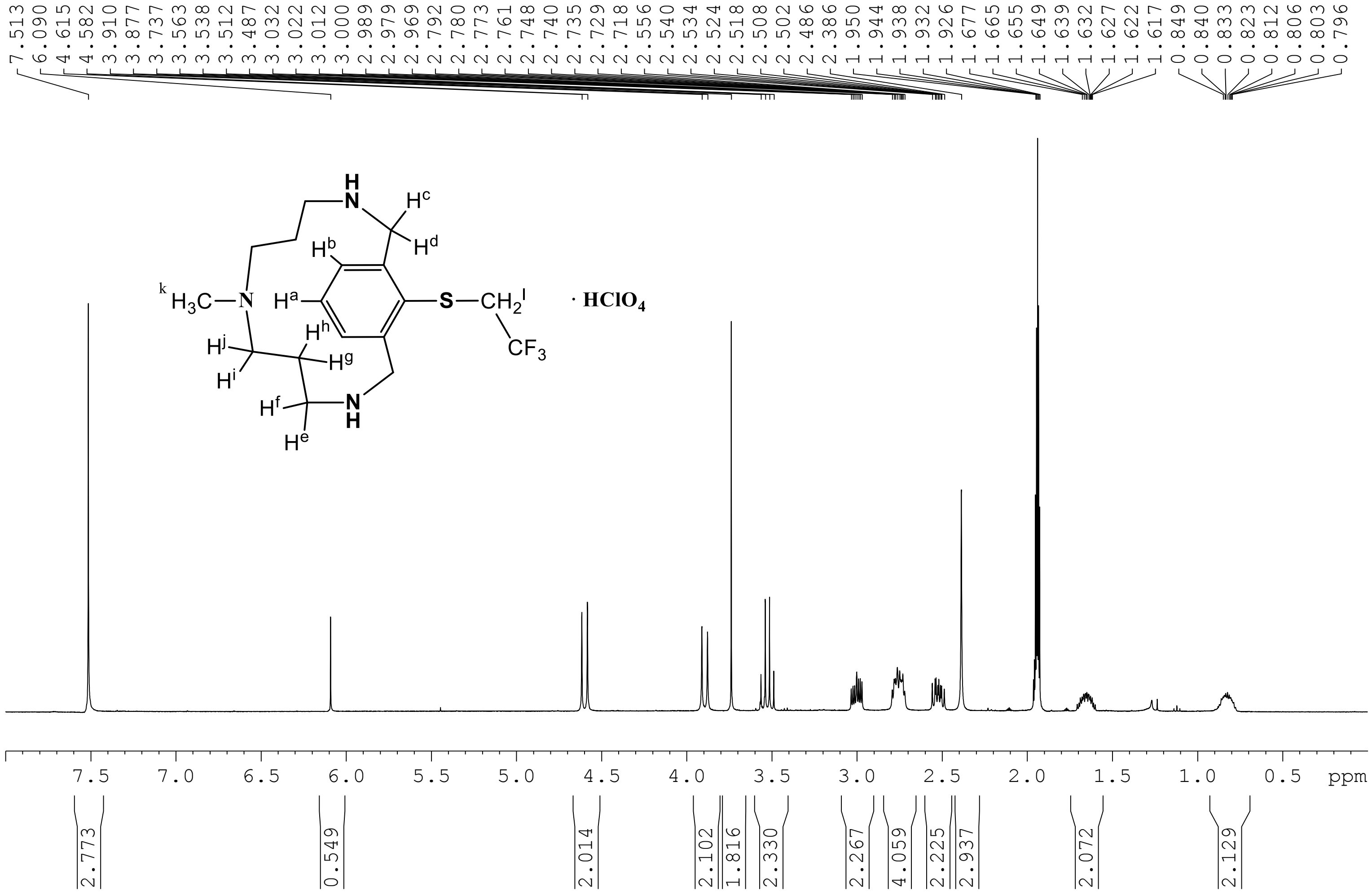

Figure S26. ^{13}C-NMR spectrum of compound **1g** in CD_3CN, 100 MHz, at 298 K.

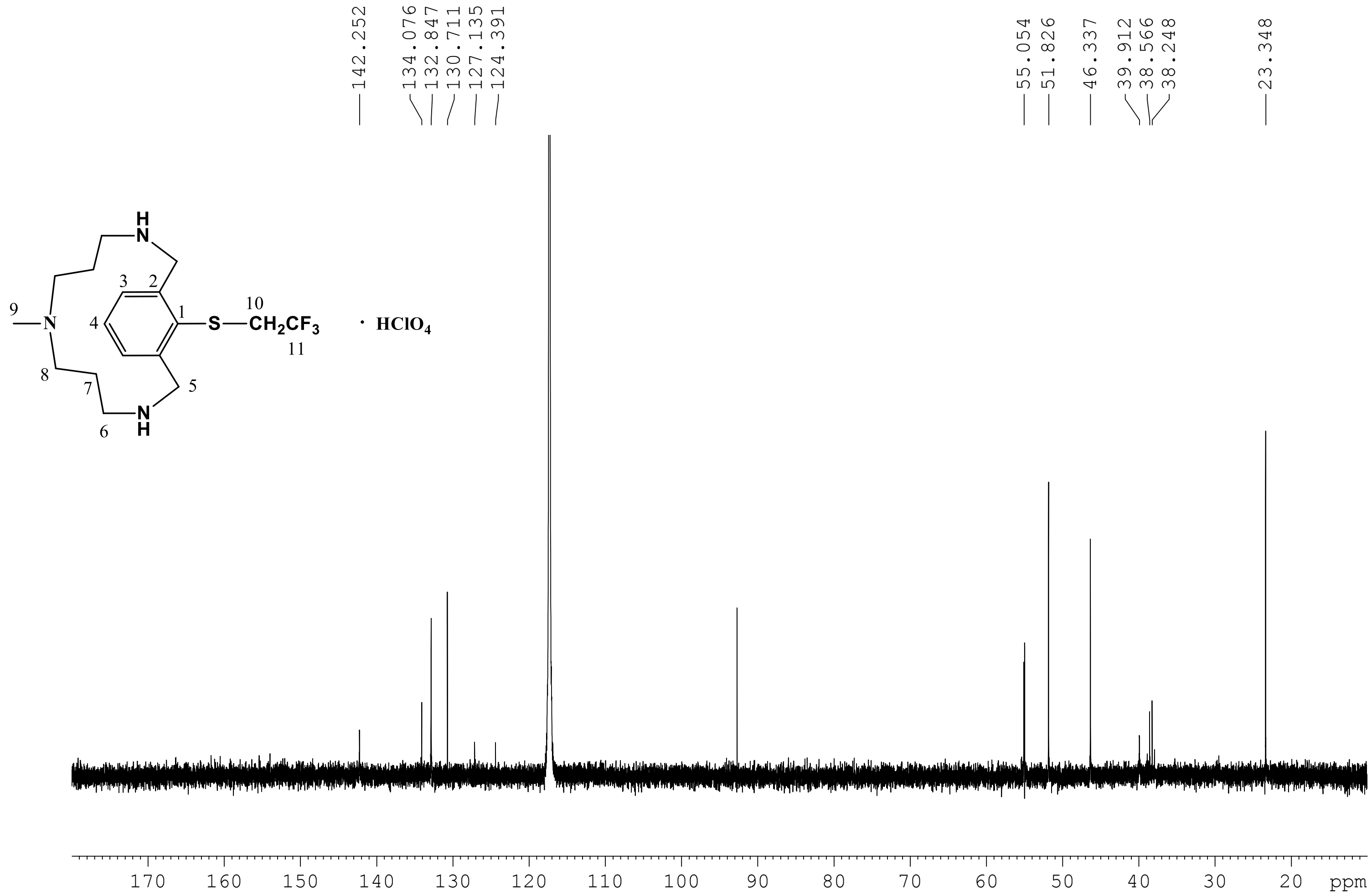

Figure S27. ^{1}H-NMR spectrum of compound **2a** in CD_3CN, 400 MHz, at 298 K.

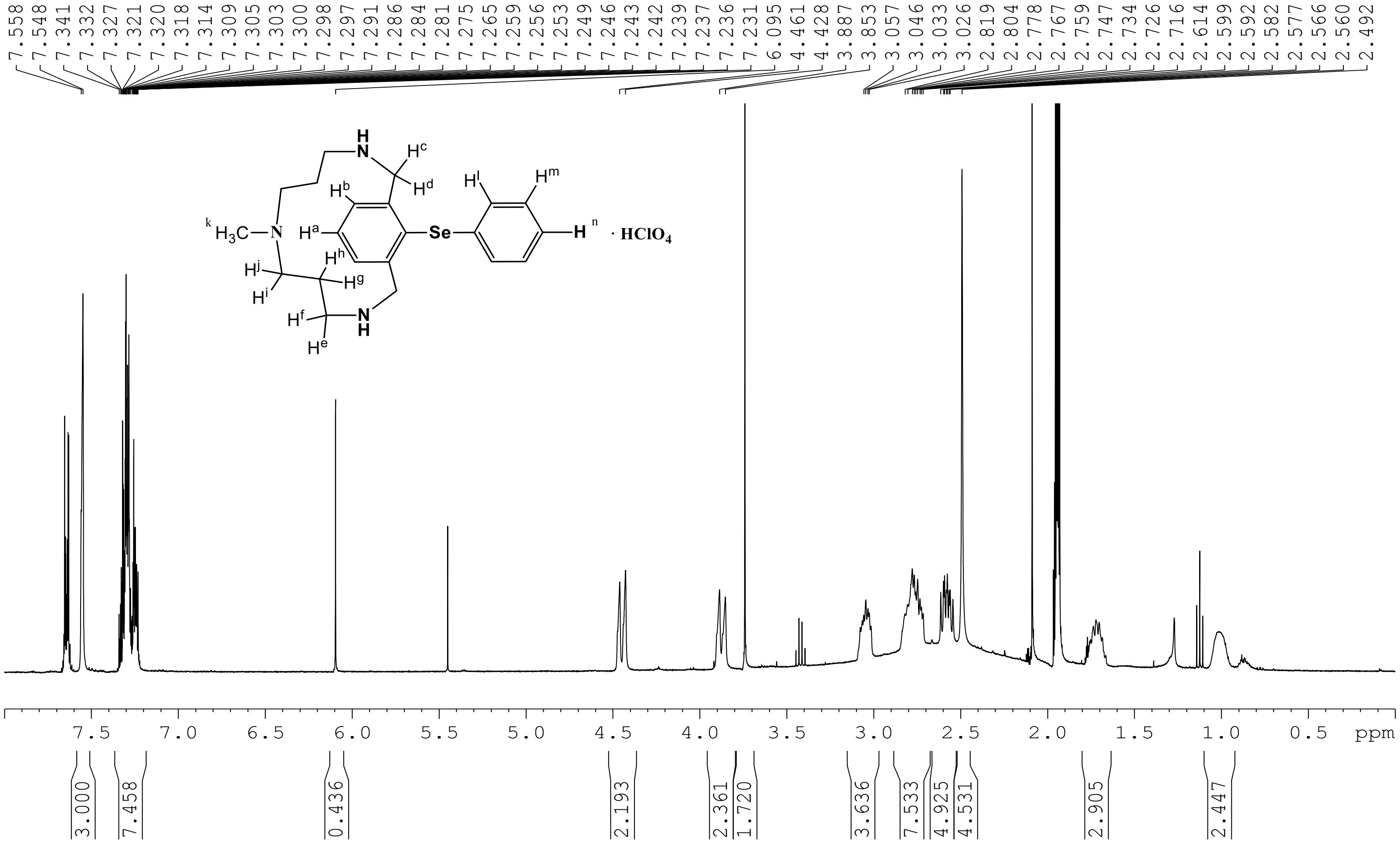

Figure S28. ^{13}C-NMR spectrum of compound **2a** in CD_3CN, 100 MHz, at 298 K.

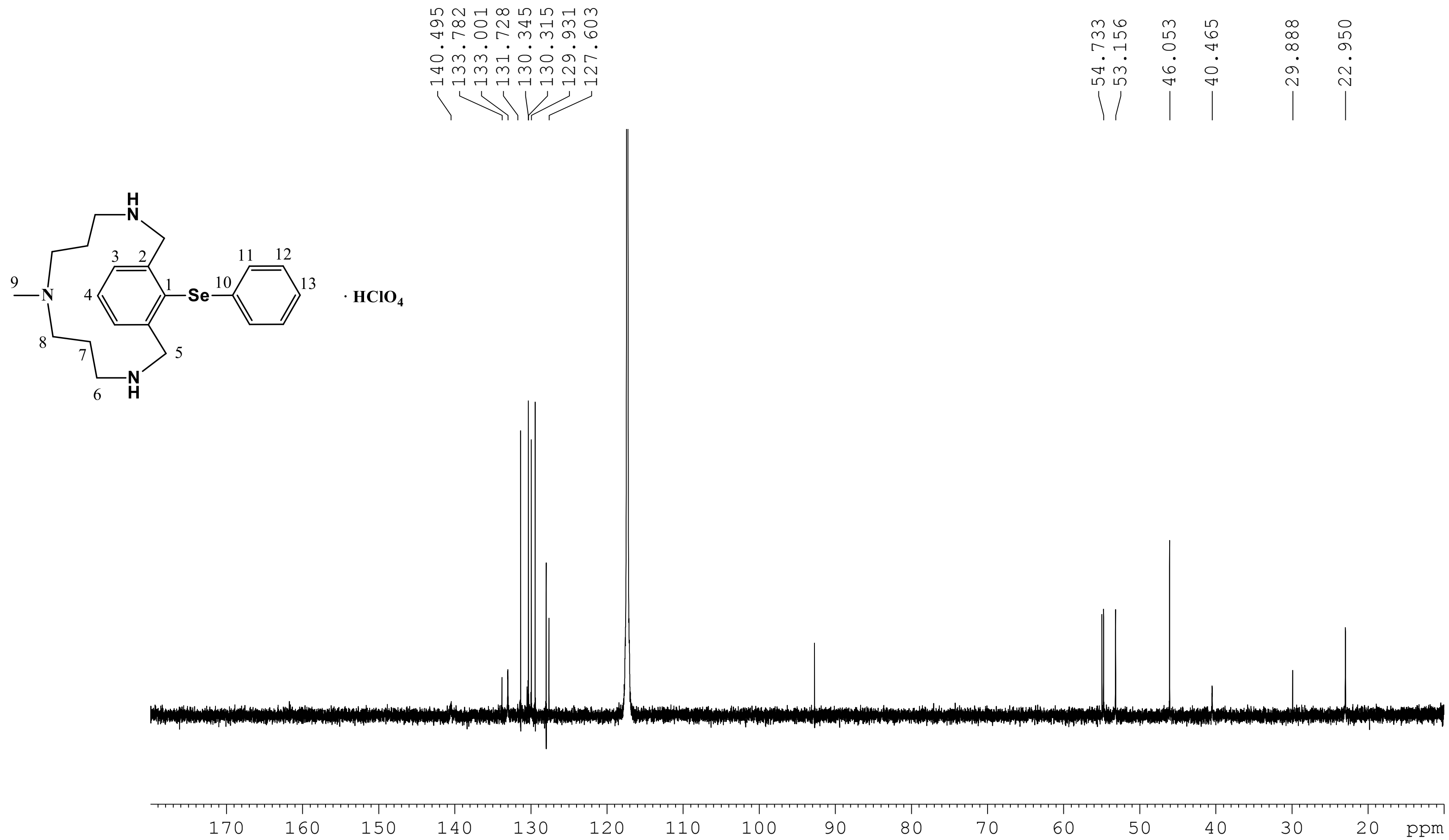

Figure S29. ^{1}H-^{77}Se HMBC spectra of compound **2a** optimized at 8 Hz (CD$_3$CN, 600 MHz, 298 K)

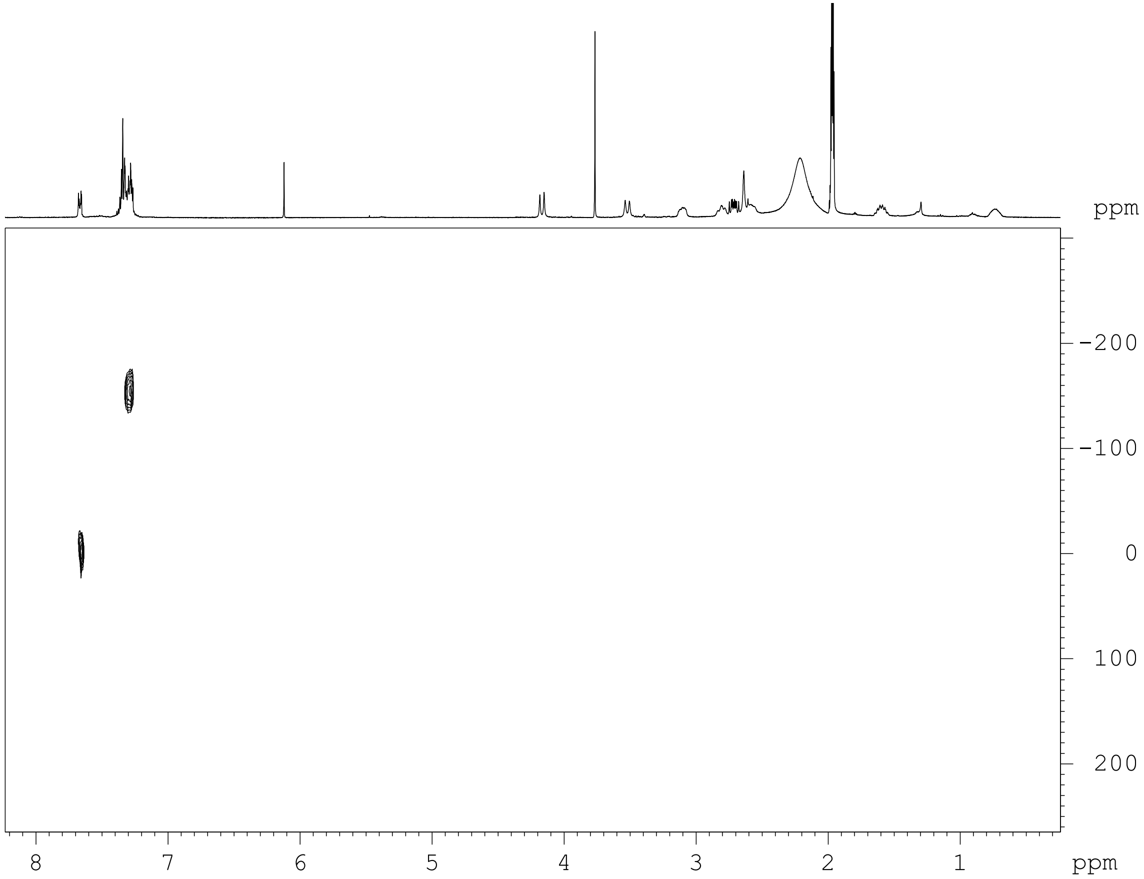

Figure S30. ^{1}H-DOSY spectra of L1-Se-Ph (CD_3CN, 600MHz, 298 K)

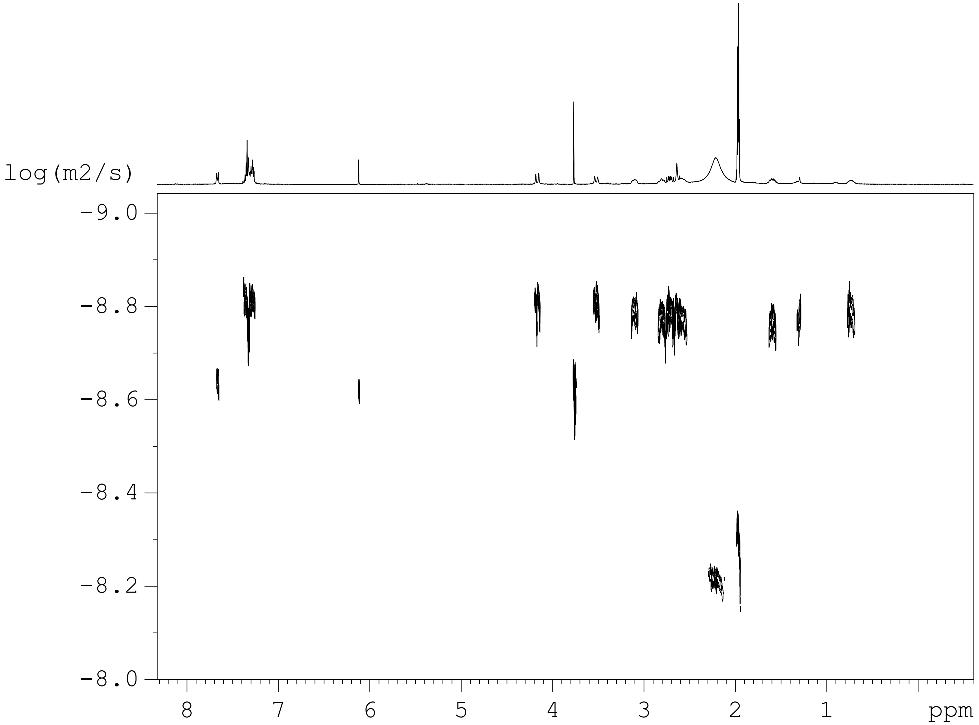

Figure S31. ^{1}H-NMR spectrum of compound **3a** in CD_3CN, 400 MHz, at 298 K.

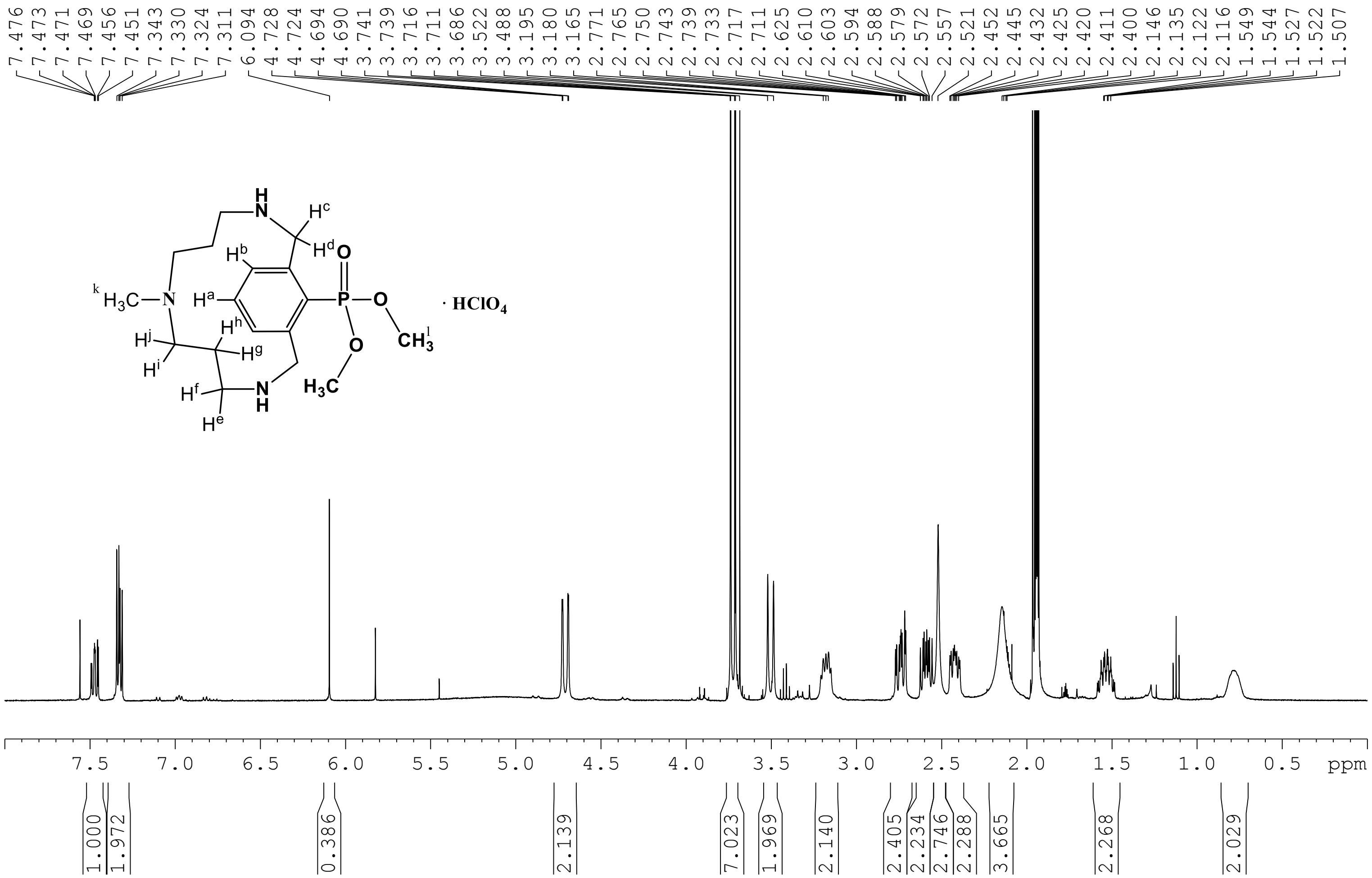

Figure S32. ^{13}C-NMR spectrum of compound **3a** in CD$_3$CN, 100 MHz, at 298 K.

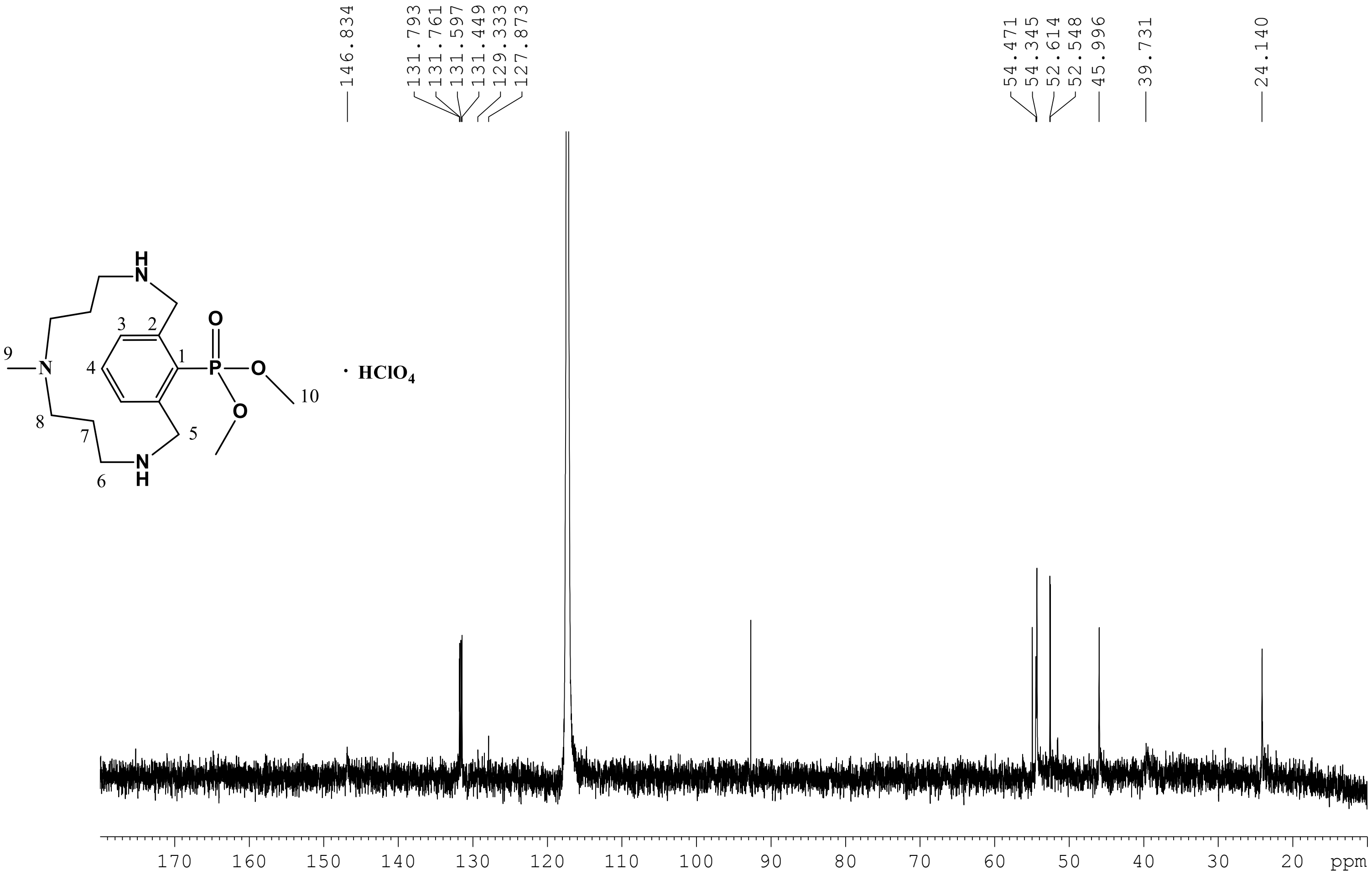

Figure S33. ^{31}P-NMR spectrum of compound **3a** in CD_3CN, 161.98 MHz on a Bruker 400 MHz, at 298 K.

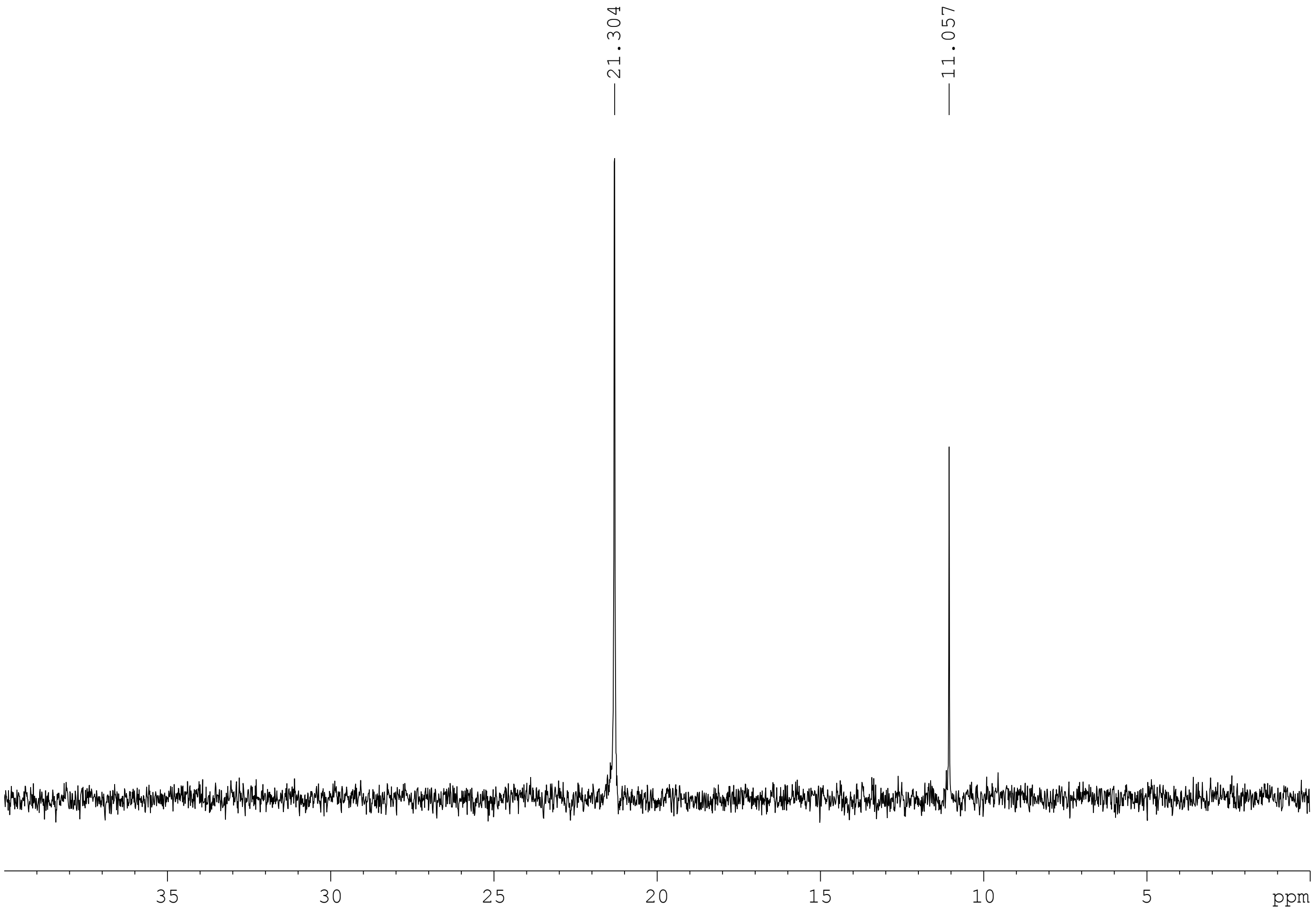

Figure S34. ESI-MS spectrum of compound **3a** and byproducts **3a.1** and **3a.2** in $CH_3CN:H_2O$ (80:20).

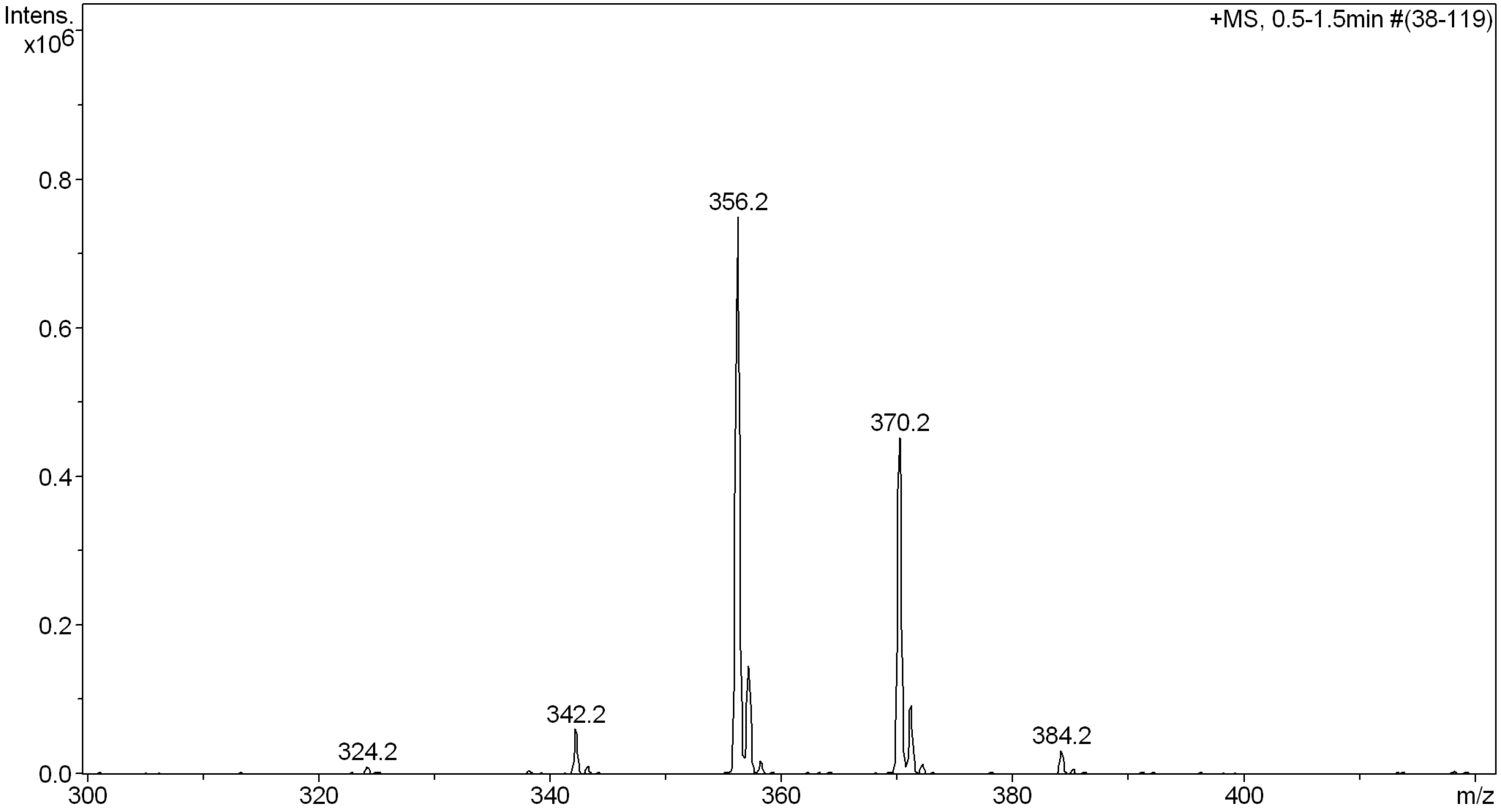

Figure S35. ^{1}H-NMR spectrum of compound **3b** in CD_3CN, 400 MHz, at 298 K.

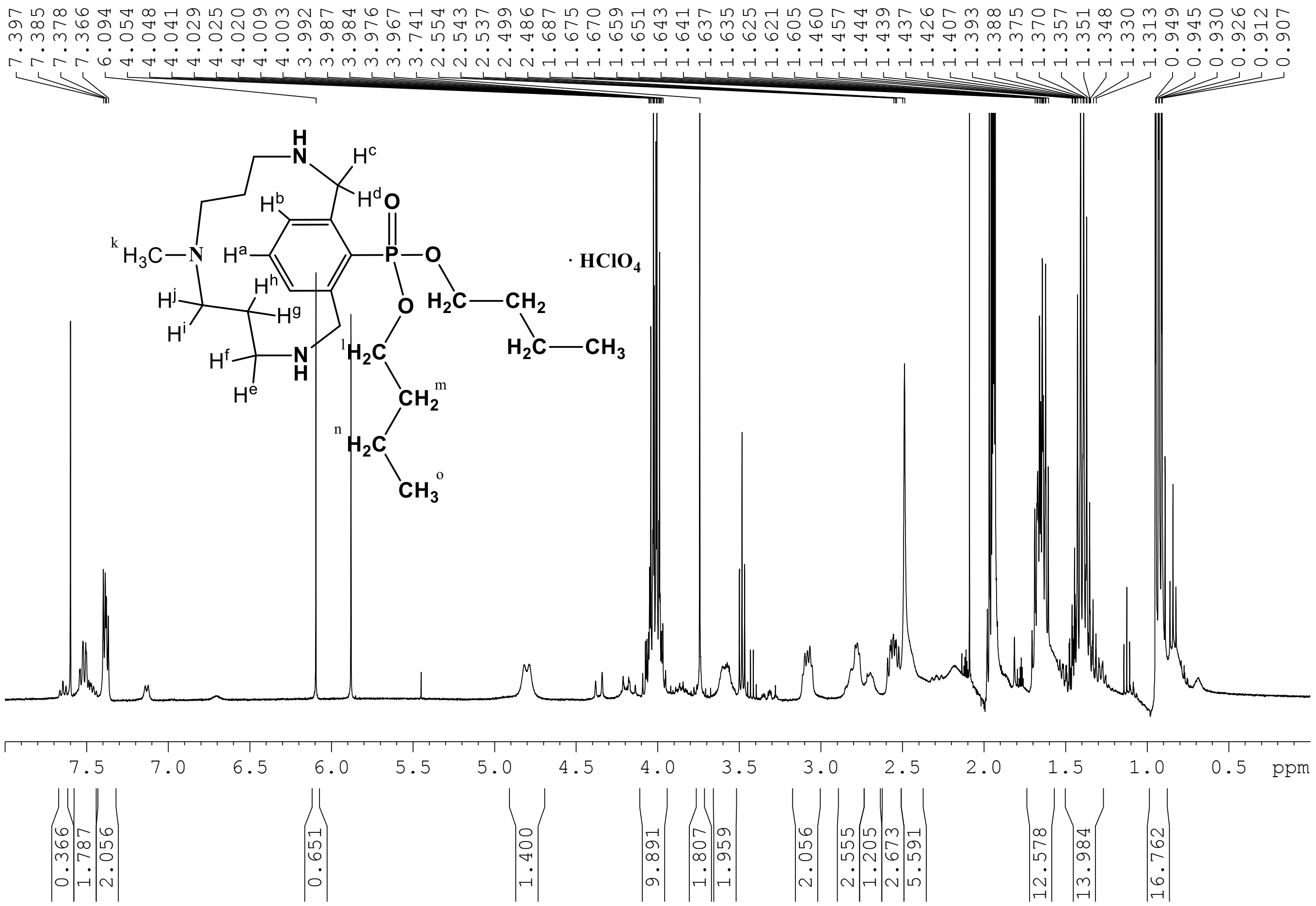

Figure S36. ^{13}C-NMR spectrum of compound **3b** in CD_3CN, 100 MHz, at 298 K.

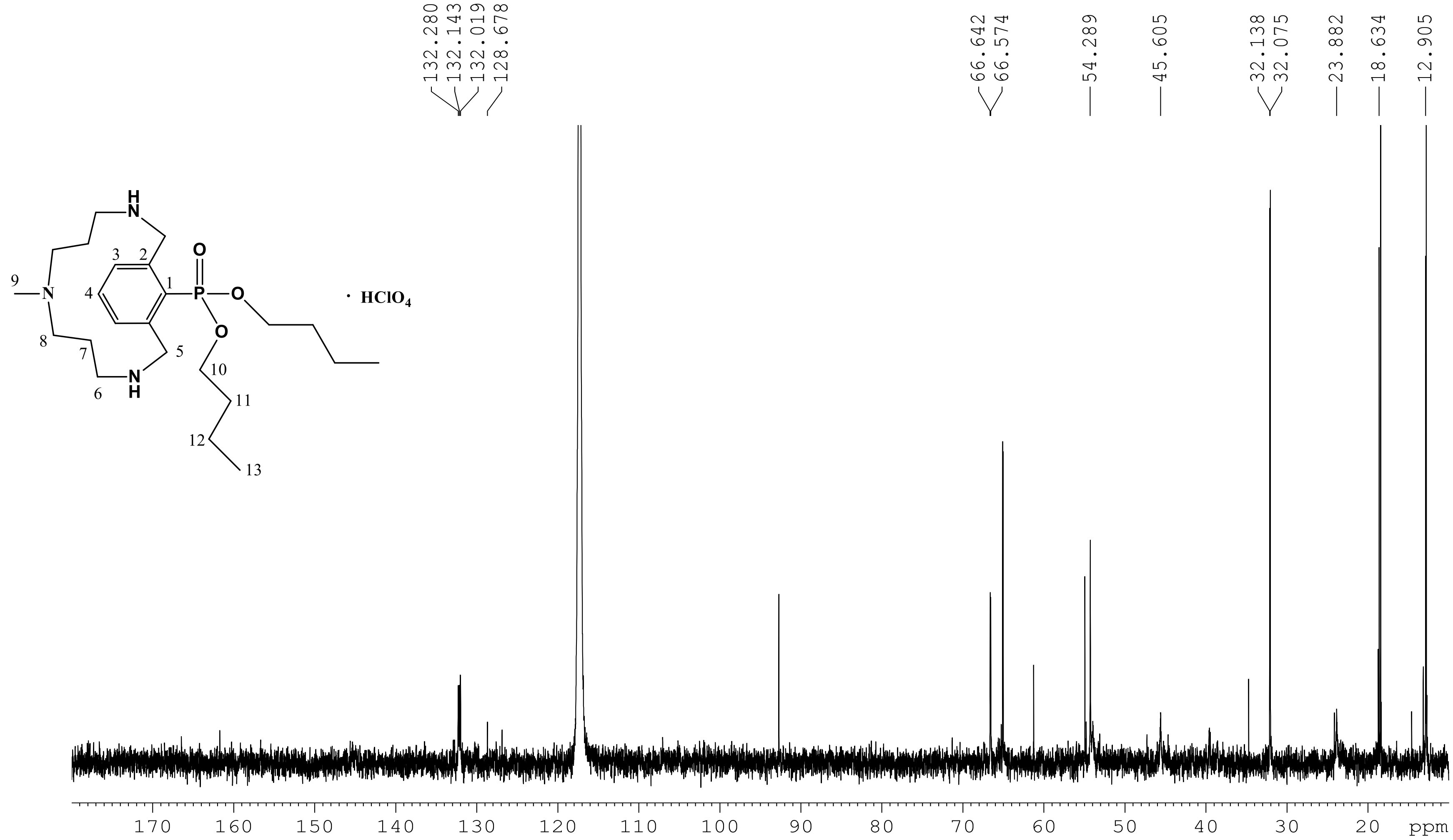

Figure S37. ^{31}P-NMR spectrum of compound **3b** in CD_3CN, 161.98 MHz, at 298 K.

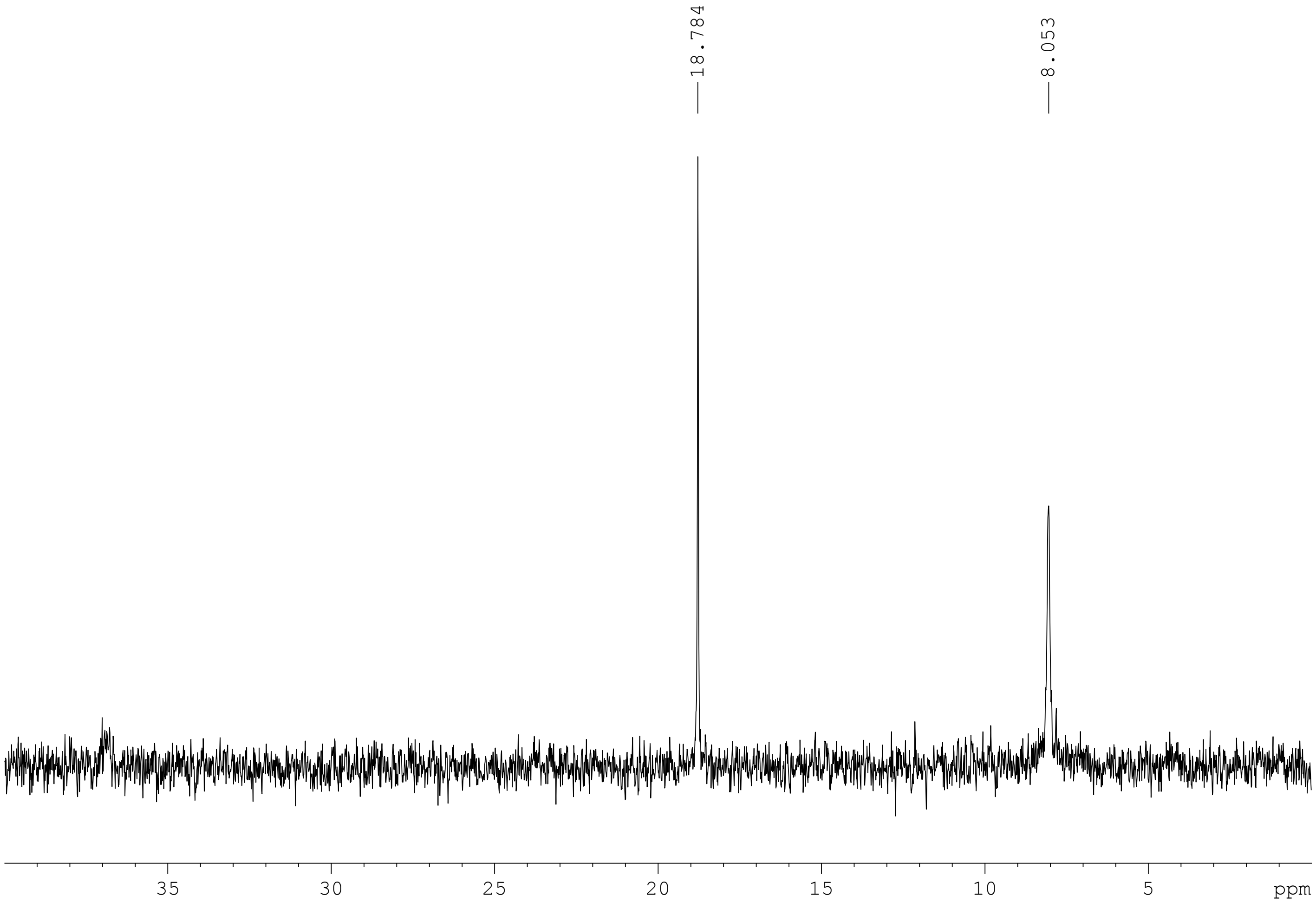

Figure S38. ^{1}H-NMR spectrum of compound **3c** in CD_3CN, 400 MHz, at 298 K.

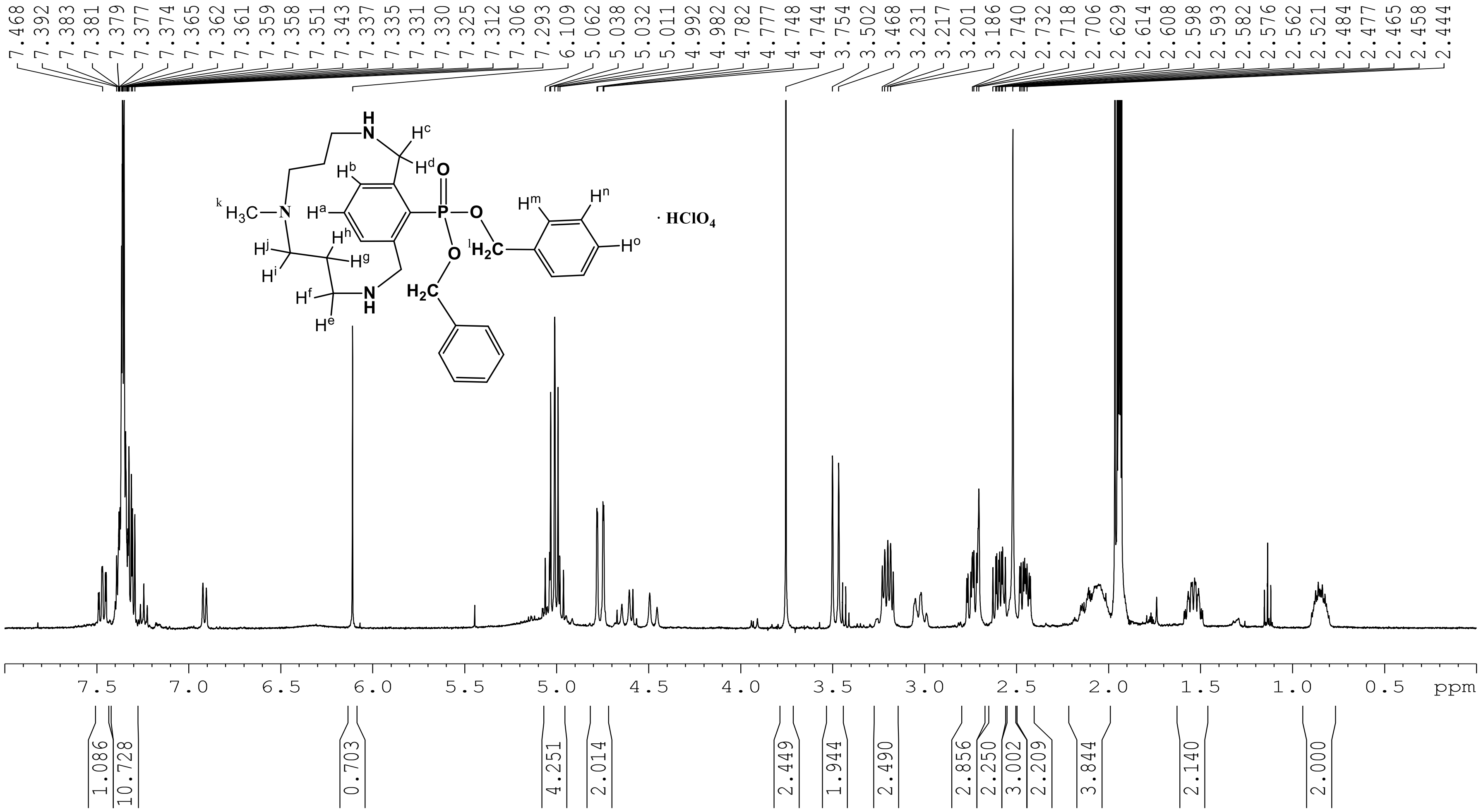

Figure S39. ^{13}C-NMR spectrum of compound **3c** in CD_3CN, 100 MHz, at 298 K.

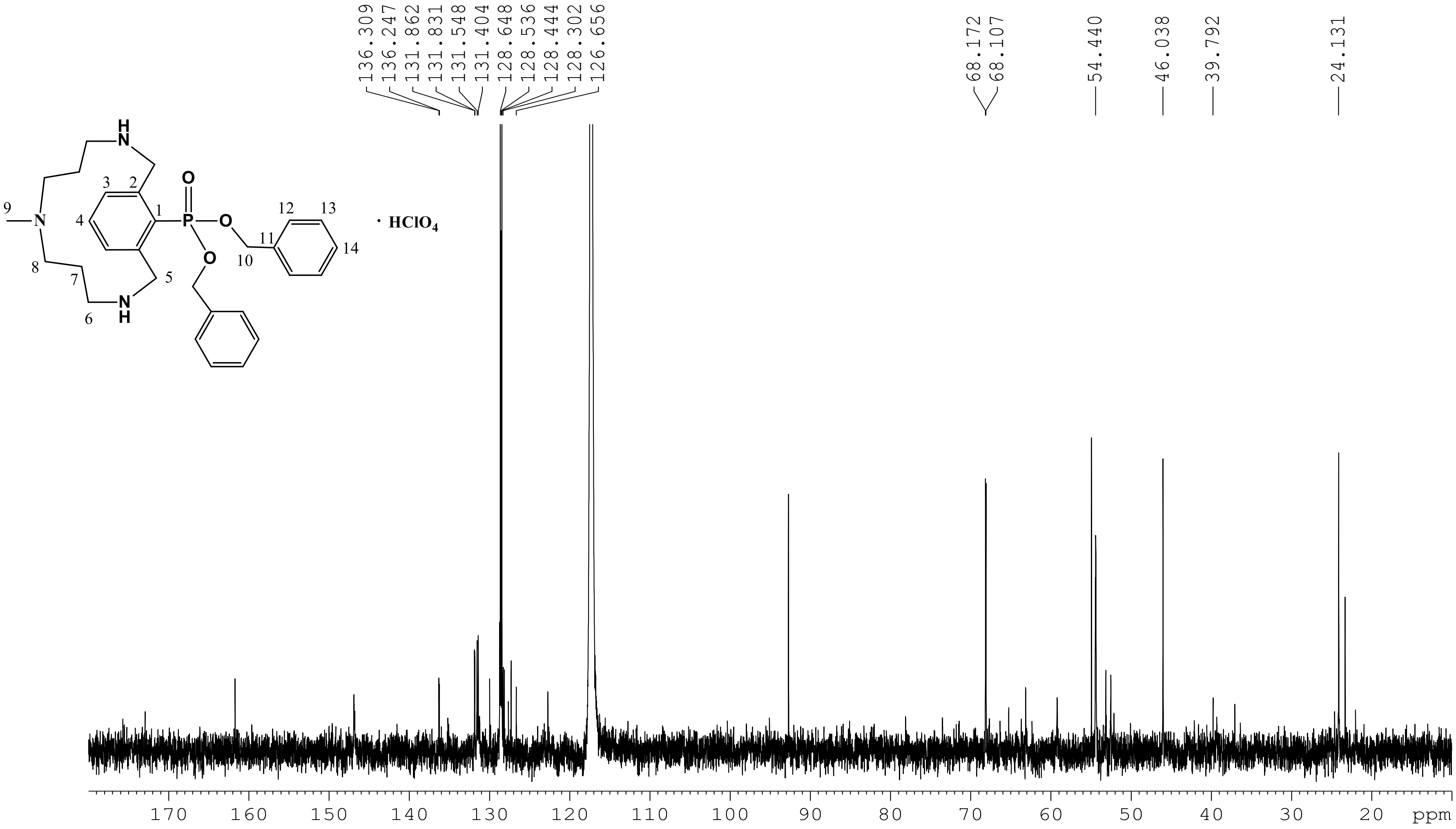

Figure S40. ^{31}P-NMR spectrum of compound **3c** in CD_3CN, 161.98 MHz, at 298 K.

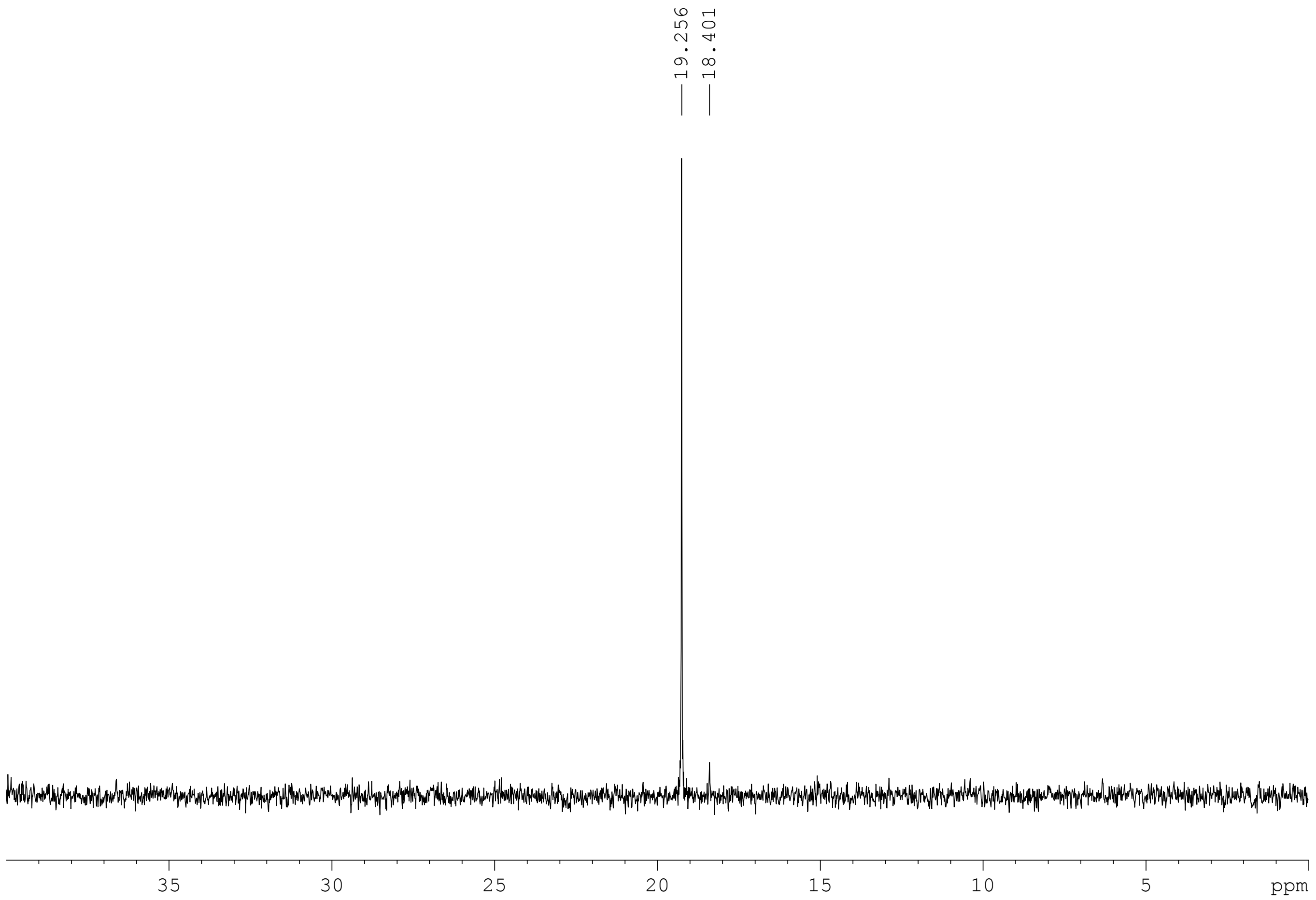

Figure S41. ESI-MS spectrum of compound **3c** and byproducts **3c.1** and **3c.2** in CH_3CN.

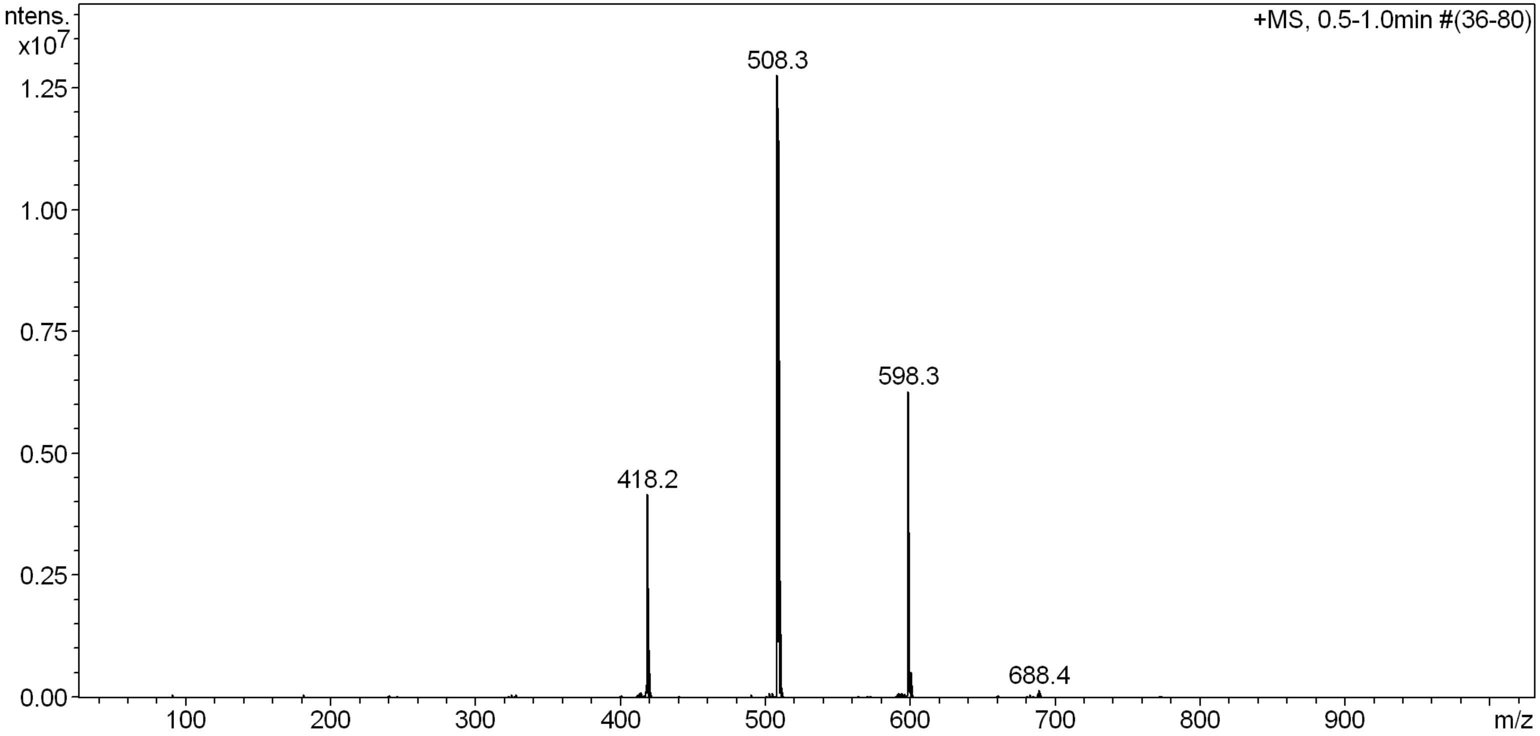

Figure S42. ^{1}H-NMR spectrum of compound **4a** in CD_3CN, 400 MHz, at 298 K.

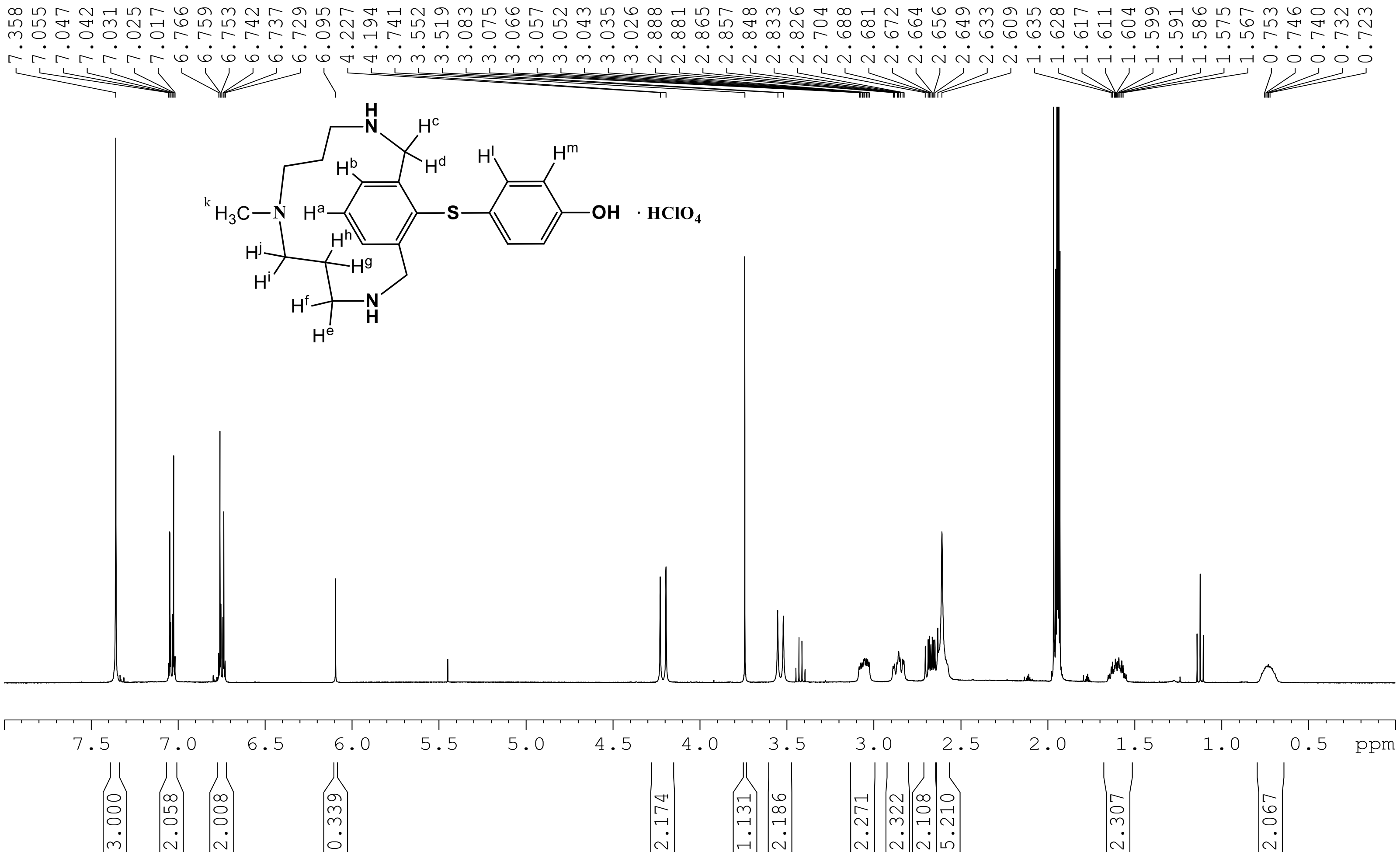

Figure S43. ^{13}C-NMR spectrum of compound **4a** in CD_3CN, 100 MHz, at 298 K.

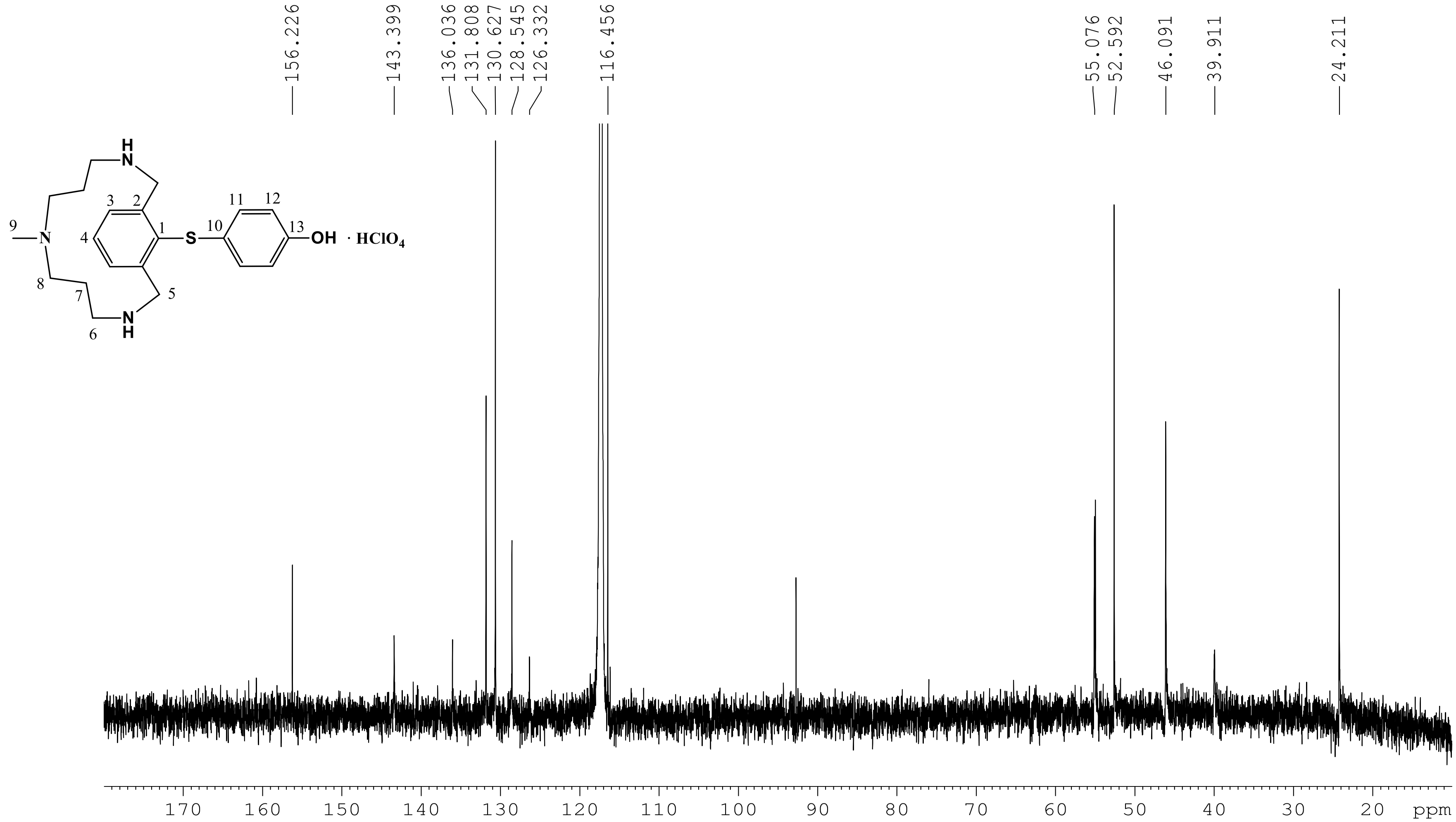

Figure S44. ^{1}H-NMR spectrum of compound **4b** in CD_3CN, 400 MHz, at 298 K.

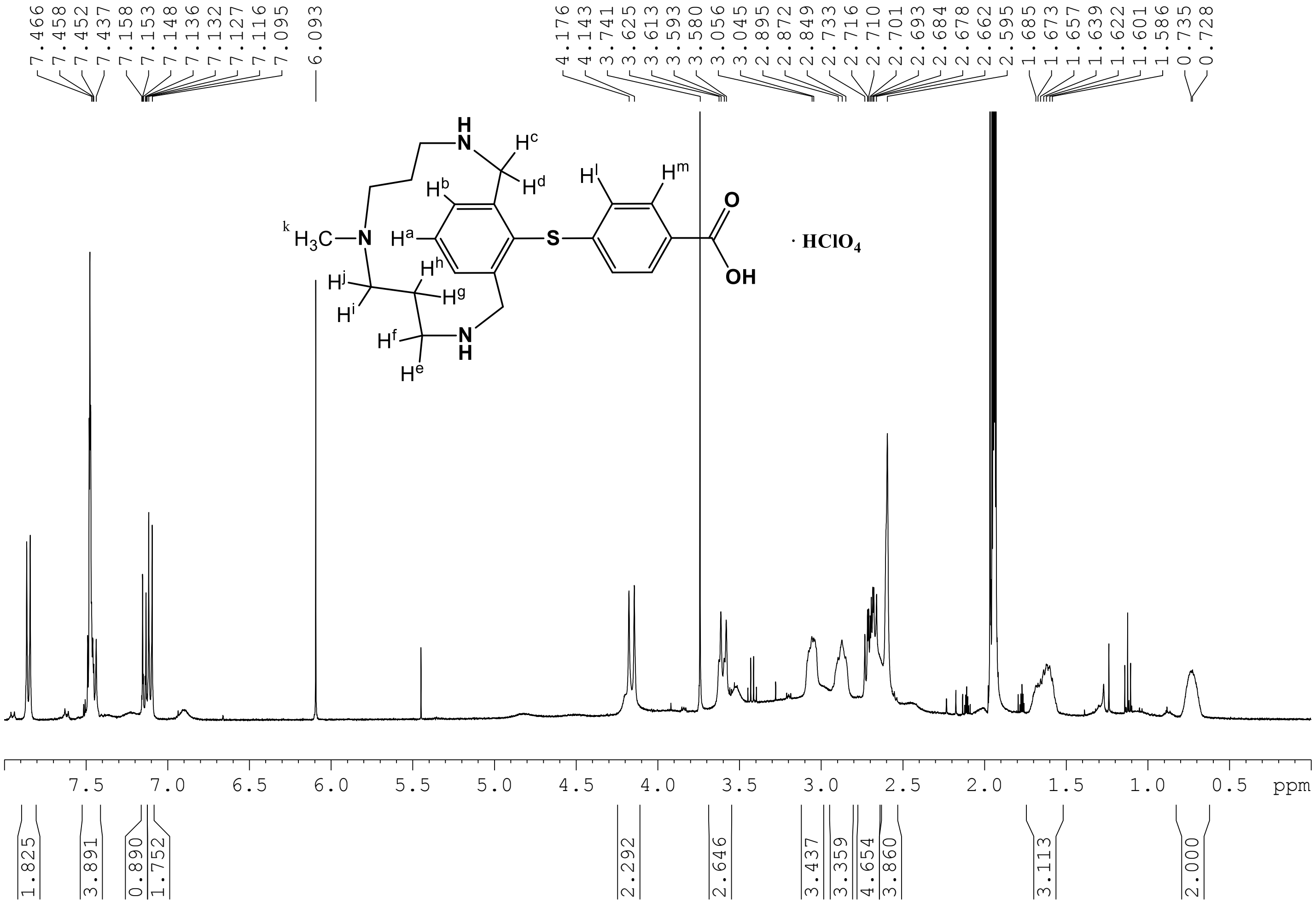

Figure S45. ^{13}C-NMR spectrum of compound **4b** in CD_3CN, 100 MHz, at 298 K.

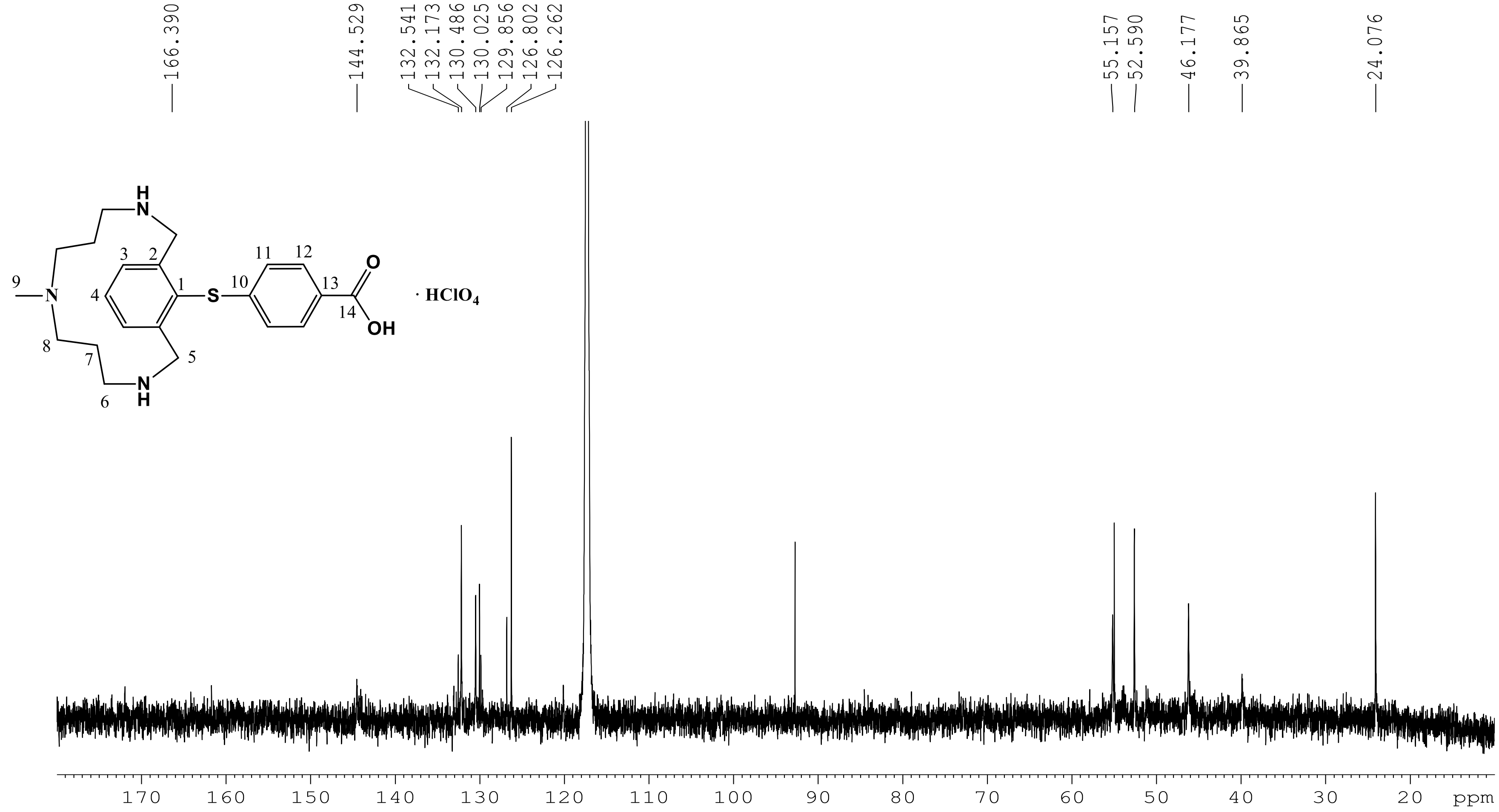

Figure S46. ^{1}H-NMR spectrum of compound **4c** in CD_3CN, 400 MHz, at 298 K.

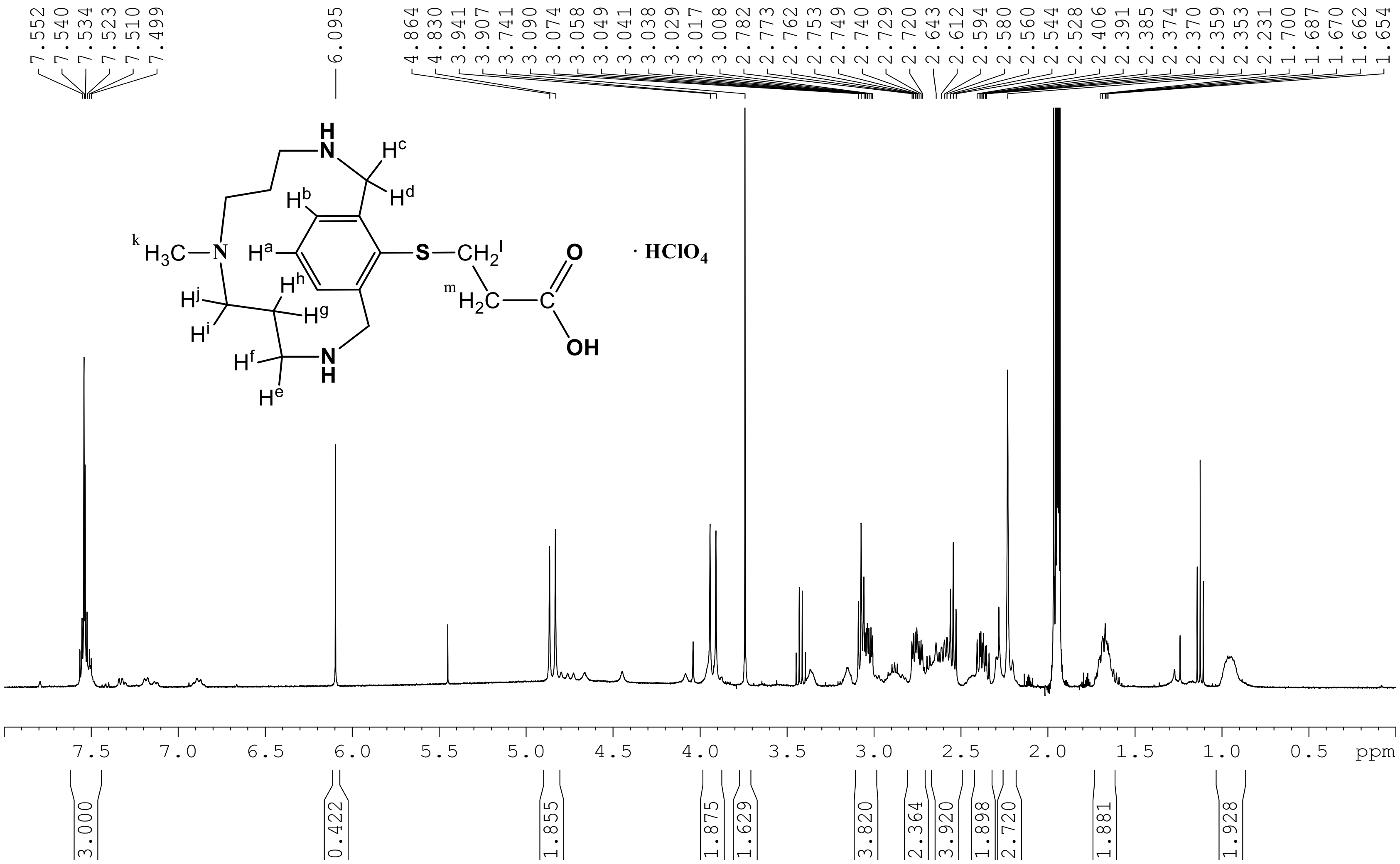

Figure S47. ^{13}C-NMR spectrum of compound **4c** in CD_3CN, 100 MHz, at 298 K.

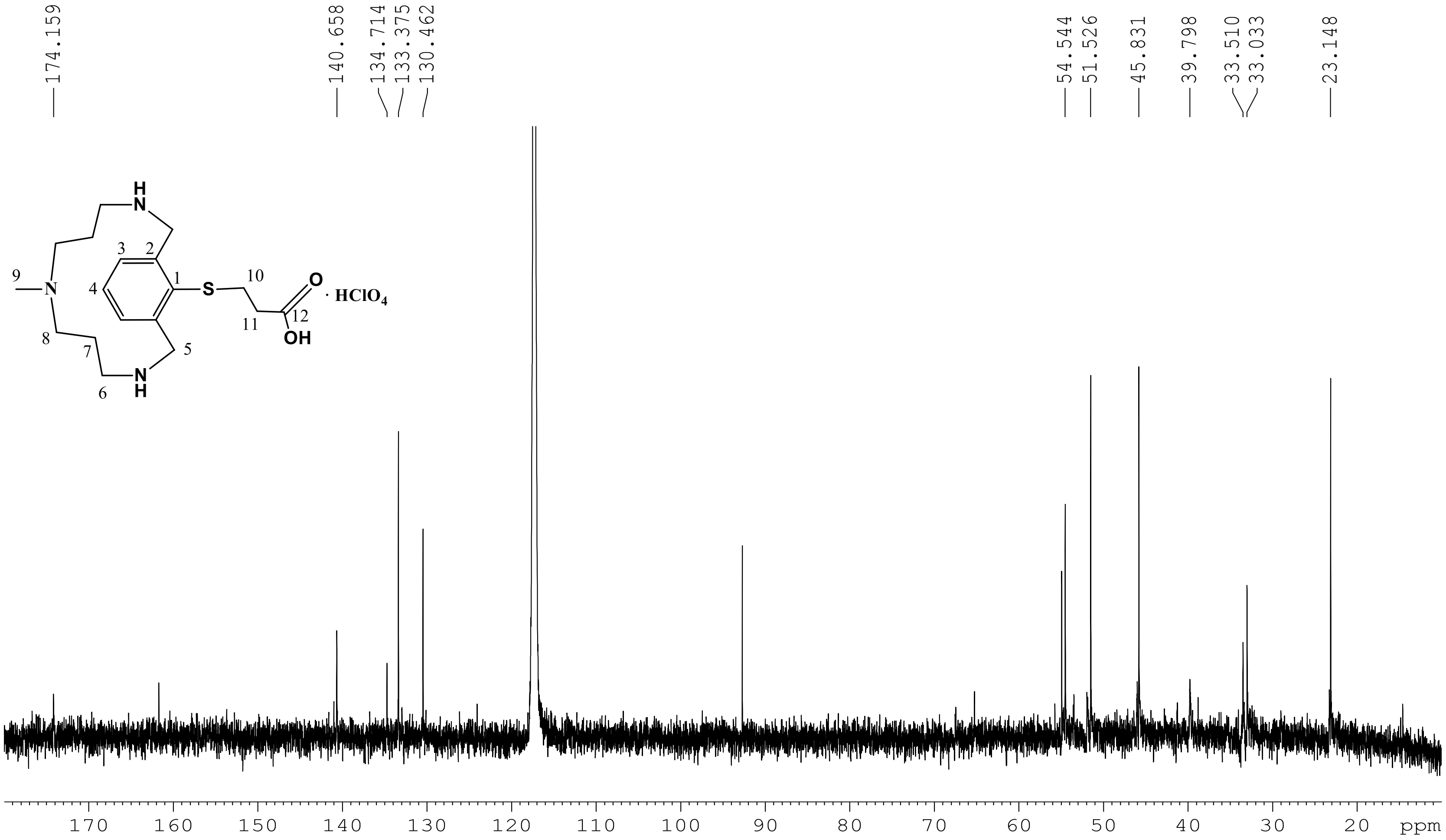

Figure S48. ^{1}H-NMR spectrum of compound **4d** in CD_3CN, 400 MHz, at 298 K.

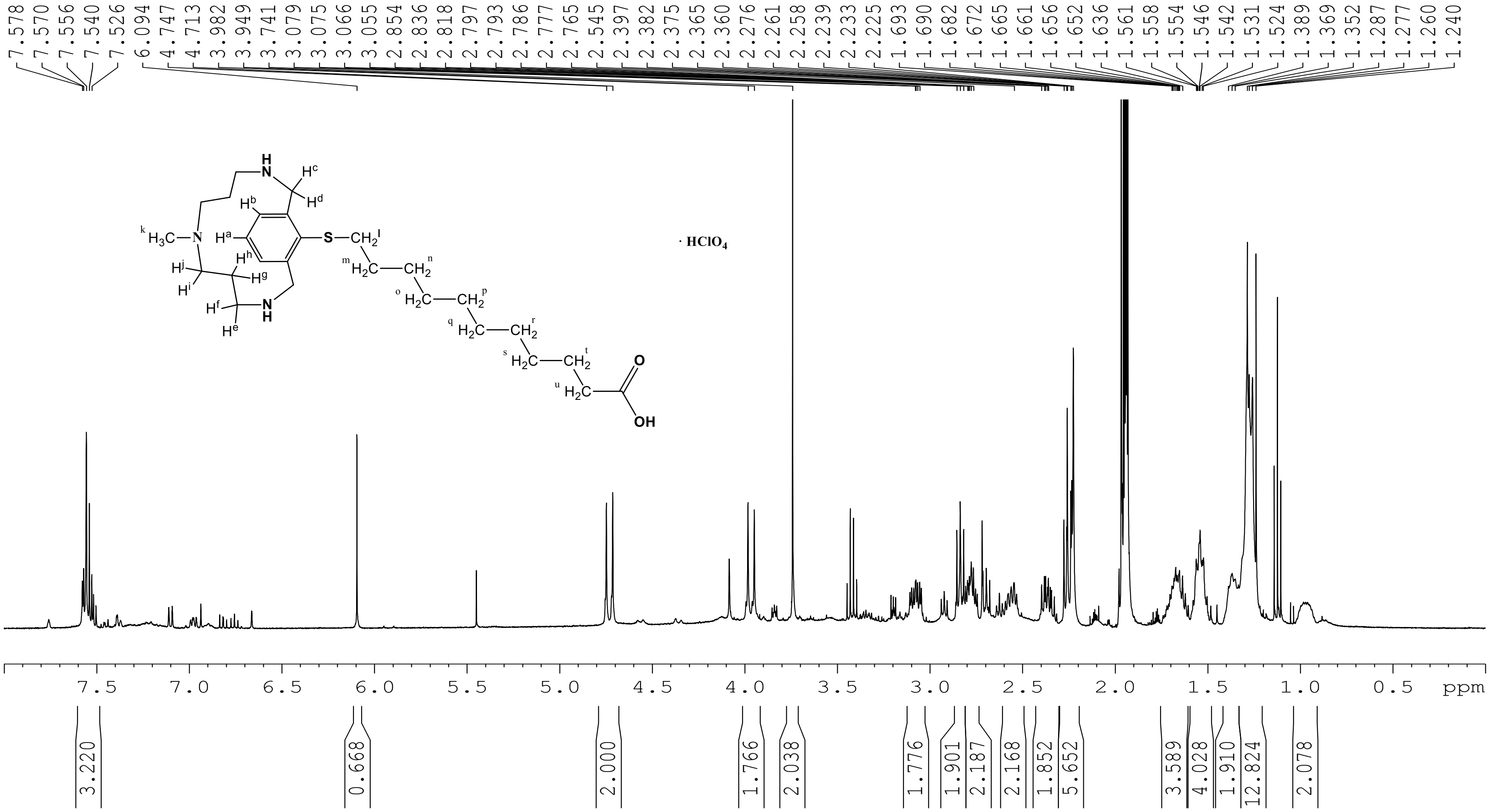

Figure S49. ^{13}C-NMR spectrum of compound **4d** in CD$_3$CN, 100 MHz, at 298 K.

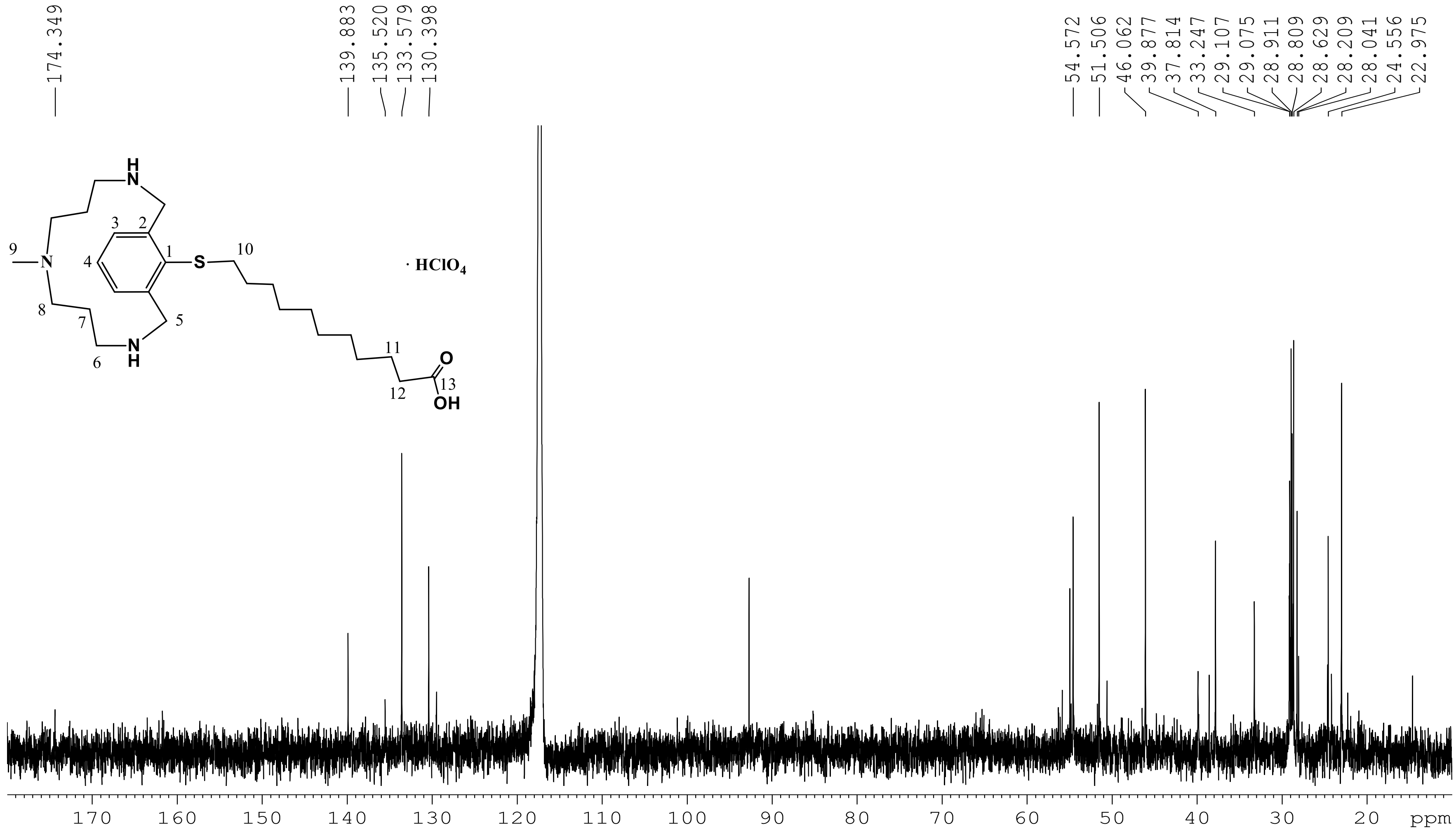

Figure S50. IR spectra of a) 11-mercaptoundecanoic acid and b) of the insoluble precipitate corresponding to the C-O coupling product between **1** and 11-mercaptoundecanoic acid (the free thiol group reacts with Cu^I to produce the insoluble product). The C=O stretching shifts from 1696 cm^{-1} for the acid moiety (spectrum a)) to 1712 cm^{-1} for the R-COO-aryl moiety (spectrum b)).

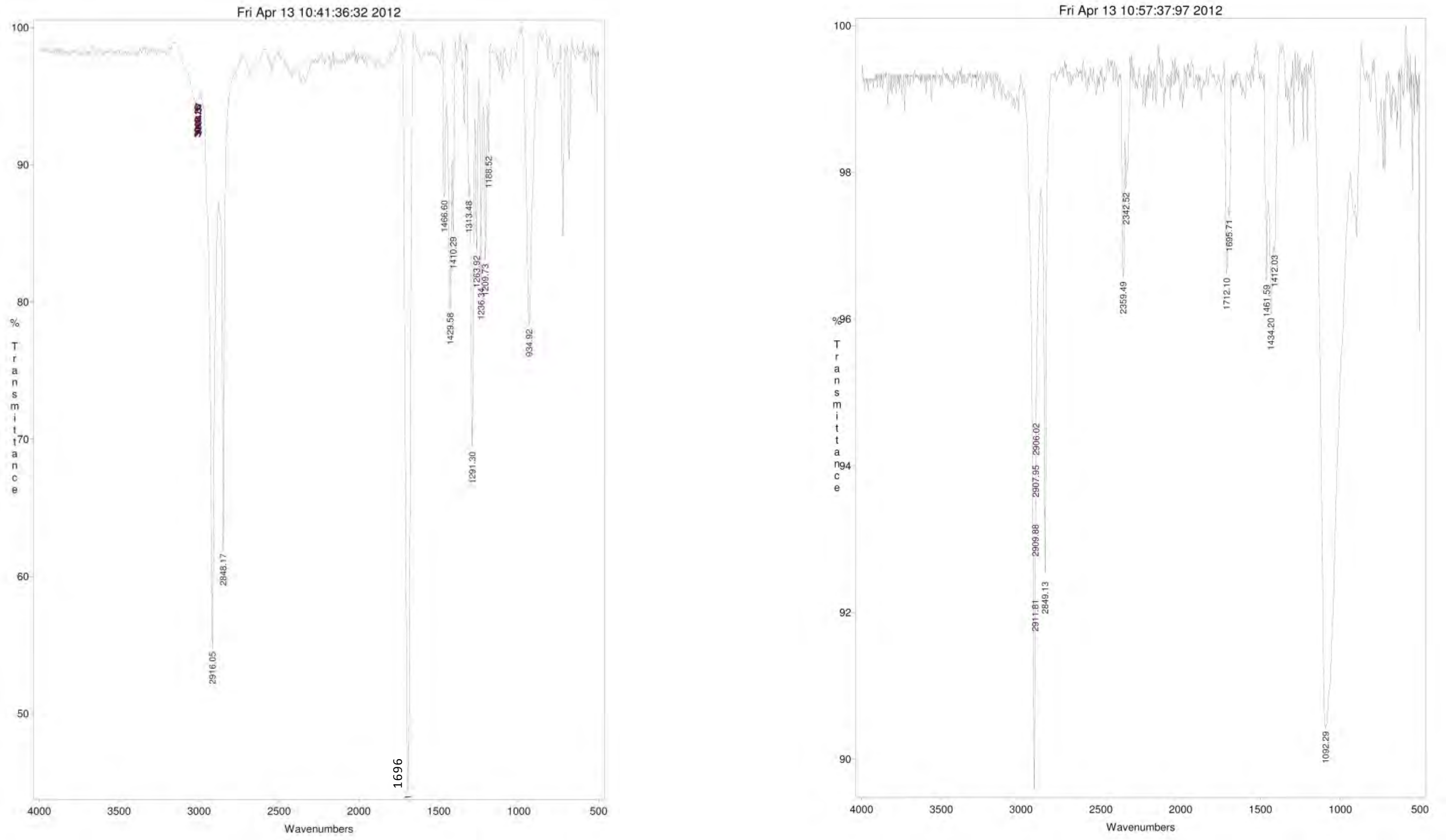

a) b)

Figure S51. Low temperature UV-vis monitoring of the initial stages of the reaction of **1** with a) benzeneselenol and b) *p*-methoxythiophenol respectively showing the formation of adduct species. Conditions: [**1**] = 0.8 mM, [Nuc] = 0.72, CH_3CN, 0 ºC for benzeneselenol, -35 ºC for *p*-methoxythiophenol.

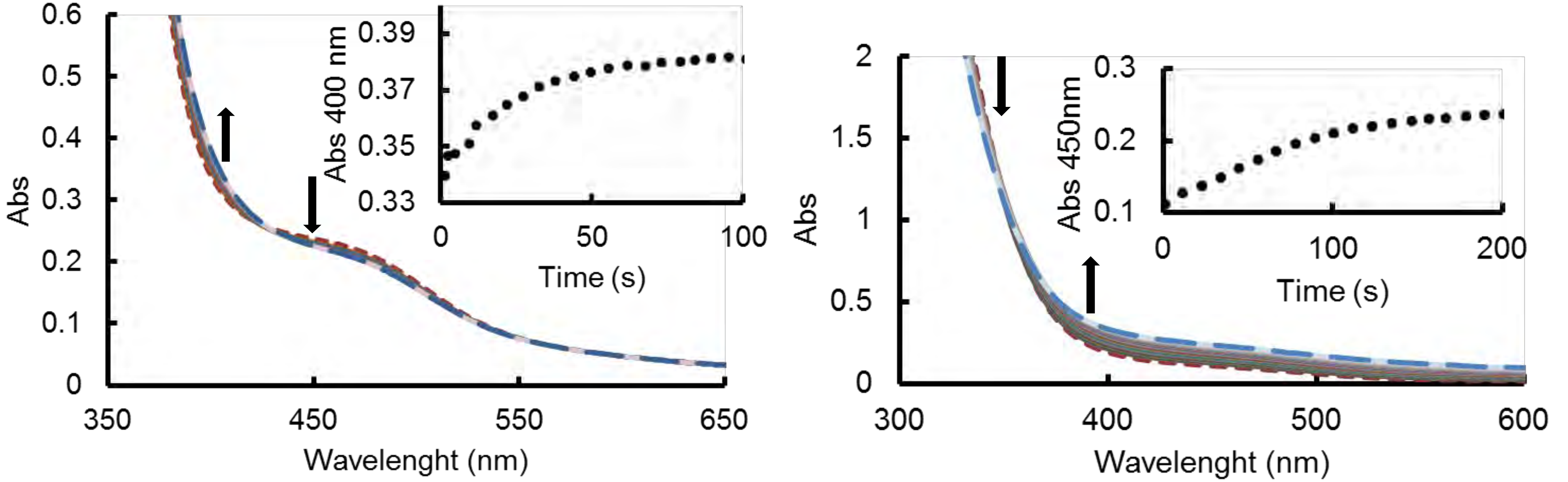

Figure S52. ^{1}H NMR spectrum of the adduct species (AD, see Figure S51) formed upon reaction of **1** with *n*BuSH at -35ºC, 5 min after mixing. Conditions: [**1**] = 4 mM, [*n*BuSH] = 3.6 mM, CD_3CN, -35ºC.

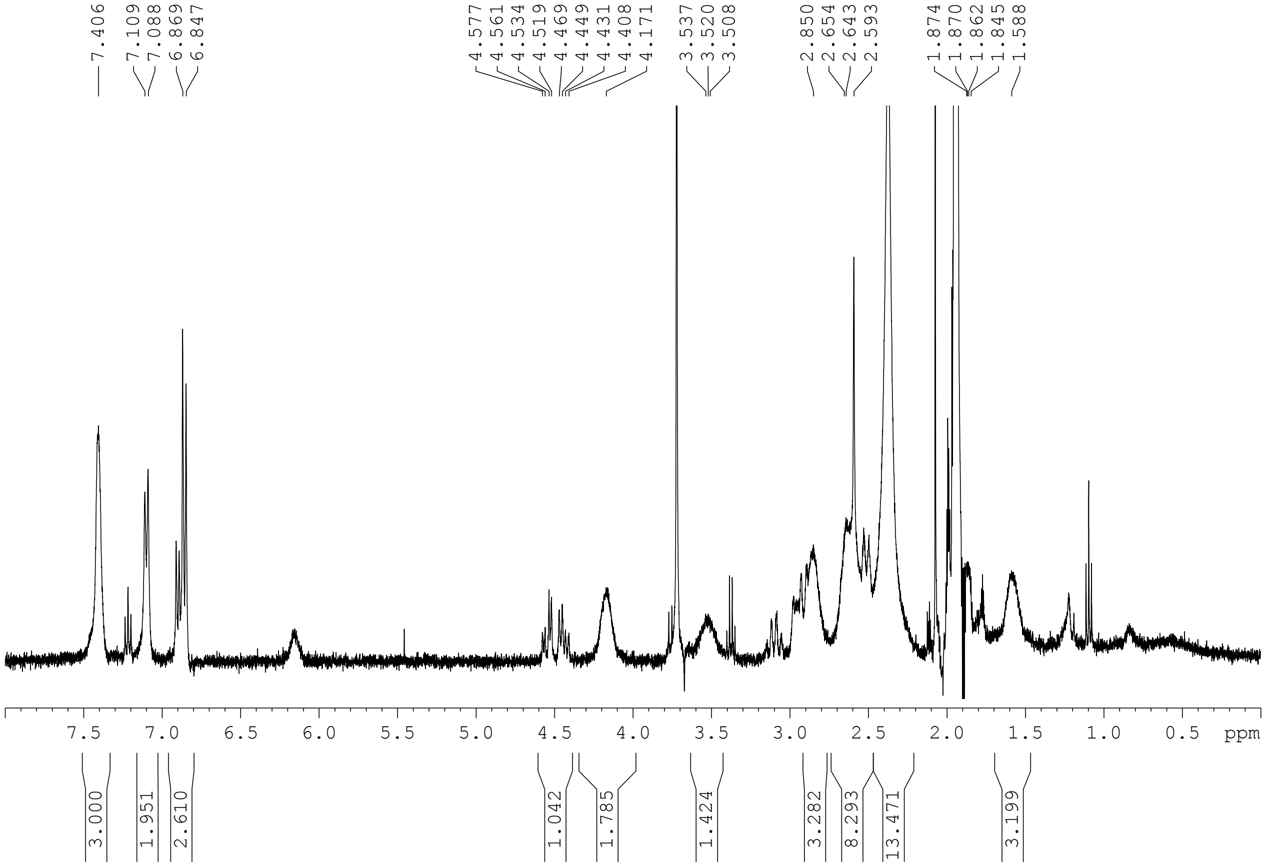

Figure S53. Low temperature ^{1}H NMR monitoring of the reaction of **1** with *p*MeO-PhSH. Conditions: [**1**] = 4 mM, [*p*MeO-PhSH] = 3.6 mM, CD$_3$CN, -38ºC.

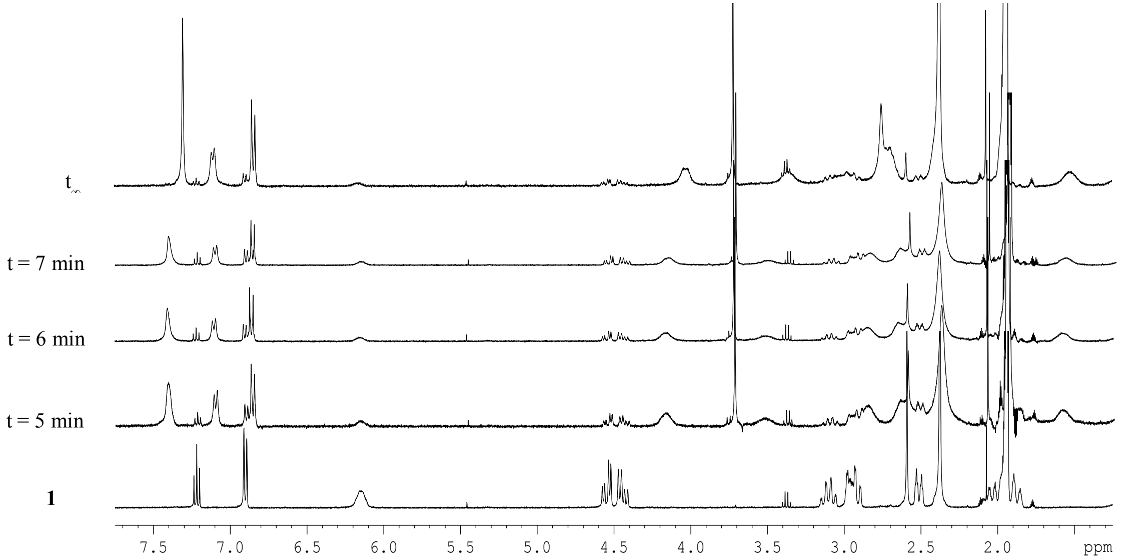

Figure S54. UV-vis monitoring of the initial stages of the copper(I)-catalyzed (Cu^I 10 mol%) C-S cross coupling reaction between **L1-Br** substrate and *p*Cl-PhSH. The formation of bands at 550 and 400 nm clearly indicates the rapid aryl-Br oxidative addition to form aryl-Cu^{III}-Br intermediate species (**2_{Br}**), The inset shows the rapid formation of **2_{Br}** and its steady-state formation during the first stages of the catalysis. (Final concentrations: [**L1-Br**] = 10 mM, [$Cu^I(CH_3CN)_4OTf$] = 1 mM, [*p*Cl-PhSH] = 11 mM, CH_3CN, 20 ºC)

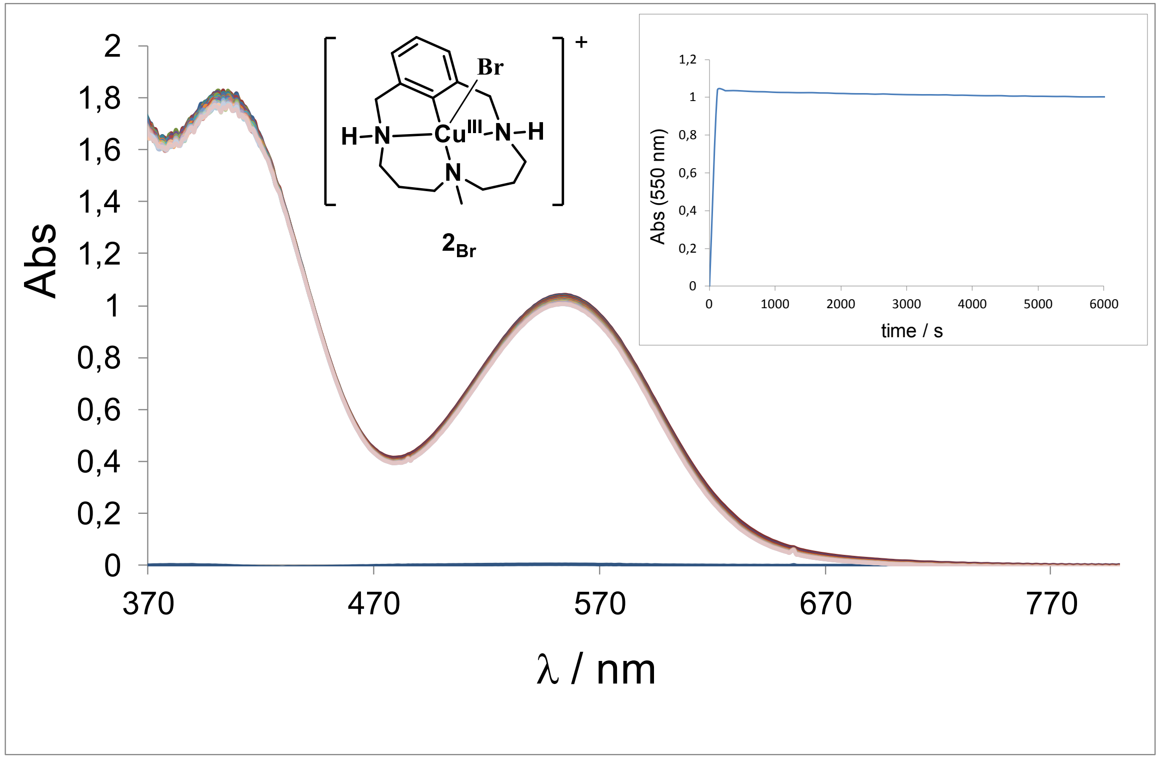

ANNEX II

Supplementary Information

Direct observation of two-electron Ag(I)/Ag(III) redox cycles in coupling catalysis

*Marc Font,[a] Ferran Acuña-Parés,[a] Teodor Parella,[b] Jordi Serra,[a] Josep M. Luis,[a] Julio Lloret-Fillol,[a] Miquel Costas [a] and Xavi Ribas [a,]**

[a] Institut de Química Computacional i Catàlisi (IQCC) and Departament de Química, Universitat de Girona, Campus Montilivi, Girona E-17071, Catalonia, Spain. [b] Servei de NMR, Facultat de Ciències, Universitat Autònoma de Barcelona, Campus UAB, Bellaterra, E-08193, Catalonia, Spain

CONTENTS

1. Supplementary Methods 172

- 1.1. Synthesis of ligands 172
- 1.2. Procedure for the oxidative addition of silver(I) salts to $\mathbf{L_1}$**-I** 172
- 1.3. Description of the C-N coupling product 172
- 1.4. Description of the C-O coupling products 173
- 1.5. Description of the C-S coupling product 175
- 1.6. Description of the C-C coupling products 176
- 1.7. Description of the C-C coupling products of boronic acids 177
- 1.8. Description of the C-halide coupling products 178
- 1.9. Identification of the amine deprotonated species $\mathbf{2_{ClO4}}$ generated during the fluorination of the $\mathbf{1_{ClO4}}$ complex 179
- 1.10. Identification of Ag^I species in the resulting mixture of the C-O bond forming cross-coupling reactions 179
- 1.11. Procedure for monitoring kinetics by UV-Vis spectroscopy 181
- 1.12. Stoichiometric fluorination of $\mathbf{L_1}$**-Br** and $\mathbf{L_5}$**-Br** model substrates 181
- 1.13. General procedure for the ^{1}H-NMR monitoring of the stoichiometric fluorination of $\mathbf{L_1}$**-Br** 183
- 1.14. General procedure for C-O bond forming cross-coupling reactions using stoichiometric amounts of Ag^I 183
- 1.15. Procedure for the ^{1}H-NMR monitoring of the catalytic C-O bond forming cross-coupling experiments 184

1.16. Procedure for the ESI-MS monitoring of the catalytic C-O bond forming cross-coupling experiments 184
2. Supplementary Discussion 185
3. Supplementary References 186
4. Supplementary Figures 188
5. Supplementary Tables 298

1. Supplementary Methods

1.1. Synthesis of ligands

Aryl halide model substrates **L_1-F**, **L_1-Cl**, **L_1-Br**, **L_1-I**, **L_5-F**, **L_5-Cl**, **L_5-Br** and **L_5-I** were prepared following procedures described in the literature.[1,2]

1.2. Procedure for the oxidative addition of silver(I) salts to L_1-I

All reagents used were weighed in a precision balance (legibility 0.01 mg) and then brought in an inert-atmosphere glove box to perform the reactions. A sample of the **L_1-I** model substrate (15.7 mg of **L_1-I**, 0.042 mmol) and 1,3,5-trimethoxybenzene as internal standard were dissolved in CD_3CN (1.4 mL). A portion of this solution (0.5 mL) was loaded into an amber vial containing 1-2 equiv. of the corresponding additive (NaOTf or TlOTf) and the reaction vial was sealed with a septum. Finally, 0.5 mL of a 0.03-0.06 M solution of AgOTf in CD_3CN were added dropwise over 1 h and the mixture was allowed to react for 1 more hour. After that time, the reaction mixture is centrifuged, filtered through Celite and then through an Acrodisc® filter. The resulting mixture was transferred to an amber NMR tube and analyzed by ^1H NMR. Final concentrations: **[L_1-I]** = 15 mM, [AgOTf] = 15-30 mM, [additive] = 15-30 mM. Reaction yields were obtained by integration of the ^1H NMR spectra of the crude reaction mixtures relative to 1,3,5-trimethoxybenbenzene as internal standard (5 mM in CD_3CN) (see Supplementary Table 1).

1.3. Description of the C-N coupling product

*The compound labelled as **2a** in this section does not correspond to the same compound **2a** in Annex I.*

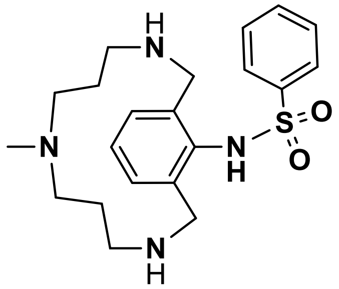

· $HClO_4$ **(2a)**

2a. ^{1}**H NMR** (400 MHz, CD_3CN, 25ºC) δ, ppm: 7.69-7.48 (m, 3H, H^l, H^m, H^n), 7.22-7.19 (m, 3H, H^a, H^b), 4.14 (d, 2H, J = 14.08 Hz, H^c or H^d), 3.51 (d, 2H, J = 14.08 Hz, H^c or H^d), 2.81-2.76 (m, 2H, H^e or H^f), 2.74-2.68 (m, 2H, H^i or H^j), 2.58-2.53 (m, 2H, H^i or H^j), 2.36-2.30 (m, 2H, H^e or H^f), 2.07 (s, 3H, H^k), 1.68-1.60 (m, 2H, H^g or H^h), 1.48-1.42 (m, 2H, H^g or H^h). ^{13}**C NMR** (100 MHz, CD_3CN, 25ºC) δ, ppm: 141.53 (C_{10}), 139.00 (C_1 or C_2), 132.83 (C_{13}), 131.32 (C_3 or C_4), 129.45 (C_{12}), 129.33 (C_1 or C_2), 126.25 (C_3 or C_4), 125.93 (C_{11}), 54.79 (C_8), 51.36 (C_5), 45.79 (C_6), 38.47 (C_9), 23.86 (C_7); HRMS (ESI-TOF, **[M-H]**$^+$) *m/z* calculated for $C_{17}H_{28}N_3O_2^+$, 403.2162, found: 403.2168.

1.4. Description of the C-O coupling products

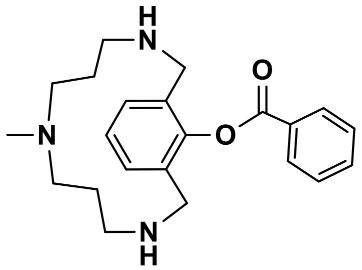

· $HClO_4$ **(2b)**

2b. ^{1}**H NMR** (400 MHz, CD_3CN, 60ºC) δ, ppm: 7.64-7.60 (m, 2H, H^m), 7.58-7.56 (m, 2H, H^l), 7.48 (m, 1H, H^n), 7.34-7.27 (m, 1H, H^b or $H^{b'}$), 7.21 (d, 1H, J = 6.84 Hz, H^b or $H^{b'}$), 6.91 (t, 1H, J = 7.48 Hz, H^a), 4.76 (br s, 2H, H^c or H^d), 4.08 (br s, 2H, H^c or H^d), 3.56 (t, 2H, J = 6.14 Hz, H^e or H^f), 2.94 (br m, 2H, H^g or H^h), 2.81-2.59 (m, 2H, H^i or H^j), 2.47-2.16 (m, 5H, H^i or H^j, H^k), 1.72 (quint, 2H, J = 5.88 –hz, H^g or H^h), 1.17 (br m, 2H, H^e or H^f). ^{13}**C NMR** (100 MHz, CD_3CN, 60ºC) δ, ppm: 154.20, 131.28, 130.19, 129.50, 128.54, 128.46, 127.95, 124.56, 120.21, 55.00, 54.07, 50.08, 46.78, 22.29; HRMS (ESI-TOF, **[M-H]**$^+$) *m/z* calculated for $C_{22}H_{30}N_3O_2^+$, 368.2333, found: 368.2358.

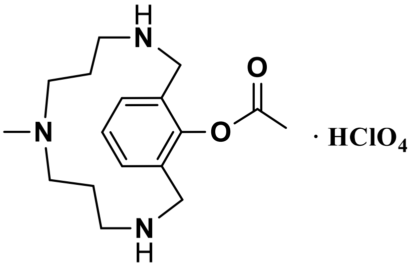

(2c)

2c. ^{1}**H NMR** (400 MHz, CD$_3$CN, 60ºC) δ, ppm: 7.30 (d, 1H, J = 7.5 Hz, H^{b} or H$^{b'}$), 7.20 (d, 1H, J = 7.3 Hz, H^{b} or H$^{b'}$), 6.91 (t, 1H, J = 7.5 Hz), 4.73 (br s, 2H, H^{c} or H^{d}), 4.09 (br s, 3H, H^{c} or H^{d}), 3.49 (br m, 2H, H^{e} or H^{f}), 2.89 (br m, 2H, H^{e} or H^{f}), 2.71 (br m, 2H, H^{i} or H^{j}), 2.6-2.35 (bb, 2H, H^{i} or H^{j}), 2.23 (s, 3H, H^{k}), 1.97 (s, 3H, H^{l}), 1.70 (quint, 2H, J = 6.2 Hz, H^{g} or H^{h}), 1.70 (br m, 2H, H^{g} or H^{h}). ^{13}**C NMR** (100 MHz, CD$_3$CN, 60ºC) δ, ppm: 171.14 (C$_{10}$), 133.26 (C$_1$), 131.25 (C$_3$), 124.84 (C$_2$), 120.24 (C$_4$), 53.49 (C$_8$), 49.52 (C$_5$), 45.99 (C$_6$), 22.23 (C$_7$), 20.92 (C$_9$), 19.41 (C$_{11}$); HRMS (ESI-TOF, **[M-H]**$^+$) *m/z* calculated for C$_{17}$H$_{28}$N$_3$O$_2$$^+$, 306.2176, found: 306.2191.

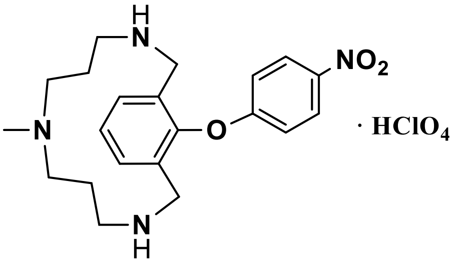

(2d)

2d. ^{1}**H NMR** (400 MHz, CD$_3$CN, 25ºC) δ, ppm: 8.13-8.11 (m, 2H, H^{m}), 7.42 (d, 2H, J = 7.36 Hz, H^{b}), 7.36-7.32 (m, 1H, H^{a}), 7.00 (d, 2H, J = 9.08 Hz, H^{l}), 3.75 (d, 2H, H^{c} or H^{d}), 3.52 (d, 2H, J = 13.52 Hz, H^{c} or H^{d}), 3.21-3.18 (m, 2H, H^{i} or H^{j}), 2.85-2.76 (m, 4H, H^{e} or H^{f}, H^{i} or H^{j}), 2.72-2.66 (m, 2H, H^{e} or H^{f}), 2.63 (s, 3H, H^{k}), 1.75-1.66 (m, 2H, H^{g} or H^{h}), 1.11-1.04 (m, 2H, H^{g} or H^{h}). ^{13}**C NMR** (100 MHz, CD$_3$CN, 25ºC) δ, ppm: 162.92 (C$_{10}$), 151.44 (C$_1$), 142.90 (C$_{13}$), 133.52 (C$_2$), 132.25 (C$_3$), 126.74 (C$_4$), 126.06 (C$_{12}$), 115.71 (C$_{11}$), 55.92 (C$_8$), 49.44 (C$_5$), 46.83 (C$_6$), 39.54 (C$_9$), 24.23 (C$_7$); HRMS (ESI-TOF, **[M-H]**$^+$) *m/z* calculated for C$_{21}$H$_{30}$N$_4$O$_3$$^+$, 385.2234, found: 385.2223.

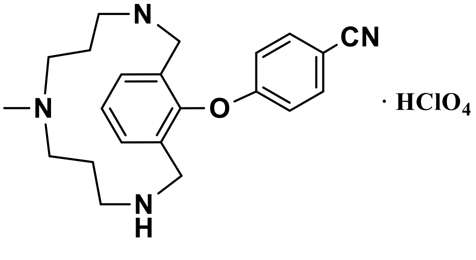

(2e)

2e. **^{1}H NMR** (400 MHz, CD_3CN, 25ºC) δ, ppm: 7.70 (d, 2H, J = 8.96 Hz, H^m), 7.40 (d, 2H, J = 7.48 Hz, H^b), 7.34-7.30 (m, 1H, H^a), 6.98 (d, 2H, J = 8.80 Hz, H^l), 3.73 (d, 2H, H^c or H^d), 3.50 (d, 2H, J = 13.52 Hz, H^c or H^d), 3.19-3.16 (m, 2H, H^i or H^j), 2.84-2.74 (m, 4H, H^e or H^f, H^i or H^j), 2.70-2.65 (m, 2H, H^e or H^f), 2.60 (s, 3H, H^k), 1.73-1.64 (m, 2H, H^g or H^h), 1.12-1.03 (m, 2H, H^g or H^h). **^{13}C NMR** (100 MHz, CD_3CN, 25ºC) δ, ppm: 160.29 (C_{10}), 151.32 (C_1), 134.57 (C_{12}), 133.58 (C_2), 132.18 (C_3), 126.58 (C_4), 118.58 (C_{14}), 116.22 (C_{11}), 105.61 (C_{11}), 55.92 (C_8), 49.47 (C_5), 46.82 (C_6), 39.52 (C_9), 24.27 (C_7); HRMS (ESI-TOF, **[M-H]$^+$**) *m/z* calculated for $C_{22}H_{29}N_4O^+$, 365.2336, found: 365.2328.

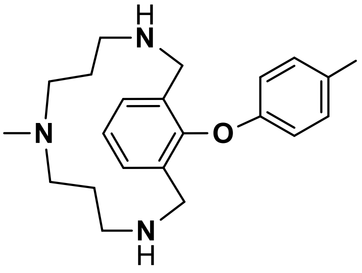

· $HClO_4$ **(2f)**

2f. **^{1}H NMR** (400 MHz, CD_3CN, 25ºC) δ, ppm: 7.42 (d, 2H, J = 7.52 Hz, H^b), 7.31 (m, 1H, H^a), 7.15 (dd, 2H, J = 8.72 Hz, J = 0.68 Hz, H^m), 6.75 (d, 2H, J = 8.6 Hz, H^l), 3.84 (d, 2H, J = 13.48 Hz, H^c or H^d), 3.58 (d, 2H, J = 13.52 Hz, H^c or H^d), 3.05-2.99 (m, 2H, H^i or H^j), 2.89-2.83 (m, 2H, H^e or H^f), 2.77-2.65 (m, 4H, H^i or H^j, H^e or H^f), 2.51 (s, 3H, H^k), 2.29 (s, 3H, H^n), 1.76-1.70 (m, 2H, H^g or H^h), 1.22-1.17 (m, 2H, H^g or H^h). **^{13}C NMR** (100 MHz, CD_3CN, 25ºC) δ, ppm: 154.58 (C_3), 152.38 (C_1), 132.52 (C_{13}), 132.45 (C_2), 132.19 (C_{10}), 130.19 (C_{12}), 126.17 (C_4), 114.80 (C_{11}), 55.86 (C_8), 49.10 (C_5), 46.90 (C_6), 39.52 (C_9), 24.01 (C_7), 19.52 (C_{14}); HRMS (ESI-TOF, **[M-H]$^+$**) *m/z* calculated for $C_{22}H_{32}N_3O^+$, 354.2540, found: 354.2548.

1.5. Description of the C-S coupling product

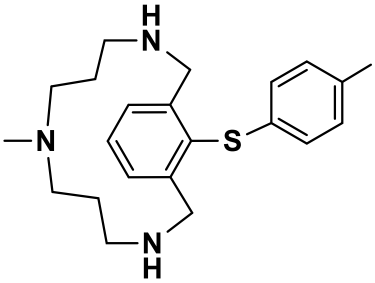

· $HClO_4$ **(2g)**

2g. **^{1}H NMR** (400 MHz, CD_3CN, 25ºC) δ, ppm: 7.73-7.68 (m, 3H, H^a, H^b), 7.16 (d, 2H, J = 8.68 Hz, H^m), 6.99 (d, 2H, J = 8.24 Hz, H^l), 4.57 (d, 2H, J = 13.68 Hz, H^c or H^d), 4.06 (d, 2H, J = 13.64 Hz, H^c or H^d), 3.24-3.18 (m, 2H, H^e or H^f), 2.94-2.88 (m, 2H, H^e or H^f), 2.65-2.59 (m, 2H, H^i or H^j), 2.50-2.43 (m, 2H, H^i or H^j), 2.34 (s, 3H, H^k), 2.29 (s, 3H, H^n), 1.85-1.74 (m, 2H, H^g or

H^h), 1.09-1.05 (m, 2H, H^g or H^h). **^{13}C NMR** (100 MHz, CD_3CN, 25ºC) δ, ppm: 138.34 (C_1 or C_2), 137.79 (C_{13}), 134.86 (C_3 or C_4), 134.10 (C_1 or C_2), 131.70 (C_3 or C_4), 130.51 (C_{12}), 129.82 (C_{10}), 127.65 (C_{10}), 54.52 (C_8), 50.84 (C_5), 46.38 (C_6), 40.29 (C_9), 22.39 (C_7), 19.95 (C_{14}); HRMS (ESI-TOF, **[M-H]**$^+$) *m/z* calculated for $C_{22}H_{31}N_3S^+$, 370.2311, found: 370.2317.

1.6. Description of the C-C coupling products

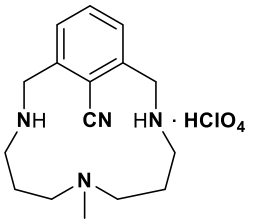

L_1-CN. ^{1}H NMR (400 MHz, CD_3CN, 25ºC) δ, ppm: 7.42 (t, 1H, J = 7.54 Hz, H^a), 7.26 (d, 2H, J = 7.64 Hz, H^b), 4.28 (d, 2H, J = 13.6 Hz, H^c or H^d), 3.61 (d, 2H, J = 13.06 Hz, H^c or H^d), 2.70-2.64 (m, 2H, H^i or H^j), 2.32-2.30 (m, 2H, H^e or H^f), 2.19-2.13 (m, 2H, H^e or H^f), 1.89-1.84 (m, 2H, H^i or H^j), 1.77 (s, 3H, H^k), 1.42-1.37 (m, 4H, H^g or H^h); **^{13}C NMR** (100 MHz, CD_3CN, 25ºC) δ, ppm: 147.17 (C_2), 131.19 (C_4), 129.13 (C_3), 117.37 (C_{10}), 112.15 (C_1), 55.27 (C_8), 52.31 (C_5), 42.95 (C_6), 38.82 (C_9), 27.26 (C_7); HRMS (ESI-TOF, **[M-H]**$^+$) *m/z* calculated for $C_{16}H_{25}N_4^+$, 273.2074, found: 273.2076.

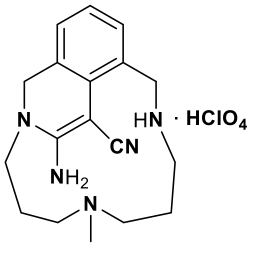

(2h)

2h. ^{1}H NMR (400 MHz, CD_3CN, 25ºC) δ, ppm: 7.25-7.12 (m, 3H, H^a, H^b, H^c), 5.64 (bb, 2H, **NH_2**), 5.00 (d, 1H, J = 13.88 Hz, H^d or H^e), 4.28-4.18 (m, 2H, H^s or H^t), 3.99 (d, 1H, J = 13.88 Hz, H^d or H^e), 3.87-3.84 (ddd, 1H, J = 15.28 Hz, J = 8.64 Hz, J = 2.52 Hz, H^q or H^p), 3.13 (ddd, 1H, J = 15.28 Hz, J = 7.28 Hz, J = 2.64 Hz, H^q or H^p), 2.83-2.78 (m, 1H, H^f or H^g), 2.57-2.42 (m, 3H, H^j or H^k, H^f or H^g, H^m or H^n), 2.41-2.34 (m, 1H, H^j or H^k), 2.20 (s, 3H, H^l), 2.08 (ddd, 1H, J = 12.64 Hz, J = 9.72 Hz, J = 5.52 Hz, H^m or H^n), 1.83-1.73 (m, 1H, H^o or H^p), 1.57-1.47 (m, 1H, H^h or H^i), 1.44-1.34 (m, 1H, H^o or H^p), 1.16-1.06 (m, 1H, H^h or H^i). **^{13}C NMR** (100 MHz, CD_3CN, 25ºC) δ, ppm: 161.69 (C_{15}), 132.32 (C_1), 131.84 (C_2), 131.13 (C_3 or C_4 or C_5), 126.39 (C_{16}), 125.22 (C_3 or C_4 or C_5), 124.30 (C_3 or C_4 or C_5), 121.36 (C_{17}), 55.26 (C_9), 53.31 (C_{14}), 52.72 (C_{11}), 49.77 (C_{13}), 49.15 (C_6), 44.63 (C_7), 40.88 (C_{10}), 26.12 (C_{12}) 22.86 (C_8); HRMS (ESI-TOF, **[M-H]**$^+$) *m/z* calculated for $C_{18}H_{26}N_5^+$, 312.2183, found: 312.2159.

1.7. Description of the C-C coupling products of boronic acids

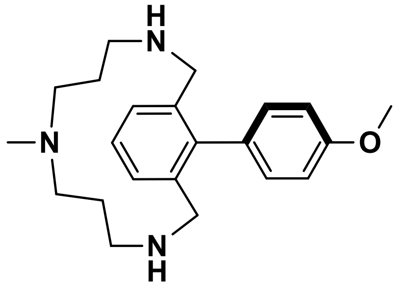

(2i)

2i. ^{1}**H NMR** (400 MHz, CD_3CN, 25ºC) δ, ppm: 7.59 (dd, 1H, J = 8.52 Hz, J = 2.24 Hz, H^{o}), 7.46-7.42 (m, 3H, H^{a}, H^{b}), 7.12 (dd, 1H, J = 8.48, J = 2.76 Hz, H^{n}), 7.01 (dd, 1H, J = 8.48 Hz, J = 2.76 Hz, H^{m}), 6.91-6.86 (m, 1H, H^{l}), 3.83 (s, 3H, H^{p}), 3.74-3.71 (m, 2H, H^{c} or H^{d}), 3.65 (d, 2H, J = 13.12 Hz, H^{c} or H^{d}), 2.71 (t, 4H, J = 6.32 Hz, H^{e} or H^{f}), 2.43-2.37 (m, 2H, H^{i} or H^{j}), 2.27-2.21 (m, 5H, H^{i} or H^{j}, H^{k}), 1.54-1.44 (m, 2H, H^{g} or H^{h}), 0.94-0.85 (m, 2H, H^{g} or H^{h}). ^{13}**C NMR** (100 MHz, CD_3CN, 25ºC) δ, ppm: 159.45 (C_{13}), 142.71 (C_1), 136.81 (C_2), 132.06 (C_{11}), 130.96 (C_3 or C_4), 129.71 (C_{15}), 129.35 (C_{10}), 127.80 (C_3 or C_4), 114.42 (C_{12}), 113.35 (C_{14}), 55.36 (C_8), 54.74 (C_{16}), 50.76 (C_5), 45.770 (C_6), 40.54 (C_9), 24.83 (C_7); HRMS (ESI-TOF, **[M-H]**$^{+}$) *m/z* calculated for $C_{22}H_{32}N_3O^{+}$, 354.2540, found: 354.2534.

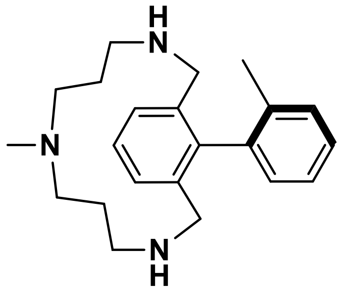

(2j)

2i. ^{1}**H NMR** (400 MHz, CD_3CN, 25ºC) δ, ppm: 7.50-7.43 (m, 3H, H^{a}, H^{b}), 7.40-7.37 (m, 2H, H^{m}, H^{n}), 7.36-7.33 (m, 1H, H^{o}), 7.22-7.19 (m, 1H, H^{l}), 3.64 (d, 2H, J = 13.16 Hz, H^{c} or H^{d}), 3.49 (d, 2H, J = 13.12 Hz, H^{c} or H^{d}), 2.75-2.71 (m, 4H, H^{e} or H^{f}), 2.39-2.33 (m, 2H, H^{i} or H^{j}), 2.27-2.20 (m, 5H, H^{i} or H^{j}, H^{k}), 1.69 (s, 3H, H^{p}), 1.56-1.45 (m, 2H, H^{g} or H^{h}), 0.93-0.84 (m, 2H, H^{g} or H^{h}). ^{13}**C NMR** (100 MHz, CD_3CN, 25ºC) δ, ppm: 141.41 (C_1), 136.77 (C_{15}), 136.25 (C_2), 131.21 (C_3 or C_4), 130.84 (C_{14}), 128.83 (C_3 or C_4), 128.51 (C_{11}), 128.06 (C_{10}), 128.01 (C_{12}), 125.63 (C_{13}), 55.27 (C_8), 50.58 (C_5), 45.86 (C_6), 40.74 (C_9), 25.01 (C_7), 18.84 (C_{16}); HRMS (ESI-TOF, **[M-H]**$^{+}$) *m/z* calculated for $C_{22}H_{32}N_3^{+}$, 338.2591, found: 338.2591.

1.8. Description of the C-Halogen coupling products

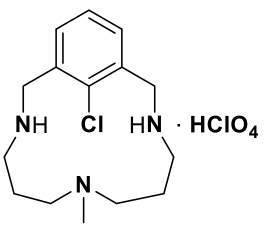

L_1-Cl. **^{1}H NMR** (400 MHz, CD_3CN, 25ºC) δ, ppm: 7.28-7.26 (m, 2H, H^b), 7.24-7.20 (m, 1H H^a), 4.34 (d, 2H, J = 13.88 Hz, H^c or H^d), 3.60 (d, 2H, J = 13.92 Hz, H^c or H^d), 2.51-2.39 (m, 4H, H^e or H^f, H^i or H^j), 2.37-2.31 (m, 2H, H^e or H^f), 2.06-2.00 (m, 2H, H^i or H^j), 1.94 (s, 3H, H^k), 1.48-1.45 (m, 4H, H^g or H^h); HRMS (ESI-TOF, **[M-H]**$^+$) *m/z* calculated for $C_{15}H_{25}N_3Cl^+$, 282.1732, found: 282.1735.

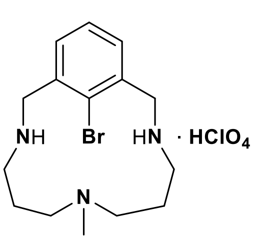

L_1-Br. **^{1}H NMR** (400 MHz, CD_3CN, 25ºC) δ, ppm: 7.21-7.14 (m, 3H, H^a, H^b), 4.25 (d, 2H, J = 13.96 Hz, H^c or H^d), 3.52 (d, 2H, J = 13.92 Hz, H^c or H^d), 2.47-2.40 (m, 2H, H^i or H^j), 2.28-2.15 (m, 4H, H^e or H^f, H^i or H^j), 1.91-1.88 (m, 2H, H^e or H^f), 1.80 (s, 3H, H^k), 1.65-1.55 (m, 4H, H^g or H^h); HRMS (ESI-TOF, **[M-H]**$^+$) *m/z* calculated for $C_{15}H_{25}N_3Br^+$, 326.1226, found: 326.1234.

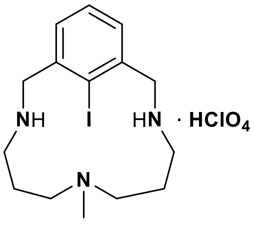

L_1-I. **^{1}H NMR** (400 MHz, CD_3CN, 25ºC) δ, ppm: 7.20-7.16 (m, 1H, H^a), 7.11-7.09 (m, 2H, H^b), 4.18 (d, 2H, J = 13.84 Hz, H^c or H^d), 3.61 (d, 2H, J = 13.84 Hz, H^c or H^d), 2.53-2.46 (m, 2H, H^i or H^j), 2.30-2.25 (m, 2H, H^e or H^f), 2.19-2.09 (m, 2H, H^e or H^f), 1.91-1.88 (m, 2H, Hi or Hj), 1.80 (s, 3H, H^k), 1.41-1.27 (m, 4H, H^g or H^h); HRMS (ESI-TOF, **[M-H]**$^+$) *m/z* calculated for $C_{15}H_{25}IN_3^+$, 374.1088, found: 374.1081.

1.9. Identification of the amine deprotonated species 2$_{\mathrm{ClO4}}$ generated during the fluorination of the 1$_{\mathrm{ClO4}}$ complex

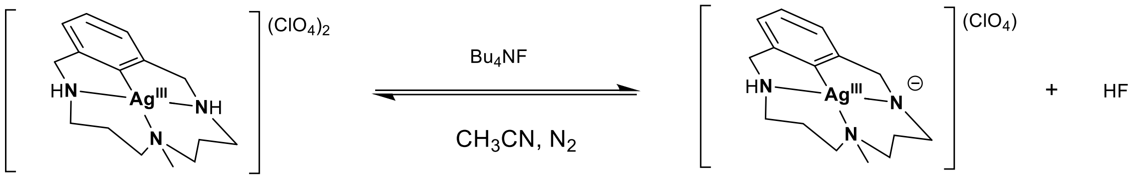

1$_{\mathrm{ClO4}}$

2$_{\mathrm{ClO4}}$

All reagents used were weighed in a precision balance (legibility 0.01 mg) and then brought in an inert-atmosphere glove box to perform the reaction. A UV-visible cuvette equipped with a Teflon stopcock was dried in an oven and cooled under vacuum. Stock solutions of tetrabutylammonium fluoride trihydrate (48 mM) and the aryl-Ag^{III} complex **1**$_{\mathrm{ClO4}}$ (4.8 mM) were prepared in dry CH_3CN (3 mL). After backfilling the cuvette with dry N_2, 0.5 mL of the aryl-Ag^{III} stock solution were added via syringe, and it was diluted with CH_3CN to a total volume of 2.9 mL. The cuvette was inserted into the spectrometer, and the reaction was started by adding the tetrabutylammonium fluoride trihydrate stock solution (0.1 mL) to the cuvette followed by rapid mixing of the combined solutions. Final concentrations: [**1**$_{\mathrm{ClO4}}$] = 0.8 mM; [$nBu_4NF \cdot 3H_2O$] = 1.6 mM. Once the orange band at 450 nm (corresponding to the deprotonated aryl-Ag^{III} (**2**$_{\mathrm{ClO4}}$) species) is stabilized (Supplementary Fig. 13), the solution in the cuvette was introduced into the mass spectrometer by direct infusion using a syringe pump and was externally calibrated using sodium formate. The instrument was operated in the positive ion mode and the expected m/z peak for **2**$_{\mathrm{ClO4}}$ was observed (Supplementary Fig. 14).

1.10. Identification of Ag^{I} species in the resulting mixture of the C-O bond forming cross-coupling reactions

Experiment A: identification of the Ag(I) species in the final reaction mixture by PPh_3 addition (Supplementary Fig. 11).

All reagents used were weighed in a precision balance (legibility 0.01 mg) and then brought in an inert-atmosphere glove box to perform the reaction. A sample of the aryl-Ag^{III} complex **1**$_{\mathrm{ClO4}}$ (11.6 mg, 21 μmol) was dissolved in CD_3CN (1.4 mL) and 0.1 mL of a solution of 1,3,5-trimethoxybenzene was added as internal standard. A portion of this solution (0.6 mL) was loaded into an amber NMR tube, and 1 equiv. of *p*-nitrophenol was added to the tube (0.1 mL, 0.084 M). Final concentrations: [**1**$_{\mathrm{ClO4}}$] = 12 mM and [*p*-NO_2phenol] = 12 mM. The tube was sealed with a septum, and the reaction was allowed to proceed at 70°C monitoring it by ^1H NMR spectroscopy until completion. Once the reaction is completed, 3 equiv. of PPh_3 were loaded into the NMR tube (0.1 mL, 0.252 M). The sample was placed in the NMR probe, cooled to -35°C and its ^{31}P-NMR acquired.

Blank experiment: All reagents used were weighed in a precision balance (legibility 0.01 mg) and then brought in an inert-atmosphere glove box to perform the reaction. A sample of PPh_3 (33 mg, 126 µmol) was dissolved in 0.5 ml of CD_3CN. A portion of this solution (0.1 mL) was loaded into an amber NMR tube containing 0.7 mL of a 12 mM solution of $Ag^{I}ClO_4$ in CD_3CN. The tube was sealed with a septum, placed in the NMR probe, cooled to -35ºC and its ^{31}P-NMR acquired.

Experiment B: observation of Ag(I) reactivity using the final reaction mixture to form aryl-Ag(III) species (Supplementary Fig. 12).

All reagents used were weighed in a precision balance (legibility 0.01 mg) and then brought in an inert-atmosphere glove box to perform the reaction. A sample of the aryl-Ag^{III} complex $\mathbf{1}_{\mathbf{ClO4}}$ (16.3 mg, 29 µmol) was dissolved in CD_3CN (2.1 mL) and 0.2 mL of a solution of 1,3,5-trimethoxybenzene was added as internal standard. A portion of this solution (0.6 mL) was loaded into an amber NMR tube, and 1 equiv. of *p*-nitrophenol was added to the tube (0.1 mL, 0.084 M). Final concentrations: [$\mathbf{1}_{\mathbf{ClO4}}$] = 12 mM and [*p*-$NO_2$phenol] = 12 mM. The tube was sealed with a septum, and the reaction was allowed to proceed at 70ºC monitoring it by ^{1}H NMR spectroscopy until completion. Once the reaction is completed, 0.5 equiv. of $\mathbf{L_1}$**-Br** were loaded into the NMR tube (0.1 mL, 0.084 M). After 18 h, the mixture was analyzed by ^{1}H NMR and the amount of aryl-Ag^{III} complex $\mathbf{1}_{\mathbf{ClO4}}$ formed was obtained by integration of the ^{1}H NMR spectra of the crude reaction mixtures relative to the internal standard (Supplementary Fig. 12). All products obtained in the reaction crude were identified by ESI-MS spectroscopy.

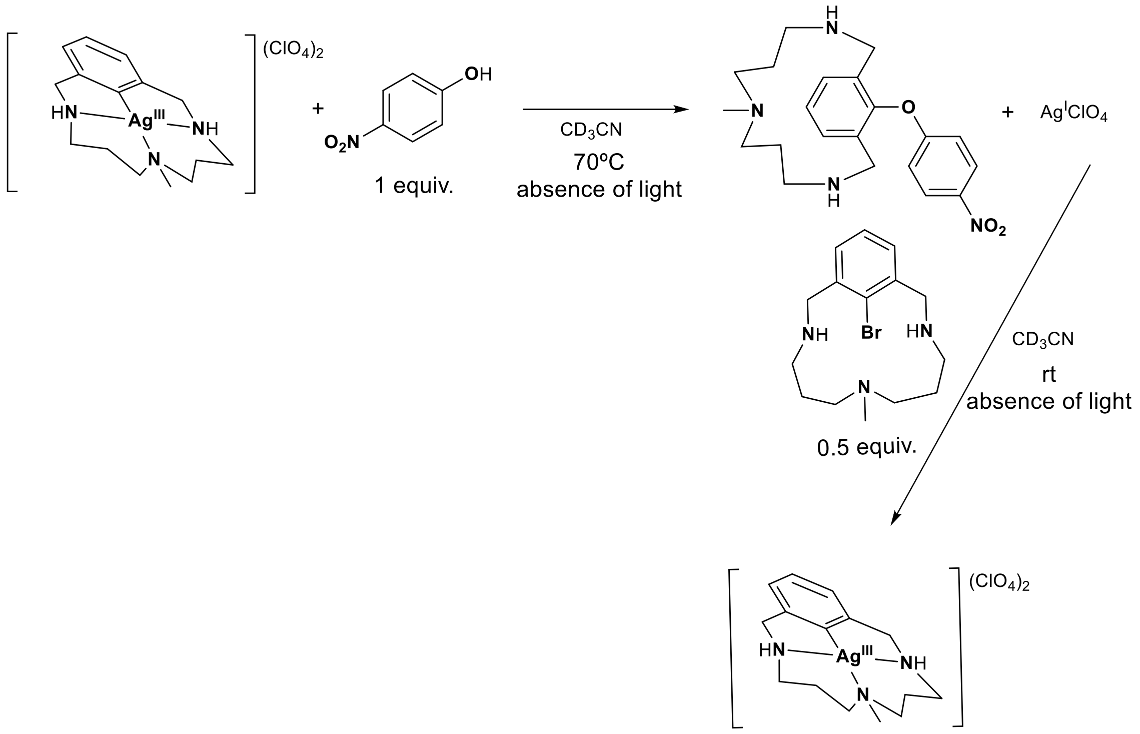

1.11. Procedure for monitoring kinetics by UV-Vis spectroscopy

All reagents used were weighed in a precision balance (legibility 0.01 mg) and then brought in an inert-atmosphere glove box to perform the reactions. A UV-Visible cuvette equipped with a Teflon stopcock was dried in an oven and cooled under vacuum. Stock solutions of *p*-cyanophenol (0.24 M) and the aryl-Ag^{III} complex $\mathbf{1}_{\mathbf{ClO4}}$ (1.2 mM) were prepared in dry CH_3CN. After backfilling the cuvette with dry N_2, 2 mL of the aryl-Ag^{III} stock solution were added via syringe, and the solution was diluted with CH_3CN to a total volume of 2.9 mL. The cuvette was inserted into the spectrophotometer and the temperature was allowed to equilibrate. The reaction was initiated by adding 0.1 mL of the stock solution of *p*CN-phenol to the cuvette under continuous stirring. Final concentrations: [$\mathbf{1}_{\mathbf{ClO4}}$] = 0.8 mM, [*p*-CNphenol] = 8 mM. The reaction progress was monitored by measuring the change in absorbance at 375 nm, and the data were fit to an single exponential decay curve using SigmaPlot 11.0 (pseudo first-order conditions) (for the Eyring plot extracted from this experiment see Supplementary Fig. 29).

1.12. Stoichiometric fluorination of L$_1$-Br and L$_5$-Br model substrates

*Stoichiometric fluorination of model substrate **L$_1$-Br**: synthesis of **L$_1$-F**.*

All reagents used were weighed in a precision balance (legibility 0.01 mg) and then brought in an inert-atmosphere glove box to perform the reactions. 4 mg of ligand **L$_1$-Br** (0.012 mmols) were dissolved in 2 mL of CH_3CN in a vial. Subsequently, this solution was added to an amber vial containing 3.1 mg of Ag^{I}OTf (0.012 mmols) and

1.5 mg of AgF (0.012 mmols) or 3.1 mg of AgF (0.024 mmols). The vial was sealed with a screw-cap and the suspension was heated to 40ºC and stirred vigorously. After 24 h of reaction, the crude was centrifuged to remove the black solids generated during the reaction. The resulting solution was evaporated under vacuum and the solids obtained were dried under vacuum for several hours. ^{1}H NMR yield of the **L_1-F** coupling product was obtained in CD_3CN and calculated using 1,3,5-trimethoxybenzene as internal standard. ^{1}H NMR and high resolution mass spectrometric analysis were obtained without isolation of the C-F coupling product.

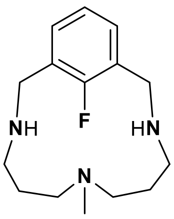

L_1-F. ^{1}H NMR (400 MHz, CD_3CN, 25ºC) δ, ppm: 7.31 (t, 2H, J = 7.28 Hz, H^b), 7.17 (t, 1H, J = 7.56 Hz, H^a), 3.98 (s, 4H, H^c, H^d), 2.51 (t, 4H, J = 6.12 Hz, H^e, H^f), 2.26-2.22 (m, 6H, H^i, H^j, **NH**), 1.97 (s, 3H, H^k), 1.52 (quint, 4H, J = 6.04 Hz, H^g, H^h); **^{19}F-NMR** (282.4 MHz, CD_3CN, 25ºC) δ, ppm: -124.5 ppm; HRMS (ESI-TOF, **[M-H]$^+$**) *m/z* calculated for $C_{17}H_{29}FN_3^+$, 266.2027, found: 266.2041.

*Stoichiometric fluorination of model substrate **L_5-Br**: synthesis of **L_5-F**.*

All reagents used were weighed in a precision balance (legibility 0.01 mg) and then brought in an inert-atmosphere glove box to perform the reactions. 5 mg of ligand **L_5-Br** (0.014 mmols) were dissolved in 2 mL of CH_3CN in a vial. Subsequently, this solution was added to an amber vial containing 3.6 mg of AgF (0.028 mmols). The vial was sealed with a screw-cap and the suspension was heated to 40ºC and stirred vigorously. After 24 h of reaction, the crude was centrifuged to remove the black solids generated during the reaction. The resulting solution was evaporated under vacuum and the solids obtained were dried under vacuum for several hours. ^{1}H NMR yield of the **L_5-F** coupling product was obtained in CD_3CN and calculated using 1,3,5-trimethoxybenzene as internal standard. ^{1}H NMR and high resolution mass spectrometric analysis were obtained without isolation of the C-F coupling product.

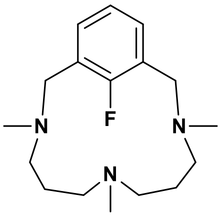

L$_5$-F. **^{1}H NMR** (400 MHz, CD$_3$CN, 25ºC) δ, ppm: 7.21 (t, 2H, J = 7.40 Hz, H^b), 7.05 (t, 1H, J = 7.46 Hz, H^a), 3.46 (s, 4H, H^c, H^d), 2.28 (s, 6H, H^l), 2.15-2.09 (m, 8H, H^e, H^f, H^i, H^j), 1.83 (s, 3H, H^k), 1.31-1.21 (m, 4H, H^g, H^h); **^{19}F-NMR** (282.4 MHz, CD$_3$CN, 25ºC) δ, ppm: -120.1 ppm; HRMS (ESI-TOF, **[M-H]$^+$**) *m/z* calculated for $C_{17}H_{29}FN_3^+$, 294.2340, found: 294.2361.

1.13. General procedure for the ^{1}H NMR monitoring of the stoichiometric fluorination of L$_1$-Br

All reagents used were weighed in a precision balance (legibility 0.01 mg) and then brought in an inert-atmosphere glove box to perform the reactions. A sample of the **L$_1$-Br** (9.1 mg, 28 μmol) was dissolved in CD$_3$CN (1.5 mL) and 0.1 mL of a solution of 1,3,5-trimethoxybenzene was added as internal standard. A portion of this solution (0.7 mL) was loaded into an amber vial containing 3.1 mg (2 equiv.) of silver fluoride (or 3.1 mg (1 equiv.) of silver triflate and 1.5 mg (1 equiv.) of silver fluoride). The resulting mixture is stirred vigorously for 5 minutes, turning yellow rapidly. The mixture is then transferred to an amber NMR tube and sealed with a septum. Final concentration: [**L$_1$-Br**] = 17.5 mM. The sample was placed in the NMR probe, heated to 40ºC and after equilibration, the monitoring of the reaction was started. The amounts of **1$_{\text{ClO4}}$**, yields and conversions were obtained by integration of the ^{1}H NMR spectra of the crude reaction mixtures relative to the internal standard (for the overlapped spectra of the ^{1}H NMR monioring of **L$_1$-Br** see Supplementary Fig. 15). All products obtained in the reaction crude were identified by ESI-MS spectroscopy.

1.14. General procedure for C-O bond forming cross-coupling reactions using stoichiometric amounts of Ag^I

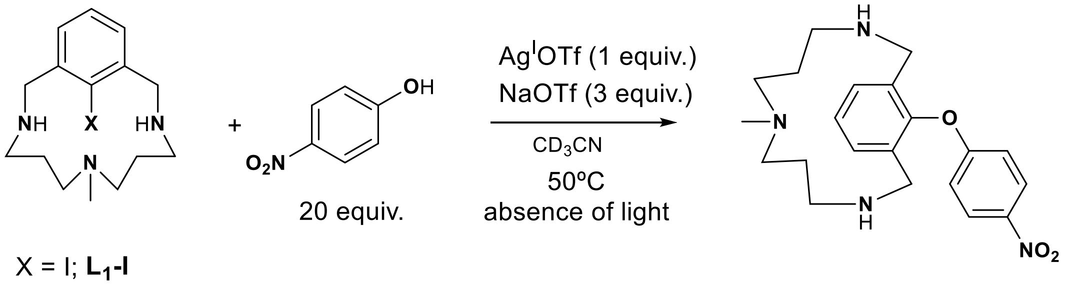

X = I; **L$_1$-I**
X = Br; **L$_1$-Br**
X = Cl; **L$_1$-Cl**

All reagents used were weighed in a precision balance (legibility 0.01 mg) and then brought in an inert-atmosphere glove box to perform the reactions. A sample of the **L$_1$-X** (X = I, Br, Cl) model substrate (9.0 mg for **L$_1$-I**, 7.8 mg for **L$_1$-Br** and 6.8 mg for **L$_1$-Cl**, 0.024 mmol) and 1,3,5-trimethoxybenzene as internal standard were dissolved in CH$_3$CN (0.8 mL). A portion of this solution (0.5 mL) was loaded into an amber vial that contained 3 equiv. of NaOTf (0.045

mmol). 20 equiv. of the corresponding phenol were subsequently added to the amber vial (0.25 mL, 1.2 M in CD_3CN). The vial was sealed with a septum and heated to 50ºC. Finally, 0.25 mL of a 0.06-0.066 M solution of AgOTf in CH_3CN were added dropwise over 1h and the mixture was allowed to react for 5 more hours at 50ºC. The resulting solution was evaporated and dried under vaccum. The crude mixture was then dissolved in 0.5 ml of CD_3CN and transferred to an amber NMR tube and analyzed by ^1H NMR. Final concentrations: [$\mathbf{L_1}$**-X**] = 15 mM, [NaOTf] = 45 mM, [*p*-NO_2phenol] = 0.3 M and [AgOTf] = 15-16.5 mM. Reaction yields were obtained by integration of the ^1H NMR spectra of the crude reaction mixtures relative to 1,3,5-trimethoxybenzene as internal standard (10 mM in CD_3CN) (Table 2, Chapter IV). All products obtained in the reaction crude were identified by ESI-MS spectroscopy.

1.15. Procedure for the ^1H NMR monitoring of the catalytic C-O bond forming cross-coupling experiments

All reagents used were weighed in a precision balance (legibility 0.01 mg) and then brought in an inert-atmosphere glove box to perform the reactions. A sample of the $\mathbf{L_1}$**-I** (13.6 mg, 36 μmol) was dissolved in CD_3CN (1.2 mL) and 0.1 mL of a solution of 1,3,5-trimethoxybenzene was added as internal standard. Stock solutions of AgOTf/PPh_3 (14/14 mM) and *p*-nitrophenol (2.8 M) were prepared in dry CD_3CN (3 mL). 0.5 mL of the $\mathbf{L_1}$**-I** stock solution (0.5 mL) was loaded into an amber NMR tube via syringe, sealed with a septum and placed in the spectrometer. The reaction was started by adding a sample of the *p*-nitrophenol stock solution (0.1 mL) and AgOTf/PPh_3 (0.1 mL) to the NMR tube. Final concentrations: [$\mathbf{L_1}$**-I**] = 20 mM, [*p*-NO_2phenol] = 0.4 M, [AgOTf] = 2 mM, [PPh_3] = 2 mM. After 30 min. of reaction, the appearance of $\mathbf{1_{ClO4}}$ is observed and the NMR probe is heated to 35ºC for the C-O bond forming cross-coupling reaction to proceed (Supplementary Fig. 18). The amounts of $\mathbf{1_{ClO4}}$, yields and conversions were obtained by integration of the ^1H NMR spectra of the crude reaction mixtures relative to the internal standard. All products obtained in the reaction crude were identified by ESI-MS spectroscopy.

1.16. Procedure for the ESI-MS monitoring of the catalytic C-O bond forming cross-coupling experiments

All reagents used were weighed in a precision balance (legibility 0.01 mg) and then brought in an inert-atmosphere glove box, where stock solutions of $\mathbf{L_1}$**-I** (30 mM), AgOTf/PPh_3 (7.5/7.5 mM) and of the *p*-nitrophenol (0.13 M) were prepared in CH_3CN. An amber vial was loaded with 0.2 mL of the AgOTf/PPh_3 stock solution and subsequently 2.3 mL of the *p*-nitrophenol stock solution and 0.5 mL of the $\mathbf{L_1}$**-X** stock solution were added. The vial was sealed with a screw-cap and allowed to react at 50ºC for 6 h. Final concentrations: [$\mathbf{L_1}$**-X**] = 5 mM, [AgOTf]

= 0.5 mM, [PPh_3] = 0.5 mM, [*p*-NO_2phenol] = 0.1 M. After 6 h of reaction the crude solution was introduced into the mass spectrometer by direct infusion using a syringe pump and was externally calibrated using sodium formate. The instrument was operated in both positive and negative ion mode and coordination complexes containing p-nitrophenol as well as diiodide monoanionic species were observed (Supplementary Fig. 22 and 25).

2. Supplementary Discussion

Supplementary text on C-O coupling catalysis optimization: Higher loadings of PPh_3 afforded lower yields of coupling product, suggesting that excess PPh_3 can sequester the active catalyst by forming non-reactive Ag(I) species (Supplementary Table 2). It is worth noticing that by increasing the amount of phenol nucleophile up to 60 equiv. or by raising the temperature to 70ºC the reaction outcome was not enhanced (Supplementary Table 2).

3. Supplementary References

1. Casitas, A.; King, A. E.; Parella, T.; Costas, M.; Stahl, S. S.; Ribas, X. *Chem. Sci.* **2010**, *1*, 326.

2. Casitas, A.; Canta, M.; Solà, M.; Costas, M.; Ribas, X. *J. Am. Chem. Soc.* **2011**, *133*, 19386.

4. Supplementary Figures

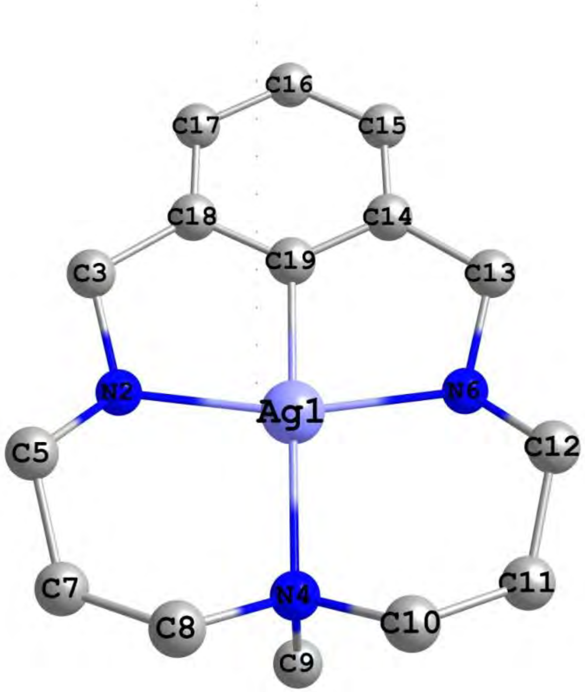
C16
C17
C15
C18
C14
C19
C3
C13
N2
Ag1
N6
C5
C12
C7
C11
N4
C8
C10
C9

Supplementary Figure 1. DFT optimized structure of the $[Ag^{III}(L_1)](ClO_4)_2$ (1_{ClO4}) complex. Hydrogen atoms and the two perchlorate anions have been omitted for clarity. Selected bond lengths [Å] and angles [º] of $[Ag^{III}(\mathbf{L_1})](ClO_4)_2$ ($\mathbf{1_{ClO4}}$): Ag-C(19) 1.993, Ag-N(2) 2.122, Ag-N(6) 2.112, Ag-N(4) 2.180; C(19)-Ag-N(2) 81.43, C(19)-Ag-N(6) 81.58, N(2)-Ag-N(4) 98.94, N(6)-Ag-N(4) 98.23, C(19)-Ag-N(4) 178.23, N(2)-Ag-N(6) 161.34.

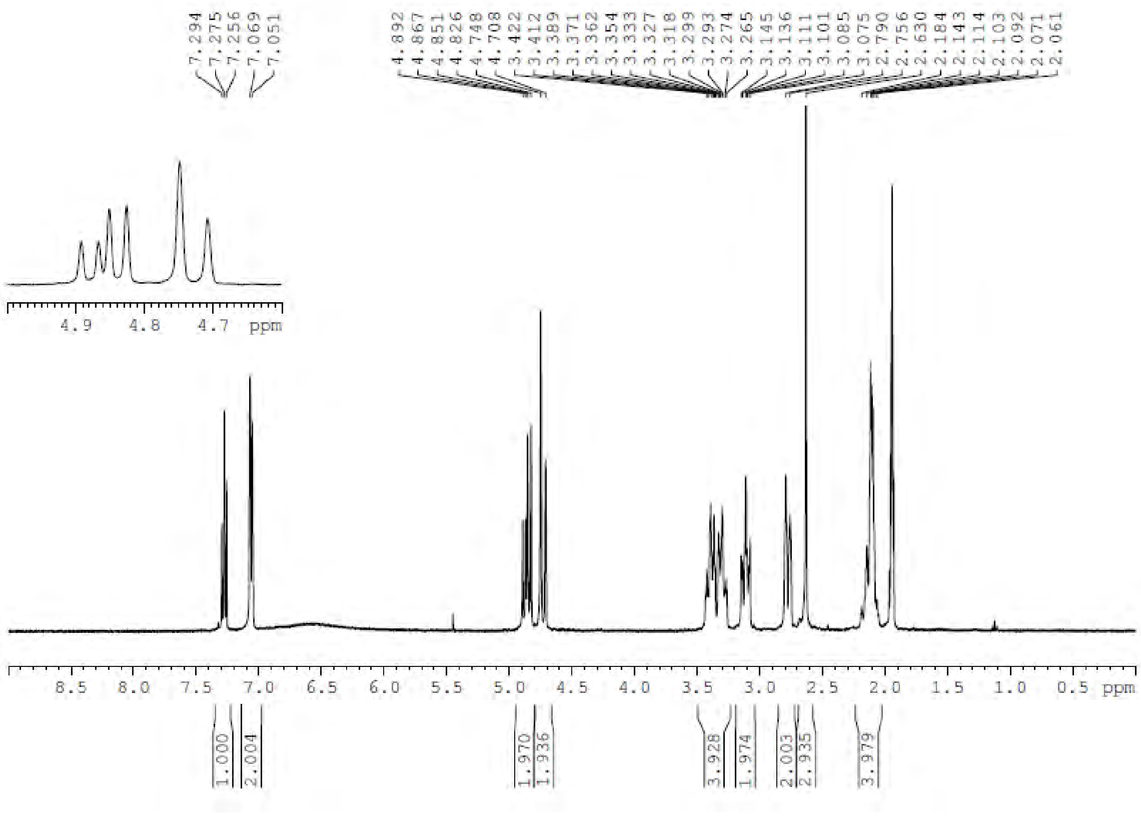

Supplementary Figure 2. ^{1}H NMR spectrum of complex [Ag^{III}(L$_1$)](ClO$_4$)$_2$ (1$_{ClO4}$). Experiment performed in CD_3CN, 400 MHz, at 298 K.

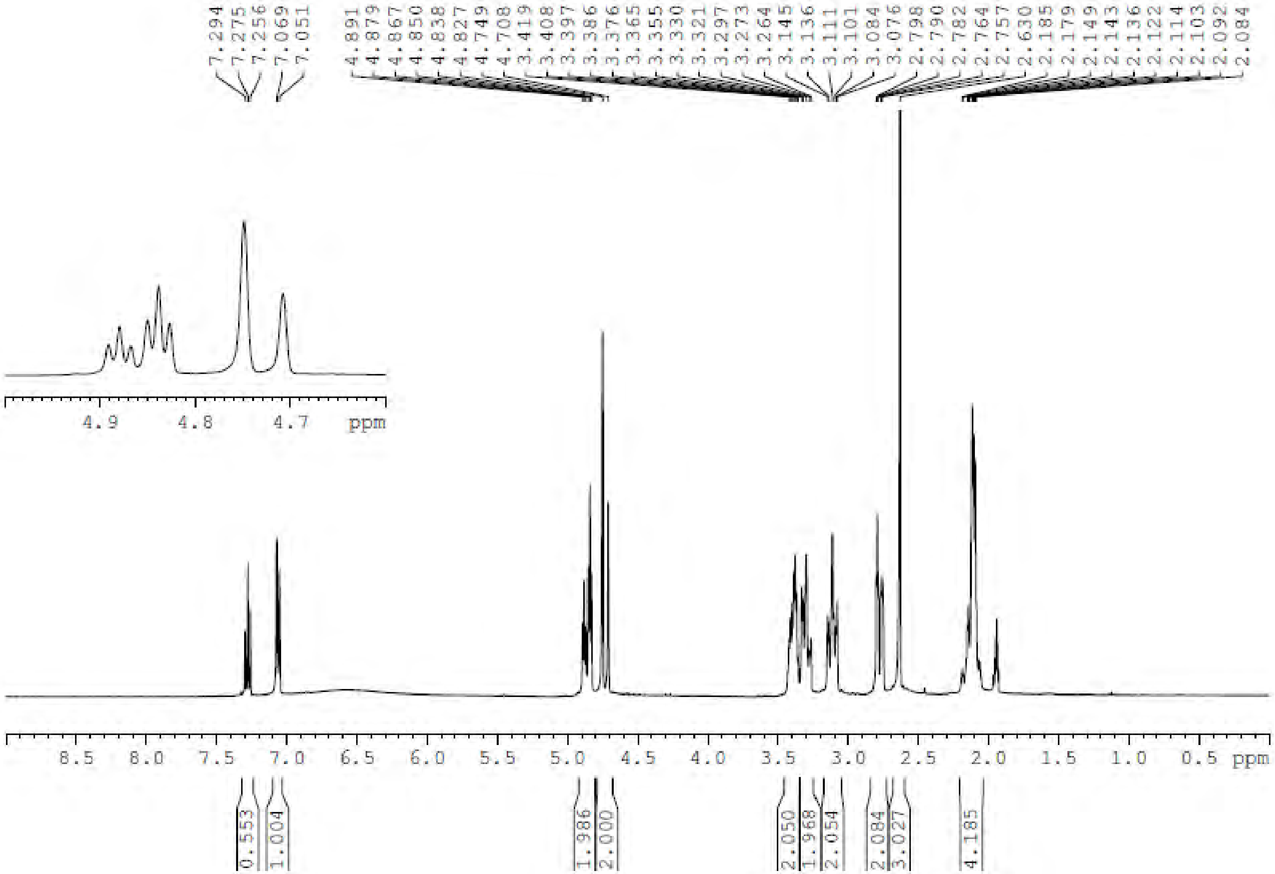

Supplementary Figure 3. ^{1}H NMR{^{109}Ag} spectrum of complex [Ag^{III}(L$_1$)](ClO$_4$)$_2$ (1$_{ClO4}$). Experiment performed in CD$_3$CN, 400 MHz, at 298 K.

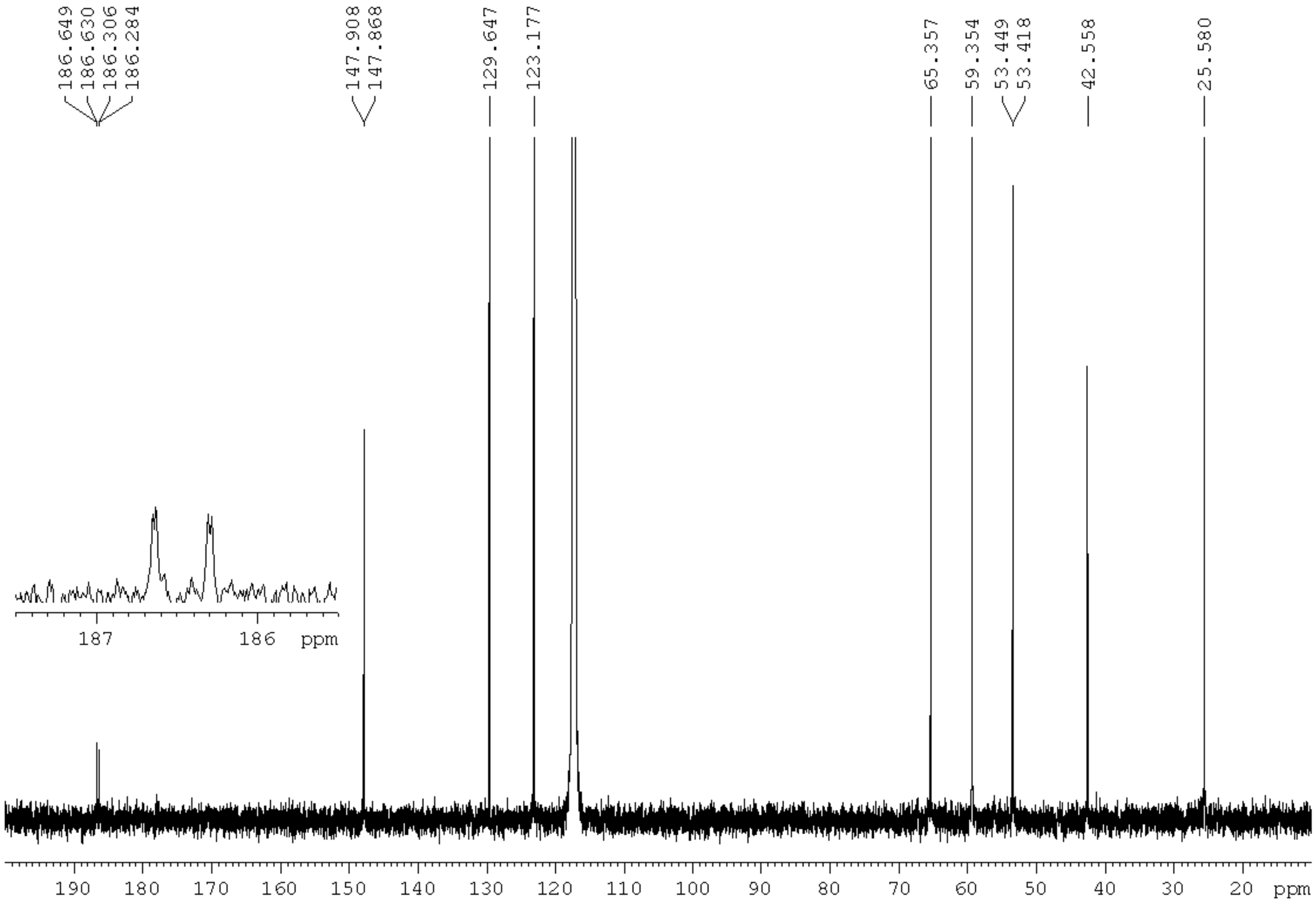

Supplementary Figure 4. ^{13}**C NMR spectrum of complex [Ag^{III}(L$_1$)](ClO$_4$)$_2$ (1$_{ClO4}$).** Experiment performed in CD$_3$CN, 100 MHz, at 298 K.

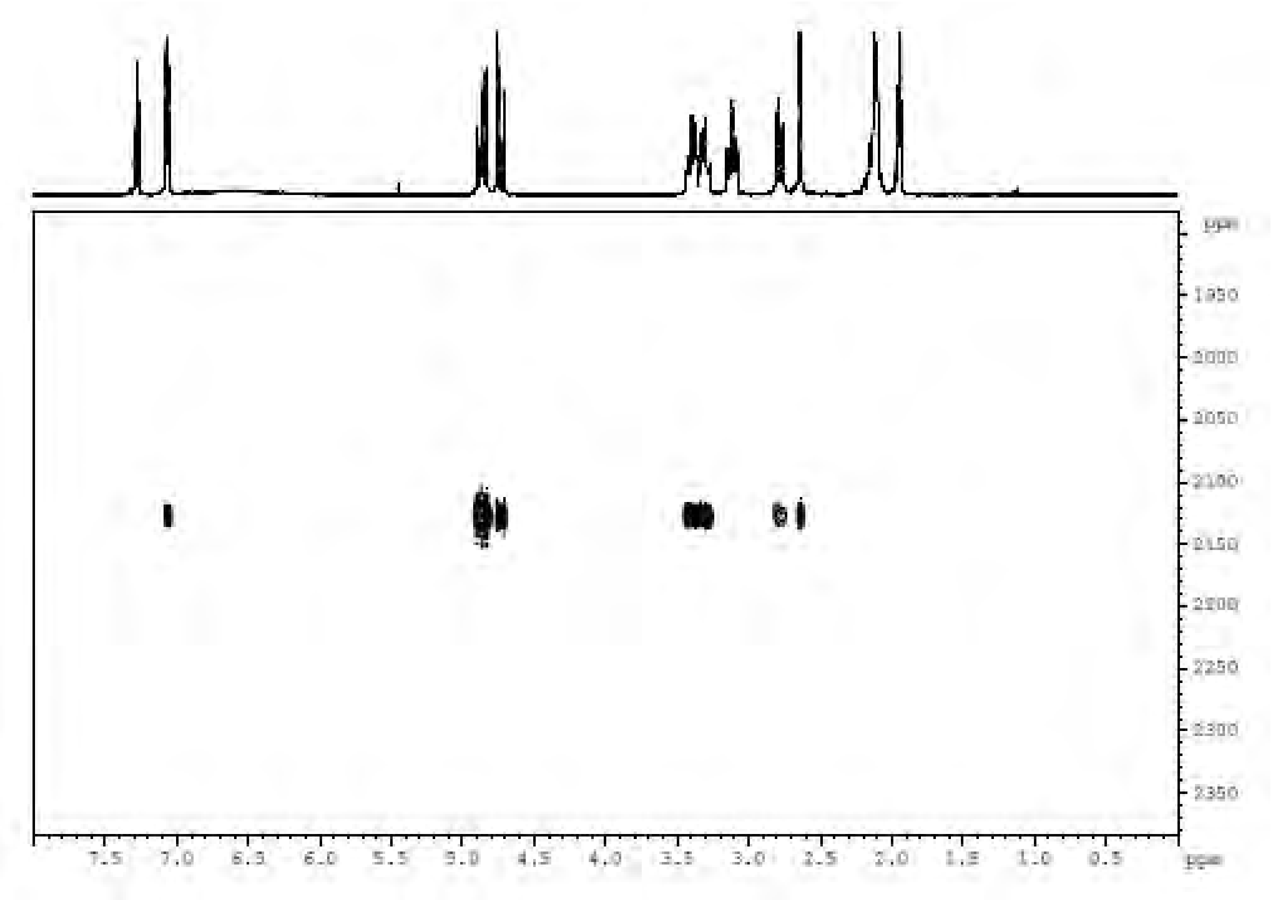

Supplementary Figure 5. ^{1}H ^{109}Ag HMBC spectrum of complex [Ag^{III}(L$_1$)](ClO$_4$)$_2$ (1_{ClO4}). Experiment performed in CD$_3$CN, 400 MHz, at 298 K.

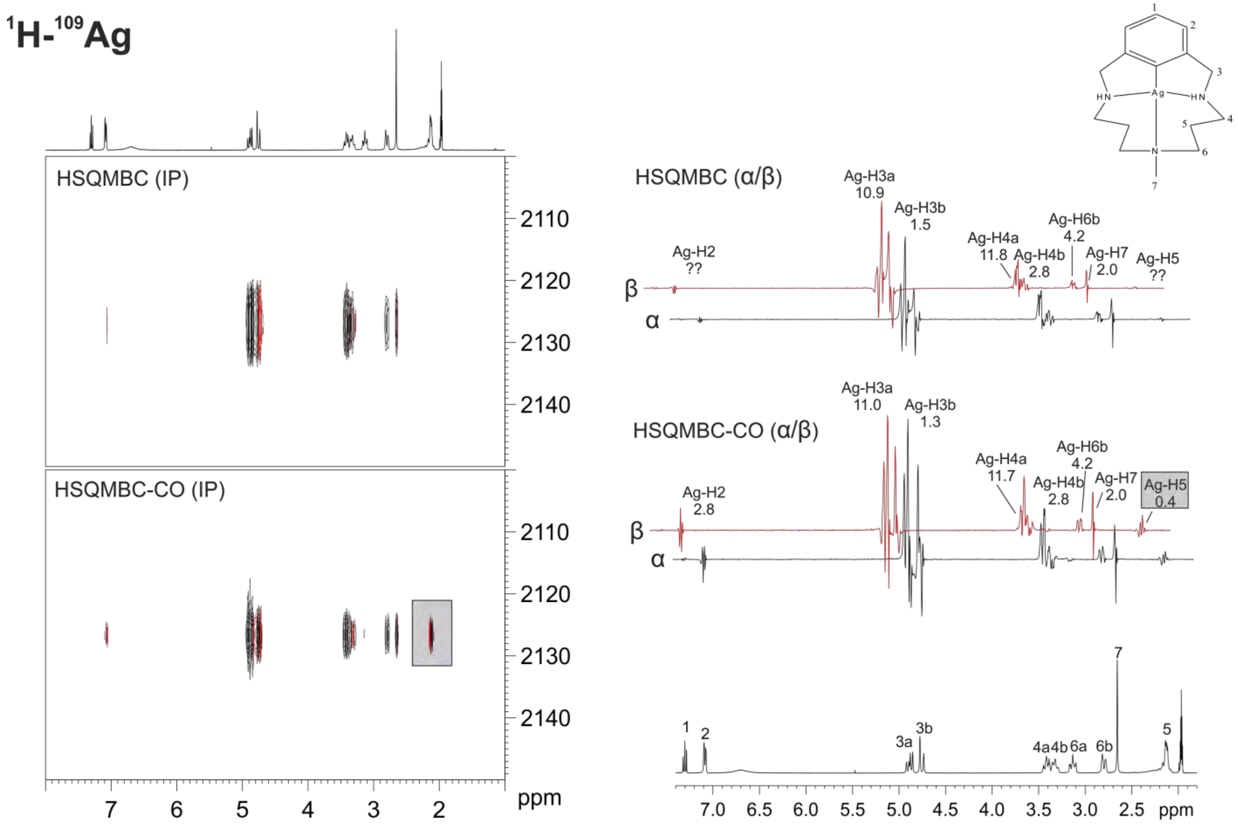

Supplementary Figure 6. 2D ^{1}H ^{109}Ag HSQMBC-IPAP and HSQMBC-COSY-IPAP experiments of complex $[Ag^{III}(L_1)](ClO_4)_2$ (1_{ClO4}). This experiment enables the quantitative measurement of J(^{1}H ^{109}Ag) coupling constants in CD_3CN, 400 MHz, at 298 K.

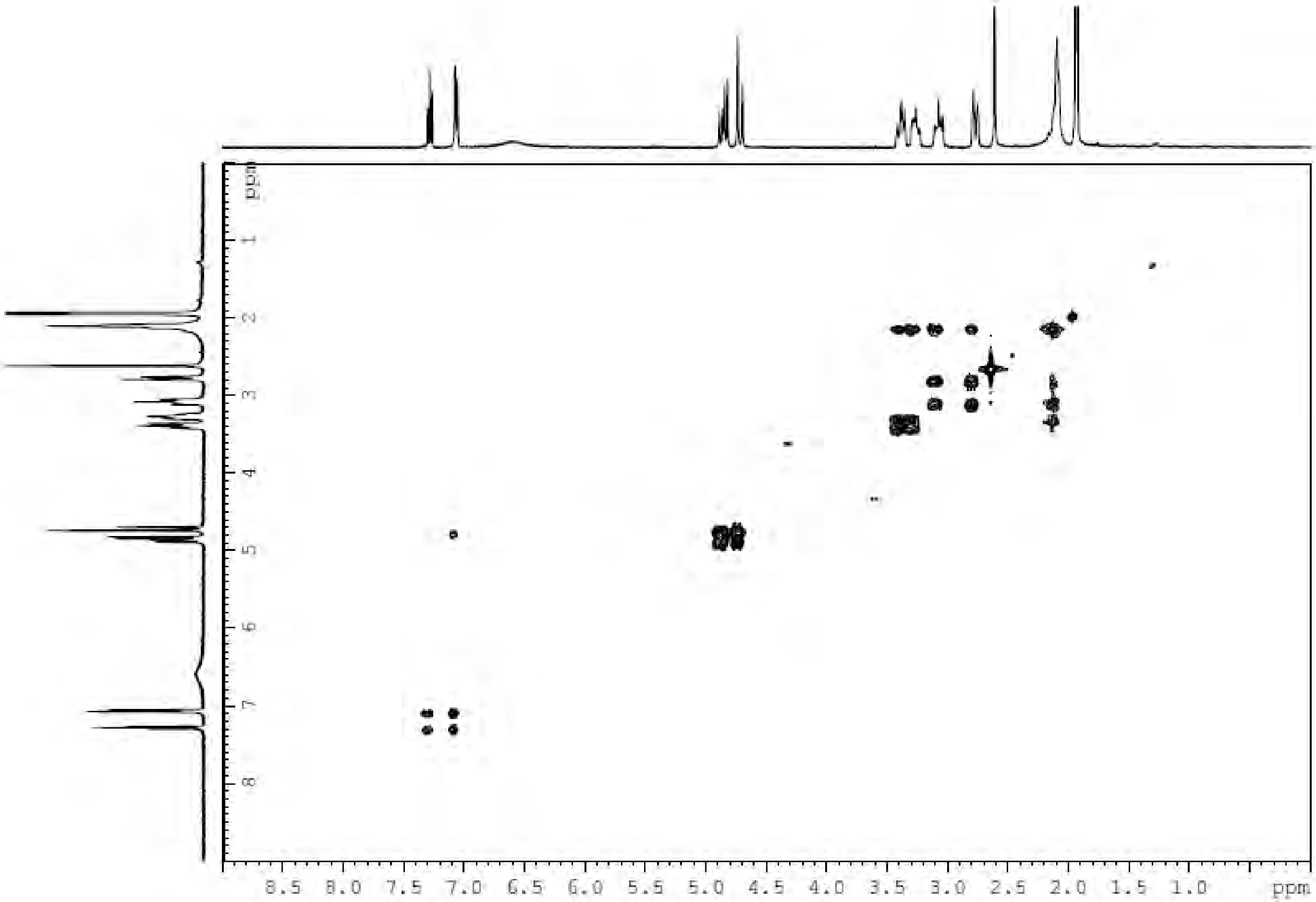

Supplementary Figure 7. COSY spectrum of complex [Ag^{III}(L$_1$)](ClO$_4$)$_2$ (1$_{ClO4}$). Experiment performed in CD$_3$CN, 400 MHz, at 298 K.

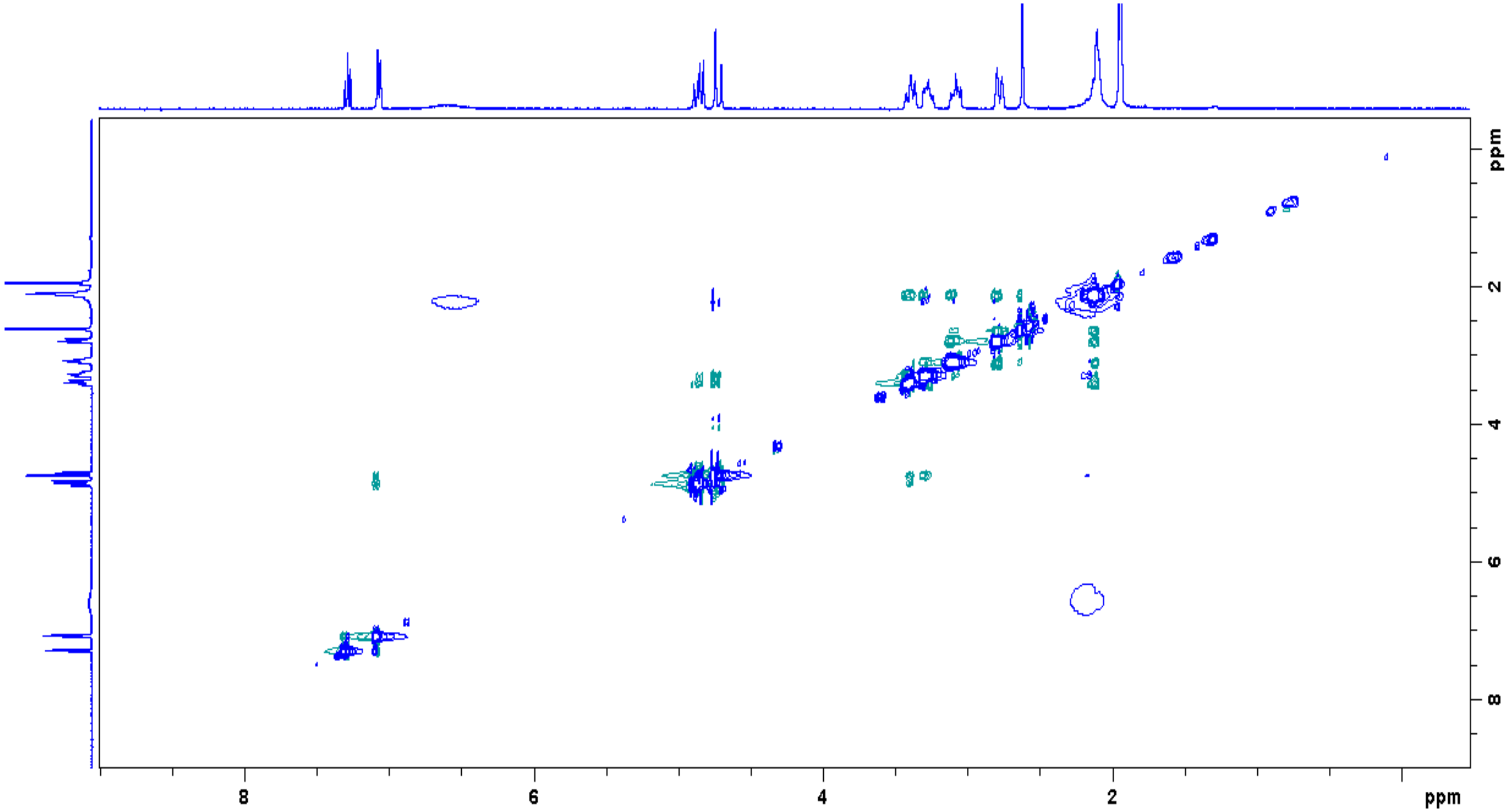

Supplementary Figure 8. NOESY spectrum of complex $[Ag^{III}(L_1)](ClO_4)_2$ (1_{ClO4}). Experiment performed in CD_3CN, 400 MHz, at 298 K.

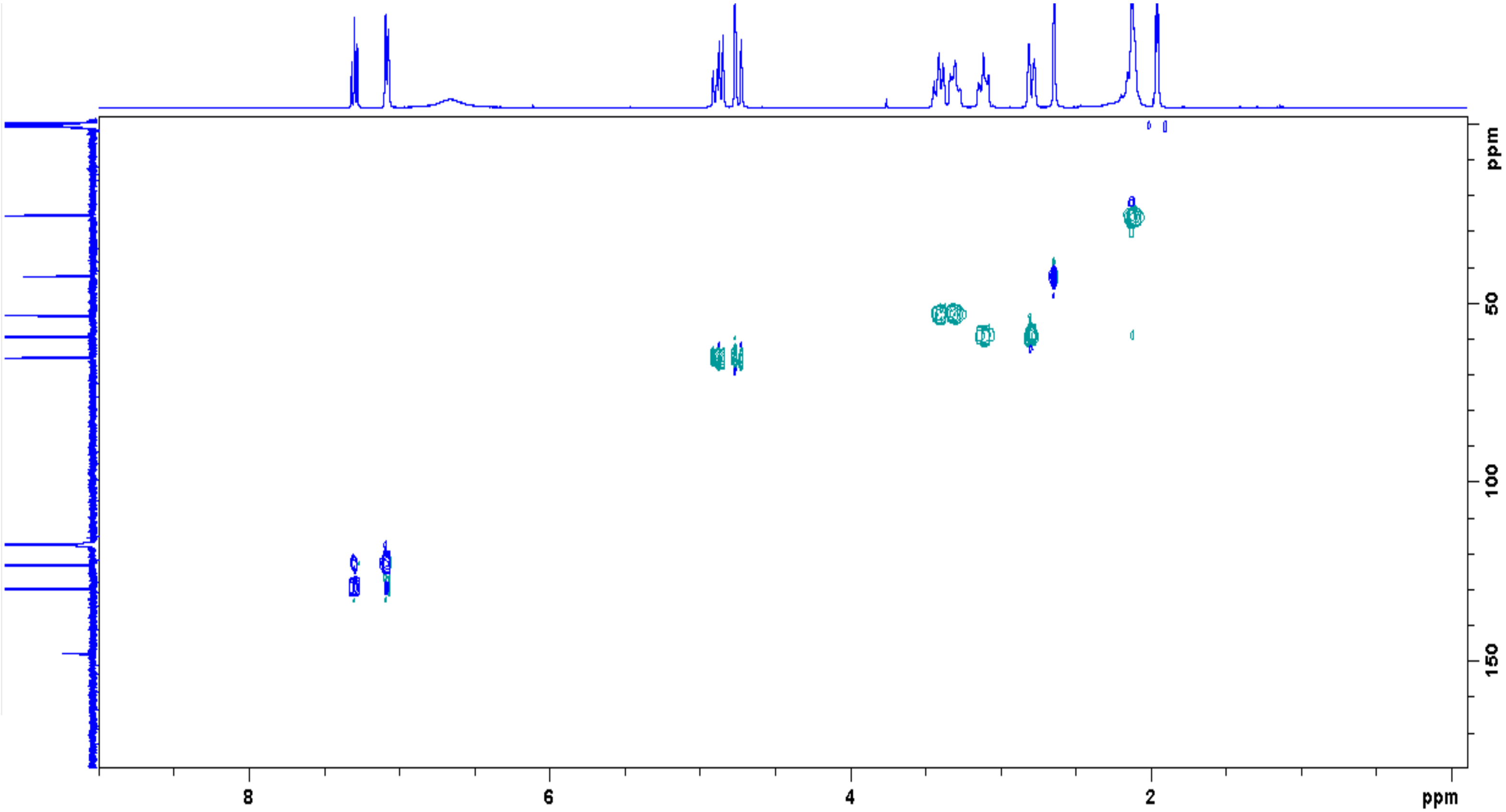

Supplementary Figure 9. ^{1}**H** ^{13}**C HSQC spectrum of complex [Ag^{III}(L$_1$)](ClO$_4$)$_2$ (1$_{ClO4}$).** Experiment performed in CD_3CN, 400 MHz, at 298 K.

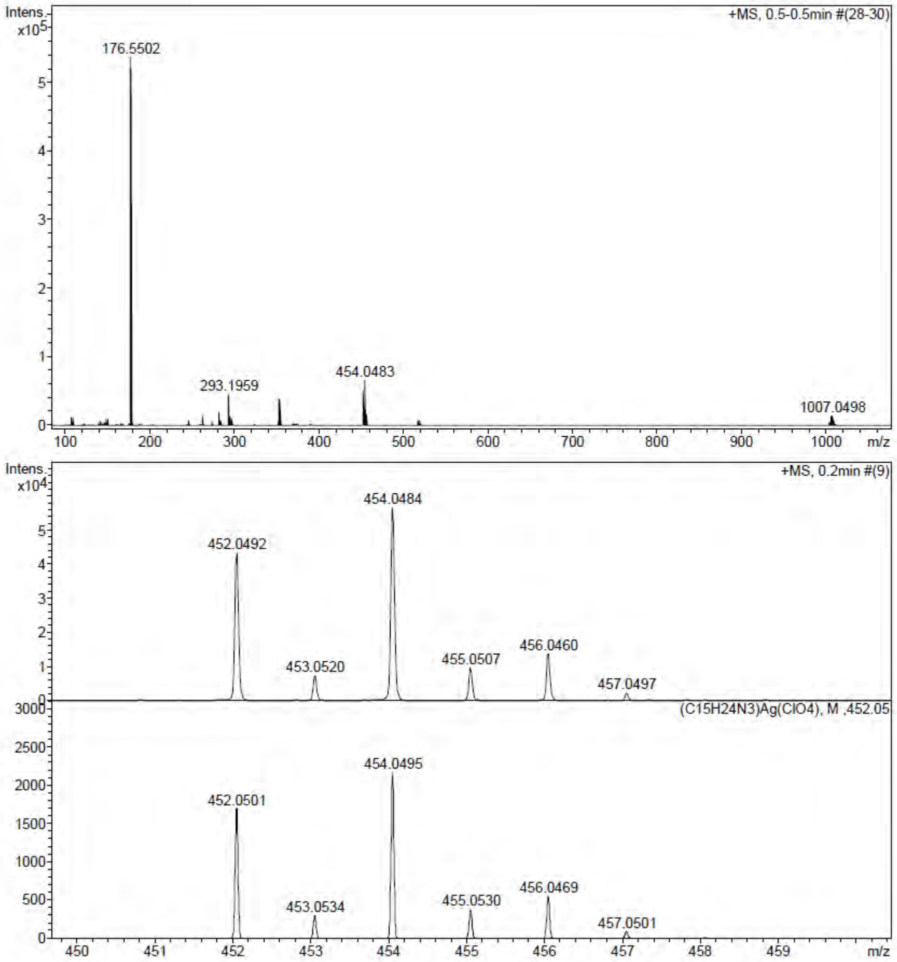

Supplementary Figure 10. HRMS (ESI-MS) spectrum of complex $[Ag^{III}(L_1)](ClO_4)_2$ (1_{ClO4}). Experiment performed in CH_3CN (spectrum at the bottom corresponds to the simulated peak).

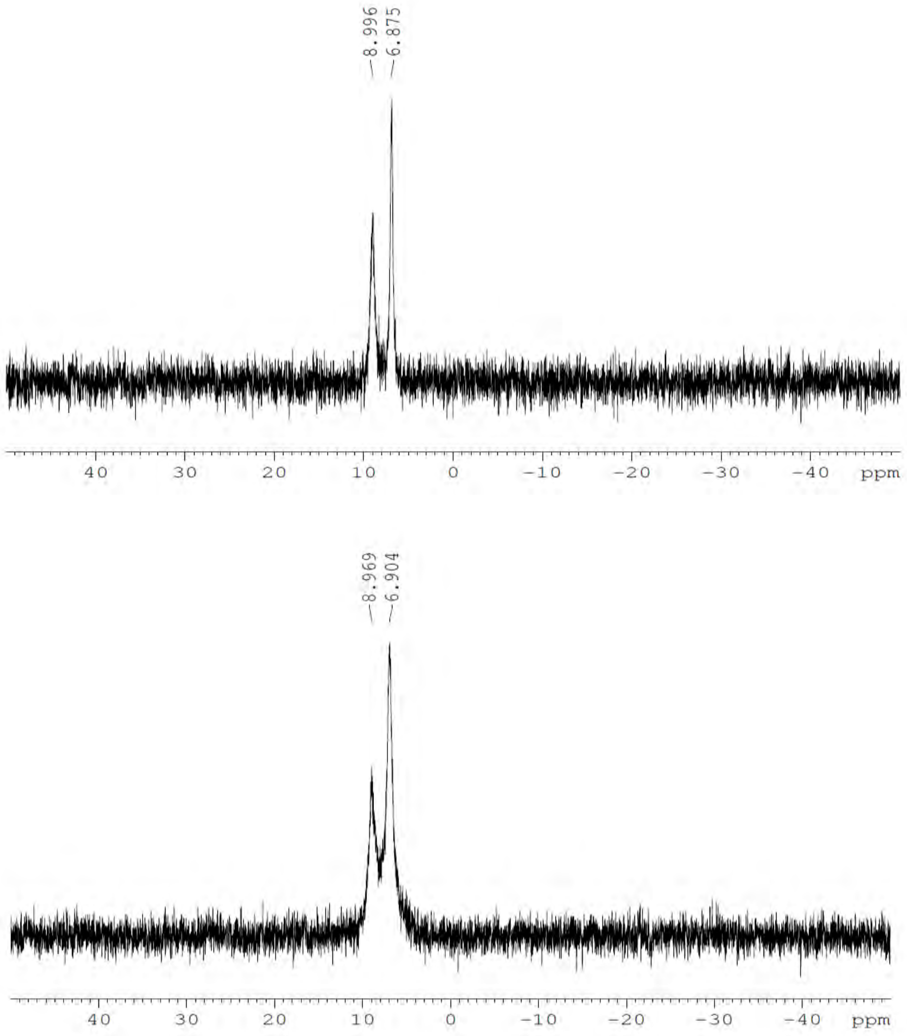

Supplementary Figure 11. **Direct detection of Ag(I) species released to the reaction media after the insertion of p-nitrophenol into $\mathbf{1}_{\mathbf{ClO4}}$**. ^{31}P-NMR of the final solution mixture of the synthesis of **2d** upon addition of 3 equiv. of PPh_3 (upper spectrum). ^{31}P-NMR of the mixture of $AgClO_4$ with 3 equiv. of PPh_3 (lower spectrum).

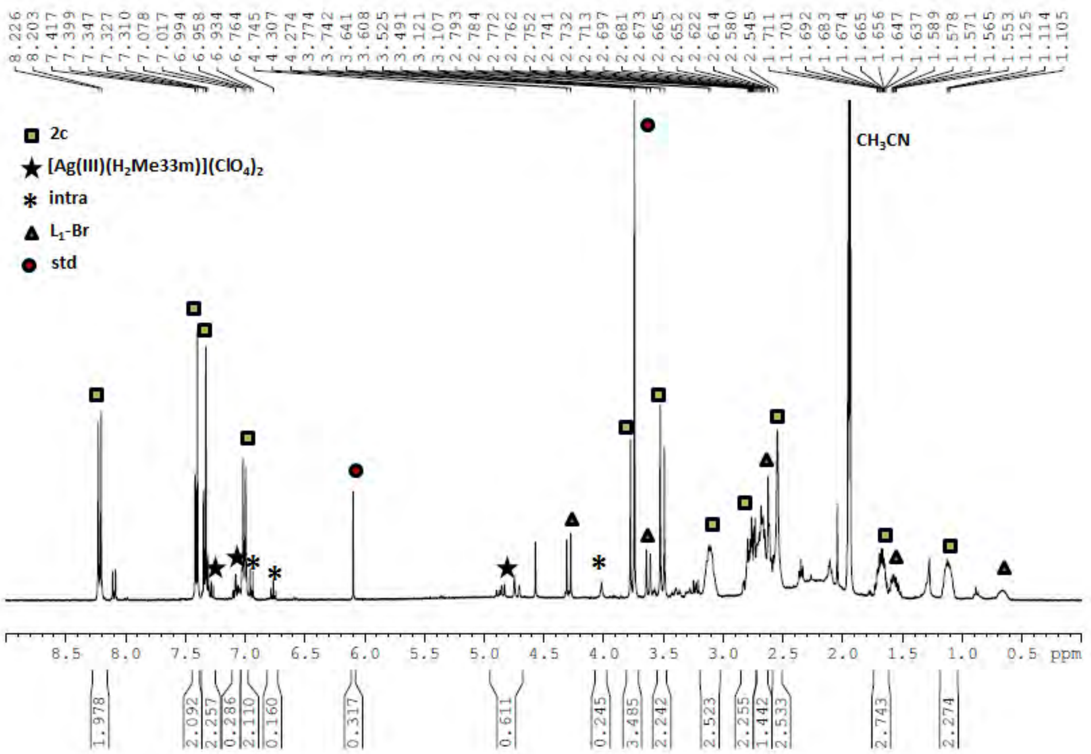

Supplementary Figure 12. Indirect detection of Ag(I) species released to the reaction media after the insertion of p-nitrophenol into 1$_{ClO4}$. NMR experiment after 18 h of the addition of 0.5 equiv. of **L$_1$-Br** showing the formation of the aryl-Ag^{III} complex **1**$_{ClO4}$ in the resulting mixture of the reaction of **1**$_{ClO4}$ with 1 equiv. of *p*-nitrophenol at 40ºC in CH$_3$CN under N$_2$. Initial conditions: [**1**$_{ClO4}$] = 12 mM, [*p*-NO$_2$phenol] = 12 mM. After the C-O bond forming event, 0.5 equiv. of L$_1$-Br added. Conditions: [**1**$_{ClO4}$] = 10.5 mM, [*p*-NO$_2$phenol] = 10.5 mM, [**L$_1$-Br**] = 5.3 mM. (**2d** = C-O coupling product, intra = intramolecular C-N coupling product,[1] std = 1,3,5-trimethoxybenzene internal standard).

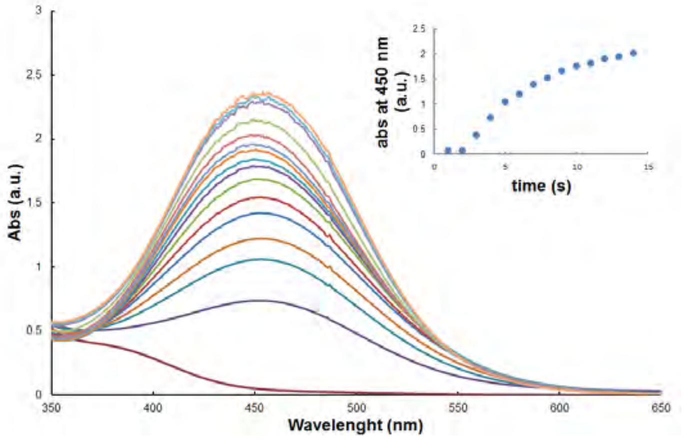

Supplementary Figure 13. **Detection of the deprotonated 2$_{\mathrm{ClO4}}$ species**. UV-Vis monitoring of the formation of orange intermediate (**2**$_{\mathrm{ClO4}}$) species upon addition of 2 equiv. of tetrabutylammonium fluoride trihydrate to complex **1**$_{\mathrm{ClO4}}$ at 25ºC in CH_3CN under N_2. Spectrum trace **a** corresponds to initial complex **1**$_{\mathrm{ClO4}}$, [**1**$_{\mathrm{ClO4}}$] = 0.83 mM. Conditions: [**1**$_{\mathrm{ClO4}}$] = 0.8 mM, [$nBu_4NF \cdot 3H_2O$] = 1.6 mM. Inset: Kinetic profile of absorbance at 450 nm.

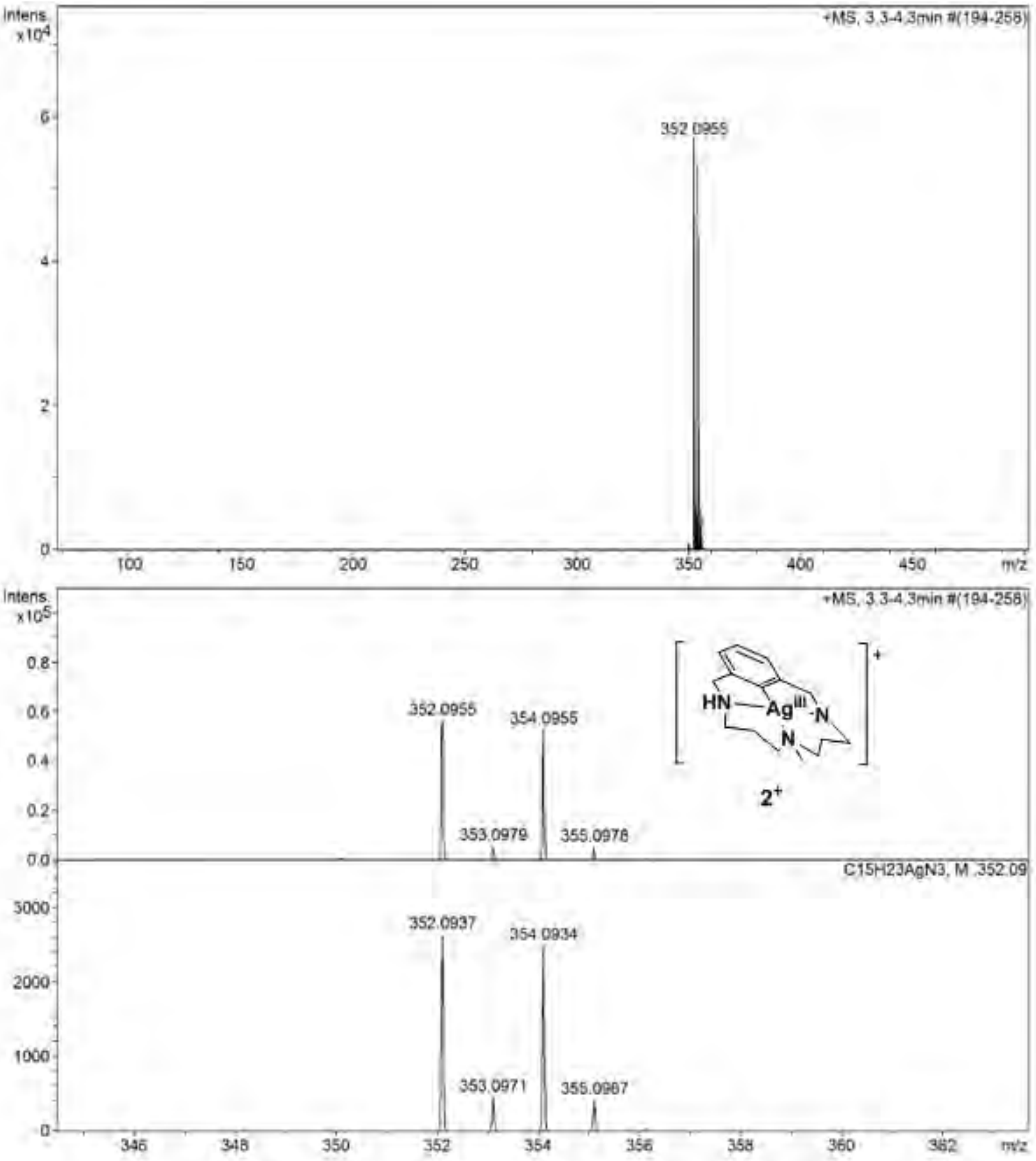

Supplementary Figure 14. **Identification of the deprotonated 2**$_{\mathbf{ClO4}}$ **species**. HRMS (ESI-MS) spectrum of the orange intermediate species (**2**$_{\mathrm{ClO4}}$) after its formation upon addition of 2 equiv. of tetrabutylammonium fluoride trihydrate to complex **1**$_{\mathrm{ClO4}}$ at 25ºC in CH_3CN under N_2 confirmed by UV-Vis spectroscopy. Conditions: [**1**$_{\mathrm{ClO4}}$] = 0.8 mM, [$nBu_4NF\cdot 3H_2O$] = 1.6 mM. Bottom: simulated spectrum.

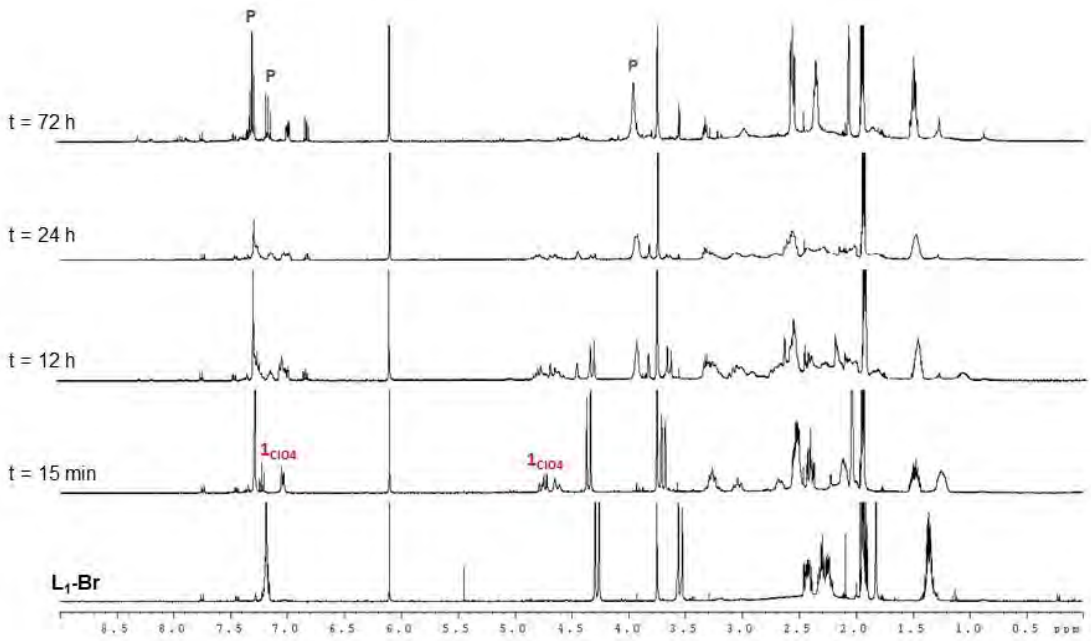

Supplementary Figure 15. **Variable temperature ^{1}H NMR monitoring of the fluorination of the model aryl halide substrate L_1-Br**. Reaction performed using 1 equiv. of AgOTf and 1 equiv. of AgF. Conditions: [**L_1-Br**] = 17.5 mM, CD_3CN, 40ºC. (**1_{ClO4}** = aryl-Ag^{III} species, P = **L_1-F**).

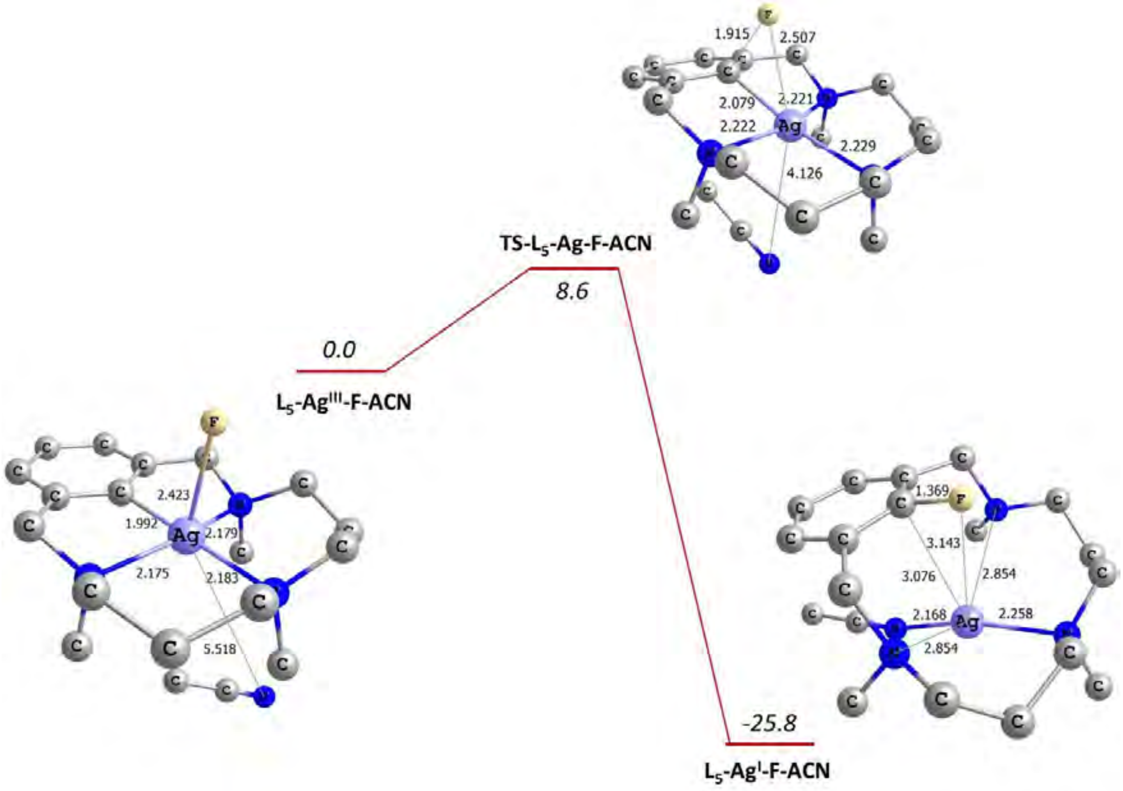
1.915
2.507
2.079
2.221
2.222
Ag
2.229
4.126
TS-L5-Ag-F-ACN
8.6
0.0
L5-AgIII-F-ACN
F
2.423
1.992
Ag
2.179
2.175
2.183
5.518
1.369
F
3.143
3.076
2.854
2.168
Ag
2.258
2.854
-25.8
L5-AgI-F-ACN

Supplementary Figure 16. DFT computed reaction profile for the reductive elimination of L_5-Ag(III)-F to Ag(I) and L_5-F. Relative Gibbs energy values are given in kcal·mol^{-1}. Selected bond distances are given in Å. H atoms are omitted for clarity.

a)

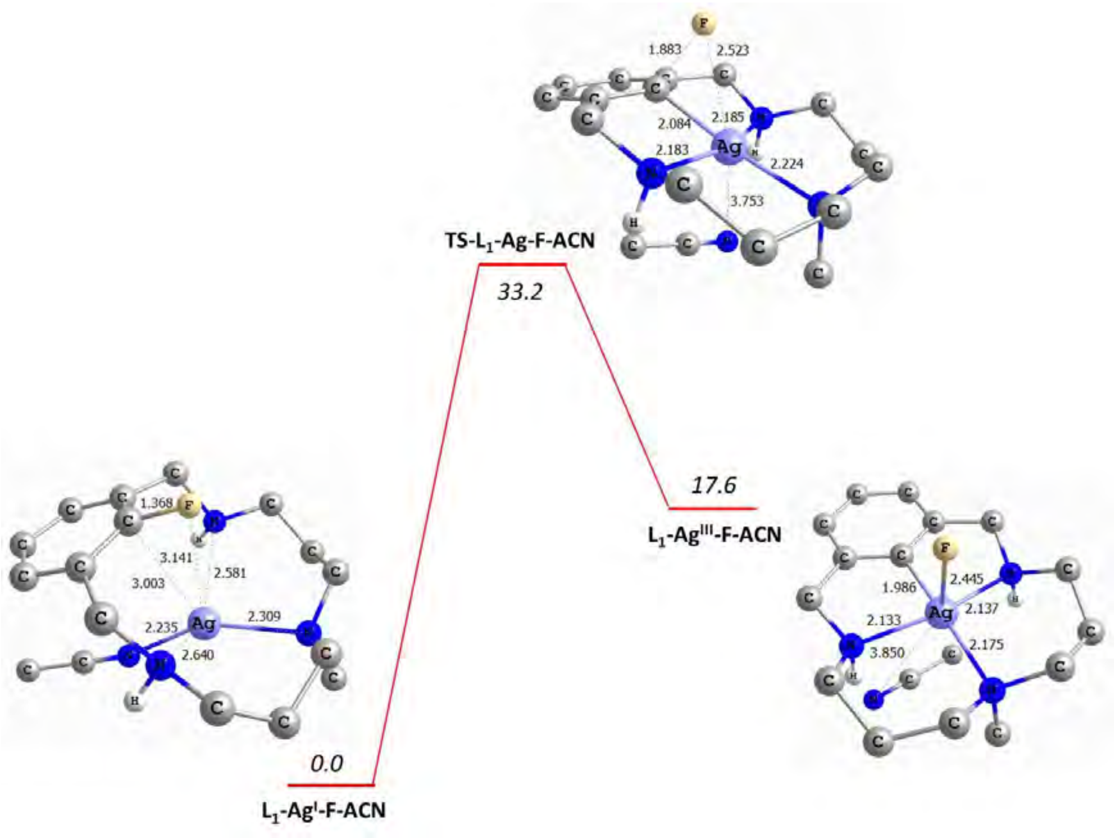

TS-L1-Ag-F-ACN
33.2
1.883
2.523
2.084
2.185
2.183
2.224
3.753
Ag
F
17.6
L1-AgIII-F-ACN
1.986
2.445
2.133
2.137
2.175
3.850
1.368
3.141
2.581
3.003
2.235
2.309
2.640
0.0
L1-AgI-F-ACN

b)

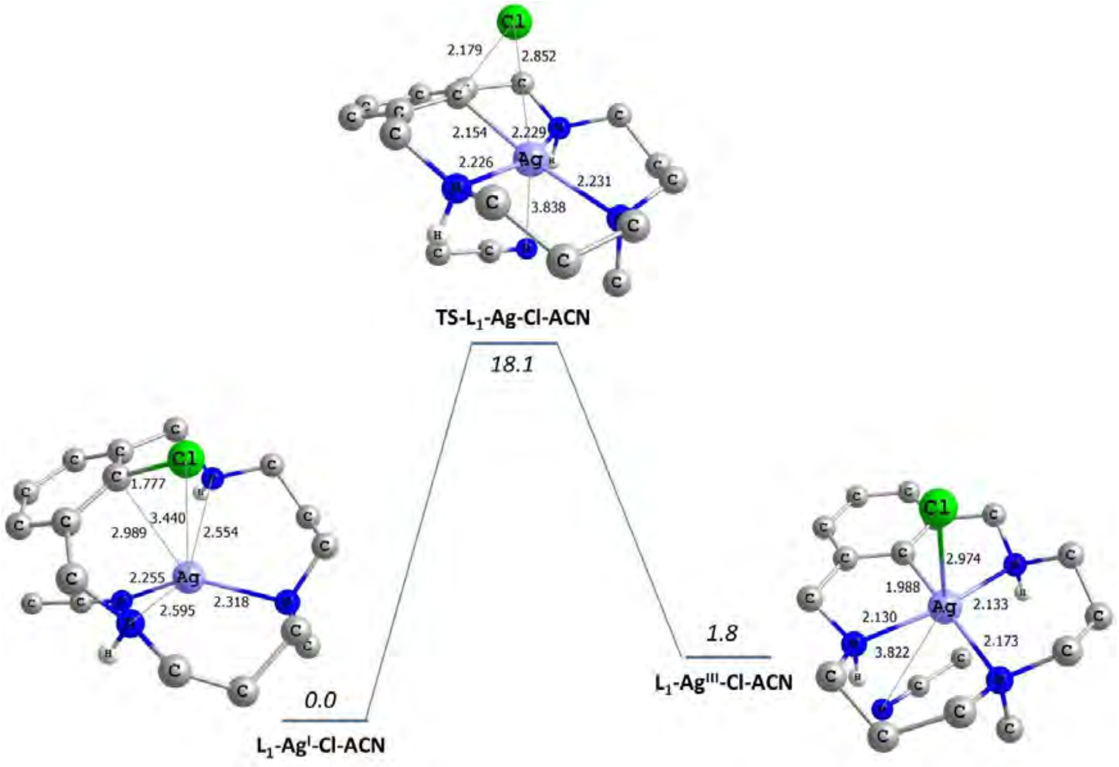
TS-L_1-Ag-Cl-ACN
18.1
L_1-Ag^I-Cl-ACN
0.0
L_1-Ag^{III}-Cl-ACN
1.8
Cl
Ag
2.179
2.852
2.154
2.229
2.226
2.231
3.838
1.777
3.440
2.989
2.554
2.255
2.318
2.595
2.974
1.988
2.130
2.133
2.173
3.822

c)

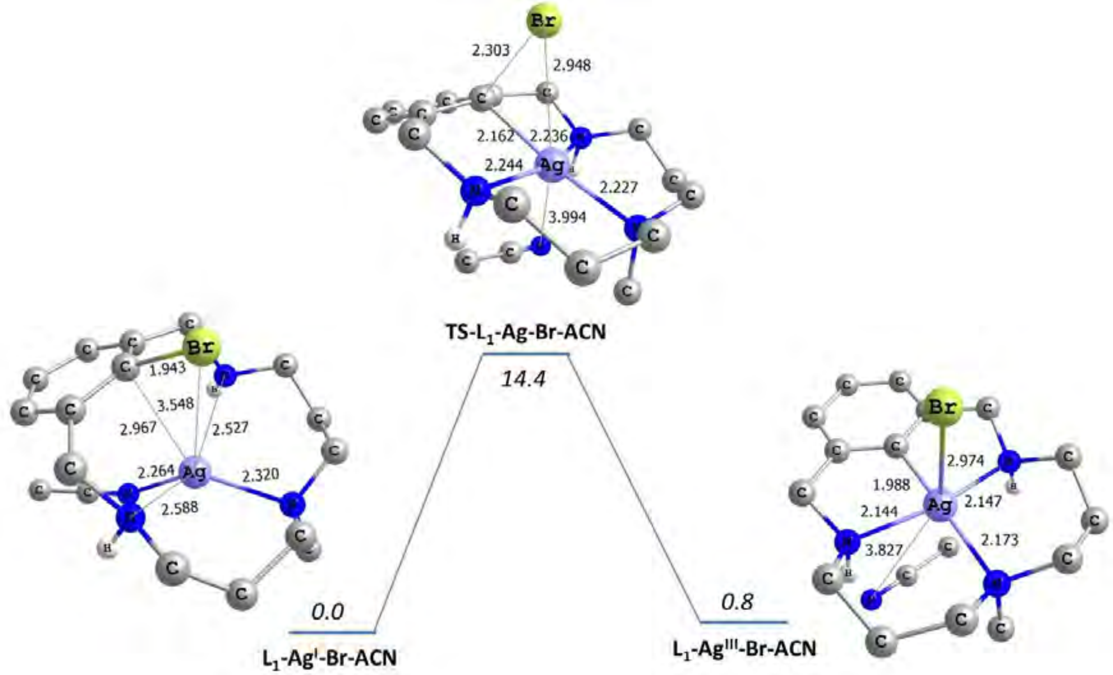
Br
2.303
2.948
2.162
2.236
2.244
Ag
2.227
3.994
TS-L$_1$-Ag-Br-ACN
14.4
Br
1.943
3.548
2.967
2.527
2.264
Ag
2.320
2.588
0.0
L$_1$-Ag^I-Br-ACN
Br
2.974
1.988
2.144
Ag
2.147
2.173
3.827
0.8
L$_1$-Ag^{III}-Br-ACN

d)

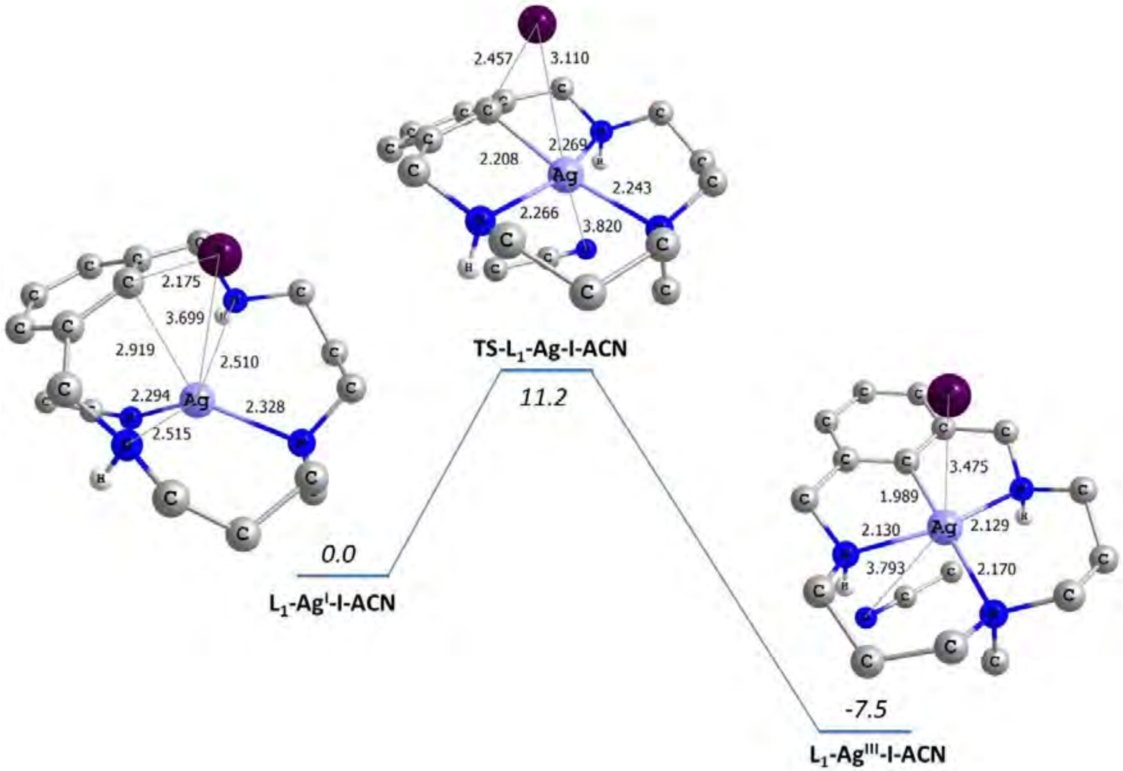
2.457
3.110
2.208
2.269
Ag
2.243
2.266
3.820
TS-L1-Ag-I-ACN
11.2
2.175
3.699
2.919
2.510
2.294
Ag
2.328
2.515
0.0
L1-AgI-I-ACN
3.475
1.989
2.130
Ag
2.129
3.793
2.170
-7.5
L1-AgIII-I-ACN

Supplementary Figure 17. DFT computed reaction profile for the oxidative addition of Ag(I) over L_1-X. a) X = F, b) X = Cl, c) X = Br and d) X = I. Relative Gibbs energy values are given in kcal·mol^{-1}. Selected bond distances are given in Å. H atoms are omitted for clarity except for N-H moieties.

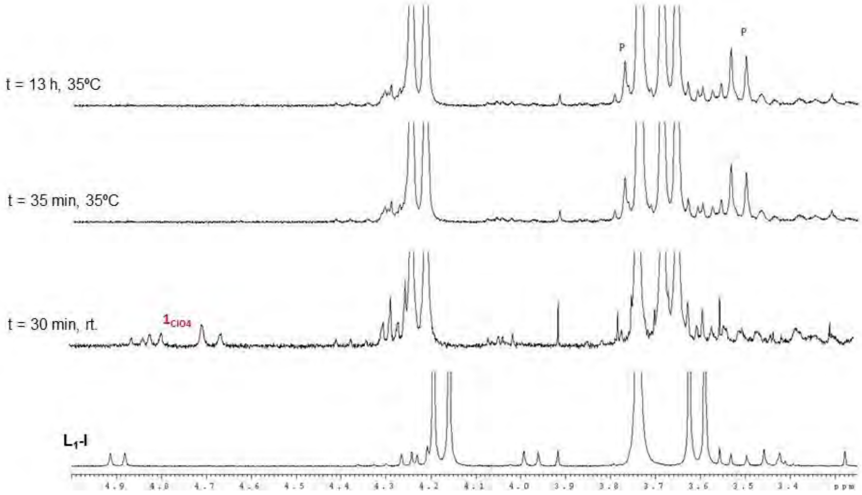

Supplementary Figure 18. **^{1}H NMR monitoring of the C-O bond forming cross-coupling catalysis of the model aryl halide substrate L$_1$-I**. Conditions: [**L$_1$-I**] = 20 mM, [*p*-NO$_2$phenol] = 0.4 M, [AgOTf] = 2 mM, [PPh$_3$] = 2 mM, CD$_3$CN, 35ºC. (**1_{ClO4}** = aryl-Ag^{III} species, P = **2d**). **1_{ClO4}** is formed in a 4% yield and **2d** in a 17% yield (the lower yield of **2d** compared to the standard catalytic procedure (Table 2, Chapter IV) can be explained by the lower temperature employed and the absence of stirring in the NMR tube).

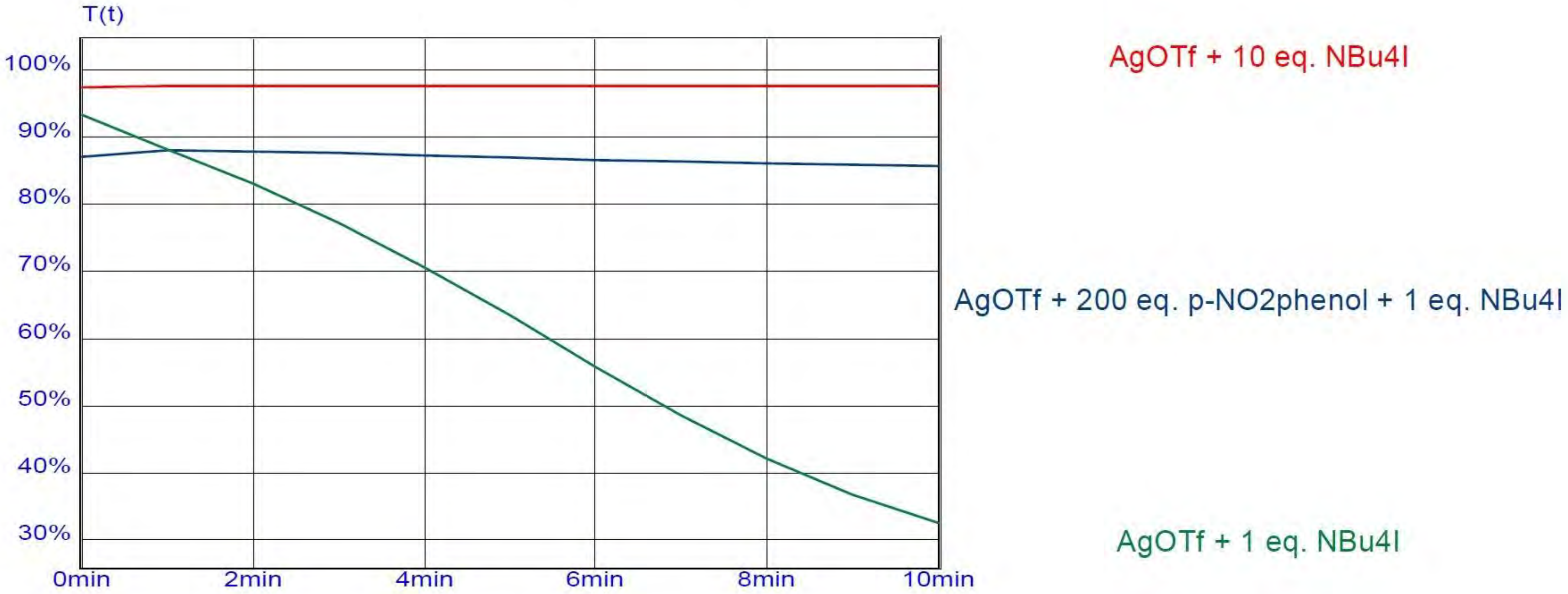

Supplementary Figure 19. Transmitted light monitoring of AgOTf solutions upon addition of nBu$_4$NI. Red line corresponds to a sample containing AgOTf and 10 equiv. of *n*BuNI in acetonitrile. Blue line corresponds to a sample containing AgOTf, 200 equiv. of *p*-nitrophenol and 1 equiv. of *n*BuNI in acetonitrile. Green line corresponds to a sample containing AgOTf and 1 equiv. of *n*Bu$_4$NI in acetonitrile. Conditions: [AgOTf] = 0.63 mM, CH$_3$CN, rt.

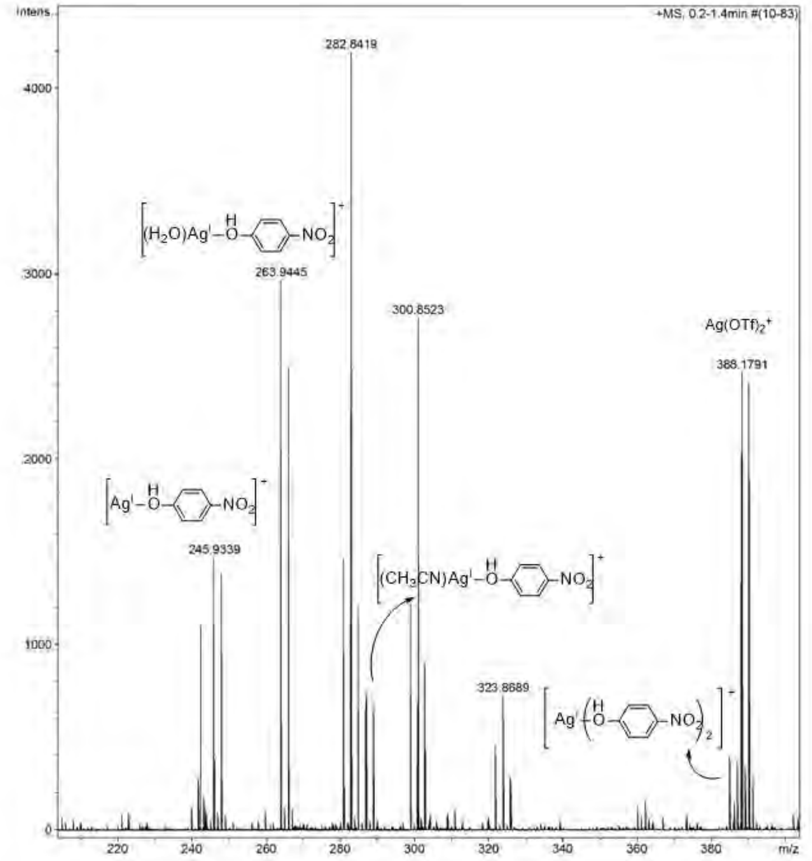

Supplementary Figure 20. **Identification of soluble Ag(I) species by HRMS**. HRMS (ESI-MS) spectrum in positive ion mode of the silver species formed upon addition of 200 equiv. of *p*-nitrophenol to a silver triflate solution at 25ºC in CH_3CN. Conditions: [AgOTf] = 2.5 mM, [*p*-NO_2phenol] = 0.5 M.

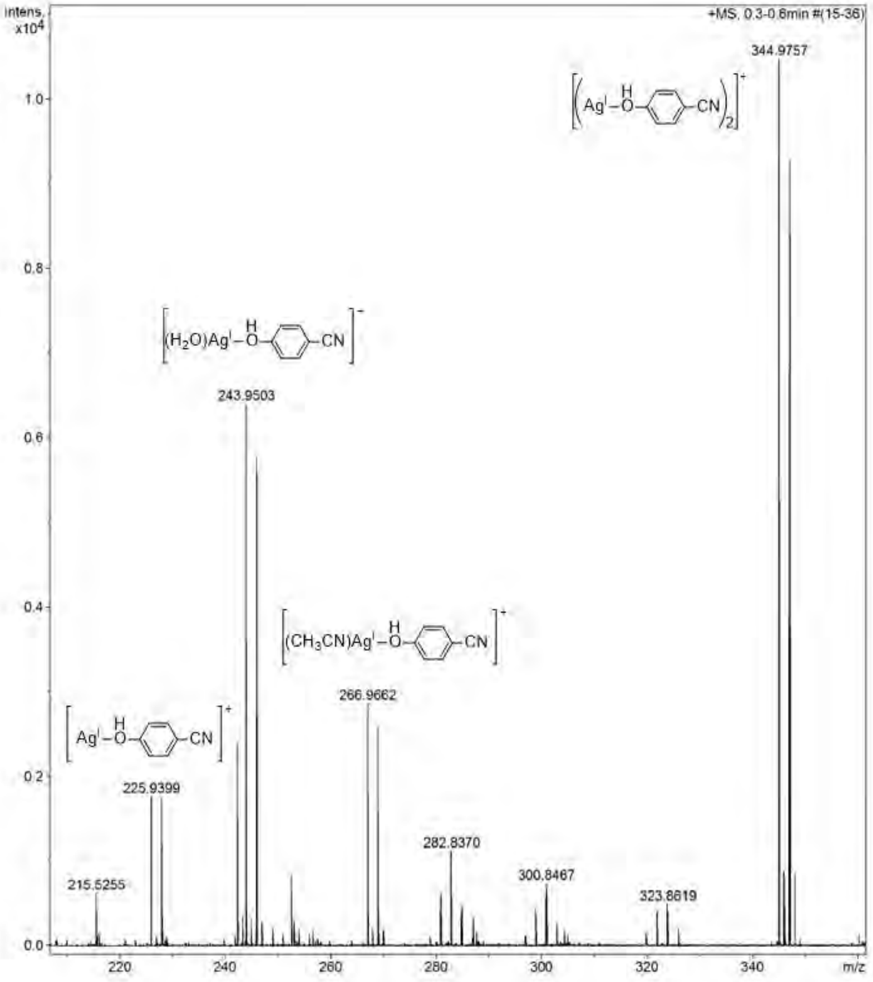

Supplementary Figure 21. **Identification of soluble Ag(I) species by HRMS**. HRMS (ESI-MS) spectrum in positive ion mode of the silver species formed upon addition of 200 equiv. of *p*-cyanophenol to a silver triflate solution at 25ºC in CH_3CN. Conditions: [AgOTf] = 2.5 mM, [*p*-CNphenol] = 5 mM.

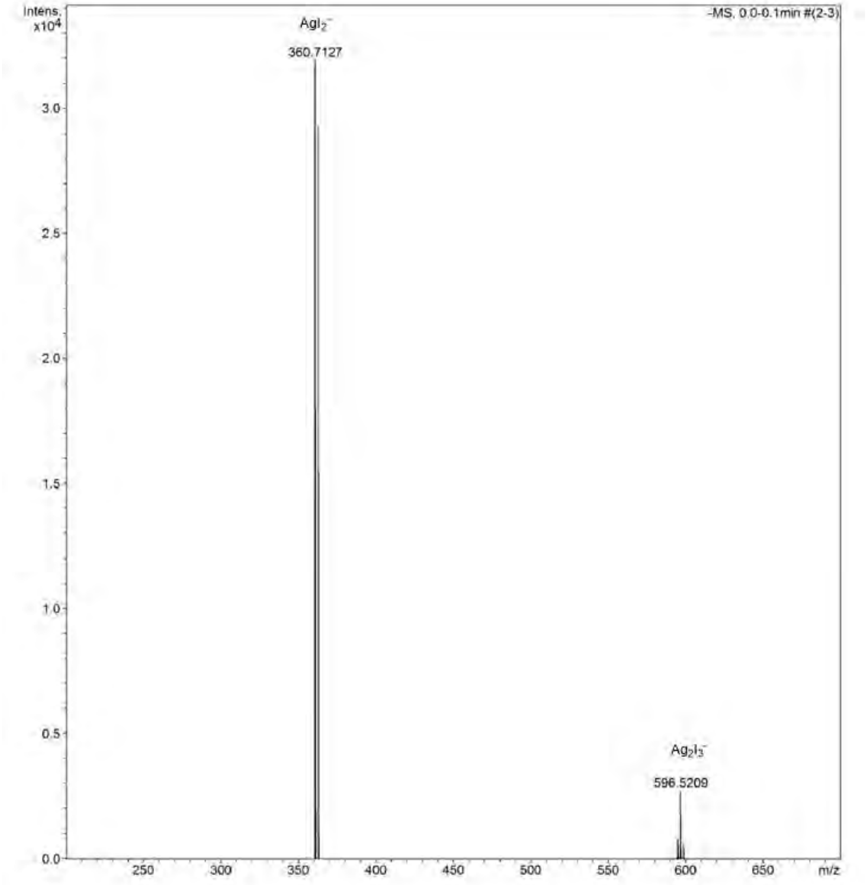

Supplementary Figure 22. **Identification of soluble Ag(I) species by HRMS** HRMS (ESI-MS) spectrum in negative ion mode of the C-O bond forming cross-coupling catalysis of the model aryl halide substrate **L$_1$-I** at 50ºC in CH_3CN under N_2 after 6 h. Conditions: [**L$_1$-I**] = 5 mM, [*p*-NO_2phenol] = 0.1 M, [AgOTf] = 0.5 mM, [PPh_3] = 0.5 mM, CH_3CN, 50ºC.

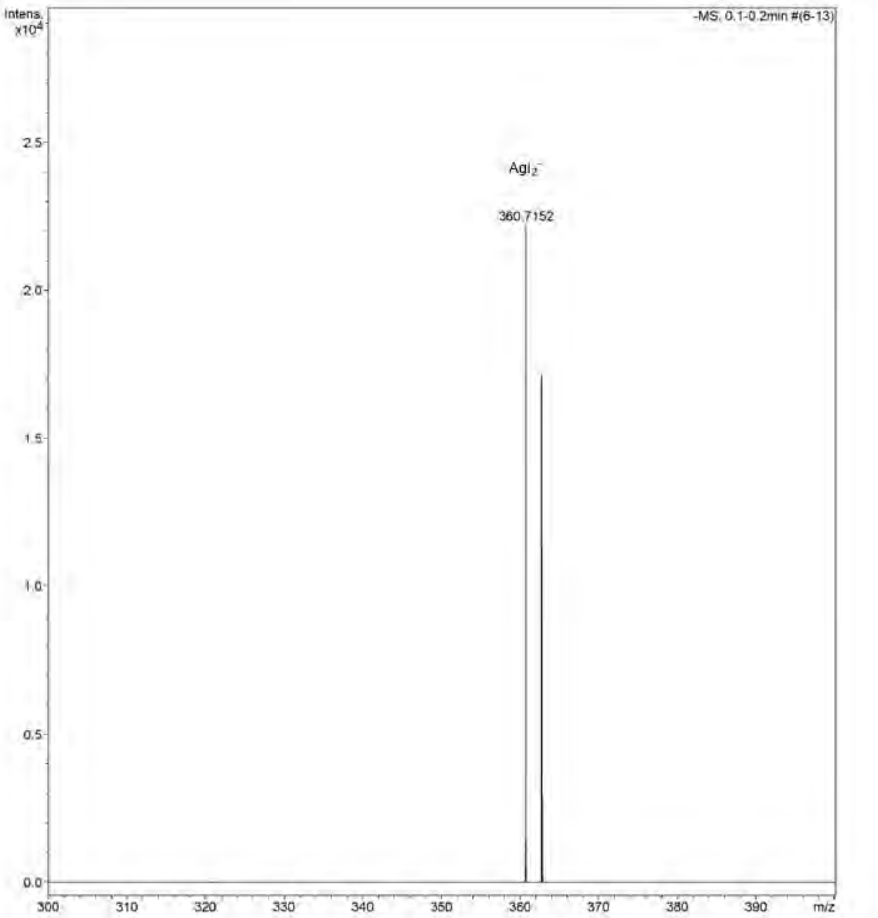

Supplementary Figure 23. **Identification of soluble Ag(I) species by HRMS.** HRMS (ESI-MS) spectrum in negative ion mode of the silver species formed upon addition of 1 equiv. of tetrabutylammonium iodide to a silver triflate and 20 equiv. of *p*-nitrophenol solution at 25ºC in CH_3CN. Conditions: [AgOTf] = 2.5 mM, [*p*-NO_2phenol] = 50 mM, [nBu_4NI] = 2.5 mM.

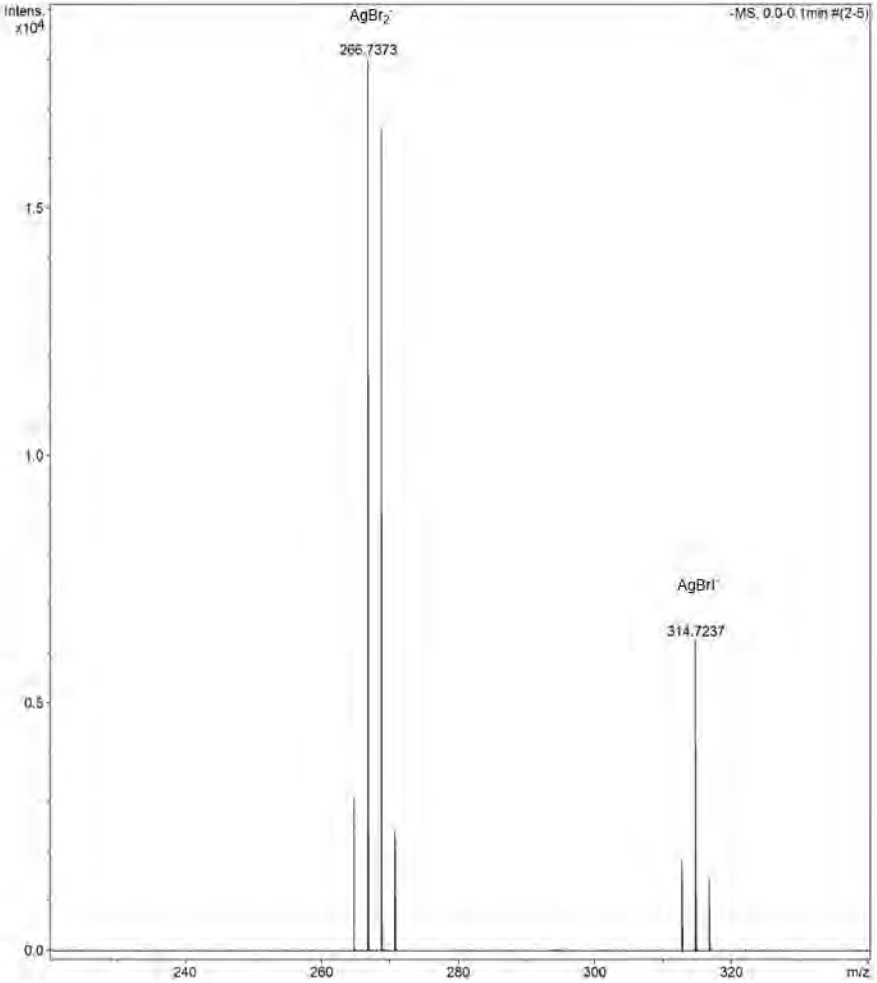
Intens.
x10^4
AgBr2⁻
266.7373
-MS, 0.0-0.1min #(2-5)
1.5
1.0
0.5
0.0
AgBrI⁻
314.7237
240
260
280
300
320
m/z

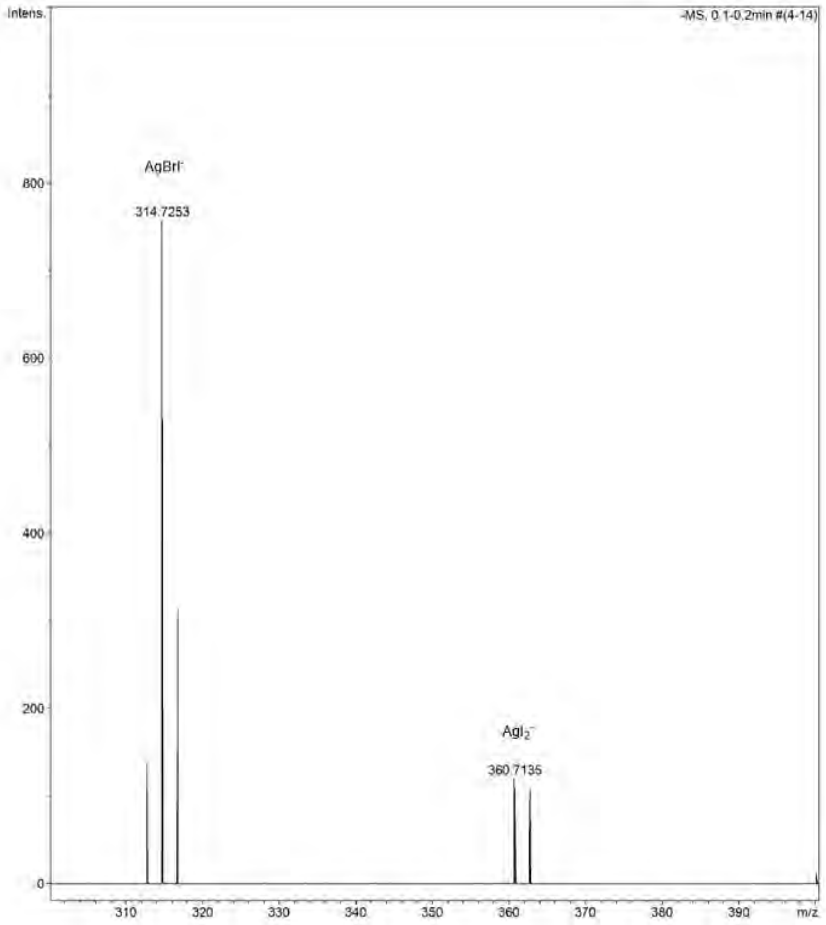

Supplementary Figure 24. **Identification of soluble Ag(I) species by HRMS.** HRMS (ESI-MS) spectrum in negative ion mode of the stoichiometric halide exchange reaction of the model aryl halide substrate **L_1-I** at 50ºC in CH_3CN under N_2 after 6 h. Conditions: [**L_1-I**] = 15 mM, [nBu_4Br] = 0.15 M, [AgOTf] = 15 mM, CH_3CN, 50ºC.

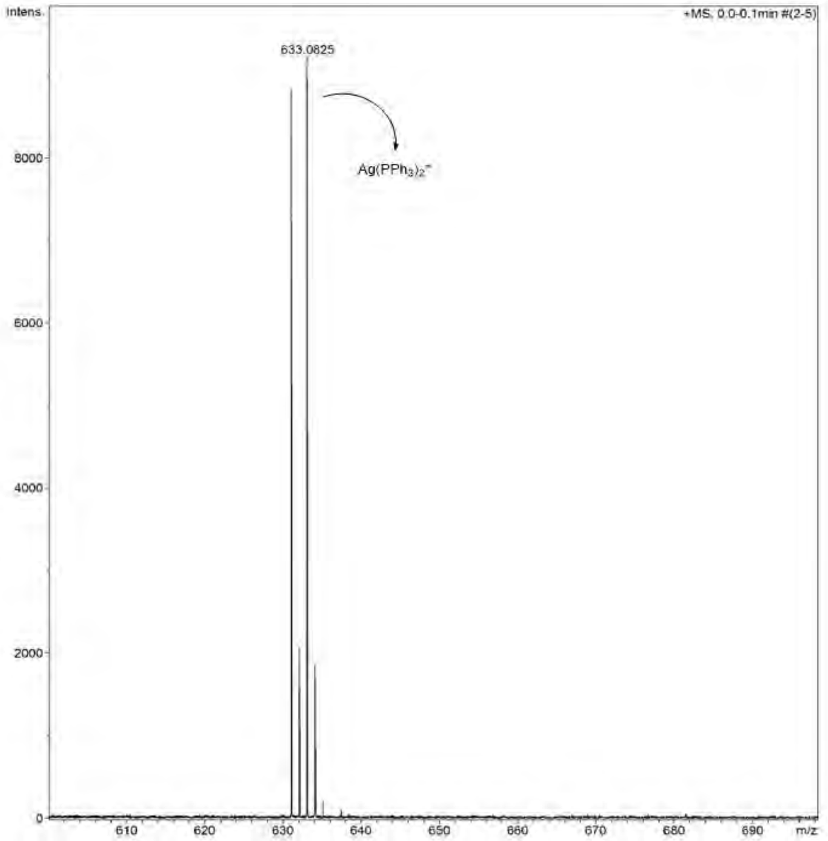

Supplementary Figure 25. **Identification of soluble Ag(I) species by HRMS**. HRMS (ESI-MS) spectrum in positive ion mode of the C-O bond forming cross-coupling catalysis of the model aryl halide substrate **L_1-I** at 50ºC in CH_3CN under N_2 after 6 h. Conditions: [**L_1-I**] = 5 mM, [*p*-NO_2phenol] = 0.1 M, [AgOTf] = 0.5 mM, [PPh_3] = 0.5 mM, CH_3CN, 50ºC.

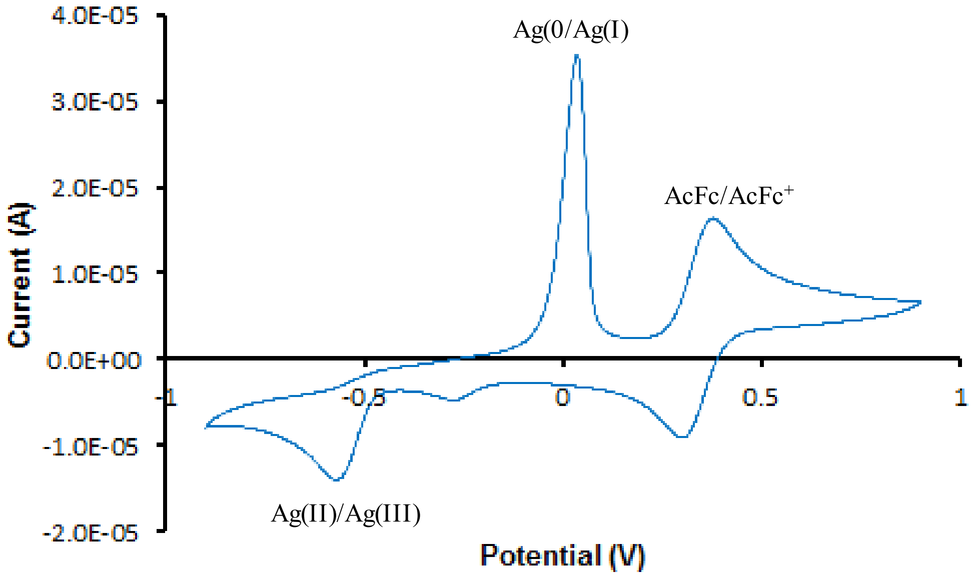

Supplementary Figure 26. Cyclic Voltammetry (CV) of complex $[Ag^{III}(L_1)](ClO_4)_2$ (1_{ClO4}). $[[Ag^{III}(L_1)](ClO_4)_2]$ = 1 mM, $[nBu_4NPF_6]$ = 0.1 M, CH_3CN, 298 K, scan rate = 0.1 V/s, using non-aqueous $Ag/AgNO_3$ reference electrode and $AcFc/AcFc^+$ as the internal reference.

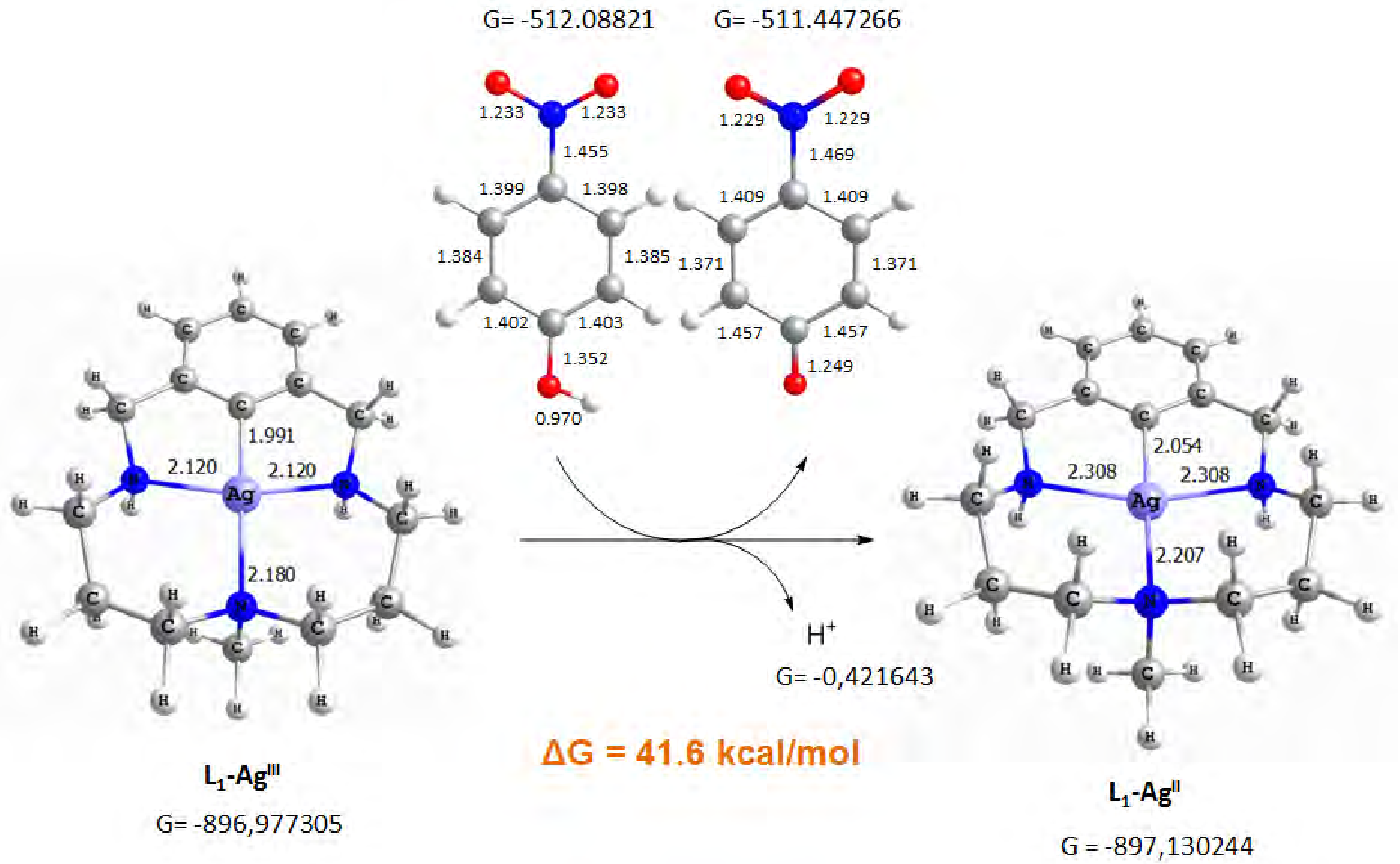
G= -512.08821
G= -511.447266
1.233
1.233
1.455
1.399
1.398
1.384
1.385
1.402
1.403
1.352
0.970
1.229
1.229
1.469
1.409
1.409
1.371
1.371
1.457
1.457
1.249
1.991
2.120
2.120
2.180
Ag
2.054
2.308
2.308
2.207
H+
G= -0,421643
ΔG = 41.6 kcal/mol
L1-AgIII
G= -896,977305
L1-AgII
G = -897,130244

Supplementary Figure 27. DFT free energy difference of the single electron transfer (SET) from the *p*NO_2-phenol to the aryl-Ag(III) complex. Relative Gibbs energy values are given in kcal·mol^{-1}. Selected bond distances are given in Å.

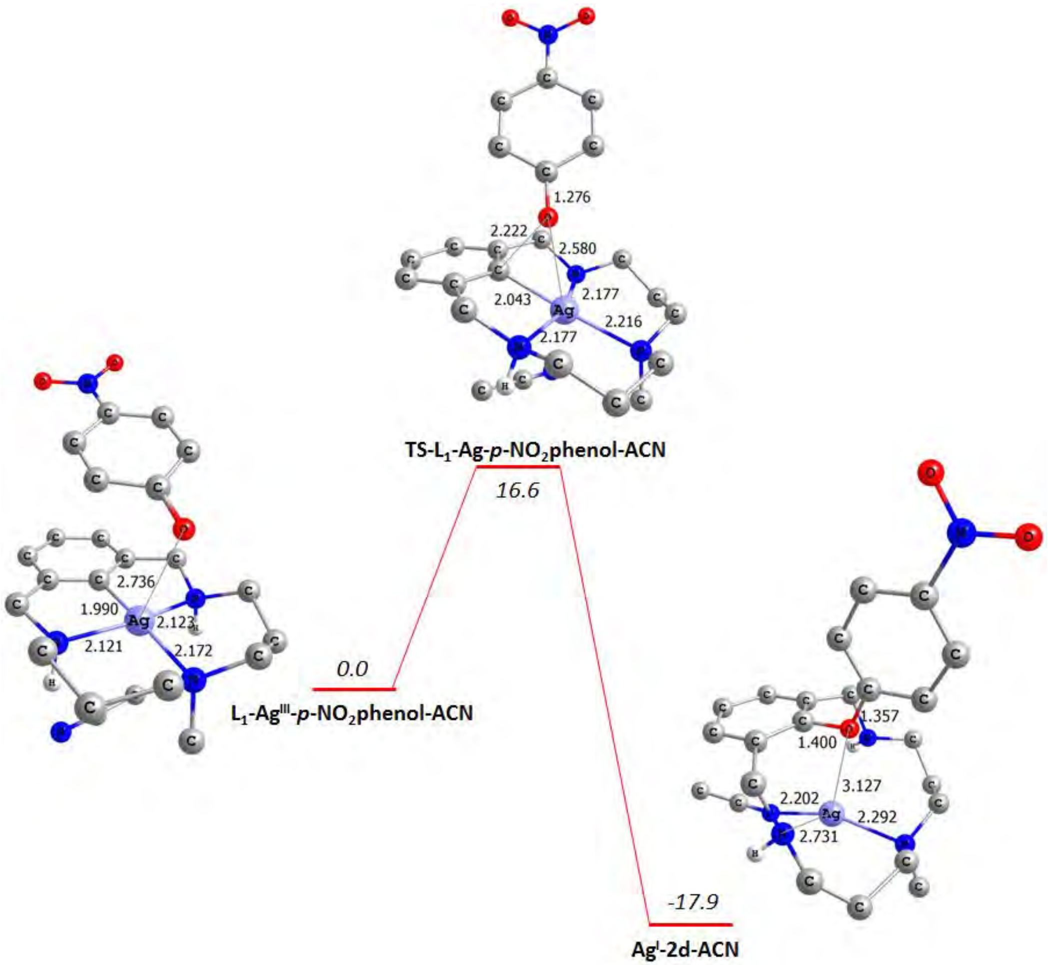
1.276
2.222
2.580
2.177
2.043
Ag
2.216
2.177
TS-L$_1$-Ag-*p*-NO$_2$phenol-ACN
16.6
2.736
1.990
Ag
2.123
2.121
2.172
0.0
L$_1$-Ag^{III}-*p*-NO$_2$phenol-ACN
1.357
1.400
3.127
2.202
Ag
2.292
2.731
-17.9
Ag^{I}-2d-ACN

Supplementary Figure 28. DFT computed reaction profile for the reductive elimination of the aryl-Ag(III) complex with *p*-nitrophenol. Relative Gibbs energy values are given in kcal·mol^{-1}. Selected bond distances are given in Å. H atoms are omitted for clarity.

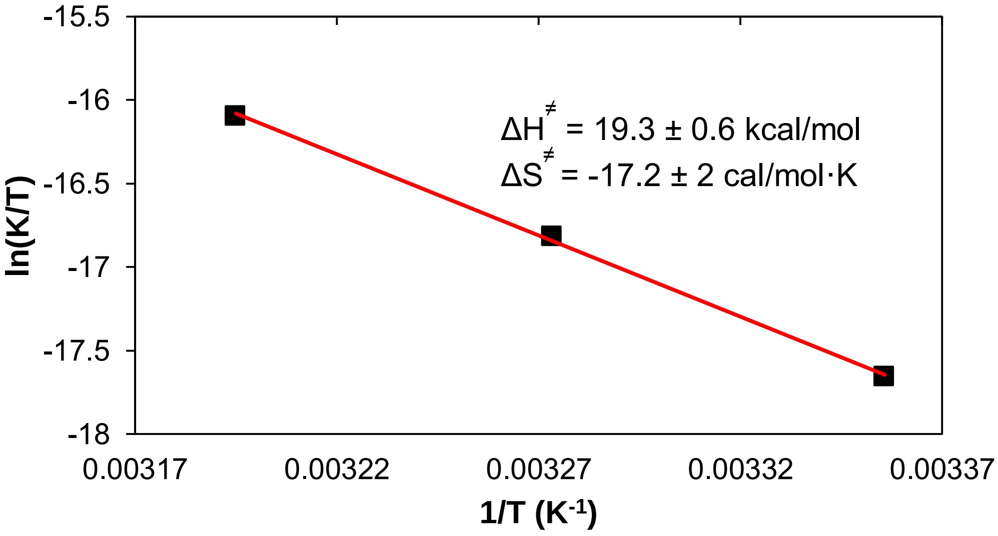

Supplementary Figure 29. **Eyring plot for the reaction of complex $\mathbf{1}_{\mathrm{ClO4}}$ with *p*-CN-phenol obtained by UV-vis monitoring**. Reaction conditions: [$\mathbf{1}_{\mathrm{ClO4}}$] = 0.8 mM, [*p*-CNphenol] = 8 mM, CH_3CN, T_{range} = 298-335.5 K.

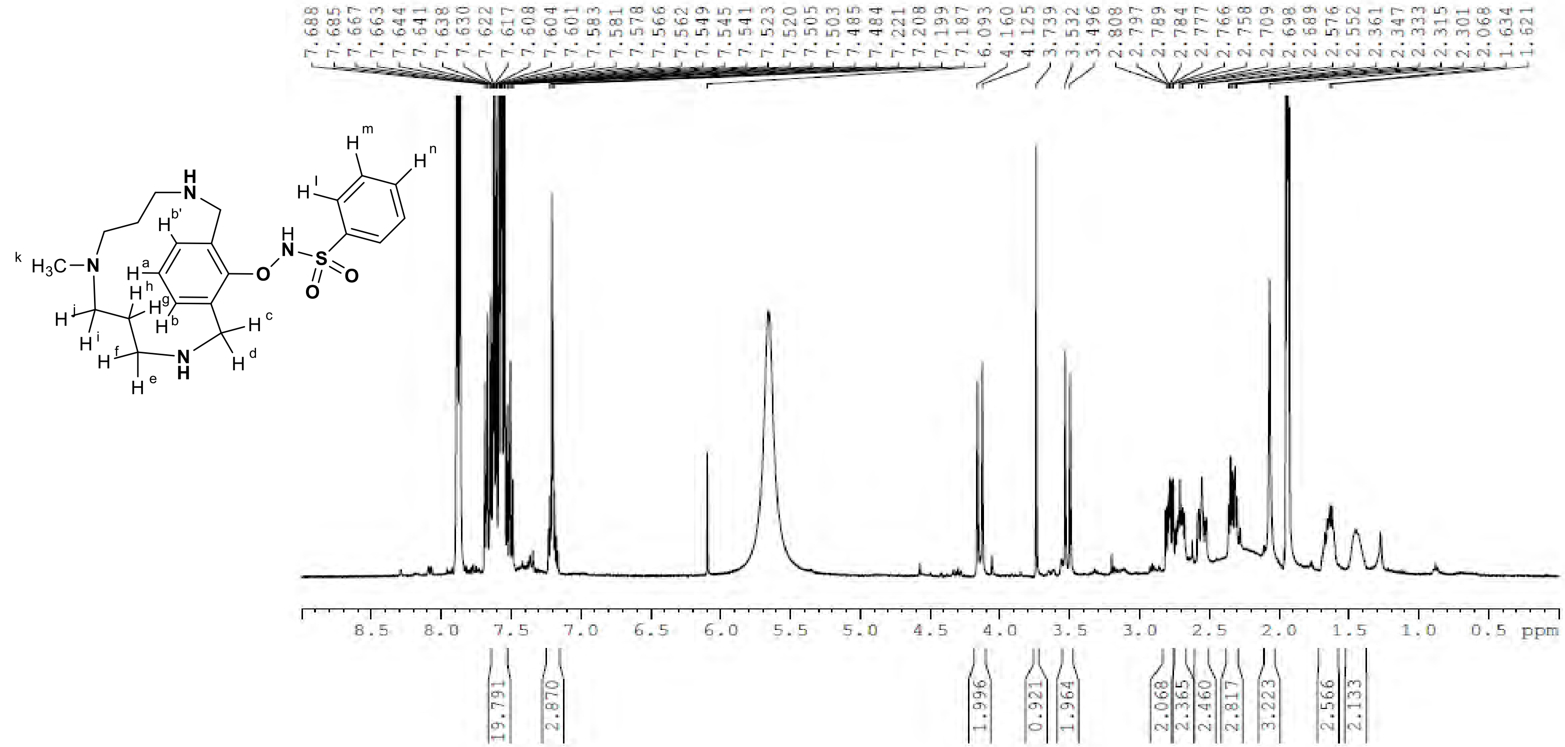

Supplementary Figure 30. ^{1}H NMR spectrum of compound 2a. Experiment performed in CD_3CN, 400 MHz, at 298 K.

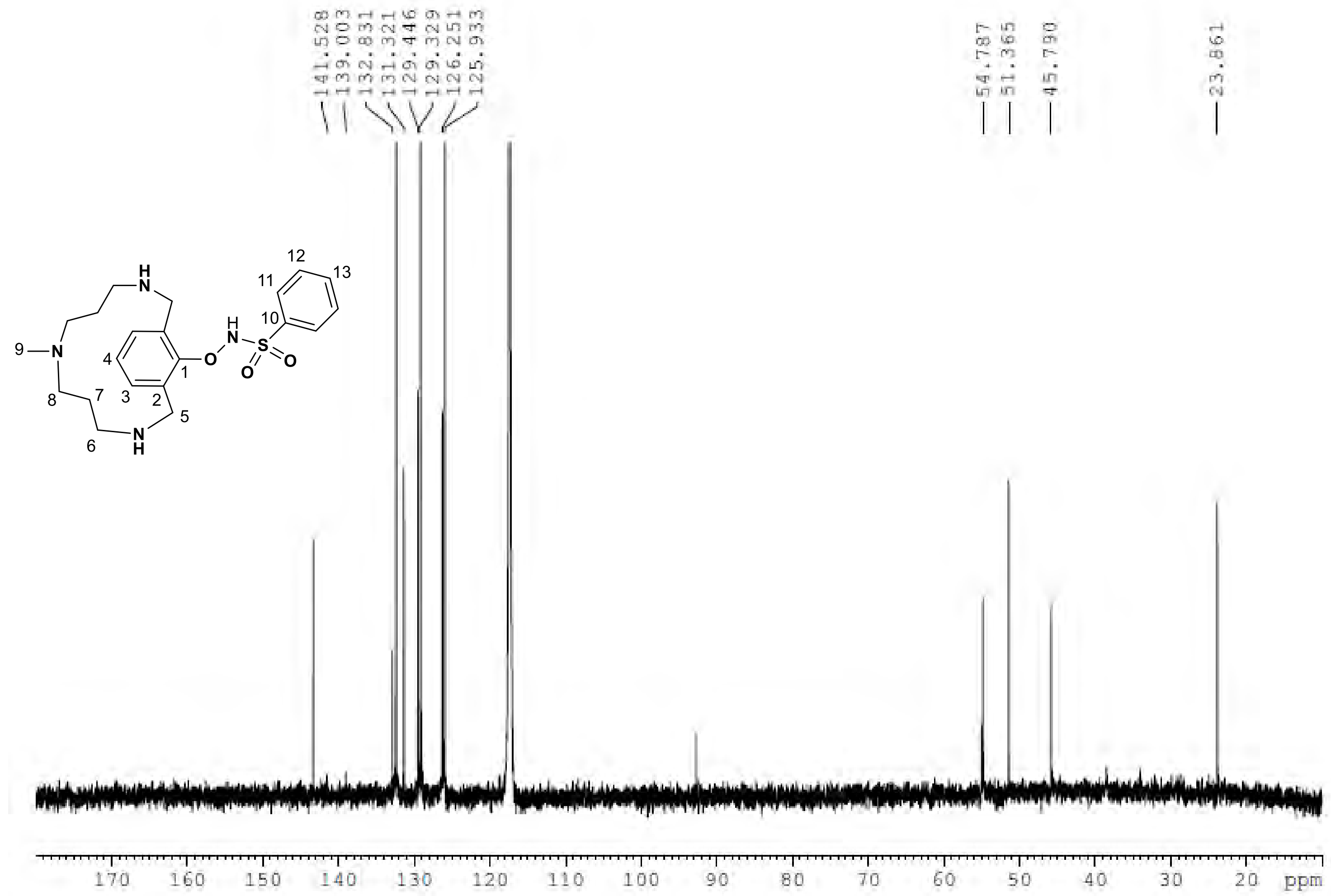

Supplementary Figure 31. ^{13}C NMR spectrum of compound 2a. Experiment performed in CD_3CN, 100 MHz, at 298 K.

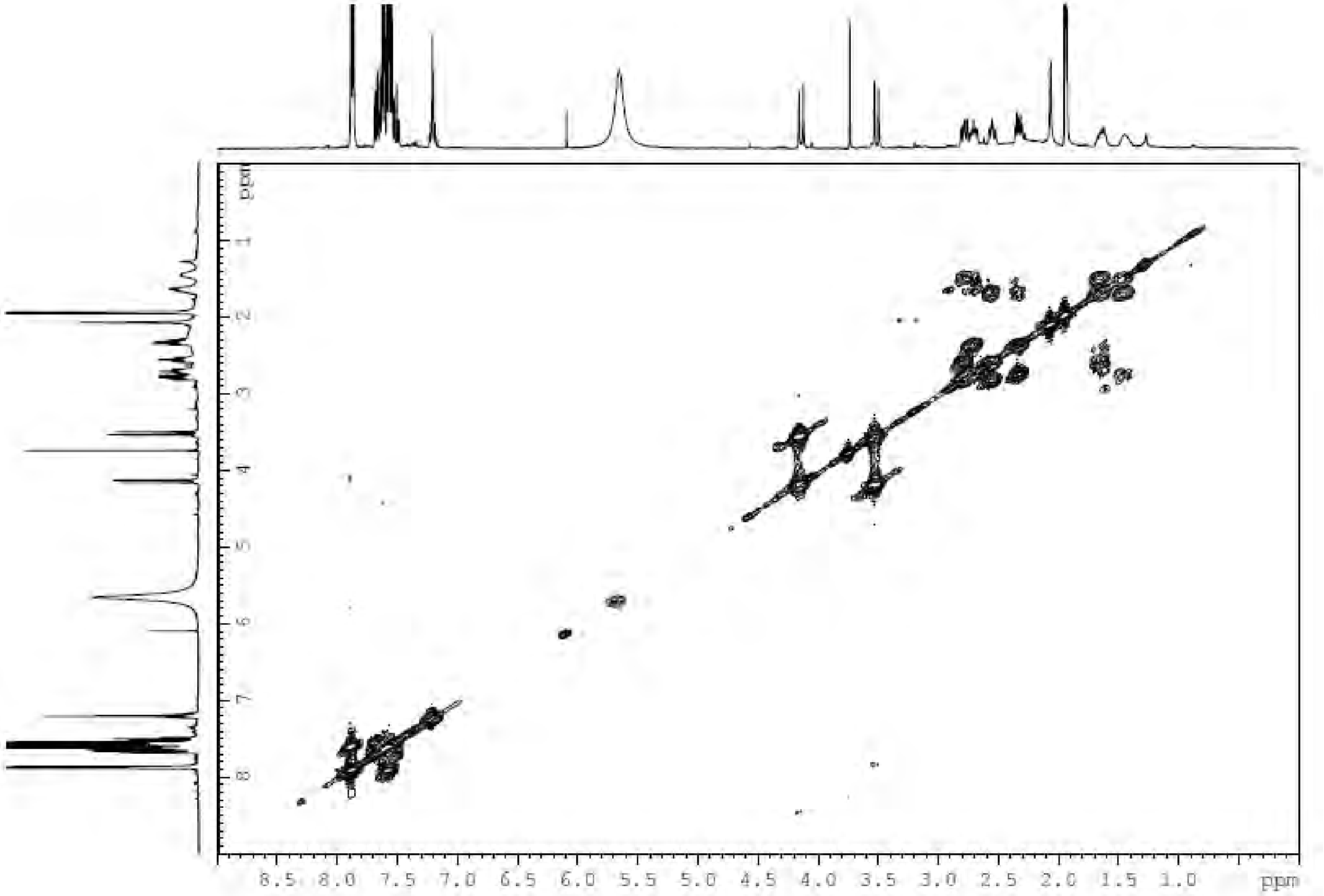

Supplementary Figure 32. COSY spectrum of compound 2a. Experiment performed in CD_3CN, 400 MHz, at 298 K.

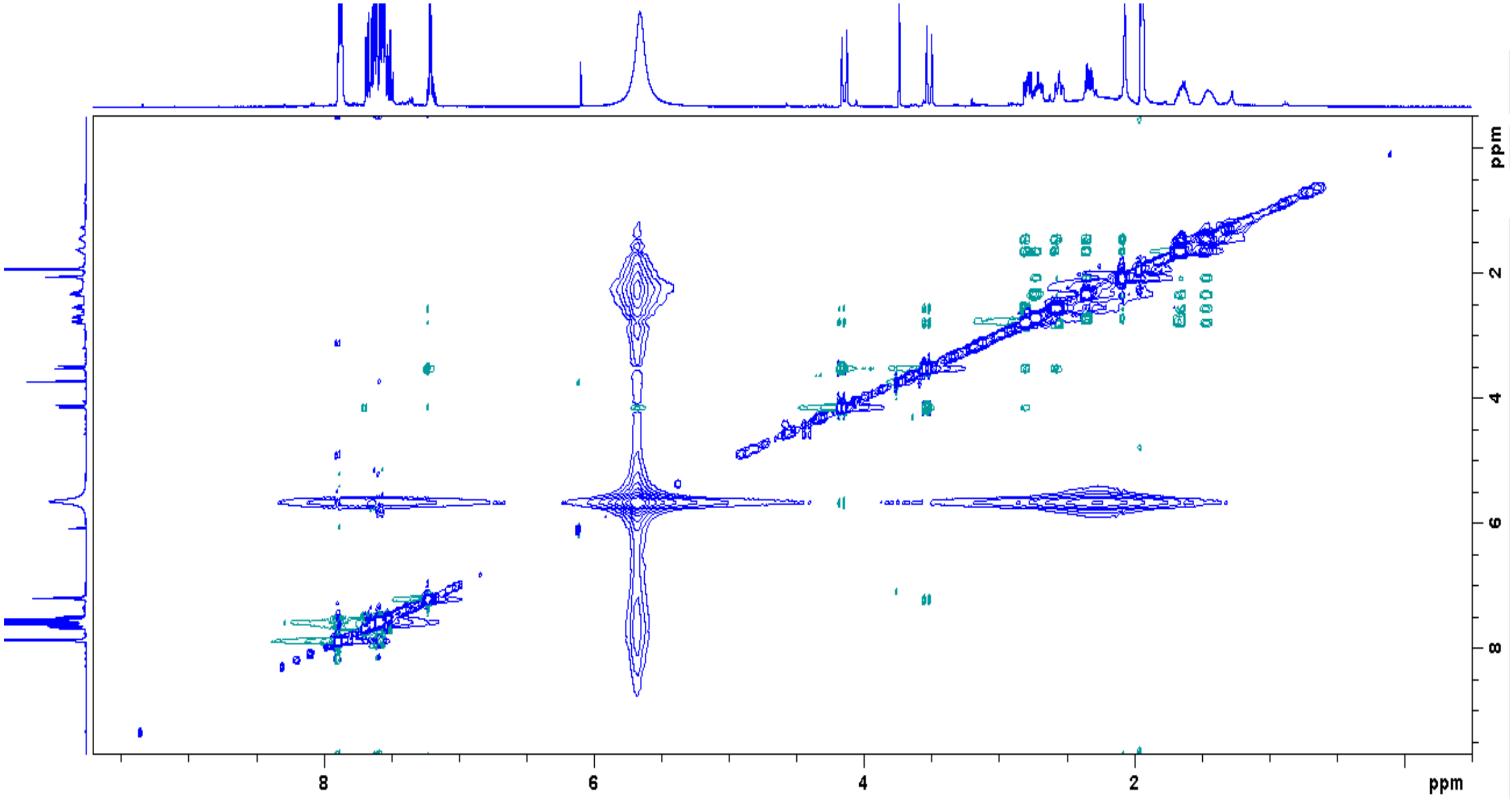

Supplementary Figure 33. NOESY spectrum of compound 2a. Experiment performed in CD_3CN, 400 MHz, at 298 K.

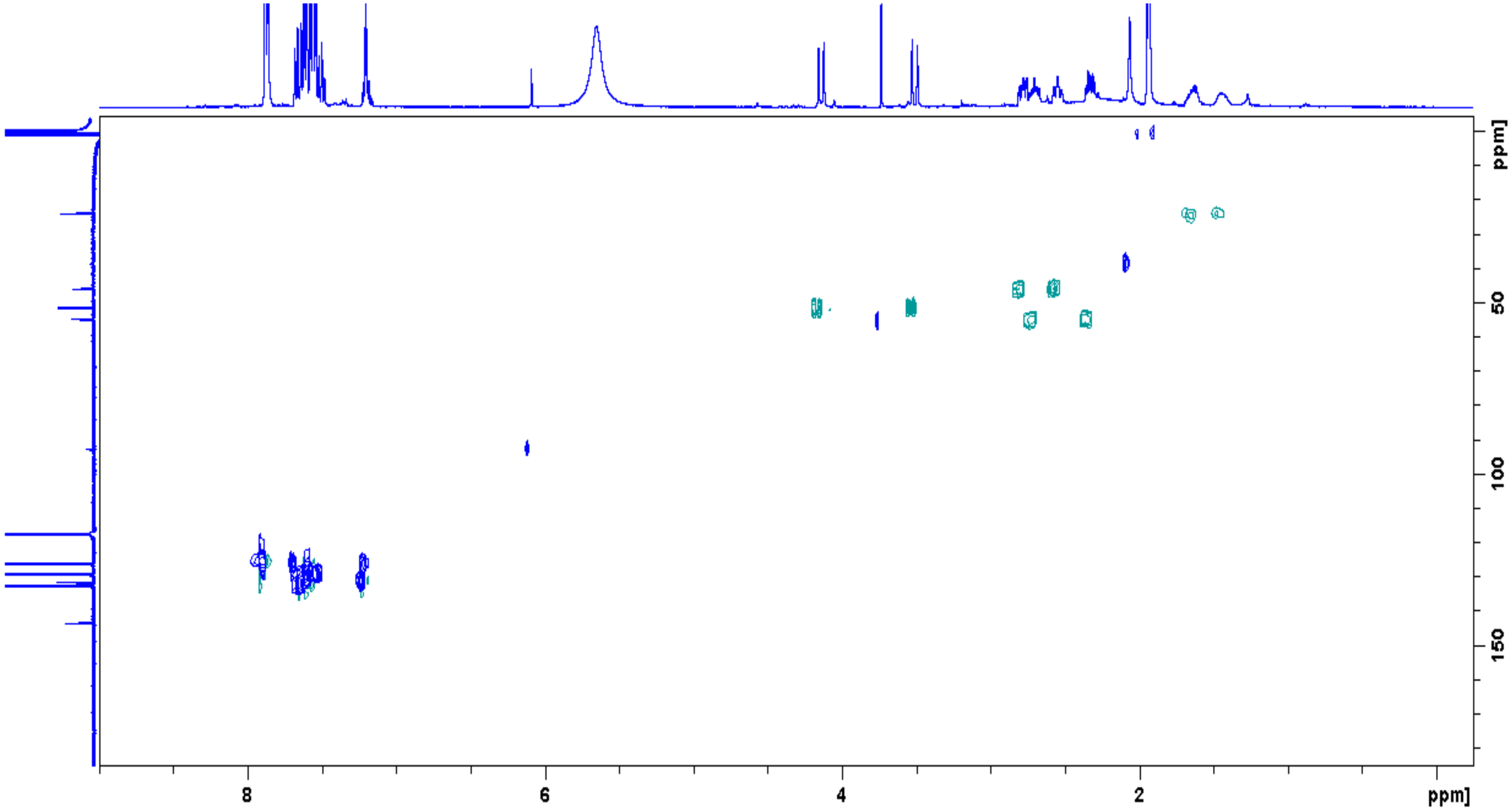

Supplementary Figure 34. ^{1}H ^{13}C HSQC spectrum of compound 2a. Experiment performed in CD_3CN, 400 MHz, at 298 K.

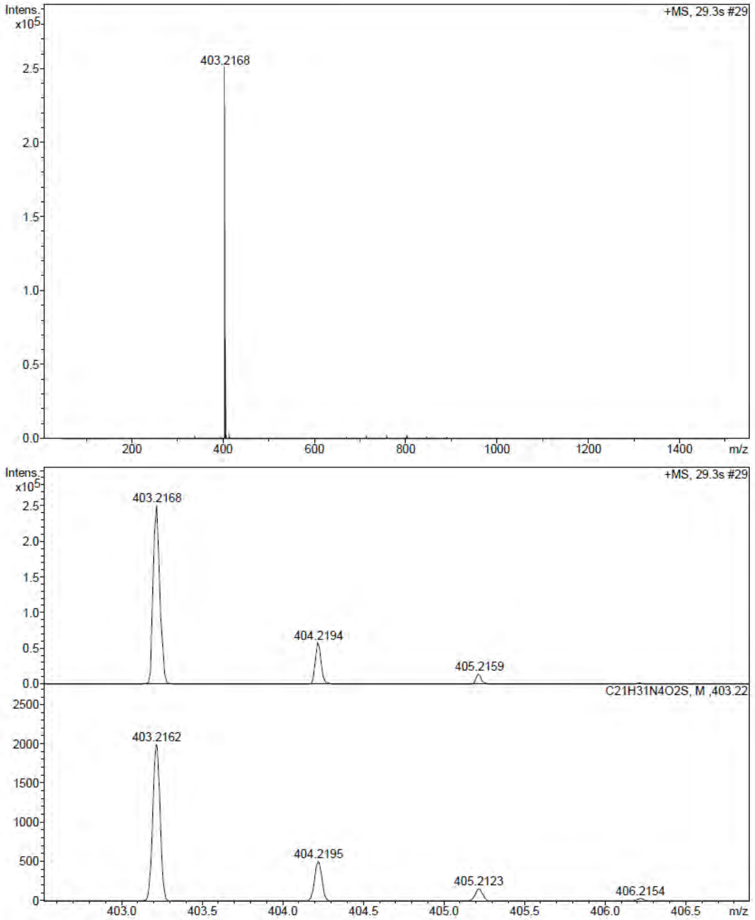

Supplementary Figure 35. HRMS (ESI-MS) spectrum of compound 2a. Experiment performed in CH_3CN (spectrum at the bottom corresponds to the simulated peak).

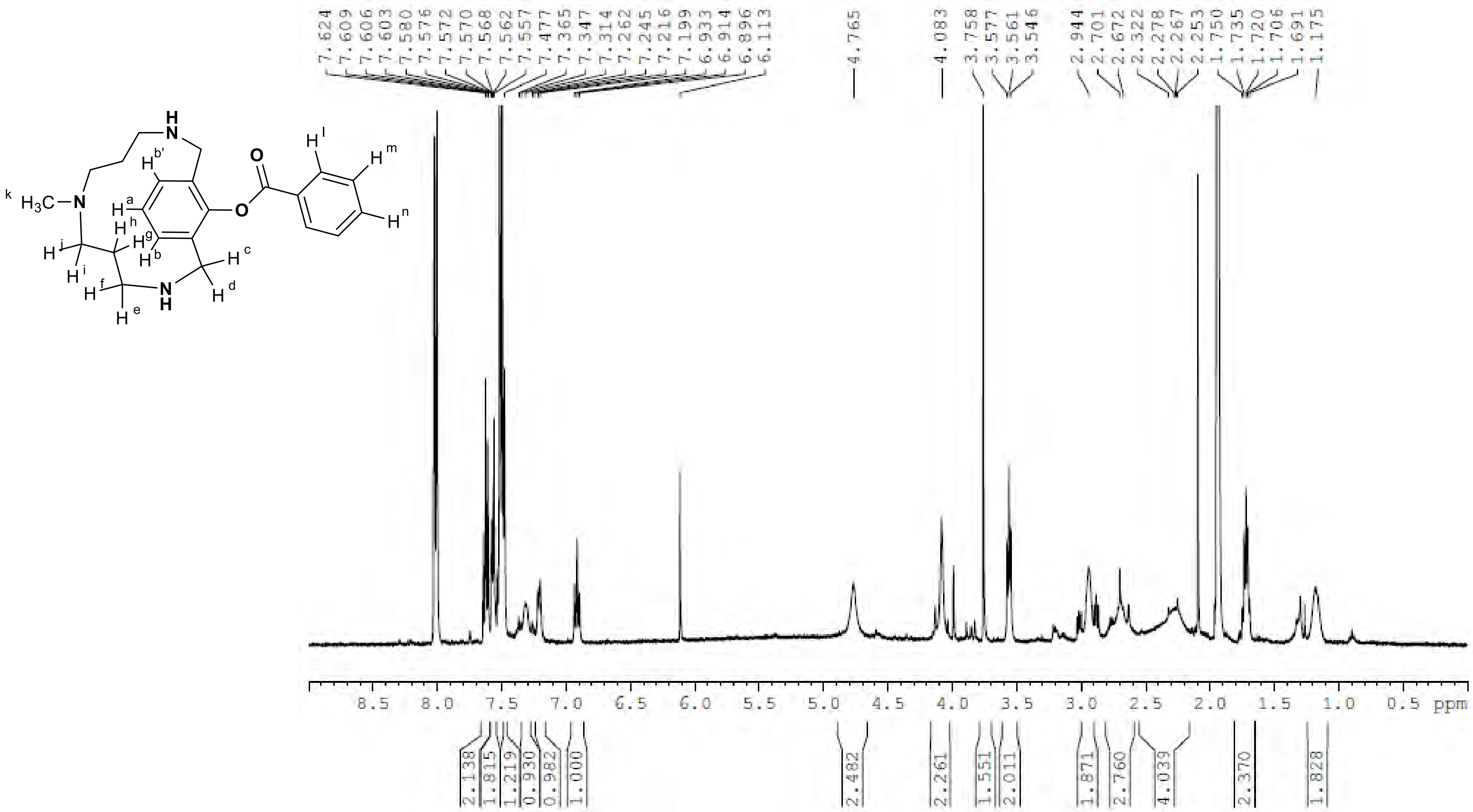

Supplementary Figure 36. ^{1}H NMR spectrum of compound 2b. Experiment performed in CD_3CN, 400 MHz, at 333 K.

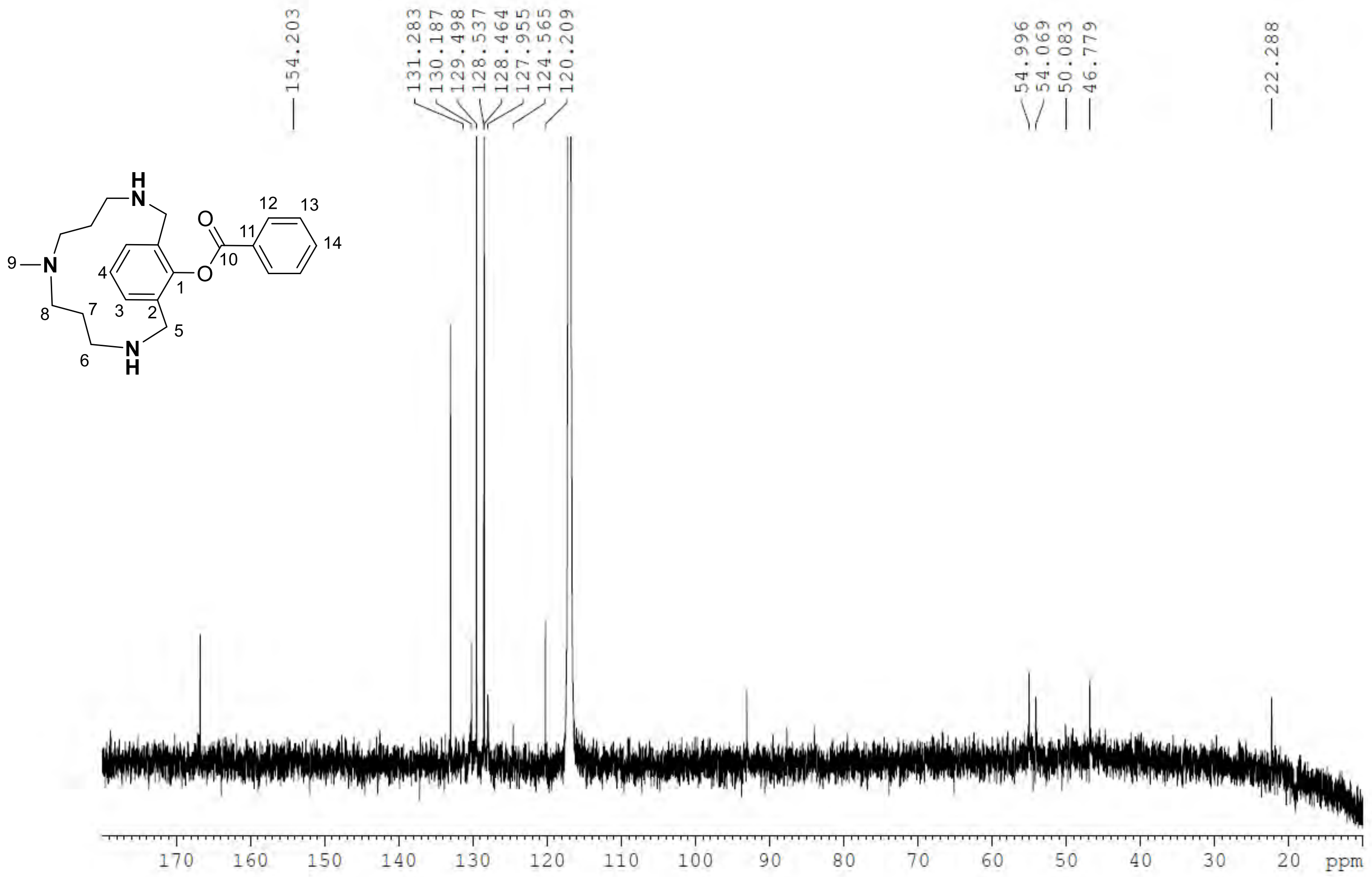

Supplementary Figure 37. ^{13}C NMR spectrum of compound 2b. Experiment performed in CD_3CN, 100 MHz, at 333 K.

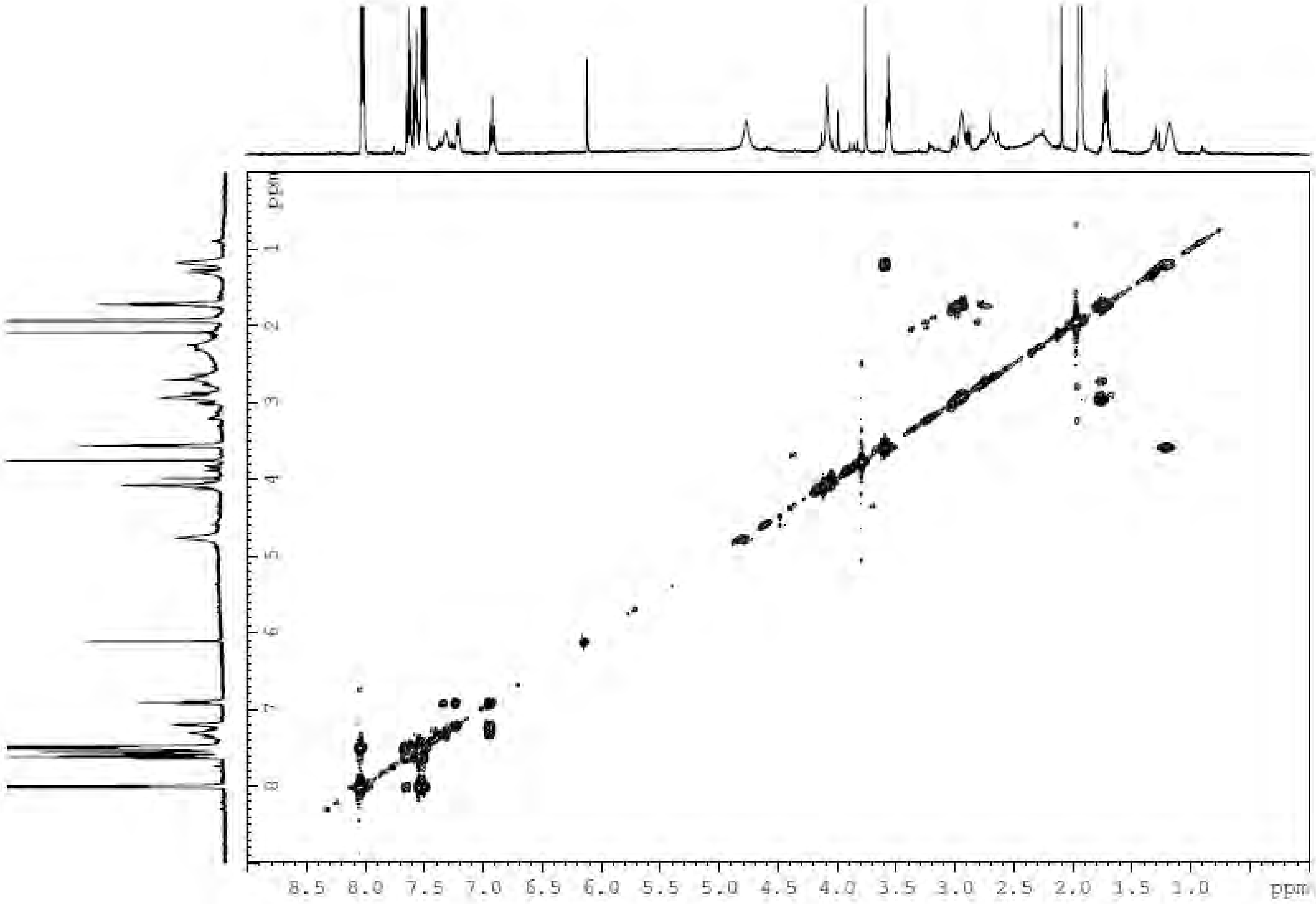

Supplementary Figure 38. COSY spectrum of compound 2b. Experiment performed in CD_3CN, 400 MHz, at 333 K.

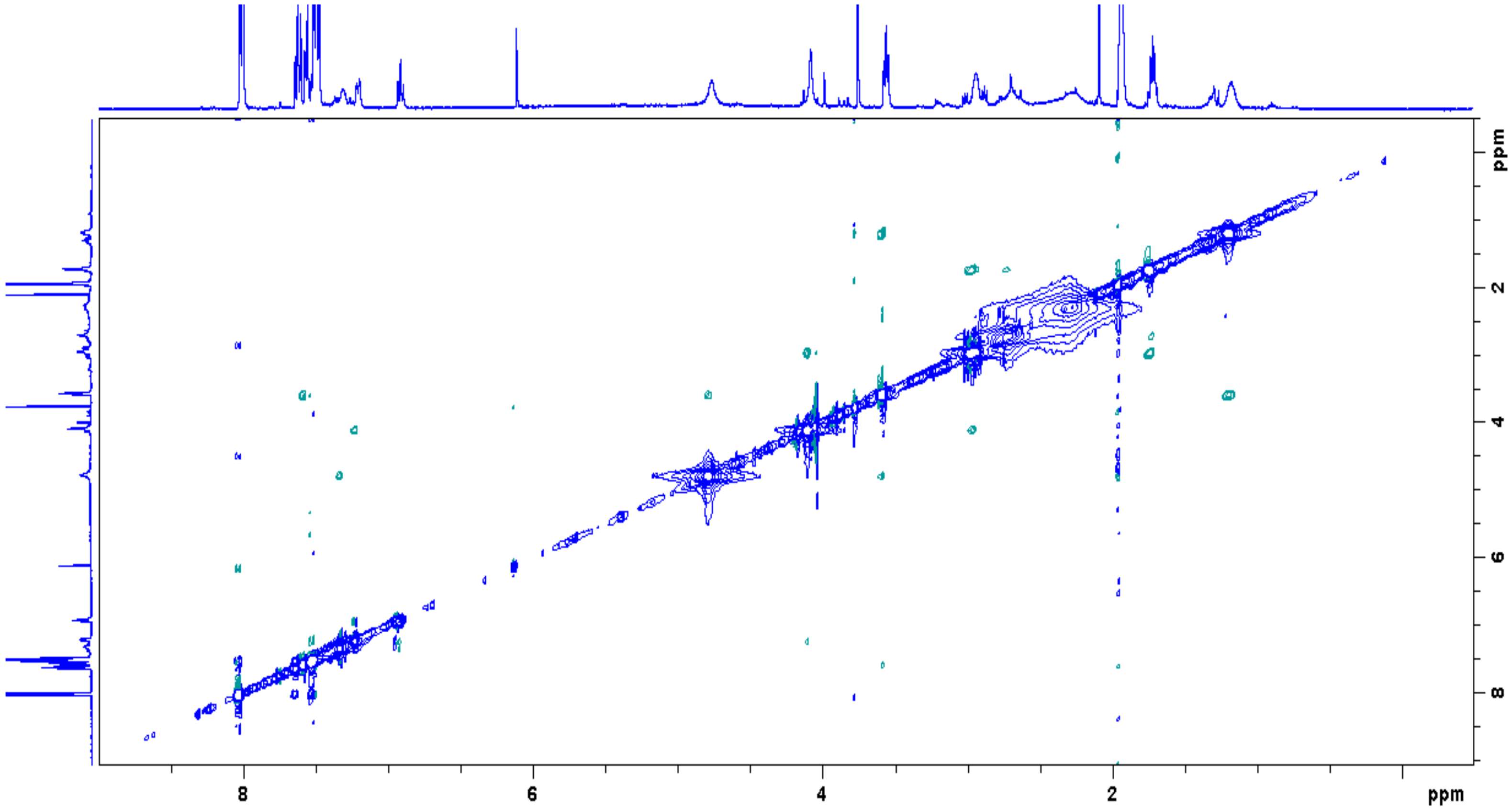

Supplementary Figure 39. NOESY spectrum of compound 2b. Experiment performed in CD_3CN, 400 MHz, at 333 K.

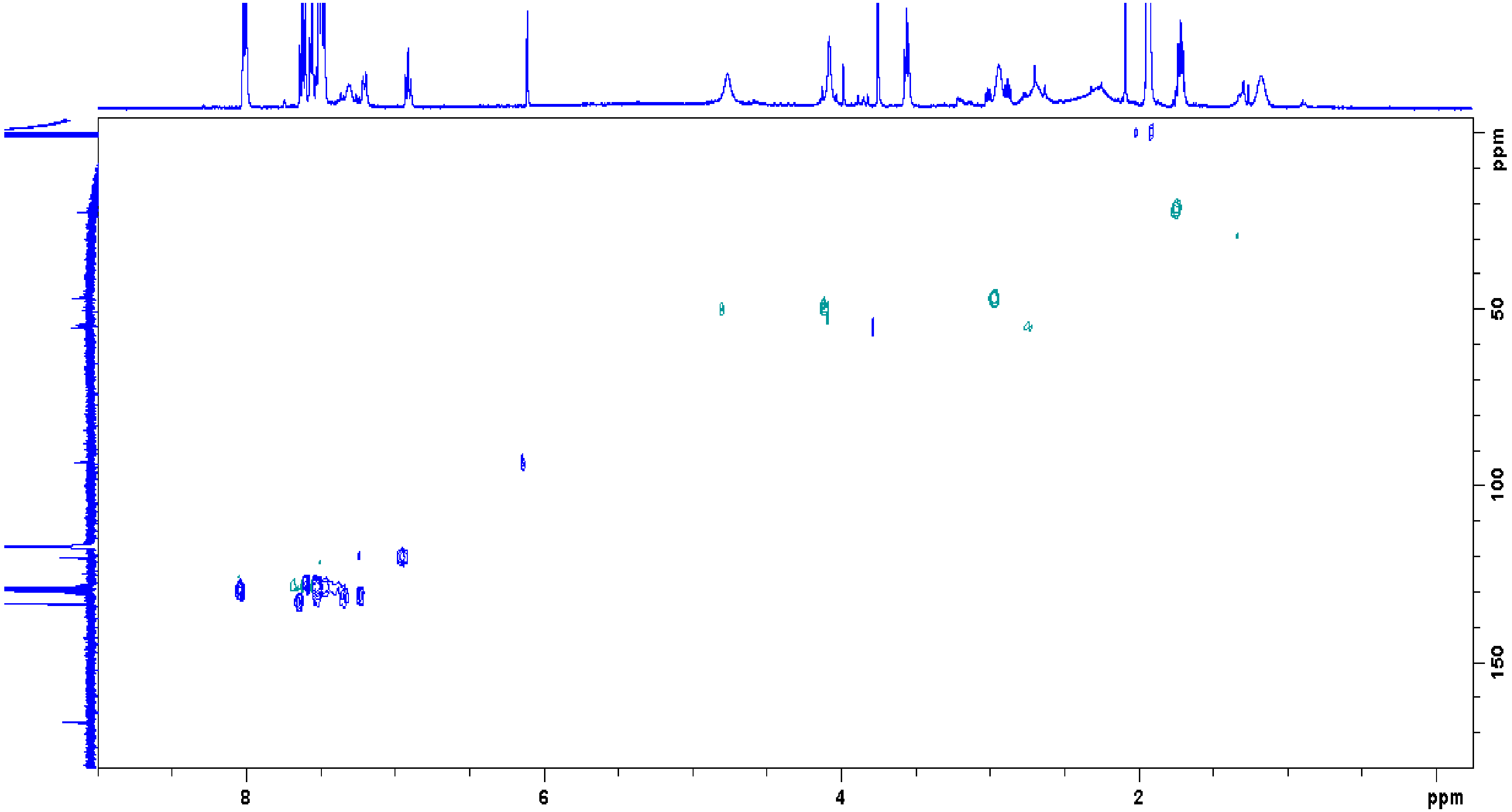

Supplementary Figure 40. ^{1}H ^{13}C HSQC spectrum of compound 2b. Experiment performed in CD_3CN, 400 MHz, at 333 K.

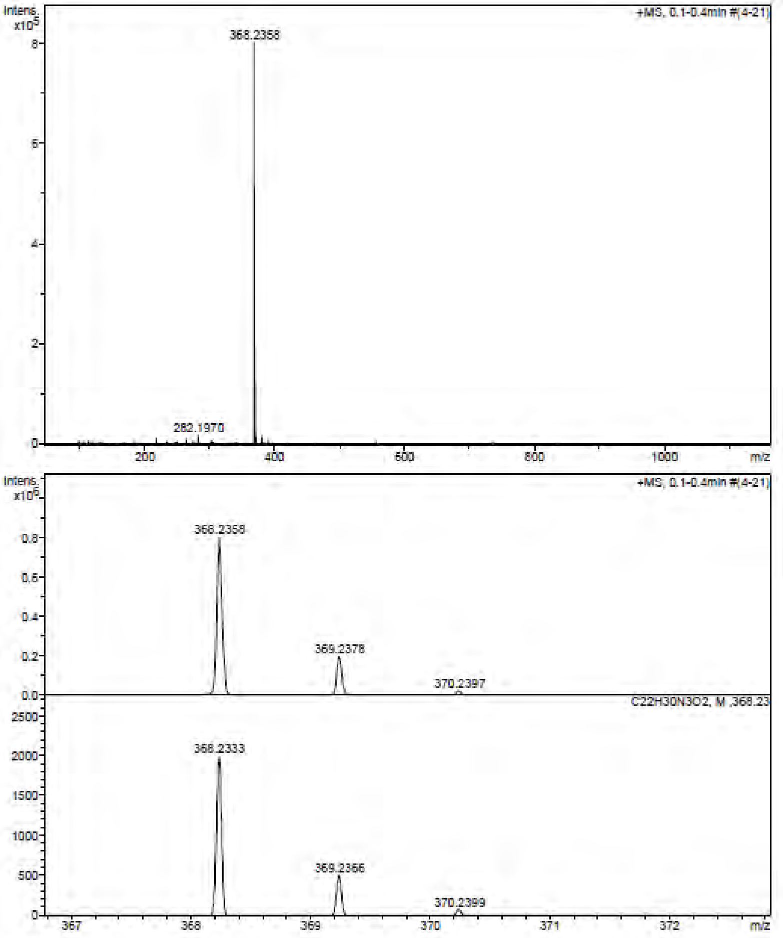

Supplementary Figure 41. HRMS (ESI-MS) spectrum of compound 2b. Experiment performed in CH_3CN (spectrum at the bottom corresponds to the simulated peak).

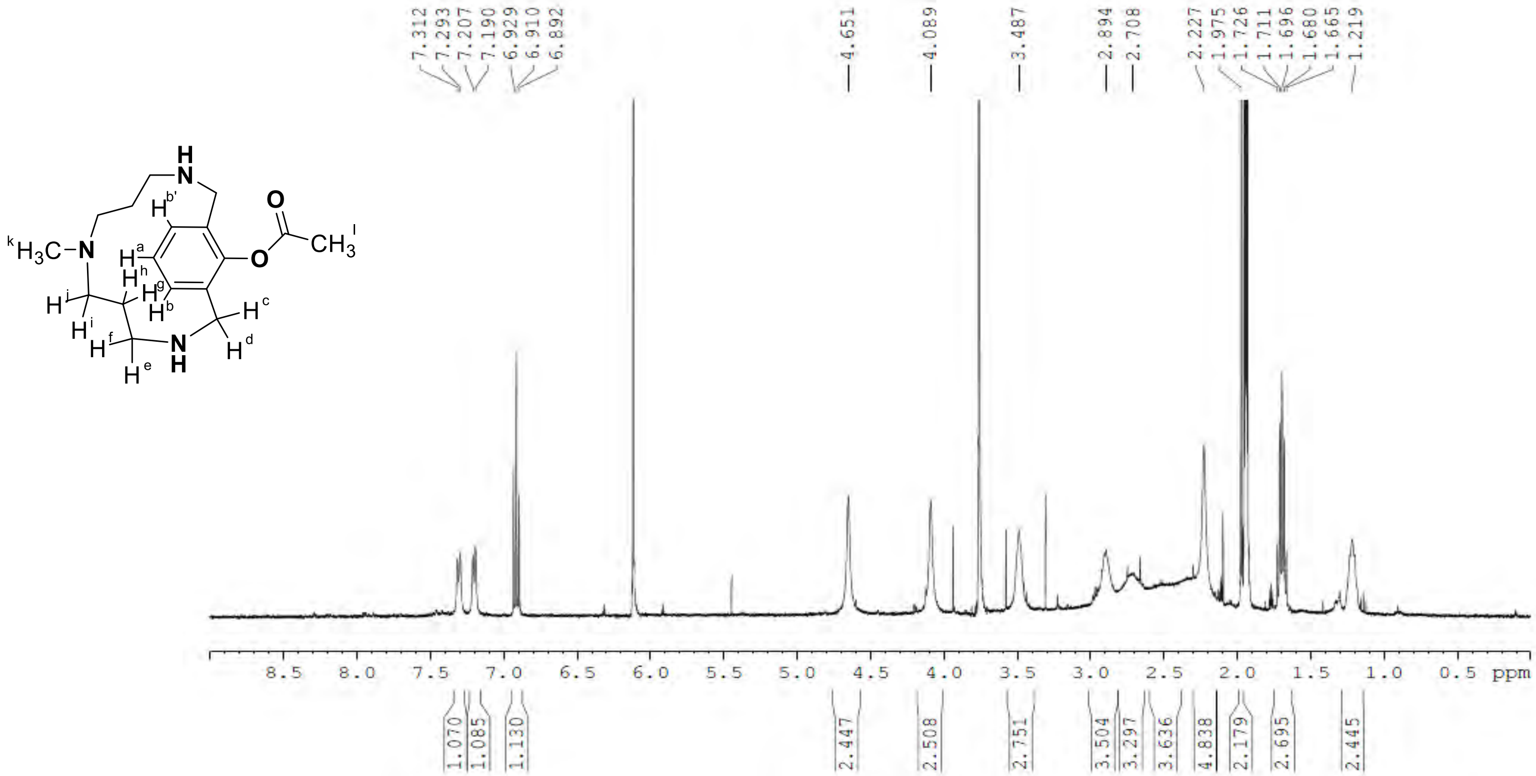

Supplementary Figure 42. ^{1}H NMR spectrum of compound 2c. Experiment performed in CD_3CN, 400 MHz, at 333 K.

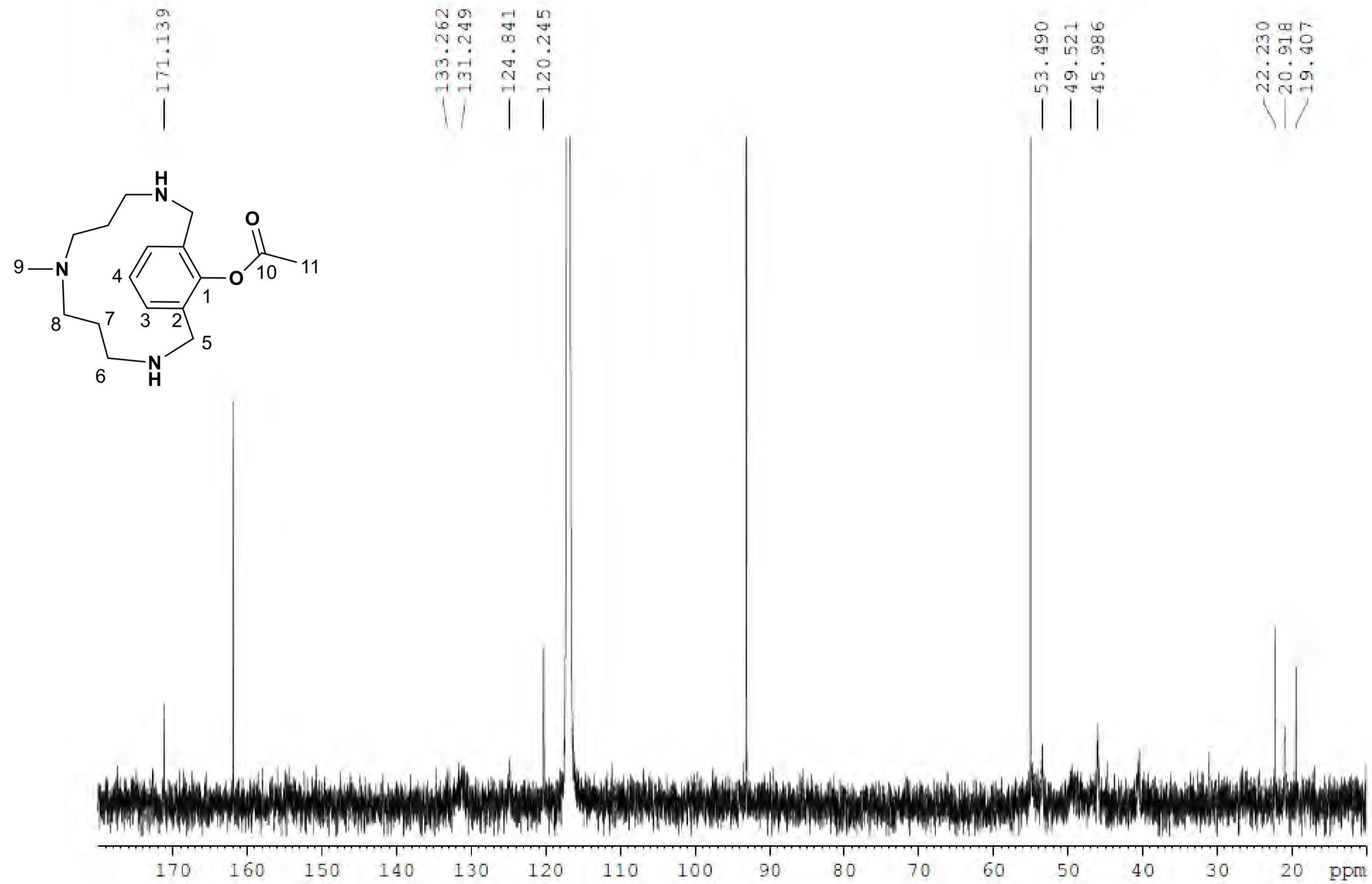

Supplementary Figure 43. ^{13}C NMR spectrum of compound 2c. Experiment performed in CD_3CN, 100 MHz, at 333 K.

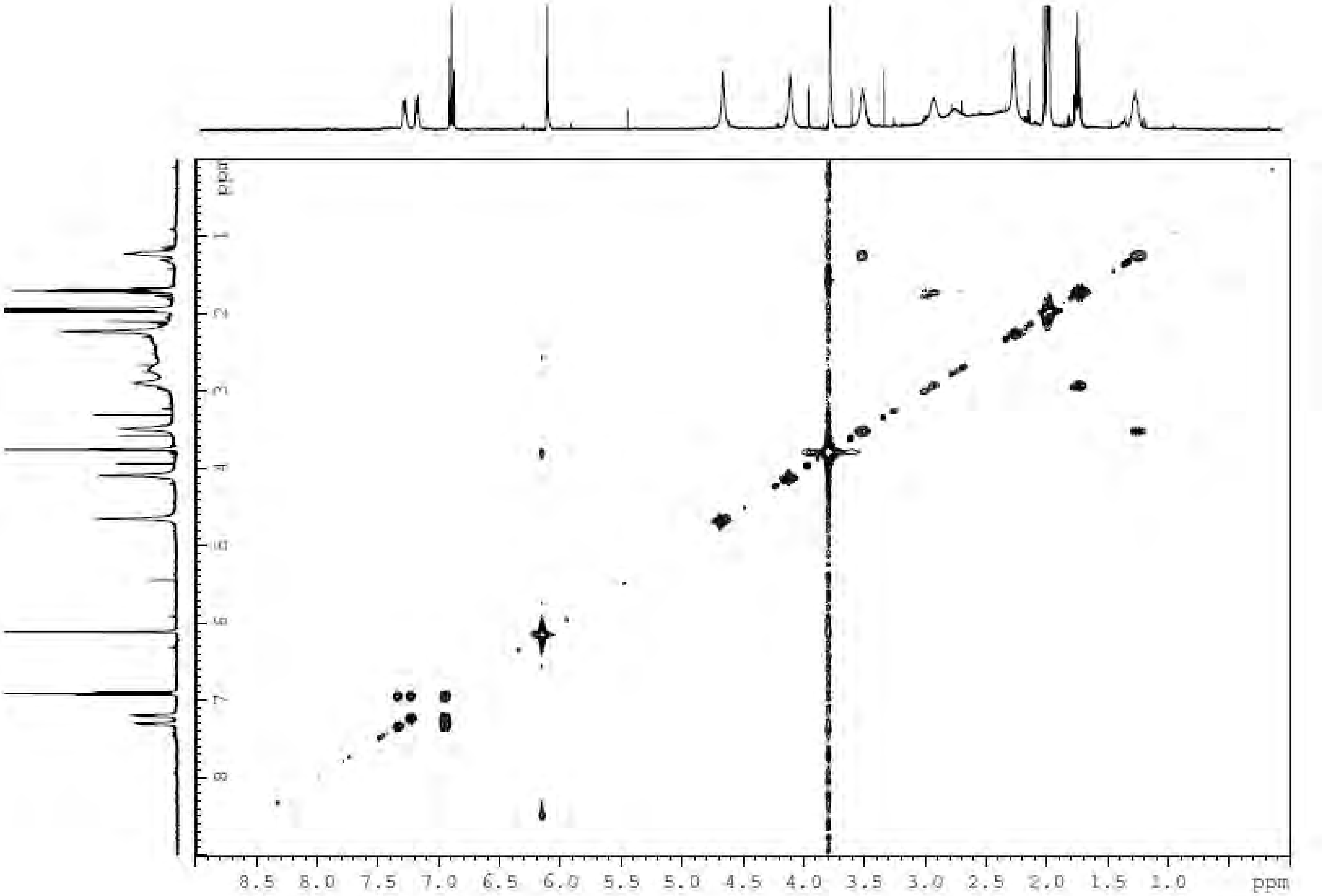

Supplementary Figure 44. COSY spectrum of compound 2c. Experiment performed in CD_3CN, 400 MHz, at 333 K.

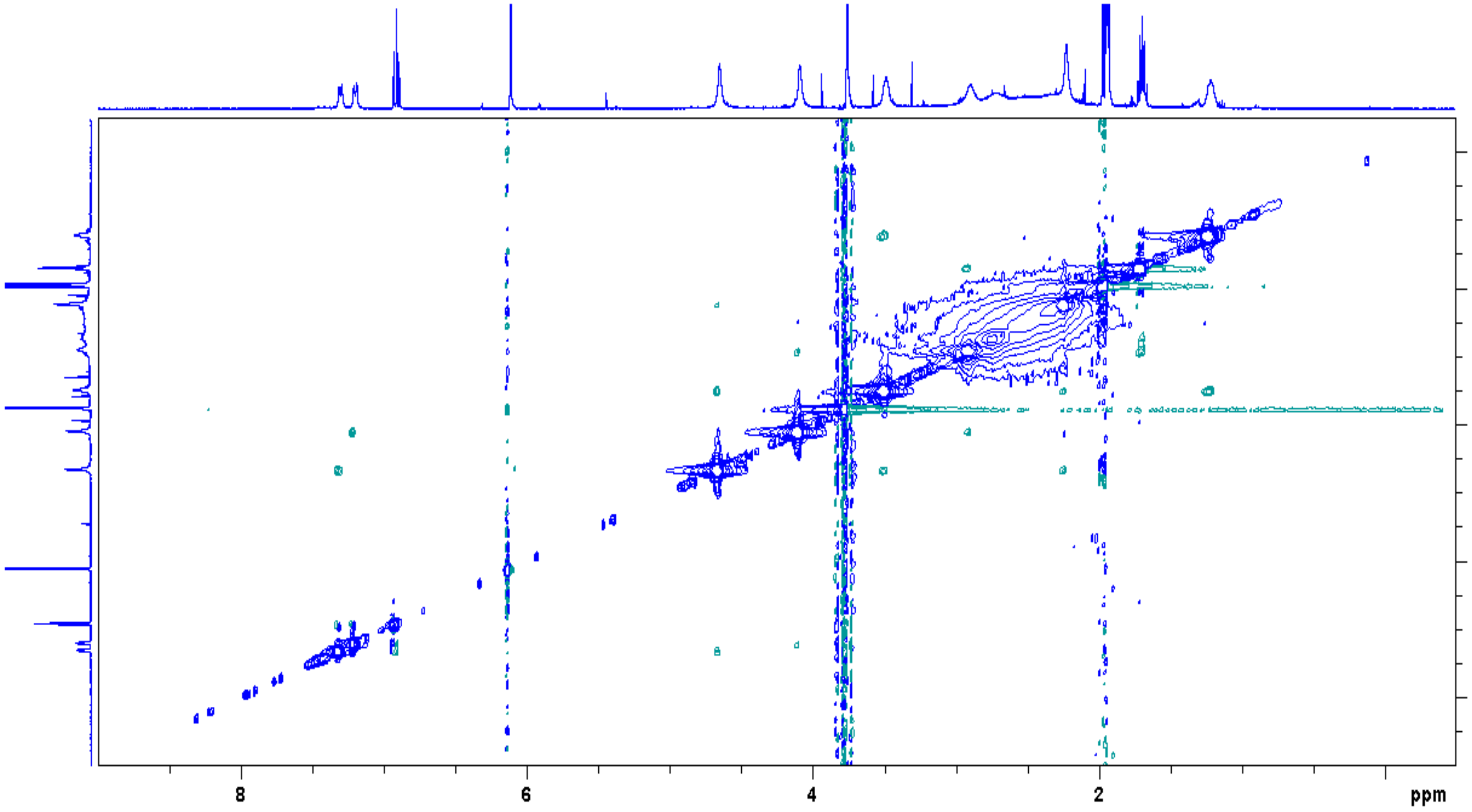

Supplementary Figure 45. NOESY spectrum of compound 2c. Experiment performed in CD_3CN, 400 MHz, at 333 K.

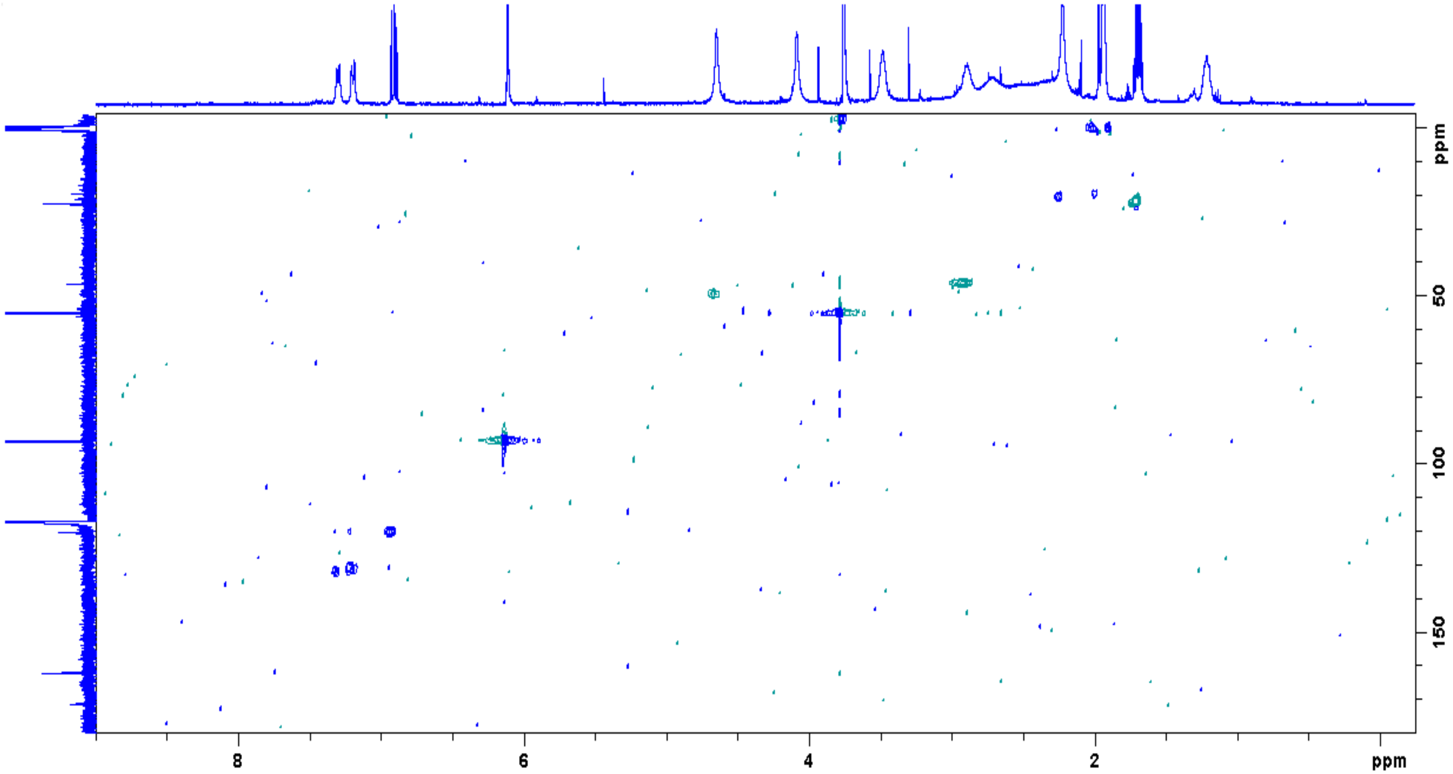

Supplementary Figure 46. ^{1}H ^{13}C HSQC spectrum of compound 2c. Experiment performed in CD_3CN, 400 MHz, at 333 K.

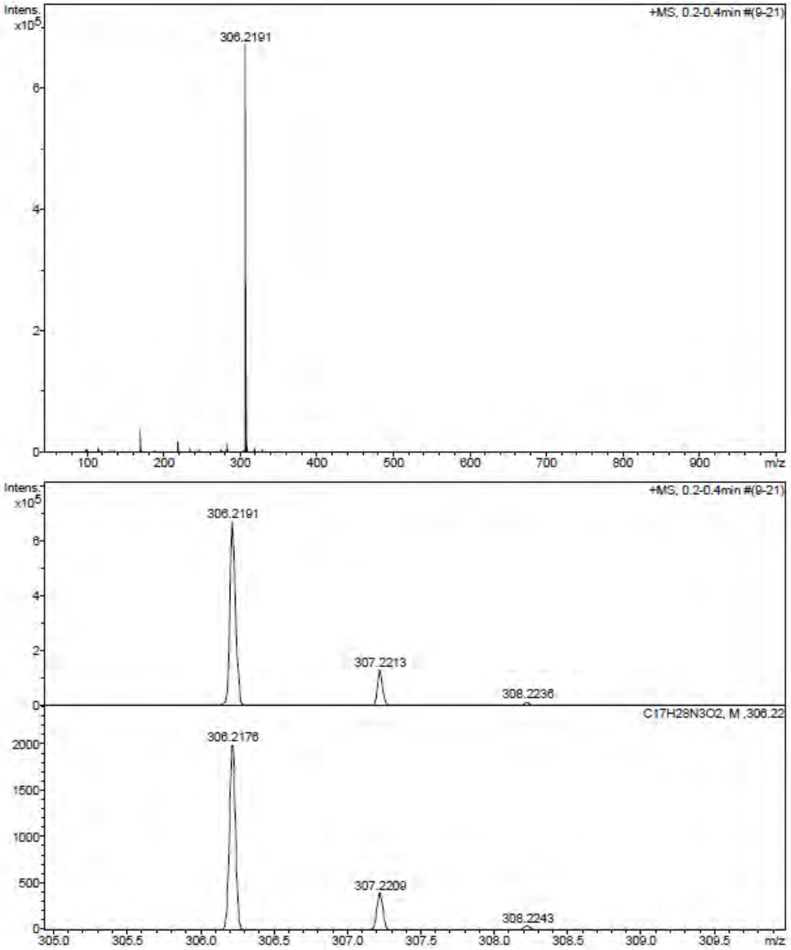

Supplementary Figure 47. HRMS (ESI-MS) spectrum of compound 2c. Experiment performed in CH_3CN (spectrum at the bottom corresponds to the simulated peak).

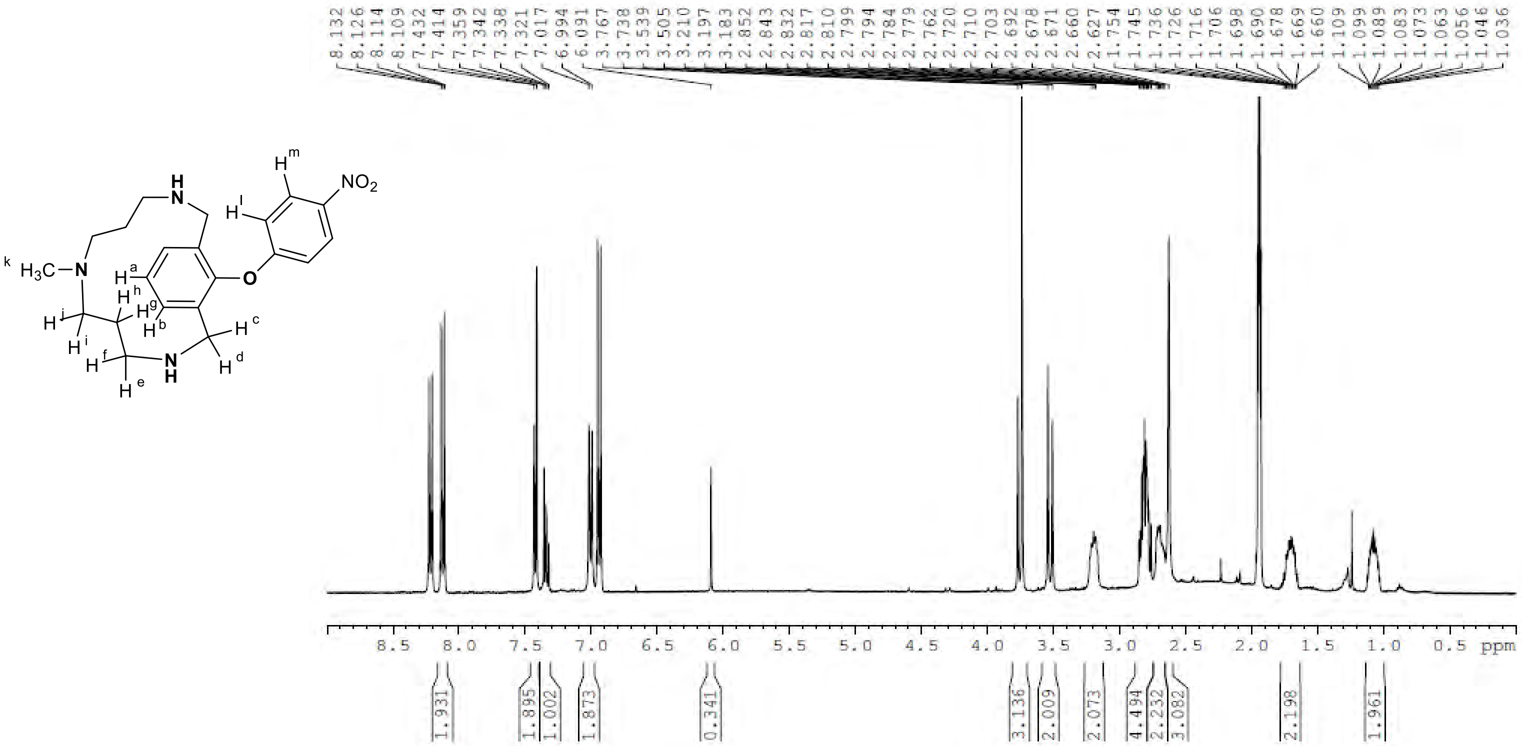

Supplementary Figure 48. ^{1}H NMR spectrum of compound 2d. Experiment performed in CD_3CN, 400 MHz, at 298 K.

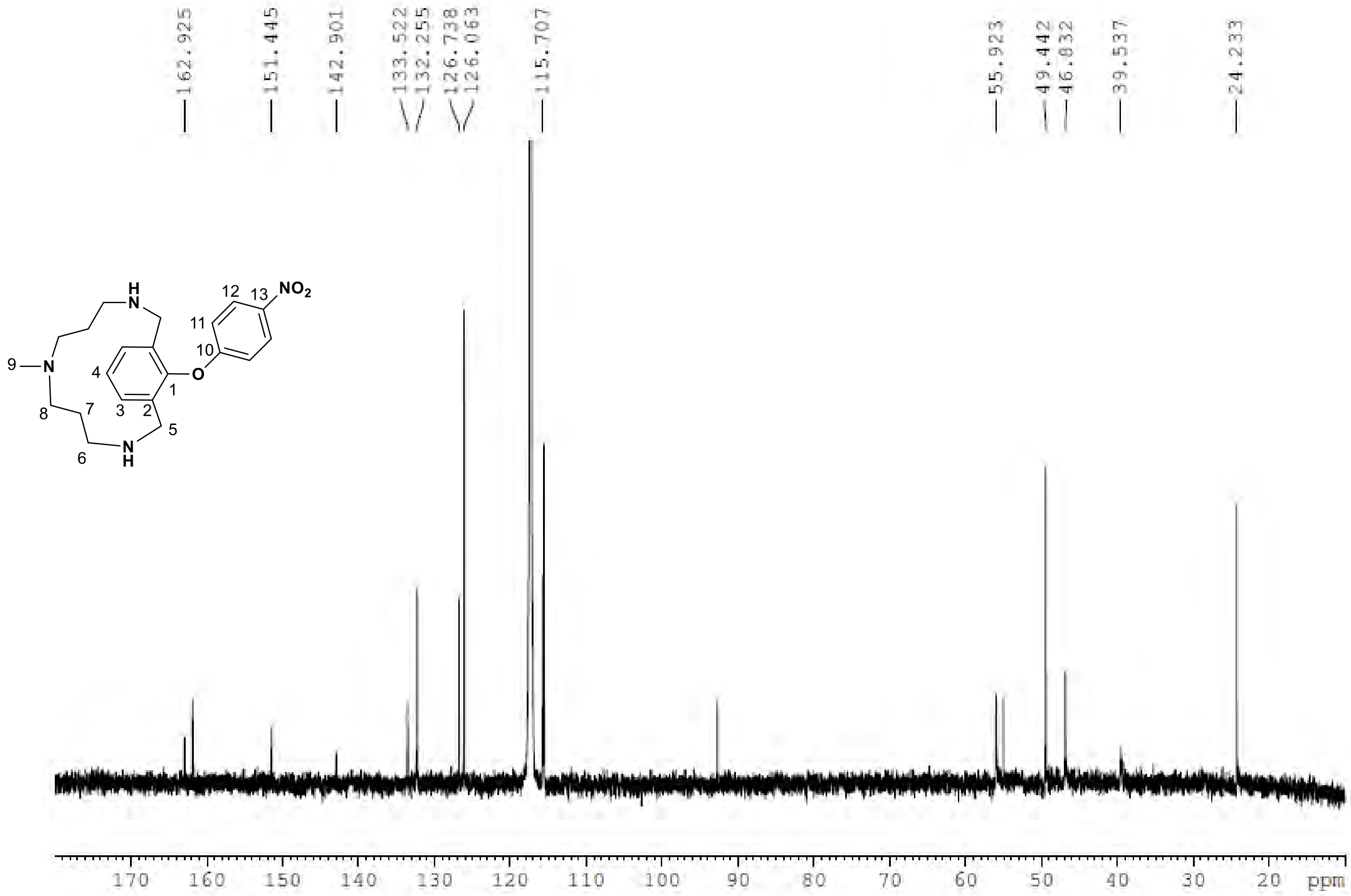

Supplementary Figure 49. ^{13}C NMR spectrum of compound 2d. Experiment performed in CD$_3$CN, 100 MHz, at 298 K.

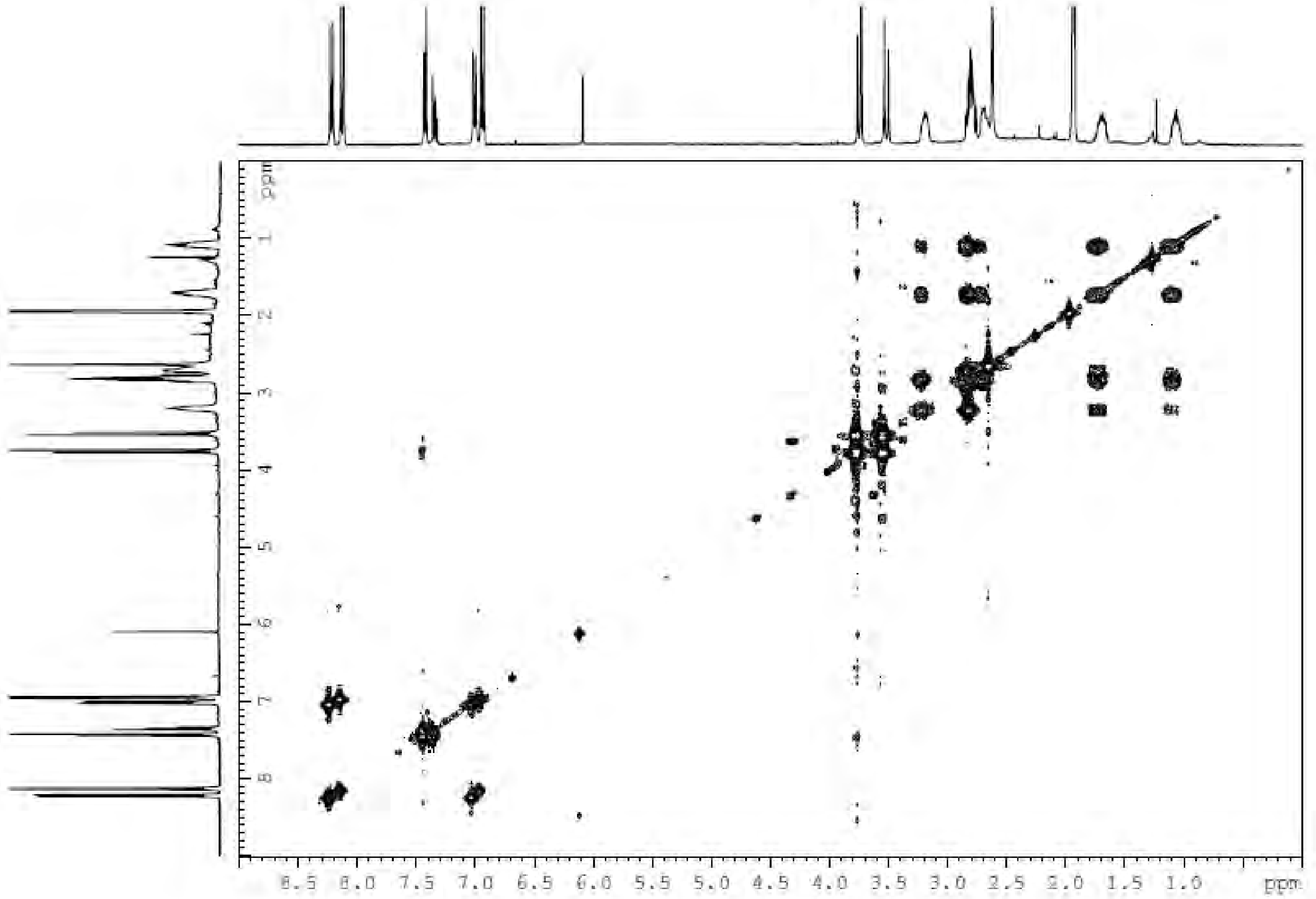

Supplementary Figure 50. COSY spectrum of compound 2d. Experiment performed in CD_3CN, 400 MHz, at 298 K.

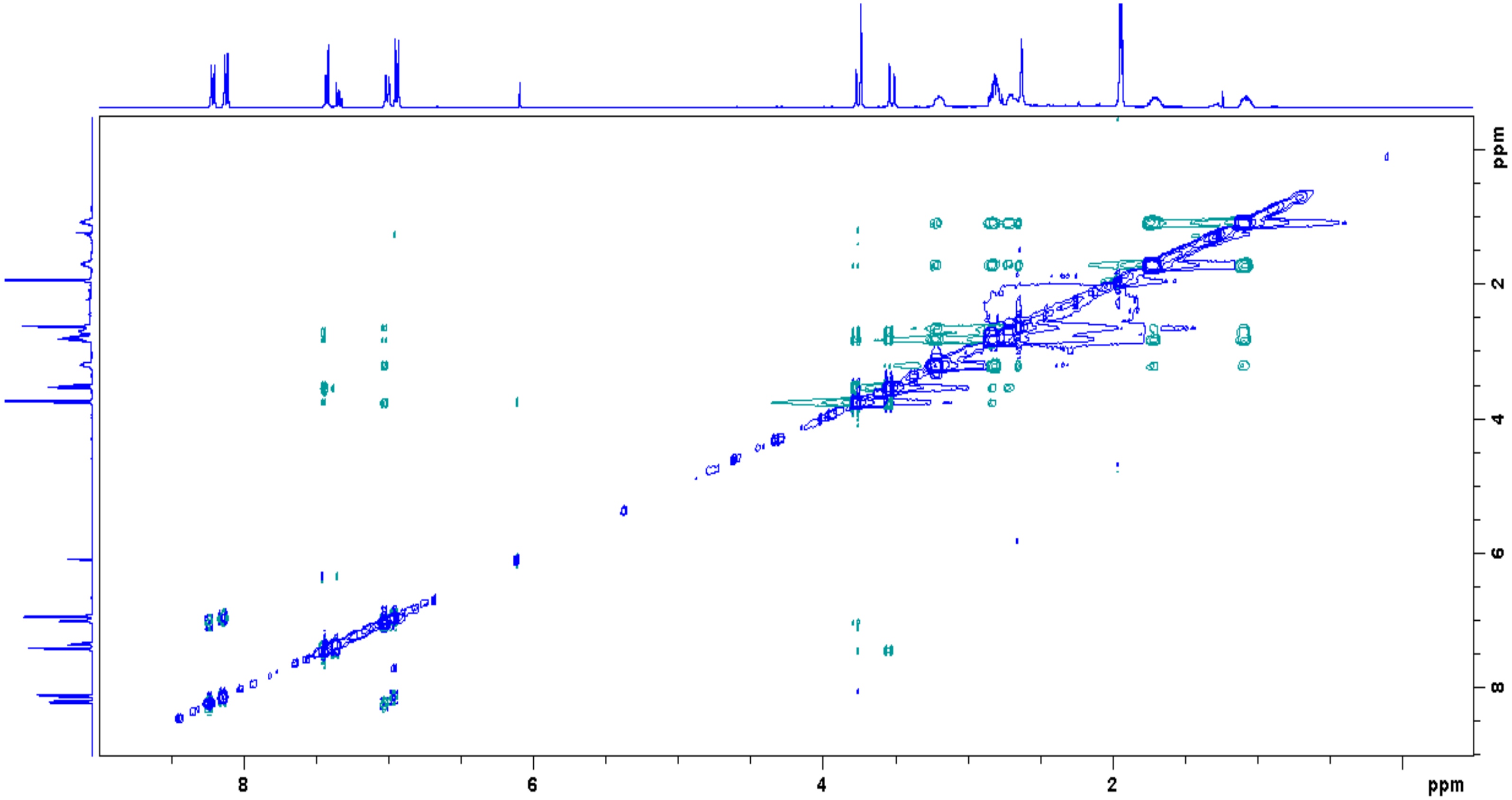

Supplementary Figure 51. NOESY spectrum of compound 2d. Experiment performed in CD_3CN, 400 MHz, at 298 K.

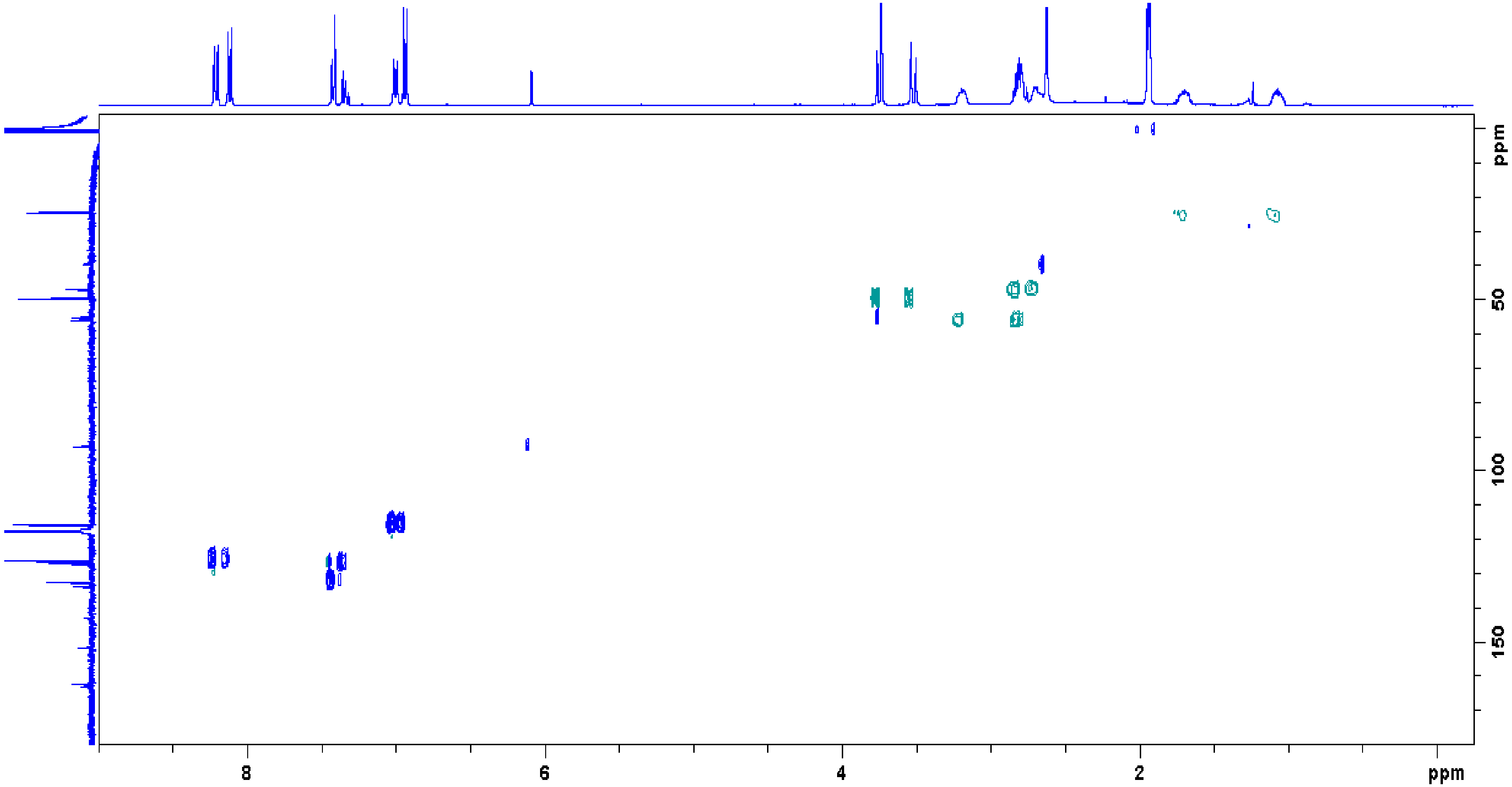

Supplementary Figure 52. ^{1}H ^{13}C HSQC spectrum of compound 2d. Experiment performed in CD_3CN, 400 MHz, at 298 K.

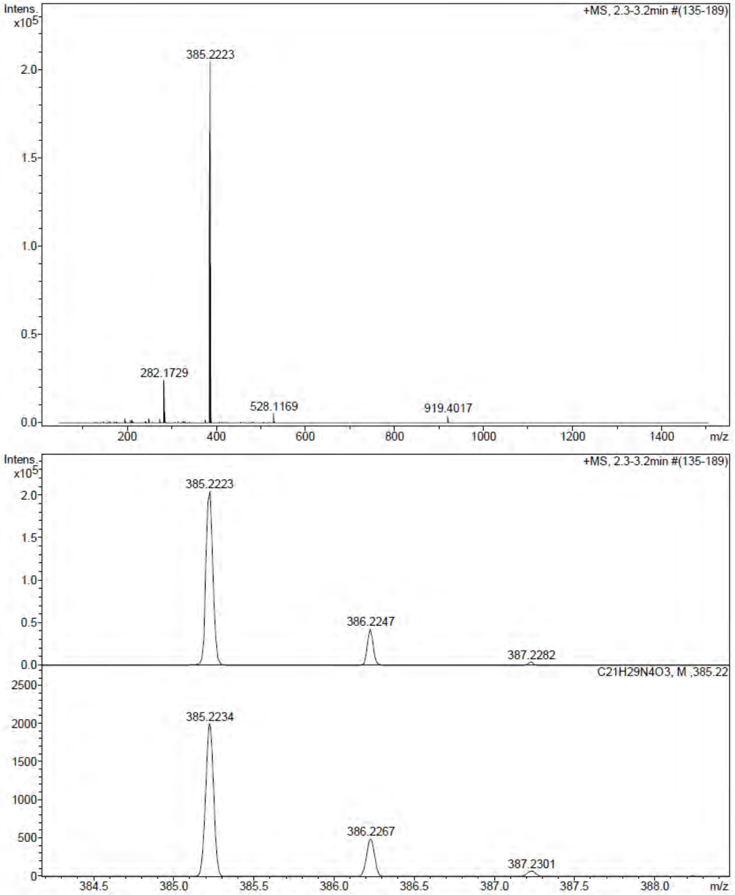

Supplementary Figure 53. HRMS (ESI-MS) spectrum of compound 2d. Experiment performed in CH_3CN (spectrum at the bottom corresponds to the simulated peak).

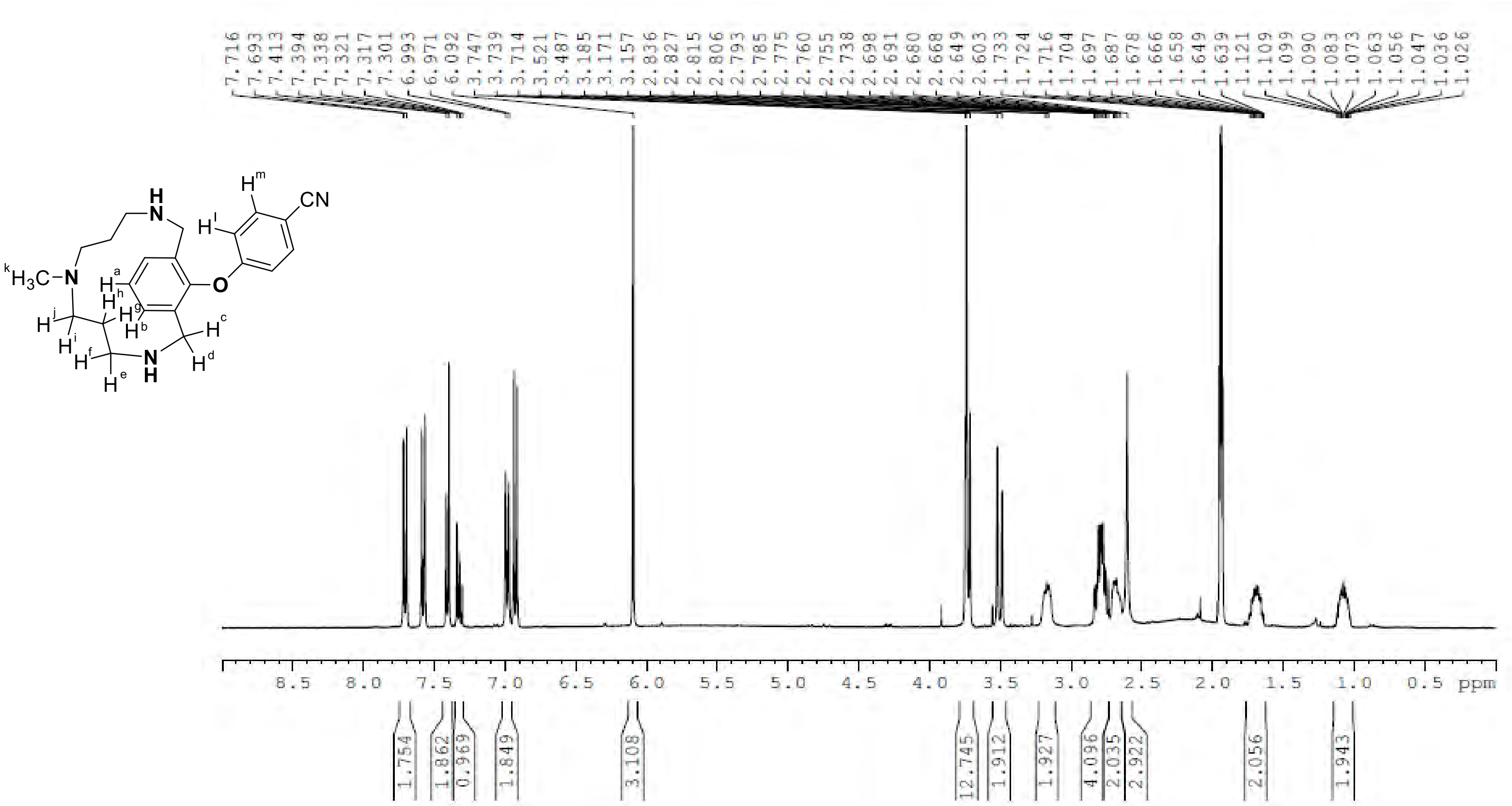

Supplementary Figure 54. ^{1}H NMR spectrum of compound 2e. Experiment performed in CD_3CN, 400 MHz, at 298 K.

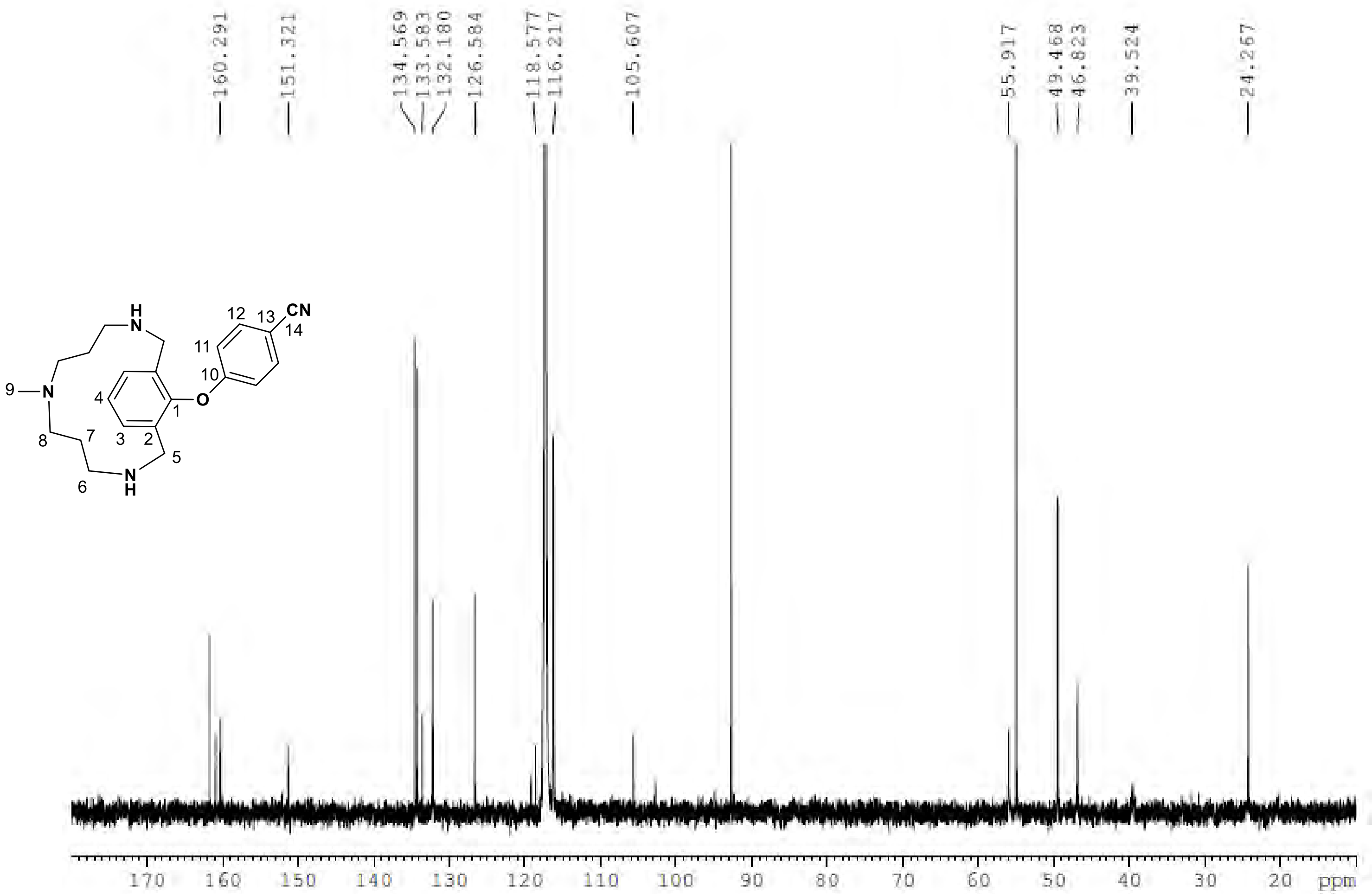

Supplementary Figure 55. ^{13}C NMR spectrum of compound 2e. Experiment performed in CD$_3$CN, 100 MHz, at 298 K.

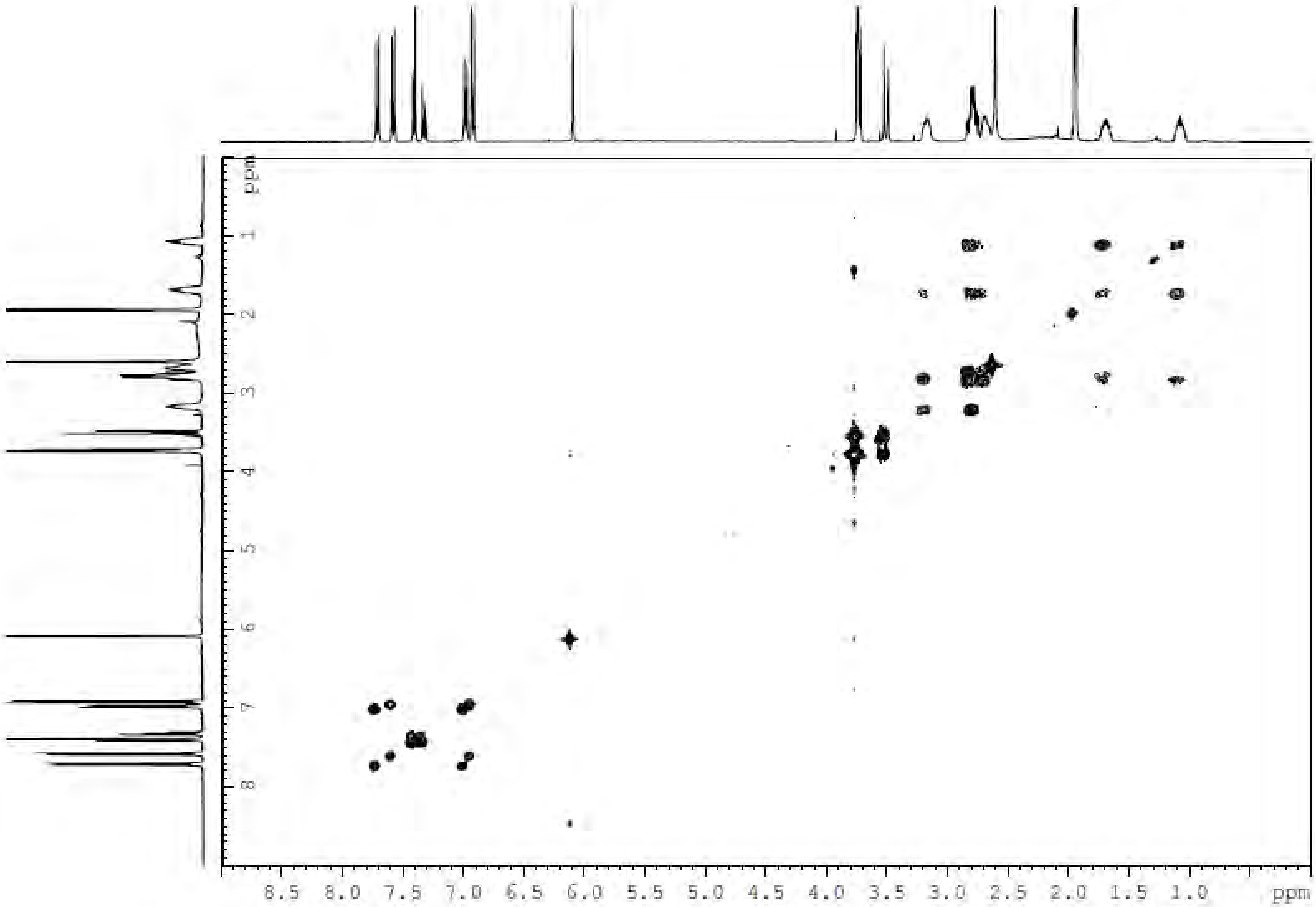

Supplementary Figure 56. COSY spectrum of compound 2e. Experiment performed in CD_3CN, 400 MHz, at 298 K.

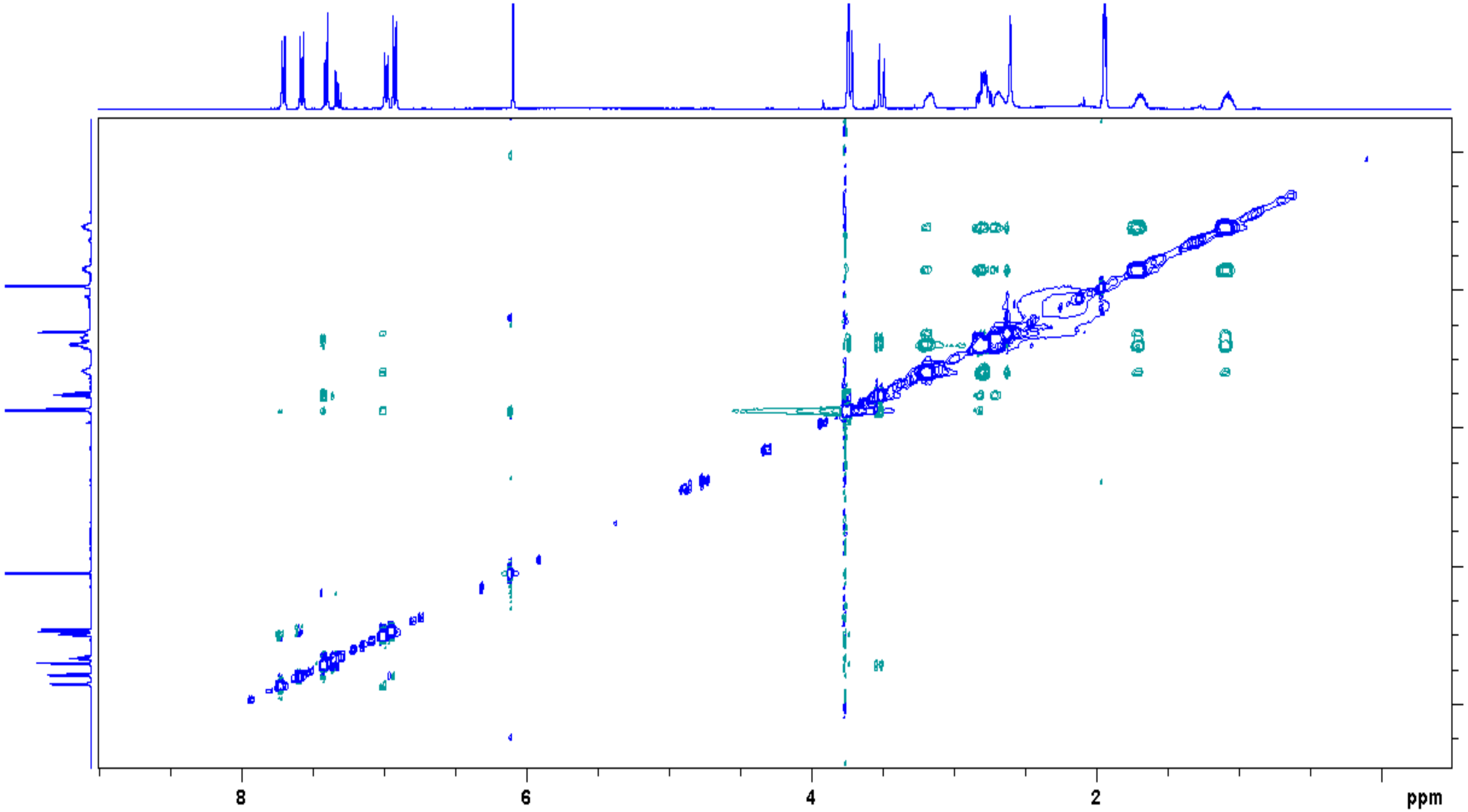

Supplementary Figure 57. NOESY spectrum of compound 2e. Experiment performed in CD_3CN, 400 MHz, at 298 K.

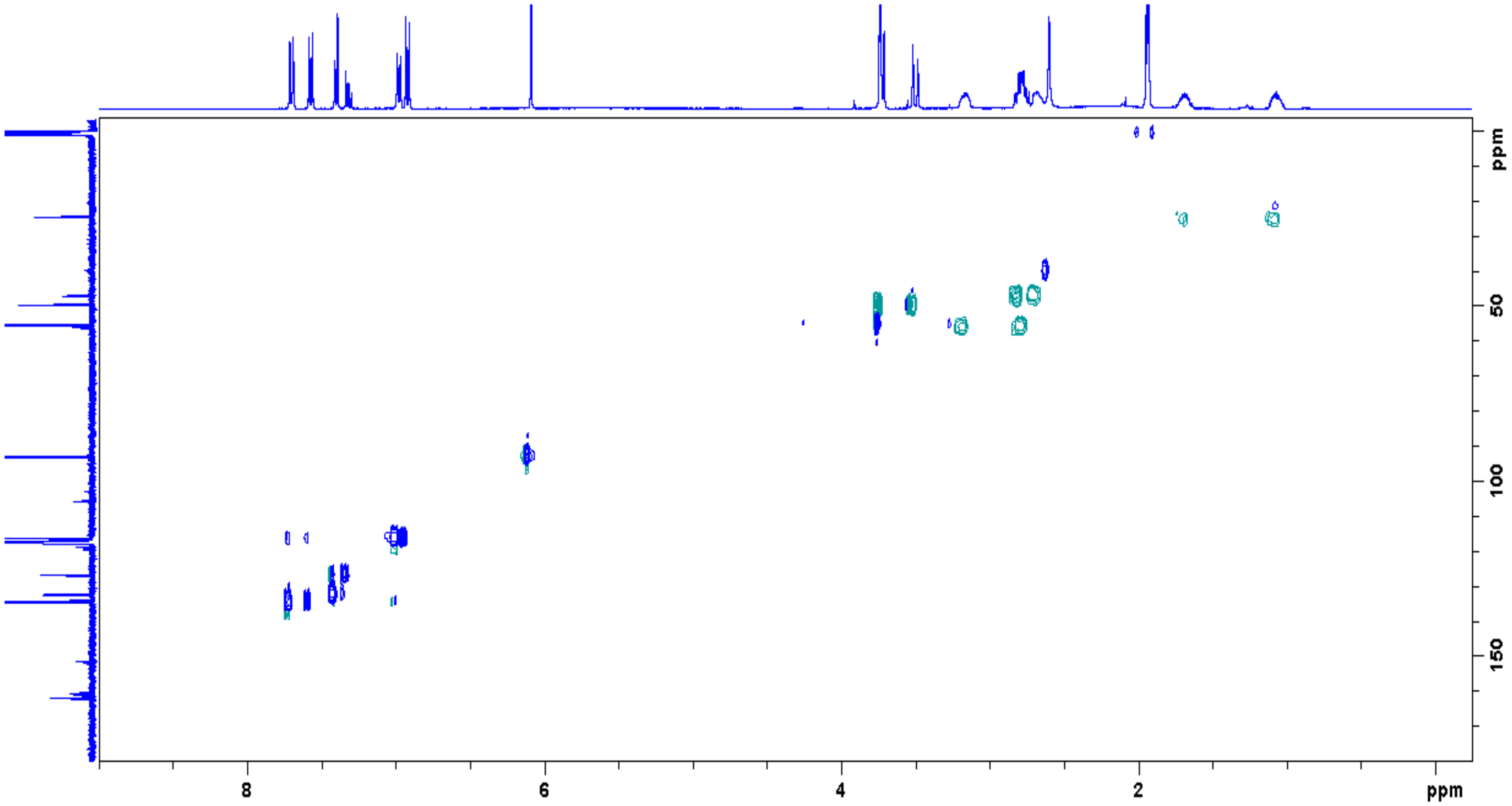

Supplementary Figure 58. ^{1}H ^{13}C HSQC spectrum of compound 2e. Experiment performed in CD_3CN, 400 MHz, at 298 K.

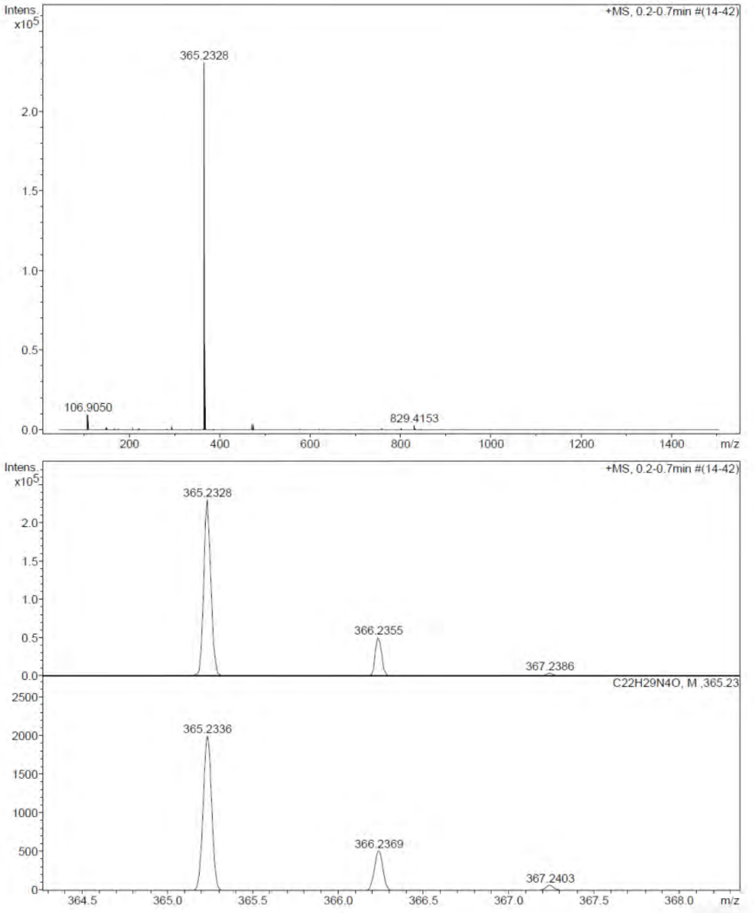

Supplementary Figure 59. HRMS (ESI-MS) spectrum of compound 2e. Experiment performed in CH_3CN (spectrum at the bottom corresponds to the simulated peak).

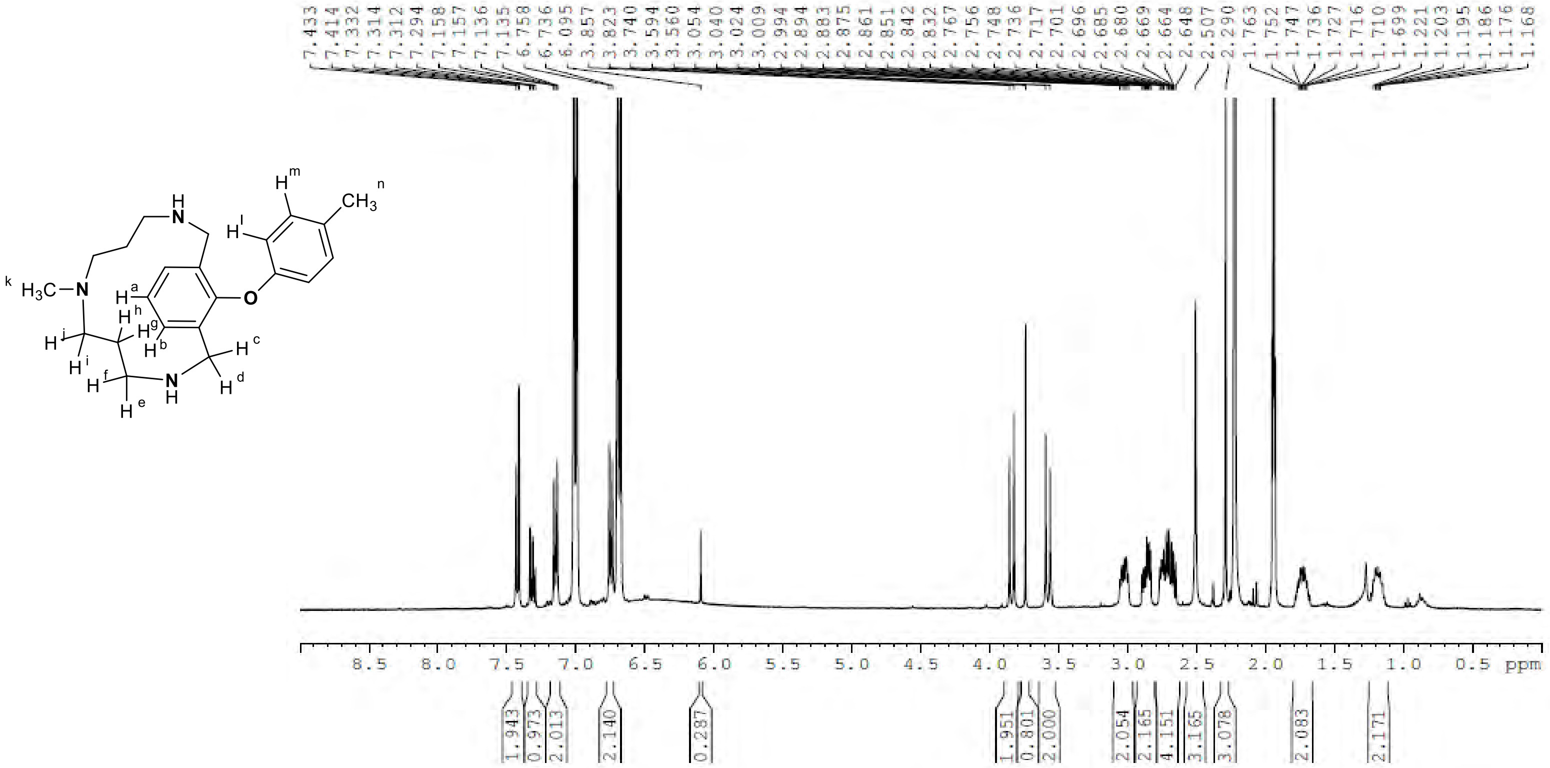

Supplementary Figure 60. ^{1}H NMR spectrum of compound 2f. Experiment performed in CD_3CN, 400 MHz, at 298 K.

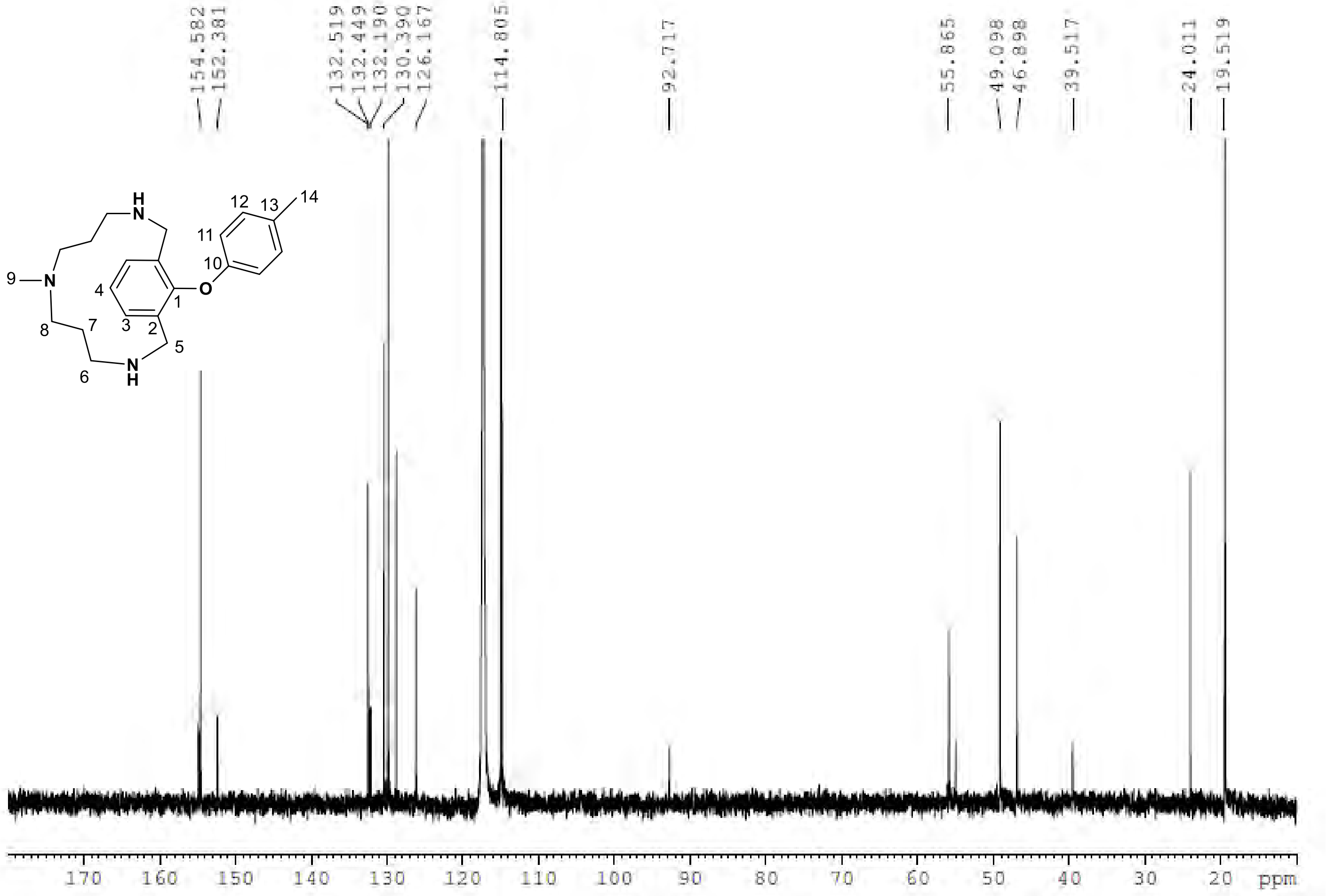

Supplementary Figure 61. ^{13}C NMR spectrum of compound 2f. Experiment performed in CD_3CN, 100 MHz, at 298 K.

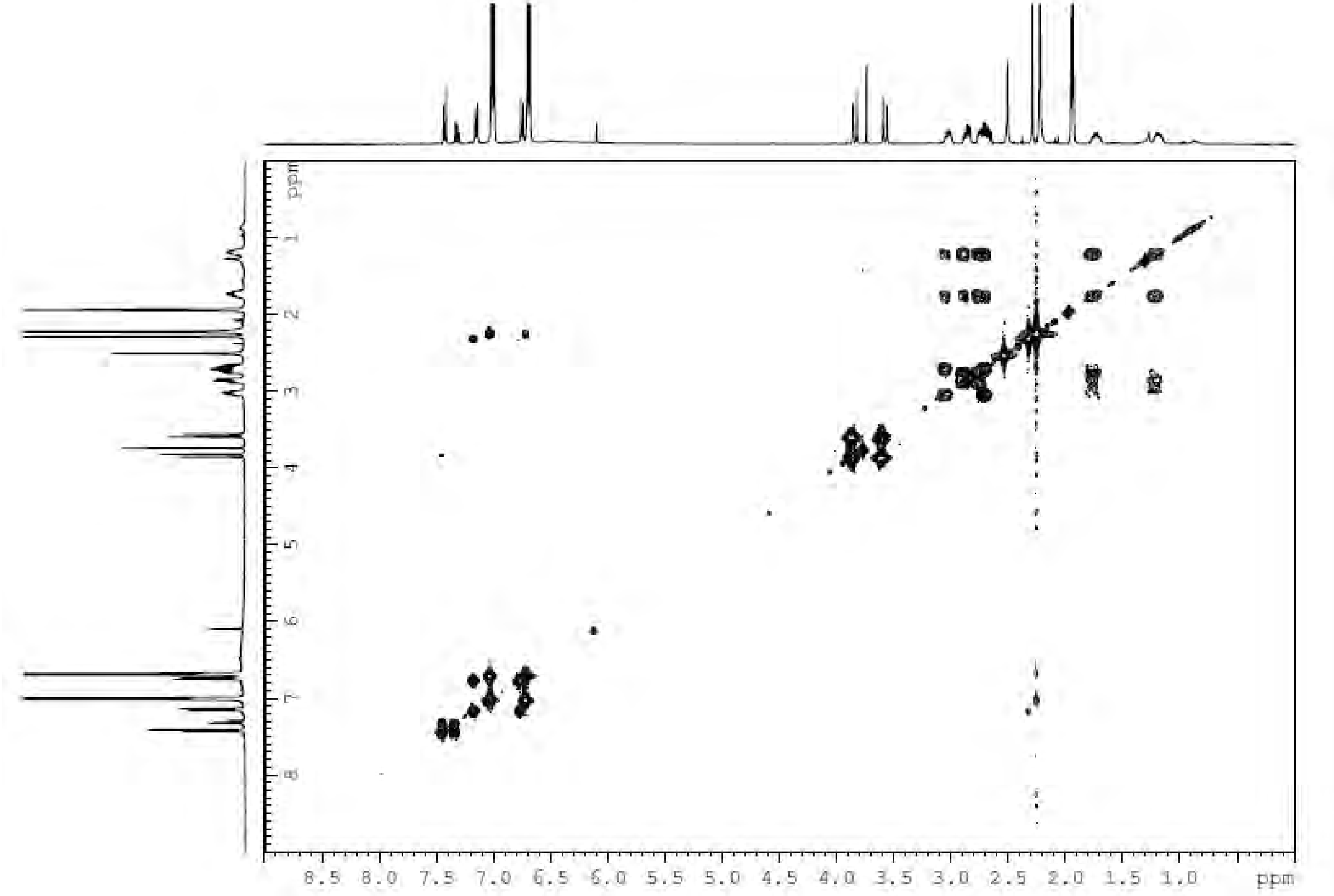

Supplementary Figure 62. COSY spectrum of compound 2f. Experiment performed in CD_3CN, 400 MHz, at 298 K.

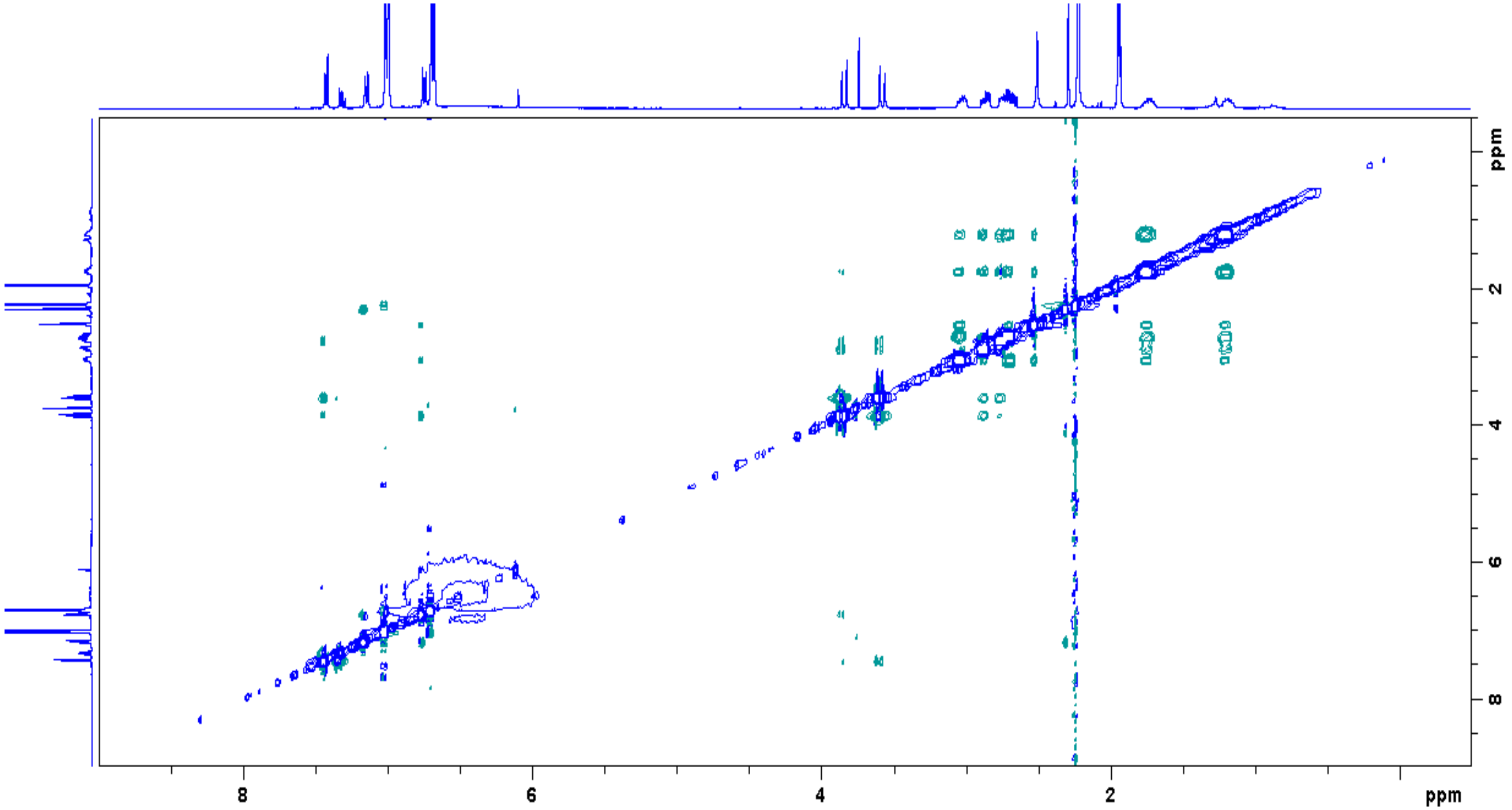

Supplementary Figure 63. NOESY spectrum of compound 2f. Experiment performed in CD_3CN, 400 MHz, at 298 K.

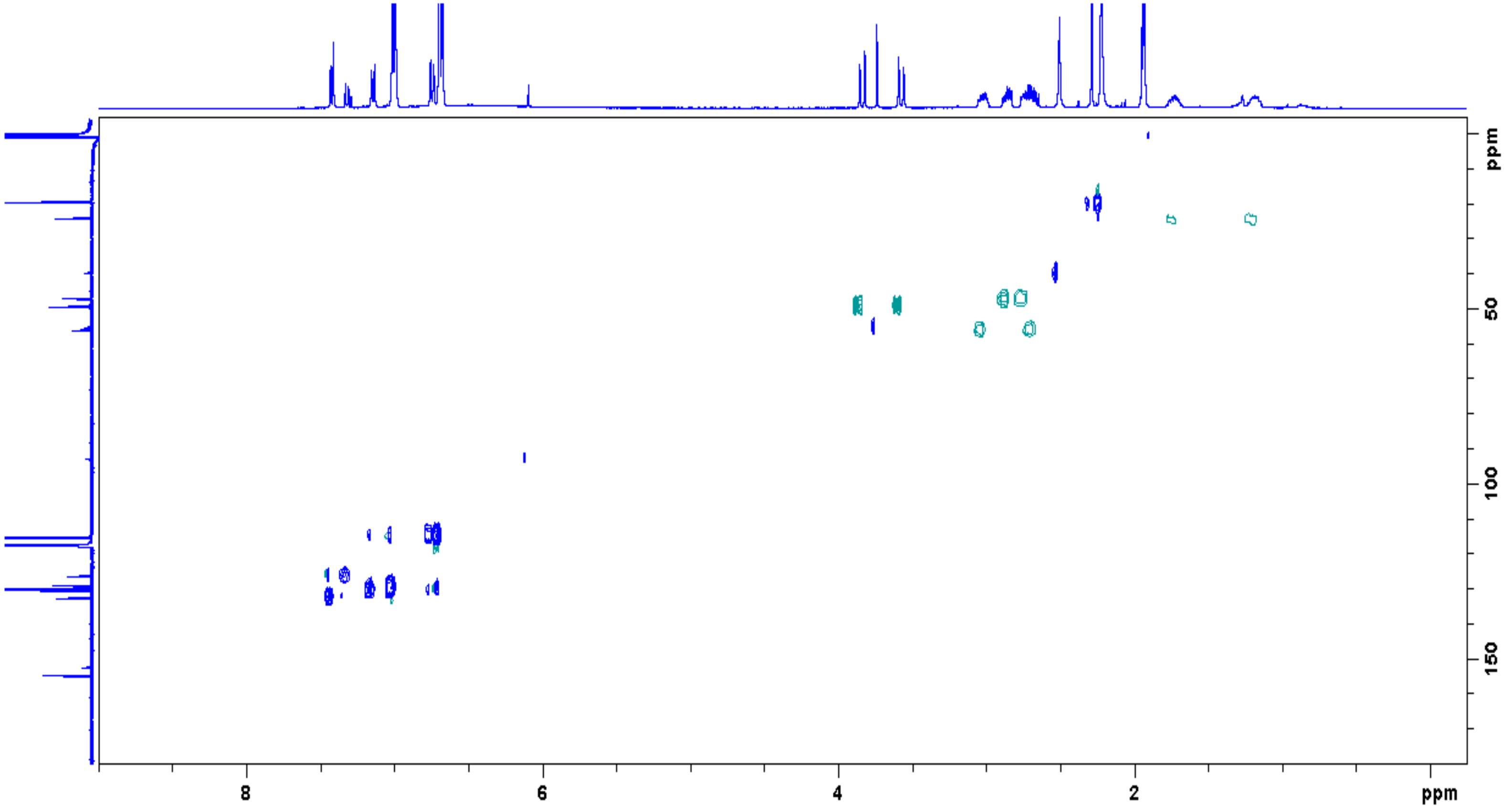

Supplementary Figure 64. ^{1}H ^{13}C HSQC spectrum of compound 2f. Experiment performed in CD_3CN, 400 MHz, at 298 K.

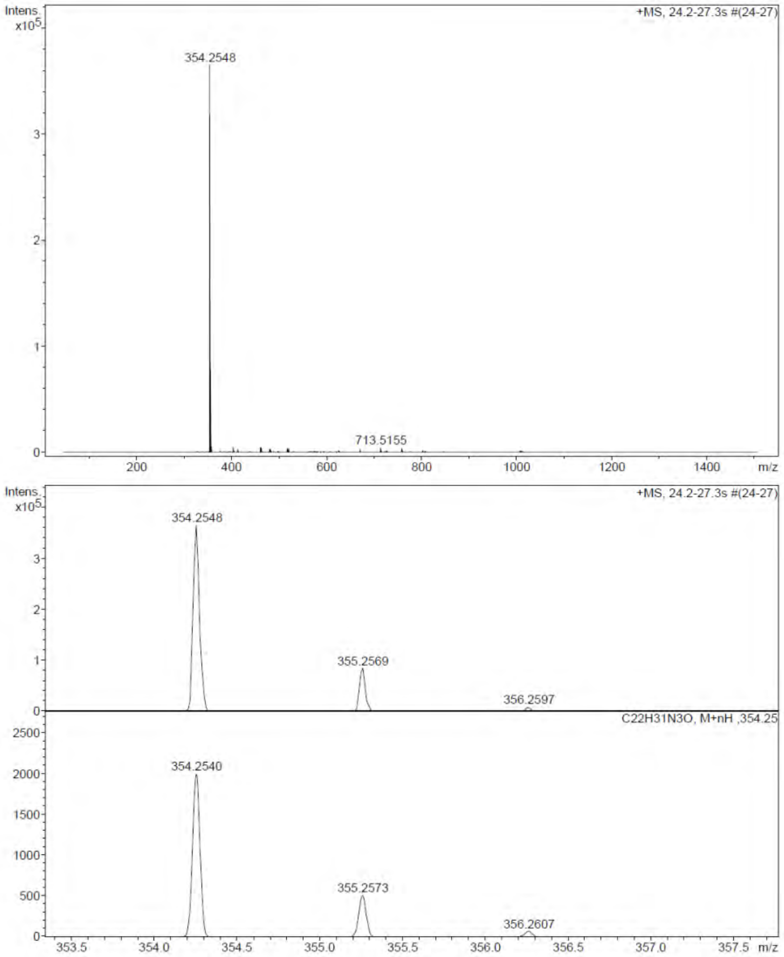

Supplementary Figure 65. HRMS (ESI-MS) spectrum of compound 2f. Experiment performed in CH_3CN (spectrum at the bottom corresponds to the simulated peak).

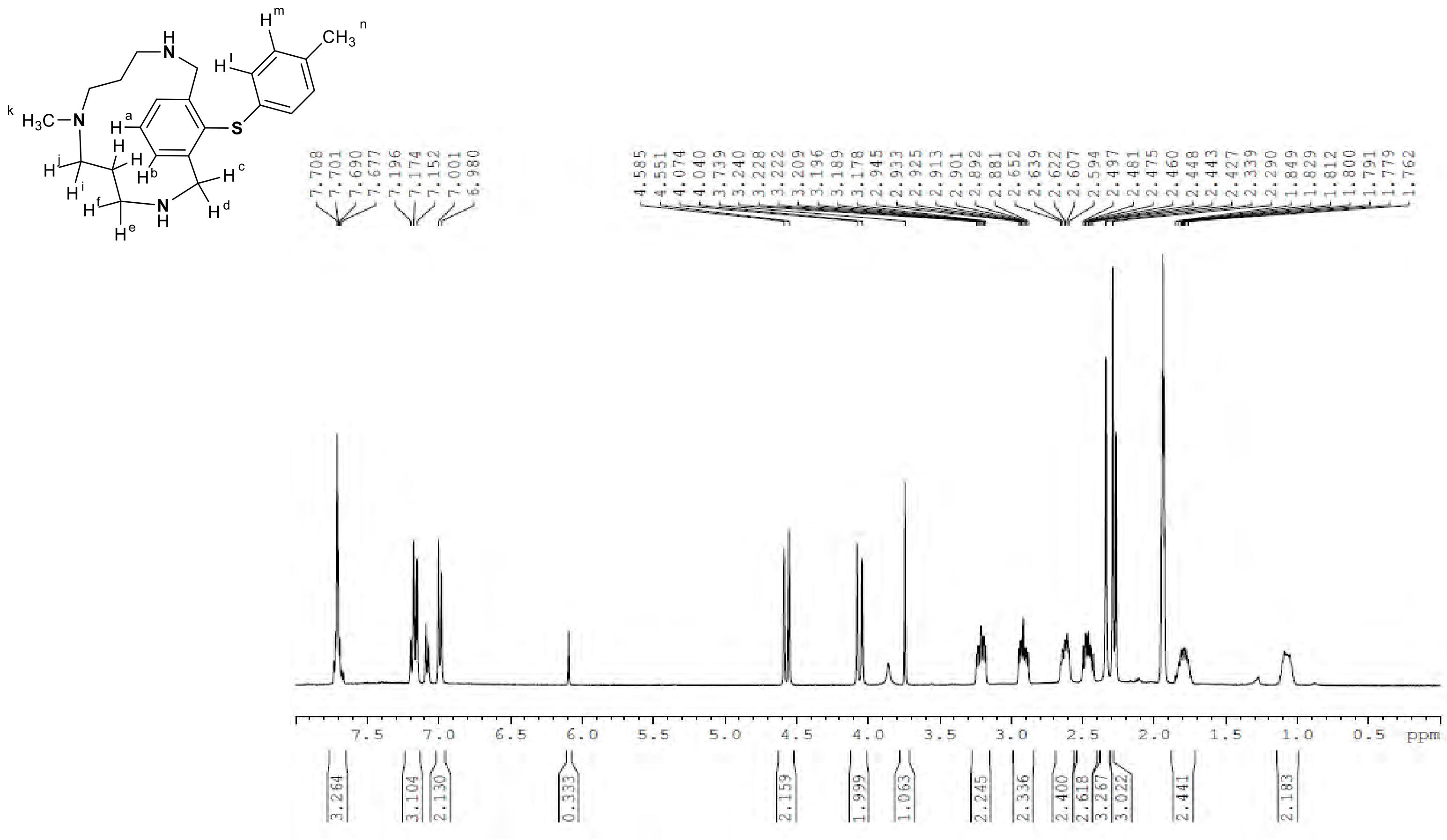

Supplementary Figure 66. ^{1}H NMR spectrum of compound 2g. Experiment performed in CD_3CN, 400 MHz, at 298 K.

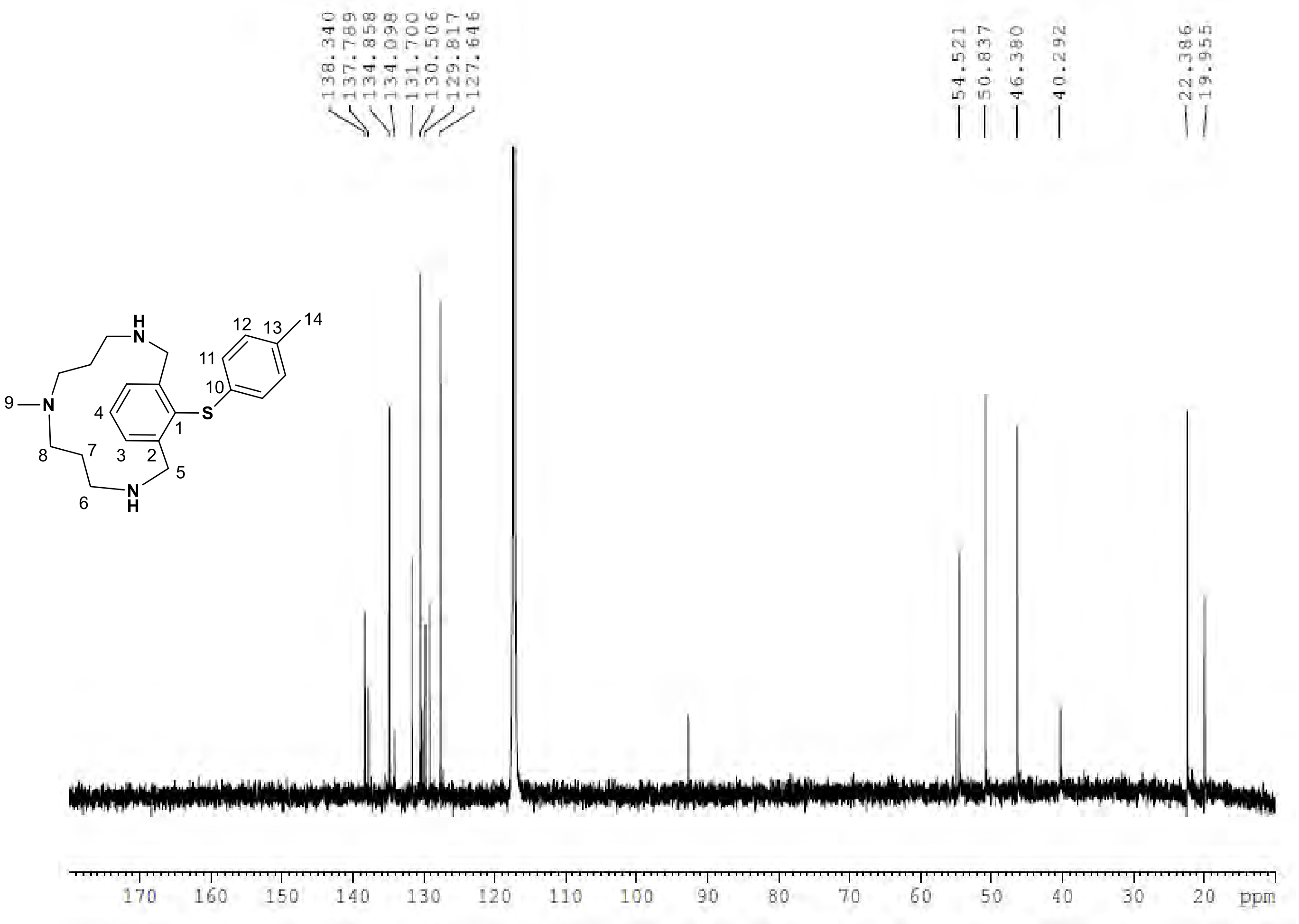

Supplementary Figure 67. ^{13}C NMR spectrum of compound 2g. Experiment performed in CD_3CN, 100 MHz, at 298 K.

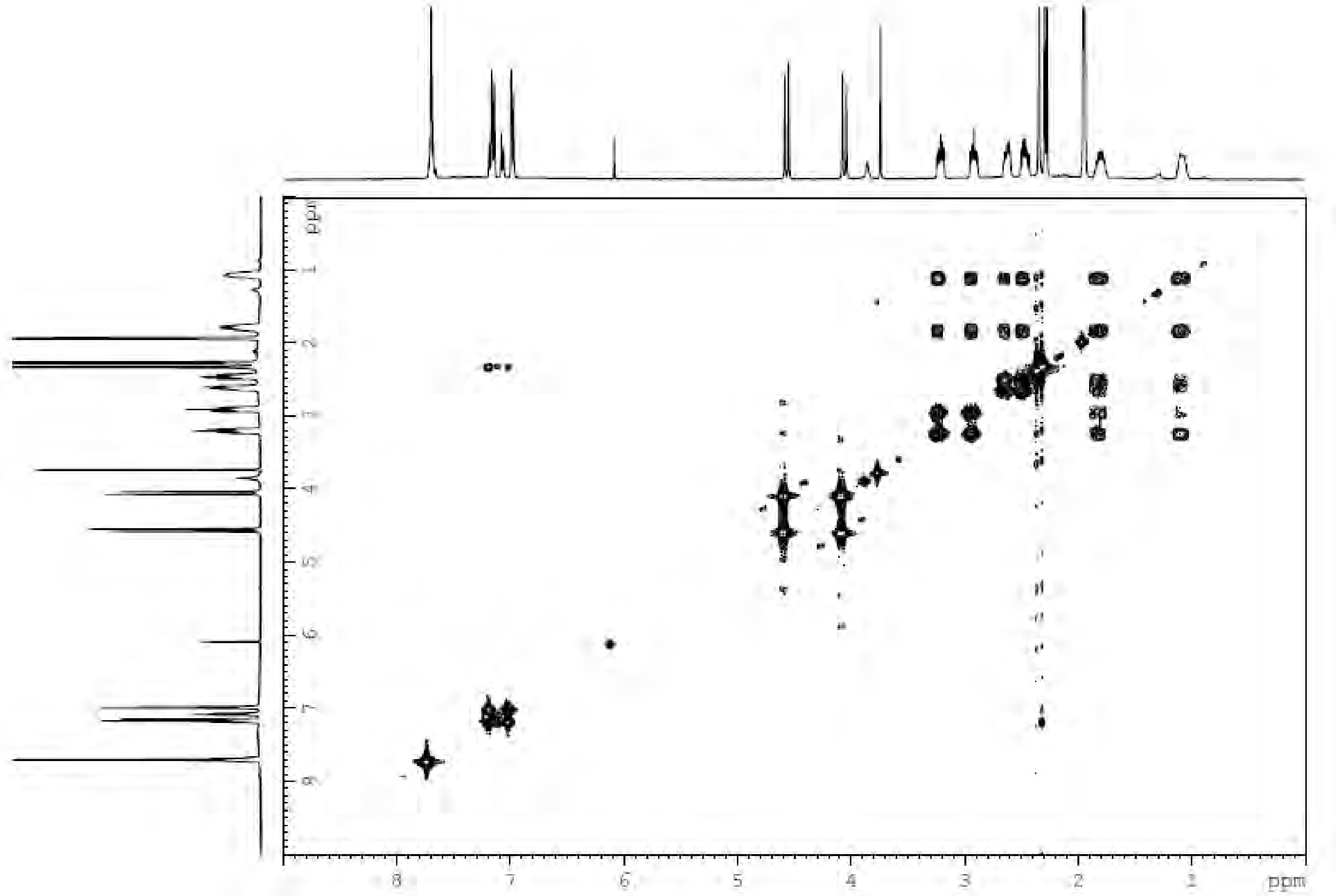

Supplementary Figure 68. COSY spectrum of compound 2g. Experiment performed in CD_3CN, 400 MHz, at 298 K.

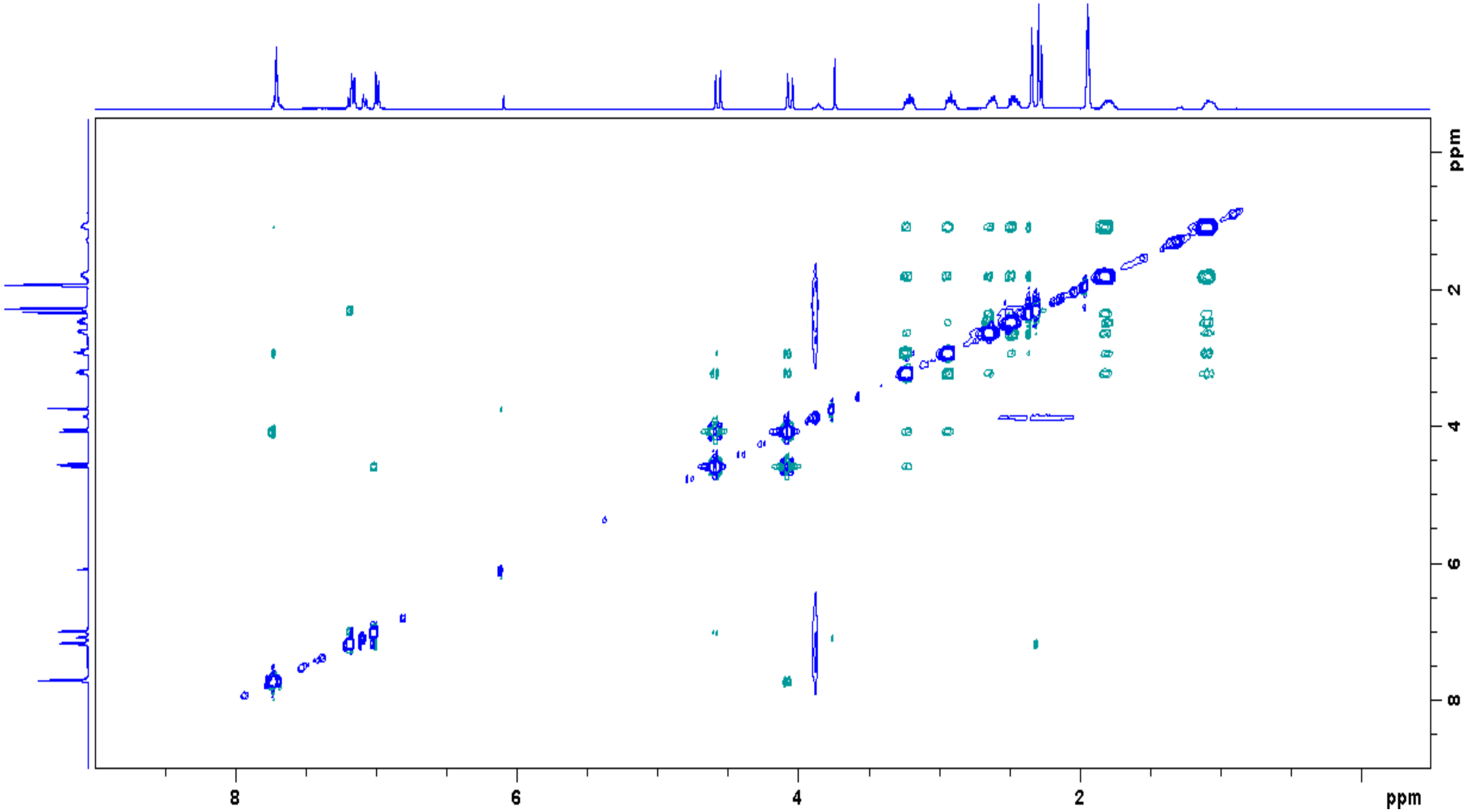

Supplementary Figure 69. NOESY spectrum of compound 2g. Experiment performed in CD_3CN, 400 MHz, at 298 K.

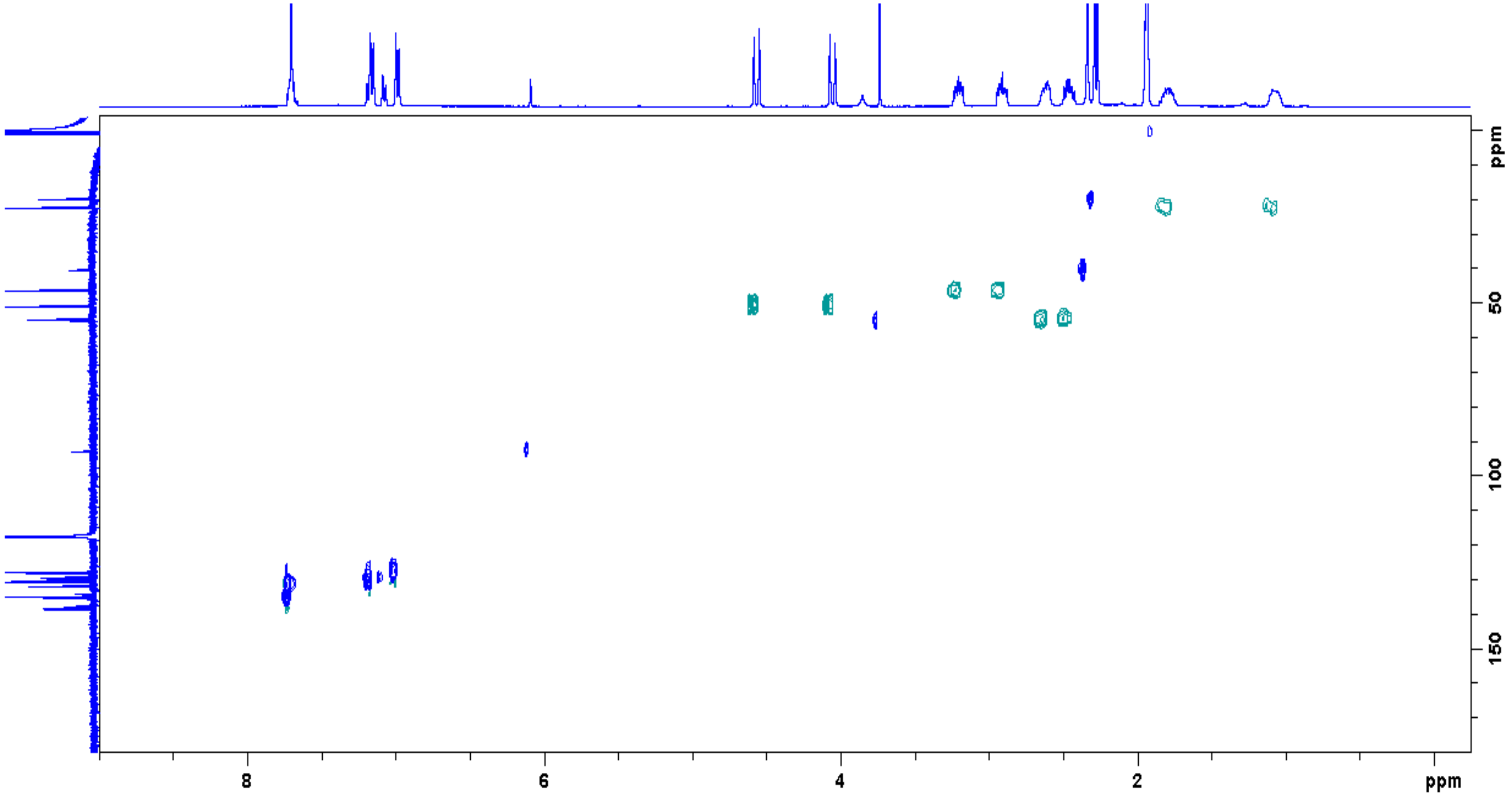

Supplementary Figure 70. ^{1}H ^{13}C HSQC spectrum of compound 2g. Experiment performed in CD_3CN, 400 MHz, at 298 K.

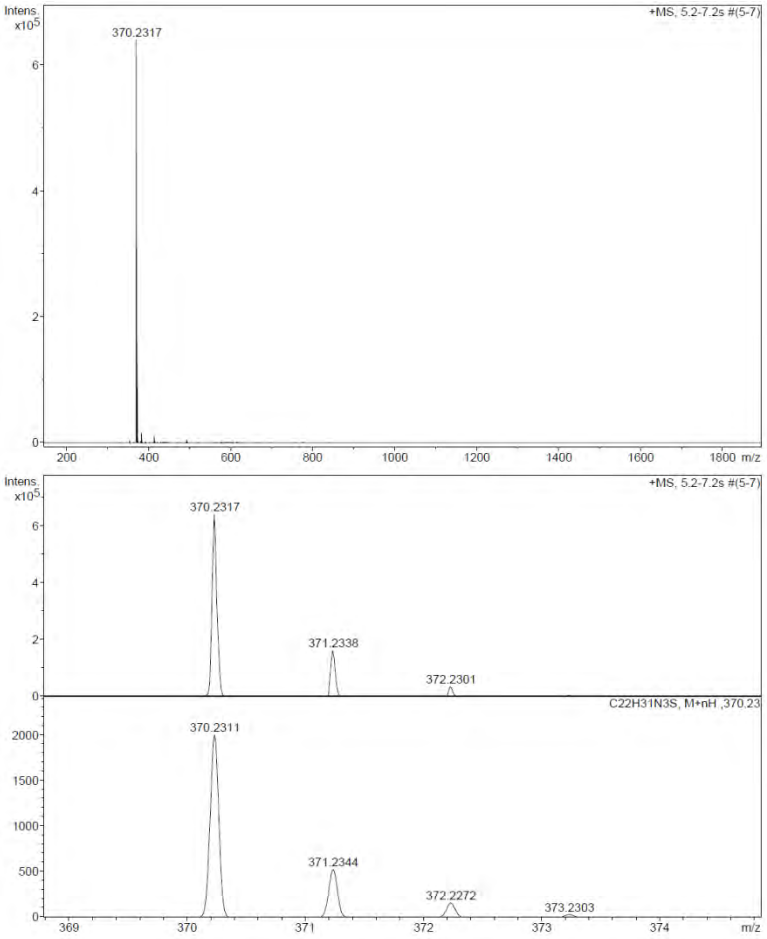

Supplementary Figure 71. HRMS (ESI-MS) spectrum of compound 2g. Experiment performed in CH_3CN (spectrum at the bottom corresponds to the simulated peak).

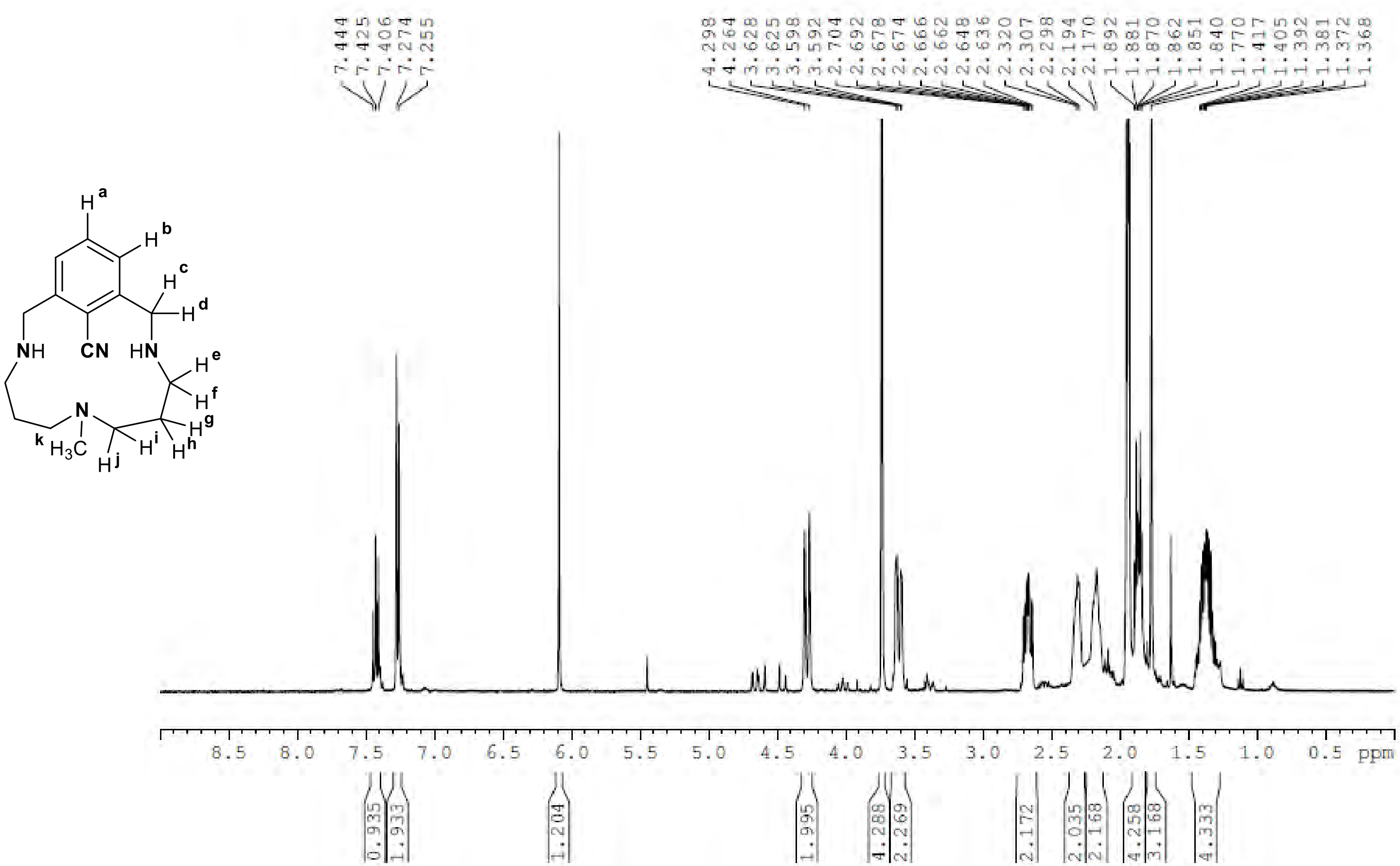

Supplementary Figure 72. ^{1}H NMR spectrum of compound L$_1$-CN. Experiment performed in CD_3CN, 400 MHz, at 298 K.

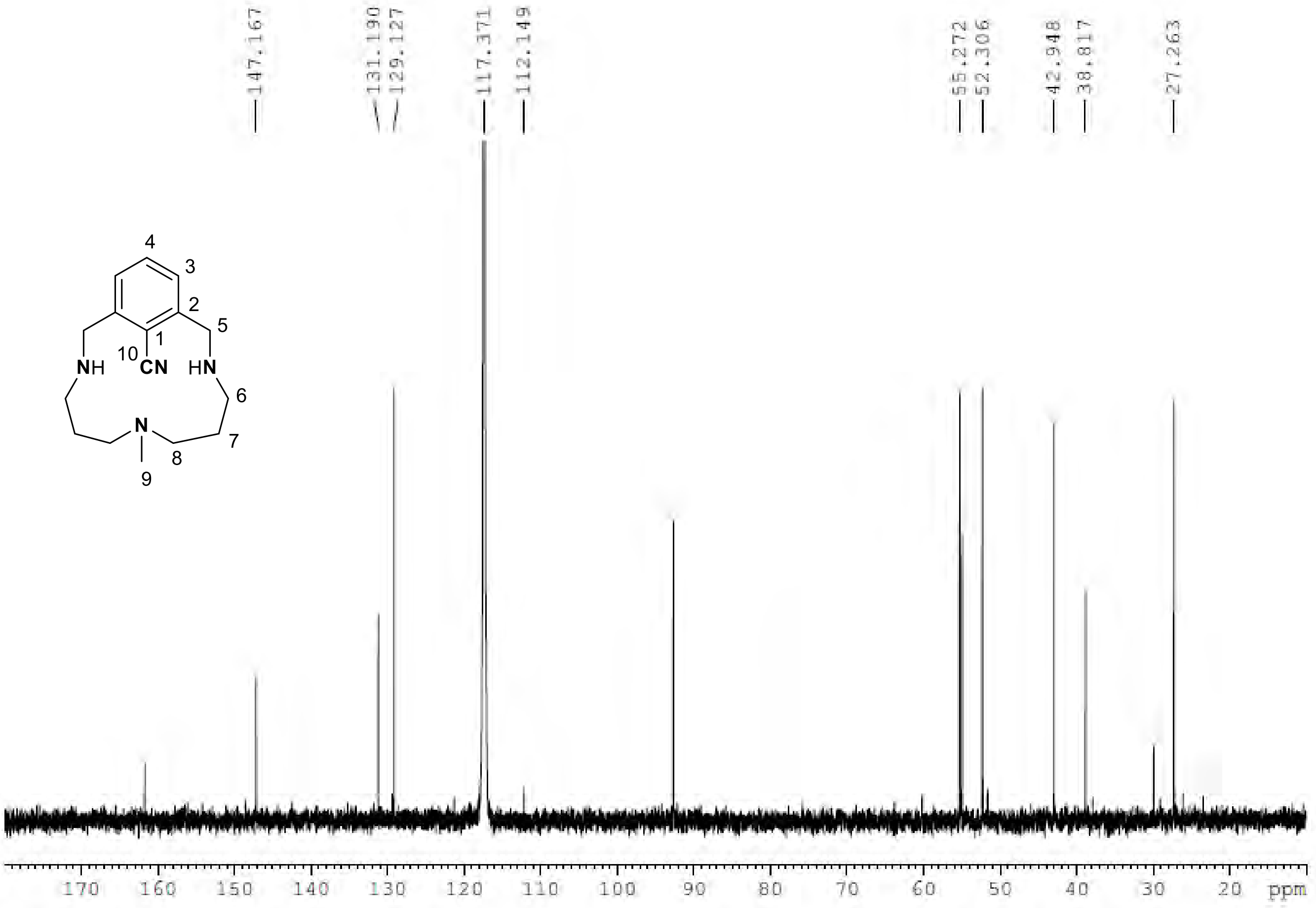

Supplementary Figure 73. ^{13}C NMR spectrum of compound L$_1$-CN. Experiment performed in CD_3CN, 100 MHz, at 298 K.

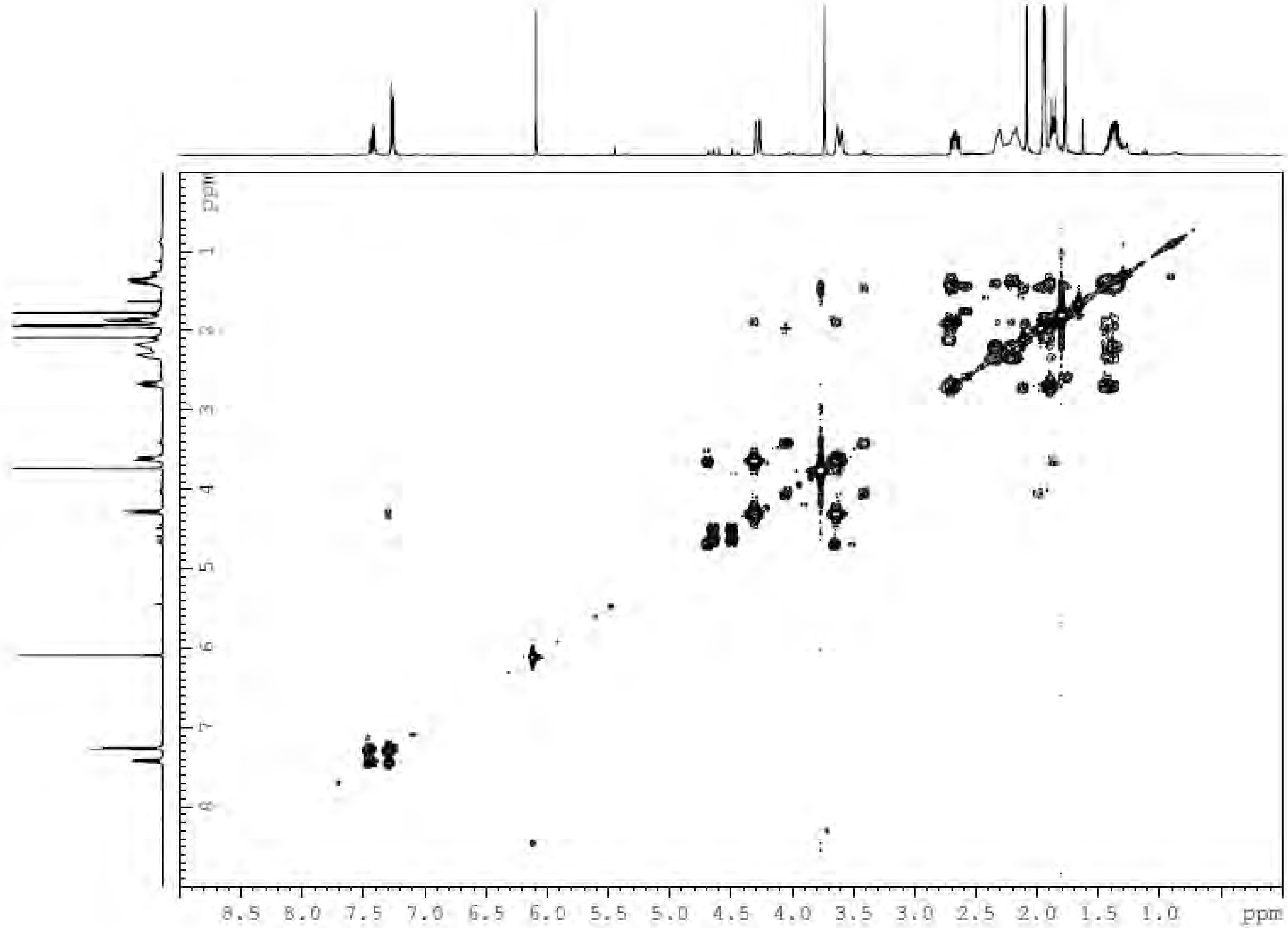
ppm
1
2
3
4
5
6
7
8
8.5
8.0
7.5
7.0
6.5
6.0
5.5
5.0
4.5
4.0
3.5
3.0
2.5
2.0
1.5
1.0
ppm

Supplementary Figure 74. COSY spectrum of compound L$_1$-CN. Experiment performed in CD$_3$CN, 400 MHz, at 298 K.

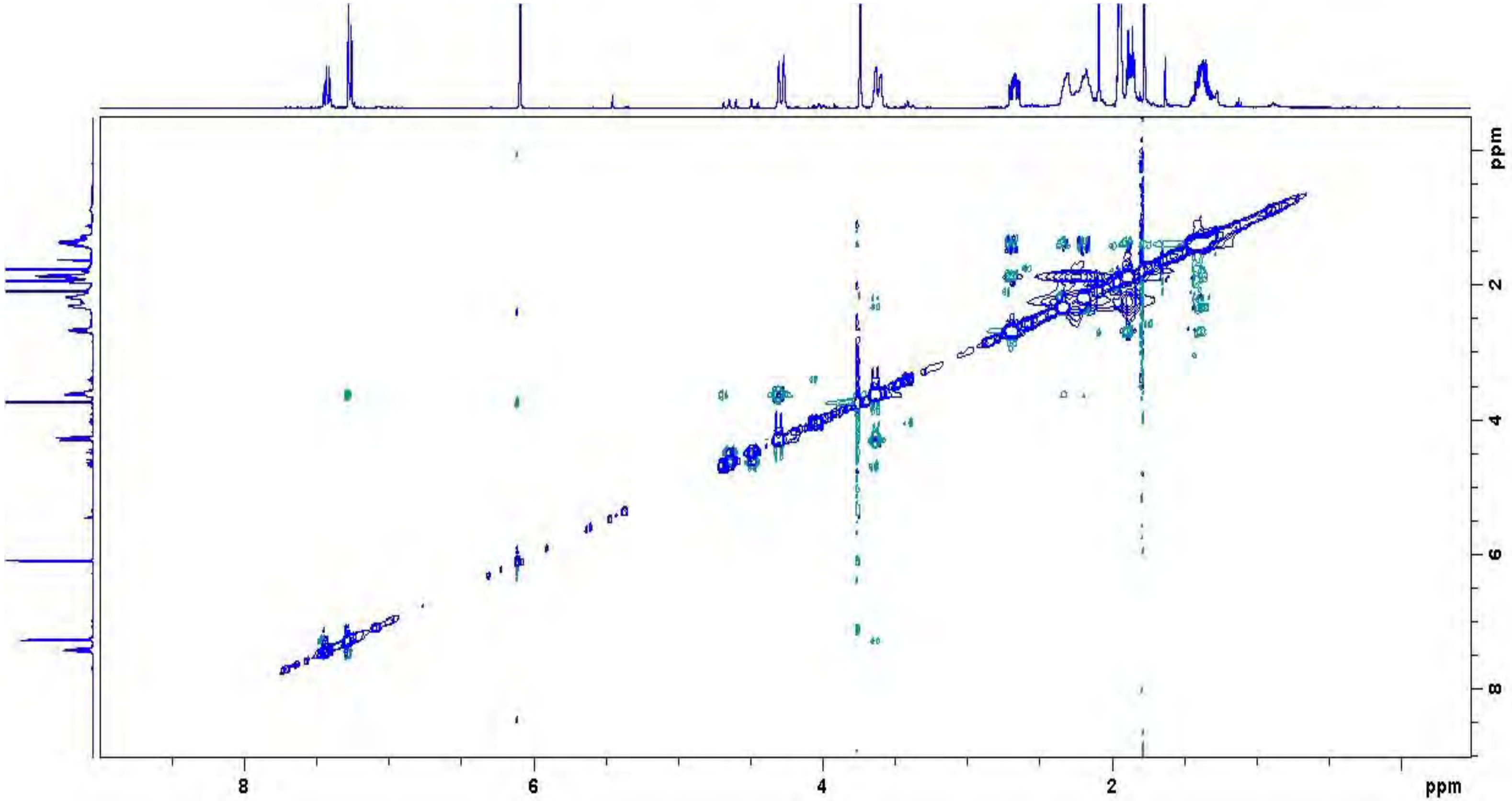

Supplementary Figure 75. NOESY spectrum of compound L$_1$-CN. Experiment performed in CD$_3$CN, 400 MHz, at 298 K.

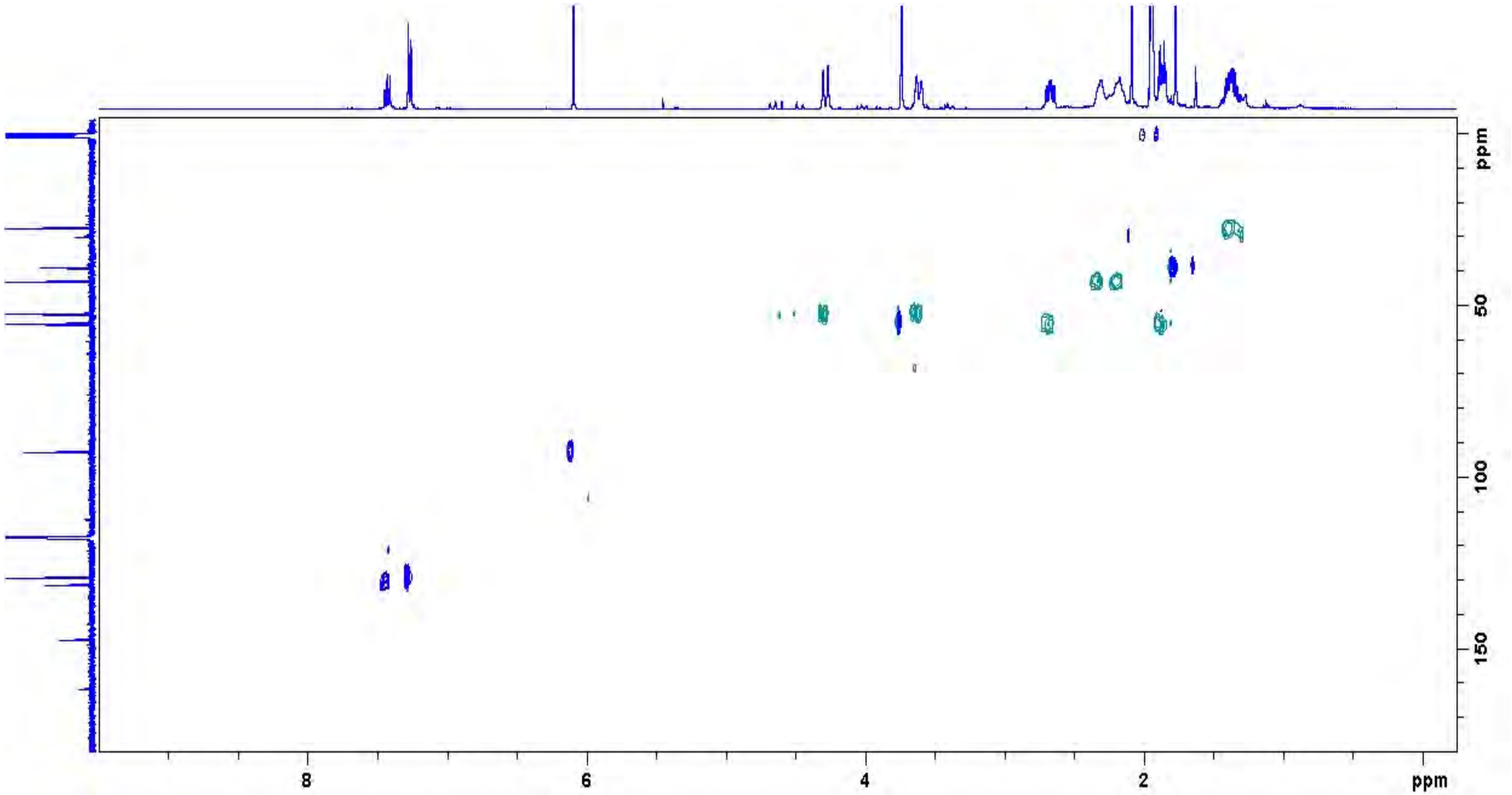

Supplementary Figure 76. ^{1}H ^{13}C HSQC spectrum of compound L$_1$-CN. Experiment performed in CD$_3$CN, 400 MHz, at 298 K.

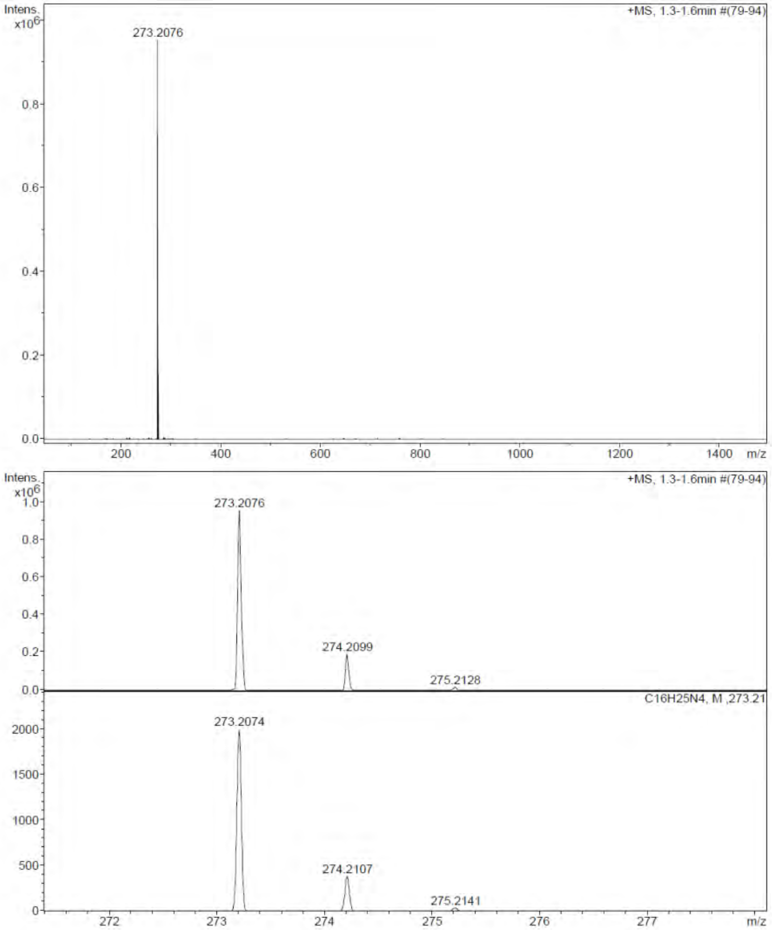

Supplementary Figure 77. HRMS (ESI-MS) spectrum of compound L_1-CN. Experiment performed in CH_3CN (spectrum at the bottom corresponds to the simulated peak).

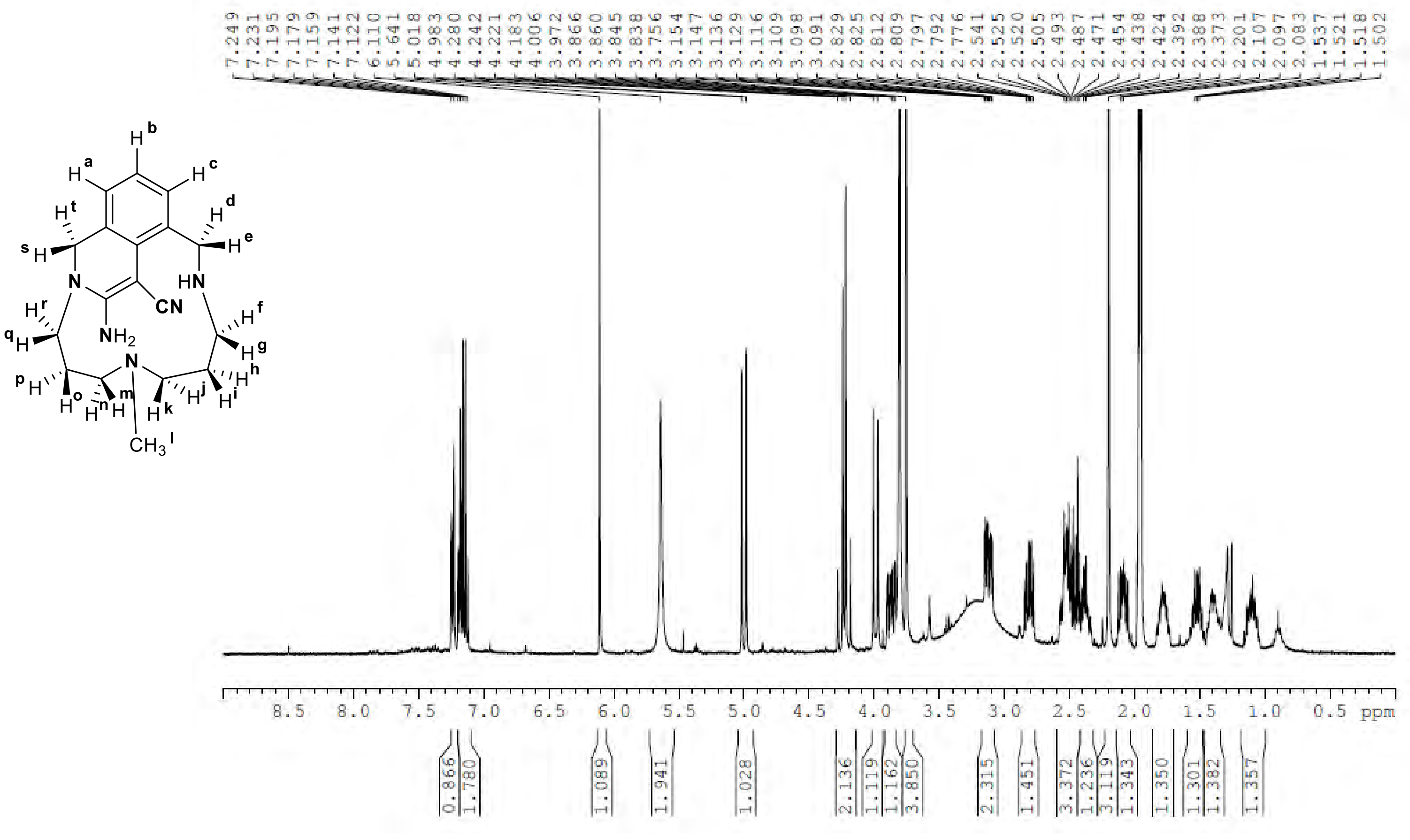

Supplementary Figure 78. ^{1}H NMR spectrum of compound 2h. Experiment performed in CD_3CN, 400 MHz, at 298 K (see ref ^{2})

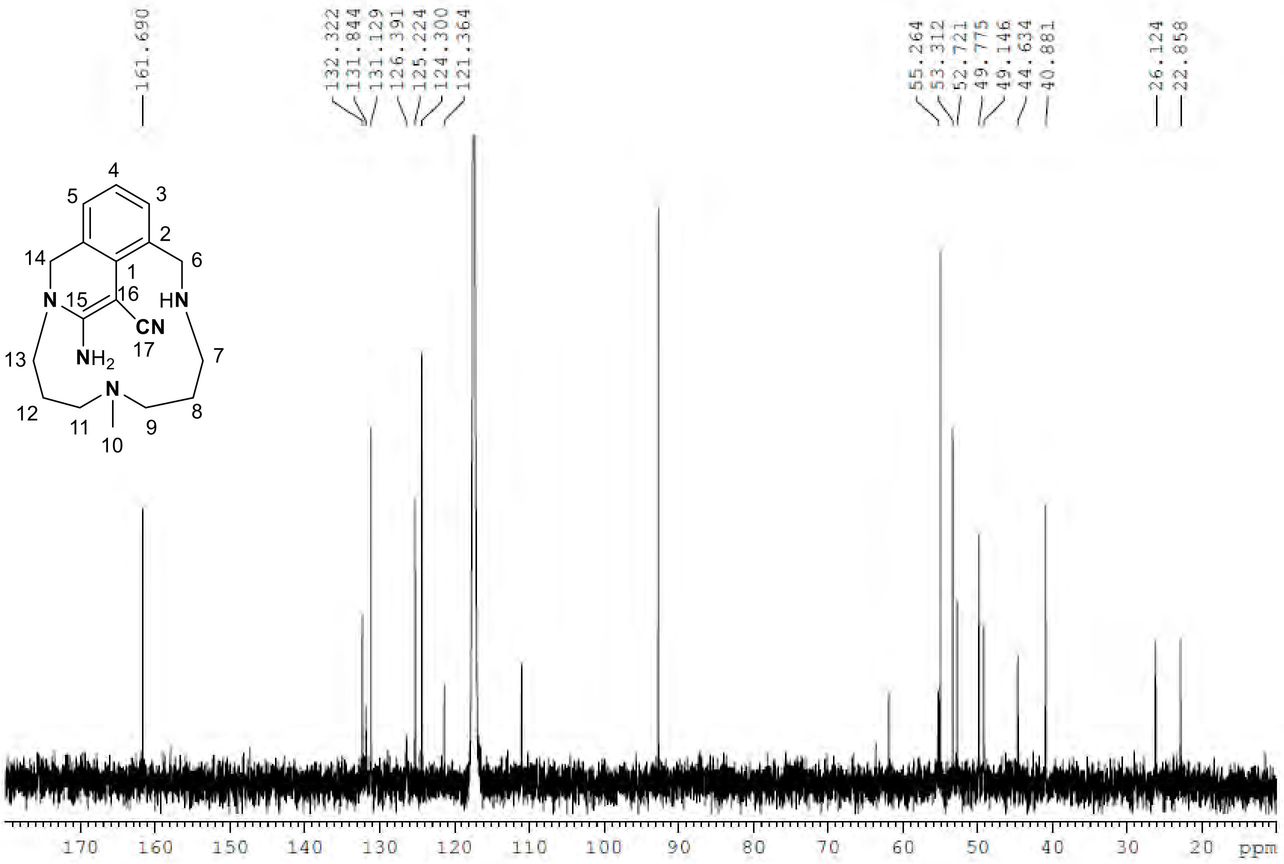

Supplementary Figure 79. ^{13}C NMR spectrum of compound 2h. Experiment performed in CD_3CN, 100 MHz, at 298 K.

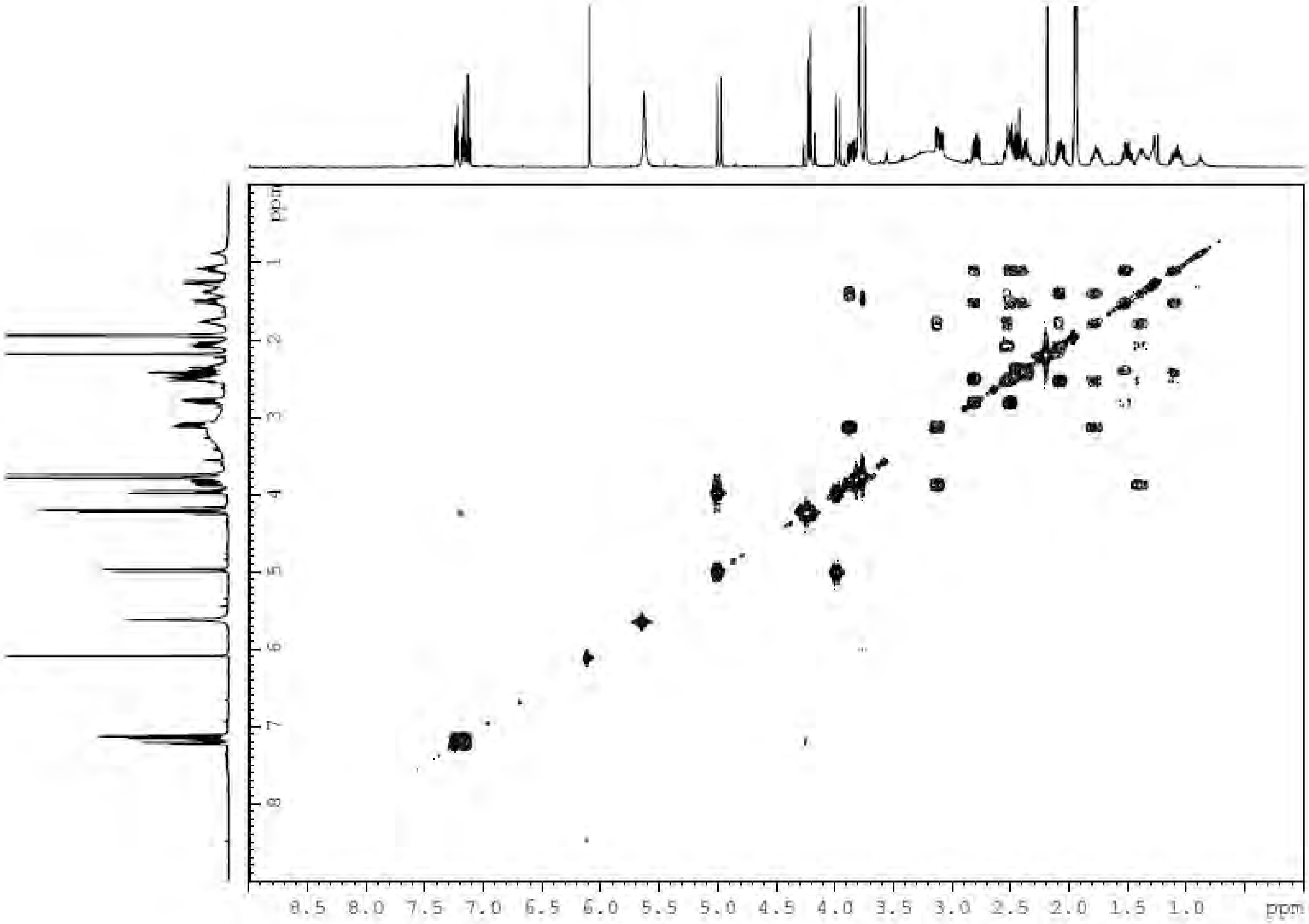

Supplementary Figure 80. COSY spectrum of compound L_1-CN. Experiment performed in CD_3CN, 400 MHz, at 298 K.

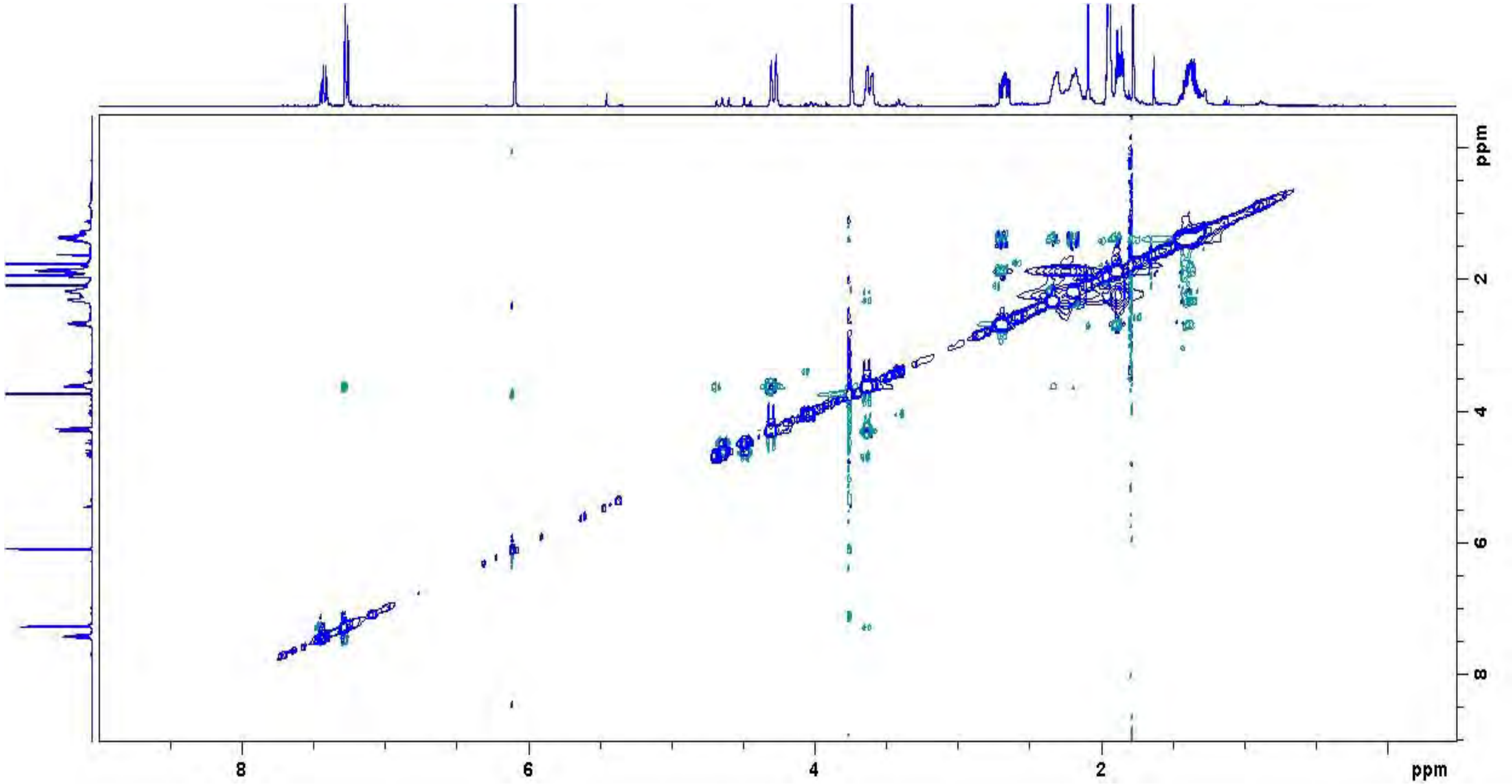

Supplementary Figure 81. NOESY spectrum of compound 2h. Experiment performed in CD_3CN, 400 MHz, at 298 K.

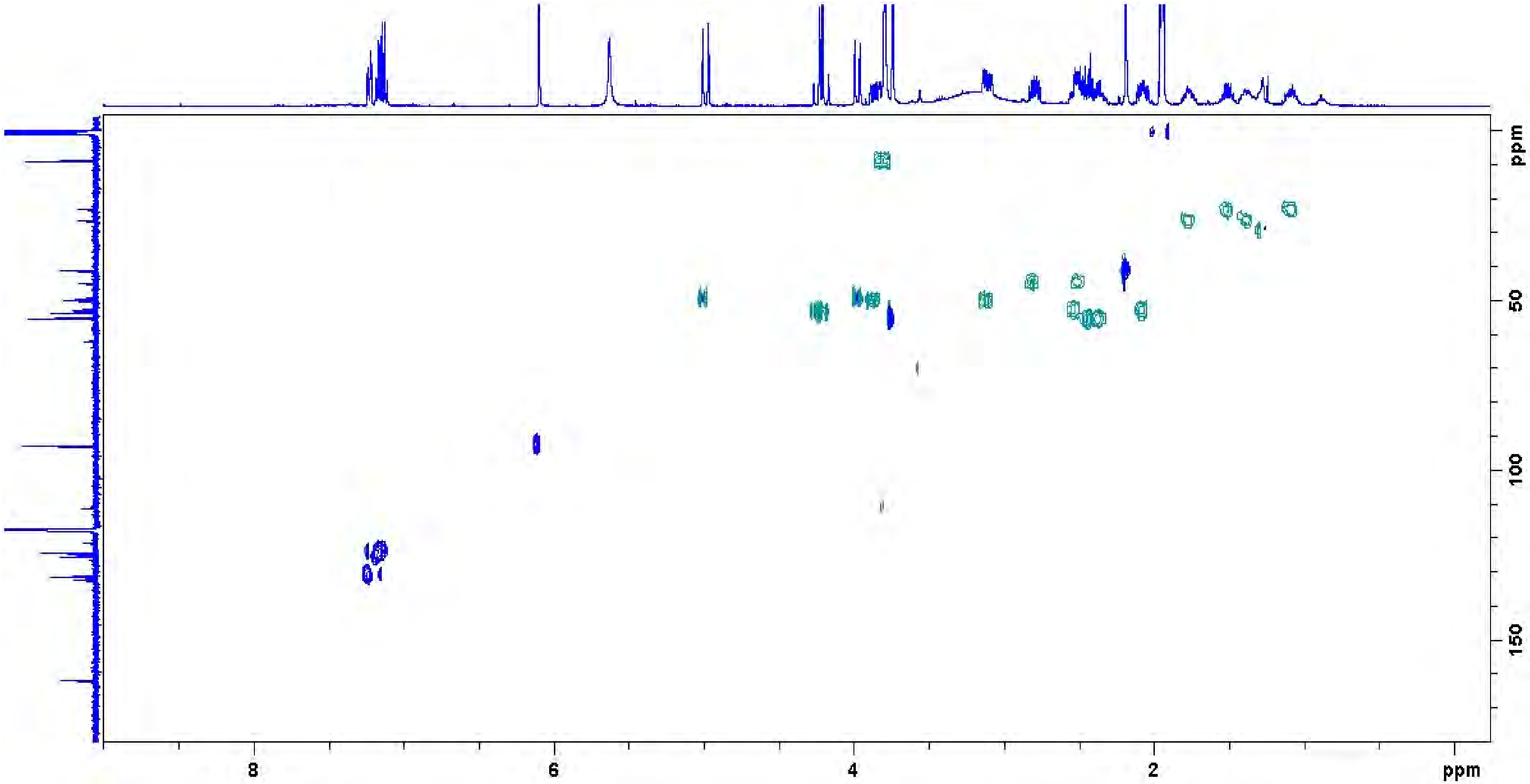

Supplementary Figure 82. ^{1}H ^{13}C HSQC spectrum of compound 2h. Experiment performed in CD_3CN, 400 MHz, at 298 K.

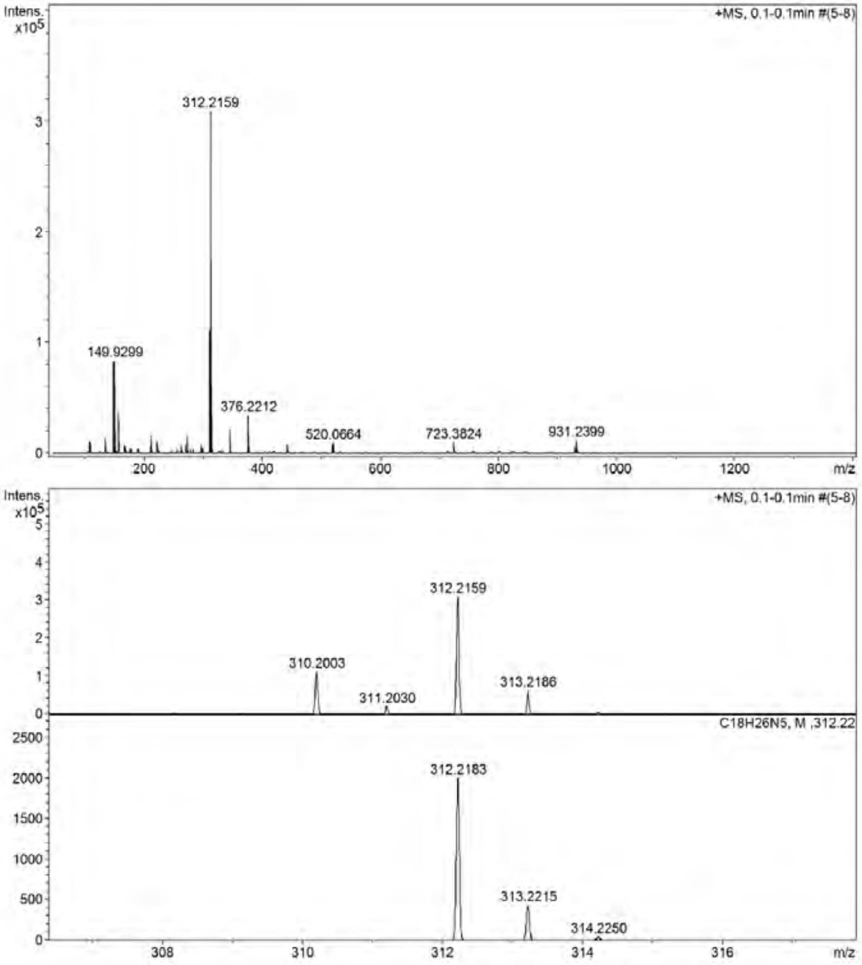

Supplementary Figure 83. HRMS (ESI-MS) spectrum of compound 2h. Experiment performed in CH_3CN (spectrum at the bottom corresponds to the simulated peak).

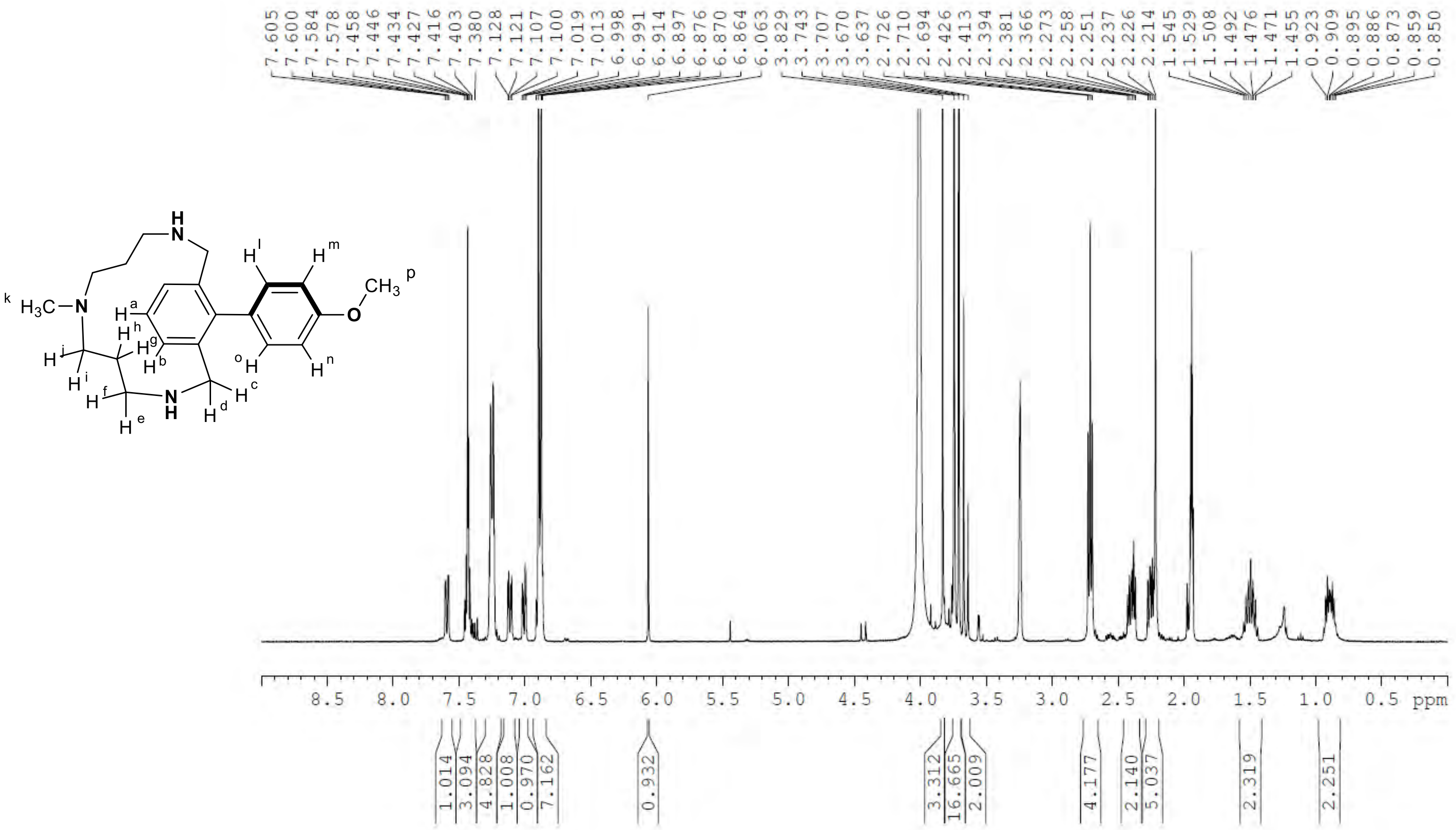

Supplementary Figure 84. ^{1}H NMR spectrum of compound 2i. Experiment performed in CD_3CN, 400 MHz, at 298 K.

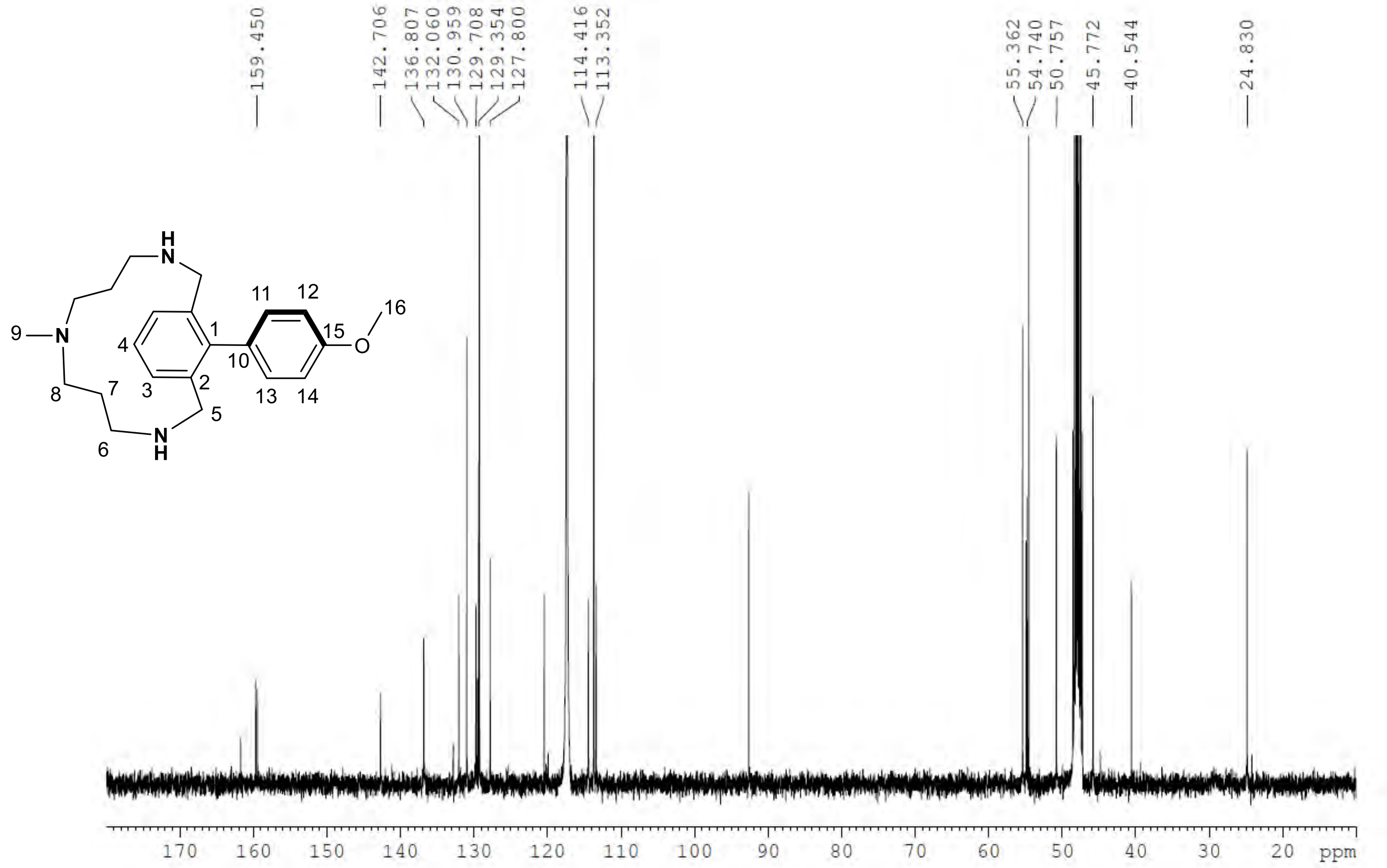

Supplementary Figure 85. ^{13}C NMR spectrum of compound 2i. Experiment performed in CD_3CN, 100 MHz, at 298 K.

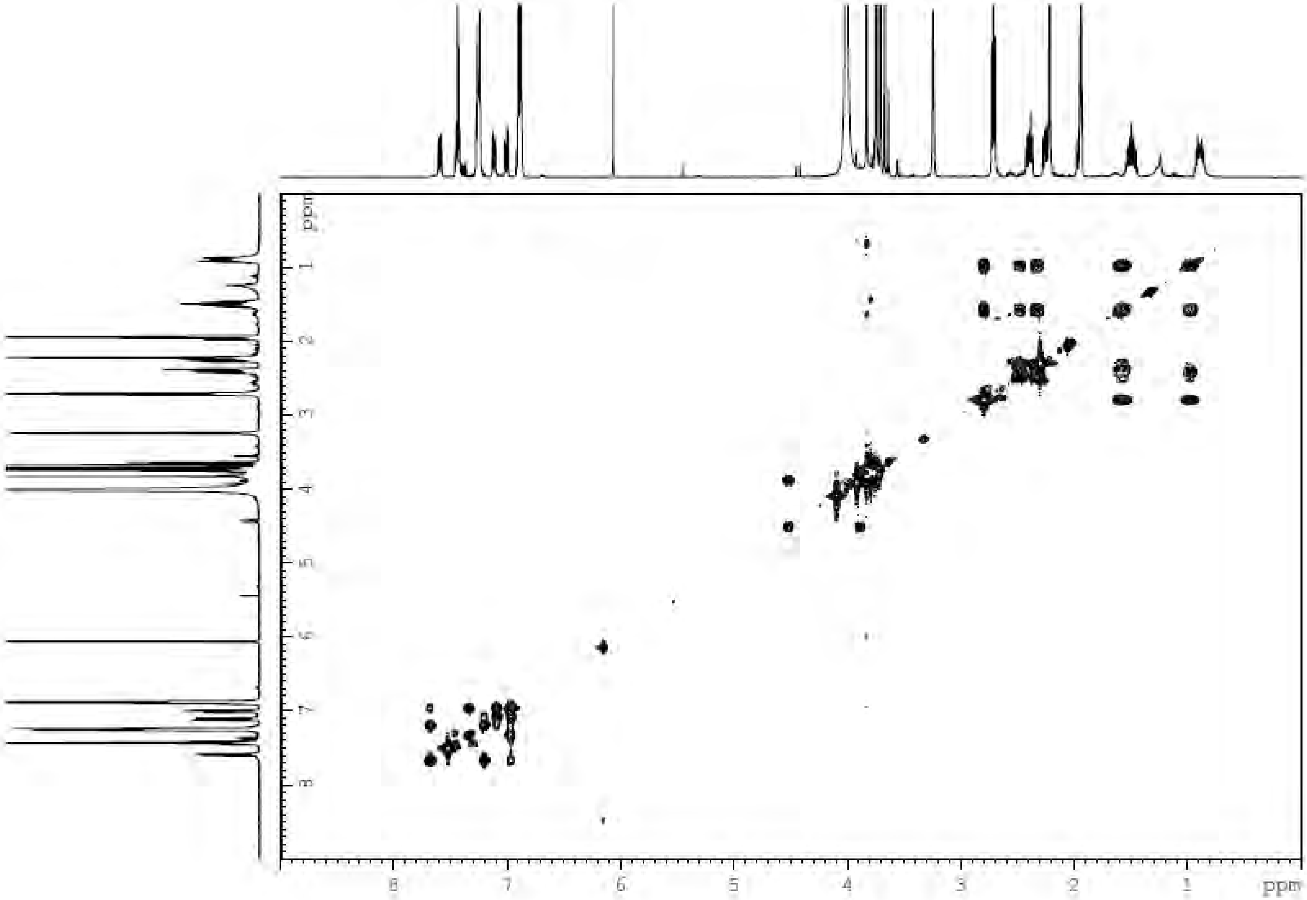

Supplementary Figure 86. COSY spectrum of compound 2i. Experiment performed in CD_3CN, 400 MHz, at 298 K.

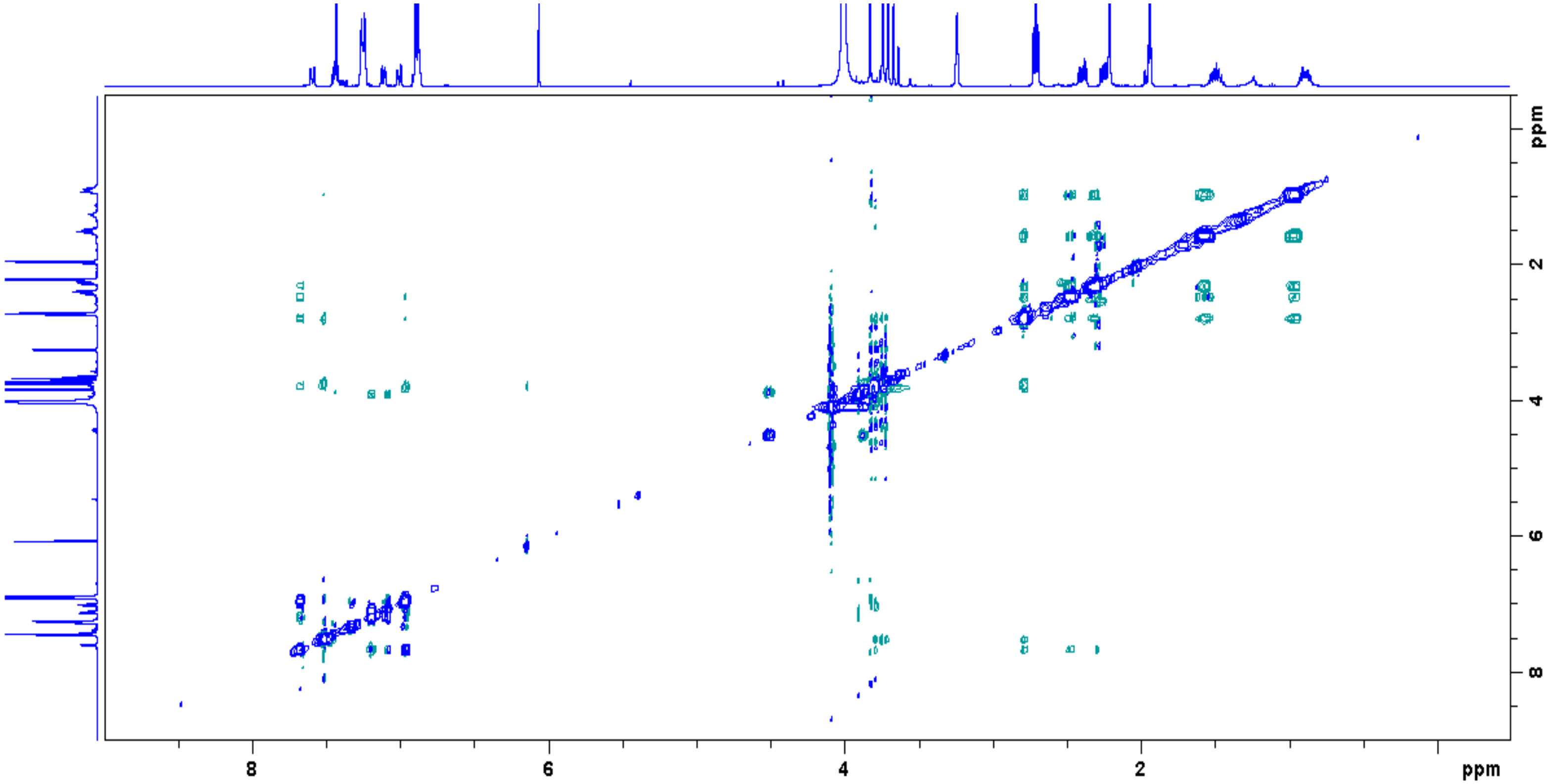

Supplementary Figure 87. NOESY spectrum of compound 2i. Experiment performed in CD$_3$CN, 400 MHz, at 298 K.

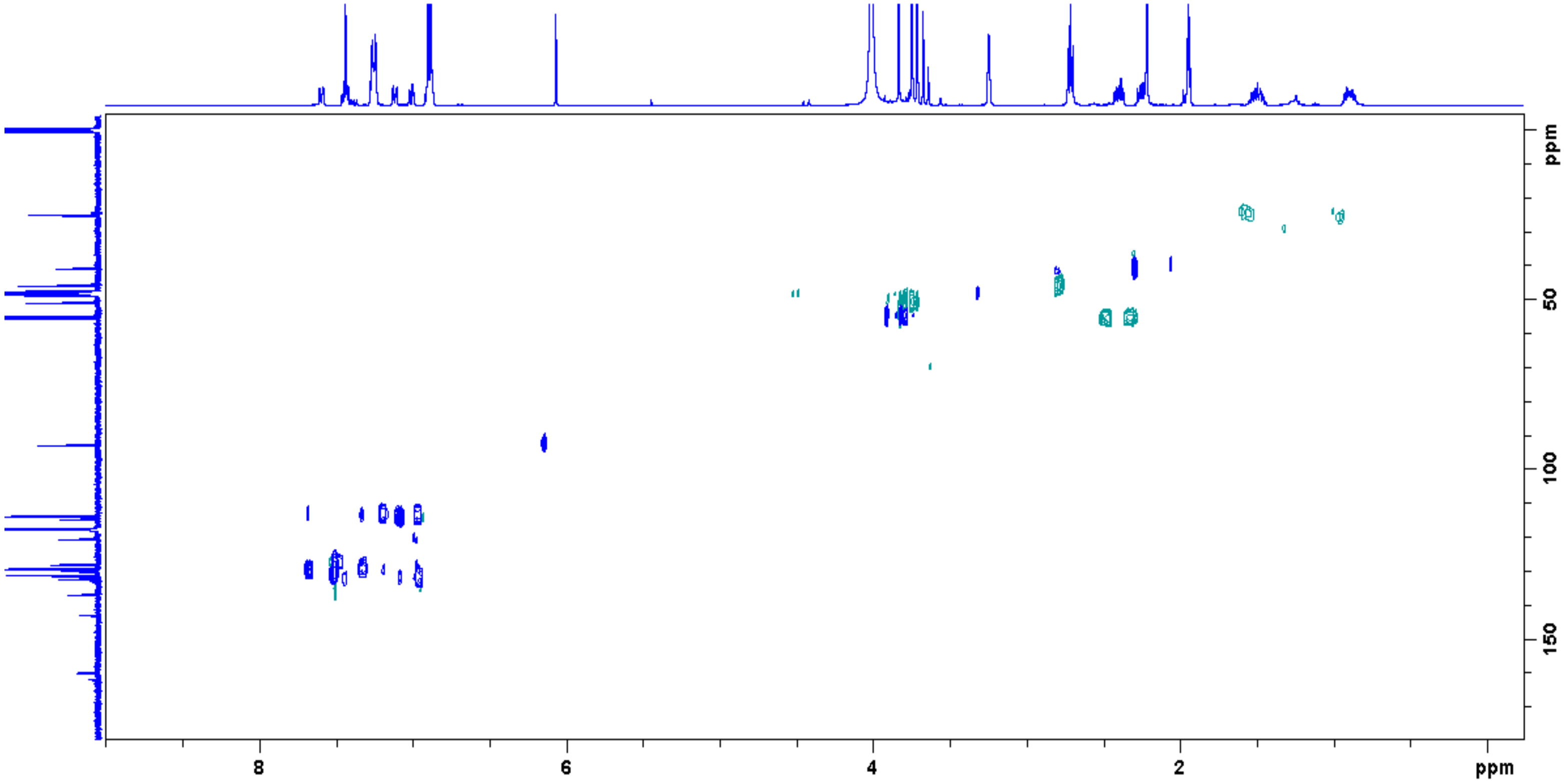

Supplementary Figure 88. ^1H ^{13}C HSQC spectrum of compound 2i. Experiment performed in CD_3CN, 400 MHz, at 298 K.

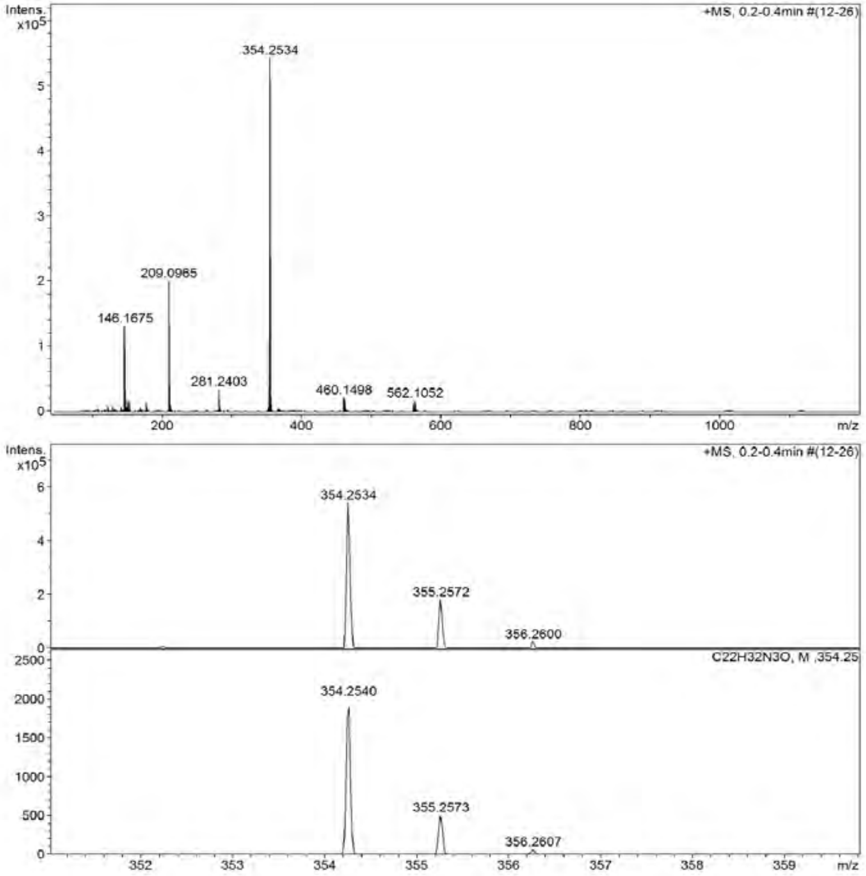

Supplementary Figure 89. HRMS (ESI-MS) spectrum of compound 2i. Experiment performed in CH_3CN (spectrum at the bottom corresponds to the simulated peak).

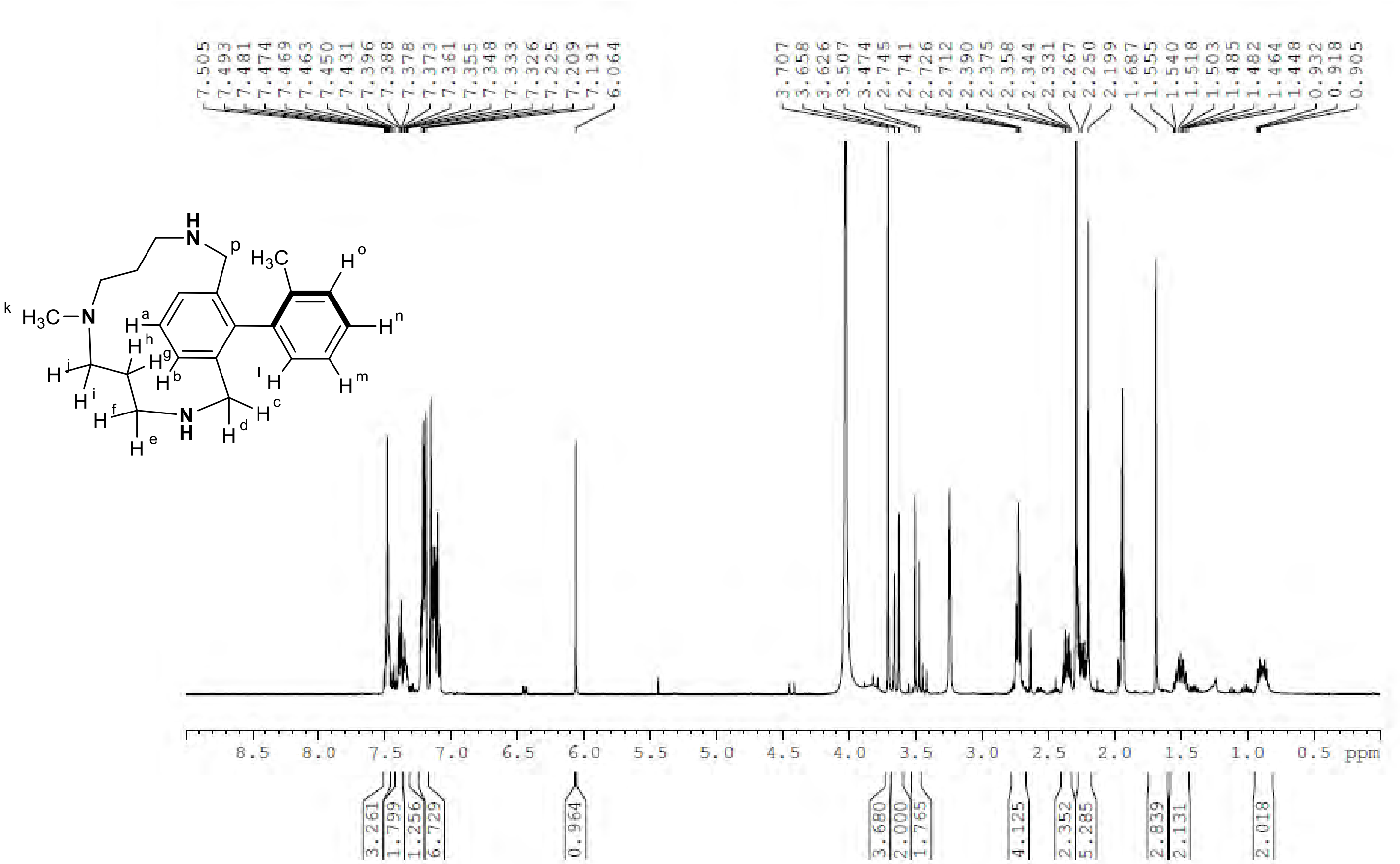

Supplementary Figure 90. ^{1}H NMR spectrum of compound 2j. Experiment performed in CD_3CN, 400 MHz, at 298 K.

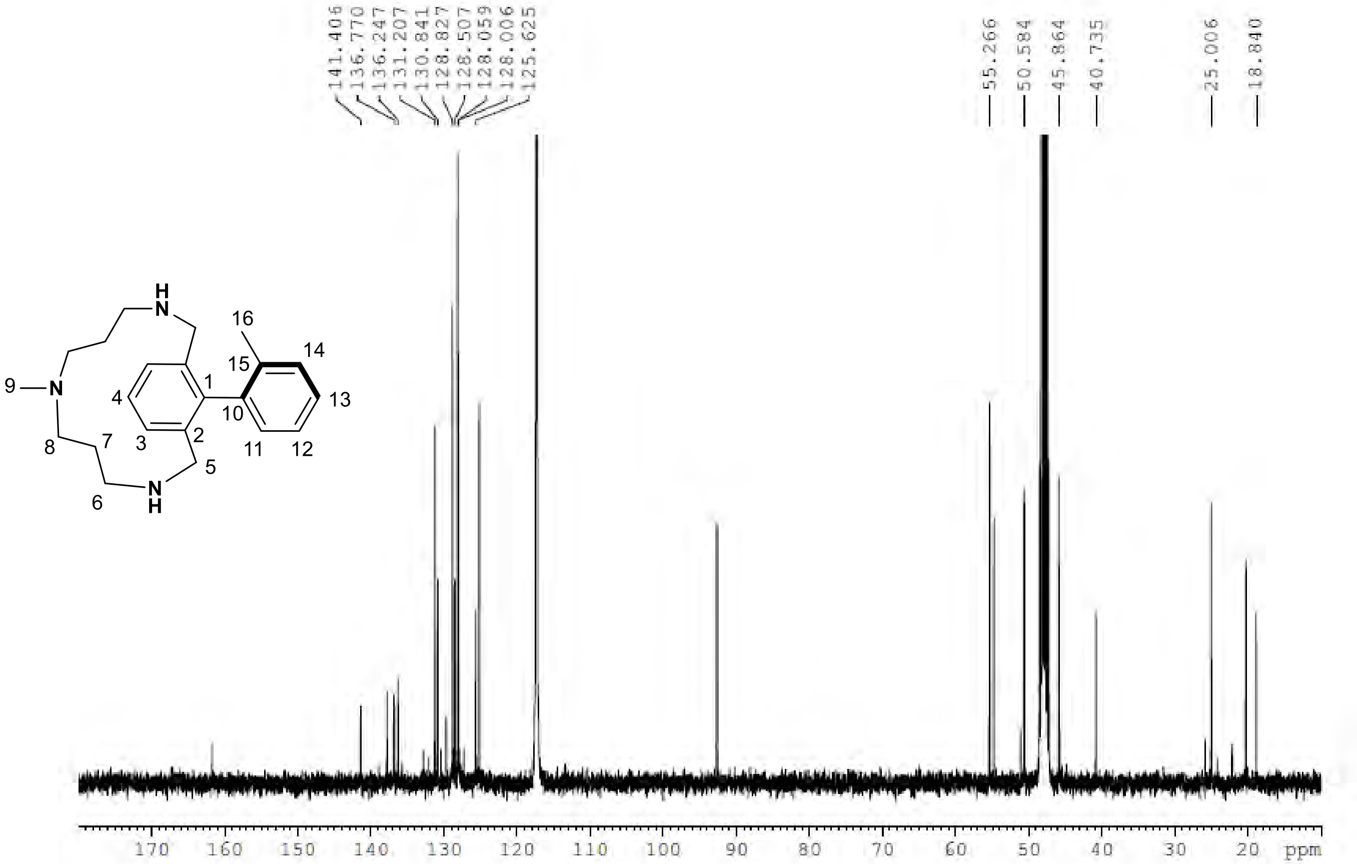

Supplementary Figure 91. ^{13}C NMR spectrum of compound 2j. Experiment performed in CD_3CN, 100 MHz, at 298 K.

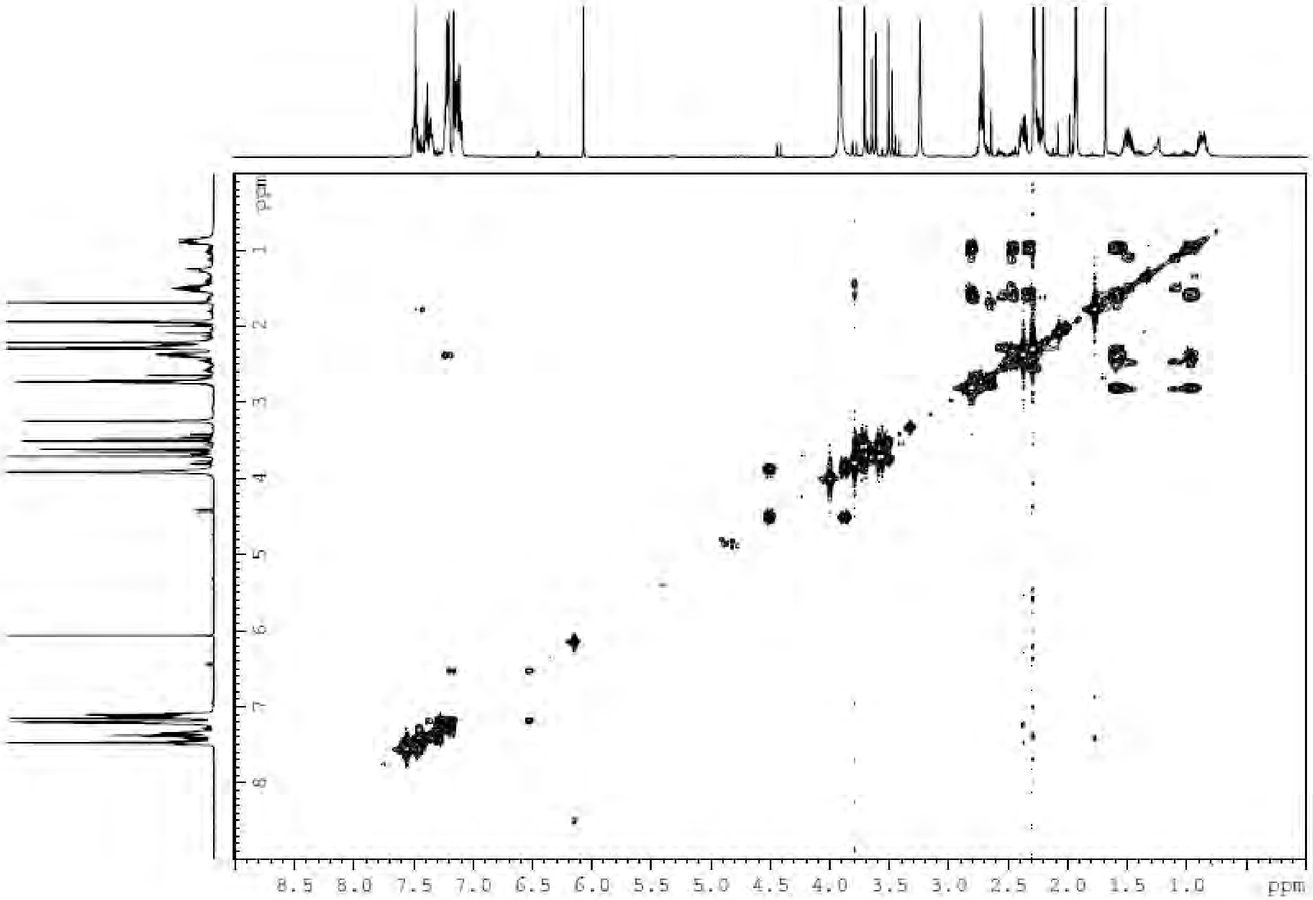

Supplementary Figure 92. COSY spectrum of compound 2j. Experiment performed in CD_3CN, 400 MHz, at 298 K.

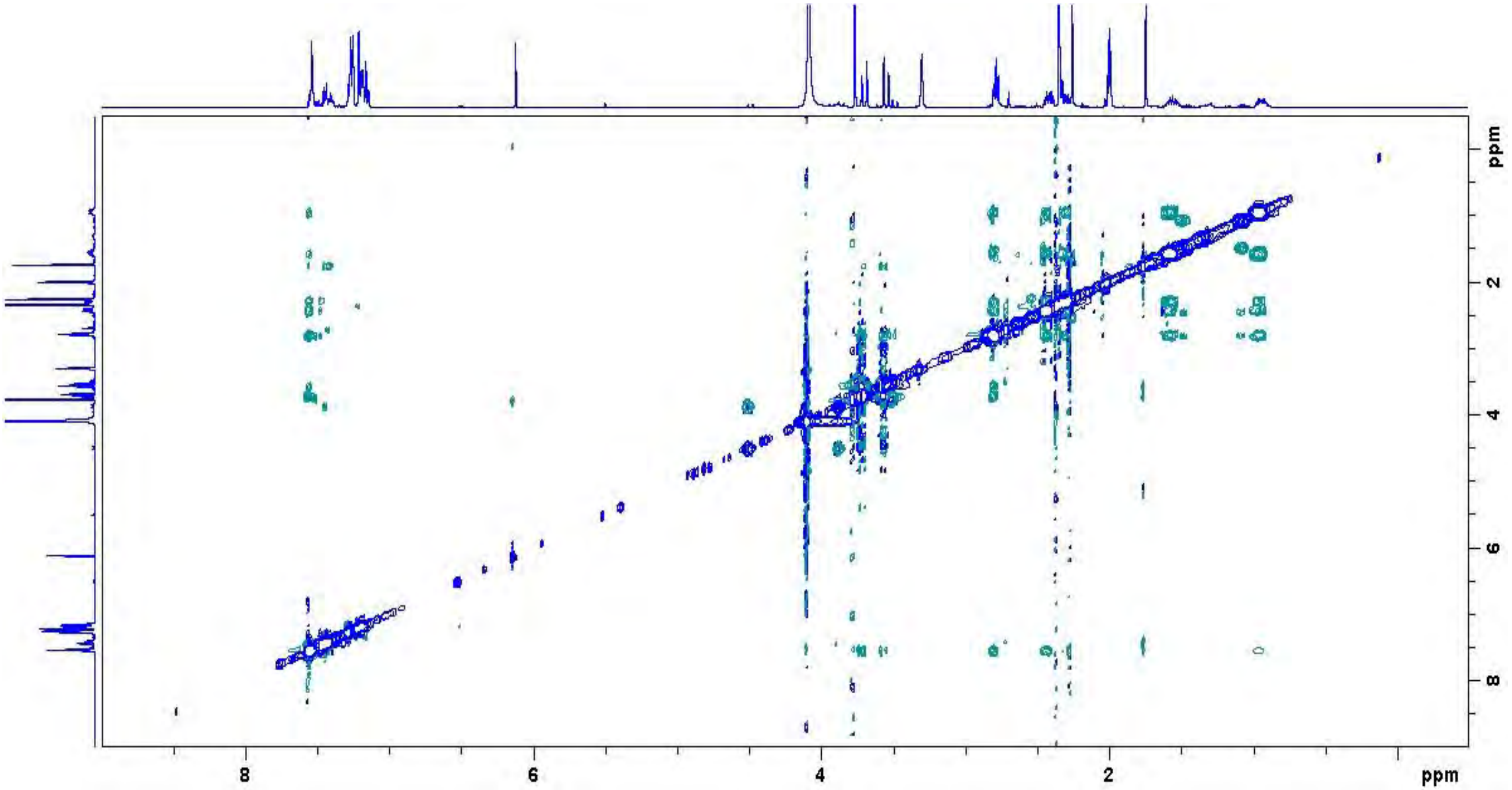

Supplementary Figure 93. NOESY spectrum of compound 2j. Experiment performed in CD_3CN, 400 MHz, at 298 K.

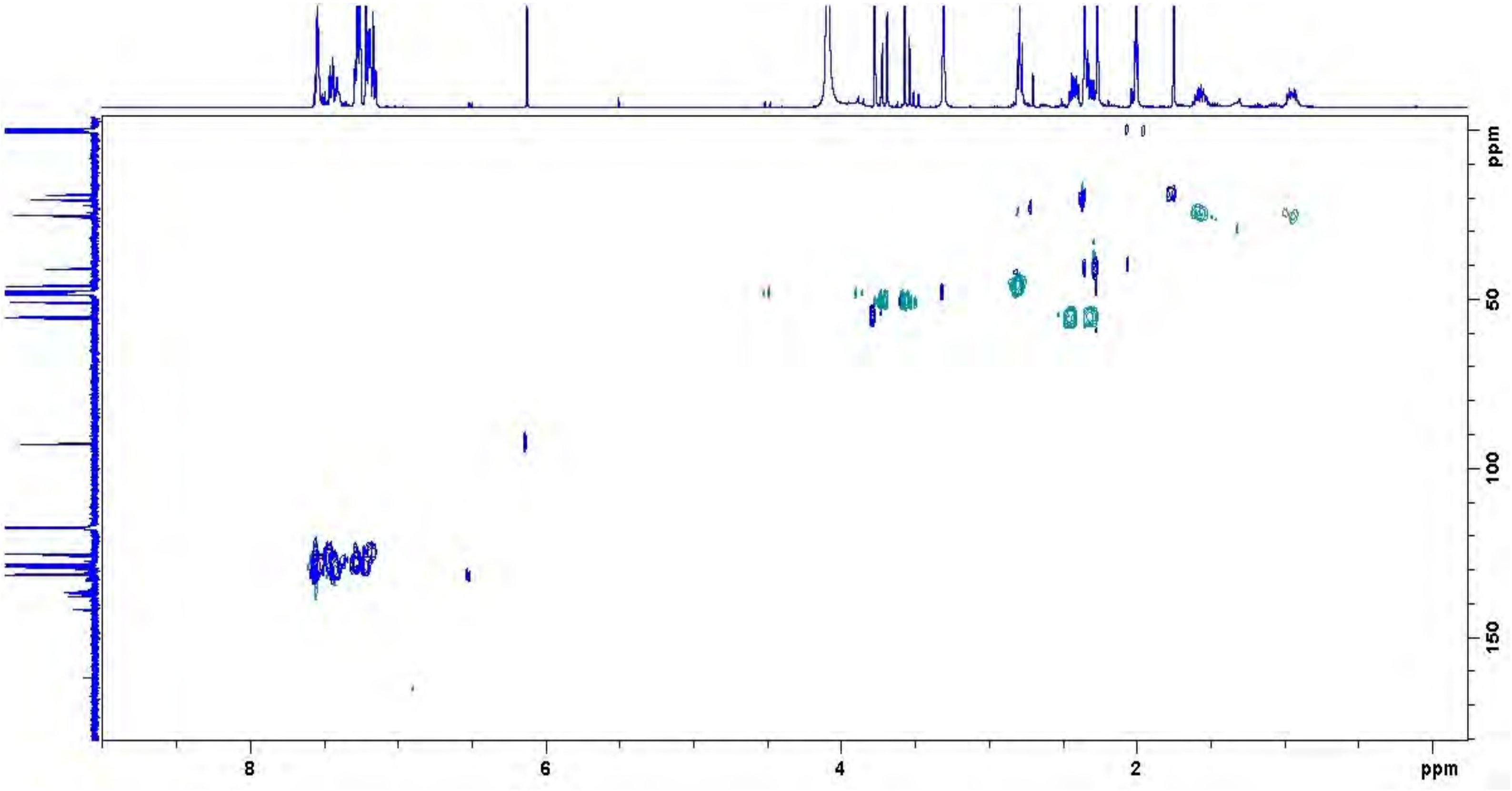

Supplementary Figure 94. ^1H ^{13}C HSQC spectrum of compound 2j. Experiment performed in CD_3CN, 400 MHz, at 298 K.

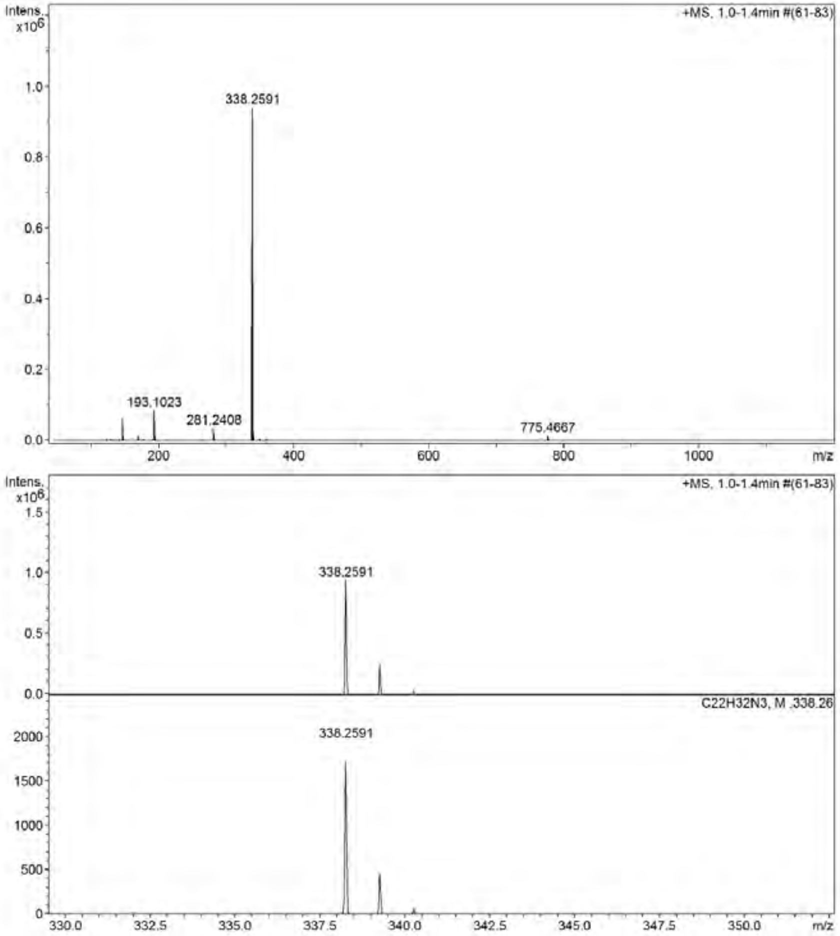

Supplementary Figure 95. HRMS (ESI-MS) spectrum of compound 2j. Experiment performed in CH_3CN (spectrum at the bottom corresponds to the simulated peak).

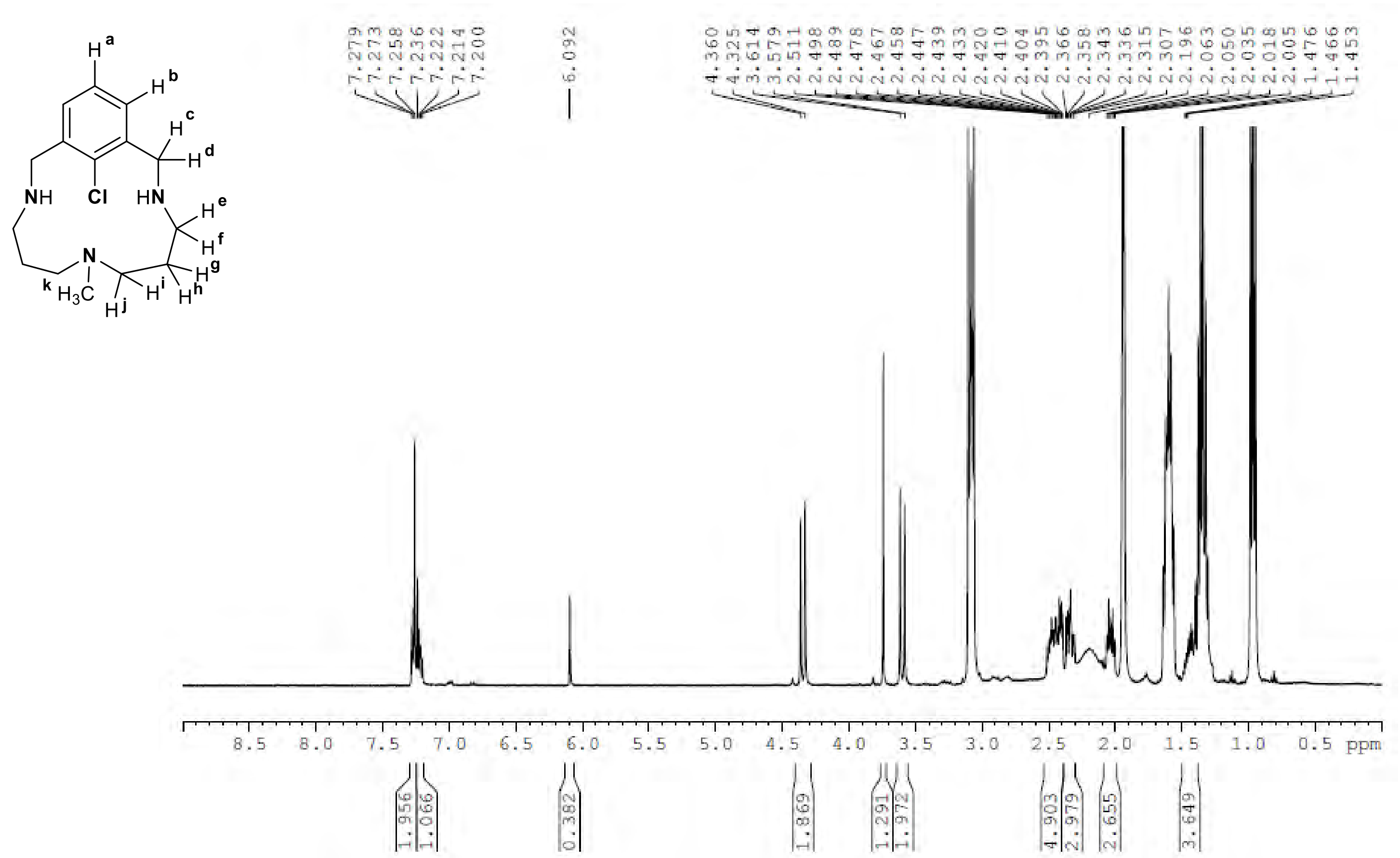

Supplementary Figure 96. ^{1}H NMR spectrum of compound L$_1$-Cl. Experiment performed in CD_3CN, 400 MHz, at 298 K.

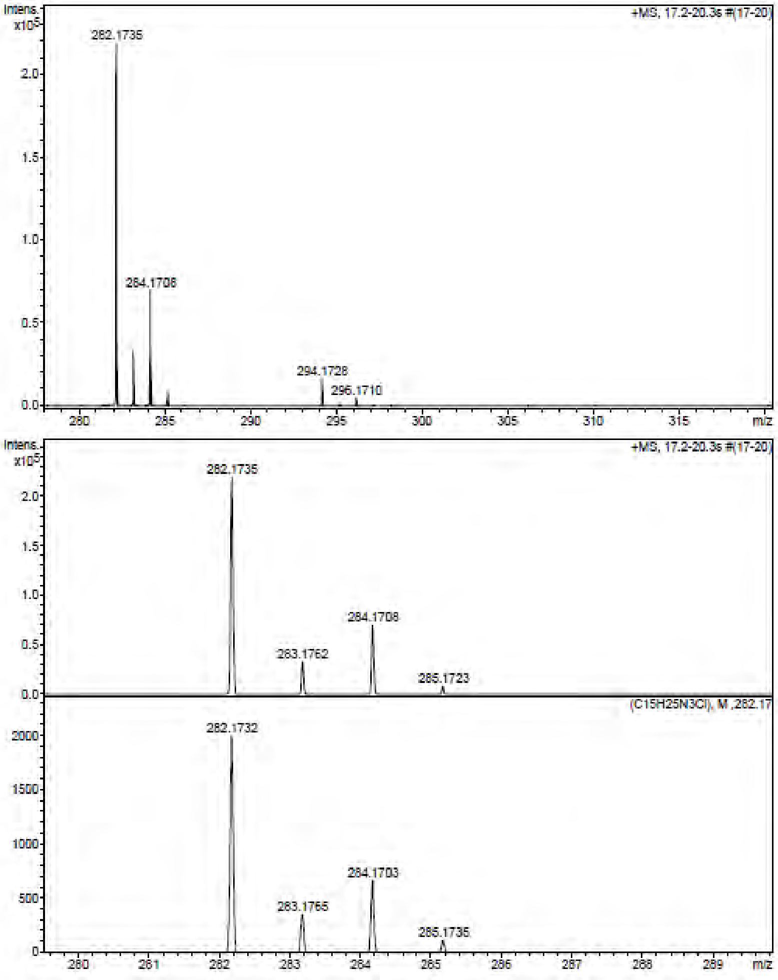

Supplementary Figure 97. HRMS (ESI-MS) spectrum of compound L_1-Cl. Experiment performed in CH_3CN (spectrum at the bottom corresponds to the simulated peak).

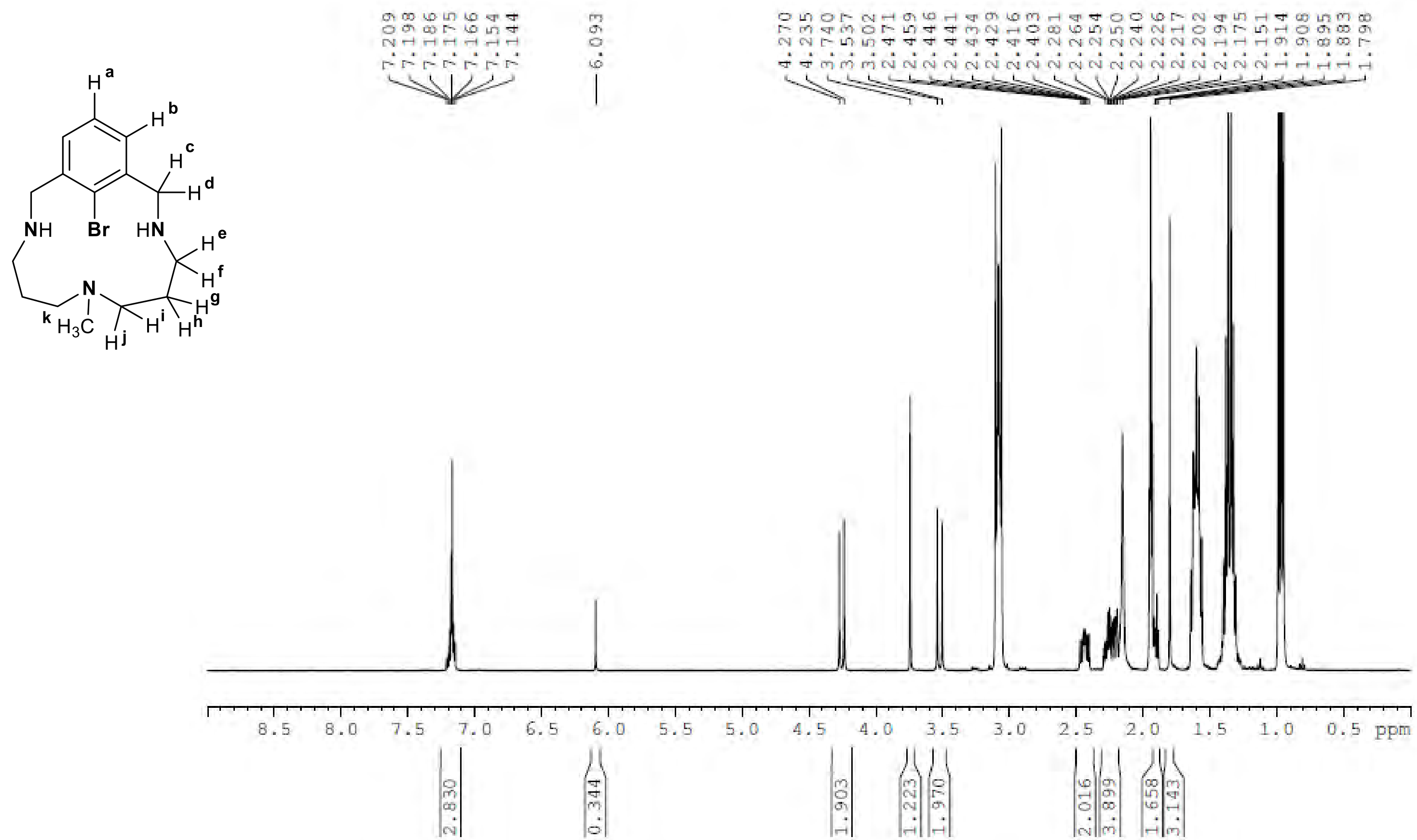

Supplementary Figure 98. ^{1}H NMR spectrum of compound L$_1$-Br. Experiment performed in CD$_3$CN, 400 MHz, at 298 K.

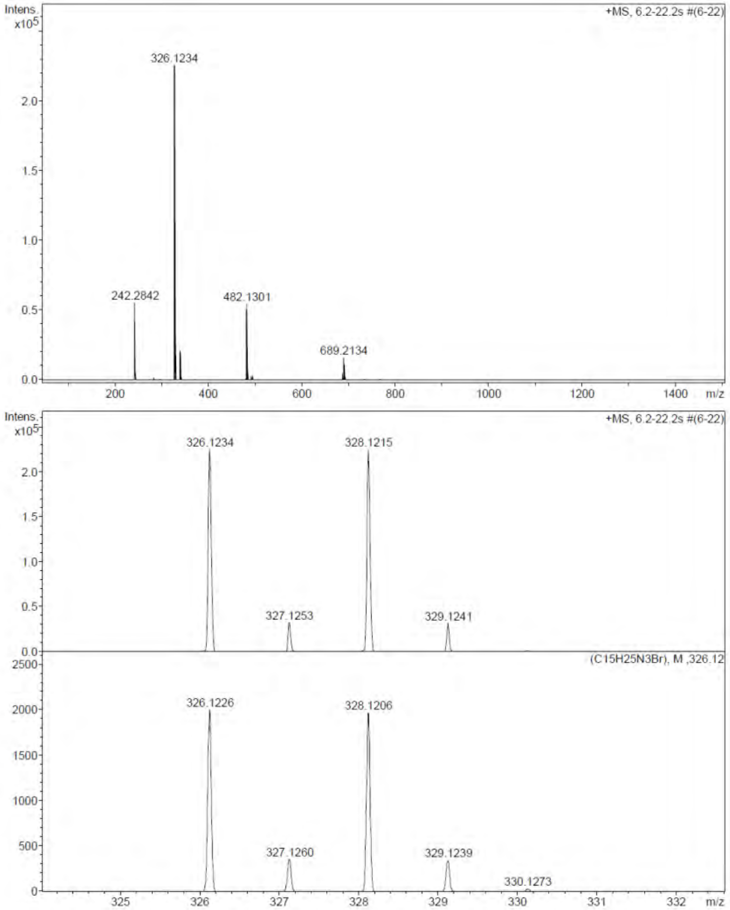

Supplementary Figure 99. HRMS (ESI-MS) spectrum of compound L$_1$-Br. Experiment performed in CH_3CN (spectrum at the bottom corresponds to the simulated peak).

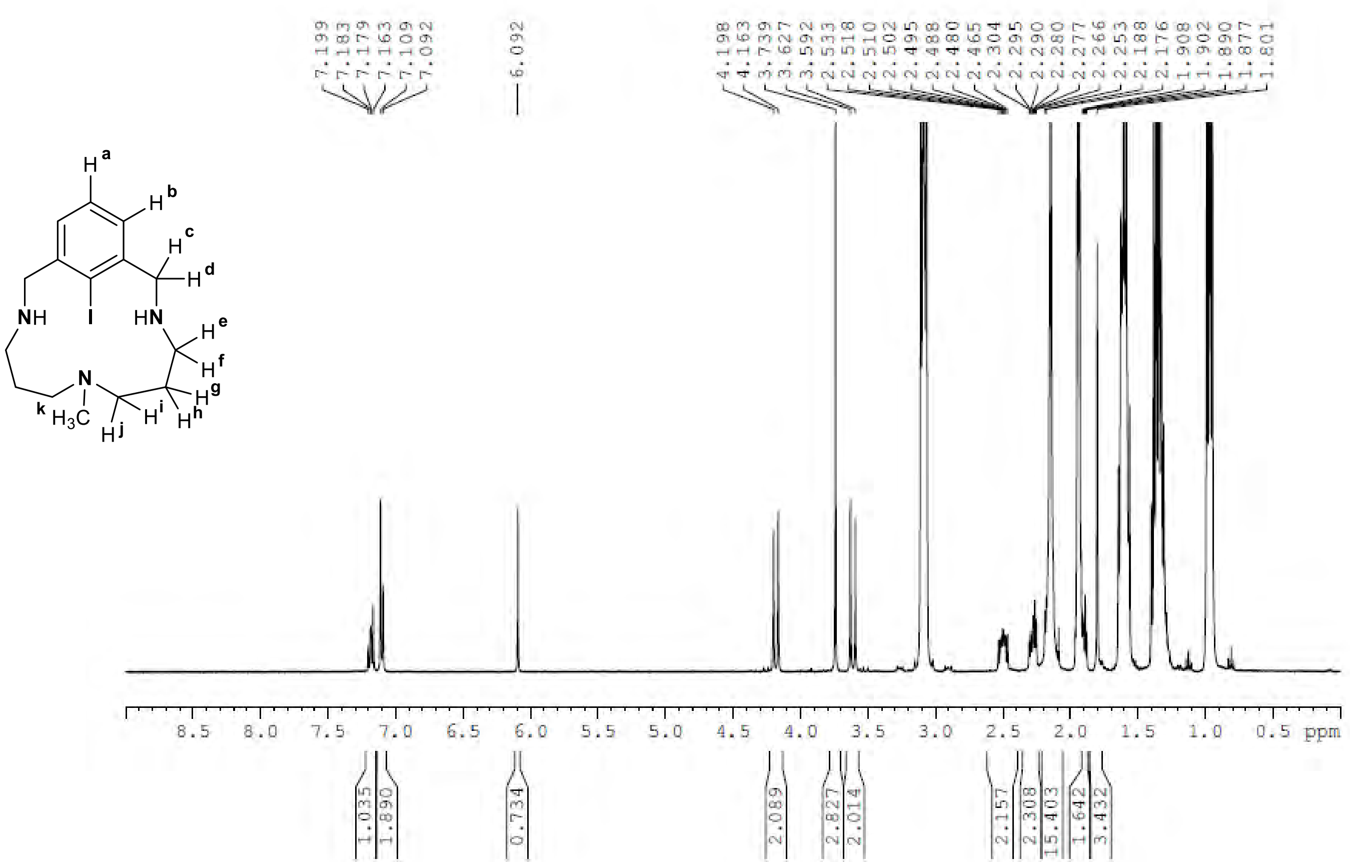

Supplementary Figure 100. ^{1}H NMR spectrum of compound L$_1$-I. Experiment performed in CD$_3$CN, 400 MHz, at 298 K.

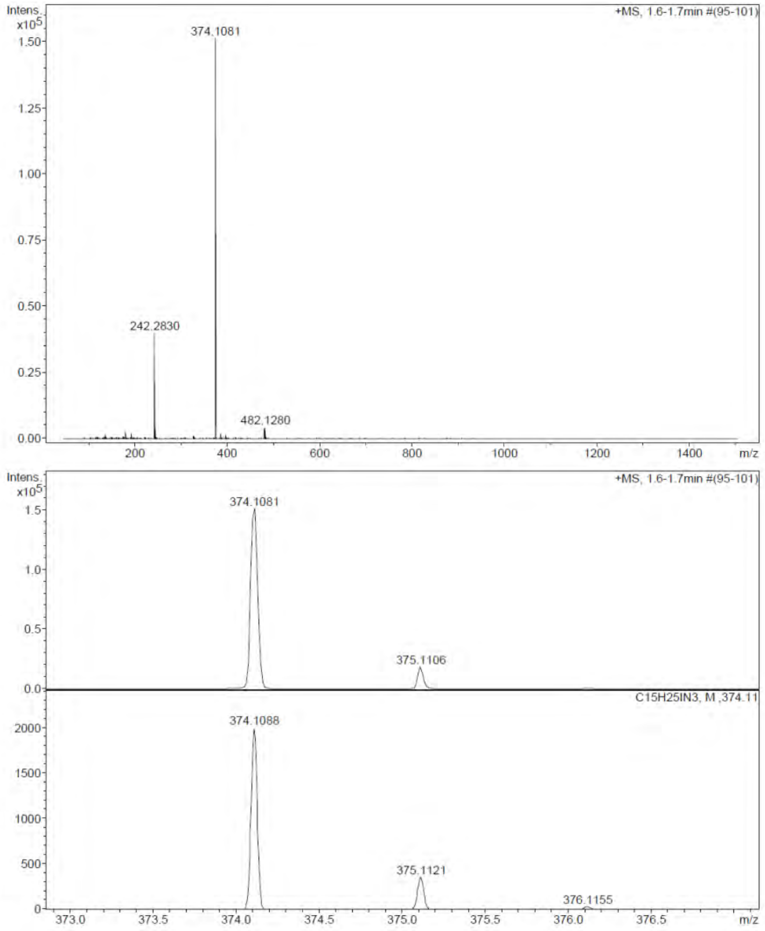

Supplementary Figure 101. HRMS (ESI-MS) spectrum of compound L$_1$-I. Experiment performed in CH_3CN (spectrum at the bottom corresponds to the simulated peak).

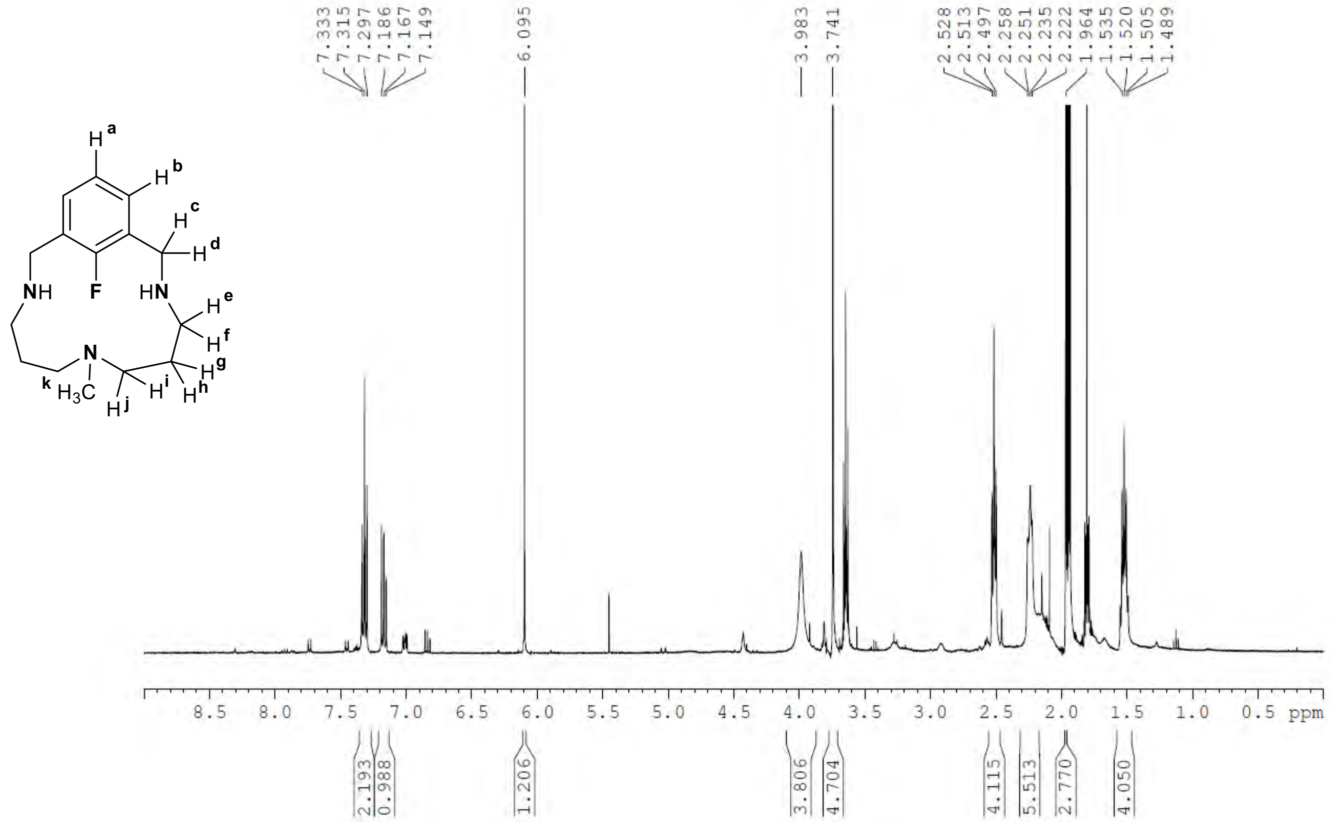

Supplementary Figure 102. ^{1}H NMR spectrum of compound L$_1$-F. Experiment performed in CD$_3$CN, 400 MHz, at 298 K.

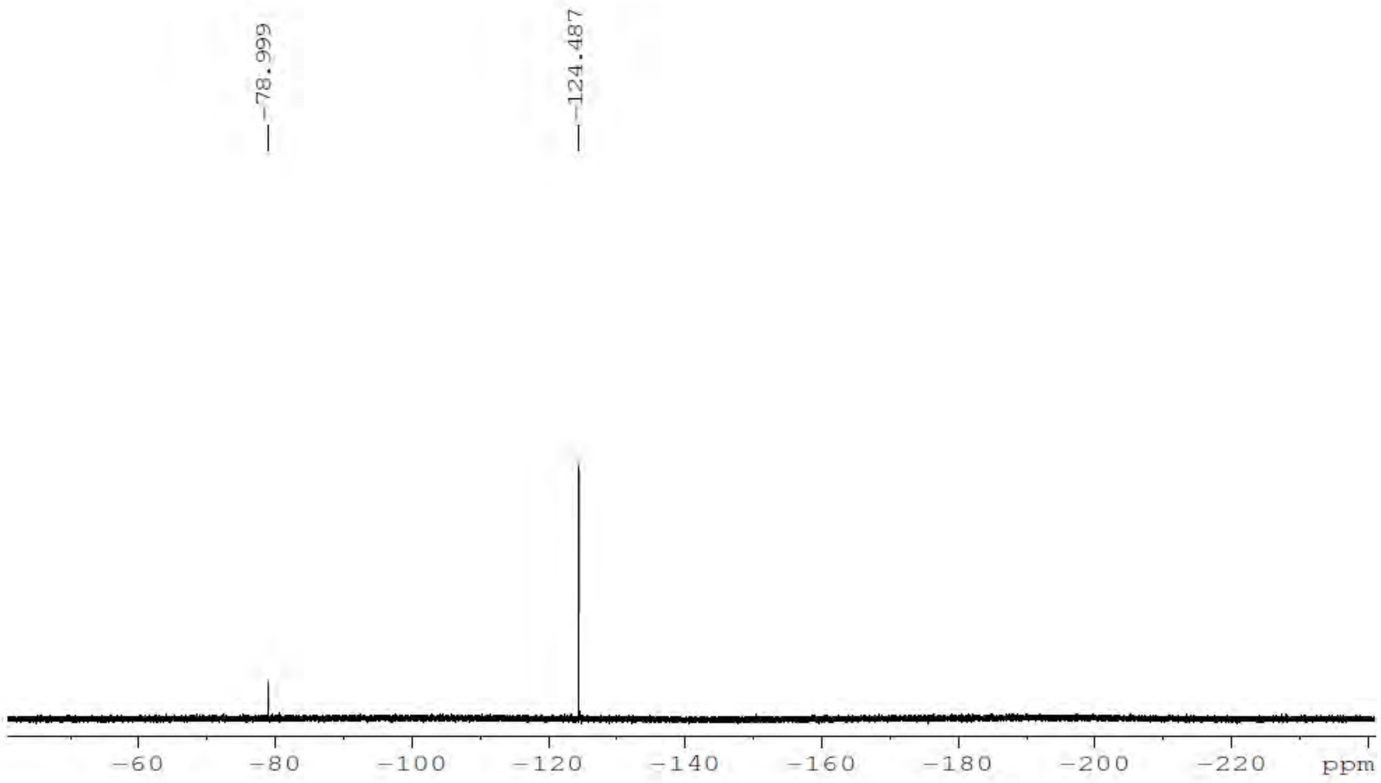

Supplementary Figure 103. ^{19}**F-NMR spectrum of compound L$_1$-F**. Experiment performed in CD_3CN, 282.4 MHz, at 298 K, using $NaCF_3SO_3$ as internal standard (-79.0 ppm).

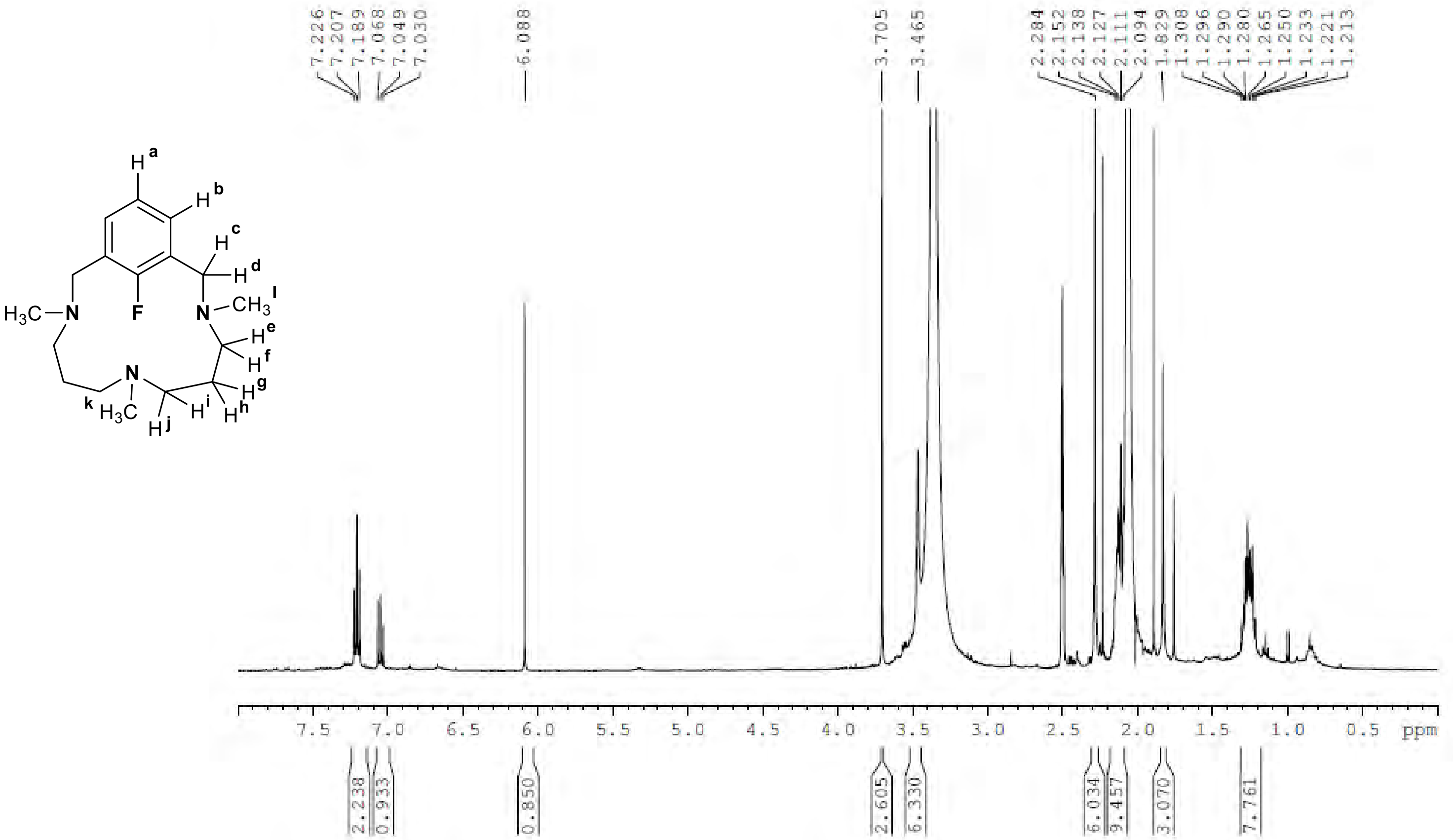

Supplementary Figure 104. ^{1}H NMR spectrum of compound L$_5$-F. Experiment performed in CD$_3$CN, 400 MHz, at 298 K.

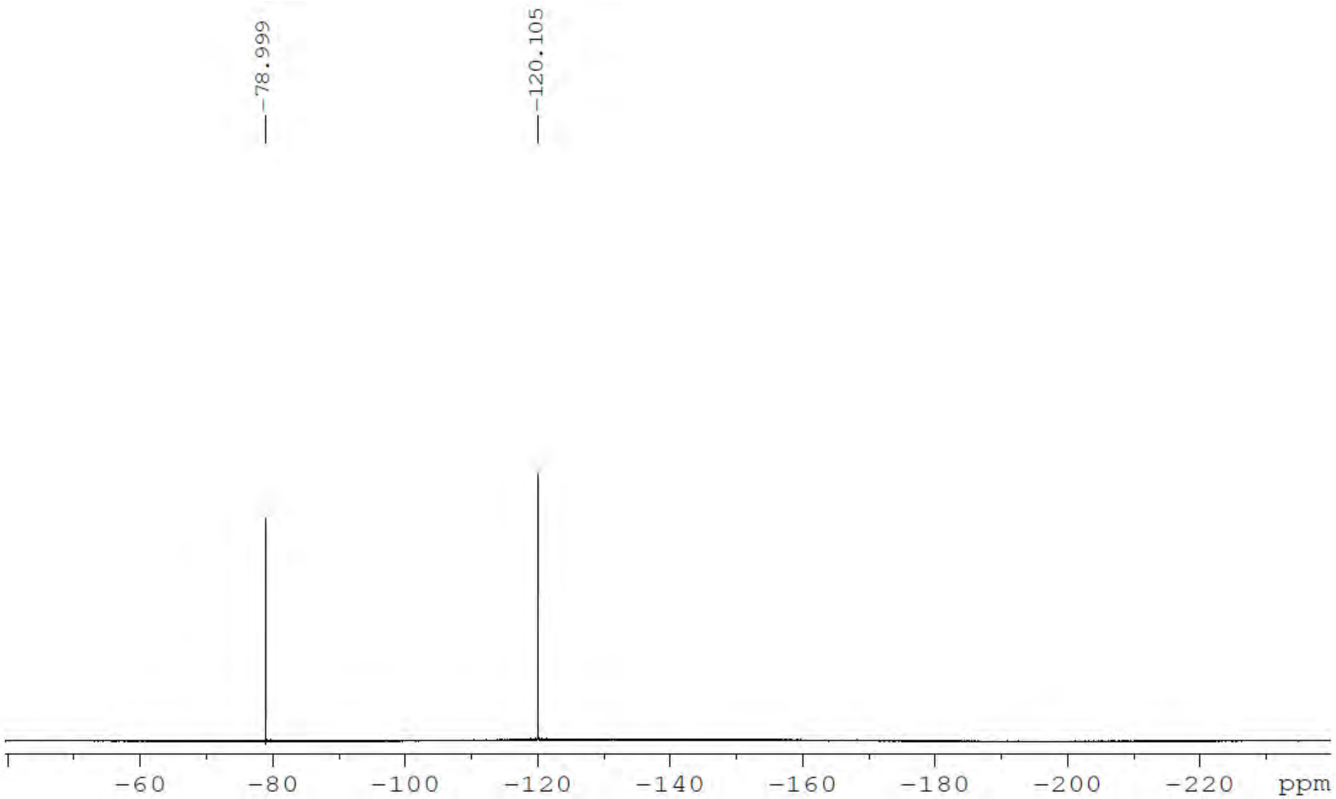

Supplementary Figure 105. ^{19}F-NMR spectrum of compound L_5-F. Experiment performed in CD_3CN, 282.4 MHz, at 298 K, using $NaCF_3SO_3$ as internal standard (-79.0 ppm).

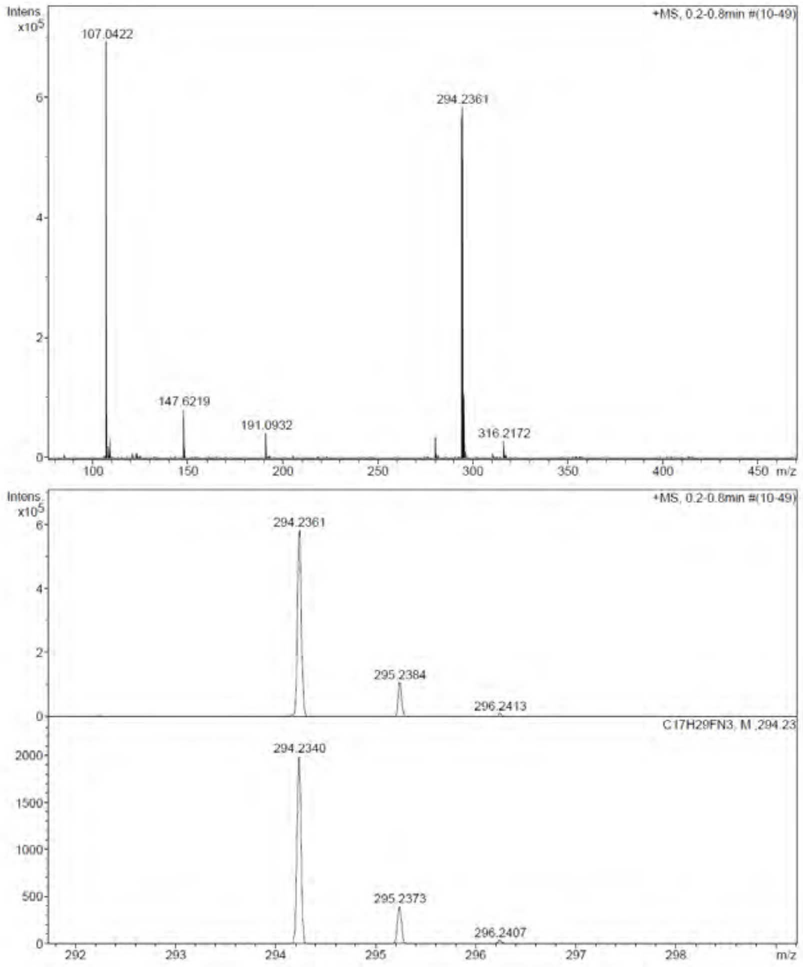

Supplementary Figure 106. HRMS (ESI-MS) spectrum of compound L_5-F. Experiment performed in CH_3CN (spectrum at the bottom corresponds to the simulated peak).

5. Supplementary Tables

Supplementary Table 1. Optimization of the oxidative addition of silver(I) salts to the model aryl-halide L_1-X ligands.[a]

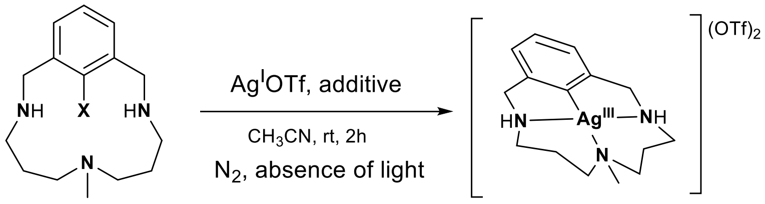

X = I; **L_1-I**
X = Br; **L_1-Br**
X = Cl; **L_1-Cl**

1_{OTf}

Entry	Ligand	Equiv. AgOTf	Additive (equiv. NaOTf)	Yield	Entry	Ligand	Equiv AgOTf	Additive (equiv. NaOTf)	Yield[b]
1[c]	**L_1-Cl**	2	0	0%	13	**L_1-Br**	1.2	0	37%
2	**L_1-Br**	0.5	0	traces	14		1.6	0	55%
3		0.8	0	15%	15		2	0	79%
4		1	0	26%	16		2	2	83%
5		1	1	32%	17		3	0	71%
6		1	1.5	36%	18[d]		1	1 (Tl(OTf))	50%
7		1	2	49%	19[d]		**1**	**10 (Tl(OTf))**	**58%**
8		1	3	45%	20[d]		0	10 (Tl(OTf))	0%
9		1	4	42%	21[d]	**L_1-I**	1	2	51%
10		1	6	40%	22[d]		2	0	97%
11		1	8	33%	23[d]		**1**	**1 (Tl(OTf))**	**68%**
12		1	10	32%	24[d]		4	4 (Tl(OTf))	78%

[a] General conditions: [**L_1-X**] = 15 mM, [Ag^I] = 7.5-30 mM, [additive] = 0-150 mM, 1 mL CH$_3$CN, rt. [b] Calculated by ^{1}H NMR spectroscopy using 1,3,5-trimethoxybenzene as internal standard. [c] Reaction performed at 70ºC. [d] Reaction performed in CD$_3$CN.

Supplementary Table 2. Silver-catalyzed cross coupling with L_1-X model substrates.[a]

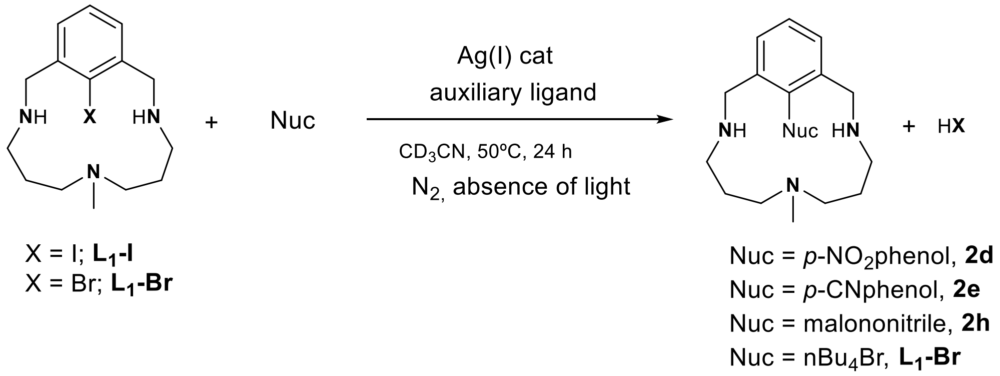
NH X HN
N
+ Nuc
Ag(I) cat
auxiliary ligand
CD$_3$CN, 50ºC, 24 h
N$_2$, absence of light
NH Nuc HN
N
+ HX
X = I; **L$_1$-I**
X = Br; **L$_1$-Br**
Nuc = *p*-NO$_2$phenol, **2d**
Nuc = *p*-CNphenol, **2e**
Nuc = malononitrile, **2h**
Nuc = nBu$_4$Br, **L$_1$-Br**

Entry	Substrate	Additive (mol%)	AgOTf (mol%)	2d Yield[b] (mol%)
1[c]	**L_1-I**	-	10 mol%	9%
2		PPh_3 (1 mol%)	10 mol%	35%
3		PPh_3 (5 mol%)	10 mol%	44%
4[d]		PPh_3 (10 mol%)	10 mol%	46%
5[e,f]		PPh_3 (10 mol%)	10 mol%	38%
6		PPh_3 (20 mol %)	10 mol%	33%
7		PPh_3 (30 mol%)	10 mol%	34%
8		PPh_3 (50 mol%)	10 mol%	23%
9		$P(C_6F_5)_3$ (10 mol%)	10 mol%	31%
10		P(*t*Bu)$_3$ (10 mol%)	10 mol%	10%
11		P(*n*Bu)$_3$ (10 mol%)	10 mol%	26%
12		$P(OMe)_3$ (1 mol%)	10 mol%	30%
13		$P(NMe_2)_3$ (10 mol%)	10 mol%	38%
14		$Ph_2P-(CH_2)_3-PPh_2$ (10 mol%)	10 mol%	12%
15		DMEDA (10 mol%)	10 mol%	40%
16	**L_1-Br**	PPh_3 (20 mol%)	10 mol%	13%
17		P(*n*Bu)$_3$ (10 mol%)	10 mol%	12%
18[g]		PPh_3 (10 mol%) + Tl(OTf) (2 equiv.)	0 mol%	<2%

[a] General conditions: [**L_1-X**] = 5 mM, [*p*-NO$_2$phenol] = 100 mM, 3 mL CH$_3$CN, 50ºC, 24 h. [b] Calculated by ^{1}H NMR spectroscopy using 1,3,5-trimethoxybenzene as internal standard. [c] [*p*-NO$_2$phenol] = 10 mM; [d] [*p*-NO$_2$phenol] = 300 mM. [e] 70ºC. [f] 18% intramolecular C-N coupling and 5% **L_1-OH**.[3] [g] TlOTf (2 equiv.) as additive, 25ºC.

Supplementary Table 3. Crystallographic data and structure refinement for complex [Ag^{III}(L$_1$)](ClO$_4$)$_2$ (1$_{ClO4}$); the Cambridge Crystallographic Data Centre (CCDC) code is 978368.

Compound	**1**$_{ClO4}$
Empirical formula	$C_{15} H_{24} Ag Cl_2 N_3 O_8$
Formula weight	553.14
Temperature, K	150(10)
Wavelenght, Å	0.71073
Crystal system	monoclinic
Space group	P21/n
Unit cell dimensions	
a, Å	8.5454(4)
α, deg	90.00
b, Å	12.5939(5)
β, deg	94.839(4)
c, Å	18.7061(8)
γ, deg	90.00
Volume, Å^3	2005.97(14)
Density (calculated), g·cm^3	1.832
Cell formula units_Z	4
Absorption coefficient, mm^{-1}	1.321
Crystal size, mm	0.31 x 0.12 x 0.08
Reflections collected	27341
Independent reflections	5122 [R(int) = 0.0333]
Final R indices [I<2σ(*I*)]^α	R1 = 0.0312 , wR2 = 0.0700
R indices (all data)	R1 = 0.0414 , wR2 = 0.0775

$R = \Sigma[F_0 - F_c] / \Sigma F_0$ $\quad$ $wR = [\Sigma(w(F_0^2 - F_c^2)^2) / \Sigma(wF_0^4)]^{1/2}$